

**Application of NEXTMap DEM Data to the  
Mapping and Interpretation of Late Quaternary  
Landforms in the Scottish Highlands**

**Chao-Yuan Chen**

**Thesis submitted for the degree of Doctor of Philosophy at the  
University of London**

**July 2012**

**Institution of study:  
Department of Geography  
Royal Holloway University of London**

## Declaration of Authorship

I **CHAO-YUAN CHEN** hereby declare that this thesis and the work presented in it is entirely my own. Where I have consulted the work of others, this is always clearly stated.

Signed: 

Date: 17-07-2012

## **Abstract**

---

This thesis examines the potential of NEXTMap imagery for the study of glacial landforms in parts of the Scottish Highlands. NEXTMap Digital Elevation Mapping (DEM) was developed in 1998 and a comprehensive set of DEMs for the British Isles generated in 2004. However, very few maps based on NEXTMap technology had been published for the British Isles before the start of this PhD, and so its full potential had not been realised. The objectives of the PhD were therefore to establish the degree to which NEXTMap imagery could improve the mapping of Quaternary landforms.

To test its capabilities, NEXTMap images were obtained for the Loch Lomond area, which had previously been mapped in some detail using both field observation and aerial photography. Appropriate protocols were therefore developed for an area where NEXTMap images could be ‘ground-truthed’ by independent ground mapping. Methods were developed for optimizing the appearance of landforms on NEXTMap images and mapping their distributions; the results show close correspondence with the results of detailed ground mapping, suggesting that confidence can be attached to landform maps derived using NEXTMap, while the latter can also provide subtle but important new geomorphological information.

The second part of the thesis applied the methodology developed in the Loch Lomond study to the study of landforms in and around Glen Roy, in the western Scottish Highlands. This area was chosen as it also had already been mapped in detail and proved to be critical for establishing the extent and timing of the last major glaciers in Scotland. The area also contains a unique set of well preserved ancient lake shorelines – the Parallel Roads of Glen Roy. These features extend for miles across the study area, providing an outstanding opportunity to test the spatial and vertical resolution of

NEXTMap images, and hence to establish the limits of maps and models based upon them. This part of the project included direct tests of the vertical resolution achievable using NEXTMap, which gives surprisingly accurate data for flat and gently-inclined surfaces. The results of trend surface analysis of nearly 32,000 altitude measurements obtained from the shoreline surfaces shows that despite the fact that they are significantly deformed and dislocated, they nevertheless retain consistent along-shore surface gradients. Both the overall gradients and the localized deformation features associated with the shorelines are attributed to a combination of regional and local isostatic stresses. The thesis finishes with a synthesis of the new evidence and perspectives that NEXTMap has provided for the Glen Roy area, and with a synopsis of where interpretations differ from those previously based on ground mapping.

## **Acknowledgements**

---

The accomplishment of this PhD thesis is attributed to many people who have been involved and provided help to the author over the course of the past 5 years. I would like to thank them all for their help and encouragement. First and foremost I would like to pass on my sincere thanks to Professor **John Lowe**, Professor **Jim Rose** and Dr. **Adrian Palmer** for their unwavering guidance and support. I really appreciate the way you have steered me through the whole process and am grateful for all the stimulating scientific questions that inspired me in this research. I also owe enormous thanks to Dr. **Xingming Meng** who introduced me to the Quaternary research world, helped me improve my GIS skills and gave me useful advice for living in the Egham area in particular, and in the UK in general.

I also acknowledge and thank the **British Geological Survey** and the **Natural Environment Research Council (NERC), UK** for providing access to the NEXTMap image data base which supported this project under the NERC's RAPID Climate Change thematic programme. Copyright of the NEXTMap DEM data used in this PhD project belongs to the NERC but **Intermap Technologies**, who flew the original air photograph sorties and developed the imagery, are also duly acknowledged throughout the thesis.

Several cohorts of students of the NERC-supported MSc degree in Quaternary Science (taught jointly by Royal Holloway and University College, University of London) have contributed by undertaking some independent field analytical tests in the Glen Roy area. Special thanks are due to the group of MSc 2009-2010 students who carried out the instrumental levelling of a section of the 'Parallel Road' surfaces for one of the key tests

of experiments reported in Chapter 7 of this thesis. Thanks also go to past MSc students **Gareth Tye, Eleri Harris, Robert Storrar** and **Richard Jones** for their company and assistance in the field. In addition to those who have directly contributed by leveling, I would also like to acknowledge the advice received from **Simon Armitage, Simon Blockley, Russell Coope** and **Brian Sissons** during field visits between 2006 and 2010.

The Short Field Meeting of the Quaternary Research Association (QRA) based in Spean Bridge and Roybridge between the 7<sup>th</sup> and 11th September, 2008, is an event that had an important impact on this PhD project. Many of the key ideas reported in this thesis were refined as a result of that trip, and indeed when preparing the contributions made to the associated field guide (see below). Discussion with **Douglas Benn** during that field meeting were particularly valuable.

Thanks also go to **Win Min Tun** for providing help with data storage and computer technical support; **Penny Rose** for kindly providing tuition in the English language during her private time; and **Richard Wallis** of Alcan Aluminium UK Limited, for supplying the altitude data for the Alcan hydroelectric scheme pipes near Fort William, used in one of the tests of the vertical resolution of NEXTMap.

I also wish to extend sincere thanks to the EMU postgraduate community crew of **Alison, Faye, Eriko, Xuejuan, Nhung, Charles, Sorayya, Chih Yuan** and **Harnng Luh**. Their regular companionship and encouragement gave me renewed energy when things got tough: all the very best to you all.

And finally to my family members and my wife, I thank them for their long-suffering patience, as well as their unending love, support and encouragement throughout the

whole of the PhD study period, which gave me the strength to overcome all kinds of difficulties.

### **Declaration of published material**

---

It is hereby declared that parts of chapters 3, 6 and 7 in this thesis provided the foundation for the following parts of the following publication:

Chen, C-Y. and Rose, J. 2008. Assessment of remote sensed imagery on the analysis of landforms in Glen Roy. In Palmer, A.P., Lowe, J.J., Rose, J. (eds.), *The Quaternary of Glen Roy and Vicinity: Field Guide*, Quaternary Research Association, London, pp. 36-45.

Chen, C-Y. and Rose, J. 2008. A DSM perspective on the geomorphology of the region around Glen Turret and the adjacent part of Glen Roy. In Palmer, A.P., Lowe, J.J., Rose, J. (eds.), *The Quaternary of Glen Roy and Vicinity: Field Guide*, Quaternary Research Association, London, pp. 150-157.

*and*

Chen, C-Y. and Rose, J. 2008. A DSM perspective on the geomorphology of the region around Caol Lairig and the Viewpoint in the lower section of Glen Roy. In Palmer, A.P., Lowe, J.J., Rose, J. (eds.), *The Quaternary of Glen Roy and Vicinity: Field Guide*, Quaternary Research Association, London, pp. 166-173.

# CONTENTS

---

<b>Declaration of Authorship</b> .....	<b>i</b>
<b>Abstract</b> .....	<b>ii</b>
<b>Acknowledgements</b> .....	<b>iv</b>
<b>List of Chapters and sections</b> .....	<b>vii</b>
<b>List of Figures</b> .....	<b>xiii</b>
<b>List of Tables</b> .....	<b>xxiv</b>
<b>List of Appendices</b> .....	<b>xxvi</b>

## **List of Chapters and sections:**

<b>1. Introduction</b> .....	<b>1</b>
<b>1.1 Inception of the project</b> .....	<b>1</b>
<b>1.2 Framing the project</b> .....	<b>5</b>
<b>1.3 Aims of the project</b> .....	<b>7</b>
<b>1.4 Structure of the project</b> .....	<b>8</b>
<b>2. Mapping the ice limits of the last (late Devensian) ice sheet in the British Isles</b> .....	<b>11</b>
<b>2.1 Introduction</b> .....	<b>11</b>
<b>2.2 The last ice sheet in Northern Europe</b> .....	<b>12</b>
<b>2.3 The last (Late Devensian) ice sheet in Britain and Ireland</b> .....	<b>19</b>
<b>2.4 The Loch Lomond and Glen Roy study areas</b> .....	<b>23</b>



2.5	Numerical modeling of Loch Lomond Readvance ice growth in Scotland.....	26
<b>3.</b>	<b>Introduction to NEXTMap: testing its capabilities.....</b>	<b>30</b>
3.1	Introduction.....	30
3.2	Remote sensing imagery available in UK.....	31
3.3	DEM Visualization Techniques.....	37
3.4	Characteristics of NEXTMap Great Britain <sup>TM</sup> .....	47
3.5	Experiments.....	48
3.5.1	Research sites.....	48
3.5.2	Evaluation of glacial landforms on ORI, DSM and DTM NEXTMap images.....	51
3.5.3	Experiments designed to examine the effectiveness of DSM images for the representation of landforms.....	55
3.5.4	Analysis of experimental results.....	56
3.6	Conclusions.....	66
<b>4.</b>	<b>Glacial landform mapping using NEXTMap: scoping exercises...68</b>	
4.1	Introduction.....	68
4.2	Mapping Procedures.....	70
4.3	Glacial landform mapping using rotating NEXTMap images and its comparison with results derived from field survey.....	74
4.3.1	Introduction.....	74
4.3.2	Glacial landform mapping using rotating NEXTMap images and its comparison with results derived from field survey: drumlins.....	75
4.3.3	Glacial landform mapping using rotating NEXTMap images and its comparison with results derived from field survey: hummocky	

moraines.....	81
<b>4.3.4</b> Glacial landform mapping using rotating NEXTMap images and its comparison with results derived from field survey: kame and kettles.....	85
<b>4.3.5</b> Glacial landform mapping from NEXTMap and its comparison with field evidence: meltwater channels.....	91
<b>4.4</b> <b>Image mosaic: the optimized method in presenting landforms.....</b>	<b>96</b>
4.4.1    Analysis of glacial meltwater channel distribution and optimized base map selection.....	96
4.4.2    Imagery mosaic method for representing landforms on a single image.....	103
<b>4.5</b> <b>Conclusions and Recommendations.....</b>	<b>111</b>
<b>5. Background to the Glen Roy area.....</b>	<b>112</b>
<b>5.1 Introduction.....</b>	<b>112</b>
<b>5.2 Site location and bedrock geology.....</b>	<b>113</b>
<b>5.3 Early studies in the Glen Roy area.....</b>	<b>117</b>
<b>5.4 Interpretations of the Glen Roy evidence by J.B. Sissons.....</b>	<b>126</b>
<b>5.4.1</b> The sequence of lake changes in Glen Roy.....	<b>126</b>
5.4.1.1    Stages 1-5: The Rising Sequence.....	127
5.4.1.2    Stages 6-8: The Falling Sequence.....	130
<b>5.4.2</b> Nature and formation of shorelines.....	<b>134</b>
<b>5.4.3</b> Differential glacio-isostatic uplift of crustal blocks at Glen Roy.....	<b>135</b>
<b>5.5 Synopsis.....</b>	<b>136</b>
<b>6. Glaciation effects in Glen Roy and vicinity.....</b>	<b>137</b>
<b>6.1 Introduction.....</b>	<b>137</b>

<b>6.2</b>	<b>Lower section of Glen Roy</b> .....	138
6.2.1	Introduction.....	138
6.2.2	Previous studies in the lower section of Glen Roy.....	139
6.2.3	NEXTMap interpretation of ice limits and marginal features in lower Glen Roy.....	142
6.2.3.1	The potential ice-flow direction in lower Glen Roy.....	142
6.2.3.2	Ice-marginal features and lake shorelines.....	145
6.2.3.3	Evaluation.....	157
<b>6.3</b>	<b>Middle section of Glen Roy</b> .....	158
6.3.1	Introduction.....	158
6.3.2	Allt Bhreac Achaidh Fan.....	158
6.3.3	The Brunachan Fan.....	162
6.3.4	The Reinich Fan.....	165
6.3.5	Evaluation of landforms in Middle Glen Roy.....	168
<b>6.4</b>	<b>Upper section of Glen Roy and Glen Turret</b> .....	170
6.4.1	Introduction.....	170
6.4.2	Published information on the Glacigenic landforms in Upper Glen Roy.....	171
6.4.2.1	Block I: the Glen Turret area.....	171
6.4.2.2	Block II: Allt a' Chomhlain and Coire Dubh.....	175
6.4.2.3	Block III: The upper Roy, upstream from the Turret Fan.....	176
6.4.3	Analysis of landforms in upper Glen Roy based on NEXTMap imagery.....	178
6.4.3.1	Introduction.....	178
6.4.3.2	Landforms in Glen Turret (Block I).....	181

6.4.3.3	Landforms in Allt a' Chomhlain and Coire Dubh (Block II)...	184
6.4.3.4	Upper Glen Roy, east of the GTF (Block III).....	190
6.4.3.5	Synthesis of evidence in upper Glen Roy.....	191
<b>6.5</b>	<b>Conclusions.....</b>	<b>196</b>
<b>7.</b>	<b>Shoreline analysis: distribution, form and architecture.....</b>	<b>199</b>
<b>7.1</b>	<b>Introduction.....</b>	<b>199</b>
<b>7.2</b>	<b>Methodology.....</b>	<b>201</b>
7.2.1	Assumptions concerning the mode of formation of the Roads.....	201
7.2.2	Mapping shoreline fragments using NEXTMap.....	203
7.2.3	Measurement of shoreline altitudes.....	205
<b>7.3</b>	<b>Distribution of the Parallel Roads.....</b>	<b>213</b>
<b>7.4</b>	<b>Variations in platform width, aspect and slope.....</b>	<b>224</b>
<b>7.5</b>	<b>Measurement of longitudinal shoreline gradients.....</b>	<b>231</b>
<b>7.6</b>	<b>Test of accuracy of NEXTMap altitudinal measurements.....</b>	<b>234</b>
7.6.1	Testing for horizontality: runways at Heathrow airport.....	236
7.6.2	Testing horizontal and near-horizontal surfaces at Loch Laggan.....	239
7.6.3	NEXTMap altitude measurements obtained from controlled inclined surface.....	244
7.6.4	Instrumental levelling of shoreline stretches in Glen Roy.....	249
7.6.5	Conclusions.....	253
<b>7.7</b>	<b>Evidence for block-tilting of the Parallel Roads of Glen Roy.....</b>	<b>255</b>
7.7.1	Sissons and Cornish, 1982.....	255
7.7.2	NEXTMap measurements.....	261
<b>7.8</b>	<b>Major localised dislocation of the Parallel Roads.....</b>	<b>271</b>
7.8.1	Area around landslip 1, Lower Glen Roy.....	271

7.8.2	Area around landslip 2, Lower Glen Roy.....	276
7.8.3	Area around landslip 3, Middle Glen Roy.....	285
7.8.4	Upper Roy, NE of the Turret fan.....	295
<b>7.9</b>	<b>Synopsis.....</b>	<b>303</b>
<b>7.10</b>	<b>Analysis of longitudinal shoreline gradients: trend-surface analysis.....</b>	<b>305</b>
<b>7.11</b>	<b>Deriving representative gradients for the Parallel Roads.....</b>	<b>317</b>
<b>8.</b>	<b>Synthesis and Conclusions.....</b>	<b>327</b>
<b>8.1</b>	<b>Introduction.....</b>	<b>327</b>
<b>8.2</b>	<b>Key issues concerning the sequence of events in the Glen Roy area during the Loch Lomond Stadial.....</b>	<b>329</b>
8.2.1	Maximum extent of glacier advance in Glen Gloy.....	329
8.2.2	Origin of the Turret fan.....	334
8.2.3	Evidence for asynchronous ice-front changes in Glen Turret, Glen Gloy, Caol Lairig and Glen Roy.....	337
8.2.4	Causes of deformation of the Parallel Roads.....	340
8.2.5	The time of formation of dislocations of the Parallel Roads.....	346
8.2.6	The locus and timing of major jökulhlaup events in the Roy-Gloy area.....	348
<b>8.3</b>	<b>The pattern and sequence of events in Glen Roy during the Loch Lomond Stadial.....</b>	<b>356</b>
<b>8.4</b>	<b>Key conclusions concerning the potential of NEXTMap imagery.....</b>	<b>364</b>
	<b>Bibliography.....</b>	<b>370</b>
	<b>Appendices.....</b>	<b>388</b>

<b>List of Figures</b>	<b>Page no.</b>
 <b>Chapter 1: Introduction</b>	
1.1 A digital surface elevation model (DSM) of the NW Scottish Highlands created using NEXTMap images (from Goodenough et al., 2009).....	4
 <b>Chapter 2: Mapping the ice limits of the last (late Devensian) ice sheet in the British Isles</b>	
2.1 Reconstruction of the limits of the Eurasian ice sheet at the Late Weichselian/Devensian glacial maximum (from Svendsen et al. 2004)....	12
2.2 Climatostratigraphic subdivision of the last 30,000 (from Lowe <i>et al.</i> , 2008).....	14
2.3 Geomorphological evidence for the maximum extent and recession of the late Weichselian Fennoscandian ice sheet in northern Europe (from Lowe and Walker 1997).....	16
2.4 Recent reconstructions of the maximum extent of the Last Glacial Maximum (Late Devensian) ice sheet over the British Isles (from Boulton and Hagdorn 2006).....	20
2.5 Inferred maximal limits of Loch Lomond Readvance glacier ice in Scotland based on numerical modeling compared with inferences based on empirical studies (from Golledge <i>et al.</i> , 2008).....	28
 <b>Chapter 3: Introduction to NEXTMap: testing its capabilities</b>	
3.1 Comparison of the imageries used in Smith <i>et al.</i> (2006).....	35
3.2 Comparison of LiDAR, NEXTMap (STAR-3i) and SPOT satellite image in terms of data unit price and vertical accuracy.....	36
3.3 Sample imageries of each DEM visualization method.....	42
3.4 Different directions of illumination used to demonstrate the effects on the image visibility and interpretation in the Moy Corrie area.....	46
3.5 Example of relief shading image using the default illumination direction and elevation (Azimuth: 315°, Elevation 45°) settings in GIS.....	47
3.6 Location of the Glen Roy and Glasgow study areas in UK.....	49
3.7 Location of the of the Glen Turret area.....	50
3.8 Location of the Glasgow area of western Central Scotland to show the regions selected for detailed examination of DEM imagery.....	51
3.9 The ORI NEXTMap image of the Glen Turret area.....	52

3.10	A DSM image of the Glen Turret area.....	53
3.11	A DTM image of the Glen Turret area.....	53
3.12	A DIFF image, created by elements of the image removed to turn the DSM into the DTM.....	54
3.13	Location of samples in the Glasgow area.....	57
3.14	Comparison of altitude angle change effects on topography.....	60
3.15	Comparison of azimuth angle change effects on topography.....	61
3.16	Comparison of the illumination effect on drumlin.....	62
3.17	Comparison of the illumination effect on cirque.....	63
3.18	Comparison of images in response to changes in the azimuthal angles of illumination.....	64
3.19	Comparison of image contrast values upon the representation of drumlin topography.....	65

**Chapter 4: Glacial landform mapping using NEXTMap: scoping exercises**

4.1	Relief-shaded images with 5° changes of angle of elevation of the light source used for the NEXTMap image.....	71
4.2	Comparison of changing levels of contrast on landforms that are part of a drumlin field.....	72
4.3	The Glasgow area of western central Scotland to show the regions selected for detailed examination of DEM imagery.....	74
4.4	Drumlins from the southeastern part of the Loch Lomond basin, western central Scotland (from Smith <i>et al.</i> , (2006).....	76
4.5	Comparison of DEM and field mapping of drumlins (take from Clark <i>et al.</i> 2009).....	77
4.6	Comparison of the results of field mapping by Rose (1965-1970) (Rose, 1982).....	78
4.7	Drumlins identified by Rose in 1965-1970 (Rose, 1982; Smith <i>et al.</i> 2006) those were not visible on the analysis of the rotating map.....	80
4.8	New potential drumlins identified in the research area plotted against the drumlins identified in the field by Rose (Rose, 1982; Smith <i>et al.</i> 2006)..	80
4.9	1:25,000 scale representation of 1:10,560 field mapping carried out J. Rose in 1965-1970 and published in Rose and Smith (2008).....	82
4.10	Digitization of the hummocky moraine and moraine ridge in the area shown on Figure 4.9 (based on Rose and Smith (2008).....	82

4.11	1:10,000 scale relief-shading images generated from NEXTMap for hummocky moraines mapping experiment.....	83
4.12	Digitalized hummocky moraines overlapping with 1:10,000 scale relief-shading map.....	84
4.13	An area of kames and kettle holes in the area near Kirkintilloch in the Kelvin Valley, western central Scotland (taken from Rose and Smith, 2008).....	86
4.14	NEXTMap images of the area shown on Figure 4.13.....	87
4.15	Digitization of the kames shown on the NEXTMap image on Figure 4.14 showing their location and distribution (with assigned number of kame and part of kettle holes).....	88
4.16	Digitization of the kames shown on the NEXTMap image on Figure 4.14 showing their location and distribution.	88
4.17	Digitization of the kettle holes shown in the NEXTMap image on Figure 4.14 showing their location and distribution (with assigned number of kettle holes).....	89
4.18	The digitalized kames and kettle holes derived from the NEXTMap image in the area of the Kelvin Valley near Kirkintilloch.....	89
4.19	Location of kames that are not visible on NEXTMap and their assigned number for the area of the Kelvin Valley near Kirkintilloch.....	90
4.20	Location of kettle holes that are not visible on NEXTMap and their assigned number for the area of the Kelvin Valley near Kirkintilloch.....	90
4.21	An example of meltwater channels represented by a slope map taken from the NEXTMap image.....	92
4.22	1:25,000 scale map of the meltwater channels shown in Figure 4.21 (form Rose and Smith, 2008).....	93
4.23	Location and distribution of digitalized meltwater channels for the area shown on Figure 4.22.....	94
4.24	Digitalized meltwater channel boundaries overlapping on original 1:25,000 scale map taken from Rose and Smith 2008.....	95
4.25	Comparison of the mapping results from slope map and field mapping...	95
4.26	Comparison of two different methods of representing meltwater channels.....	97
4.27	Frequency distribution of each azimuth group (meltwater channels).....	98
4.28	Distribution and frequency of dissected meltwater channels.....	99
4.29	Comparison of optimized image for each separated azimuth angle group	100



	(Original).....	
4.30	Comparison of optimized image for each separated azimuth angle group (With 20% contrast ratio).....	100
4.31	Distribution of visible and poorly visible meltwater channel sections.....	101
4.32	Comparison of the visibility of meltwater channel section on NEXTMap.....	102
4.33	Frequency distribution of the visibility of drumlins using different directions of light source.....	104
4.34	Frequency of drumlins plotted against angles that or orthogonal to the trend of the lineament.....	105
4.35	Location of Figure 4.36 and 4.37 in southeastern corner of the Loch Lomond basin.....	106
4.36	Illumination tolerance testing.....	107
4.37	Comparison of light from top (10°) and bottom (190°).....	107
4.38	Distribution of two main drumlin groups. (Blue group's azimuth: 340°~40°, Green group's azimuth: 270°~330°).....	108
4.39	Illustration of merged part.....	109
4.40	Comparison of the original imageries with merged imagery.....	110
<b>Chapter 5: Background to the Glen Roy area</b>		
5.1	Topographic map of Glen Roy, Glen Gloy and the Glen Spean valley, constructed in the present project using NEXTMap.....	115
5.2	Geology map of the Glen Roy area based upon DiGMapGB-625-Bedrock geology v.5 (March 2010).....	116
5.3	Reconstructions of the former lakes in Glen Roy based on interpretations of the 'parallel roads' and associated geomorphological features (taken from Rudwick, 2009).....	125
5.4	The ice limits and lake surfaces during the rising sequence of lake formation, based on the Sissons (1979) model (adopted from Palmer <i>et</i> <i>al.</i> , 2008).....	131
5.5	Ice-marginal positions and the key catchment controlling cols in Glen Roy area.....	134
<b>Chapter 6: Background to the Glen Roy area</b>		
6.1	Site locations and section boundaries in Glen Roy.....	137

6.2	Locations of the Viewpoint and Caol Lairig.....	138
6.3	Geomorphological map of lower Glen Roy, including Caol Lairig, from Sissons (1979) and Peacock and Cornish (1989).....	140
6.4	View of the pronounced terminal moraine, the 325 and 350 m shorelines taken from the head of Caol Lairig, looking south-west.....	142
6.5	Vertical NEXTMap images of the Caol Lairig and Viewpoint area.....	143
6.6	3D perspective of the Caol Lairig area viewed from the NW.....	144
6.7	Ice-dammed lake shorelines in lower Glen Roy (digitized from the 1:25,000 scale Ordnance Survey map and NEXTMap images).....	150
6.8	3D perspective of the Caol Lairig area from the SE direction.....	151
6.9	3D perspective of the Caol Lairig area from the NW direction.....	152
6.10	Digitised map of the distribution of landforms in lower Glen Roy as depicted on Hillshade NEXTMap imagery.....	154
6.11	3D perspective of southern flank of Bohuntine Hill viewed from SW direction.....	155
6.12	3D perspective of southern flank of Bohuntine Hill viewed from S direction.....	156
6.13	Location of the Allt Bhreac Achaidh Fan, the Brunachan Fan and the Reinich Fan in the middle section of Glen Roy.....	158
6.14	The Allt Bhreac Achaidh Fan and adjacent landforms (from Peacock and Cornish 1989, Figure 9).....	159
6.15	The surface and margins of the Allt Bhreac Achaidh Fan and preserved parts of the Parallel Roads on adjacent slopes, mapped using NEXTMap imagery.....	160
6.16	The 334 m and 343 m minor shorelines at Allt Bohaskey as depicted on NEXTMap imagery.....	161
6.17	Geomorphological map of the Brunachan Fan (from Peacock, 1986).....	164
6.18	Surface form and margins of the Brunachan Fan and distribution of preserved parts of the Parallel Roads on adjacent slopes, mapped using NEXTMap imagery.....	164
6.19	Geomorphological maps of the Reinich Fan (from Sissons and Cornish, 1983 and Peacock, 1986).....	166
6.20	The form and margins of the Reinich Fan mapped using NEXTMap imagery.....	167
6.21	Comparison between the mapped distributions of the Parallel Roads in	169

	the middle part of Glen Roy.....	
6.22	The three prominent fans of the middle sector of Glen Roy and the distribution of well preserved parts of the Parallel Roads, mapped using NEXTMap imagery.....	170
6.23	A vertical NEXTMap image of parts of Glens Gloy, Turret and upper Roy.....	171
6.24	Glacial landforms and sediments in upper part of Glen Roy (from Peacock 1986).....	172
6.25	The distribution of the Parallel Roads in upper Glen Roy, digitalized from the 1:25,000 scale Ordnance Survey Map.....	173
6.26	Geomorphological map of the fans and river terraces of the northern part of upper Glen Roy(from Sissons and. Cornish, 1983).....	177
6.27	Vertical NEXTMap images of the upper Glen Roy area.....	180
6.28	Geomorphological map of the area around the Turret-Roy confluence based on NEXTMap imagery.....	183
6.29	View of the landforms in the Allt a' Chomhlain-Coire Dubh tributary valley.....	185
6.30	3D perspective of the Glen Turret area from the NE direction.....	186
6.31	3D perspective of the Glen Turret area from the SSW direction.....	188
6.32	3D perspective of the Glen Turret area from the W direction.....	189
6.33	Preserved remnants of major fans and distribution of the Parallel Roads in upper Glen Roy mapped using NEXTMap imagery.....	190
6.34	A simulation of the 260 m lake in upper Glen Roy.....	194
6.35	A simulation of the 325 m lake in upper Glen Roy.....	194
6.36	A simulation of the 350 m lake in upper Glen Roy.....	195
 <b>Chapter 7: Shoreline analysis: distribution, form and architecture</b>		
7.1	Generalised model of wave-cut platform and bluff formation ( from Schaeztl <i>et al.</i> , 2002).....	202
7.2	Hill-shaded and slope factor image of the area close to the Viewpoint in Glen Roy.....	206
7.3	Fragments of the shorelines mapped at scale of 1:10,000 and 1:1,000.....	207
7.4	Continuous stretches of fragments recognised for the 260 m shoreline....	210

7.5	Continuous stretches of fragments recognised for the 325 m shoreline....	211
7.6	Continuous stretches of fragments recognised for the 350 m shoreline....	212
7.7	Illustration of typical density of randomly distributed measured points on stretches of Parallel Roads.....	213
7.8	Digitised map of the distribution of the Parallel Roads of Glen Roy as depicted on 1:25,000 O.S. maps.....	214
7.9	Distribution of Parallel Roads in Glen Roy using NEXTMap imagery at a scale of 1: 45,000.....	214
7.10	Distribution and widths of Parallel Roads of Glen Roy as surveyed by Sissons (1978).....	215
7.11	Digitised transform, based on 1:25,000 O.S. maps, of the shorelines mapped by the O.S. in the vicinity of the Turret-Roy confluence, shown on DEM image.....	218
7.12	Simplified map version of the digitised O.S. shoreline distributions shown in Figure 7.11.....	218
7.13	Shorelines in the vicinity of the Turret-Roy confluence mapped from NEXTMap images at a scale of 1:25,000.....	219
7.14	Simplified map of the shoreline distributions shown in Figure 7.13.....	219
7.15	Shorelines in the middle reach of Glen Roy digitised from 1:25,000 O.S. maps.....	220
7.16	Shorelines in the middle reach of Glen Roy mapped using NEXTMap images.....	220
7.17	Shorelines in the vicinity of the Allt Chonnal-Roy confluence digitised from 1:25,000 O.S. maps.....	223
7.18	Shorelines in the vicinity of the Allt Chonnal-Roy confluence based on NEXTMap images.....	223
7.19	Altitude data for the 260 m shoreline on the eastern side of Glen Roy plotted orthogonally on to a northing axis extending between NN840000 and NN920000.....	232
7.20	Altitude data for the 260 m shoreline on the eastern side of Glen Roy plotted orthogonally on to an easting axis extending between NN300000 and NN360000.....	232
7.21	Location of sites for test the accuracy of NEXTMap altitudinal measurements.....	235
7.22	NEXTMap images of the runways at Heathrow Airport selected for measurement for a test of NEXTMap depiction of a horizontal surface...	237

7.23	Location of points selected for altitudinal measurement on Heathrow runways 27R and 27L.....	237
7.24	Plot of altitudinal measurement of Heathrow airport runway 27R, derived using 2360 NEXTMap data-points.....	238
7.25	Plot of altitudinal measurement of Heathrow airport runway 27L, derived using 2638 NEXTMap data-points.....	238
7.26	Location of transects of altitudinal measurements on terrace features at the western end of Loch Laggan.....	241
7.27	Plot of altitudes obtained from 3054 measured points along the Loch Laggan 1 transect.....	242
7.28	Plot of altitudes obtained from 2523 measured points along Loch Laggan 2 transect.....	243
7.29	Scatter plot of measured spot-heights along one of the pipes and on the bare ground surface adjacent to the selected pipe, superimposed on NEXTMap-ORI image.....	246
7.30	NEXTMap altitudinal measurements obtained from the pipe surface and adjacent ground surface shown in Figure 7.28.....	247
7.31	NEXTMap altitudinal measurements obtained on pipeline surface between anchor points 2 and 4 on the Alcan pipelines, Fort William.....	248
7.32	Location and ranges of shoreline stretches selected for instrumental leveling in Glen Roy.....	249
7.33	Plot of instrumentally-based altitudinal measurements and NEXTMap-generated data for stretches of the three Parallel Roads in the middle sector of Glen Roy (from Frings, 2010).....	251
7.34	Departures of altitudinal measurements from sector means based on instrumental measurement and NEXTMap data for stretches of the 260 m, 325 m and 350 m shorelines in the central Roy valley (from Frings 2010).....	252
7.35	Altitude measurements obtained by Sissons and Cornish (1982) for surveyed stretches of the 260 m, 325 m, and 350 m shorelines in Glen Roy.....	256
7.36	Results of instrumental levelling and re-levelling of three stretches of shoreline by Sissons & Cornish, 1982).....	258
7.37	Evidence for differential block movement of the Parallel Roads of Glen Roy reported by Sissons and Cornish (1982b).....	259
7.38	Altitudes of all three shorelines on either side of a major landslip scar located on the eastern side of the Glen, close to the Loch Lomond Readvance ice limit near the Viewpoint (from Sissons and Cornish,	260

	1982b).....	
7.39	NEXTMap altitude measurements obtained for selected stretches of the Parallel Road of Glen Roy.....	270
7.40	Location of 6 small landslides in glens Roy and Gloy and of the positions of Loch Lomond Stadial glacier termini.....	271
7.41	The location of Landslide 1 and the measured altitudes of adjacent shorelines as reported by Sissons and Cornish (1982b).....	272
7.42	Stretches of the Parallel Roads from which NEXTMap altitude measurements were derived for Figure 7.43.....	274
7.43	Projected shoreline surface altitudes of the 325 and 260m Parallel Roads in the vicinity of landslide 1.....	275
7.44	The location of Landslide 2 and the measured altitudes of adjacent shorelines as reported by Sissons and Cornish (1982b).....	276
7.45	Stretches of the Parallel Roads from which NEXTMap altitude measurements were derived for Figures 7.46 and 7.47.....	277
7.46	Projected shoreline surface altitudes of the Parallel Roads in the vicinity of landslide 2 on the eastern flank of the valley.....	281
7.47	Projected shoreline surface altitudes of the Parallel Roads in the vicinity of landslide 2 on the western flank of the valley.....	284
7.48	Stretches of the Parallel Roads from which NEXTMap altitude measurements were derived for Figures 7.49 and 7.50.....	286
7.49	Projected shoreline surface altitudes of the Parallel Roads in the vicinity of landslide 3 on the north-western flank of the Middle Roy valley.....	291
7.50	Projected shoreline surface altitudes of the Parallel Roads in the vicinity of landslide 3 on the south-eastern flank of the Middle Roy valley.....	294
7.51	Stretches of the Parallel Roads from which NEXTMap altitude measurements were derived for Figures 7.52 and 7.53.....	296
7.52	Projected shoreline surface altitudes of the Parallel Roads on the north flank of the Upper Roy, up-valley from the Turret fan.....	299
7.53	Projected shoreline surface altitudes of the Parallel Roads on the southern flank of the Upper Roy, up-valley from the Turret fan.....	302
7.54	Trend surface data for the Glen Roy shoreline surfaces.....	306
7.55	Example of the density of altitudinal information available for shoreline fragments.....	307
7.56	Isobase contours for the 260 m shoreline in Glen Roy generated using NEXTMap-based altitudinal measurements.....	310
7.57	Isobase contours for the 325 m shoreline in Glen Roy generated using NEXTMap-based altitudinal measurements.....	311

7.58	Isobase contours for the 350 m shoreline in Glen Roy generated using NEXTMap-based altitudinal measurements.....	311
7.59	Comparison of the isobase maps generated by Dawson <i>et al.</i> (2002) and in the present research.....	312
7.60	Arrows point towards the centre of glacio-isostatic load at the time of formation of each of the three Parallel Roads of Glen Roy, as concluded by Dawson <i>et al.</i> (2002) based on trend-surface analysis.....	315
7.61	Arrows point towards the inferred centre of glacio-isostatic load at the time of formation of each of the three Parallel Roads of Glen Roy, based on trend-surface analysis of NEXTMap altitudinal data undertaken in the present research.....	316
7.62	Location of selected shoreline sections in Glen Roy for surface gradient experiment.....	318
7.63	Projected shoreline surface altitudes of the 260m_D, 325m_C and 350m_C shoreline sections in Glen Roy.....	320
7.64	Comparison of the altitudinal data obtained using N-S and SW-NE axial projection planes.....	324

## **Chapter 8: Synthesis and Conclusions**

8.1	Different representations of the maximum ice stands in the Gloy-Roy area during the Loch Lomond Stadial (after Sissons, 1979; Sissons and Cornish, 1982; and Peacock, 1986).....	329
8.2	A general overview of the landforms and other features referred to in Chapters 6 and 7, including ice-moulded lineaments attributed to the Late Devensian ice sheet.	330
8.3	Locations referred to in text, where key geomorphological features occur that help to resolve the sequence of events in Glens Gloy and Roy during the Loch Lomond Stadial.....	331
8.4	Diagram used by Jarman (2008) to illustrate the distribution of, and to explain the concept of, rock slope failures (RSFs) in the Glen Roy-Loch Lochy area.....	342
8.5	The Spean-Roy ice-dammed lake and proposed jökulhlaup route, with the locations of associated fan deposits at Fort Augustus and Inverness (from Sissons, 1981).....	349
8.6	Reconstructed lake water levels, glacier ice margin and associated fluvial terraces formed after jökulhlaup drainage according to Sissons (1979c).....	350
8.7	Landforms in the area around (A) the Glen Roy Viewpoint from Sissons	353

	1979c); (B) Spean Bridge and Gairlochy (from Sissons, 1979a); (C) Loch Treig/Roybridge (from Sissons, 1979c); (D) Triage valley and part of the Spean valley (from Sissons, 1979d).....	
8.8	NEXTMap imagery for the area around Glen Roy and Glen Gloy.....	354
8.9	Modern catchment and topographic details in Glen Spean and Glen Gloy, on NEXTMap-derived base image.....	355
8.10	The sequence of ice advance and the rising lake sequence and of ice decay and the falling lake sequence in the Gloy-Roy-Spean area, according to the author's observations and interpretation.....	358



<b>List of Tables</b>	<b>Page no.</b>
<b>Chapter 2: Mapping the ice limits of the last (late Devensian) ice sheet in the British Isles</b>	
2.1	Definition of the termination, onset and duration of climatic events during the Late Devensian (from Lowe et al., 2008)..... 15
<b>Chapter 3: Introduction to NEXTMap: testing its capabilities</b>	
3.1	Imagery used in Smith et al. (2006) with the resolution of the methods... 33
3.2	Methods for visualizing DEM data (after Lidmar and Bergström,1991; Smith, 2003; and Smith, 2005). 38
3.3	Numerical comparison of different DEM image conditions (from Smith, 2003). 44
3.4	NEXTMap Great Britain technical data (from Li <i>et al.</i> , 2002 and 2004; Mercer, 2001) 48
<b>Chapter 4: Glacial landform mapping using NEXTMap: scoping exercises</b>	
4.1	Basic geometry characters of the dissected meltwater channels..... 98
4.2	Frequency of each separated meltwater channel group’s azimuth range... 98
4.3	Comparison of main meltwater channel group with the other sub-groups 99
4.4	Frequency of visible drumlins observed by using light sources with a different azimuthal angle..... 103
<b>Chapter 5: Background to the Glen Roy area</b>	
5.1	Catalogue of the symbols used in Figure 5.2..... 116
5.2	Important field investigators and their contributions to the development of ideas on the formation of the Parallel Roads of Glen Roy..... 119
<b>Chapter 6: Background to the Glen Roy area</b>	
6.1	Estimated dimensions of the preserved fragments of the major fans in upper Glen Roy..... 191
<b>Chapter 7: Shoreline analysis: distribution, form and architecture</b>	
7.1	Summary of measurements made by Sissons (1978) on the horizontal widths of the Parallel Roads of Glen Roy outside the Loch Lomond Readvance ice limits..... 225
7.2	Summary of measurements of the horizontal widths of the Parallel Roads made in this research using NEXTMap images..... 225

7.3	Width of the Glen Roy and Gloy shorelines related to aspect as reported by Sissons (1978).....	229
7.4	Widths of the Glen Roy and Caol Lairig shorelines related to aspect from the results obtained in this thesis.....	229
7.5	Inclination of platform slopes of Parallel Roads lying outside the Loch Lomond Readvance limits measured by Sissons (1978).....	230
7.6	Inclination of platform slopes of Parallel Roads lying outside the Loch Lomond Readvance limits measured in current study.....	231
7.7	Gradients and regression $r^2$ values computed for shoreline stretches using instrumental and NEXTMap-generated data.....	252
7.8	Statistical data for the 260 m shoreline from Sissons and Cornish (1982).....	257
7.9	Statistical data for the 325 m shoreline from Sissons and Cornish (1982).....	257
7.10	Statistical data for the 350 m shoreline from Sissons and Cornish (1982).....	258
7.11	NEXTMap-generated altitude measurements for the surface of the 260 m shoreline in Glen Roy.....	263
7.12	NEXTMap-generated altitude measurements for the surface of the 325 m shoreline in Glen Roy.....	264
7.13	NEXTMap-generated altitude measurements for the surface of the 350 m shoreline in Glen Roy.....	265
7.14	Calculated gradients for Glen Roy shorelines based on NEXTMap altitudinal measurements using linear and 2nd order polynomial regression.....	305
7.15	Isobase contour parameters obtained by Dawson et al., 2002 for the surfaces of the Parallel Roads of Glen Roy.....	308
7.16	Calculated shoreline surface gradients for the sector of Glen Roy shown in Figure 7.62, obtained using different projection axes.....	321
7.17	Variation in gradient of the surfaces of the Glen Roy shorelines after incremental 5° angle changes in the direction of the plane of projection through the NE quadrant.....	322
7.18	Comparison of shoreline surface gradients calculated for the three Parallel Roads using a N-S axial projection plane (top line) and a SW-NE axial projection plane (middle line).....	323

<b>List of Appendices</b>	<b>Page no.</b>
 <b>Appendix 1</b>	
1.0 Creating the rotating map.....	376
 <b>Appendix 2:Rotating maps ( See attached CD in the back cover of the thesis)</b>	
2.1 Drumlin mapping experiment.....	CD
2.2 Kame and Kettle mapping experiment.....	CD
2.3 Meltwater channel mapping experiment.....	CD
 <b>Appendix 3:Shoreline surface analysis data</b>	
3.1 Analysis of shoeline width and slope.....	CD
3.2 NEXTMap capability test 1 - Heathrow airport.....	CD
3.3 NEXTMap capability test 2 - Loch Laggan.....	CD
3.4 NEXTMap capability test 3 - Alcan Hydroelectrical pipes.....	CD
3.5 Shoreline surface analysis-measure points.....	CD
3.6 Shoreline surface trend analysis.....	CD
 <b>Appendix 4</b>	
4.0 MSc students levelling of Parallel Road sections T and U., Glen Roy-Patrick Frings.....	CD
 <b>Appendix 5</b>	
5.0 MSc students levelling of Parallel Road sections T and U., Glen Roy-Stephen Bate.....	CD

**Appendix 6**

6.0 Glen Roy - Shoreline surface gradient -260D\_325C\_350C..... CD

**Appendix 7**

7.0 Glen Roy - Shoreline surface gradient - 260-All\_325-All\_350-All..... CD

**Appendix 8**

8.0 Glen Roy - Overall landforms -NEXTMap..... CD

**Appendix 9**

9.0 Glen Roy - Overall landforms -OS map..... CD

# 1. Introduction

---

## 1.1 Inception of the project

This thesis reports the results of an examination of the capability of NEXTMap technology, a remote sensing methodology that generates digital terrain models. Here it is tested for its capabilities and advantages in the precise mapping of glacial landform suites associated with the waning of the last (Devensian) glaciation in Scotland. The project was initiated in 2007, soon after this type of technology had become available to the UK research community. At that time NEXTMap represented the most affordable imaging data-set available that covered the PhD areas of interest. It is gradually being superseded by LiDAR imagery, which provides much greater image resolution, but which is more expensive and did not cover the whole of the PhD areas of interest. NEXTMap represented the latest step in a revolution of the manner in which the landscape, as well as individual landforms, could be mapped, manipulated and represented. In recent years it has become possible to examine representations of the topography of large tracts of land at high spatial resolution, through digital terrain images captured from satellites or aircraft. When combined with GIS facilities, it becomes possible to view, interpret and model the landscape with increasing ease. But questions arise as to the degree of faithfulness with which the landforms are represented in such images, and the limits of spatial resolution that they can realistically convey. These are the kind of questions that stimulated the study reported in this thesis.

GIS and digital imaging were already being widely employed prior to 2008 to map landform assemblages that enabled the limits of the last ice sheet that occupied the British Isles to be reconstructed, and to trace the margins of possible retreat stages during the dissipation of the ice. The BRITICE project (Clark *et al.*, 2004), for example, is a GIS-based compilation of all the available evidence for the last British ice sheet

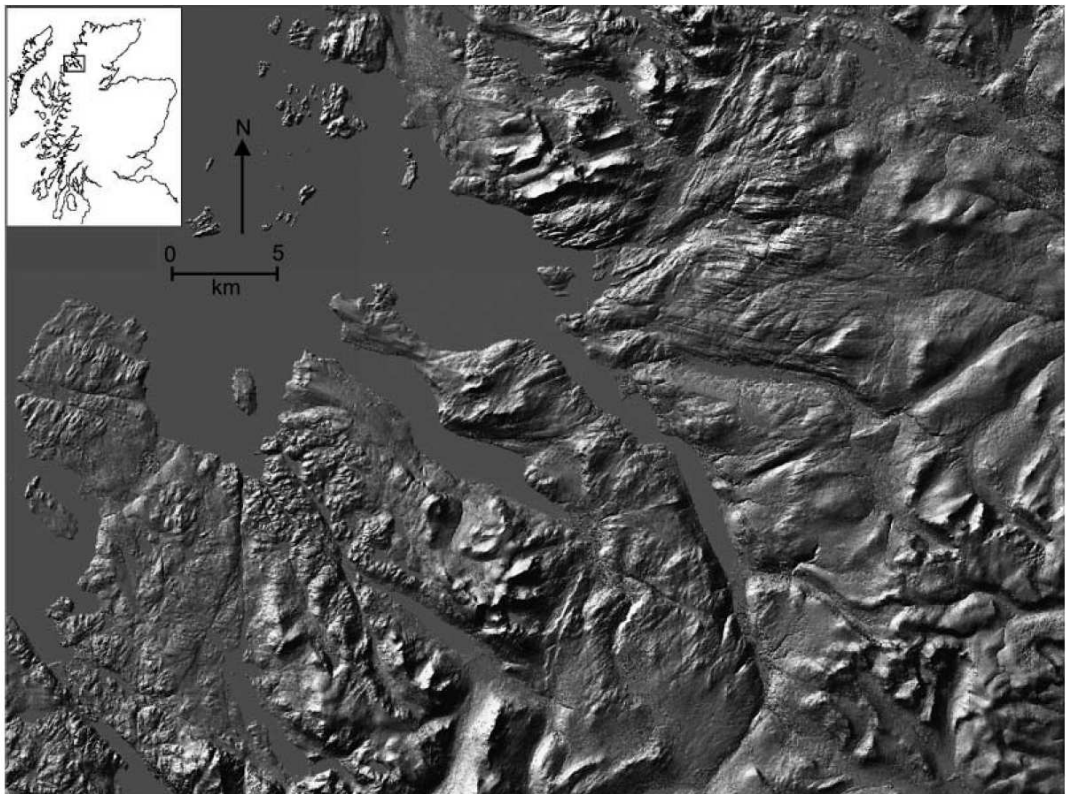
from which ice-marginal limits and ice-flow patterns can be inferred (Clark 1997 and Everest *et al.*, 2005). The observations are based on high-quality satellite imagery that allows suites of landforms to be viewed at both regional and national scales, while evidence obtained from published maps with relevant interpretations of landforms were also incorporated. Attention was focused on the identification of moraines, eskers, drumlins, meltwater channels, tunnel valleys, trimlines, clear limits to the distribution of glacial features, glaciolacustrine deposits, and ice-dammed lakes and associated shorelines. To this was added information from the literature that could not be directly observed on the images, such as erratic dispersal patterns, lithostratigraphic information and subaqueous features, for example major fans along the continental shelf margin. Altogether some 20,000 features were plotted into GIS using a number of thematic layers, the results being made publicly available ([http://www.shef.ac.uk/geography/staff/clark\\_chris/britice.html](http://www.shef.ac.uk/geography/staff/clark_chris/britice.html)), while periodic up-grades are generated as additional information becomes available (e.g. Evans *et al.*, 2005). This comprehensive compilation of published and observational landform patterns provides a useful first approximation of the overall dimensions and flow patterns of the last British-Irish ice sheet (BIIS) at its maximum extent. However, not all of the features have been 'ground-truthed', and there has been no direct testing of the limits of spatial resolution with which landforms in the British Isles can be mapped using the satellite imagery on which BRITICE is based, while the features have been generalized on a national map at a scale of 1:625,000.

A parallel study of the last British ice sheet illustrates the potential of GIS-based modeling. Fretwell *et al.* (2008) used ARCGIS programs to project different configurations of the last British ice sheet on to the Ordnance Survey grid, and combined this compilation with offshore bathymetric data obtained from the National Geophysical Data Centre (NGDC 2005). They used the results, which model the overall

anatomy of the ice sheet, to compute ice area and volume and predict the isostatic response, which could then be compared with independent glacio-isostatic models based on reconstructions of local and regional sea-level change. Although the grid-size for the models is still rather crude (ranging in grid-square size from a typical 500m to 90m at best), this study nevertheless shows the potential power of GIS-based modeling for integrating evidence of different physical effects on the landscape – in this instance the growth and dissipation of an ice sheet and its concomitant stress load on the underlying crust, as well as on the resulting reconfiguration of adjacent shorelines.

Shortly after these studies were published, the author came across the first published examples of the use of NEXTMap DEM data for illustrating landforms in the Scottish landscape, and became aware of the technology and its apparent potential. A series of papers published in 2008 (but available on-line in 2007) included arresting images of streamlined bedforms and large-scale mega-grooves. For example, Bradwell *et al.* (2008a) included NEXTMap plot of large-scale mega-grooves and streamlined bedrock in the Ullapool area of NW Scotland, which they used in association with new multi-beam bathymetric images to reconstruct a former major ice stream flowing out towards the Minch in the west, over a 20 km-wide corridor. A related but more comprehensive study of suites of both submarine and land surface features in and around the Loch Broom-Summer Isles region by Bradwell *et al.* (2008b) was based on a combination of multi-beam Geoswath imagery, boomer seismic profiling, colour aerial photography and NEXTMap digital surface terrain models. Both of these publications illustrated how detailed maps of streamlined features could convey immediate visual impressions of strong ice-flow patterning from which ice-sheet dynamics (e.g. ice-flow convergence and divergence; variations in ice-stream flow strength) can be inferred.

Further exploration of the literature and enquiries concerning the availability of NEXTMap DEM data led to the growing realization, on the part of the author, of the stunning clarity afforded by the images and the ability to use them for the construction of high quality, and perhaps highly spatially- resolved, digital terrain models. One of the earliest published images to convey this potential was that of Goodenough *et al.* (2009), again of the NW Scottish Highlands close to Ullapool (Figure 1.1). They used such images to classify different types and scales of streamlined bedforms, and to analyse their variations with respect to differences in underlying or constituent bedrock. However, the most revealing aspects of the paper concerned the artificial manipulation of direction of illumination to emphasise the topographic variation and individual features (Figure 1.1).



**Figure 1.1** A digital surface elevation model (DSM) of the NW Scottish Highlands created using NEXTMap images flown by Intermap Technologies Inc. using Interferometric Synthetic Aperture radar with artificially-altered hill-shading to emphasise topographic forms (from Goodenough *et al.*, 2009).



These publications revealed that NEXTMap images had been flown for the whole of the British Isles, and were available for research purposes via the Natural Environment Research Council (NERC). The spatial resolution of the images was quoted as 2 to 5 m, affording “unprecedented opportunities for interpreting the landscape, since they have a far higher resolution than most widely available satellite imagery, and can provide a broader overview than stereographic aerial photos” (Goodenough *et al.*, 2009, p. 99). This seemed evident from the published examples, but in none of the studies cited above, or encountered since, was this potential fully tested by either (a) ground-truthing the results against field-based maps or (b) establishing the full spatial and vertical resolution with which the images could be interpreted, and thereby to establish the degree of subtlety with which landforms and landscape could be modeled using NEXTMap technology. These, then, became the broad aims of this present PhD study, with more specific aims outlined in section 1.3.

## **1.2 Framing the project**

In order for the above general aims to be met, it was important to select a study area for which detailed geomorphological maps already existed, and against which interpretations derived using NEXTMap DEM data could be stringently compared. Other requirements were unhindered access to NEXTMap images and the opportunity to test NEXTMap results in the field. Fortunately these requirements could all be met. Professor J. Rose had previously mapped the area to the immediate south of Loch Lomond in great detail and the results were made available for the current research. Furthermore, more recent mapping conducted in the area by Smith *et al.* (2006) and Rose and Smith (2008) provided additional detail that could be exploited for testing the NEXTMap results generated in the present research. It was therefore decided to use the Loch Lomond area as an initial test case for examining the capabilities of NEXTMap.

In 2007, when this PhD programme of study commenced, several members of the Centre of Quaternary Research (CQR) at Royal Holloway, University of London (RHUL) were funded to undertake new research in both the Loch Lomond and Glen Roy areas under the NERC's Rapid Climate Change thematic research programme (Holmes *et al.*, 2011). Dr. A. Palmer of the CQR had also previously completed a PhD study of laminated (varved) sediments in the Glen Roy area (Palmer, 2005). Aspects of these investigations have subsequently been published (Palmer *et al.*, 2008a, 2010, 2012; MacLeod *et al.*, 2011). At the same time, the Glen Roy area is regularly used as the main centre where the annual MSc Quaternary Science degree programme, taught at RHUL, is based.

This established level of activity by CQR members in both the Loch Lomond and Glen Roy areas had three important benefits for the research project reported in this thesis. First, because members of the CQR were in receipt of NERC funds for research, and because the MSc degree programme was recognized and part-funded by the NERC at that time, unlimited access to NEXTMap images was granted free of charge. NEXTMap coverage of the British Isles was initially commissioned by the Norwich Union Insurance company for the estimation of flood risks, but the full coverage was subsequently acquired by the British Geological Survey, under an agreement whereby the images are made available to researchers funded by the NERC. Secondly, regular opportunities became available to visit these field areas to examine features in the field. And thirdly, new information was being generated continuously that stimulated new questions about the history of glaciation in Scotland, and that brought added impetus to the NEXTMap-focused research reported here.

A further advantage of the Glen Roy area, as far as the research reported in this thesis is concerned, is that the Glen Roy area had previously been mapped in quite some detail by J. B. Sissons (1977, 1978, 1979a, 1979b and 1979c) and Sissons and Cornish (1982a, 1982b and 1983) during the 1970's and early 1980's, with additional details supplied by Peacock (1986) and Peacock and Cornish (1989). Furthermore, the area is famous for the 'Parallel Roads', lake shorelines formed when local glacier ice had blocked drainage escape routes. These features had been instrumentally leveled by Sissons (1977, 1978; Sissons and Cornish, 1982a, 1982b) and their near-horizontal surfaces presented particular challenges for the application of NEXTMap technology. It was therefore decided to use the Glen Roy area as a further test area in the PhD project. The strategy therefore emerged that the Loch Lomond area would be used to gain a grounding in the capabilities that NEXTMap technology had to offer, and to develop approaches that were considered useful for wider application in geomorphological mapping. The Glen Roy area would subsequently be employed to apply the principles and approaches developed in the Loch Lomond study.

### **1.3 Aims of the project**

This PhD research project aims to examine the potential and limitations of NEXTMap technology for the mapping and interpretation of palaeoglacial landforms. The objectives are to establish (a) the vertical and spatial resolution that can be realistically achieved, (b) how well various landforms can be represented in NEXTMap images, (c) how to optimize the manipulation of artificial light incidence in order to enhance both visualization of landforms and mapping approaches, and (d) assess the reliability of gradient and other altitudinal measurements obtained using NEXTMap.

The specific aims of this research related to these objectives were as follows:

1. To test the effects of illumination angle changes on NEXTMap DEM data for visualizing terrain features on NEXTMap;
2. To assess and develop appropriate glacial landform mapping protocols using NEXTMap DEM data, and to compare the results with geomorphological maps based on field mapping;
3. To develop appropriate analytical protocols for deriving terrain surface altitude measurements from NEXTMap-DEM data;
4. To determine vertical error ranges of NEXTMap-DEM data by comparing measured results with fixed natural or artificial surfaces;
5. To test published estimates of the surface gradients, distributions and degree of deformation of well developed lake shorelines in Glen Roy (the ‘Parallel Roads’) as a special case study;
6. If possible, to assess whether the new results, based on NEXTMap DEM data, add to existing interpretations of the mode of formation and age of the glacial landforms of the Glen Roy area.

#### **1.4 Structure of the project**

The thesis is structured as follows. Chapter 2 provides the temporal and palaeoglacial context relevant to the two test-case study areas selected, i.e. Loch Lomond and Glen Roy. According to current interpretations, both are critical in that they include evidence for the former margins of the final phase of glaciation in Scotland, the Loch Lomond Readvance (equivalent to the Younger Dryas Readvance of NE continental Europe), but also landforms attributed to the time when both areas were subsumed under the last ice sheet to occupy Britain. A brief introduction is therefore provided in Chapter 2 to the background, terminology and age-span of limits of glaciation in NW Europe during the Dimlington Stadial to Loch Lomond Stadial. Greater focus is given to the evidence for

the Loch Lomond Readvance in Scotland, as most of the features examined in this thesis are associated with that phase of glaciation.

Chapter 3 reviews remote sensing and digital elevation models (DEM) and imagery available in the UK, and their visualisation capabilities, with particular reference to glacial landform mapping. Methods for image optimization are also explored in this chapter, and protocols developed for their application.

Chapter 4 uses the protocols developed in Chapter 3 and tests them by mapping landforms in the area immediately south of Loch Lomond, and by comparing the results with detailed geomorphological maps generated by field-based mapping. The results obtained from the adoption of several different mapping approaches are compared with a NEXTMap-based method of optimized representation of linear glacial landforms.

Chapter 5 introduces the second study area, Glen Roy and adjacent valleys, providing information on its bedrock geology and topography, and important features in key drainage catchments that are crucial for understanding the sequence of events in this area. It also provides a synopsis of key developments of understanding of the glacial history of the Glen Roy area. The most widely-accepted model of the sequence of events in Glen Roy is then highlighted, and this model is the subject of scrutiny in the chapters that follow.

Chapter 6 examines the evidence for the glacial history of Glen Roy in more detail, and uses NEXTMap DEM data both to illustrate key features, and to identify a number of unresolved questions about the age and mode of formation of some key landforms. Some alternative interpretations are suggested on the basis of observations made from NEXTMap DEM data, aided by an experiment in which the former ice-dammed lakes

are superimposed on the maps to examine more clearly the precise relationships between the glacier limits, the lakes, and key landforms.

Chapter 7, the largest chapter in the thesis, is devoted to the most exacting study undertaken in this project, that of defining the distribution, form and gradients of the Parallel Roads. After reporting the results of some tests undertaken to evaluate the reliability and precision of NEXTMap altitude measurements, the focus is trained on an examination of the surfaces of the Parallel Roads based on almost 32,000 individual spot-height altitudinal measurements obtained from NEXTMap data. The results are used to assess (a) the degree of vertical precision with which the shorelines can be mapped using NEXTMap-generated data; (b) the degree to which the shorelines are deformed or dislocated; and (c) whether, despite the effects of localised dislocation or deformation, regional glacio-isostatic trends along the former lake shorelines can be discriminated using the extensive data-set of surface measurements generated by this project.

Finally, the results and conclusions of the work reported in chapters 6 and 7 are integrated in Chapter 8 to highlight important new ideas about the sequence of events in Glen Roy, with particular attention paid to any new observations or developments arising from the NEXTMap study. Some general conclusions about the capabilities of NEXTMap and suggestions for further work are also made.

## **2. Mapping the ice limits of the last (late Devensian) ice sheet in the British Isles**

---

### **2.1 Introduction**

This chapter provides the wider context for appreciating the nature of the glacial landform evidence in the Loch Lomond and Glen Roy areas and its importance for the development of ideas concerning the glaciation of the Scottish Highlands during the last cold stage. It will also therefore provide an explanation of why these two areas were selected for particular study in this thesis, in terms of their suitability for testing the proficiency of NEXTMap DEM data as a mapping medium. Some key terminology is also defined, with respect to glacial and palaeoclimatic events relating especially to the interval between the attainment of maximum ice cover during the last glacial stage and the final melting of the ice at the start of the Holocene (see below), the period of most relevance to the focus of this thesis. Glacial developments during this interval are better resolved than for any other glacial period, because the evidence is fresh and largely undisturbed, while a range of dating methods can be applied to provide a reasonably precise chronology for the sequence of events at a regional scale. Although not the primary concern of this thesis, more refined reconstructions of the distribution and timing of glacial ice during the most recent glacial stage are important for understanding the Earth's oceanic and atmospheric circulation at that time, which in turn contributes to the effort of generating better numerical models of Earth system processes. It is important, therefore, to determine whether the use of NEXTMap DEM data can make a significant contribution in that regard, by helping to refine models of past glacial ice cover.

## 2.2 The last ice sheet in Northern Europe

The last cold stage, which dates from ca. 100 ka to 11.7 ka BP, is called the Devensian in the British Isles and the Weichselian in much of continental Europe (Lowe and Walker 1997). The history of the expansion and contraction of the north European ice sheet during the Devensian is complex (see e.g. Ehlers and Gibbard, 2004) and details concerning the precise limits of the ice at its maximum stand are changing all of the time, as new evidence is discovered. It is therefore difficult to represent the maximal limits of the last Eurasian ice sheet in overall view with accuracy. Figure 2.1, for example, is based on a synthesis of the data available to Svendsen *et al.* in 2004, but is already out of date, for more recent evidence has led to reassessment of the limits in the Barents Sea, NW Russia, northern Poland, the North Sea and SW Ireland (see various papers in Ehlers *et al.*, 2011). At present, there is no overview map available that incorporates this latest information.

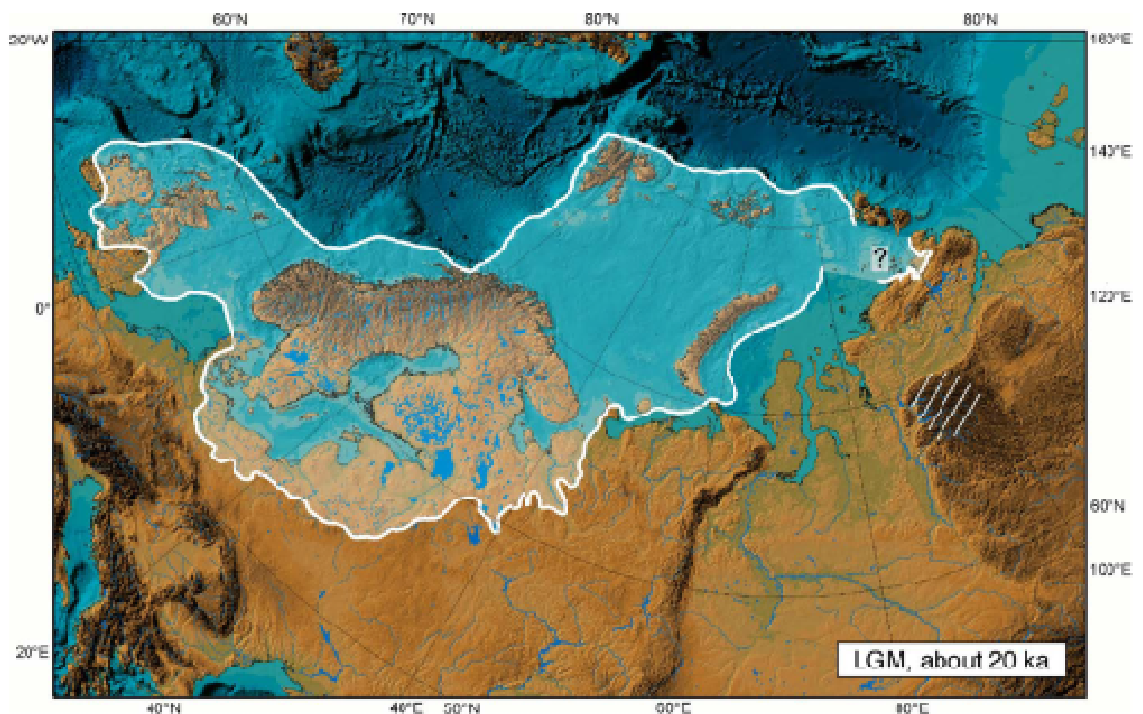


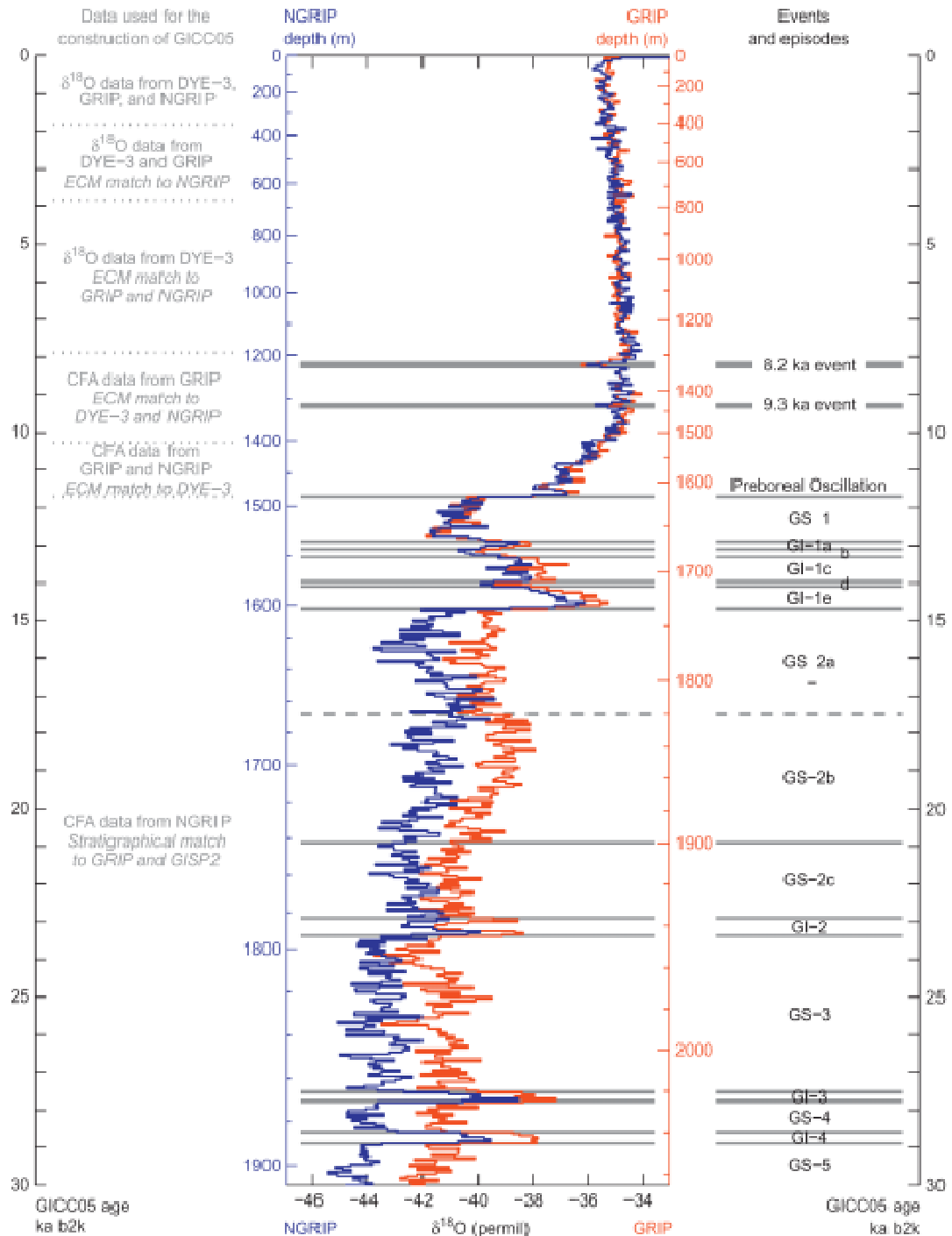
Figure 2.1 Synthesis of the limits of the Eurasian ice sheet at the Late Weichselian/Devensian glacial maximum based on evidence available to Svendsen *et al.* (2004).



The term widely employed in the literature for the maximum expansion of ice during the last cold stage is the 'Last Glacial Maximum', or LGM, originally defined on the basis of marine oxygen isotope records, for the time when ocean sediments record maximal O<sup>18</sup> enrichment, initially considered to date to ca. 20 to 18 ka BP (Shackleton, 1987). However, the timing of maximum glacial expansion appears to have varied world-wide, while the maximum globally-integrated expansion of ice according to recent models of sea-level lowering appears to have been at around 25 ka BP (Peltier and Fairbanks, 2006). The term LGM therefore does not have a universal application. In the British Isles, however, the maximum stand of Devensian ice appears to have been achieved by around 22 ka BP (Bowen *et al.*, 2002), and this date will be adopted when referring to the timing of the LGM in the Scottish Highlands. Nevertheless, there is growing evidence that indicates that the last ice sheet in northern Europe did not achieve its maximal limits contemporaneously, while the pattern of ice-margin retreat is complicated by readvances or stillstands of ice. This evidence is important, as it may reflect important climatic controls over the changing ice mass.

The late Weichselian stage in northern Europe is broadly divided into 3 cold episodes, the Pleniglacial, Older Dryas and Younger Dryas Stadials, separated by two warm intervals, the Bølling and Allerød Interstadials (Lowe and Walker 1997). Although the Greenland ice-core records indicate that this period experienced a more complex series of climatic oscillations (Rasmussen *et al.*, 2008; Lowe *et al.*, 2008a), this terminology has persisted in the literature. The Pleniglacial Stadal is roughly equivalent to the interval in the Greenland ice cores spanning Greenland Stadal 2a to Greenland Stadal 2c (GS-2a~GS-2c), to marine oxygen isotope Stage 2 (MIS-2) and to the LGM, as used in its general sense. The Younger Dryas Stadal is roughly equivalent to the cold interval GS-1 in the Greenland ice core records, and is termed the Loch Lomond Stadal (LLS) in the British Isles terminology (Figure 2.2 and Table 2.1). The significance of

these terms will become apparent in discussions below. First, a summary account is provided of reconstructions of the ice behaviour over continental NW Europe from the LGM onwards.



**Figure 2.2** Climatostratigraphic subdivision of the last 30,000 years at a 50-year resolution based on isotope variations in the NGRIP and GRIP ice-core records (from Lowe *et al.*, 2008a). GS = Greenland Stadial episodes and GI = Greenland Interstadial episodes.

Research has suggested that northern Europe was covered by a major ice dome which formed over the north-western Barents Sea shelf and eventually expanded to the western and northern continental shelf margins during the Pleniglacial (Lubinski *et al.*, 1996; Polyak *et al.*, 1997; Landvik *et al.*, 1998; Kleiber *et al.*, 2000; Svendsen *et al.*, 2004) (Figure 2.1).

**Table 2.1 Definition of the termination, onset and duration of climatic events during the Late Devensian based on the Greenland ice-core isotopic illustrated in Figure 2.2, and which forms the prototype event stratigraphy for this period (from Lowe *et al.*, 2008b).**

<b>Event</b>	<b>Termination (GICC05 ageb2k)</b>	<b>Onset (GICC05 ageb2k)</b>	<b>Duration of event</b>
Holocene	-	11, 703	11, 703
GS-1	11, 703	12,896	1,193
GI-1a	12, 896	13, 099	203
GI-1b	13, 099	13, 311	212
GI-1c	13, 311	13, 954	843
GI-1d	13, 954	14, 075	121
GI-1e	14, 075	14, 692	617 (1996 for GI-1)
GS-2a	14, 692	Not defined	?
GS-2b	Not defined	20, 900	?
GS-2c	20, 900	22, 900	2000
GI-2	23, 340	27, 540	4200
GS-3	27, 540	27, 780	240
GI-3	27, 780	28, 600	820
GS-4	28, 600	28, 900	300
GI-4	28, 900	-	-

The maximum extent of the Pleniglacial-LGM ice sheet is mainly delimited by linear moraine ridges and end moraines. The southern ice-marginal zone is characterized by several prominent moraine belts extending from northern Denmark through Germany into Poland, and then northwards through the Baltic states and into European Russia (Rinterknight *et al.*, 2005). In Germany, recession of the LGM ice margin is delimited by three sub-parallel moraines named (from south to north) the Brandenburg, Frankfurt

and Pomeranian Moraines (Figure 2.3). Recent cosmogenic radionuclide dating of boulders on these moraines suggests that the last ice sheet retreated northwards from the Brandenburg Moraine around 19 ka BP, and from the Frankfurt and Pomeranian moraines by c. 18 ka and 16 ka BP respectively (Heine *et al.*, 2009).



**Figure 2.3** Geomorphological evidence for the maximum extent and recession of the late Weichselian Fennoscandian ice sheet in northern Europe (from Lowe and Walker 1997).

Major moraine ridges in Denmark have been correlated with those in Germany: the Mid Jutland or Main Stationary Line moraine is considered the equivalent of the Frankfurt Moraine, whilst the more northerly East Jutland Line is considered to be a continuation of the Pomeranian Moraine (Lundquist, 1986; Houmark-Nielsen, 1989). In Poland, the Leszno Moraine has been judged to be an extension of the Brandenburg Moraine, while the Poznan Moraine and Pomorze Moraine have been correlated with the Frankfurt Moraine and the Pomeranian Moraine respectively. Retreat from the 'Pomeranian Moraine' in Poland appears to have been more recent than previously supposed, as cosmogenic nuclide dating suggests a delay in retreat until c. 14.3 ka BP (Rinterknecht *et al.*, 2005). The eastern margin of the last ice sheet is in part indicated by the Orsha Moraine in Belarus, and by other moraines around the southern margin of the eastern Baltic. Cosmogenic nuclide dating suggests that the last ice sheet in this region advanced after c. 25 ka BP, reached its maximal extent by c. 21 ka BP, and began to retreat by c. 19 ka BP (Rinterknecht *et al.*, 2006). It appears to have retreated from the Orsha Moraine by c.17.7 ka BP (Rinterknecht *et al.*, 2007). Overall, therefore, it appears that the maximum expansion and key phases of retreat of the last Eurasian ice sheet was not synchronous across the lowlands of Denmark, Germany, Poland and the Baltic region.

Following the Pomeranian stage, the north European ice sheet continued to retreat during the Bølling Interstadial, Older Dryas Stadial and Allerød Interstadial (GI-1 substages a to e in Table 2.1 and Figure 2.2). During this interval, the dwindling ice sheet left a series of sub-parallel moraines across northern Denmark and south-west Sweden, named the Halland (coastal) Moraines (c. 18 ka to 16 ka BP ), Göthenburg Moraines (c. 15.4 ka to 14.5 ka BP), Berghem Moraines (c. 14.4 ka to 14.2 ka BP), Trollhättan Moraines (c. 14.2 ka BP), and Levene Moraines (c. 13.4 ka BP) in SW Sweden (Lundquist and Wohlfarth, 2001); the Hvaler Moraine in southern Norway

(Anderson *et al.*, 1995) and the Little Fiskebank Moraine in Denmark (Nesje and Sejrup, 1988). The precise correlation of moraine ridges from these different sectors is not yet clear, for there are significant errors attached to the dates that have been obtained so far. In turn, this makes it difficult to establish the precise manner of the response of the ice sheet to the climatic sub-stages defined in the Greenland ice-core records. It is safe to assume that the ice sheet was responding to a general climatic improvement during Greenland Interstadial 1, but the extent to which individual moraine ridges during this period reflect minor reversals in climate is difficult to establish.

More confidence can be attached to a significant readvance of the ice sheet margin during the Younger Dryas (YD) Stadial (GS-1 in Table 2.1), which is attributed to a significant climatic downturn. YD ice limits have long been recognized, as for example those that can be traced continuously in northern Norway (the Tromsø–Lyngen Moraines), along the west coast of Norway, particularly in the Bergen area (Herdla Moraines) and in southern Norway (Ra Moraines). The ice margin during the YD in South Sweden is marked by the Middle Swedish Moraines and in Finland by the Salpausselkä Moraines (Figure 2.3). While there is a widespread view that the ice margins of the last European ice sheet did readvance during the Younger Dryas Stadial, again this does not appear to have been a synchronous event. Parts of the ice sheet margin in western Norway appear to have reached their readvance limits later than elsewhere (Bondevik and Mangerud, 2002), while the Salpausselkä Moraines form at least three distinct ridges, are composed largely of deltaic deposits and were associated with a large ice lake that developed in the Baltic basin. They may have been abandoned at an earlier stage than in western or northern Norway (Björck, 1995; Rainio *et al.*, 1995). Thus, although the ice sheet expanded as a result of general climatic deterioration, local factors may have influenced the exact manner in which the ice margins behaved.

### 2.3 The last (Late Devensian) ice sheet in Britain and Ireland

The stratigraphic definition for the period of maximum ice expansion in the British Isles during the Late Devensian, which is broadly equivalent to the 'Pleniglacial' of continental Europe, is the Dimlington Stadial (Rose, 1985). The ice cover that developed over the British Isles during that time was initially based on morphological evidence on land, by contrasting the evidence for 'Newer Drift' in England and Wales (Bowen *et al.*, 2002) and for the 'South Irish End Moraine' in Ireland (McCabe, 1987) with older, less well preserved features. More recently, however, new evidence has been obtained from offshore, in the form of ice-marginal landforms and sedimentary units, that enable former ice margins to be detected on the sea floor (e.g. Bradwell *et al.*, 2007, 2008c; Graham *et al.*, 2007). Evidence for decay of the ice and recession from the maximal ice margin can be found in the form of recessional moraines on land and glaciomarine (deltaic) formations that mark where the ice melted into shallow marine conditions (e.g. Bowen, 1981; O'Cofaigh and Evans, 2007; Hiemstra *et al.*, 2006; Phillips *et al.*, 2008; Chiverell and Thomas, 2010). Despite the wealth of evidence that has been amassed over recent decades, however, the precise position of the maximum expanse of ice during the Dimlington Stadial remains a topic of considerable debate, as reflected in Figure 2.4, which shows the degree of variation in proposed maximal ice limits published within the past 30 years or so. The picture is further complicated by the more recent suggestions that the last ice sheet over Ireland may have been twice as large as previously thought, covering the entire island and more (Gibbard and Clark, 2011).

A further point of contention concerns whether or not the last ice sheet in NW continental Europe was confluent with the last ice sheet in Britain and Ireland. Several of the reconstructions shown in Figure 2.4 assume that the two ice masses were separate, whereas the model shown in Figure 2.1 assumes that they converged. New evidence reported by Carr *et al.* (2006) suggests the British and Fennoscandian ice sheets

converged some time between 28 and 22 ka BP, though the matter remains contentious. In view of the marked disparity between the models presented in Figures 2.1 and 2.4, it may be some time before the overall configuration of the maximum extent of the last British ice sheet can be confidently portrayed.

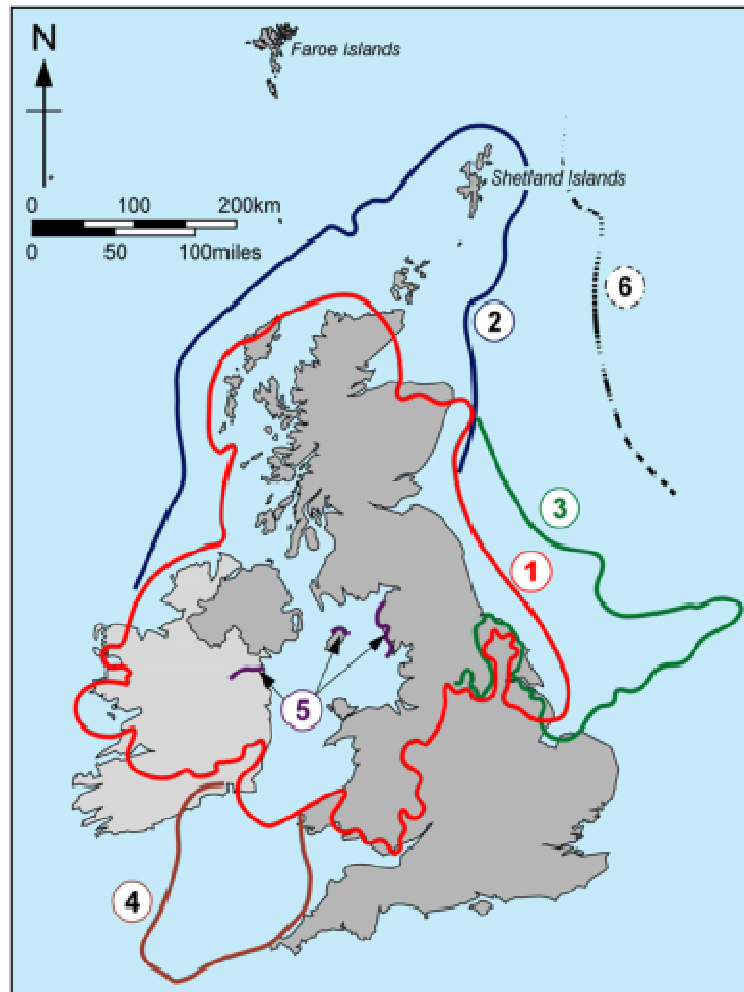


Figure 2.4 Recent reconstructions of the maximum extent of the Last Glacial Maximum (Late Devensian) ice sheet over the British Isles (from Boulton and Hagdorn 2006). (1—Bowen *et al.*, 2002; 2—Hall, 1997; 3—Balson and Jeffrey, 1991; 4—Scourse and Furze, 2001). Lines marked 5 show the extent of readvances in the Irish Sea Basin, in Ireland (Synge, 1977), the Isle of Man (Dackombe and Thomas, 1991) and Cumbria (Huddart, 1991). 6—possible western margin of the Scandinavian ice sheet at the LGM (Hall, 1997).

A number of recessional features have been proposed throughout the British Isles, some of which have been interpreted as representing significant local readvances of the ice margin after it withdrew from its maximum position. The evidence is too detailed and



complex to summarise in this short section, but is reviewed by Sutherland (1984a and 1984b) and more recently by Evans *et al.* (2005). Virtually all of the proposed readvance events are dismissed because the available evidence provides insufficient or unambiguous evidence that fails to prove that the ice readvanced; in most cases the evidence could equally be interpreted as representing a temporary halt in ice dissipation, the climatic significance of which is difficult to assess. There is evidence, however, for at least two readvance events in Scotland. One is represented by a distinctive boulder-strewn ridge that can be traced over much of Wester Ross in NW Scotland and which is termed the Wester Ross Moraine. It has been dated to c. c. 16.3 ka BP by Everest *et al.* (2006) and subsequently to c. 14.0 to 13.5 ka BP by Ballantyne *et al.* (2009). Both estimates are based on cosmogenic nuclide dating and the disparity in the estimates in part reflects different assumptions for local cosmogenic nuclide production rates. So far, evidence for an equivalent glacial margin has not been convincingly reported for other parts of Scotland, so it is not known (a) whether this moraine represents a major readvance of the ice margin or (b) whether it is of local significance only. Furthermore, if the age suggested by Everest *et al.* (2006) is correct, it would imply that the last ice sheet persisted till quite late, perhaps even into the GI-1 (Bølling) interval, a view supported by Bradwell *et al.* (2008b, 2008c) but criticized by Ballantyne (2012).

The only significant readvance which has left clear evidence throughout various parts of Scotland is the Loch Lomond Readvance, which is attributed to the Younger Dryas Stadial (the Loch Lomond Stadial in the British terminology). Evidence for this event was first proposed in the 1860's, when the 'Glacial Theory' was still embryonic in conception, but its significance was not firmly established until J.B. Simpson demonstrated in 1933 that the sediments in terminal deposits near the southern shores of Loch Lomond contain marine shells, demonstrating that the ice had advanced over

marine sediments (Sutherland, 1984b). Equivalent evidence has subsequently been found in association with several other former glacial readvance margins in Scotland, the marine shells providing radiocarbon dates that confirm that the ice readvanced some time after c. 11.0 to 11.7 k radiocarbon years BP. Presently there is a wealth of information to show that ice in Scotland had dwindled by about c. 13 ka BP to an extent that it either disappeared entirely from Scotland or was confined to within the Grampian Highlands, though it remains difficult to distinguish between these two possibilities (Sutherland, 1984b; Golledge *et al.*, 2008). It is now widely accepted that the ice had receded into the Highlands significantly during GI1, termed the Windermere Interstadial in Britain (the Bølling-Allerød period in continental Europe), and then readvanced significantly during the Younger Dryas Stadial (Loch Lomond Stadial, or GS-1).

The landforms of the Loch Lomond Readvance have been mapped in numerous parts of the Highlands, because they are the best preserved glacial landforms in the British Isles. Because they were laid down during the last cold episode to affect the British Isles, the resulting landforms have not been subjected to severe periglacial conditions. They therefore retain much fine detail, are frequently sharp-crested, characteristically display perched boulders, and can be dated directly by a range of methods (Benn, 1997; good examples of the fineness of detail that can be mapped in the field are provided in Benn and Ballantyne 2005). The quality of the mapped information has made possible the reconstruction of individual cirque and valley glaciers and the realization that the biggest mass of ice accumulated in the western Highlands of Scotland, with large icefields centred over the SW Highlands, the Rannoch Moor plateau, the Nevis Range and the mountains to the north-west and west of the Great Glen (Figure 2.5). By comparison, much smaller ice masses developed over the Cairngorm Mountains, the far north of Scotland and the Southern Uplands (Sissons, 1979e). This overall pattern of ice distribution remains to be refined in a number of places, but the evidence is particularly

clear in the Loch Lomond and Glen Roy areas, and it was therefore to these two areas in particular that attention was turned when selecting case areas for testing the capabilities of NEXTMap technology.

#### **2.4 The Loch Lomond and Glen Roy study areas**

In view of the complications and uncertainties that surround the nature of ice-marginal retreat in Europe at the end of the last glacial stage, illustrated in sections 2.2 and 2.3, care had to be exercised when selecting test-case areas for the application of NEXTMap imagery. Areas in which the landforms were of uncertain origin and/or subdued in form should be avoided, as far as is possible, while the study was not intended to be purely one of morphological description, but one which could make a contribution to the advancement of understanding of the late Quaternary history of the British Isles. Hence the decision was made to focus on two areas: the Loch Lomond and Glen Roy areas, both of which have been mapped at a high spatial resolution, and both of which contain clear evidence for the terminal positions of major ice margins of the Loch Lomond Readvance. The former is non-controversial in terms of providing a pinning position and age for the limit of the Loch Lomond Readvance. The latter, as explained in subsequent chapters, has proved to be more controversial, and somewhat more complex.

Landforms in the Loch Lomond area are key to understanding the glacial history of Scotland. The pioneering work of Simpson (1933), which led to the coining of the term Loch Lomond Readvance, has already been alluded to. Subsequent mapping throughout much of Scotland by J.B. Sissons (e.g. 1974, 1979b, 1979d, 1979e, 1980a, 1980b, 1982) led to the pattern of ice cover in Scotland during the Loch Lomond Readvance becoming more refined, including confirmation of the position of the ice limit in the

Loch Lomond area. The most detailed maps for glacial landforms in the Loch Lomond area, however, were developed by Rose (1981), who also placed the evidence in a wider context, by combining the morphological with lithostratigraphical observations. As a result, he has established the evidence in this area as the stratotype sequence for the Loch Lomond Readvance. The evidence confirms that during that period a large valley glacier, fed by ice formed in cirques throughout the SW Scottish Highlands, advanced down the length of the Loch Lomond basin, eventually to splay out as a piedmont lobe on to the low ground just to the south of the present shore of Loch Lomond (Figure. 2.5).

The key features in this area that enable the former ice limit to be reconstructed are a major end-moraine complex that can be traced over the ground to the south of Loch Lomond, and extensive fields of drumlins, some formed during the Loch Lomond Readvance that lie within (to the north/north-west of) the terminal moraine, and some attributed to Late Devensian ice sheet times. Those in the latter category either lie wholly outside the Loch Lomond Readvance terminal moraine, or have been over-run by Loch Lomond Readvance ice, which has modified their surface appearance. Distinction between drumlins attributed to either category has been made on morphological grounds, by detailed field mapping and remote sensing methods, the results of which can be tested by lithostratigraphical records (Rose, 1981; Rose *et al.*, 1988; Rose and Lloyd-Davies, 2003). This evidence is discussed in more detail in Chapter 4. The area was considered most suitable as a test-case for the application of NEXTMap technology because the morphological features have been independently mapped in the field and subsequently using remote sensing methods, the results of which show clear concordant spatial patterns in drumlin form and axial trends (Smith *et al.*, 2006; Rose and Smith, 2008). The original maps used for the field mapping were

made available by Professor Rose for comparison with interpretations based on NEXTmap.

This area therefore provided a relatively straightforward case in which the morphological features presented (a) a distinct ice-marginal context and (b) contrasts between features formed by Dimlington Stadial ice and younger landforms formed by Loch Lomond Readvance ice. Furthermore the age and position of the terminal moraine has been refined by a combination of varve chronology and radiocarbon dating, while detailed analysis of the varves confirms the position of the ice margin, in the manner in which it blocked local drainage (MacLeod *et al.*, 2011). Hence the area appeared to provide a non-controversial test-case for ‘ground-truthing’ maps and interpretations based upon NEXTMap DEM data (Chapter 4).

The Glen Roy area is also an iconic location in the development of the history of glaciation in Scotland. Indeed, Agassiz visited the area during his travels in Scotland in 1840, and was the first to suggest that the famous ‘Parallel Roads of Glen Roy’ (ancient lake shorelines) were formed by lakes that had been impounded by glacial ice. Subsequent research by J.B. Sissons (Chapter 3) led to the detailed mapping of the glacial landforms throughout the area, and to the most detailed examination yet undertaken of the distribution and form of the Parallel Roads. His conclusion was that the majority of fresh glacial landforms, as well as the ‘Roads’ themselves, were formed during the Loch Lomond Stadial, a conclusion corroborated by dating based on varved lake sediments preserved in the area (Palmer *et al.*, 2010) and by cosmogenic nuclide dates obtained from boulders on some of the landforms in Glen Roy (Fabel *et al.*, 2010).

As with the Loch Lomond area, a suite of landforms suggests that Loch Lomond Readvance ice terminated in the Glen Roy area, in the vicinity of location 13 in Figure

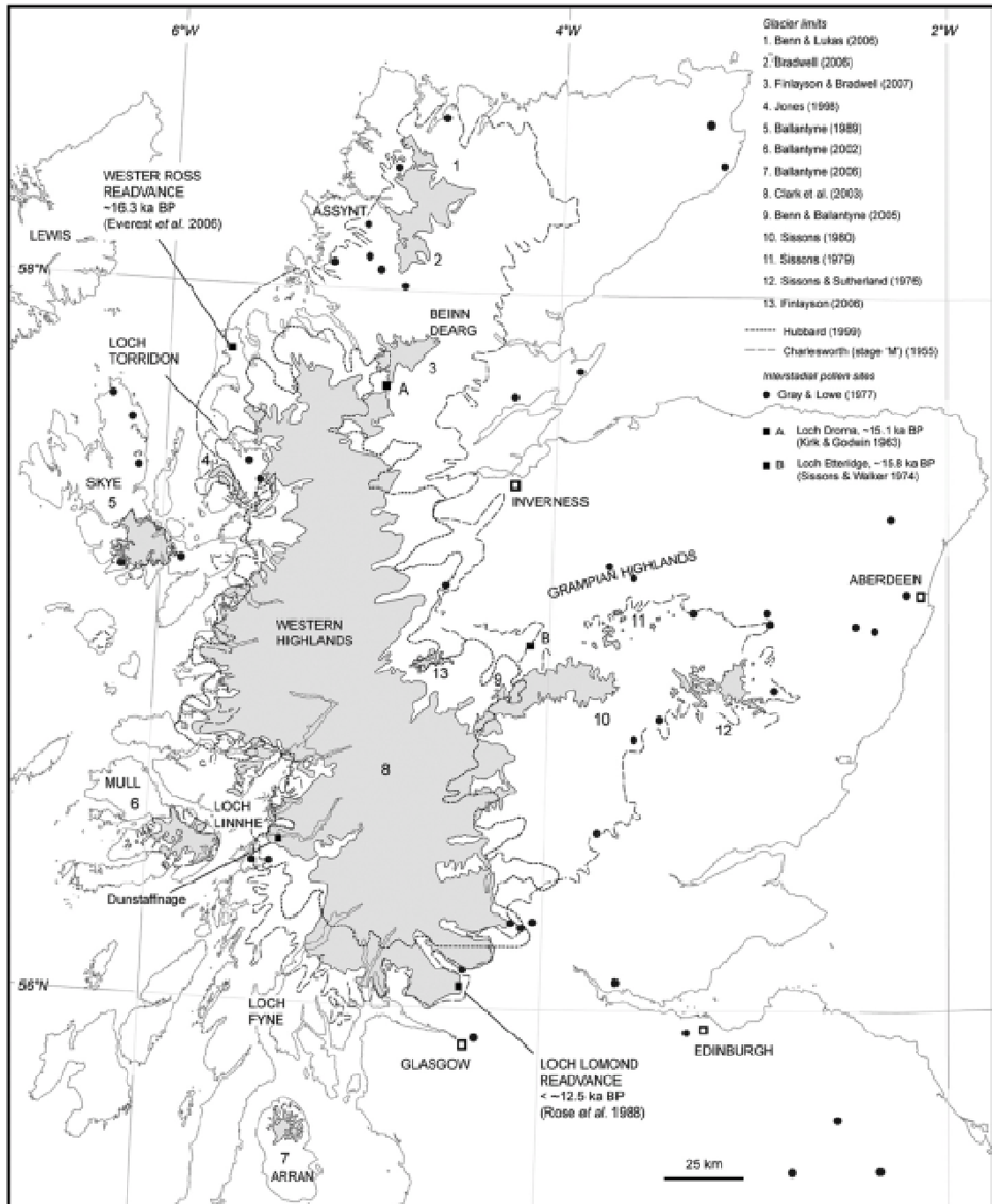
2.5. The precise location of the maximum ice advance into Glen Roy itself is generally agreed by those who have previously mapped the glacial features in this area (Sissons, 1979b; Sissons and Cornish, 1982b; Peacock, 1986), but some differences of opinion surround the interpretation and age of other ice-marginal features in adjacent valleys, while the ages and mode of formation of major fans in Glen Roy are also disputed. The ancient lake shorelines also provide unique near-horizontal features that can be traced throughout the area, and which intersect the glacial features, providing some information on the order of formation of different landforms. Hence this area was selected for further study, to provide a further test of the capabilities of NEXTMap technology. The aims in this part of the study (reported in Chapters 6 and 7) were to (a) apply the mapping methods developed in the study of the Loch Lomond test case, and compare the resulting landform interpretations with previous results for the Glen Roy area based on field mapping and aerial photography; (b) test the degree to which the technology could be used to map near-horizontal surfaces; and (c) examine whether the new evidence helps to resolve some of the existing disputes concerning the sequence of events in Glen Roy at the end of the last glacial stage. These aims were considered important, because the evidence in the Glen Roy area is proving crucial for testing numerical models of the growth of ice in Scotland during the Loch Lomond Readvance, as explained next.

### **2.5 Numerical modeling of Loch Lomond Readvance ice growth in Scotland**

Although the broad pattern of the ice masses that developed during the Loch Lomond Readvance is emerging from the abundant geological evidence that exists, some disputes and enigmas remain. As already mentioned earlier in this chapter, a long-held view was that the Late Devensian ice sheet completely melted during the Windermere Interstadial (Bølling-Allerød or GI-1), and that ice was re-generated anew during the

Loch Lomond Stadial, building up the western Highland ice mass and smaller cirque glaciers afresh (Sutherland, 1984a). This has never fully been accepted, however, even by proponents of this explanation, because there has always been a question over the time available to build up this large mass of ice from ‘scratch’. The Younger Dryas interval, as defined by isotopic signals in the Greenland ice-core records, is estimated to have lasted about 1200 years (12.9 to 11.7 GICC05 ka BP), which many regard as too short a period to generate such a large body of ice. The alternative view, based on reconstructions of the pattern of ice retreat in the Loch Broom area in NW Scotland (north of the Glen Roy area), is that the LLR was a short-lived reactivation of the residual mass of the down-wasting Late Devensian ice sheet, which persisted in large parts of the Scottish Highlands (Bradwell *et al.* 2008b, 2008c). Furthermore, some of the published reconstructions of Loch Lomond Readvance glaciers have been questioned on the grounds of improbable glacier dynamics (e.g. Golledge and Hubbard, 2005). In order to address questions such as these, increasing use is being made of numerical models of the growth of glacier ice in Scotland during the Loch Lomond Readvance. These use estimates of prevailing climatic conditions, especially snow supply, topographic parameters, and glaciological dynamics to ‘grow’ the ice sheet over prescribed intervals, in an attempt to establish what is feasible under given forcing conditions (e.g. Hubbard 1999; Golledge *et al.*, 2008; Golledge 2010). One of the outputs of such numerical modeling exercises is illustrated in Figure 2.5.

A comparison between the ice limits based on numerical modeling compared with those based on empirical studies shows an encouraging degree of general agreement, but some important differences in detail. The former seem to exceed the latter in the north and east, but under-estimate them in the west and south. Of importance to the current study: the empirical and modeled data provide closely matched inferences in the Loch Lomond area, but are significantly different in the Glen Roy and adjacent areas.



**Figure 2.5** Inferred maximal limits of Loch Lomond Readvance glacier ice in Scotland based on numerical modeling (dashed lines) compared with inferences based on empirical studies (grey shaded area, solid lines) published between 1955 and 2007 (from Golledge *et al.*, 2008)

There are also differences in the suggested timing of maximum glacier expansion, with the models suggesting this was achieved in the early part of the Loch Lomond Stadial (Golledge, 2010), while empirical evidence from Loch Lomond and Glen Roy suggest



maximal positions were attained towards the end of the cold phase (Palmer *et al.*, 2010; MacLeod *et al.*, 2011).

It is not the intention here to review the relative merits of numerical versus empirical reconstructions of the Loch Lomond Readvance ice cover in Scotland, as clearly both approaches offer some important insights. However, the latter provide key pinning points for testing the validity of the models, which is certainly the case in the Loch Lomond area, where the ice position can be pin-pointed in space and time with a high degree of confidence (MacLeod *et al.*, 2011). Strong empirical evidence also exists in the Glen Roy area, but is not currently as clear-cut as the evidence from Loch Lomond. A major question addressed in this thesis, therefore, is whether NEXTMap DEM data can resolve some of the questions surrounding aspects of the evidence in Glen Roy, and whether, as a result, greater confidence can be attached to the use of the geomorphological evidence in this area to provide a pinning point for numerical models of the Loch Lomond Readvance ice cover in Scotland.

### **3. Introduction to NEXTMap: testing its capabilities**

---

#### **3.1 Introduction**

A precise and accurate base map is critical in all kinds of geography research. With traditional ground-based surveys it is difficult to accurately determine the topography of physically complex landscapes in remote areas. It is also time consuming and it is easy to miss significant elements of the landscape depending upon the type of survey carried out. Remote sensing techniques have widely been adopted in contemporary landform survey, especial for large and remote areas. Traditionally, in the field of palaeo glacier dynamics and ice sheet reconstruction, researchers normally use contours as the base information (Rose and Letzer, 1975) and record field survey results upon paper-based topographic maps (Rose and Smith, 2008). However, most of the glacial landform evidence covers large areas and is in remote areas which require the synthesis of regional data sets and many problems exist with the derivation of data from paper-based topographic maps. These have now been largely replaced by remote sensing techniques such as aerial photography, satellite imagery and the digital elevation models (DEMs).

The aim of this chapter is to determine and evaluate which are the best methods for mapping glacial landforms in the UK. This chapter will start by reviewing image sources that are available in UK and evaluate their effectiveness for glacial landform mapping. Elements that effect the visualizion and landform representation capabilities of the selected image data will also be examined and evaluated through a series of experiments in selected areas. In the final part of this chapter, a new method will be presented that will allow the selected landform to be present most effectively on a single image.

### **3.2 Remote sensing imagery available in UK**

Remote sensing imagery available for the UK can be grouped into aerial photography, satellite imagery and digital elevation models (DEMs). Aerial photography has been used extensively for high resolution landform visualization and mapping since 1860 (Lillesand *et al.*, 2004; p60). It gives us a bird's-eye view and enables us to see Earth surface features in their spatial context for what may be a large area. However the limitations of photo range, flying time and photogrammetric processing makes aerial photography a high cost option for much glacial landform mapping.


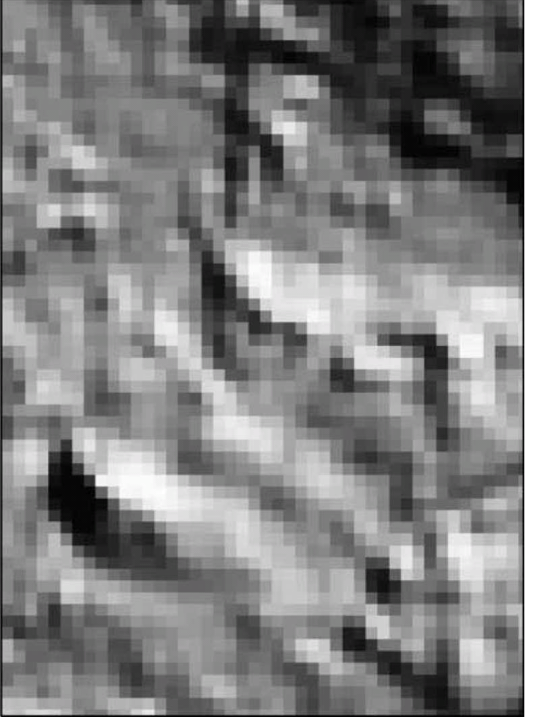
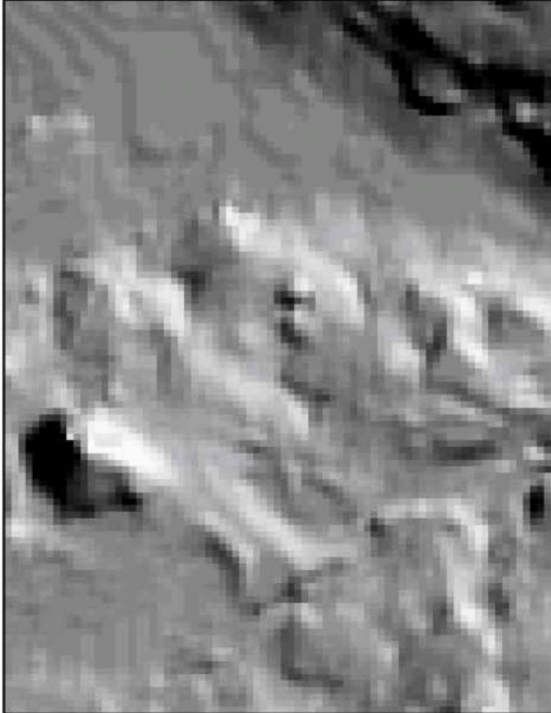

Satellite imagery here refers to Earth resource satellite imagery launched after 1972. The National Aeronautics and Space Administration (NASA) of USA launched Landsat-1 on July 23, 1972 (Lillesand *et al.*, 2004; p404). This provided a new method for researchers in observing the earth surface. In comparison with aerial photography, satellite imagery has large areal coverage, relatively low cost and enables relatively rapid rates of mapping (Punkari, 1982; Clark, 1997). Resolution of satellite imagery improved rapidly from 80 m (Landsat-1, MSS) to 2.44 m (Quickbird, MSS) in 3 decades (Lillesand *et al.*, 2004). Classified by the imagery resolution we can divide satellite imagery into 3 groups, the low resolution multi-spectral satellite imagery (e.g. Landsat 1~7), which offered maximum spatial resolutions up to 30 m (MSS, TM, ETM and ETM+); the medium resolution imagery which provides spatial resolution range from 20 m (SPOT 1~4, XS) up to 10 m (SPOT-5, XS) giving moderate detail. Very high resolution imagery, which refers to spatial resolution smaller than 5 m, is represented by IKONOS, with 4 m MSS and Quick-Bird with 2.44 MSS. These kinds of imagery provide spatial resolutions close to large scale aerial photography (1–4 m), but it is more expensive than other scales of satellite imagery.

In recent years DEMs have become perhaps the most popular data source for landform mapping as they record absolute elevation information which traditional aerial photography and satellite imagery can not provide. Using GIS software, the analysis of DEMs allows researchers to view the landforms from any perspective and change the illumination angle, in order to highlight particular landform features. Commonly, DEMs are generated from three source types. i) Using spot height data from field survey or GPS survey. ii) Acquiring elevation data from the contours of topographic maps. Satellite image capture operates in stereo-pair acquisition mode (eg. SPOT-5 and ASTER). iii) From space or aircraft transported active microwave or light detection and ranging (LiDAR) sensing techniques. Imagery such as Shuttle Radar Topography Mission data (SRTM) and NEXTMap are typical examples of this source.

Smith *et al.* (2006) collected one satellite image (Landsat Thematic Mapper) and six DEM data sets (including LiDAR, NEXTMap Great Britain (refer to NEXTMap in the following text), Ordnance Survey Panorama and Profile (refer to OS Panorama and OS Profile), Landmap and Shuttle Radar Topography Mission (refer to SRTM) (Table 3.1 and Figure 3.1) of a 100-km<sup>2</sup> region north of Glasgow, west central Scotland, UK (Figure 3.8). Among selected DEMs, OS Panorama and Profile are generated from the contours of topographic contours. SRTM, Landmap and NEXTMap are active microwave based data sets and the first two are free DEMs for use by the academic community in the UK. An experiment was carried out to compare glacial geomorphological mapping derived from remote sensing imagery with 1: 10,000 scale field mapping (Smith *et al.*, 2006). The results show that of the results derived from the remote sensing data sets, only NEXTMap provided information that showed any approximation to the field mapping. OS Panorama and OS Profile provided very poor approximations, and the other images fail to provide any information of value.

**Table 3.1 Imagery used in Smith *et al.* (2006) with the resolution of the methods. The image reference refers to the parts of Figure 3.1 of this thesis.**

	Image reference	Horizontal resolution (m)	Vertical resolution (m)
Landsat Thematic Mapper	A	30	--
Shuttle Radar Topography Mission C-band (SRTM)	B	90	6
OS Panorama	C	50	5
Landmap	D	25	20
OS Profile	E	10	5
NEXTMap	F	5	1
LiDAR	G	2	0.25
Field mapping	H	<1.0	1

<p><b>A. Landsat Thematic Mapper</b></p>	<p><b>B. Shuttle Radar Topography Mission C-band (SRTM)</b></p>
	
<p><b>C. OS Panorama</b></p>	<p><b>D. Landmap</b></p>
	

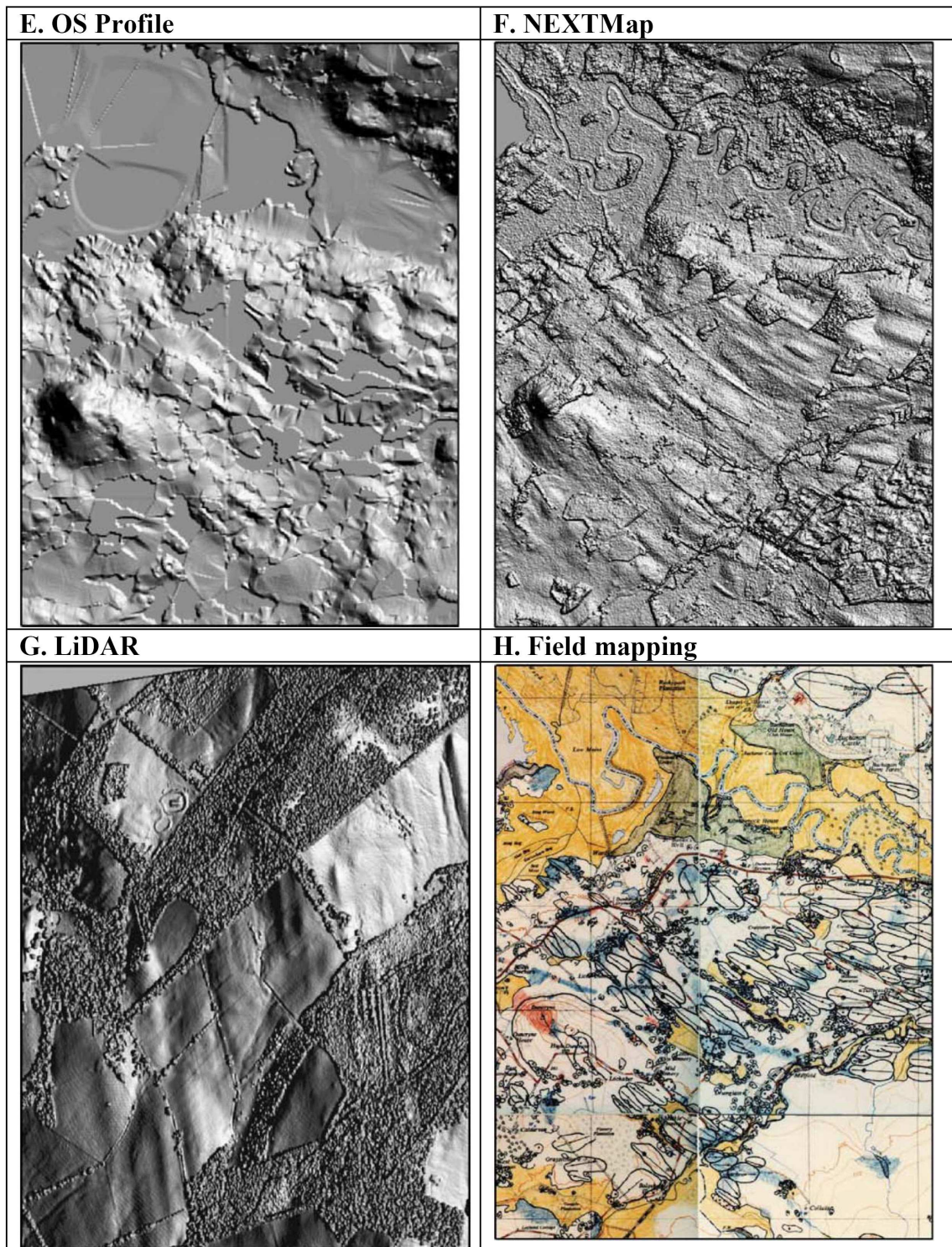


Figure 3.1. Comparison of the imageries used in Smith *et al.* (2006). Except the LiDAR image, the other images samples are present the same area.

Mercer (2001) compared NEXTMap and LiDAR DEM data in terms of the methodologies and the price factor. His main conclusions can be summarized as follows.

1. The NEXTMap wavelength is X-Band (3 cm) which allows it to penetrate cloud and haze; LiDAR wavelengths are in the near Infra Red (1 nm) waveband which does not penetrate cloud, and are heavily absorbed by water.
2. Unlike NEXTMap using side-looking geometry, LiDAR viewing is centred on the lowest point which limits problems associated with occlusion by buildings and other solid objects.
3. The unit price of LiDAR is close to the areal photography but is about 5 times greater than NEXTMap and around 100 times greater than the SPOT satellite image (Figure 3.2).

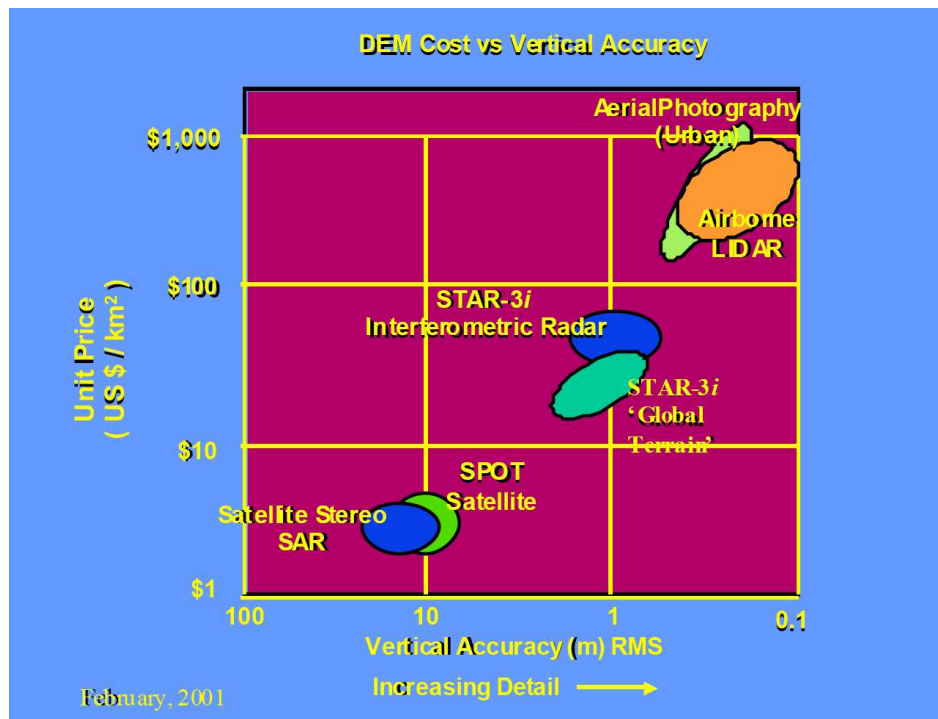


Figure 3.2 Comparison of LiDAR, NEXTMap (STAR-3i) and SPOT satellite image in terms of data unit price and vertical accuracy (Mercer 2001).

With the improvement in spatial resolution of DEMs from 90 m (SRTM) to 2 m (LiDAR), DEM data have become a progressively more important data source.



NEXTMap is the highest resolution DEM to cover the whole UK at the time of writing this thesis but a variety of organisations (Environment Agency, Natural Environment Research Council (NERC)) currently fly survey aircraft to acquire LiDAR DEM data. In the future, it could be expected that the whole UK may be covered by very high resolution LiDAR DEM data.

### **3.3 DEM Visualization Techniques**

DEM visualization is the graphical recreation of a real world scene through numerical modelling and visualisation on a computer monitor. Estes *et al.* (1983) mentioned that human eye is particularly good at perceiving subtle grey scale changes in an image. Thus relief shading can be used very effectively to highlight topographic variation and help to map landforms from DEMs. Lidmar and Bergström (1991) state that linear landforms will be less visible when shaded from a direction that is parallel to the orientation of the linear landforms, but will become more visible when the light source changes to an azimuth at angles to the landform long axis. However, they did not discuss the implications of how relief shading could be implemented within a broad mapping programme without the bias they had mentioned, or how shape can change for those landforms that are not purely linear, when viewed under different light source azimuths. These problems have been further discussed and illustrated in Smith (2003, 2005).

Smith (2003, 2005) compared 11 different DEM visualizing methods (Table 3.2) and tried to determine the optimal method for geomorphological mapping. Among the visualizing methods described, relief shading images, including orthogonal, parallel and intermediate illumination, are the most common and simple but have the “illumination bias problem” introduced above. This means the shape of the landform can become

distorted and possibly even hidden depending on the azimuth direction and elevation of light source. The Dynamic Illumination Variability (Rotating Map) method consists of a constantly changing direction (azimuth) of illumination in order to produce the relief shading imagery. This provides the potential to eliminate problems of bias caused by the direction of light source, by generating a changing pattern of light sources and hence a changing pattern of images, so providing a full visual depiction of the landform being studied

Smith and Wise (2007), stated that the representation of a landform is controlled by three main elements, which are relative size, azimuth biasing and landform strength. The relative size is the landform in relation to the resolution of the image; the azimuth biasing is the orientation of the landform with respect to the incident solar illumination azimuth; and landform signal strength refers to the tonal and textural definition of the landform on an image. These three variables interact, producing a complex “surface” representing the landform.

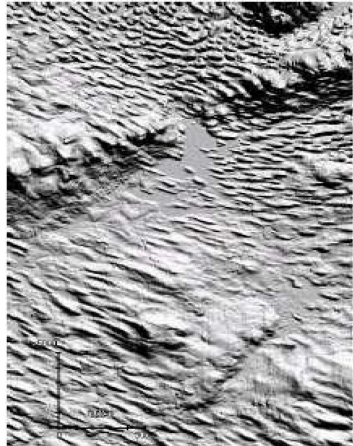
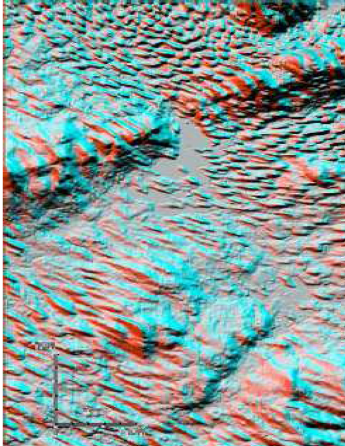
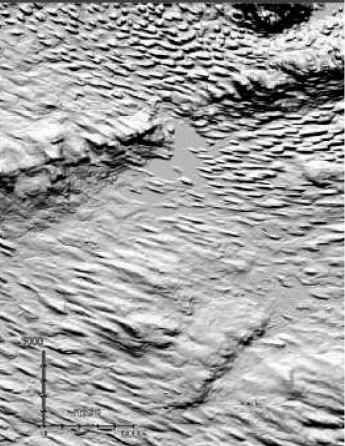
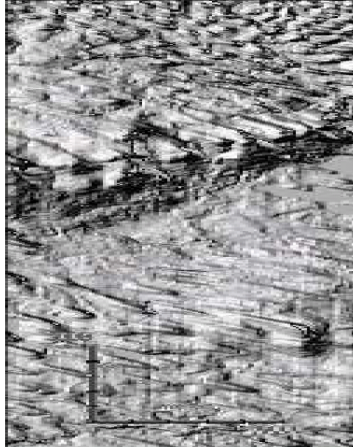

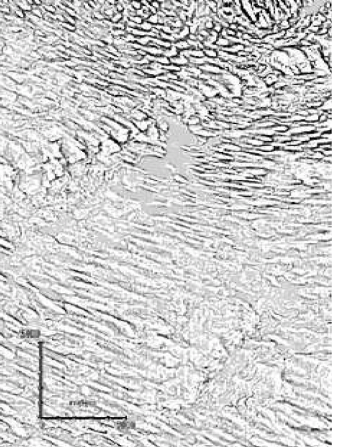
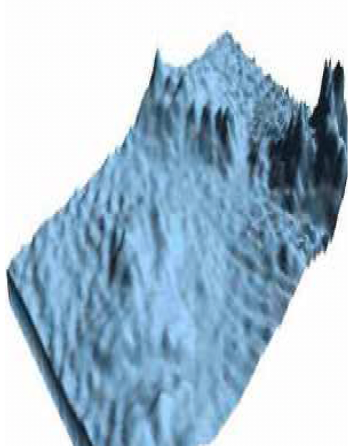
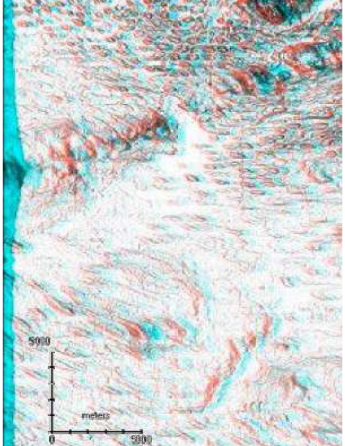
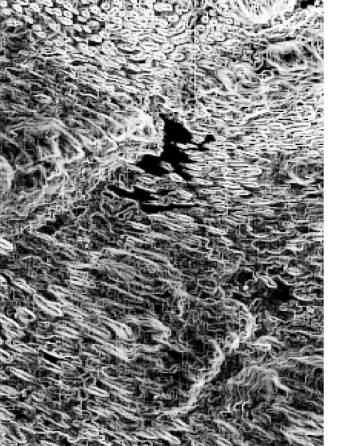
**Table 3.2 Methods for visualizing DEM data (after Lidmar and Bergström 1991; Smith, 2003; and Smith 2005). Image samples are show in Figure 3.3.**

<b>Method</b>	<b>Procedure used to generate image</b>	<b>Advantages</b>	<b>Disadvantages</b>
<b>1. Relief shading (Hillshading)</b>	This method requires the creation of at least two relief shaded images from a DEM - parallel and orthogonal to the principal lineament direction.	This arrangement should allow the visualisation of all landforms on the image.	All the relief shading imagery has azimuth bias problems.
<b>2. False colour composite</b>	In this method two relief shaded images were created as in method (1), and	This has the effect of colouring areas of the image that appear in only one, or both,	Unsatisfactory as the variation in colour distracts the eye from the underlying

	assigned to a different monitor colour (i.e. image 1 is viewed as blue, and image 2 as green).	images.	terrain making mapping difficult.
<b>3. Statistical Analysis (Mainly use Principal Component Analysis - PCA)</b>	Methods include addition, subtraction, minimum, maximum and mean between different images. The <i>parallel</i> and <i>orthogonal</i> relief shaded images were used to run the PCA program	Can be used to isolate and emphasize traits or features from 2 or more input images.	1. This is relative within the small scale study area (i.e. a global or continental scale) and does not highlight smaller, localised, elevation variations 2. The transverse ridges might become subtle such that an inexperienced observer would not identify them properly
<b>4. Combination Viewing</b>	Using Remote sensing software to load several images, <i>layered</i> on top of each other to fade or flicker between these layers.	This technique can be used to jointly map two alternatively shaded DEMs to facilitate a visual Comparison.	
<b>5. Dynamic Illumination Variability (Rotating map)</b>	Generate the relief shading images with a constantly changing illumination azimuth range from 0° - 360°. Put all those images together to become an animated GIF file.	Providing a full, visual, depiction of landform representation change with azimuth.	There is currently no easy method by which mapping can take place.

<p><b>6. Gradient</b></p>	<p>Created in the same way as <b>relief shading</b>, except using a solar elevation of 90°.</p>	<p>Lineaments are topographically distinct as a result of their elevation difference from the surrounding terrain. The brightness of each pixel is directly related to slope angle so that bright areas are flat, and dark areas are steep.</p>	<p>The transverse landforms in this imagery are less distinct.</p>
<p><b>7. Slope Curvature</b></p>	<p>Calculated in ARC/INFO, based on the method of Zevenbergen and Thorne (1987)</p>	<p>1. Regional outlines and ridges are clearly discernible and not only are they highlighted but they are also normalised for elevation. 2. This image is not illuminated, there is no azimuth bias.</p>	<p>There are hints that transverse ridge landforms can be observed, however they are not visually strong and might be considered as noise.</p>
<p><b>8. 3D Perspective Viewing</b></p>	<p>The DEM provides elevation data, it is possible to generate 3D view in GIS software using Arc Scene or overlay it with thematic information (map or satellite image)</p>	<p>Typically used to view a landscape obliquely and generate “fly-throughs”.</p>	<p>1. No software is available to direct digitising from such imagery at present. 2. The process is time consuming and is not suitable for rapid mapping.</p>
<p><b>9. Stereo Viewing</b></p>	<p>Create stereo-pair image from the DEM and then overlay with thematic data</p>	<p>1. Normally used to introduce parallax effects into the resultant image making it viewable as a 3D scene 2. Direct digitisation is possible and it can also perform stereo</p>	

		perspective viewing and “fly-throughs”.	
<b>10. Localised Spatial Enhancement- Adaptive Filtering</b>	The input image is partitioned into windows, and the transformation parameters are calculated for each pixel as a linear interpolation of the stretch parameters for adjoining blocks.	Local topographic variations can be selectively enhanced, by using this method.	Transverse landforms are not clearly outlined although a small number can be observed by using this method.
<b>11. Localised Spatial Enhancement - Texture Filter</b>	Textural information within gridded elevation data is typified by small, apparently random, changes in elevation. For lineaments these are spatially correlated so that texture filtering can highlight them. This procedure can be done by using imagery process software (Erdas Imagine)	Can be used to selectively highlight textural elements within imagery	The produced results similar to <b>slope curvature</b> .

<b>1. Relief shading</b>	<b>2. False colour composite</b>	<b>3. Statistically generated (PCA)</b>
		
<b>4. Combination Viewing</b>	<b>6. Gradient</b>	<b>7. Slope Curvature</b>
		
<b>8. 3D Perspective Viewing</b>	<b>9. Stereo Viewing</b>	<b>10. Localised Spatial Enhancement</b>
		

**Figure 3.3** Sample imageries of each DEM visualization method. (all imageries are from Smith (2003)). Further details on each of these methods are given in the Table 3.2 and in the text

In theory, the rotating map will provide the optimal imagery for landform mapping because it contains full information (including orthogonal, parallel and intermediate illumination) for each landform. This map is included in this thesis as Appendix 1, and can be viewed on the CD enclosed in the folder at the end of the thesis. However, this method was abandoned by Smith (2003, 2005) and only used to demonstrate “illumination bias”. The reason given was that there was no practical software by which it is possible to map directly onto the rotating image.

Smith (2003, 2005) then selected 7 DEM visualization methods (Table 3.3) to compare their effectiveness as sources for geomorphological mapping. He concluded that all the single image methodological approaches have limitations and provide an incomplete representation of the terrain being mapped. Among these visualization methods, orthogonal and parallel illuminations are most effective for identifying lineaments, ridges and hillocks. The orthogonal illumination data performs well at identifying lineaments and hillocks, but poorly for ridges, while the parallel illumination data performs well for hillocks and ridges, but poorly for lineaments. However, Smith (2003) suggested beginning mapping with slope curvature data due to the fact that it is bias free with respect to orientation and provides satisfactory results arising from the study of lineaments, hillocks and ridges. Smith (2003) also mentioned that the mapping results need to be revised with parallel and orthogonal illumination data as the process of mapping progresses. The remaining images have different advantages and weaknesses but are less informative than slope curvature, orthogonal illumination and parallel illumination.

The findings of Smith (2003) indicate that images produced through relief shading have the potential to satisfy most of the demands of glacial landform mapping. Although relief shading has the so call “azimuth illumination bias” problem this can be overcome

by using the rotating map technique (Appendix 2). The rotating map method not only has the potential to solve the illumination bias problems, but it also provides a full, visual depiction of the landforms with the change of azimuth. Another advantage of using the rotating map is that it uses relief shading imagery which can be manipulated by most GIS analytical models (Spatial Analyst and 3D Analyst). However the slope curvature imagery can be only generated by special software such as ESRI ArcInfo, which is the full function version of ESRI Arc GIS and is more expensive than the essential Arc View including spatial or 3D analyst model. Therefore, from the financial-and user's-accessibility point of view, the rotating map method produced from the relief shaded imagery is more economic and convenient than slope curvature imagery.

**Table 3.3 Numerical comparison of different DEM image conditions (from Smith, 2003).**

Landform	Lineament	Hillock	Ridge	Total Lineament Length (km)
Slope Curvature	361	84	10	297
PCA	271	89	10	218
Orthogonal Illumination	371	101	0	289
Parallel Illumination	176	120	20	146
Intermediate Illumination	330	75	0	146
Local Contrast Stretch	267	45	0	234
Overhead Illumination	273	102	0	218
<b>Truth</b>	<b>442</b>	<b>109</b>	<b>25</b>	<b>263</b>
Control (Orthogonal Illumination)	382	117	0	260

As a result of these conclusions the relief shading method will be used in this research for DEM representation, and the ability and procedures of using rotating maps for landform analysis will be evaluated and defined in the following section of this chapter.



In addition to the points described above, another very important factor needs to be considered in using relief-shading. This is the direction from which the illumination is derived. This is shown in Figure 3.4 which is the Moy Corrie area at the eastern side of Glen Roy in the northwestern Highlands, Scotland. The NEXTMap image on Figure 3.4B is produced by using illumination from the south (Azimuth 180°) while the illumination of Figure 3.4C is from the north (Azimuth 0/360°). Preliminary analysis of Figure 3.4B reveals problems in determining what the valley bottom is and what the hill top is. This is because for normal vision, illumination comes from the front (north hemisphere; 0°~90° and 270°~360°). Thus terrain facing the north will appear in brighter tones while that facing south will be in dark tones (Figure 3.4C). If the illumination is from the opposite direction, our interpretation become confused and it is difficult to make a correct interpretation (Figure 3.4B). It is for this reason that most general texts suggest illuminating from the NW (315°; GIS software is normally set to this value as a default in generating relief shading image). However, from the point of view of geomorphological interpretation the direction of illumination is most effective when it is normal to the dominant landform lineaments. Several authors have commented on the bias that may be introduced by single azimuth illumination (Graham and Grant, 1991; Lidmar-Bergström *et al.* 1991) and the suggestion has been made that two illumination angles should be used: orthogonal to one another, and parallel and normal to the dominant lineament orientation.

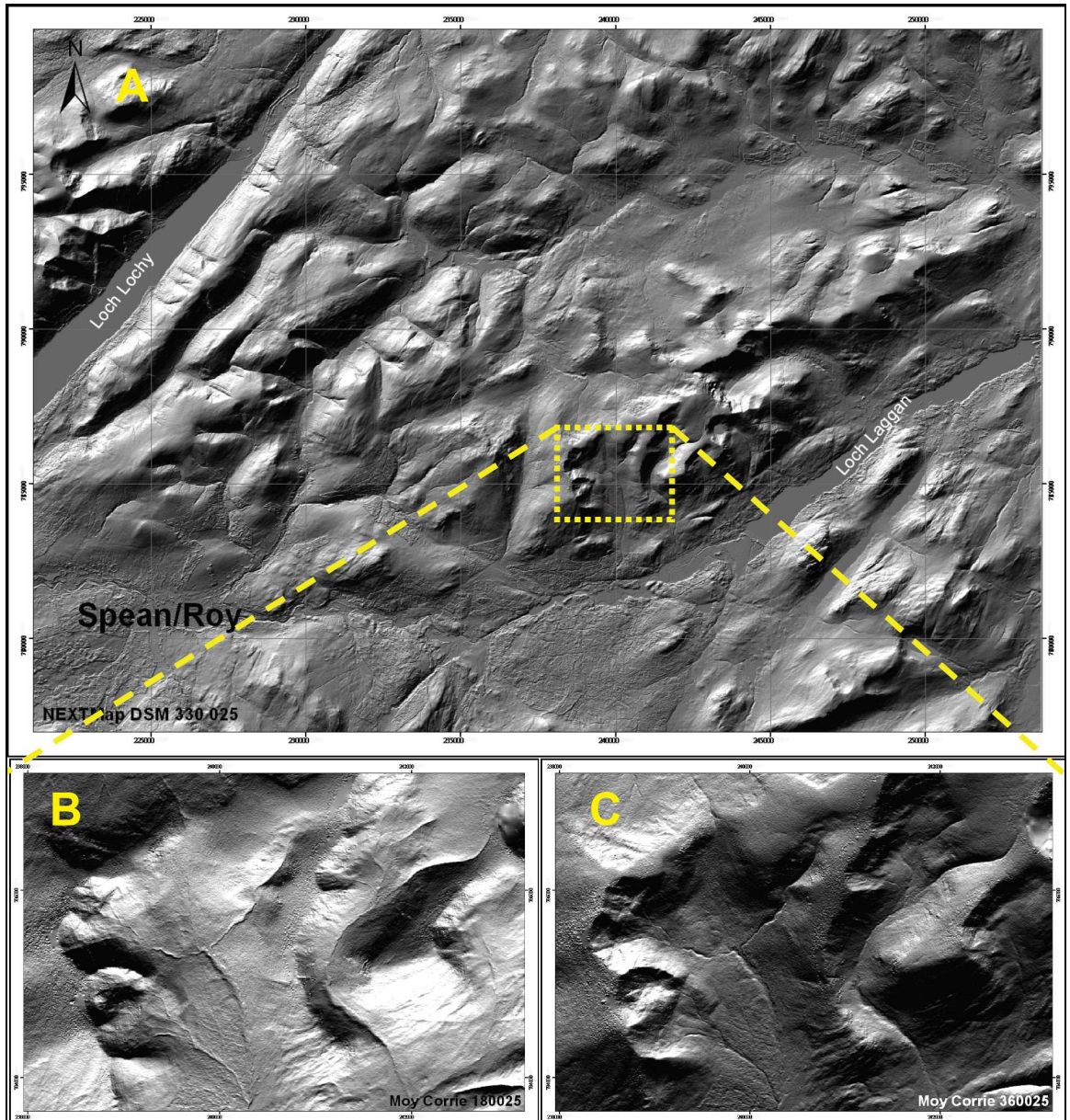


Figure 3.4 Different directions of illumination used to demonstrate the effects on the image visibility and interpretation in the Moy Corrie area at the eastern side of Glen Roy, northwestern Highlands, Scotland. Image B is produced by using illumination from the south direction (Azimuth  $180^\circ$ ) while the illumination of image C is from the north direction (Azimuth  $0/360^\circ$ ). This figure is related to Figure 3.5 which uses the default setting of the azimuth and altitude angle in GIS software.



**Figure 3.5** Example of relief shading image using the default illumination direction and elevation (Azimuth: 315° , Elevation 45°) settings in GIS. The Location of this image is in the Moy Corrie area at the eastern side of Glen Roy northwestern Highlands, Scotland as shown in Figure 3.4A.

### **3.4 Characteristics of NEXTMap Great Britain™**

NEXTMap Great Britain™ (NEXTMap) is one kind of airborne IfSAR (Interferometer Synthetic Aperture Rader) image generated by Intermap Technologies Inc. This programme of mapping was commissioned by Norwich Union plc for insurance purposes, but has since been widely used in Earth Science research (INTERMAP product handbook and quick start guide, version 3.3., 2004). IfSAR is an active microwave earth sensing technique, it employs x-band radiation which can penetrate cloud, rain and smoke (Li *et al.*, 2002). Compared to the other kinds of sensor, IfSAR imagery is good at detecting topographic variation due to the oblique viewing angle of the sensor, whereas the visible and near infra-red (VIR) sensors use near-vertical viewing angle. Another advantage of IfSAR imagery is that it does not have fixed illumination and azimuth angles unlike optical imagery (for instance: Landsat) and,

therefore, can be viewed with the light source at varying directions (azimuths) and angles of elevation on different images, according to choice. Details of NEXTMap technical data are given in Table 3.4.

**Table 3.4 NEXTMap Great Britain technical data (from Li *et al.*, 2002 and 2004; Mercer, 2001)**

Sensor	Intermap Star-3i Airborne Interferometric SAR
Flying Height	9144 ~ 6096 m above mean ground level
Band	X-Band
Acquisition Date	Dec/2002 ~ May/2004
Spatial Accuracy	5 m (DSM, DTM) ; 2.5 m (ORI)
Vertical Accuracy	0.5~1 m

Basically, NEXTMap contains three types of image:

1. Orthorectified radar image (ORI)
2. Digital terrain model (DTM)
3. Digital surface model (DSM)

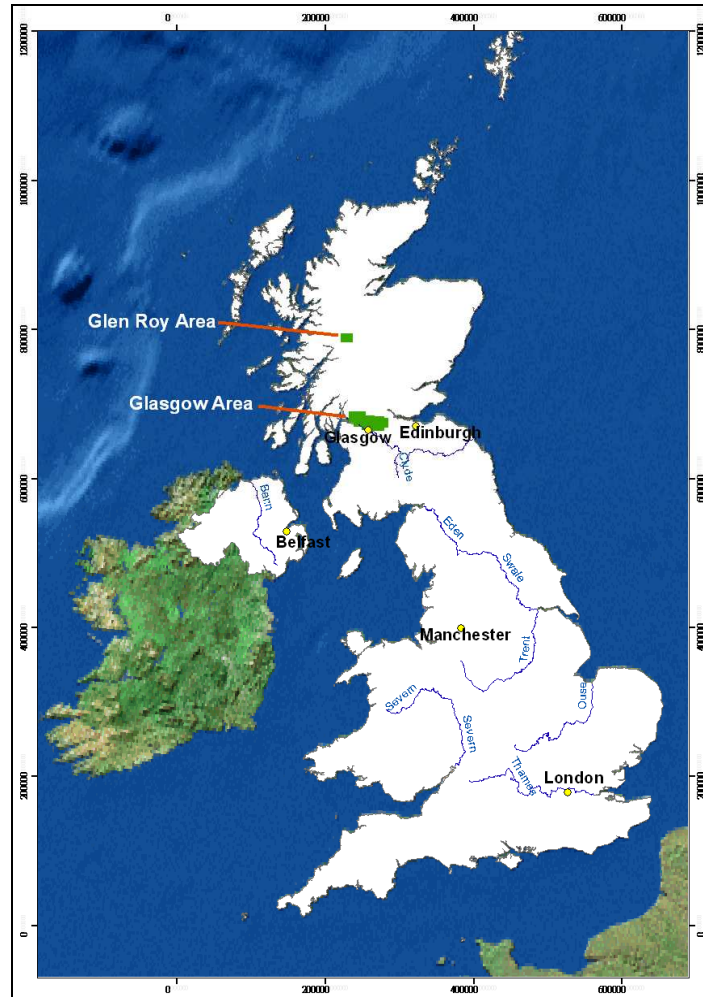
These properties can be illustrated by work from the area around the southern part of Loch Lomond just south of the western Highlands (Glasgow area), and in the area around Glen Roy in the northwest Scottish Highlands. This latter work, which is part of this thesis, has been published in part in Chen and Rose (2008a, 2008b and 2008c).

### **3.5 Experiments**

#### **3.5.1 Research sites**

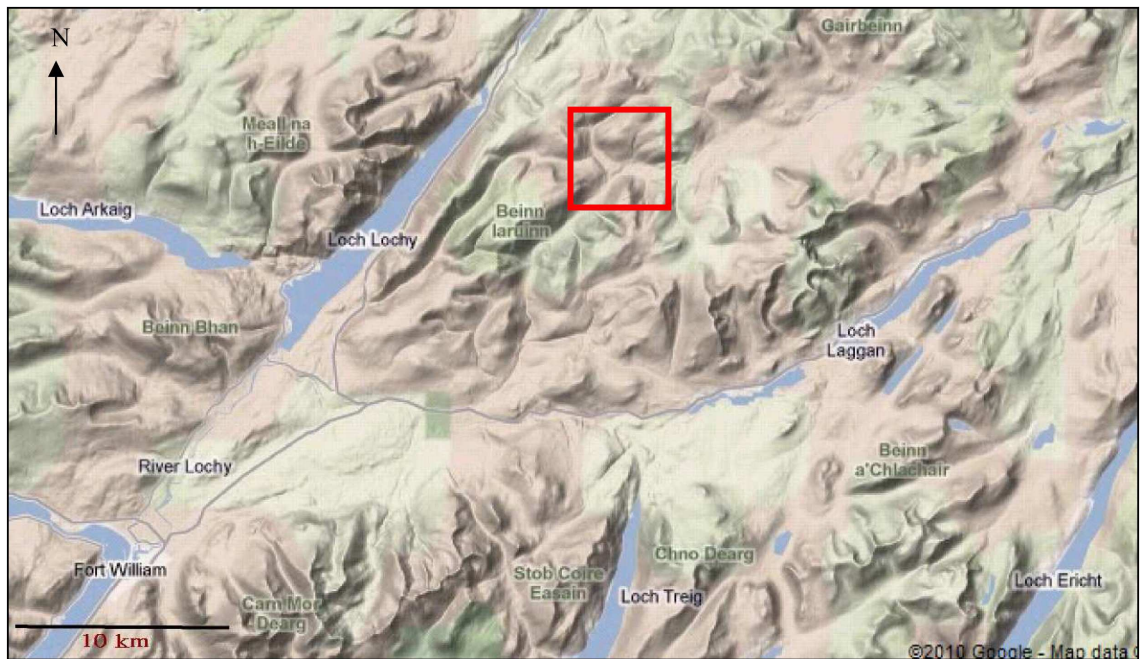
This section will re-evaluate elements controlling the representation of landforms as proposed by Smith and Wise (2007), and will mainly focus on the effects of the azimuth, altitude angle and image contrast changes. To achieve this NEXTMap DEM data have been used to provide the most realistic approximation of field mapping at a 1:10,000

scale, compared to other remote sensing imageries (Smith *et al.*, 2006). Glacial landforms from the Glasgow and Glen Roy areas have been selected for the experiments (Figures 3.6, 3.7 and 3.8).



**Figure 3.6** Location of the Glen Roy and Glasgow study areas in UK. (This map is re-generated using ESRI sample data in Arc GIS 9.2)

i) The Glen Roy area (Figure 3.6), is situated in the west Highlands of Scotland, approximately 15 km to the northeast of Fort William and the mountain range of Ben Nevis. In this chapter, different types of images (DSM, DTM and DIFF) are used to represent the area at Glen Turret near the head of Glen Roy (Figure 3.7) and to evaluate the characteristics of NEXTMap DEM data.



**Figure 3.7** Location of the of the Glen Turret area at the northern end of Glen Roy, north West Highlands, Scotland. (This image is taken from Google-Map, July 2010)

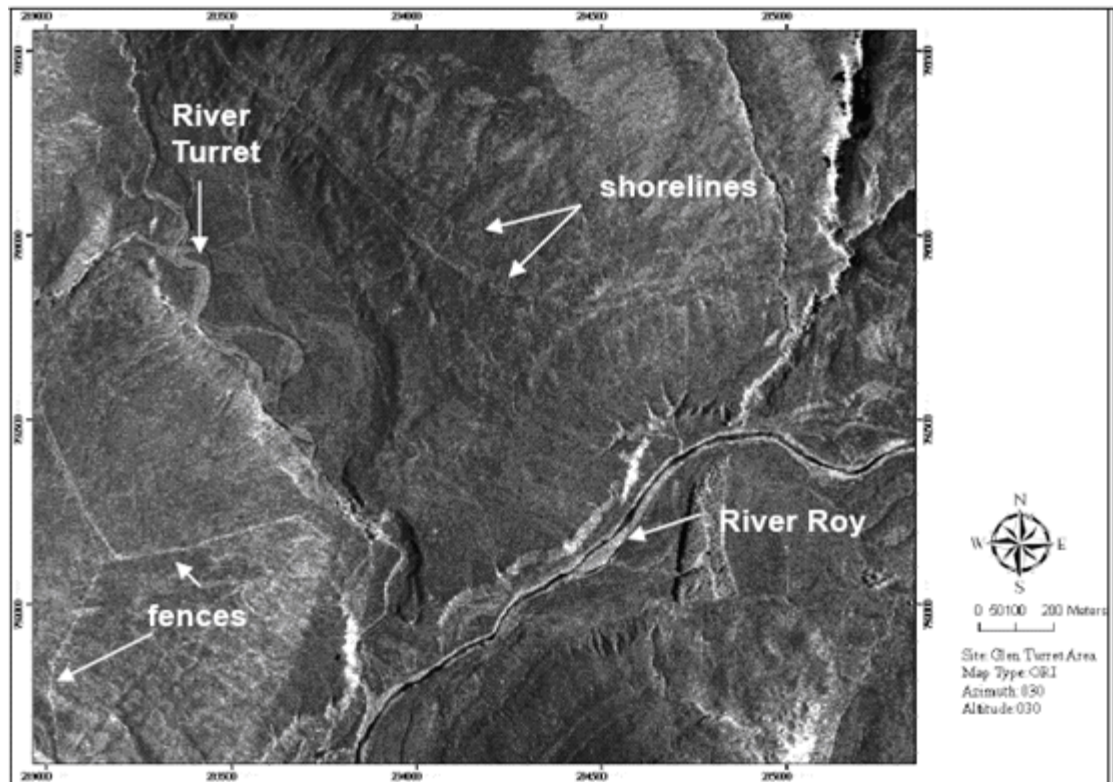
ii) The Glasgow area, including the southern Loch Lomond region (Figure 3.6 and 3.8) is in the western part of the Midland Valley of Scotland, just south of the western Highlands. The study area covers about 750 km<sup>2</sup> and was initially mapped by Rose in the 1960s and 1970s (Rose and Smith, 2008) and then used to evaluate the mapping ability of remote sensing imageries acquired by different sensors (Smith *et al.*, 2006). In this section, this area was chosen for testing the effects of azimuth, altitude angle and image contrast change.



**Figure 3.8** Location of the Glasgow area of western Central Scotland to show the regions selected for detailed examination of DEM imagery (This image is taken from Google-Map, July 2010)

### **3.5.2 Evaluation of glacial landforms using ORI, DSM and DTM NEXTMap data**

i) An ORI image resembles an orthorectified, black and white aerial photograph, with a 1.25 metre pixel size (Li *et al.*, 2004). This is illustrated in Figure 3.9 from the Glen Turrett area of Glen Roy. From this image, features like roads and fences are clearly visible. Water bodies, dry river beds, cliffs with rock exposures and steep valley trenches are also distinct on this image. In contrast the proglacial lake shorelines on the right-hand side of Figure 3.9 are hardly visible. Overall, the ORI image is good for features with strong colour and texture contrast and therefore can be used to extract road and river channels, but features such as shorelines which are covered by the same vegetation are poorly represented.



**Figure 3.9** The ORI NEXTMap image of the Glen Turret area at the northern end of Glen Roy, northwestern Highlands, Scotland (from Chen and Rose, 2008a).

ii) The digital surface model (DSM) displays the first surface on the ground that the radar strikes. These include terrain features, buildings and vegetation such as forests and large trees (Li *et al.*, 2004). Figure 3.10 is a sample of a DSM image. This type of image has widely been adopted for much topographic mapping. Its main advantage is that it display the first surface on the ground that is struck by the radar wave – including terrain features and features such as buildings, power lines and large trees or forests.

iii) Figure 3.11 is the digital terrain model (DTM), which was created from the DSM, by digitally removing all the vegetation and man-made features. The DSM has a vertical accuracy of 1 metre root mean squared error (RMSE) and the DTM has a vertical accuracy specification of 2 metre RMSE. Spatial resolution for both images is 5 metres (Li *et al.*, 2004).



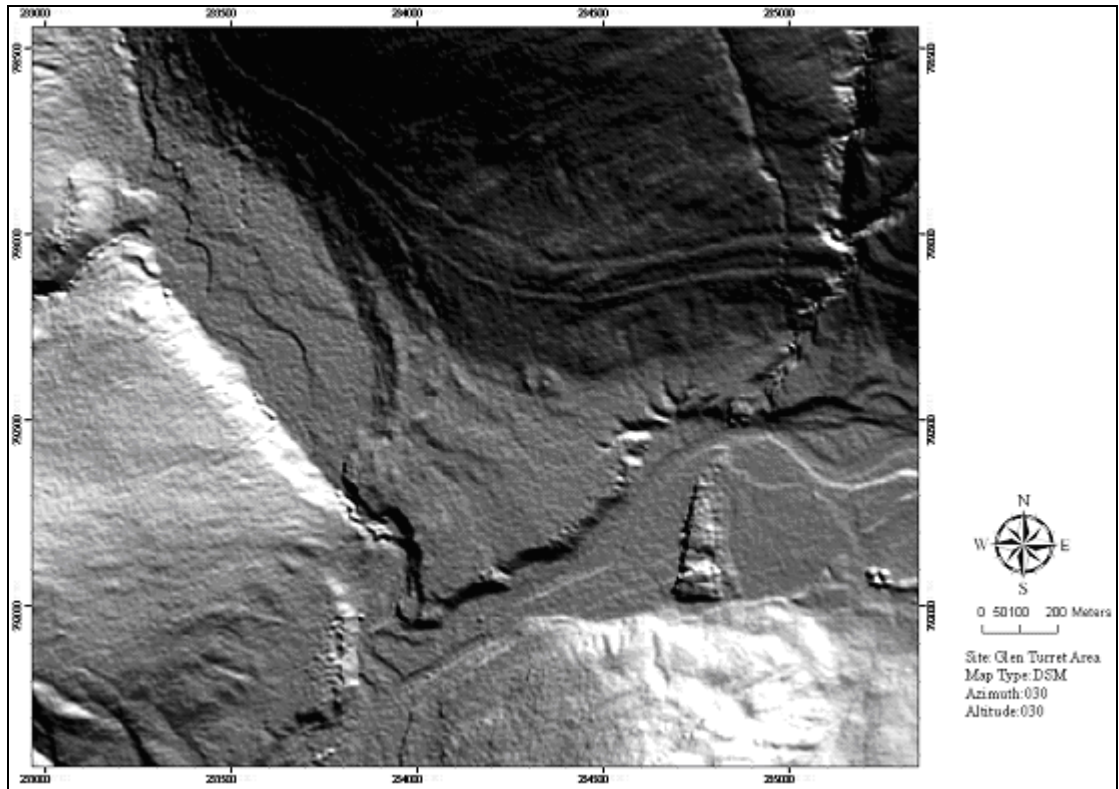


Figure 3.10 A DSM image of the Glen Turret area at the northern end of Glen Roy northwestern Highlands, Scotland (from Chen and Rose, 2008a).

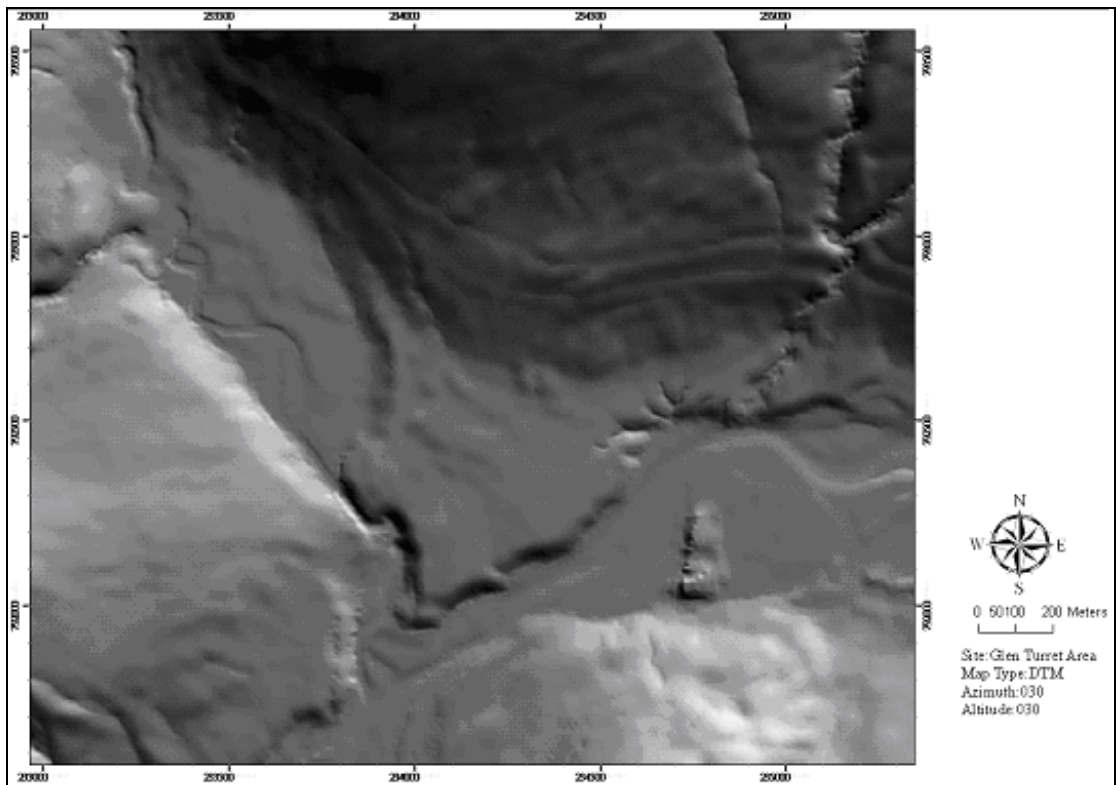


Figure 3.11 A DTM image of the Glen Turret area at the northern end of Glen Roy northwestern Highlands, Scotland (from Chen and Rose, 2008a).

iv) A DIFF image has been created to show the features that had been removed from the DSM to create the DTM (Figure 3.11). It is apparent by studying Figure 3.11 which shows many of the fine resolution features, and some landforms such as shorelines, moraine ridges, meltwater channels and river terrace edges are clearly visible. This means that the process of removal has not only removed the vegetation and man-made features, but also a number of landforms, or at least part of the landform image. Thus the DTM images must be used with caution when they are used to describe and interpret the geomorphology.

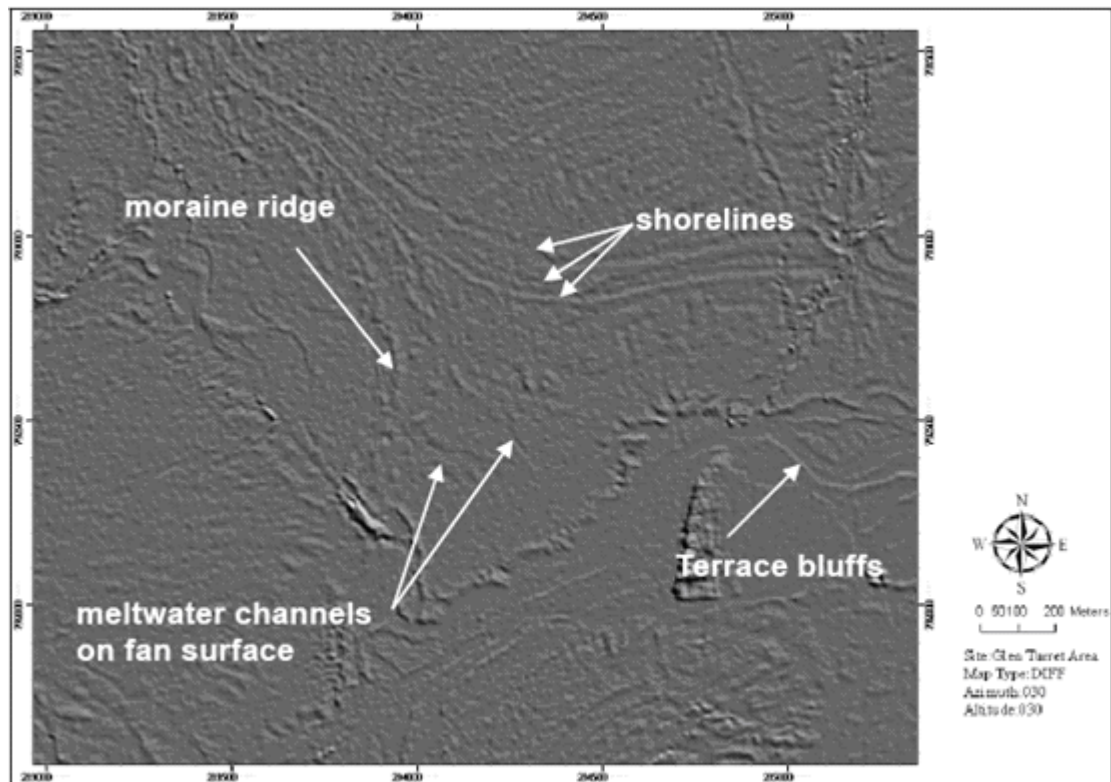


Figure 3.12 A DIFF image, created by elements of the image removed to turn the DSM into the DTM. This shows shorelines, moraine ridges, meltwater channels and river terrace bluffs indicating that on the DTM these features are represented by a degraded image. Based on the Glen Turret area at the northern end of Glen Roy northwestern Highlands, Scotland (from Chen and Rose, 2008a) and should be related to Figures 3.9, 3.10 and 3.11.

A comparison of the DSM, DTM and ORI images demonstrates that ORI images have the ability to represent artificial features such as fences very effectively, whereas geomorphological features such as moraine ridges and shorelines and river terraces are clearly identified on the DSM image. Although the ORI image has the finest spatial resolution of the three image types, features with just slight elevation and small slope variation and are covered by vegetation, are hard to identify. Thus, the ORI image looks more “flat” than the other two images and landforms such as shorelines, moraine ridges and river terraces are relatively indistinct.

From the above comparison, it can be seen that the DSM data are more effective in representing glacial and fluvial landforms than the other two data types. The DSM data will therefore be used for future analysis.

### **3.5.3 Experiments designed to examine the effectiveness of DSM data for the representation of landforms**

#### **i) Altitude testing (Landform Signal Strength testing)**

In order to assess the effect of varying solar elevations on the representation of landform on DEM data, relief shading imageries with different solar elevations were created. All the relief shading plots in this experiment have fixed the azimuth angle at  $360^\circ$  and set the imagery contrast as +60% . This test is mainly applied to drumlin landforms and previous studies have suggested that low solar elevation is more suitable for the representation of linear features (Smith and Wise, 2007). The altitude testing range in this research is from  $0^\circ$  to  $45^\circ$  with changes at a  $5^\circ$  interval.

#### **ii) Azimuth testing (Azimuth Biasing Effect testing)**

There are two tests within this experiment. The first is to assess the effect of changing the azimuth angle. In this test images are given an azimuth that varies in 40° steps. The altitude angle is fixed at 25° and set the imagery contrast as +60% . The testing range varies from 40° to 360°. A relative comparison was then performed between the imageries.

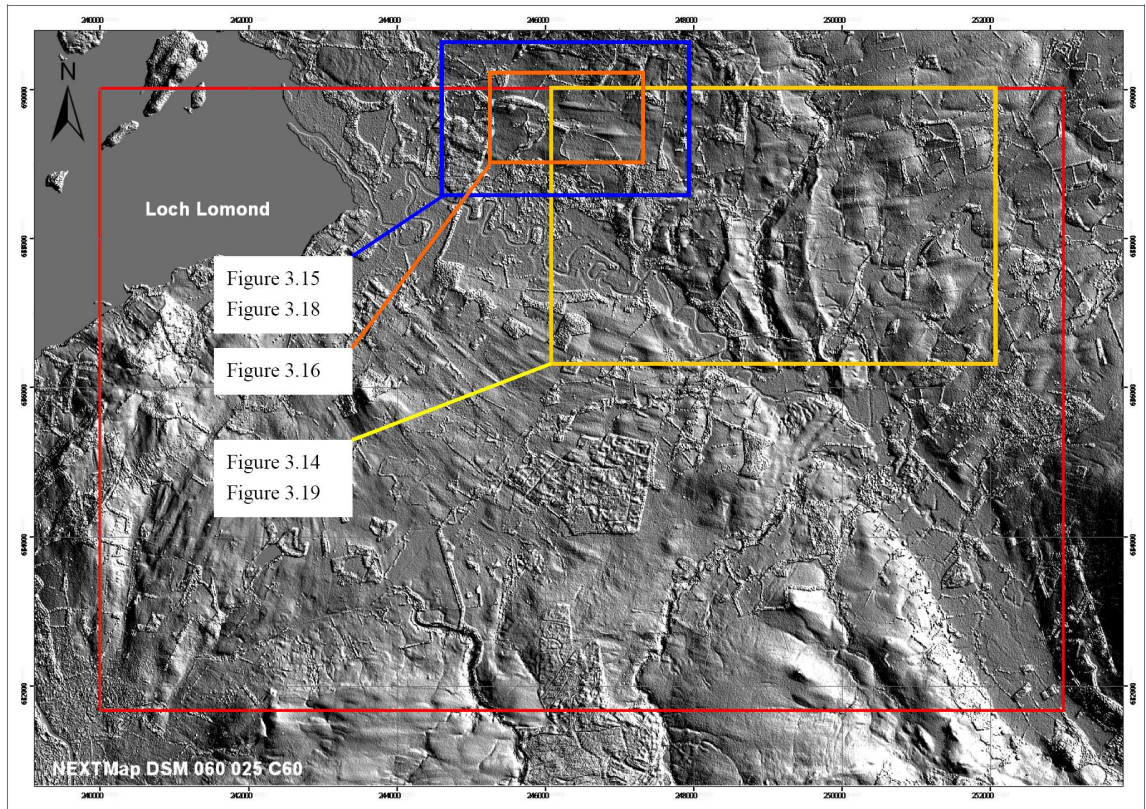
The second test is to evaluate the effect of the size of the steps between changes in azimuth for landform mapping. In this test, the illumination azimuth was changed at 10°, 20°, 30° and 40° intervals. The altitude angle and imagery contrast setting were same as the first test. Illumination directions were 330°, 340°, 350°, 360°, 10°, 20°, 30°, 40° and 50°.

### **iii) Contrast**

In order to assess the effect of varying contrast on plots of landform representation, compilations of DEM data plots of varying contrast setting were compared. A constant altitude and azimuth angle was maintained and was set as 360° and 25° respectively. Although the range in GIS environment can be changed from +100% to -100% (+100% means all black; -100% means all white) the negative value will make the imagery lose its diversity and decrease the ability of the image to represent the landforms. In this experiment, tests were carried out from 10% to 90% with changes at 10% intervals.

### **3.5.4 Analysis of experimental results**

In this section the relief shading images in the northern Glasgow area of western Central Scotland (Figure 3.8 and 3.13) are used to evaluate how the main factors that determine the ability of plots to represent landforms.



**Figure 3.13** Location of samples in the Glasgow area of western Central Scotland, UK.

### **i) Altitude testing**

Figure 3.14 demonstrates the altitude effect on landform representation. This figure shows that drumlins become less distinct as the angle of the elevation of the light-source increases. A suitable angle in which the light-source effectively illuminates the drumlins is between  $5^{\circ}$  and  $25^{\circ}$ . Although drumlins can be most clearly seen with an altitude angle of  $5^{\circ}$  this is not recommended for the following reasons: 1) Although the low elevation light-source does enhance some landforms which have high relief difference, it will also make the low relief landforms become less distinct. 2) The effect of low elevation light-source can be simulated by adjusting the contrast ratio. From the author's experience it is recommended that the  $25^{\circ}$  altitude angle is most effective as the initial setting, particularly on a relatively flat area. However, it should be noted that this setting can be changed later if there are different mapping purposes.

### **ii) Azimuth changing effects**

Figure 3.15 is used to assess the effect of changes in the azimuth angle. From this figure, landforms (drumlins) are well represented with azimuth  $40^\circ$ ,  $160^\circ$ ,  $200^\circ$  and  $360^\circ$ , but hard to distinguished with azimuths of  $80^\circ$  and  $280^\circ$ . This is because of the main orientation of drumlins is west - east. The azimuth angle which is orthogonal with main orientation of the landform intersects the largest surface area and thus reflects most light. In contrast, when the light source is parallel to the landforms the amount of light is minimal and the landforms are less obvious. This is called the “azimuth illumination bias”. Here, the author would like to propose a new concept and interpretation to minimise the problems caused by illumination bias.

Figure 3.16 illustrates the effects of azimuth illumination bias on the representation of drumlin landforms. It is clear that Figures 3.16.2 and 3.16.4 provide most of the landform information, whereas Figures 3.16.1 and 3.16.3 are ineffective. Normally, images Figures 3.16.1 and 3.16.3 would be abandoned in the process of using the relief shading imagery for landform mapping. However, if we look closer we can see that Figures 3.5.1 and 3.16.3 show the stoss part of the drumlins more successfully as this part is orthogonal to the light source. Figure 3.17 illustrates the illumination effect on cirque landforms. In contrast to the near linear shape of drumlins, where the main boundaries can be represented with an orthogonal light source, the rounded shape of the cirque means that no single illumination angle can show most of the boundaries. Consequently, this kind of landform needs a different approach and the use of a wide range of images with a wide range of azimuthal directions. Since there are no real “points” or “linearities” in the real world landforms should be treated as “polygons”. Hence, the true orthogonal angle of each landform should vary around the boundary. Each individual image provides information which the other illumination angles cannot represent. Thus although the “illumination bias” causes some problems for landform boundary delimitation it also provides some useful information. Therefore it is

recommended that no image should be abandoned. The only way to acquire sufficient information is to systematically organize the images with different azimuthal directions and put all of the images together to generate Dynamic Illumination Variability Imagery which is renamed as “the rotating map” in this research.

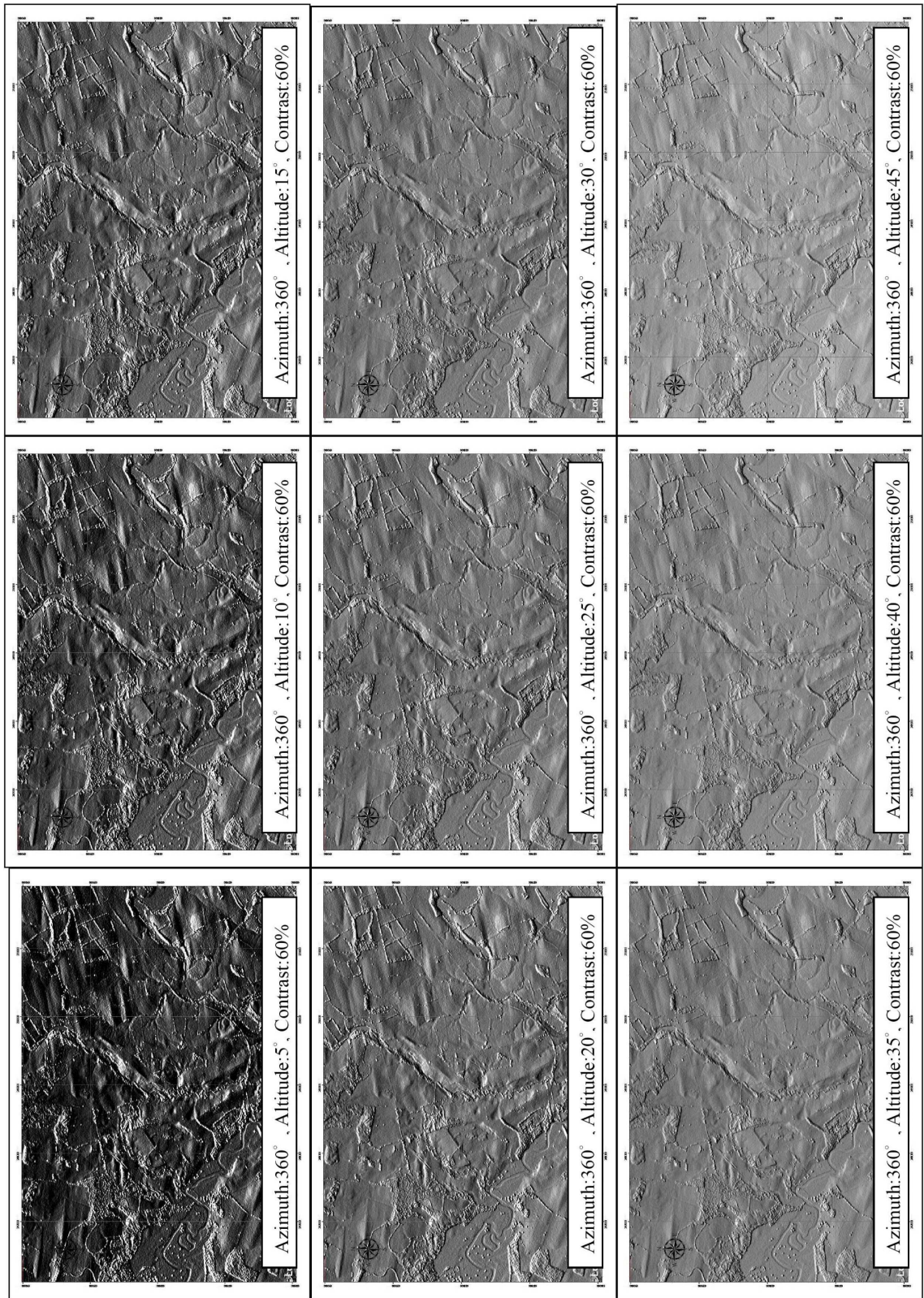


Figure 3.14 Comparison of altitude angle change effects on topography.



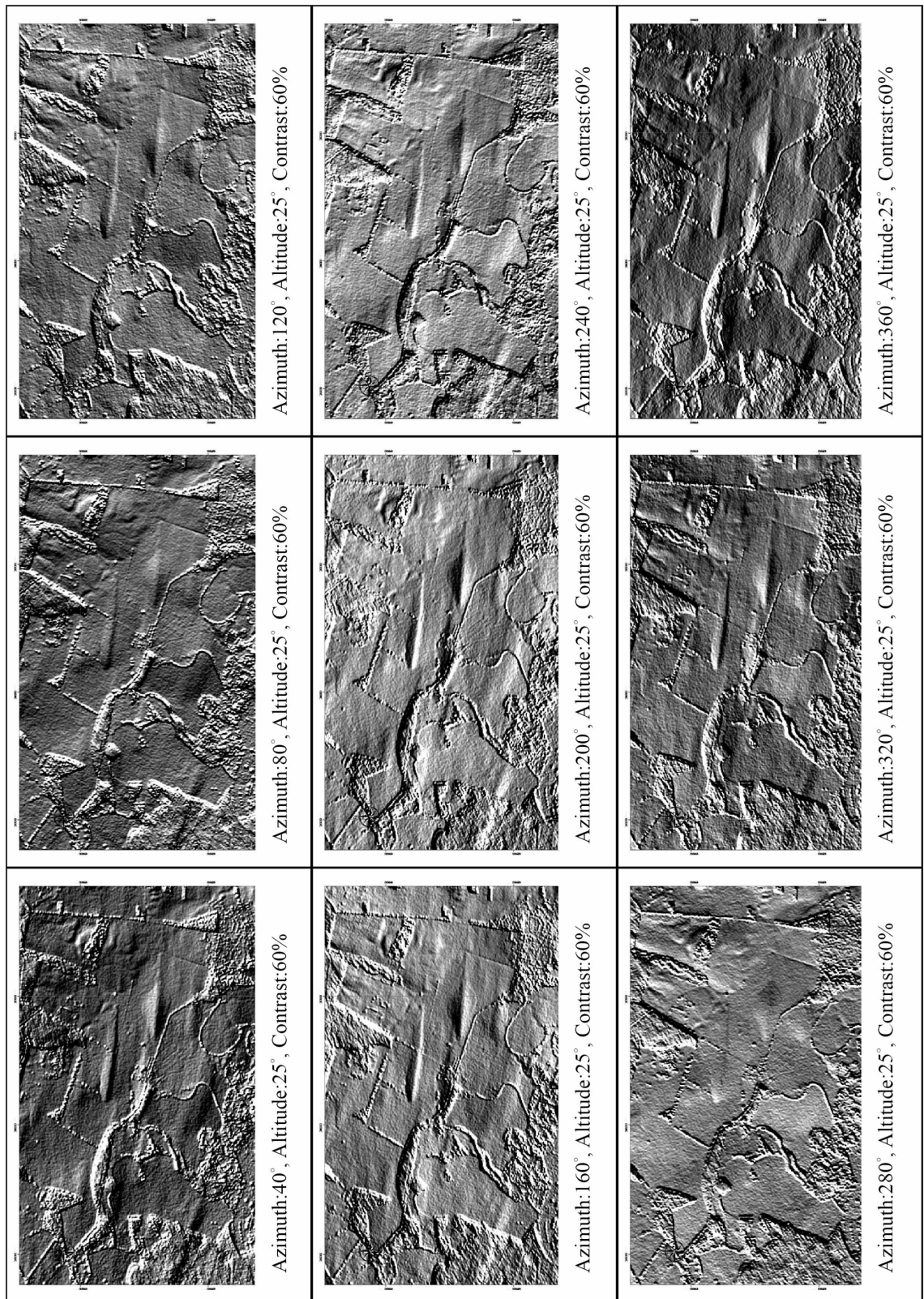
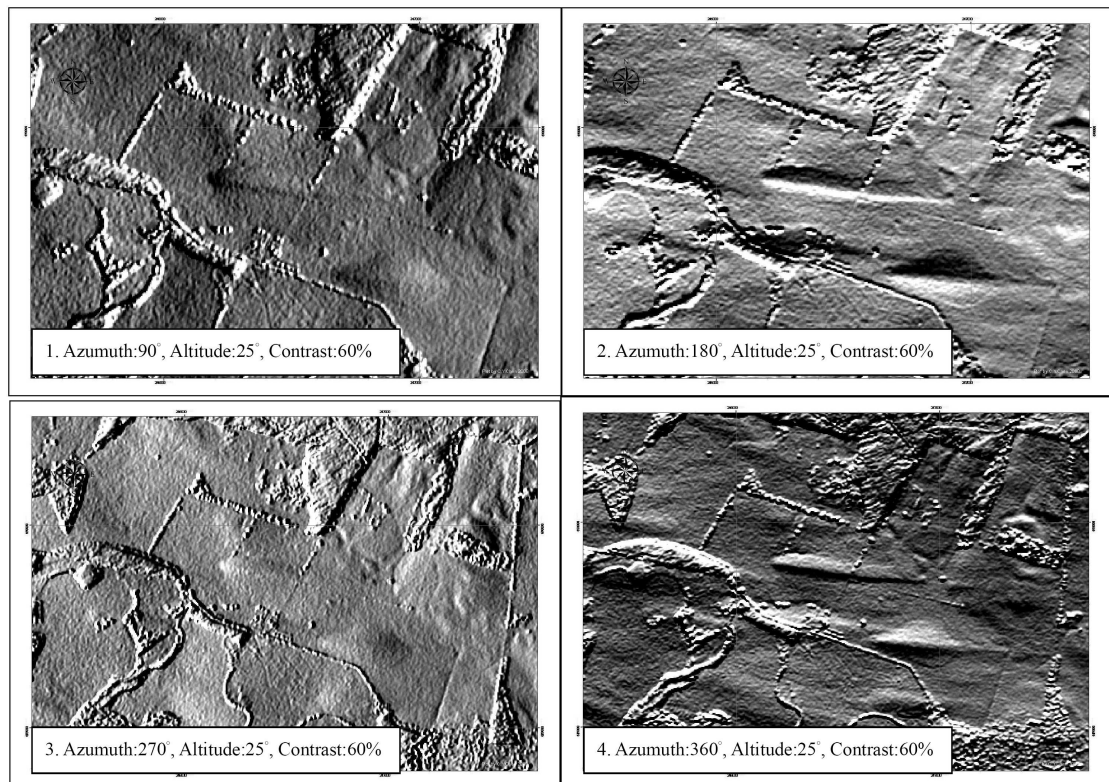
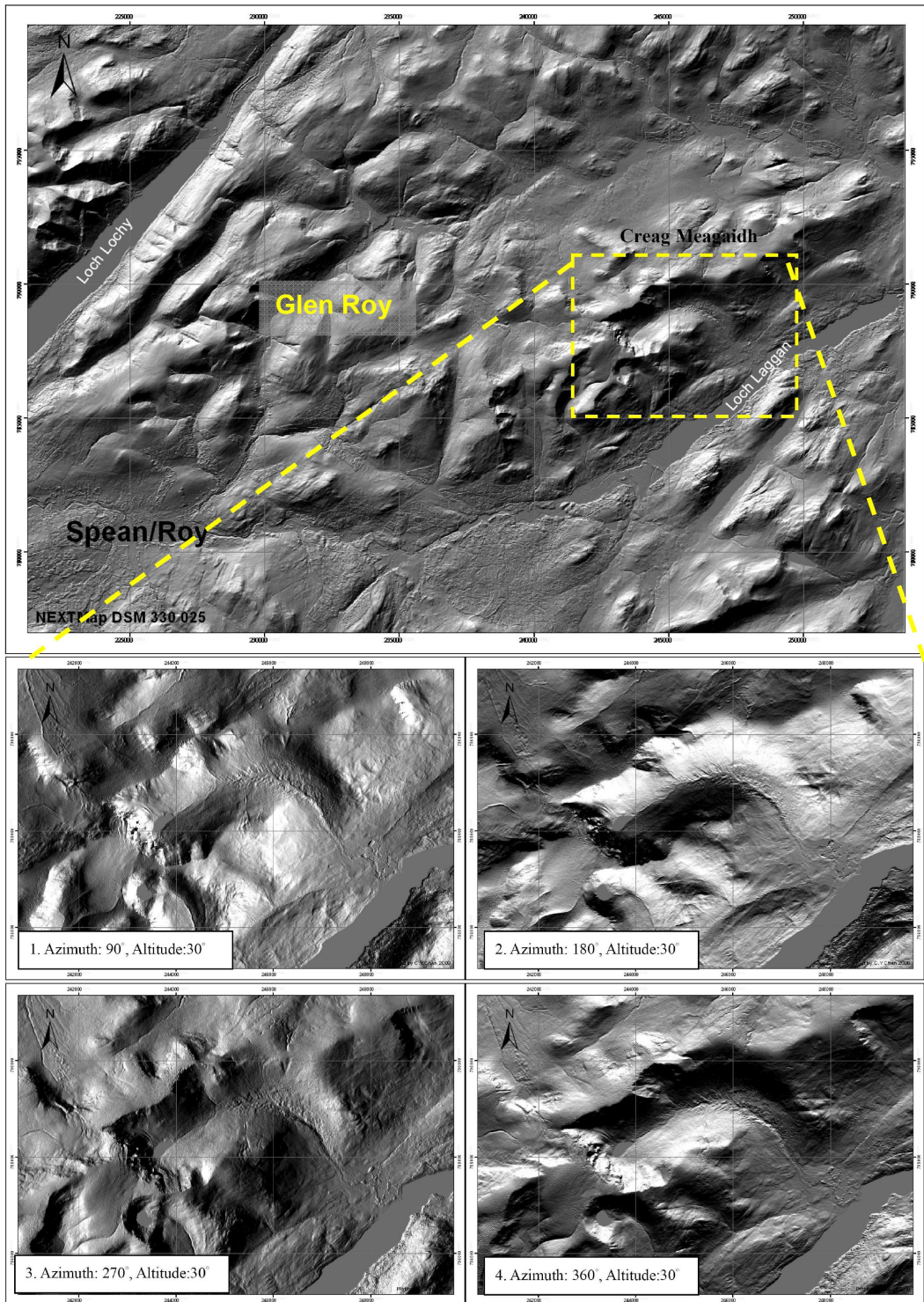


Figure 3.15 Comparison of azimuth angle change effects on topography.

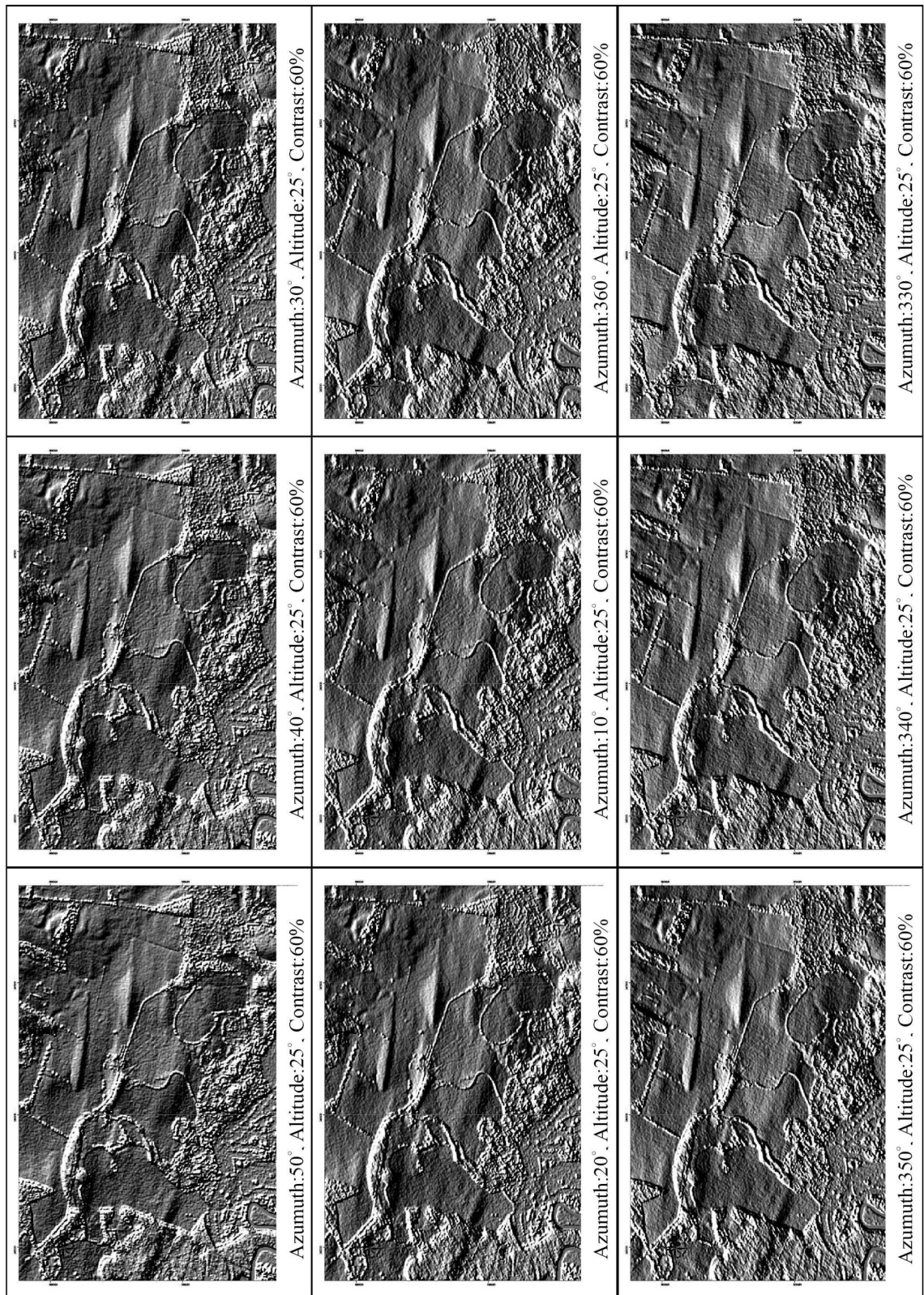


**Figure 3.16 Comparison of the illumination effect on drumlin**

It is necessary to establish the concept of an acceptable tolerance range for the azimuth angle that represents a single landform, especially when we are concerned about the use of single or limited images to represent most of the ground truth. Figure 3.18 has been constructed to answer this question. This figure shows three groups arranged horizontally with  $10^\circ$  changes in azimuthal angle. The images in this figure show little variation, one from another. This is because each of the images shown is within the acceptable tolerance range for the landform type, depending upon the size, shape and environment surrounding of the image. If, in this case, we treat the image with azimuth  $10^\circ$  as “truth”, the acceptable tolerance range is azimuth  $10^\circ \pm 30^\circ$ . It is interesting to note that with imageries with azimuth  $330^\circ$  and  $50^\circ$ , and especially that the azimuth  $330^\circ$ , some elements of the boundary features are lost in some of the low relief drumlins.



**Figure 3.17 Comparison of the illumination effect on cirque (Creag Meagaidh is located at northwestern Highlands of Scotland. Close to the Glen Roy valley).**



**Figure 3.18 Comparison of images in response to changes in the azimuthal angles of illumination. The values range from 10° at ±40° intervals.**

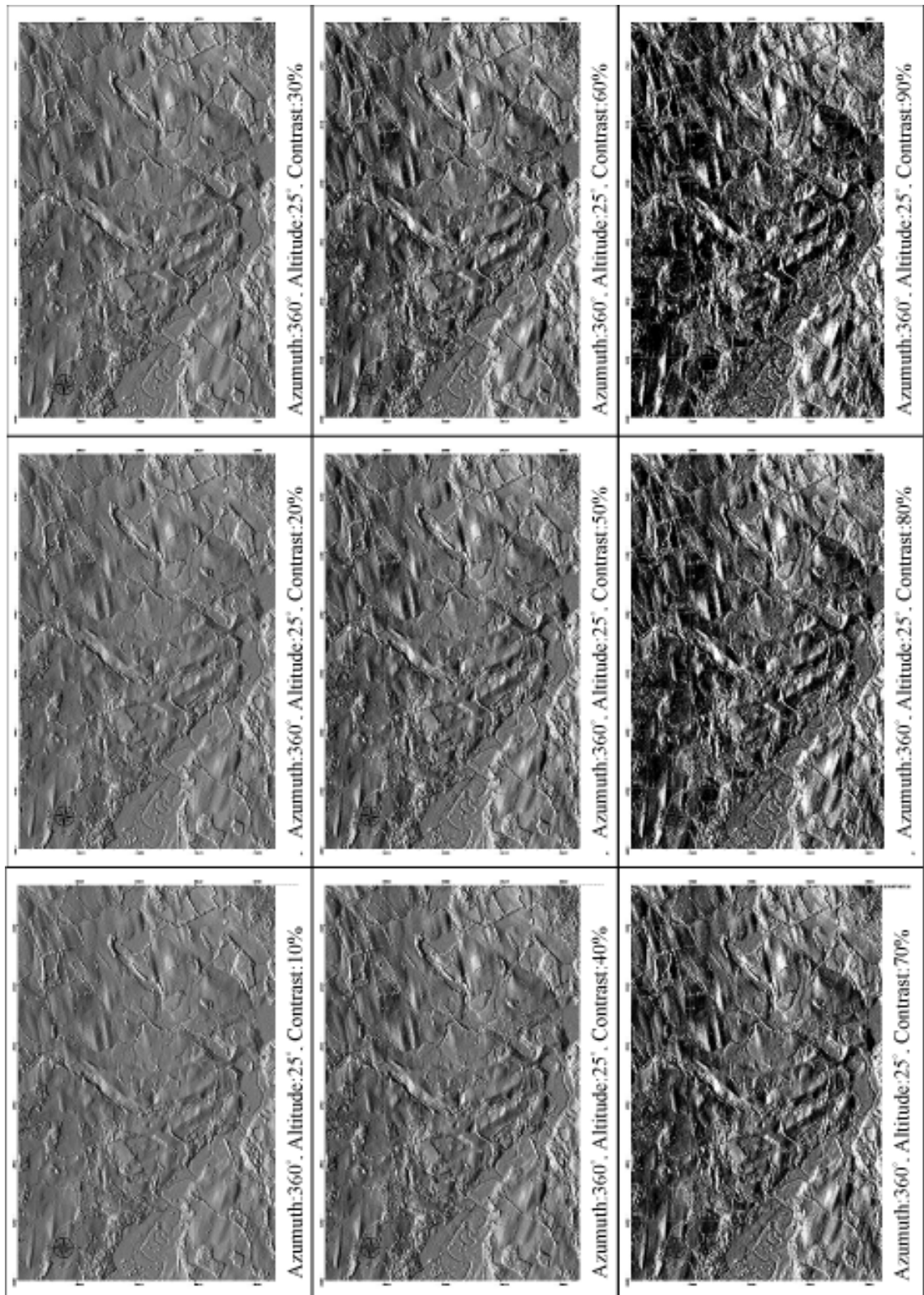


Figure 3.19 Comparison of image contrast values upon the representation of drumlin topography

### **iii) Effects of changing image contrast**

The contrast value is mainly applied to enhance the ability to detect relevant information from images. In Figure 3.19 drumlins become more and more distinct as the contrast is increased. However, although this can highlight some landforms, the increase in contrast may also obscure part of the detail, especially for those landforms which have low relief. In this experiment, the main landform within the test area is well developed drumlins. It is the opinion of the author that suitable contrast rates are 50%, 60% and 70%, but 60% is selected in this case.

### **3.6 Conclusions**

As the advent of cheap and high resolution DEM data is rapidly increasing and approaching, new methods are needed to make best use of this resource. The most important conclusion to draw from the above results is that although a variety of methods can be used to visualize map landforms from DEM (NEXTMap) data, relief-shading imagery, especially in conjunction with the rotating map is the most economic and powerful method to achieve the demands of most kinds of geomorphological mapping.

The rotating map, with constantly changing illumination azimuths, is the only method that can not only provide a full, visual, depiction of landform information, but also information that can be used to test the quality of existing mapping.

A comparison of the DSM, DTM and ORI images of NEXTMap data demonstrates that ORI images have the ability to represent artificial features such as fences very effectively, whereas geomorphological features such as moraine ridges and shorelines and river terraces are clearly identified on the DSM data. Although the ORI data have

the finest spatial resolution among three image types, features with just slight elevation and small slope variation that are covered by vegetation are hard to identify. Thus, the ORI data look “flatter” than the other two data-types and landforms such as shorelines, moraine ridges and river terraces are relatively indistinct. The DIFF image shows many of the fine resolution features and some landforms such as shorelines, moraine ridges, meltwater channels and river terrace edges are clearly visible. This means that the process of generating the DTM data has not only removed the vegetation and man-made features from the DSM image, but also removes parts of the Earth surface which are not vegetation or man-made features. Thus the DTM data must be viewed with caution when used to describe and interpret the Earth’s surface. DSM data are recommended for use in glacial and fluvial landform research.

## **4. Glacial landform mapping using NEXTMap: scoping exercises**

---

### **4.1 Introduction**

When climate change issues appear as newspaper headline titles more and more often, the need to know how the Earth's climate system works becomes more than an academic exercise. It is impossible to understand exactly how this system works and its range of climate styles, solely from modern environments or limited historical archives. Systematic reconstruction and analysis of the palaeoenvironment is an additional way of investigating this problem. Among these reconstructions, an understanding of the extent, flow geometry and topography of former ice sheets is crucial because of the increasing perception of the importance of the cryosphere in the Earth–ocean–atmosphere system and as a consequence of, and control of climate change (Shin and Barron, 1989), sea level change (Denton and Hughes, 1981; Boulton *et al.*, 1985, 1991; Lambeck, 1993a, 1993b, 1995), glacial-isostasy (Lambeck, 1991, 1993a, 1993b, 1995; Shennan *et al.*, 2000, 2002; Smith *et al.*, 2006) and neotectonics (Sissons, 1972; Sissons and Cornish, 1982; Ringrose, 1989b; Firth, 1992; Firth and Stewart, 2000).

Basically, methods for reconstructing former ice sheets can be divided into empirically-based models and numerically-based models. Empirically-based models use evidence collected from field survey or remote sensing imagery to build a sequential pattern of ice dynamics (Ballantyne and McCarroll, 1995; Ballantyne and Hallam, 2001; Stone and Ballantyne, 2006). Numerically- based models are mainly based on the factors that control mass balance (temperature, precipitation amount and spatial gradients) and other influential factors such as sea level and typical geothermal heat flux (Hubbard, 1999; Golledge, 2006, 2007, Golledge *et al.*, 2008). However, in both methods, detailed ground truthing in the form of glacial landform evidence, often in the form of maps, is essential for model building and testing.



Clark *et al.* (2004) collected information from around 2000 published papers, reports and maps that relate to the Last (Late Devensian) British Ice Sheet. Geomorphological evidence of glaciation in Britain was entered into the BRITICE GIS, from which the 'Glacial Map of Britain' has been produced. This database contains most glacial geomorphological evidence for the UK although much published information is substantiated. Data collected in this project were not tested or assessed against other information or by other methods. Therefore it is crucial to apply higher resolution imagery with efficient mapping methods and robust and systematic assessment procedures, to test mapped results.

Mapping results obtained from DEMs are a reflection of the operator's mapping ability and experience, physical characteristics of the imagery and the visualization method applied. The effect of operator's mapping ability and experience has been studied and demonstrated to be highly variable between different observers (Smith and Wise, 2007). Although it is hard to remove this variability completely it can be mitigated by well defined and meticulous mapping procedures.

The aim of this chapter is to develop a mapping procedure for the use of NEXTMap and use it to examine and evaluate glacial landform mapping capabilities through a series of experiments in selected areas. This chapter will start by defining the mapping procedure followed by a series of experiments using NEXTMap to examine and evaluate the topography of moraine ridges, hummocky moraines, kame and kettle assemblages and meltwater channel mapping. The sample region is the area of northern Glasgow in west central Scotland, mapped originally by Rose in the 1960s and 1970s (Rose and Smith, 2008). A new method by which landform shape can be optimized on single images has been developed and is discussed and illustrated in the final part of this chapter.

## **4.2 Mapping Procedures**

A well defined and meticulous mapping procedure will mitigate errors due to operator bias. This mapping method is based on relief shading generated from NEXTMap and applies the principle of a rotating light source, thus testing the full range of visual perspectives of any landform. The main software used for this process is ESRI Arc GIS 9.2 with the Spatial Analyst extension. Adobe-Imagine Ready CS2 is also used to generate the rotating map (see Appendix 1). The process of carrying out this mapping procedure is described in the following sequence:

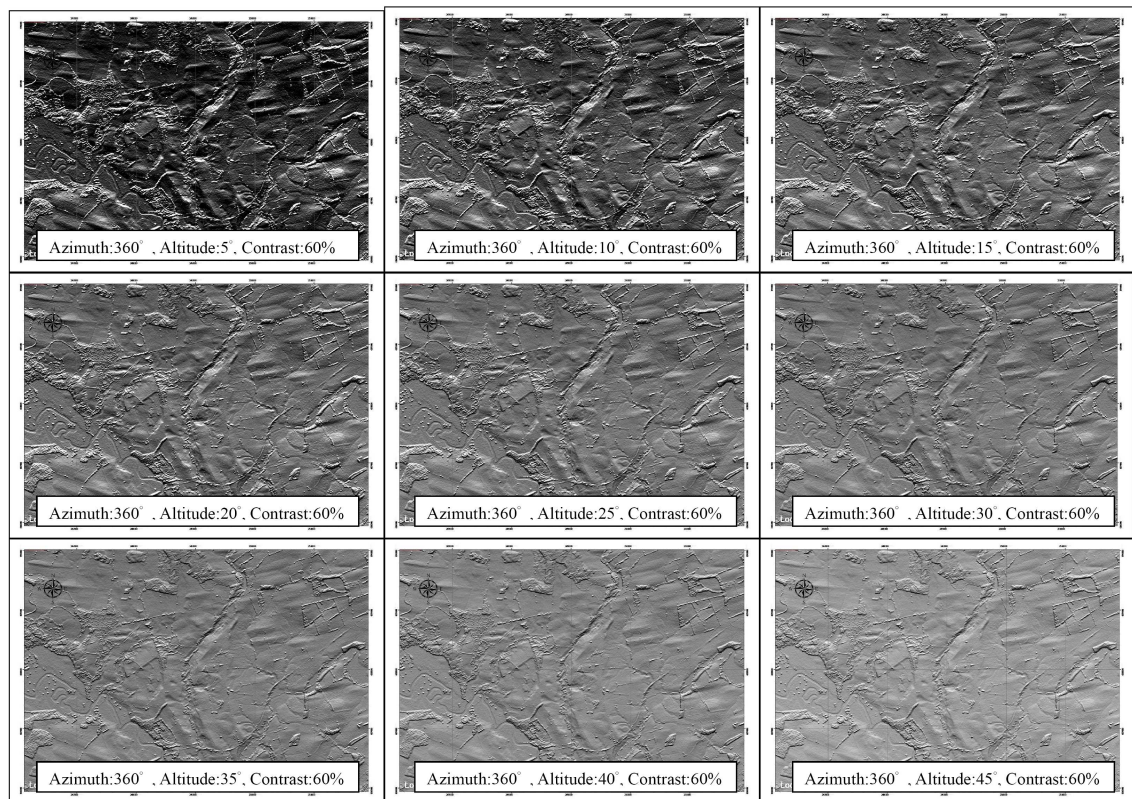
### **Step 1: Choosing the angle of altitude of the light source.**

The procedure starts by determining the angle of altitude of the light source. This process begins with the user generating imageries using a light source with different angles of elevation, but with a constant azimuthal direction. The azimuth was set as  $360^\circ/0^\circ$  and the angle of elevation was changed at  $5^\circ$  intervals (Figure 4.1). Based on this experiment it is recommended that the angle of elevation of the light source should be  $25^\circ$  from the horizontal, for an area that is relatively flat, although it should be noted that this setting can be changed for different relief and different mapping purposes.

### **Step 2: Generating relief shading with fixed angle of light source and variable angle of azimuth.**

After the angle of the light source has been determined, the next step is to generate relief shaded on NEXTMap DEM plots. In this step, the angle of the light source is fixed ( $25^\circ$  in this case, but an alternative can be used if that is more suitable), but the direction from which the light source is derived (azimuth angle) is changed. In this

experiment we use steps of  $10^\circ$ , from  $10^\circ$  to  $360^\circ$ , so that each image has a  $10^\circ$  difference in azimuth angle setting.



**Figure 4.1 Relief-shaded plots with  $5^\circ$  changes of angle of elevation of the light source used for the NEXTMap plot. The azimuth angle is fixed at  $360^\circ/0^\circ$ . The contrast ratio is set at 60%. An image with a light source at a  $25^\circ$  altitude is recommended as a start point for NEXTMap studies. The area illustrated in the above figures is in the region around Drymen southeast of Loch Lomond, and described in Smith *et al.* (2006), Rose and Smith (2008).**

Although a small difference in azimuth angle will give a finer resolution of the differences caused by the illumination, this also increase the number of images and hence the size of the document. Based on the author's experience, the size of the document should not exceed 350 MB, otherwise there are problems in generating the rotating map.

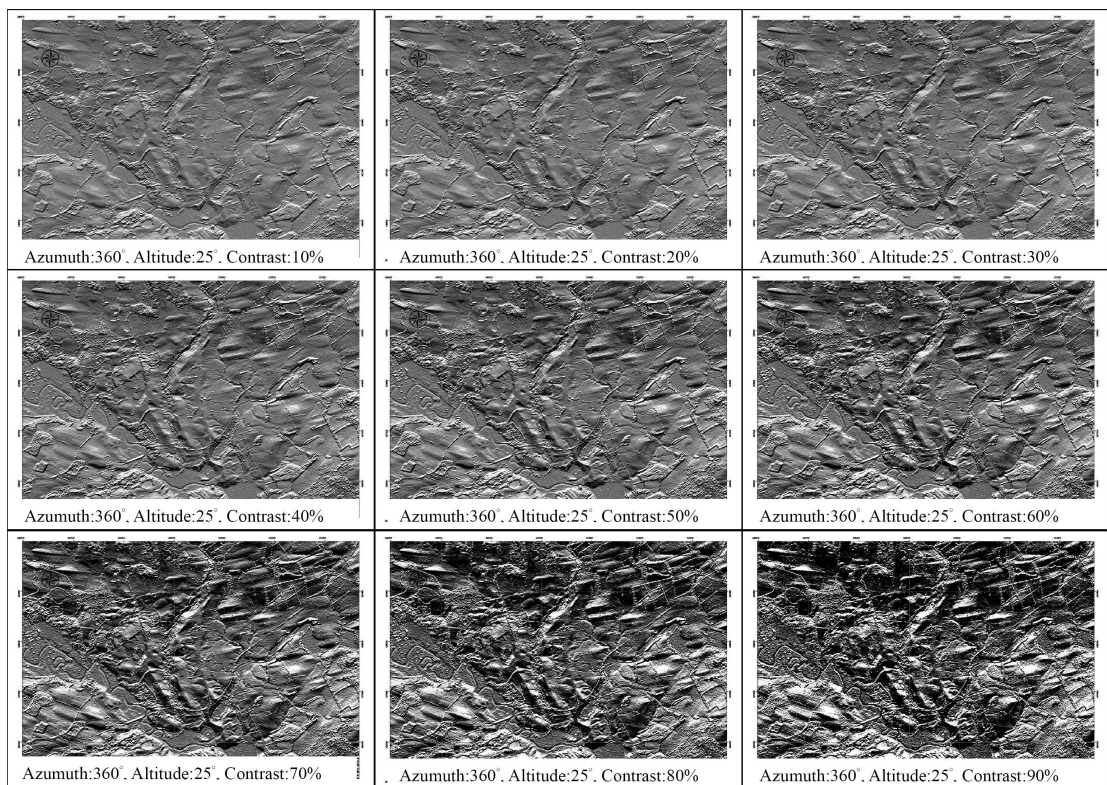
### **Step 3: Landform mapping.**

Before starting the mapping, the operator needs to chose one of the azimuthally defined images that gives the best representation of the geomorphology that is being studied. Using this image, mapping is carried out by drawing the landform boundaries in a GIS

environment. Generally speaking, the optimal imagery for linear landforms (such as drumlins) is when the trend of the target landform is orthogonal to the light source (Smith, 2003). It is not necessary that the base map should be the optimal imagery as all the mapped results can be tested and corrected at a later occasion, by the use of the rotating map.

**Step 4: Determining the effects of contrast.**

As mentioned in Step 1, the variations in contrast can be used to highlight boundaries of high relief landforms. This is Step 4 and the effects of contrast variations are illustrated in Figure 4.2. From the author’s experience, contrast at the 60% level is most effective for the identification of low relief landforms such as moraine and drumlins.



**Figure 4.2 Comparison of changing levels of contrast on landforms that are part of a drumlin field. The azimuth angle is fixed at 360°/ 0°. The contrast ratio is set at 60% because it enhances the visibility of low relief landforms. The angle of the light source is at a 25°. The area illustrated in the above figures is in the region around Drymen southeast of Loch Lomond, and described in Rose, (1981), Smith *et al.* (2006), Rose and Smith (2008).**

**Step 5: Creating the rotating map.**

In order to generate the rotating map, the DEM plots must have constant altitude, constant contrast and equal spacing in the intervals in which the azimuth angle of the light source changes from 0° to 360°. The image will be constant and hence overlap as the changes take place from 0° to 360° or vice versa. This process will be carried out with image processing software capable of creating an animation file. In this research, all rotating maps were created by using Adobe- Imagine Ready. Azimuth resolution is 10°, delay time for the change of each image (azimuthal direction of light source) is set at 1 second (see Appendix 1). It is important to stress that all the properties of the images need to be constant except for the direction of the light source. If the images do not overlap, jumping will take place when rotating.

**Step 6: Testing the rotating map.**

As discussed above, although the differences in the images caused by the changes in the direction cannot be mapped directly on screen, the rotating map is the only method which can readily highlight landforms from all directions; orthogonal, intermediate and parallel. Smith (2003) used this method to demonstrate the illumination bias problem. Here, this technique will be treated as a mapping testing platform. Two rotating maps will be needed to test mapping results as outlined in Step 3: a set with changes in direction of light source and a set with changes in contrast.

**Step 7: Correction and analysis.**

From the testing procedure landform boundaries can be identified with confidence using the changes in contrast and direction of illumination. As mentioned above, there are no technical methods that can be used to map directly onto the rotating map. Therefore, the user can only record geomorphological properties using the most effective angle of

illumination and contrast. Corrections and remapping can be done in a GIS environment (Step 3). This process can continue until satisfactory results are obtained.

### 4.3 Glacial landform mapping using rotating NEXTMap plots and comparison with results derived from field survey

#### 4.3.1 Introduction

The new mapping concepts and procedures experimented on and developed in this chapter were used to test the detection and delimitation of glacial landforms in the region to the southeast of Loch Lomond in western central Scotland (Figure 4.3).

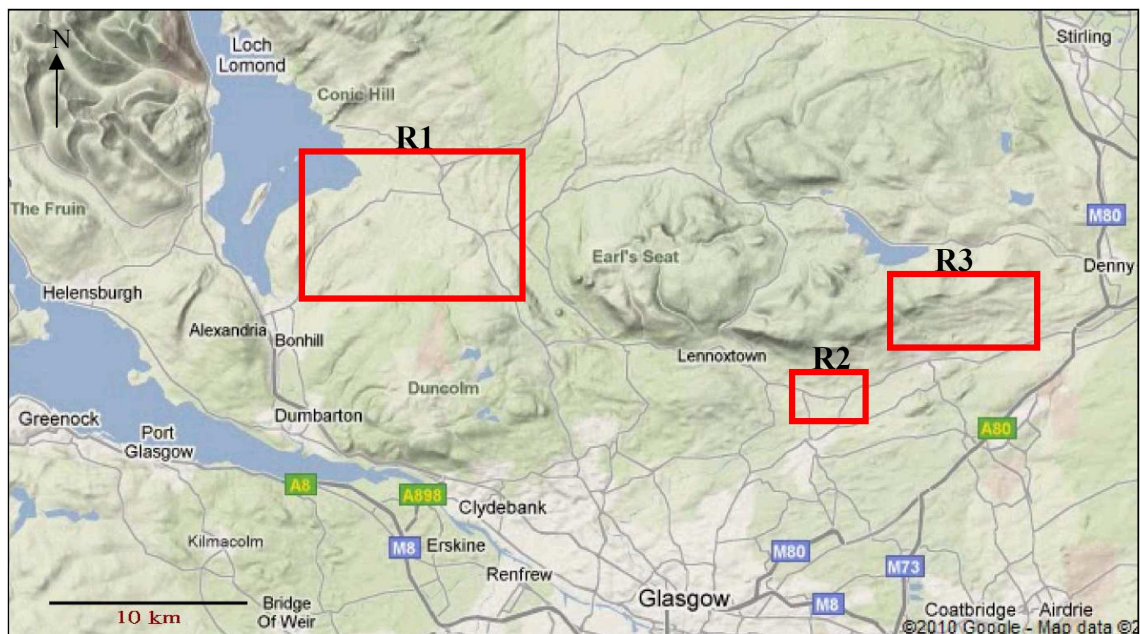


Figure 4.3 The Glasgow area of western central Scotland to show the regions selected for detailed examination of DEM imagery (R1 for drumlins and hummocky moraine, R2 for kames and kettle holes, R3 for meltwater channels. (Background image is taken from Google-Map, July/2010).

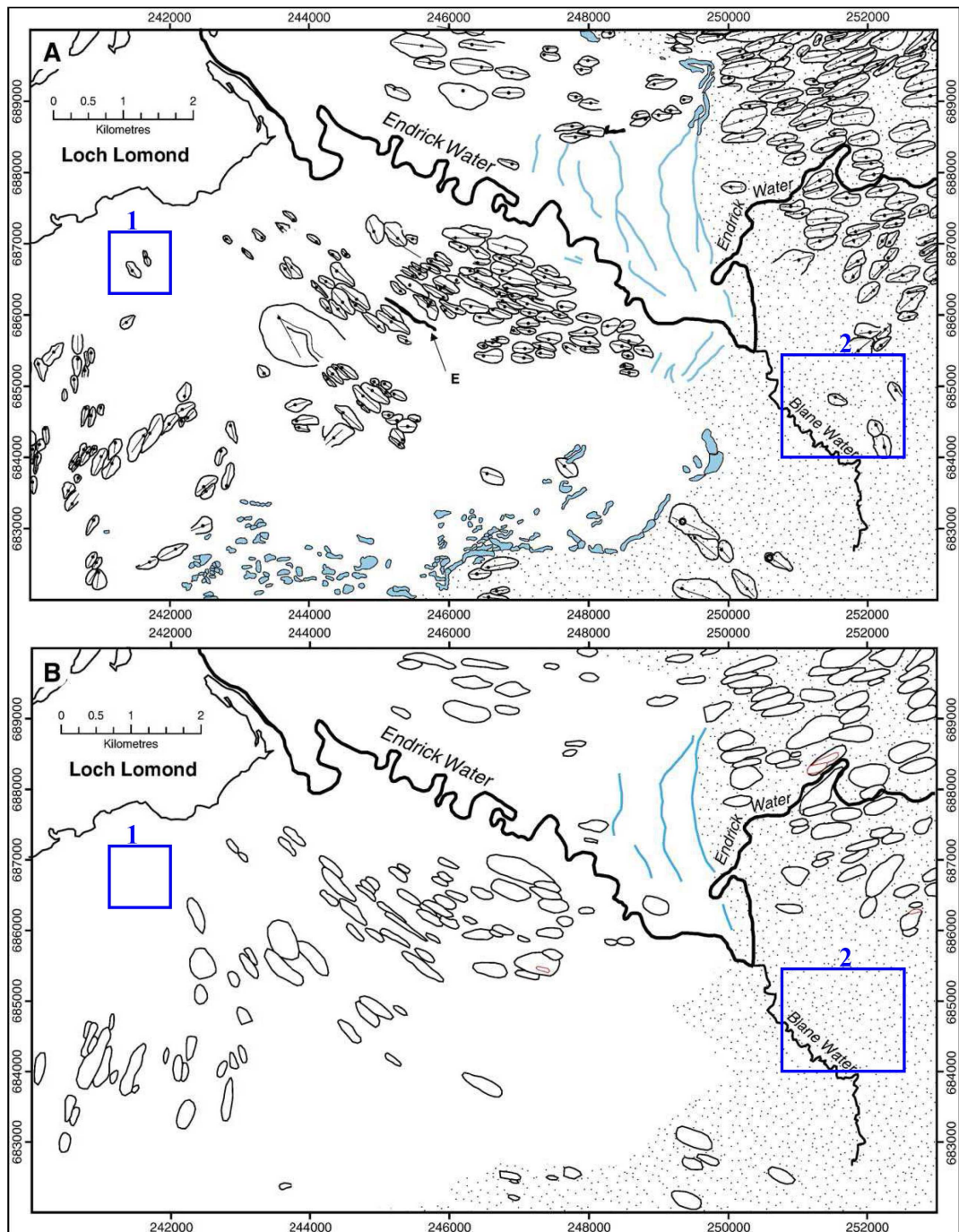
This mapping was undertaken by Jim Rose in the 1960s and early 1970s as part of his PhD research which used detailed field survey, examining landforms from different perspective (Rose, 1981). The shape of the landforms was recorded on Ordnance Survey

(OS) 1:10,560 scale topographic maps. The area contains abundant glacial landforms (crag and tail hills, drumlins, irregular till hillocks and hummocky moraine) and glaciofluvial landforms (meltwater channels, kames, kettle holes, outwash terraces and kame terraces) and is ideal for testing the mapping of glacial landforms. Smith *et al.* (2006), Rose and Smith (2008) and Clark *et al.* (2009) remapped and re-evaluated glacial landforms in this area based on the relief-shading-images generated by NEXTMap. Their work provided a good sample by which it is possible to compare the outcomes of mapping by traditional field survey methods, modern DEM mapping methods and the new mapping method from rotating maps proposed in this thesis. Quantitative inter-method comparisons have been carried out in terms of numbers, shape and spatial distribution of mapped landforms. In order to test the effectiveness of the rotating map procedure using NEXTMap imagery, selected glacial landforms (including drumlins, hummocky moraines, meltwater channels, kames and kettle holes) published in Rose and Smith (2008) were digitized and compared with the results of the rotating map procedure.

#### **4.3.2 Glacial landform mapping using rotating NEXTMap images and its comparison with results derived from field survey: drumlins**

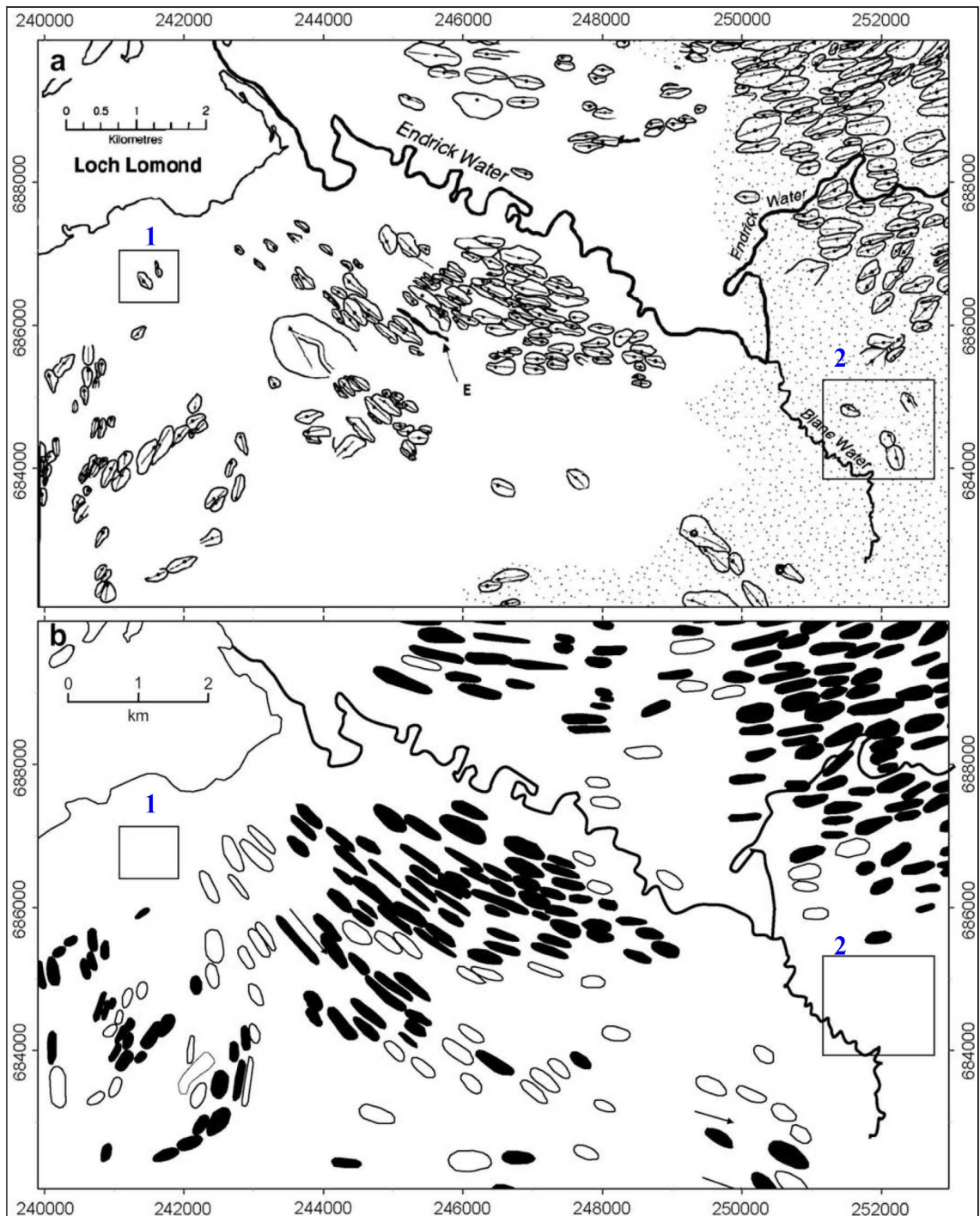
Drumlins from the southeastern part of the Loch Lomond basin (Smith *et al.*, 2006) have been used to test the rotating NEXTMap method (Figure 4.4). The field mapping in Smith *et al.* (2006) was initially mapped by Rose in 1965 to 1970 and is the most detailed mapping of this area. It is treated as “ground truth” in Smith *et al.* (2006). Clark *et al.* (2009) also take this map for their comparison of mapping methods. The digital imagery in Smith *et al.* (2006) was based on images derived from relief-shading from NEXTMap. However no mention was made of the precise illumination settings and numbers of images they used for mapping. Their paper states that 189 drumlins can be delimited from the NEXTMap and this number is much higher than the number of

drumlins identified by other remote imaging methods such as Shuttle Radar Topography Mission C-band, Landmap, OS Panorama, OS Profile and Landsat Thematic Mapper.

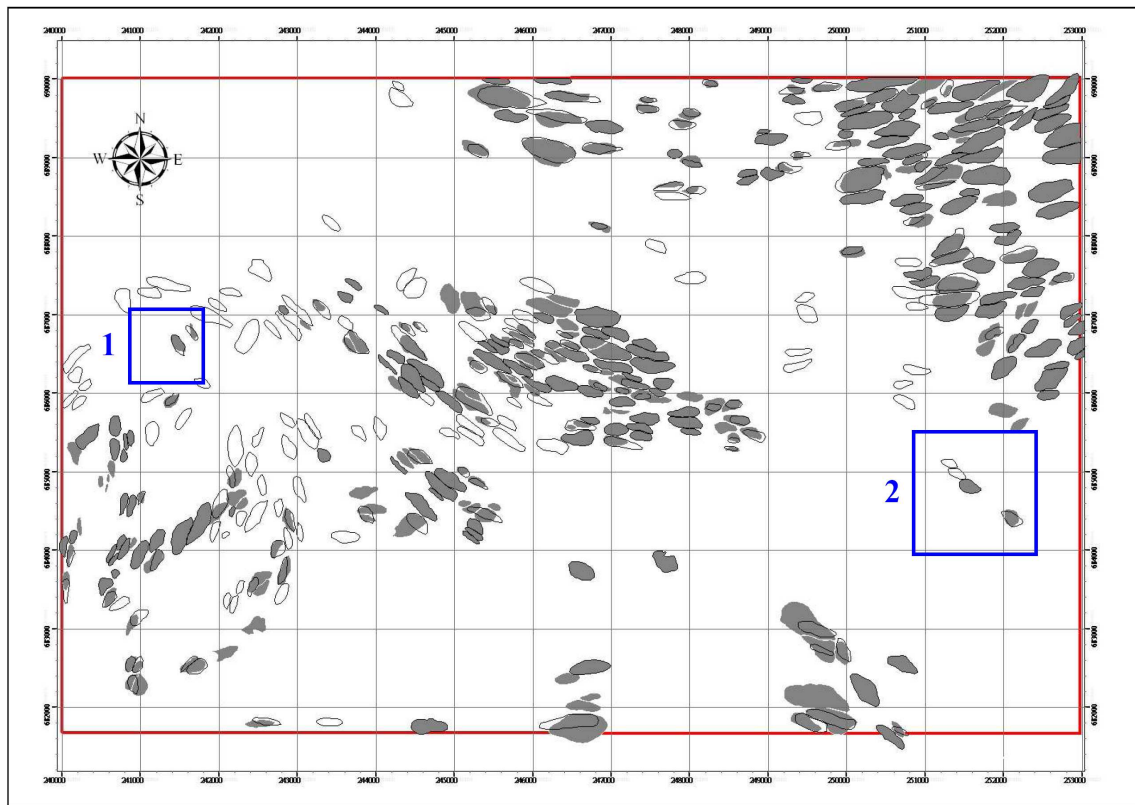


**Figure 4.4** Drumlins from the southeastern part of the Loch Lomond basin, western central Scotland. Map A is a field map by Rose (1982), digitized and published in Smith *et al.* (2006) which contains 304 drumlins in total. Map B is the results of mapping by Smith *et al.* (2006) based on NEXTMap, and 189 drumlins are recognised. This figure is from Smith *et al.*, (2006). The blue boxes highlight areas where field mapping recorded drumlins, that were not seen on the NEXTMap image (also see Figures 4.5 and 4.6).





**Figure 4.5** Comparison of DEM and field mapping of drumlins. a is the results of field mapping by Rose in 1965–1970 (Rose, 1981). An esker is marked as ‘E’. b is the results of mapping by Clark *et al.* (2009) from the NEXTMap DEM dataset. Solid black annotation for the drumlins that coincide with the results of field mapping (218 count by the present research), black outline for those found in DEM but not in the field (59-count by the present research), and the boxes highlight areas where field mapping found examples that were not seen in the NEXTMap imagery (also see Figures 4.4 and 4.6). (This figure is taken from Clark *et al.* 2009).



**Figure 4.6 Comparison of the results of field mapping by Rose (1965-1970) (Rose, 1981). Where there are similar findings with the rotating map experiment the drumlins are shown in solid gray, and drumlins only identified by the rotating map experiment are shown in black outline. The blue outline boxes identify areas with where (Clark *et al.* 2009) reported that drumlins identified by field mapping were not seen in the NEXTMap. Most of drumlins within these two areas can be found from the rotating map (also see Figures 4.4 and 4.5).**

Clark *et al.* (2009) used digital elevation models (DEMs; including NEXTMap, Ordnance Survey Panorama DEM, Landmap DEM, Shuttle Radar Topographic Mission (SRTM) DEM) and satellite images (including Landsat and SPOT image) to map some of the same drumlins field as those included in Smith *et al.* (2006). In their research, DEMs images were generated using three illumination sources from two orthogonal directions (NW and NE; no numerical azimuthal angle was provided), and from an overhead illumination (altitude = 90° or slope map; no detailed description is given in their research). Figure 4.5b shows their mapping results in comparison with the field map of Rose (Figure 4.5a). Detailed statistical mapping results were not provided in their research. In order to have a basic comparison, simple counts of the number of

drumlins was carried out for this thesis research. There are 277 drumlins in total; 218 drumlins that coincide with the results of field mapping, and 59 new drumlins that were not found by field mapping.

The new mapping procedures developed in the present study was then used to map drumlins in the same area as Smith *et al.* (2006) (Figure 4.4) and Clark *et al.* (2009) (Figure 4.5). The rotating map used to test the mapping results was set with the light source having a 25° angle of inclination, a 10° interval for changes in azimuth angle and a 60% contrast ratio. (Rotating maps were provided in CD, Appendix 2.1). Figures 4.6 to 4.8 show the results of this new research in the form of a comparison with the results of Smith *et al.* (2006) and Clark *et al.* (2009). Among the 307 drumlins that are identified for present research (in Smith *et al.* (2006), there are 304 drumlins, but 3 drumlins on the boundaries of the research that were omitted from Smith *et al.* (2006) are included in this thesis study), 268 can be observed but 39 are invisible. Of the drumlins identified by field mapping 124 have boundaries that do not coincide with the boundaries that were determined from the rotating map. 78 potentially new drumlins have been identified as a result of the rotating map experiment. The total number of drumlins in the present research is 334 (some drumlin polygons have been merged, so the total number has been reduced from 346 to 334). Basically, results from the present research almost equal the combination of results of field mapping and the mapping by Clark *et al.* (2009). In the areas identified by the blue boxes Clark *et al.* (2009) reported that drumlins found by field mapping could not be seen in the NEXTMap analysis. However, the rotating map experiment successfully visualize all the drumlins recorded by the field mapping. These ‘controversial’ drumlins are relatively small in size and their orientations trends NW-SE, which is parallel to one of the images adopted by Clark *et al.* (2009), thus reducing their visibility. Although further field investigation regarding

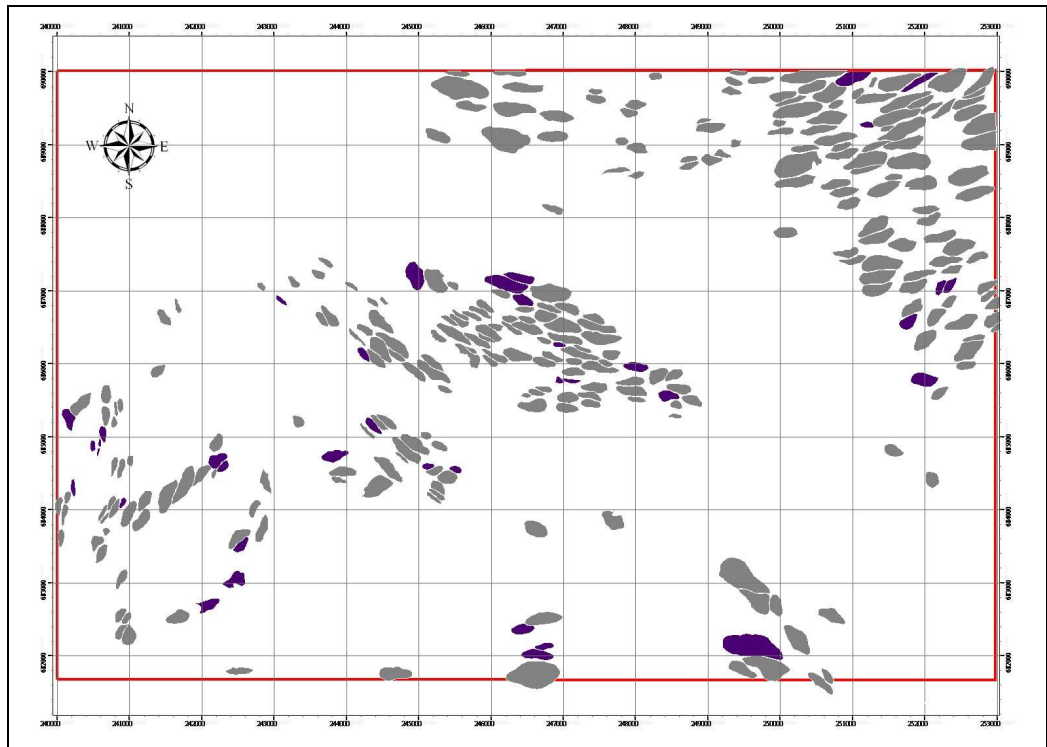


Figure 4.7 Drumlins identified by Rose in 1965-1970 (Rose, 1981; Smith *et al.* 2006) those were not visible on the analysis of the rotating map. These are shown in purple, and there are 39 in total.

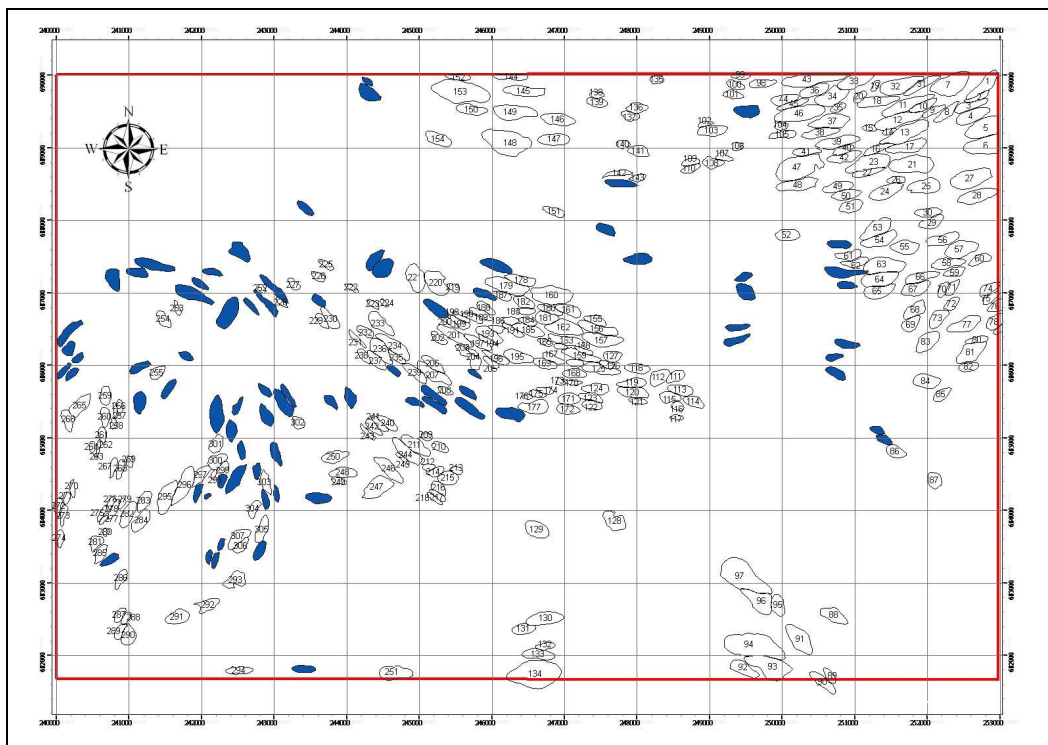


Figure 4.8 New potential drumlins identified in the research area (shown in solid blue - 78 in total) plotted against the drumlins identified in the field by Rose (Rose, 1981; Smith *et al.* 2006) (shown in black outline).

the new drumlins needs to be carried out, there is no doubt that the rotating map method of mapping has greater ability to detect drumlin landforms than other methods that have been used or are currently in use.

#### **4.3.3 Glacial landform mapping using rotating NEXTMap images and its comparison with results derived from field survey: hummocky moraines**

The term hummocky moraine has been used to describe '*moundy, irregular morainic topography 2-70 m in relief and exhibiting varying degrees of order, ranging from entirely chaotic assemblages of mounds, 15-400 m in diameter, to suites of nested transverse ridges*' (Benn and Evans, 2010, p 520). Hummocky moraine can be formed when the sediments are deposited in or against active or stagnant ice or glaciotectionic deformation processes. However, some researchers only used this term to refer to moraines deposited during the melt-out of debris-mantled glaciers (Benn and Evans 2010).

In this section, 2243 hummocky moraine landforms were mapped within the same area as that used to test the drumlins (Figures 4.3 and 4.9). All the hummocky moraines were digitized (Figure 4.10) to test the mapping ability of the new rotating map procedure. Unlike drumlins, hummocky moraines do not have a uniform shape. Normally, their shape is irregular although some research says they do have some characteristic "shape" and "pattern". Most hummocky moraines observed in this research area were irregular and it was hard to see any patterns from available imagery or field mapping. The scale is much smaller than drumlins and the length of the majority of hummocky moraines in this research area varies from 20 m to 100 m. The hummocky moraines mapping proved to be much harder than mapping drumlins both theoretically and practically.

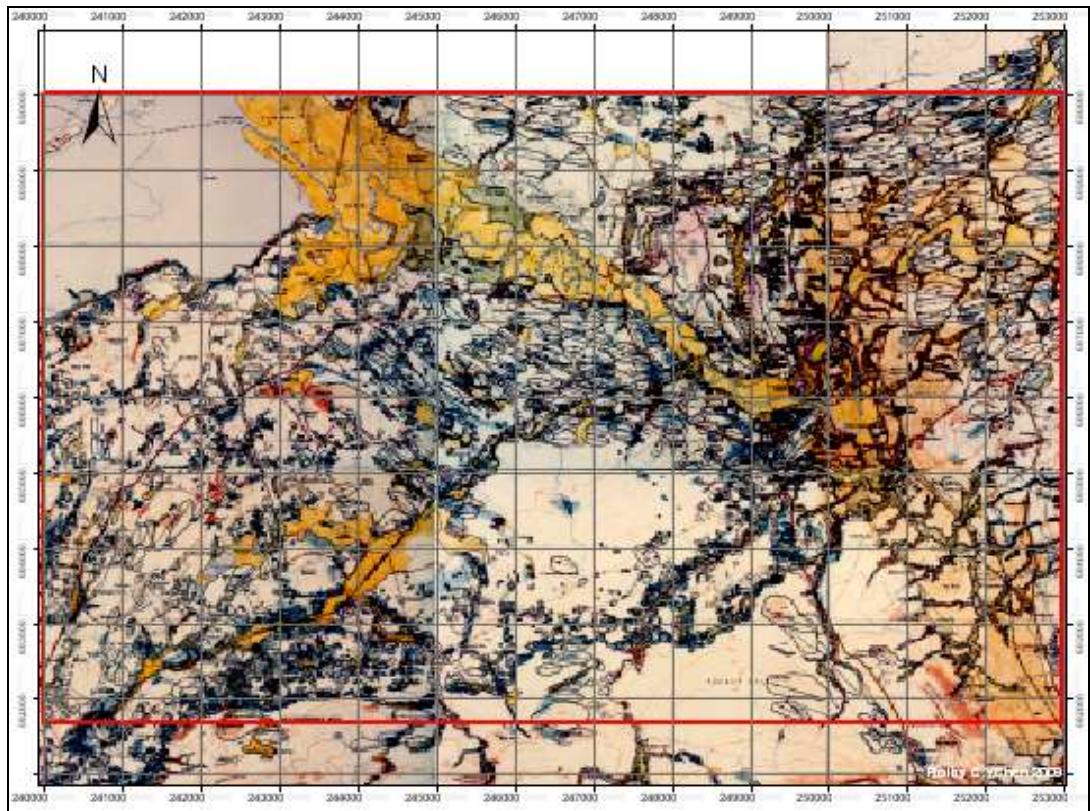


Figure 4.9 1:25,000 scale representation of 1:10,560 field mapping carried out J. Rose in 1965-1970 and published in Rose and Smith (2008)

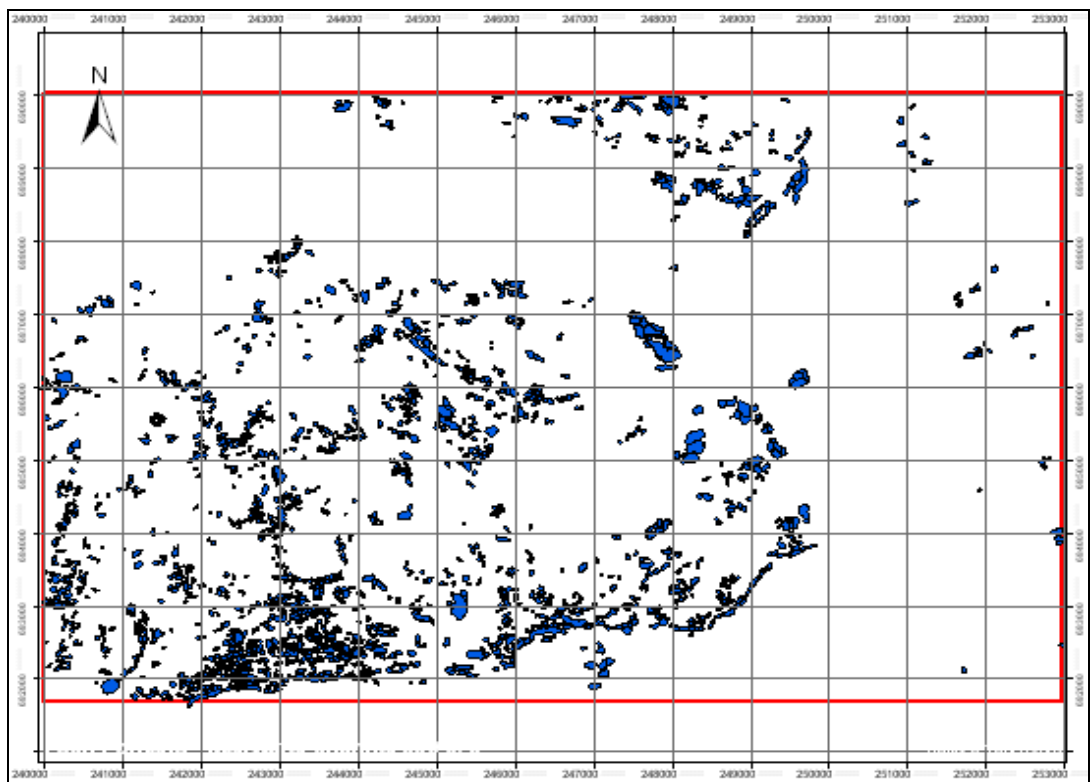


Figure 4.10 Digitized hummocky moraine and moraine ridge in the area shown on Figure 4.9 (based on Rose and Smith (2008)).

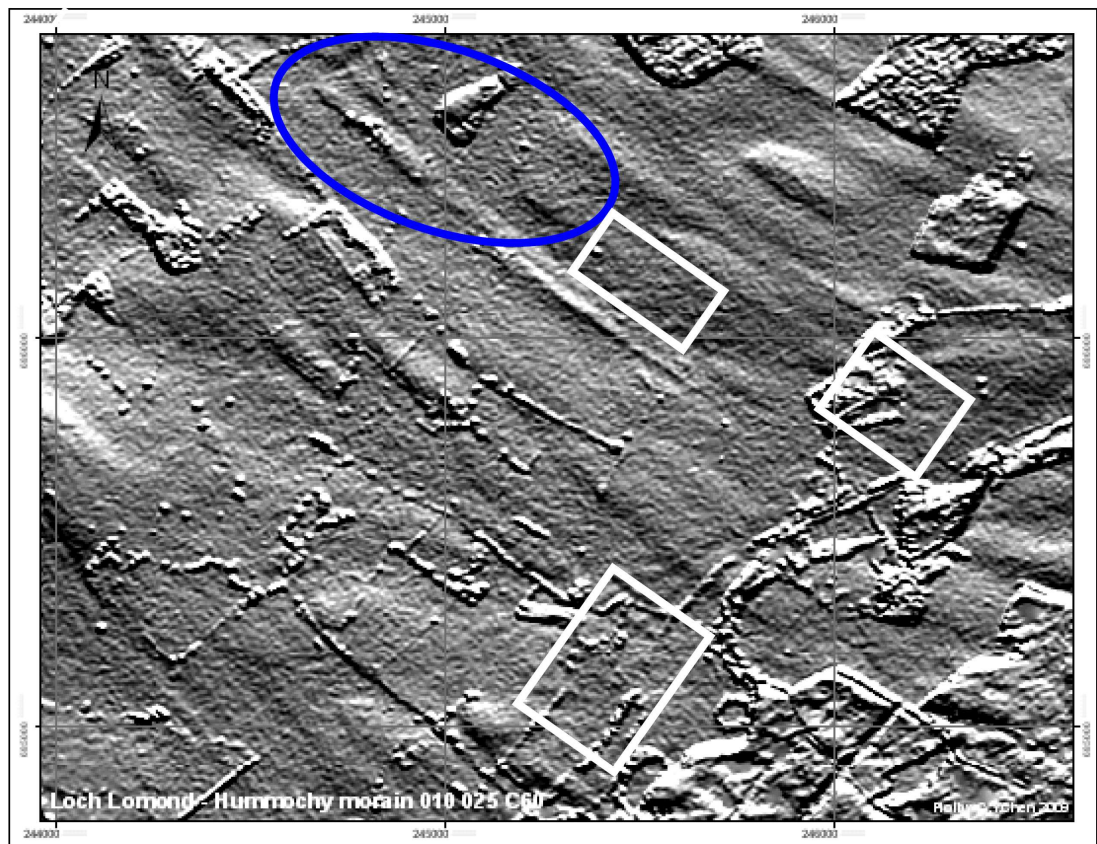
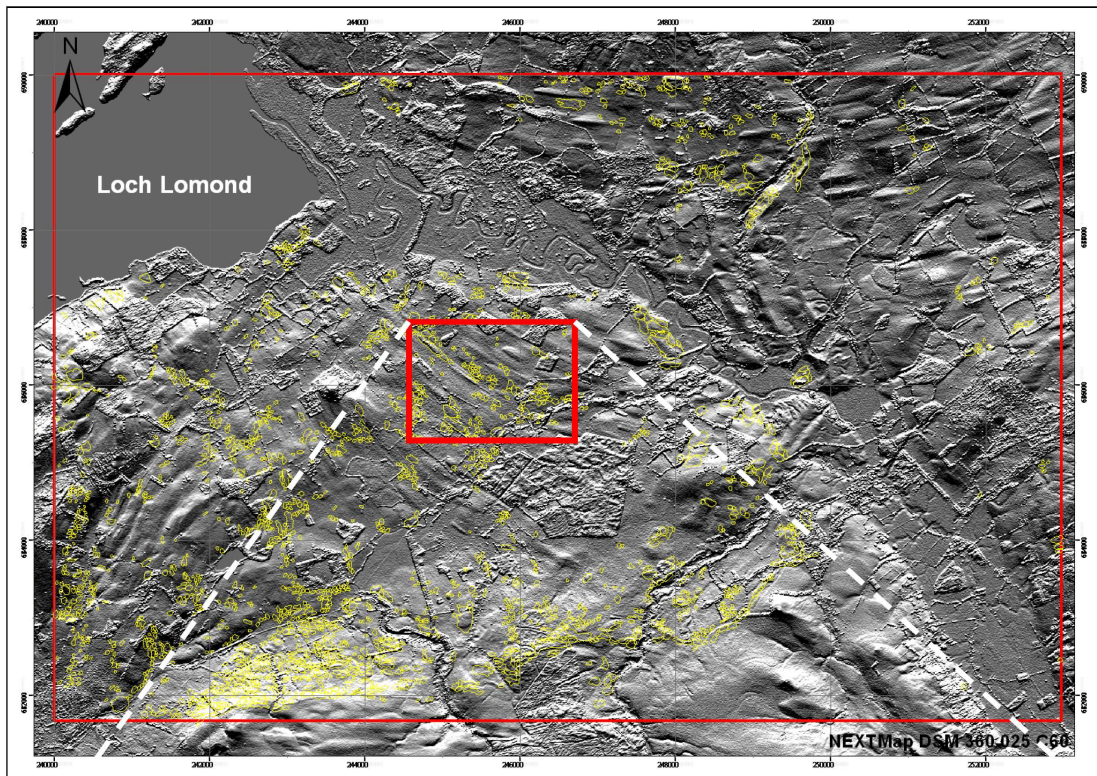
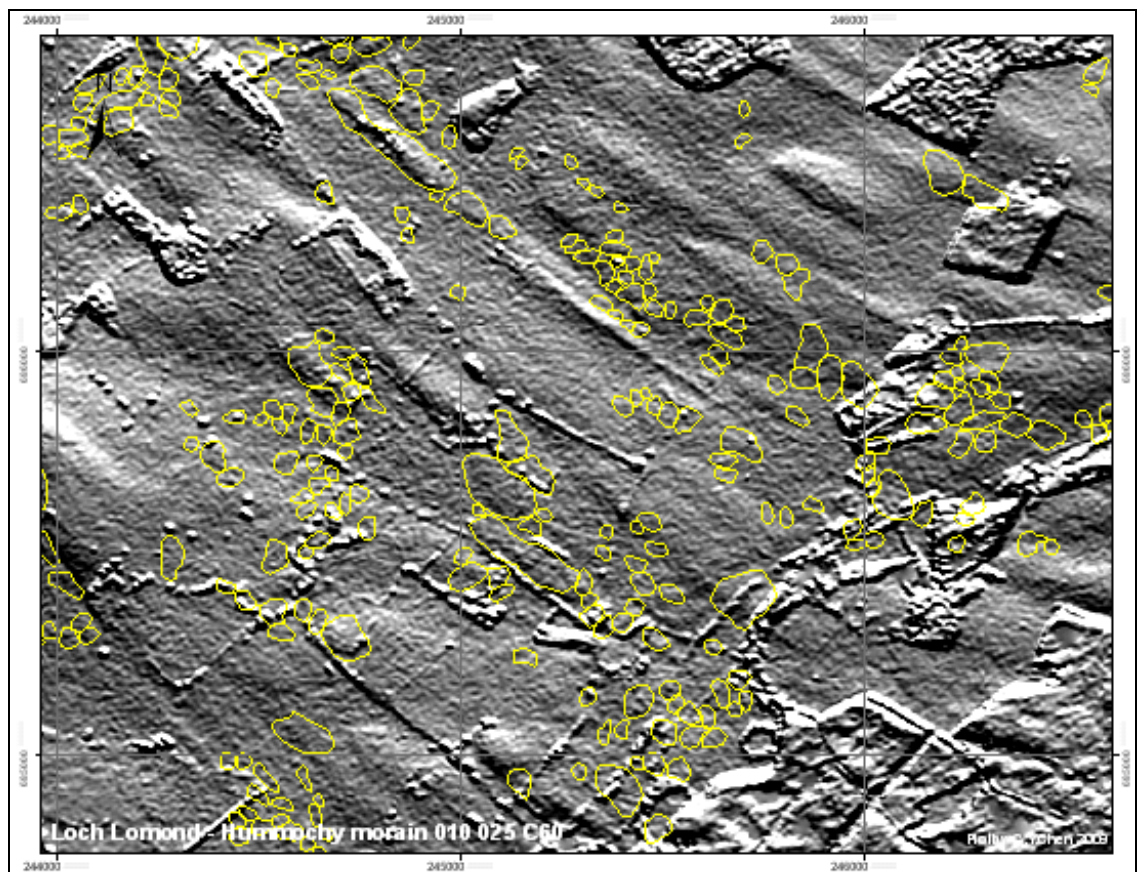


Figure 4.11 1:10,000 scale relief-shaded images generated from NEXTMap for hummocky moraines mapping experiment. Hummocky moraines in the blue oval can be discerned while those in white rectangle box are hard to see due to the resolution.

Figures 4.11 and 4.12 are relief-shading images generated from NEXTMap with a light source showing a 10° azimuth variation, a 25° angle of altitude and a 60% contrast ratio. Scale was set at 1:10,000 as it this the maximum reliable scale that can be obtained from NEXTMap (Smith *et al.*, 2006). The yellow linework in Figure 4.11 is hummocky moraine that has been digitized from the published 1:25,000 scale map of Rose and Smith (2008) (this is based on 1:10,560 field mapping field slips, redrawn at the smaller scale by Rose for publication). The lower part of Figure 4.11 is an enlargement of the area shown in red on the upper figure highlighting areas where the hummocky moraine is either well developed or incapable of identification.



**Figure 4.12** Digitalized hummocky moraines (yellow) overlapping with 1:10,000 scale relief-shading map. Compare to Figure 4.11, hummocky moraines were hard to delimit from NEXTMap.



Figure 4.12 shows the distribution of the field mapped hummocky moraine at the 1:10,000 scale, and although drumlins are clearly represented the majority of hummocky moraines mapped in the field survey are not visible on NEXTMap, due to the resolution of the remote sensed imagery. Therefore, the process of mapping hummocky moraine from NEXTMap imagery is not reliable. Higher resolution imagery, such as LiDAR does have the ability to provide sufficient information for hummocky moraines mapping (Smith *et al.*, 2006) and can be tested against the new rotating map procedure proposed in this chapter, at a future date. However at present (2012), most areas of the UK lack LiDAR imagery and until a higher resolution imagery is launched, field mapping is the most reliable way to map hummocky moraines.

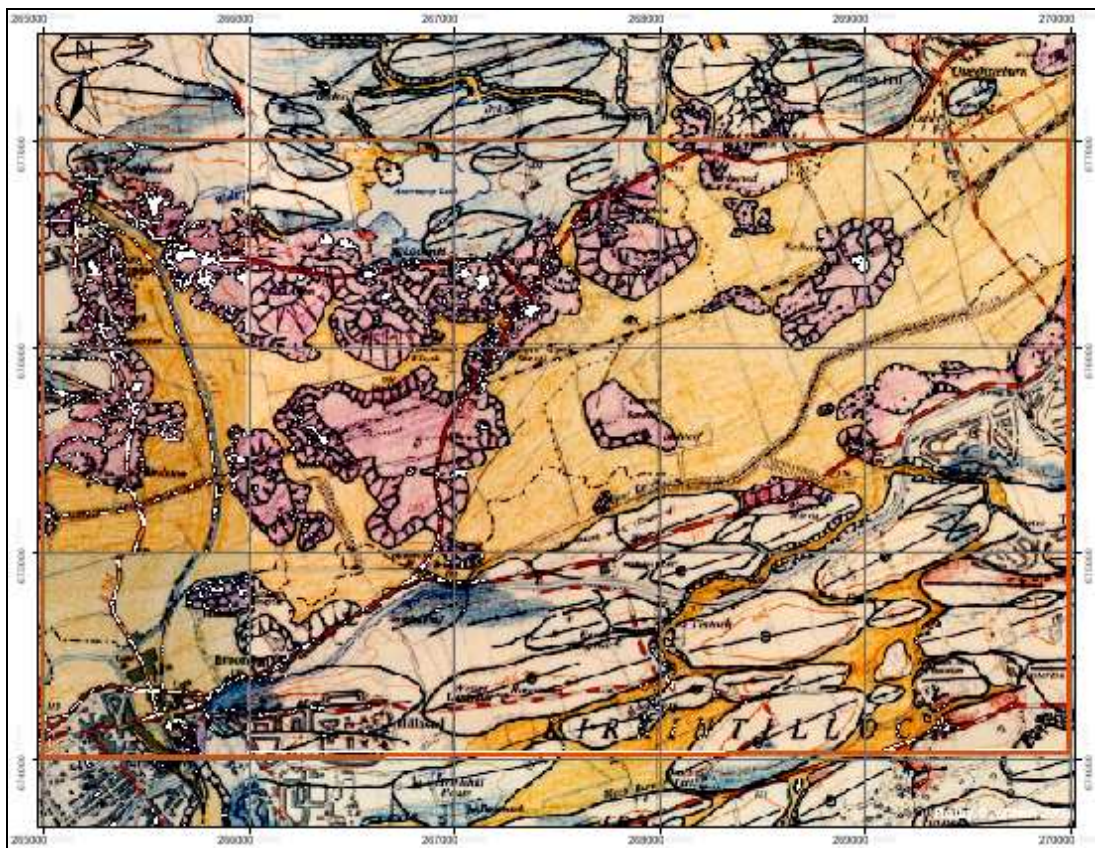
#### **4.3.4 Glacial landform mapping using rotating NEXTMap images and its comparison with results derived from field survey: kame and kettle**

*'Kames are variously shaped mounds, composed chiefly of sand and gravel, and formed by supraglacial or ice-contact glacialfluvial deposition'* (Benn and Evans, 2010, p 526). Kames may occur as isolated hills but more generally each kame is one mound in a low-lying terrain of many hummocks, terraces, ridges and hollows. Kames often occur in association with kettle holes in kame and kettle topography. Eskers may also occur between the kames. Meltwater channels may be cut into and between the kames. These associations indicate that kames are formed close to ice margins in situations where there are large volumes of both meltwater and debris. Kame terraces are normally defined as *'gently sloping depositional terraces perched on valley sides, and are deposited by meltwater streams flowing between glacier margins and the adjacent valley wall'* (Benn and Evans, 2010, p 528). Kame terraces form when sediment accumulates in ponds and lakes trapped between lobes of glacier ice or between a glacier and the valley side. Typically, the sediment comprises well-bedded and

well-sorted sand and gravel. In this research, kames and kame terraces will be called kames.

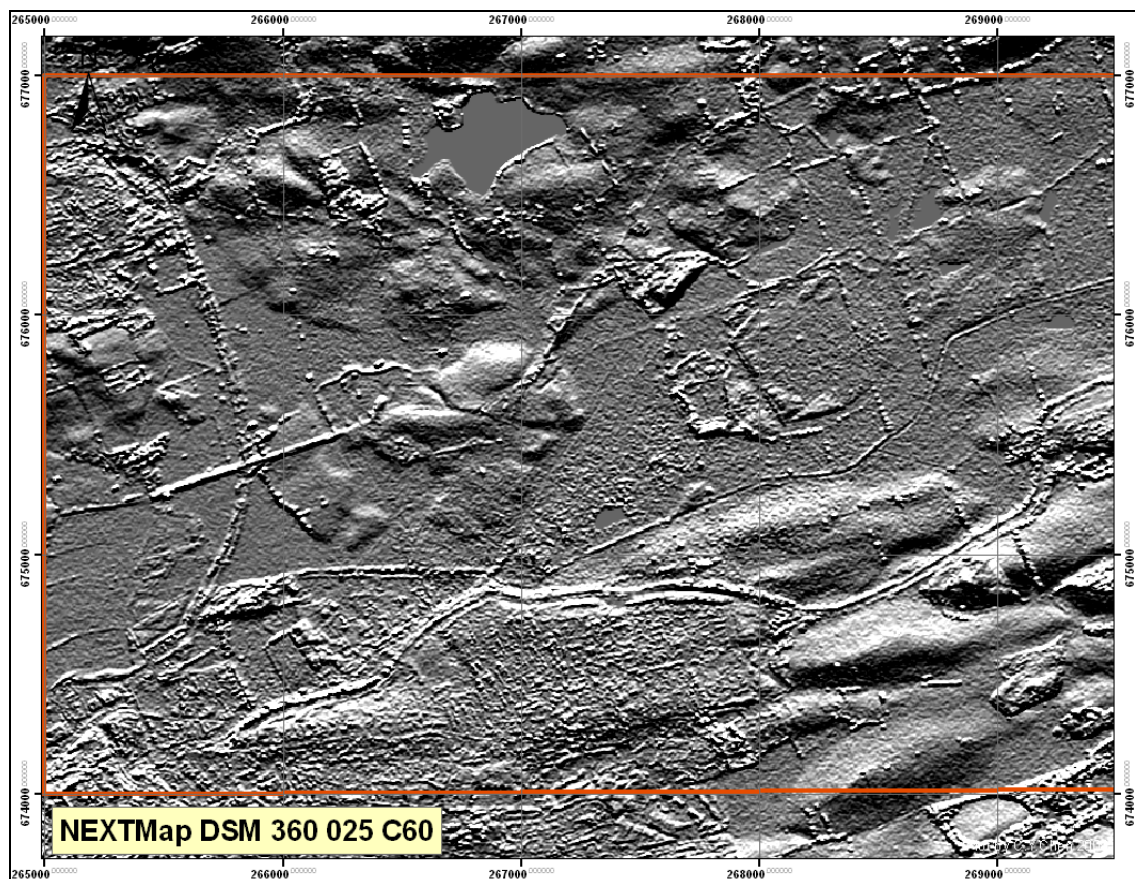
Kettles are glaciofluvial landform occurring as the result of blocks of ice calving from the front of a receding glacier and becoming buried partially to wholly by glacial outwash. When the ice blocks eventually melt they leave behind holes or depressions that fill with water to become kettle hole lakes or ponds.

In this research, area R2 in Figure 4.3 was selected to test the mapping of kames and kettle holes from NEXTMap imageries. There are 42 kames and 25 kettle holes recorded in Rose and Smith (2008) in this area (Figures 4.13 to 4.18).



**Figure 4.13** An area of kames and kettle holes in the area near Kirkintilloch in the Kelvin Valley, western central Scotland. This map is taken from Rose and Smith (2008) and is at 1:25,000 scale , reduced manually from 1:10,560 field maps produced as a result of surveys between 1965 and 1968.

As a result of the test (Rotating maps are provided on the CD, Appendix 2.2), it was found that 7 kames (numbers 6, 12, 13, 26, 27, 28, 29) (Figure 4.19) and 7 kettle holes (numbers 1, 3, 6, 7, 9, 13, 18) (Figure 4.20) were not visible on the NEXTMap imagery. Kames numbered 6, 12 and 13 kames were too small in size, while kames numbered 26, 27, 28 and 29 were covered by forest. Kames can be successfully delimited by NEXTMap, but the detection rate was highly reliant on the relief of the landforms. It is hard to delimit kettle holes without any guide or knowledge of the research area (field experience). Kettle holes are relatively small in area, a fact that also hinders their detection. The relief of the kames surrounding the kettle holes is not sufficient to allow them to stand out in NEXTMap imagery.



**Figure 4.14** NEXTMap images of the area shown on Figure 4.13, showing kames and kettle holes in the region of the Kelvin Valley near Kirkintilloch, north of Glasgow.

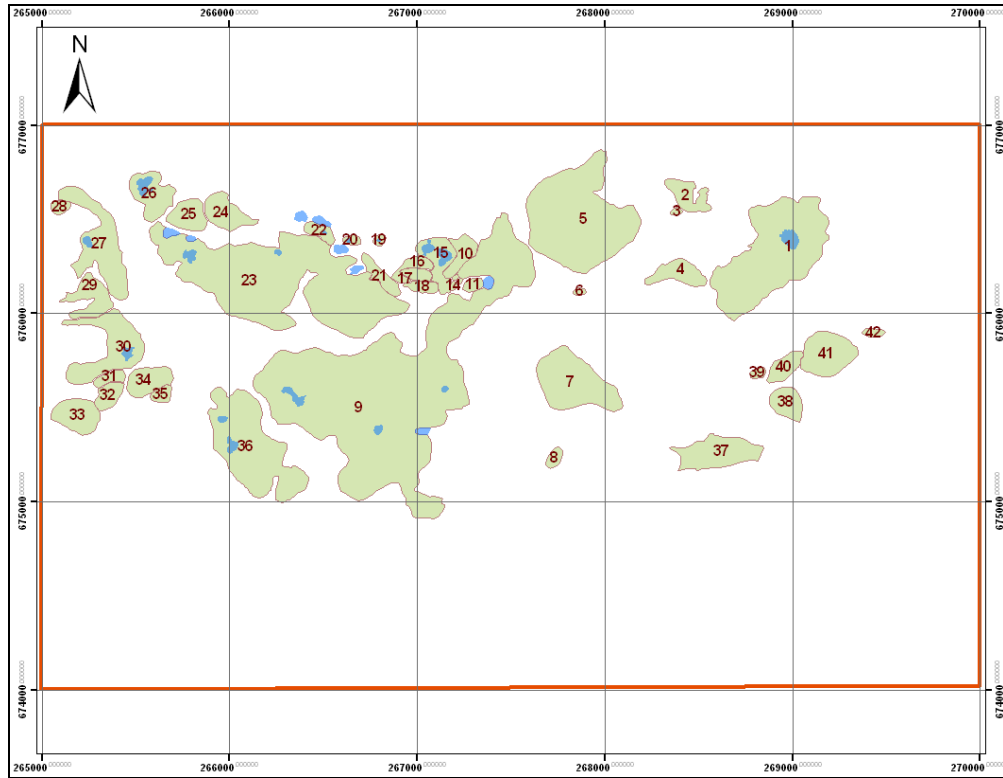


Figure 4.15 Digitization of the kames shown on the NEXTMap image on Figure 4.14 showing their location and distribution. Each kame has been assigned a number and the parts show the location of kettle holes.

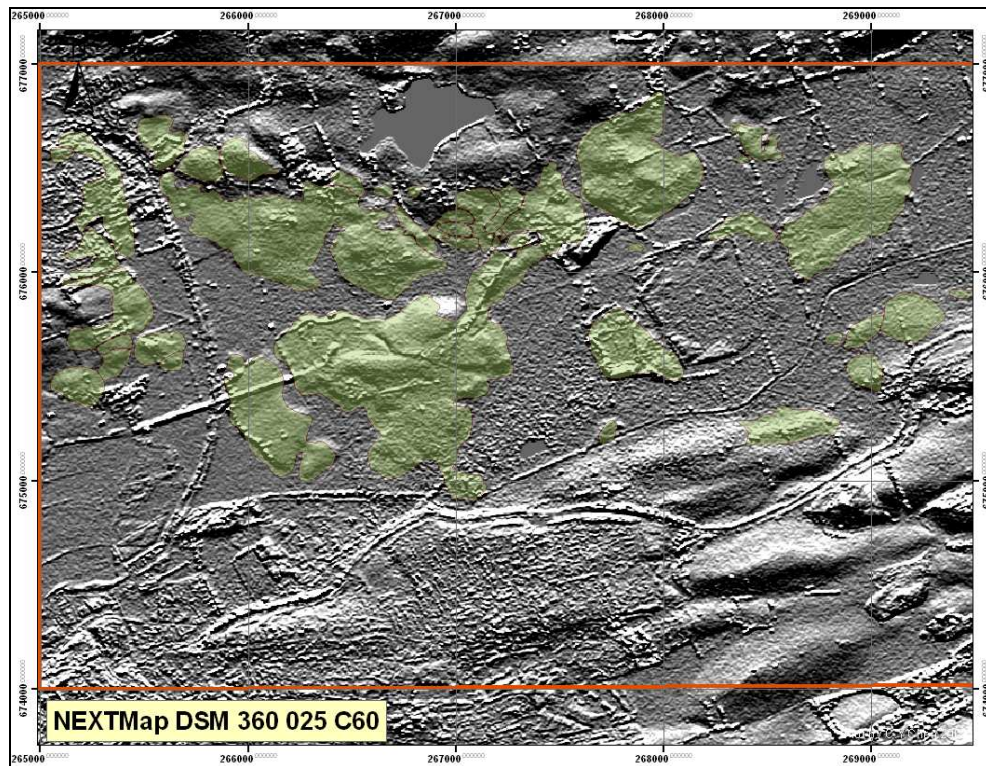


Figure 4.16 Digitization of the kames shown on the NEXTMap image on Figure 4.14 showing their location and distribution.

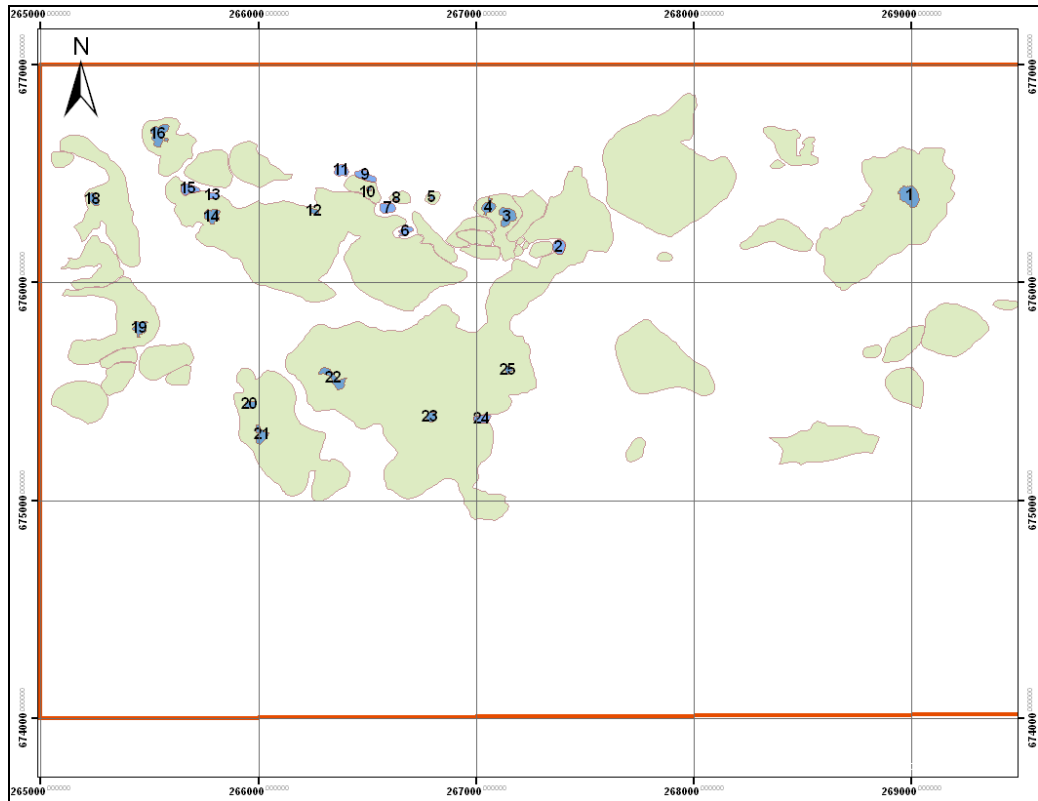


Figure 4.17 Digitization of the kettle holes shown in the NEXTMap image on Figure 4.14 showing their location and distribution. Each kettle hole has been assigned a number.

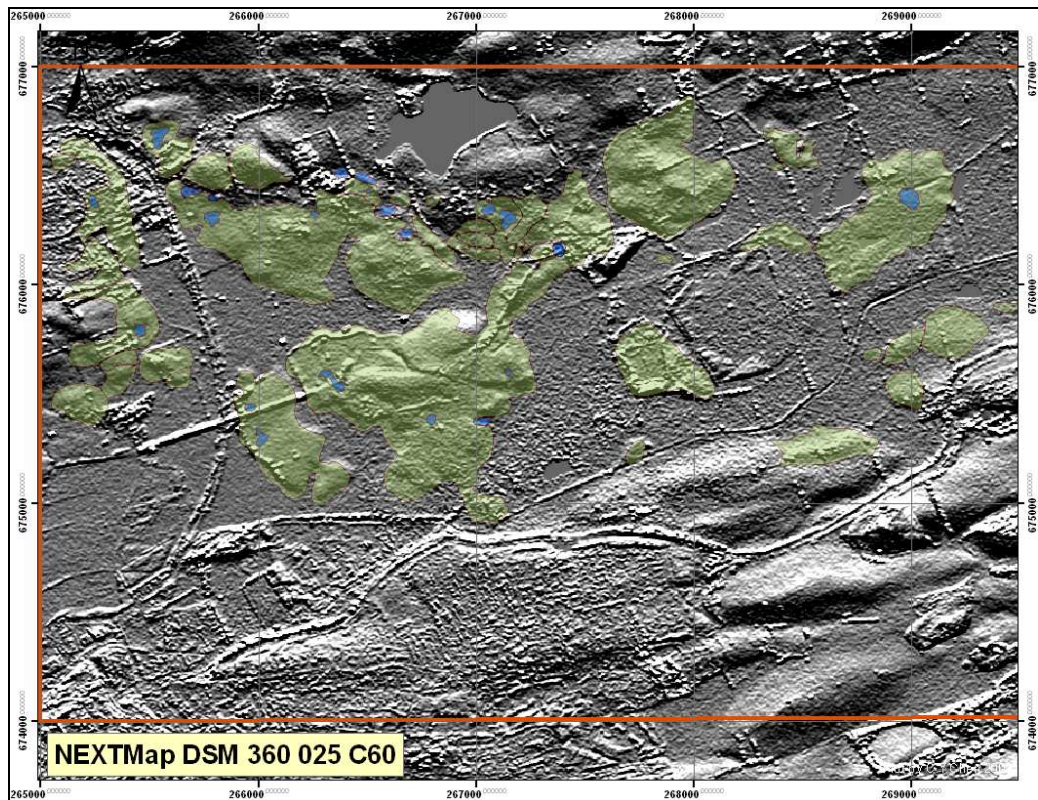


Figure 4.18 The digitalized kames (green) and kettle holes (blue) derived from the NEXTMap image in the area of the Kelvin Valley near Kirkintilloch.

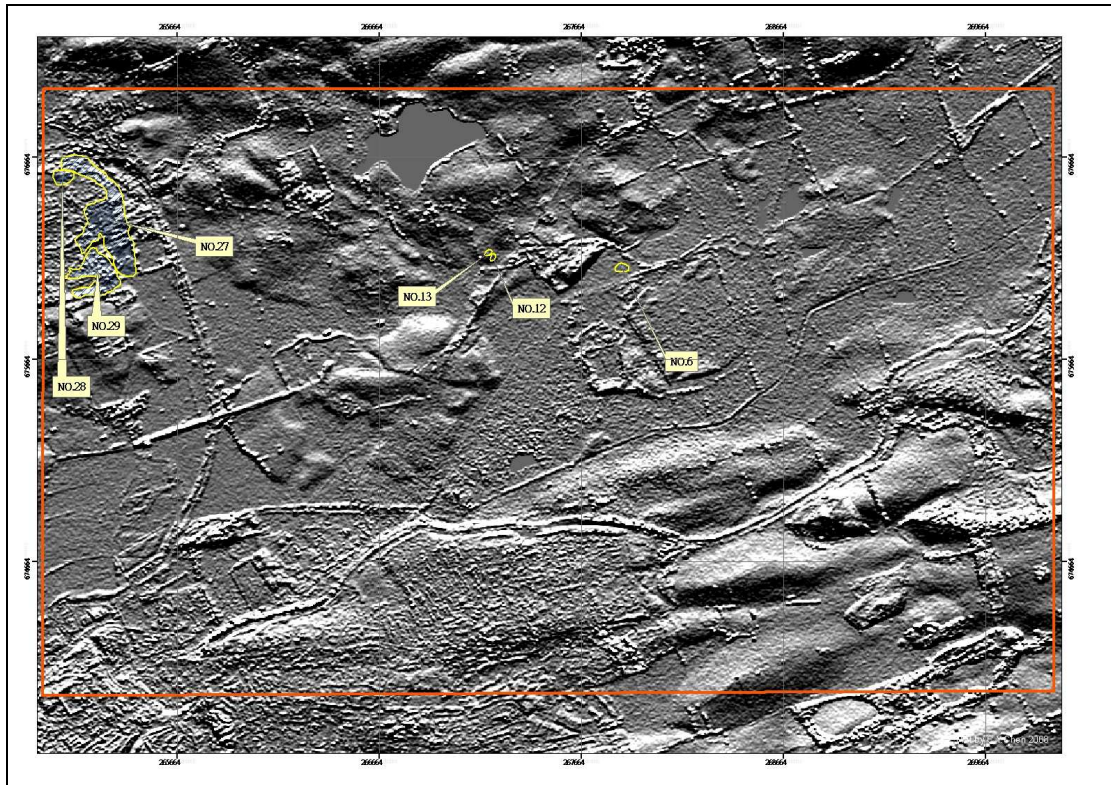


Figure 4.19 Location of kames that are not visible on NEXTMap and their assigned number for the area of the Kelvin Valley near Kirkintilloch, shown on Figure 4.13.

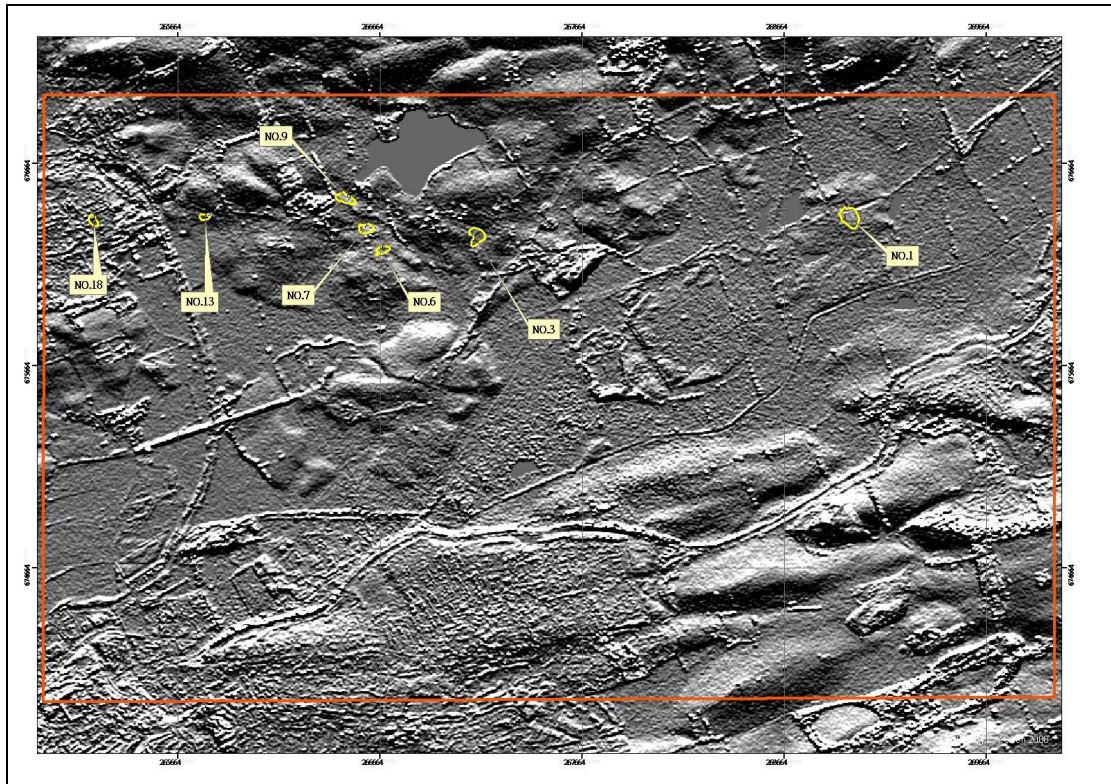


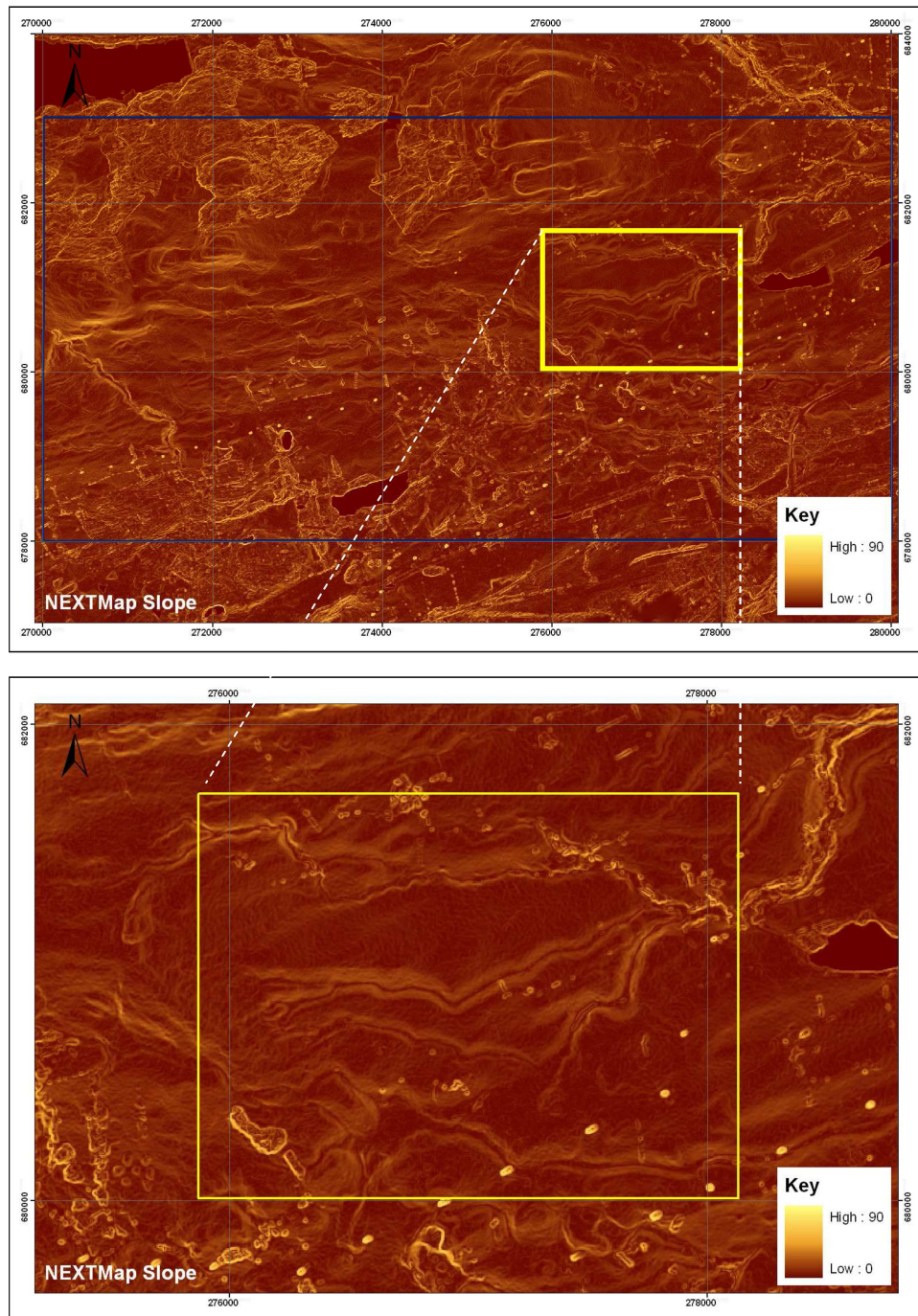
Figure 4.20 Location of kettle holes that are not visible on NEXTMap and their assigned number for the area of the Kelvin Valley near Kirkintilloch, shown on Figure 4.13.

#### **4.3.5 Glacial landform mapping from NEXTMap and its comparison with field evidence: meltwater channels**

Glacial meltwater channels are valleys eroded by glacial meltwater, and typically survive in the present landscape as dry channels or channels with underfit streams. Some contain present day streams, and in these cases independent evidence is needed to identify a glacial meltwater origin. Channels are formed in a number of contexts: subaerially at ice margins or at ice fronts in the proglacial zone; sub-marginally along valley sides and where the meltwater river is constrained by the glacier ice and beneath the ice in subglacial conduits (Röthlisberger, 1972; Schreve, 1972). The distribution and patterns of glacial meltwater channels provide information that can be used to determine the direction of ice movement and the character of ice wastage. In contrast to 'normal' surface drainage, the glacial meltwater channels may begin and end abruptly, and they lack a catchment. The size of glacial meltwater channels is typically unrelated to subaerial catchments. Normally, they are used as an evidence of former meltwater discharge routes. In the UK, marginal and sub-marginal channels have been used to reconstruct the pattern of ice sheet recession (Clark *et al.*, 2004; Greenwood *et al.*, 2007).

Characteristically well-developed meltwater channels have a relatively low gradient and steep channel walls. In comparison with drumlins and kames, the mapping target (thalweg) is lower than its surrounding environment. The width/ length ratio is small and the channels can be treated as a linear feature. These characteristics increase the difficulty of using the relief-shading imagery for mapping, because the mapping target will be seriously affected by the shadow when the illumination source is normal to the trend of the channel. This problem is accentuated when the channel is deep and narrow. Although the rotating map method still works for correcting the boundary of the channel,

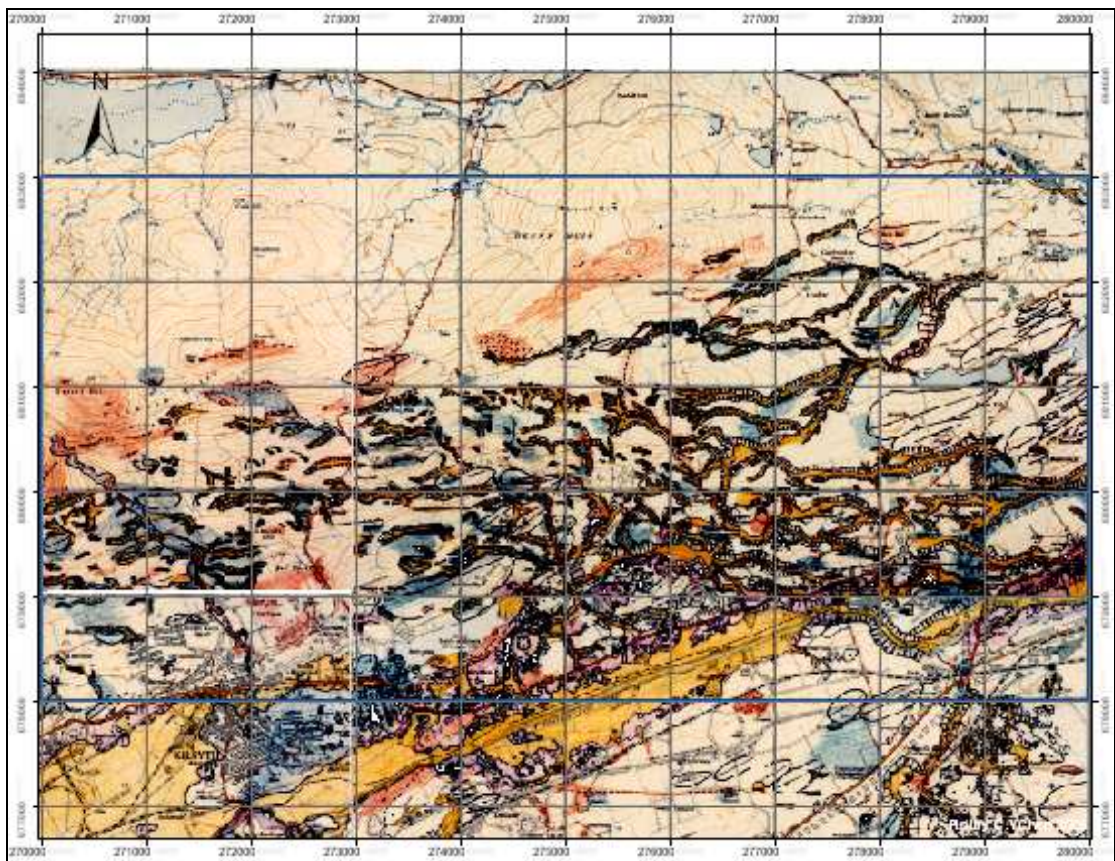
it is clear that we need a more efficient method of identifying the channels in the “draft” mapping stage.



**Figure 4.21** An example of meltwater channels represented by a slope map taken from the NEXTMap image. The thalweg of the channels and the surrounding terrain are shown in red colour, while the channel sides, which are much steeper are shown in yellow. This image has provided a very effective method for mapping the boundary of meltwater channels. The area of analysis is the region north of Kilsyth at the southeastern end of the Campsie Fells in Central Scotland

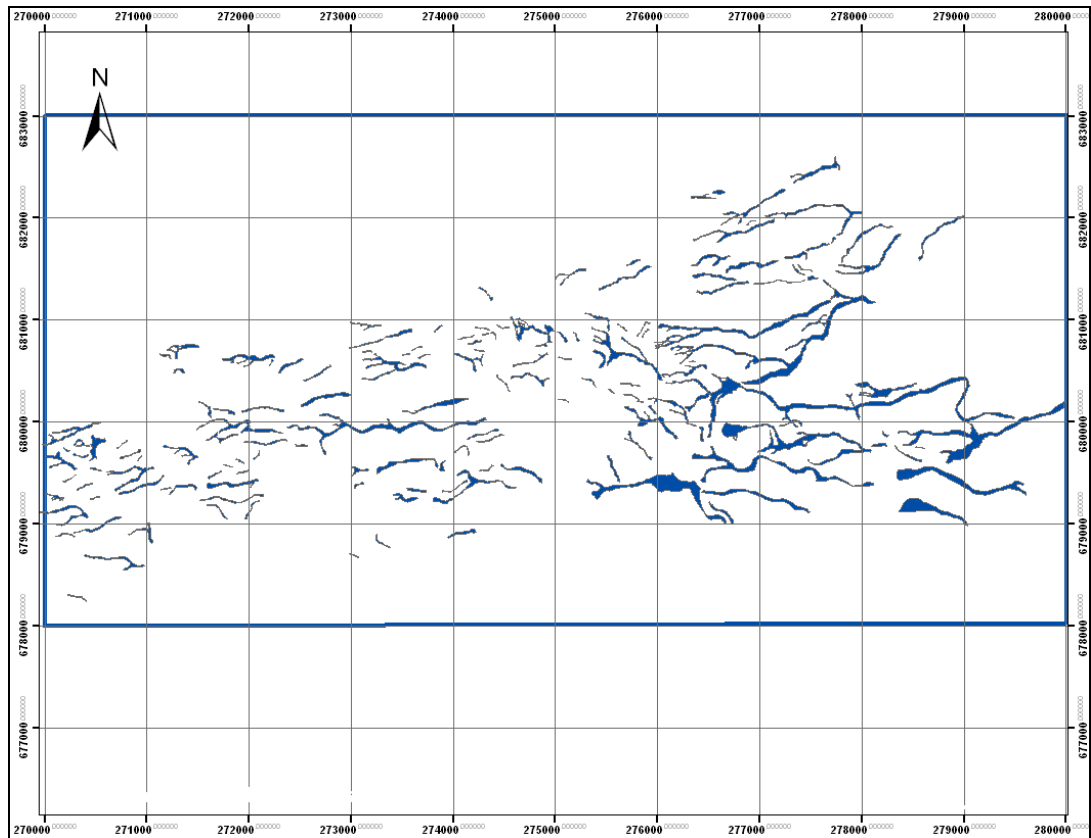


Figure 4.21 is a slope map generated from the NEXTMap. In this map, areas which have similar surface gradient are shown with similar colours, and these colours can, in turn, be used to differentiate “flat” and “steep” terrains. The terrain is not subject to an illumination problem. Hence, in the present research, slope map has been used in the draft mapping stage of the meltwater channel studies. Relief-shaded imagery and rotating map analyses have also been used to assist the image interpretation and as a tool to check boundaries.



**Figure 4.22 1:25,000 scale map of the meltwater channels shown in Figure 4.21 Rose and Smith (2008). This map is based on 1:10,560 scale mapping carried out in the field between 1965 and 1968 for the region north of Kilsyth, at the southeastern end of the Campsie Fells in Central Scotland.**

A test of the use of the NEXTMap slope map was carried out in the area north of Kilsyth at the southeast end of the Campsie Hills in central Scotland (research area R3)



**Figure 4.23** Location and distribution of digitalized meltwater channels for the area shown on Figure 4.22. This area is the region north of Kilsyth, at the southeastern end of the Campsie Fells in Central Scotland.

(Figures 4.3; 4.22 and 4.23). Some 169 meltwater channels were identified and digitized. The digital method consisted of drawing the outline of the thalweg of the channels (the blue lines in Figure 4.24). A rotating map with a  $10^\circ$  azimuth interval angle,  $25^\circ$  altitude angle and 20% contrast ratio were used as a testing platform (Rotating maps are provided on the CD, Appendix 2.3). The tested result shows that although the majority of channels can be delimited from the NEXTMap imagery some small channels cannot be identified (Figure 4.25). Generally speaking, the slope map is very successful in mapping at the draft stage of analysis, but its value diminished in areas where the gradient was low and the changes of terrain angle are small. It is easy to cause misinterpretations when viewing hills with flat tops. The relief-shaded imagery or rotating map is needed to rectify these problems, but there is no doubt that

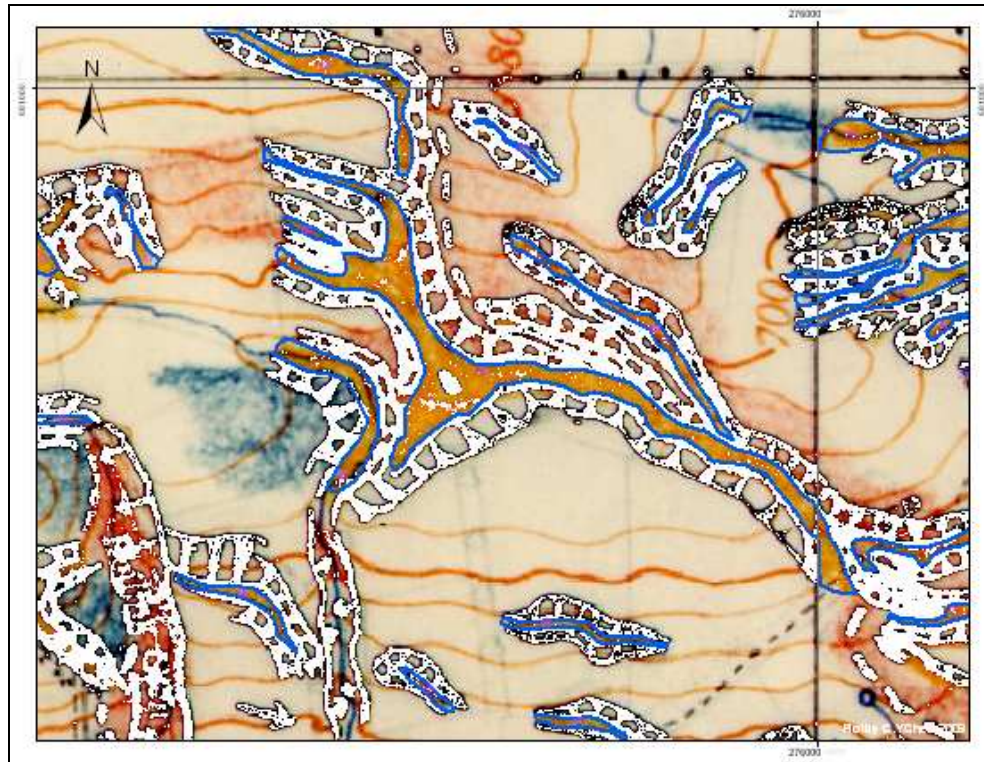


Figure 4.24 Digitized meltwater channel boundaries (in blue) overlapping on original 1:25,000 scale map taken from Rose and Smith 2008, based on original field mapping by Rose 1965-1968. All the channels were digitized along the thalweg. This sample area is from the region north of Kilsyth, at the southeastern end of the Campsie Fells in Central Scotland shown on Figure 4.22.

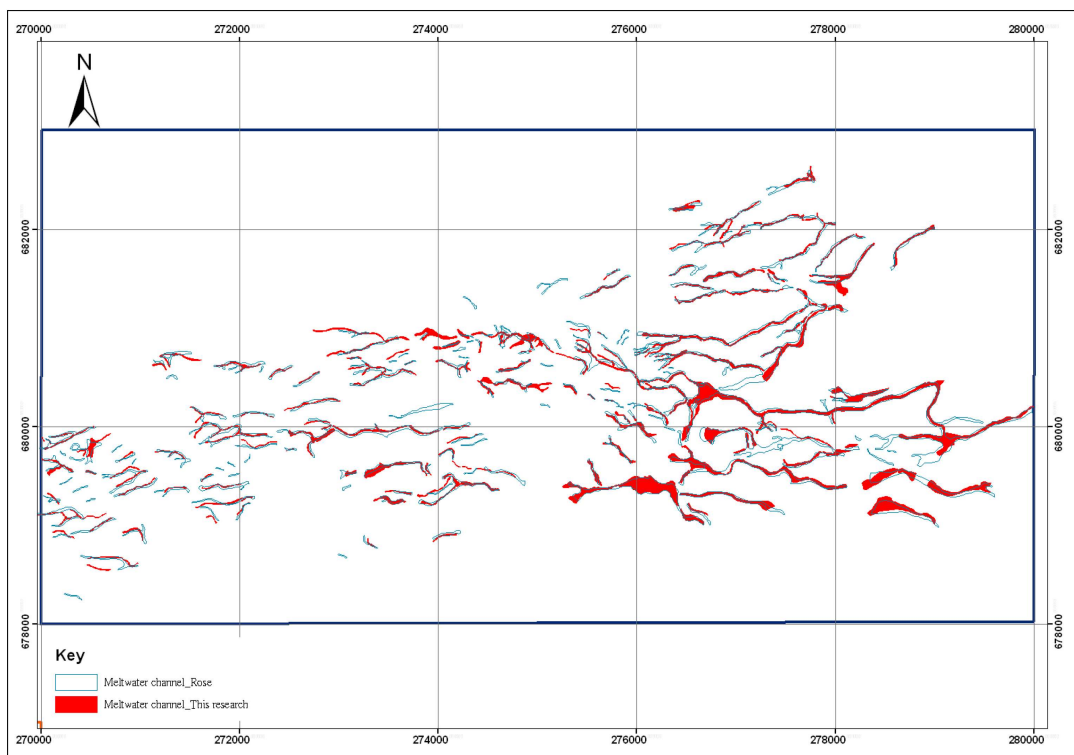


Figure 4.25 Comparison of the mapping results from slope map (solid red) and field mapping (blue line).

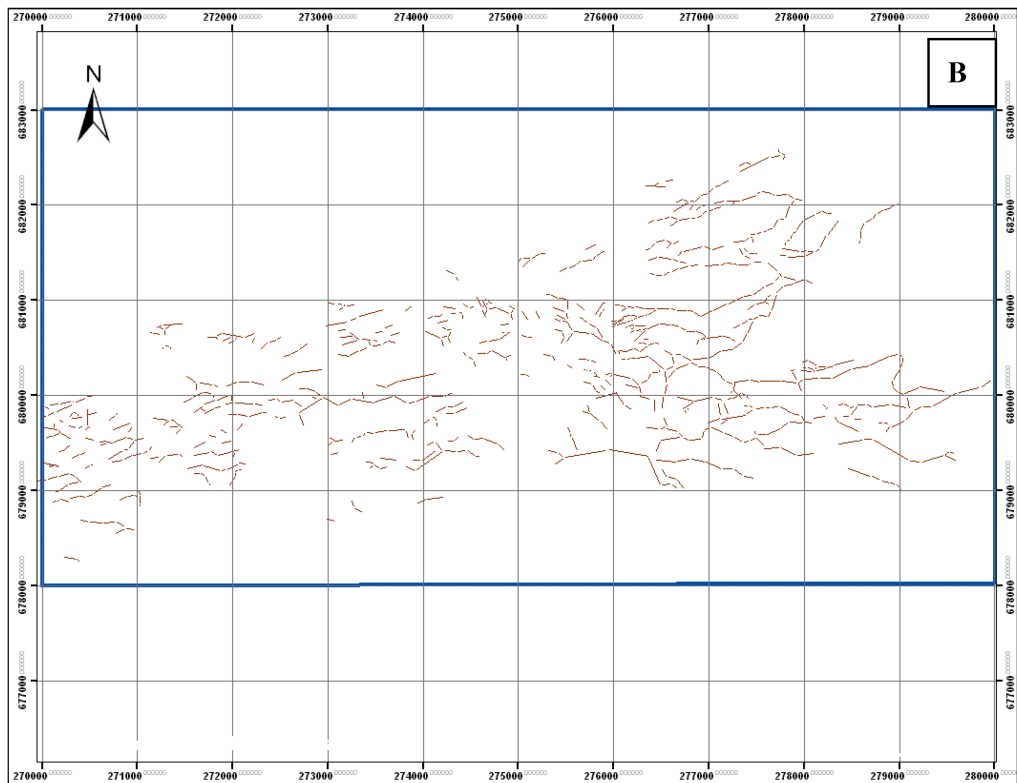
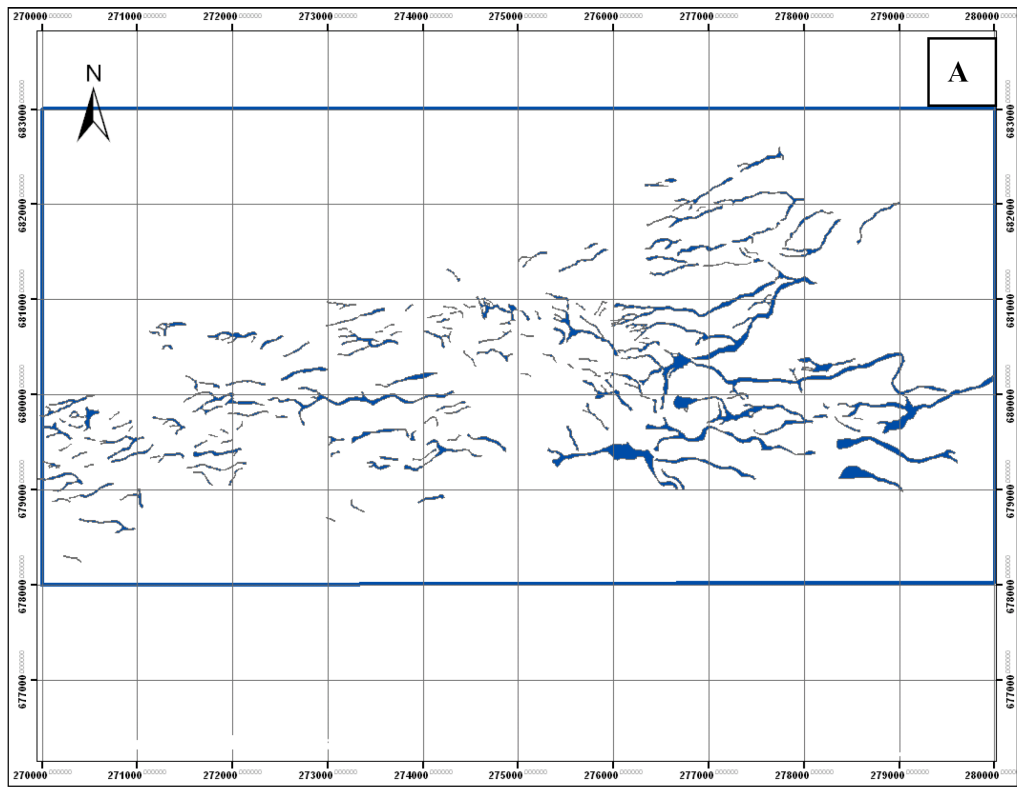
the slope map can make meltwater channel mapping more efficient. Landforms that have similar characteristics to meltwater channels can also use this mapping method and procedures.

#### **4.4 Image mosaic: the optimized method in presenting landforms**

##### **4.4.1 Analysis of glacial meltwater channel distribution and optimized base map selection**

From previous discussions we have concluded that the rotating map is the most successful mapping and visualizing method relative to the other methods that have been applied so far. However, this kind of imagery can be only demonstrated in a digital environment. It is not practical to see the illumination change effect, caused by the rotating map, on paper. Therefore, a simple and practical method has been developed which can demonstrate most landforms as a single image. The 169 meltwater channels that were mapped in the previous section will be used for further study. The first step consists of dissecting all the meltwater channels from polygons into polylines. The reason for this is that line features are more convenient for measuring and analysis of the geometrical characters. The method of re-mapping was carried out by drawing the centre line of the original polygons. In this procedure, meltwater channels were dissected into 777 sub-sections (Figure 4.26). Geometry characteristics such as length and orientation of each sub-section were then measured and calculated.

Tables 4.1 and 4.2 summarise data representing the basic geometric description and frequency of each equal separated azimuth ranges. From Table 4.3; Figure 4.27 and 4.28, we can see that the orientation of the majority of the meltwater channels is trending east to west ( $61^{\circ}\sim 120^{\circ}$ ,  $241^{\circ}\sim 300^{\circ}$ ). 84% of the sections of the meltwater



**Figure 4.26 Comparison of two different methods of representing meltwater channels. A is the digitalized meltwater channels in a polygon format; B is digitized meltwater channels in a polyline format.**

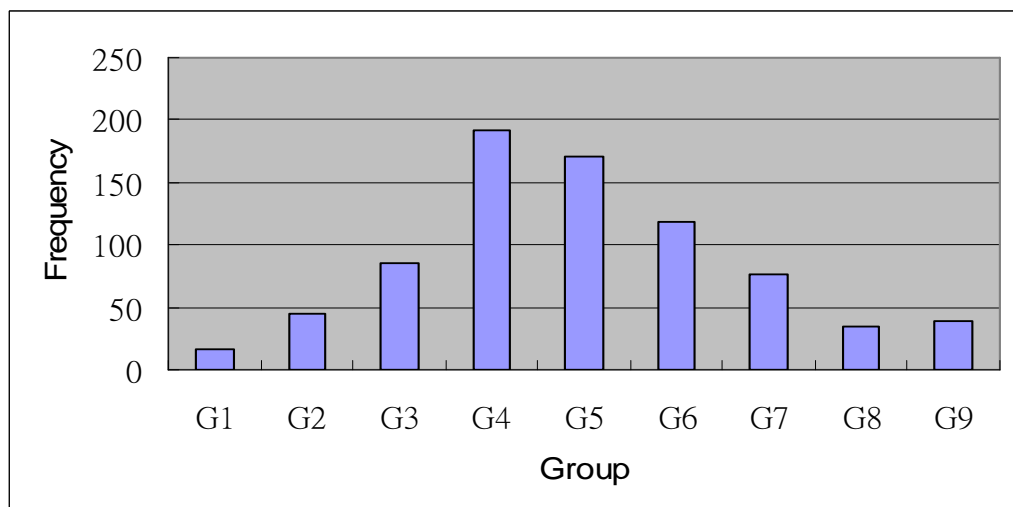
channels are trending within the range from 41°~140° and 221°~320°(Table 4.3). Although the range of trends is narrow, the distribution pattern is random. It is suitable to represent landforms by using a single illumination angle.

**Table 4.1 Basic geometry characters of the dissected meltwater channels.**

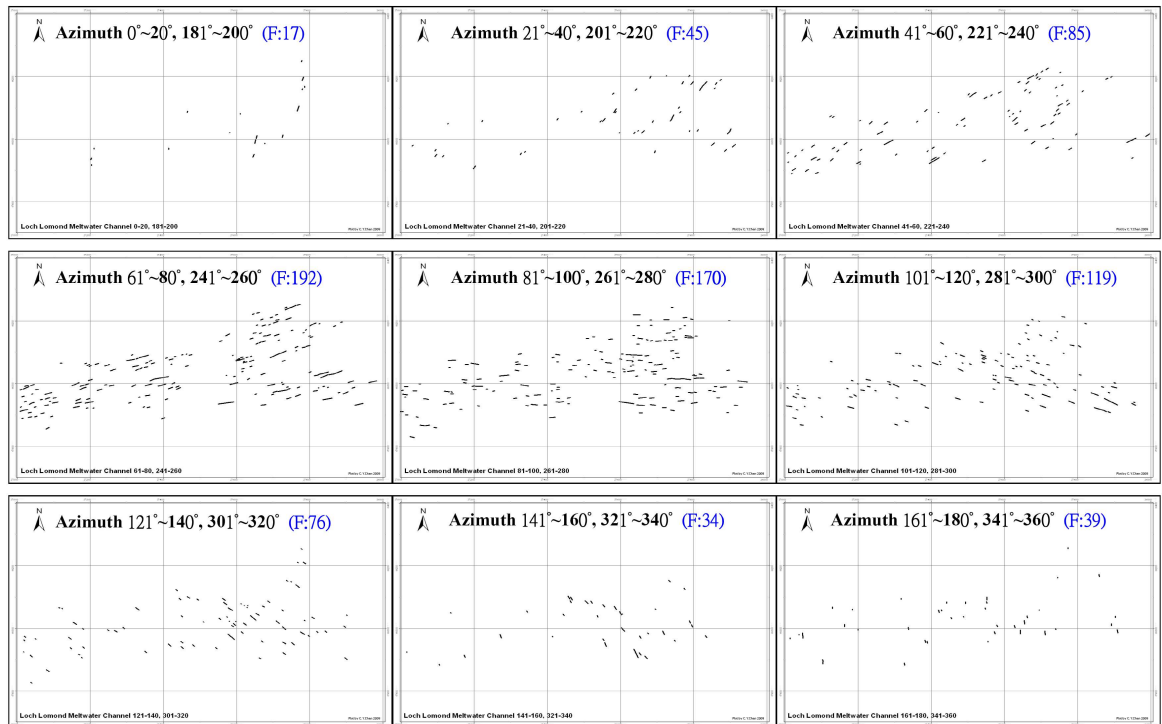
Counts	Minimum (m)	Maximum (m)	Mean (m)	Total Length (m)
777	10.69	433.65	85.77	66645.16

**Table 4.2 Frequency of each separated meltwater channel group's azimuth range**

Group	G1	G2	G3	G4	G5
<b>Azimuth</b>	0°~20° 181°~200°	21°~40° 201°~220°	41°~60° 221°~240°	61°~80° 241°~260°	81°~100° 261°~280°
<b>Orientation</b>	10°-190°	30°-210°	50°-230°	70°-250°	90°-270°
<b>Orthogonal</b>	100°,280°	120°,300°	140°,320°	160°,340°	180°,360°
<b>Frequency</b>	<b>17</b>	<b>45</b>	<b>85</b>	<b>192</b>	<b>170</b>
Group	G6	G7	G8	G9	
<b>Azimuth</b>	101°~120° 281°~300°	121°~140° 301°~320°	141°~160° 321°~340°	161°~180° 341°~360°	
<b>Frequency</b>	<b>119</b>	<b>76</b>	<b>34</b>	<b>39</b>	
<b>Orientation</b>	110°-290°	130°-310°	150°-330°	170°-350°	
<b>Orthogonal</b>	190°,20°	220°,40°	240°,60°	260°,80°	



**Figure 4.27 Frequency distribution of each azimuth group the properties of which are given in Table 4.2.**

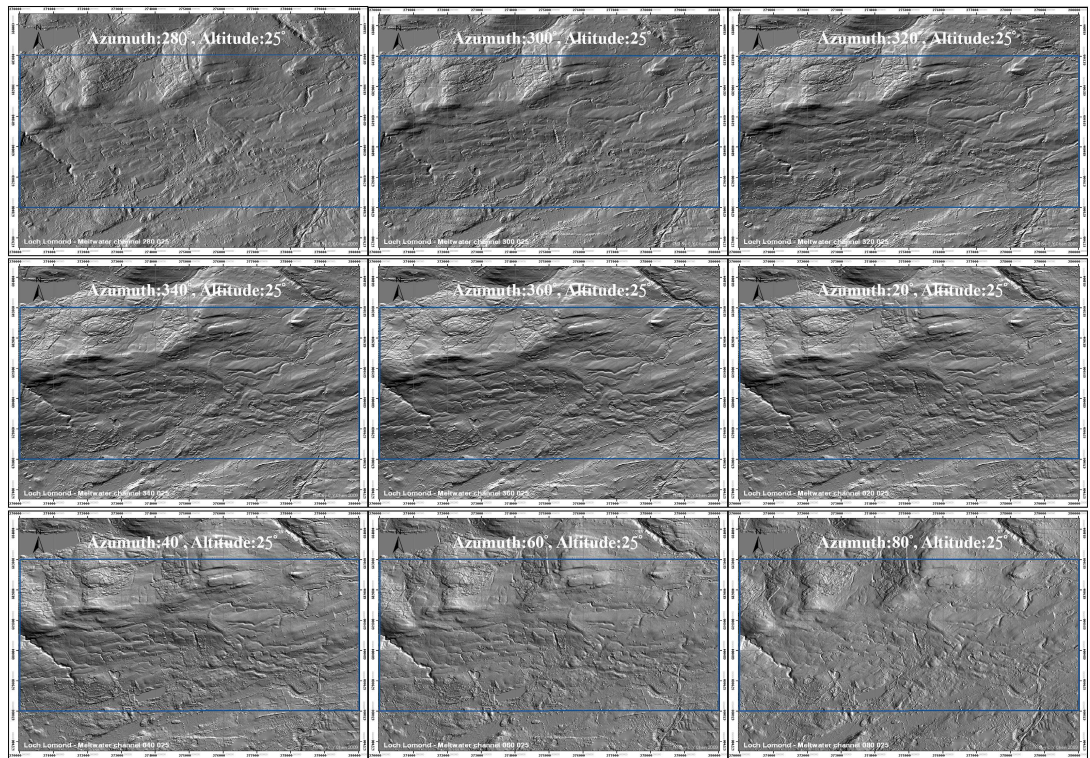


**Figure 4.28 Distribution and frequency of dissected meltwater channels. (F=Frequency)**

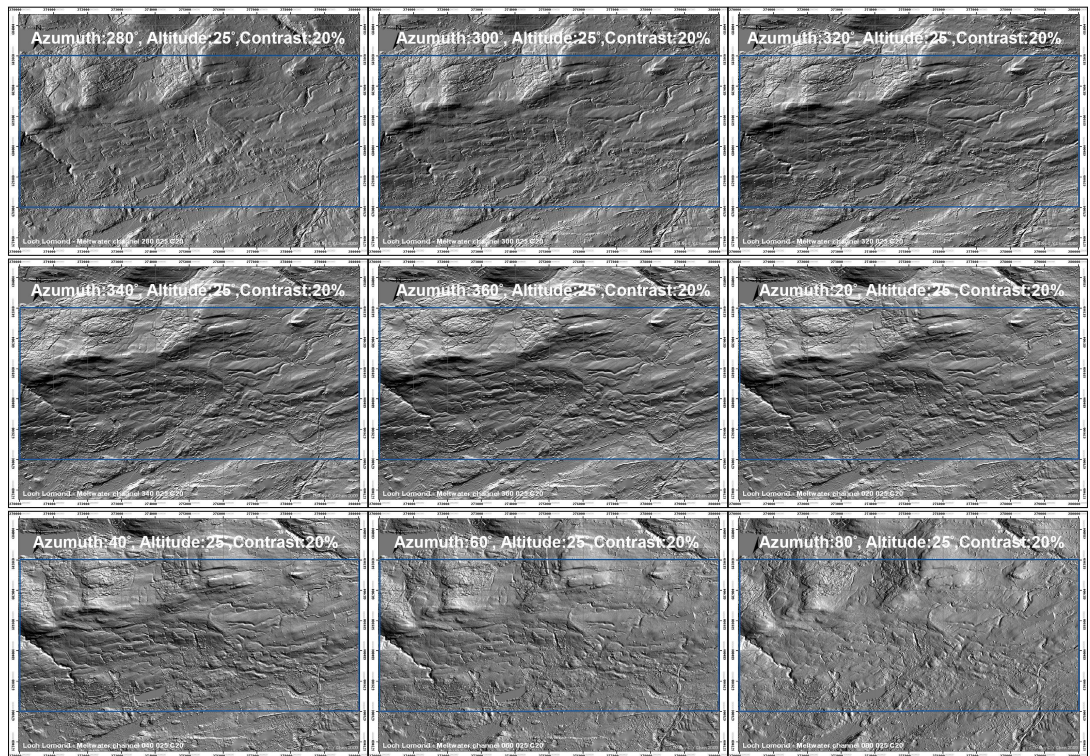
**Table 4.3 Comparison of main meltwater channel group with the other sub-groups**

<b>Azimuth</b>	41°~140° 221°~320°	Others	Sum
<b>Frequency</b>	630	147	777
<b>Length (m)</b>	56490.3 m	10154.87 m	66645.16 m
<b>Length (%)</b>	84.76%	15.24%	100%
<b>Frequency (%)</b>	81.08%	18.92%	100%

For linear landforms, the optimal light source angle for demonstrating or highlighting landforms should be orthogonal to the landforms under consideration. This means that the optimal image for representing landforms in a specific area needs a light source angle that is orthogonal or intermediate to the majority of landforms. In the case under consideration with the meltwater channels in the Campsie Fells, the optimal azimuthal angles are 350° and 170° (Figure 4.27, middle angle of G4 and G5). However, as the naked eye is used to/ familiar with a light source projecting from the front, it is recommended 350° should be used, but not 170°. Figures 4.29 and 4.30 are

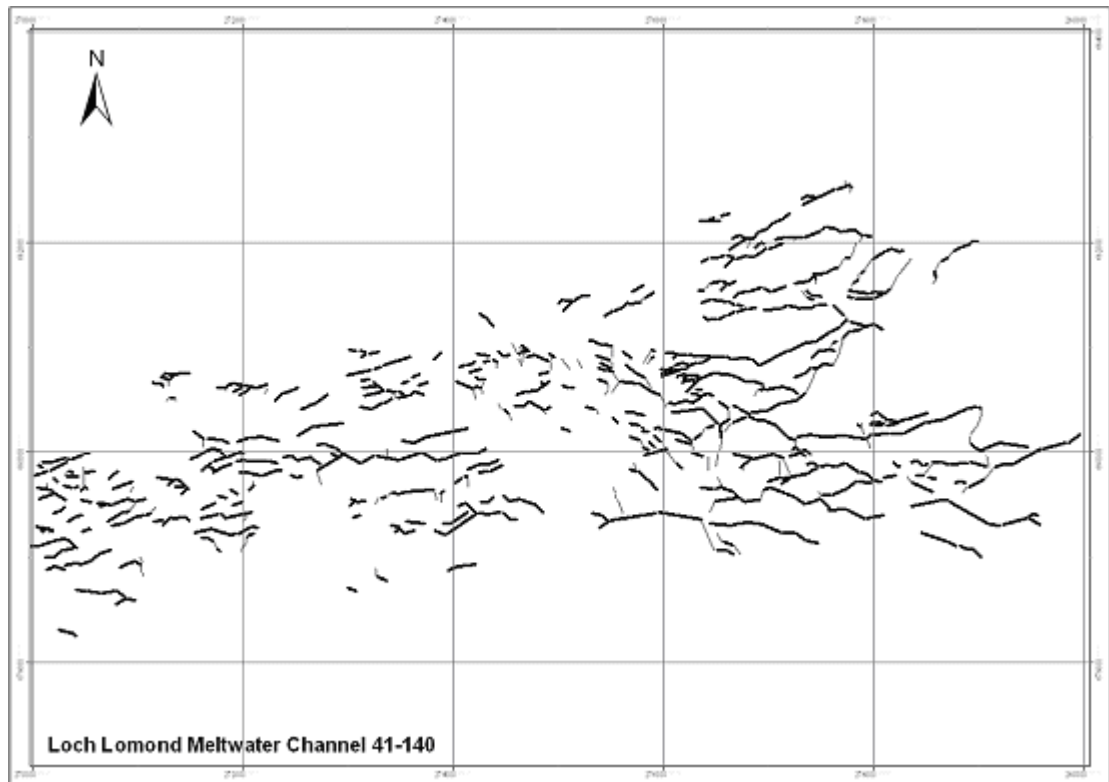


**Figure 4.29 Comparison of optimized image for each separated azimuth angle group. (Original). The area under consideration is the southeastern end of the Campsie Fells, north of Kilsyth.**



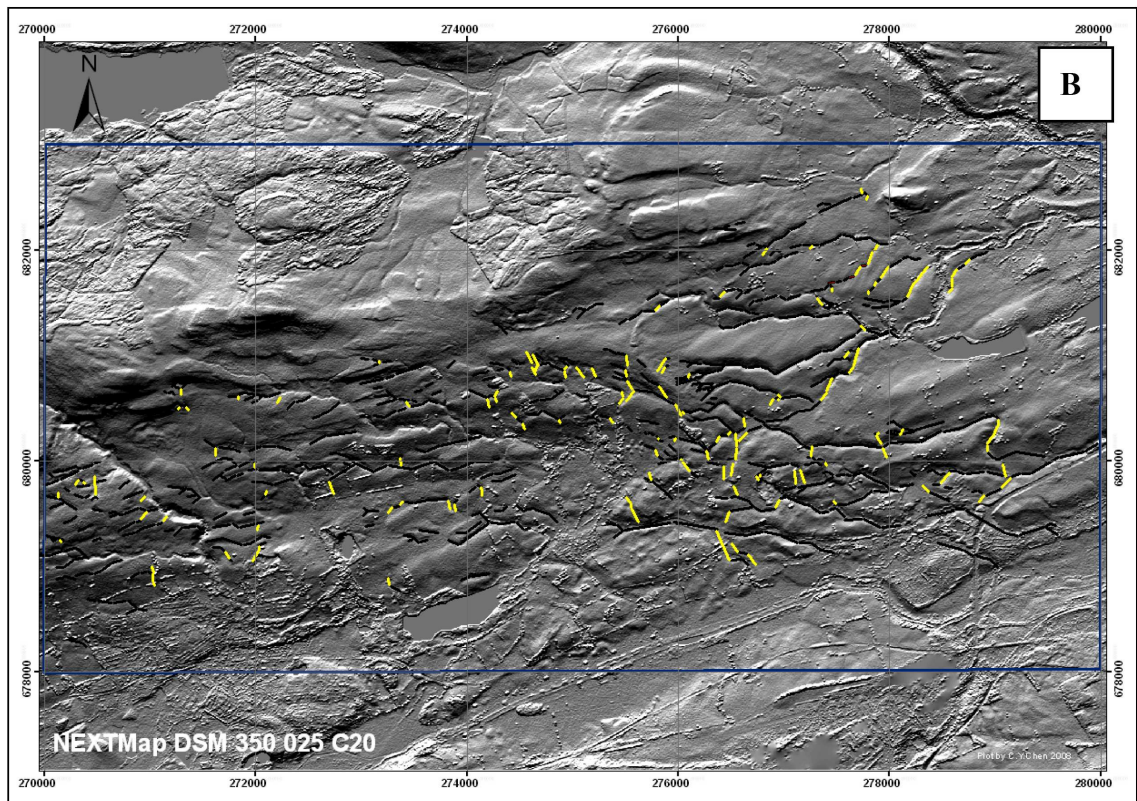
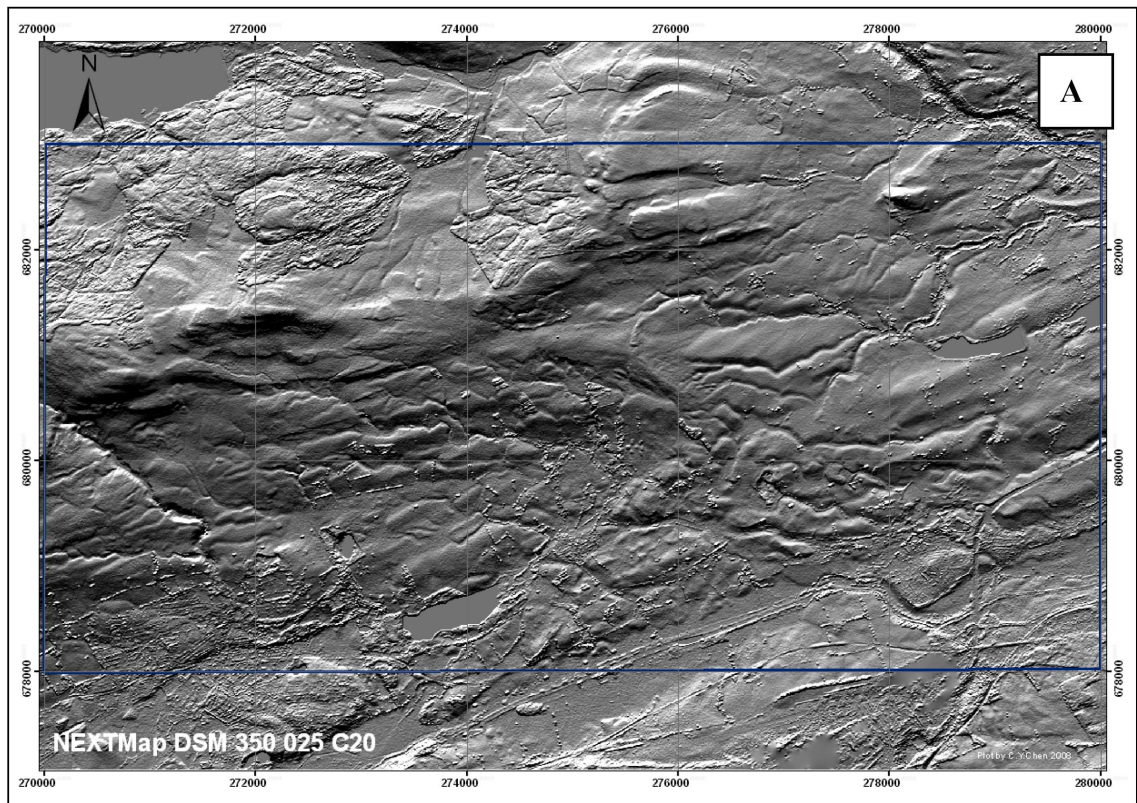
**Figure 4.30 Comparison of optimized image for each separated azimuth angle group. (With 20% contrast ratio). The area under consideration is the southeastern end of the Campsie Fells, north of Kilsyth.**





**Figure 4.31 Distribution of visible (in black) and poorly visible (in gray) meltwater channel sections. The area under consideration is the southeastern end of the Campsie Fells, north of Kilsyth and is shown in Figures 4.22, 4.23, 4.26, and 4.27.**

relief-shading imagery with orthogonal illumination angles for each separated azimuth angle group. Most of the meltwater channels were qualitative on images with illumination angles of  $320^{\circ}$ ,  $340^{\circ}$ ,  $360^{\circ}$ ,  $20^{\circ}$  and  $40^{\circ}$ . From amongst these, the image with  $360^{\circ}$  azimuth and  $25^{\circ}$  altitude illumination angle plus 20% contrast ratio is recommended for landform representation, because it generates the sharpest boundaries and can represent over 80% of the meltwater channel sections. Figures 4.31 and 4.32 demonstrate the orientation and visibility of the main and sub group of meltwater channel sections on the NEXTMap imagery. Meltwater channel sections with orientation (azimuth) angles from  $0^{\circ}\sim 40^{\circ}$ ,  $141^{\circ}\sim 200^{\circ}$  and  $341^{\circ}\sim 360^{\circ}$  may be difficult to see on relief shading image with  $360^{\circ}$  azimuth illumination angle due to their orientation being parallel to the light source. In this comparison, it is also found that



**Figure 4.32 Comparison of the visibility of meltwater channel section on NEXTMap. A is the original NEXTMap image; B is showing distribution of visible (black) and Poorly-visible (yellow) meltwater channels on NEXTMap image.**

channel sections with high relief from top and bottom were still clearly represented, although they do lose some of their visibility. Therefore, the true number of meltwater channels sections visible on NEXTMap is higher than the theoretically calculated number (84.76%).

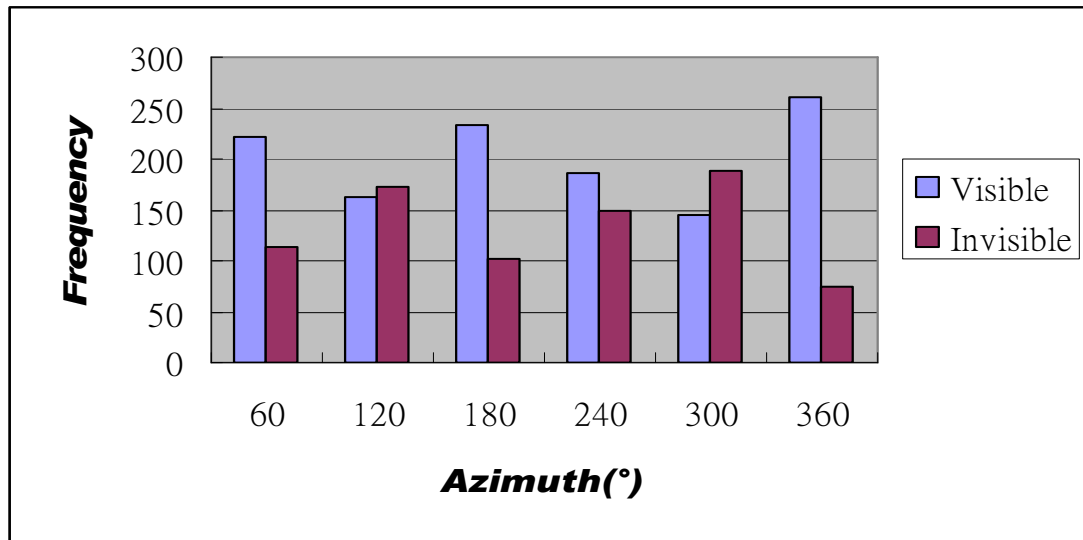
#### **4.4.2 Imagery mosaic method for representing landforms on a single image**

From the previous discussion we demonstrated and concluded that the rotating map method is the best way of mapping glacial and glaciofluvial landforms and is superior relative to all other methods. However, this kind of imagery can be only demonstrated in a digital environment. It is not practical to see illumination change effect on paper. Therefore, a simple and practical method which can demonstrate most of the landforms on a single image is necessary. In this part of the thesis, 334 drumlins that were mapped using the new mapping method in the southern Loch Lomond area will be studied further to develop this concept.

For the linear-like landform such as drumlins, the optimal light source angle necessary to demonstrate landforms is orthogonal to the lineament. However, in most situations a researcher will find that mapping targets have multi-orientations. Single imagery with single light source is therefore not sufficient. Using multi-light source in single image is the only way to represent landform objects properly.

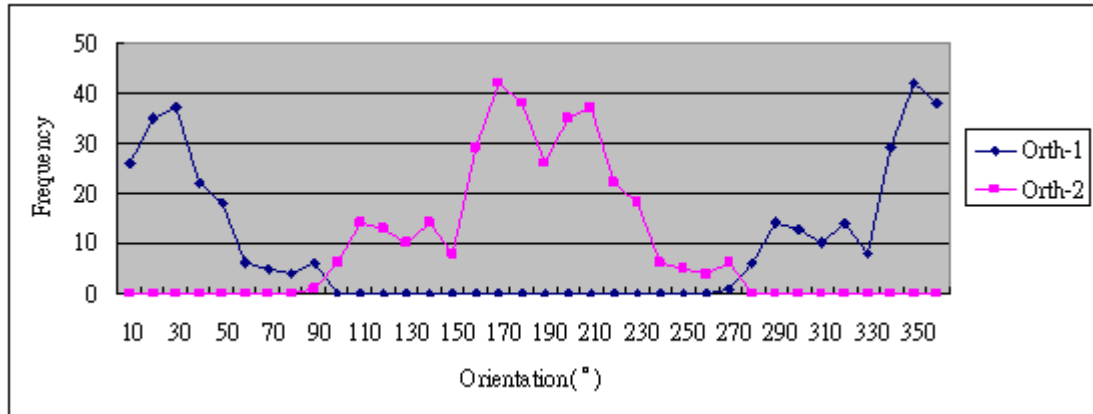
**Table 4.4. Frequency of visible drumlins observed by using light sources with a different azimuthal angle.**

<b>Azimuth</b>	<b>60°</b>	<b>120°</b>	<b>180°</b>	<b>240°</b>	<b>300°</b>	<b>360°</b>
<b>Visible</b>	222	162	234	186	146	260
<b>Invisible</b>	112	172	100	148	188	74



**Figure 4.33** Frequency distribution of the visibility of drumlins using different directions of light source.

Table 4.4 and Figure 4.33 illustrate the frequency distribution of the visibility of drumlins from different azimuth illumination angles. It is clear that the visibility of drumlins will change when the azimuth illumination angle changes. In this experiment, the poorest azimuth illumination angle can only represent 48.5% (162/334) drumlins while the best illumination angle enabled to represented 77.84% (260/334) of the drumlins. This result proves the importance of using a multi-directional light source in order to derive the best ground truth on a single image. From Figure 4.33 we can also observe an interesting phenomenon that the landform visibility improved when the light source is comes from top ( $270^{\circ}\sim 360^{\circ}$ ,  $0^{\circ}\sim 90^{\circ}$ ). In theory, linear features will have two orthogonal angles. Both angles should have equal visibility. Hence  $360^{\circ}$  should have the same frequency as  $180^{\circ}$  (same as  $300^{\circ}$  vs.  $120^{\circ}$ ;  $60^{\circ}$  vs.  $240^{\circ}$ ). However, the visibility with  $360^{\circ}$  light source increased 7.8% (26/334) relative to the visibility with  $180^{\circ}$ . In a similar fashion the visibility with  $60^{\circ}$  increased 10.78% (36/334) in comparison with  $240^{\circ}$ , but with a light source of  $300^{\circ}$  the visibility decreased 4.8% in comparison with the visibility derived from a light source with  $120^{\circ}$ . Although this phenomenon will need further investigation it is recommended that the analysis of



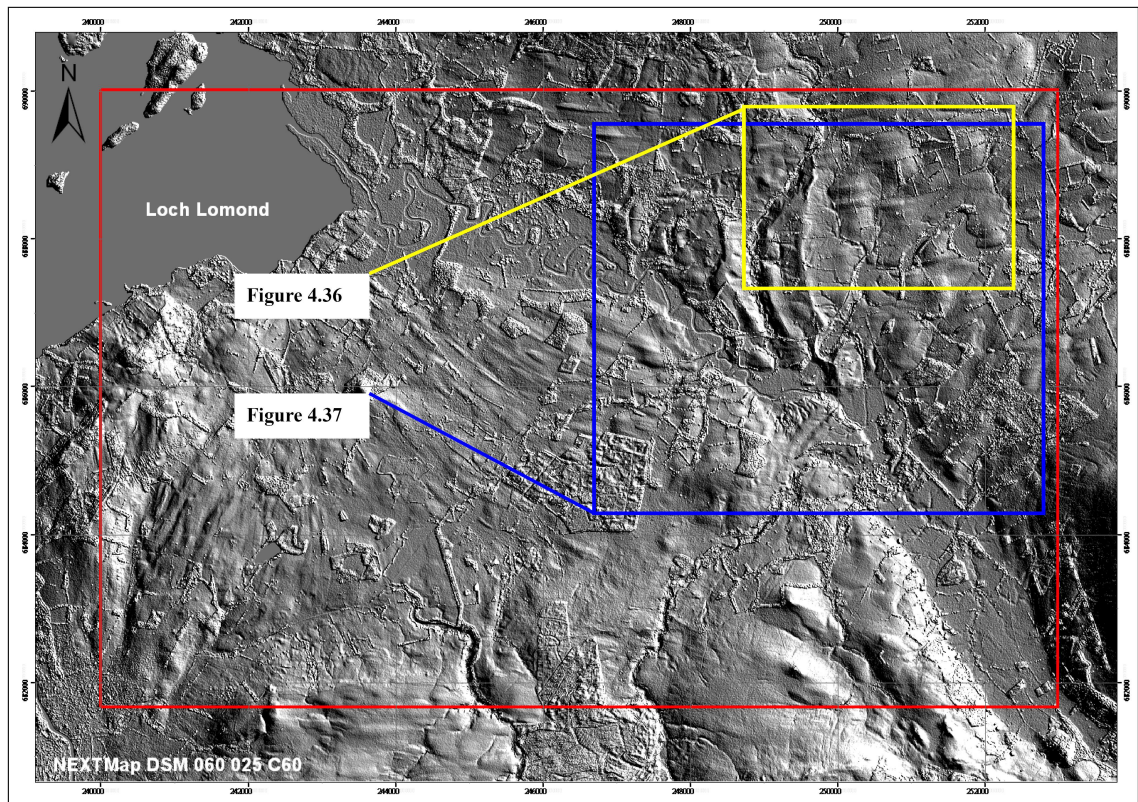
**Figure 4.34** Frequency of drumlins plotted against angles that or orthogonal to the trend of the lineament. The X axis is the illumination orientation angle in 10° intervals, the Y axis is the frequency of drumlins for each orthogonal angle.

landforms is best carried out with a light source from top, as this is the optimal azimuth illumination angle. Furthermore, because this aspect fits in with natural vision using the naked eye there is greater potential to get higher visibility.

From Figure 4.34 it is possible to observe that light source Orth-1 located between 90°-270° and light source Orth-2 located between 270°-90° and the whole data is divided into two main groups. For example in the Orth-1 data set, illumination angles from 270°~330° can be identified as a small group, whereas the angles from 340°~040° is the main group. The highest frequency of single illumination angle is located on 170° and 350°, yet the lowest frequency is located on 90°- 100° and 270°-280°.

For the single light source imagery, 170° and 350° seems to fit the demand best as these illumination angles have the highest frequency. I would like to suggest 10° should be chosen as the illumination angle setting for the single light source imagery. The reasons are as follow:

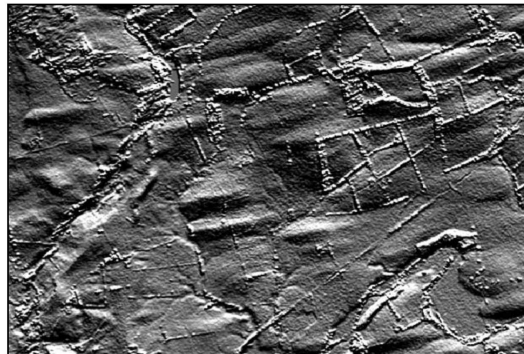
1. According to author's experience, the acceptable visualization tolerance is  $\pm 30^\circ$  spanning from the main orthogonal angle for the landform (Figure 4.35 and 4.36). The illumination range (orthogonal  $\pm 30^\circ$ ) which contains most landforms will be treated as the optimal illumination angle. In this case, optimal choices are  $190^\circ$  and  $10^\circ$ .
2. Our naked eye is used to and expects to see the light source come from the front or top part ( $270^\circ \sim 90^\circ$ ) of the imagery. Imagery with light source from back (bottom) will make terrain appear up-side-down. Valley bottom and hill top will look completely reversed (Figure 4.37). Hence,  $10^\circ$  is more suitable than  $190^\circ$ .



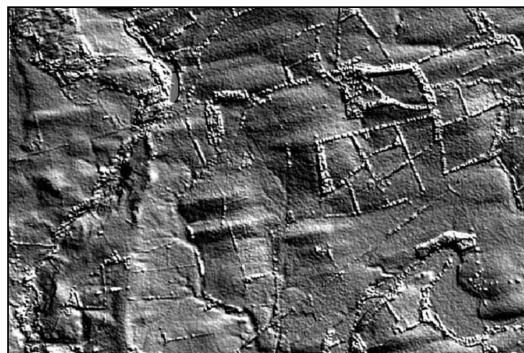
**Figure 4.35** Location of Figure 4.36 and 4.37 in southeastern corner of the Loch Lomond basin.



Azimuth 340°, Altitude:25°

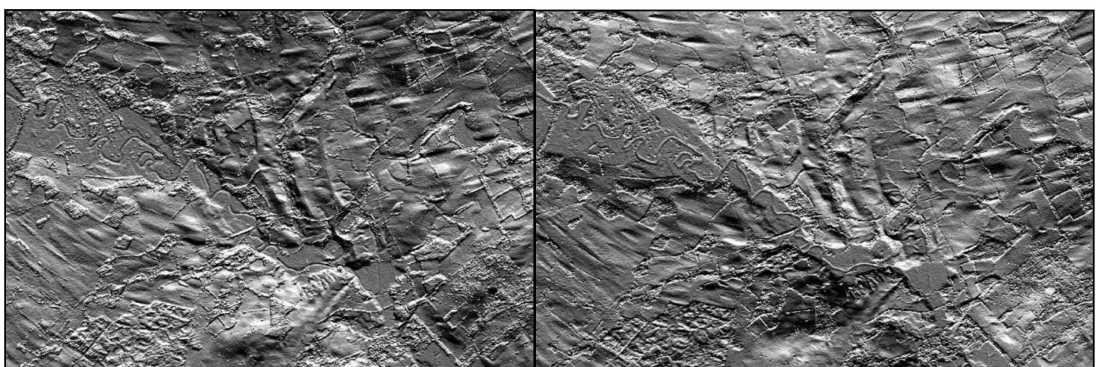


Azimuth 10°, Altitude:25°



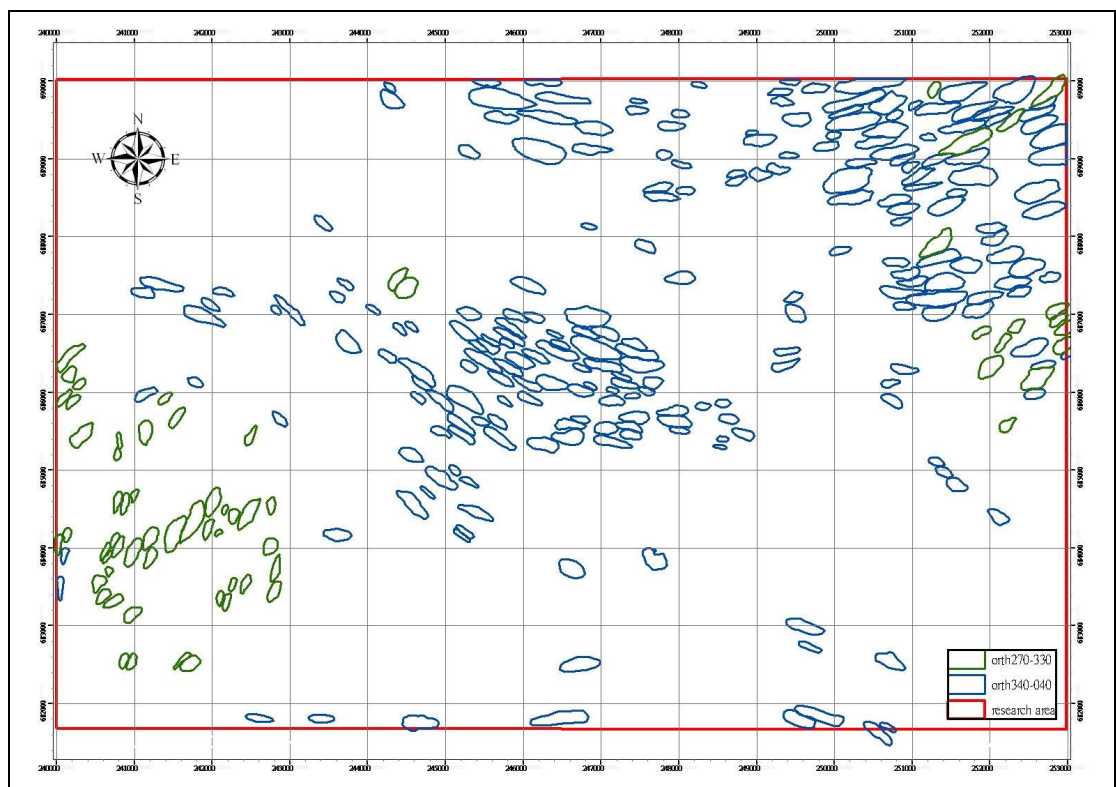
Azimuth 40°, Altitude:25°

**Figure 4.36 Illumination tolerance testing. Landforms visibility changes within  $\pm 30^\circ$  spans from the main orthogonal angle to the drumlins (Azimuth:  $10^\circ$ ) (also see Figure 4.34). The area represented is to the east of Drymen in the southeastern corner of the Loch Lomond basin in western central Scotland**



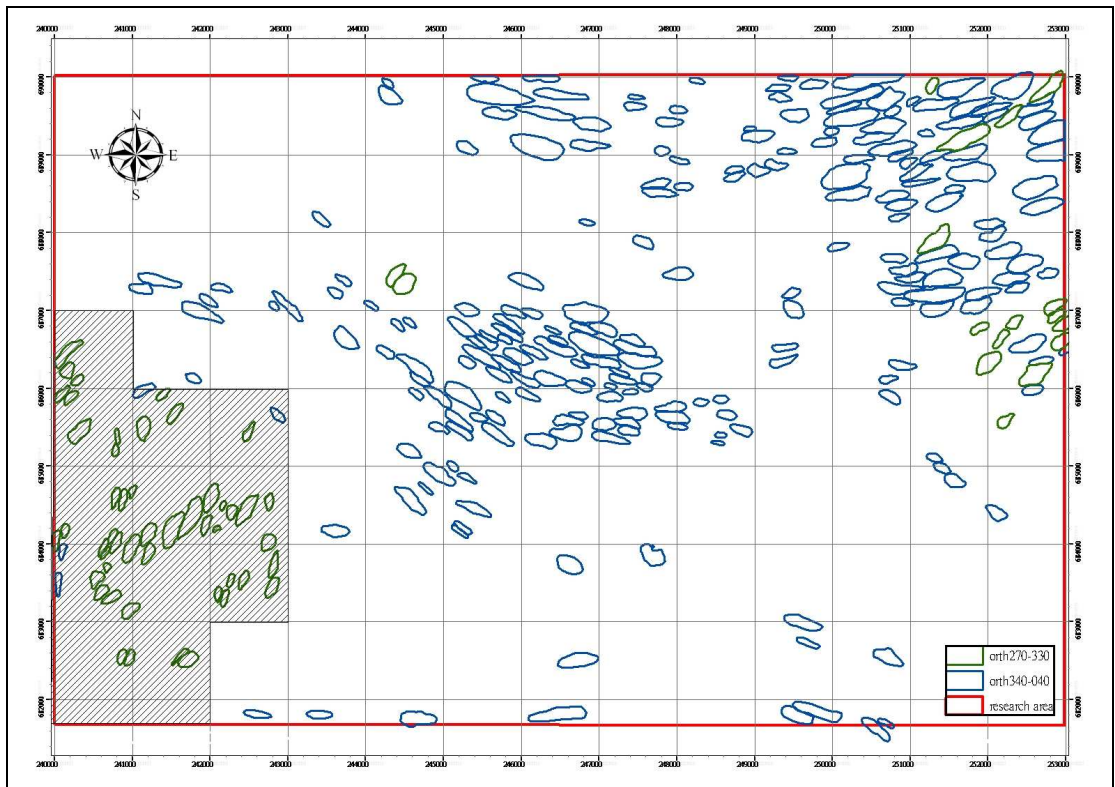
**Figure 4.37 Comparison of light from top ( $10^\circ$ ) and bottom ( $190^\circ$ ). The area represented is to the east of Drymen in the southeastern corner of the Loch Lomond basin in western central Scotland**

Figure 4.38 represented the main pattern of landforms in this study area. One group (in blue, in the northeastern corner of the figure) trend west to east which is in the direction of glacier movement during LGM. A second group (in green and blue) which trend north to south and northeast to southwest respectively was formed by the YD glaciation within this area (Rose, 1981, 1987, 1989; Rose and Smith, 2008). Since landforms have two main orientations, it is impossible to represent both groups by using single light source within single imagery. To solve this problem, two images with different light sources ( $10^\circ$  for blue group and  $300^\circ$  for green group) were used (merged) to derive a multi-light sources imagery. The  $10^\circ$  illumination was treated as base imagery for it has the orthogonal light source for the blue group of landforms.

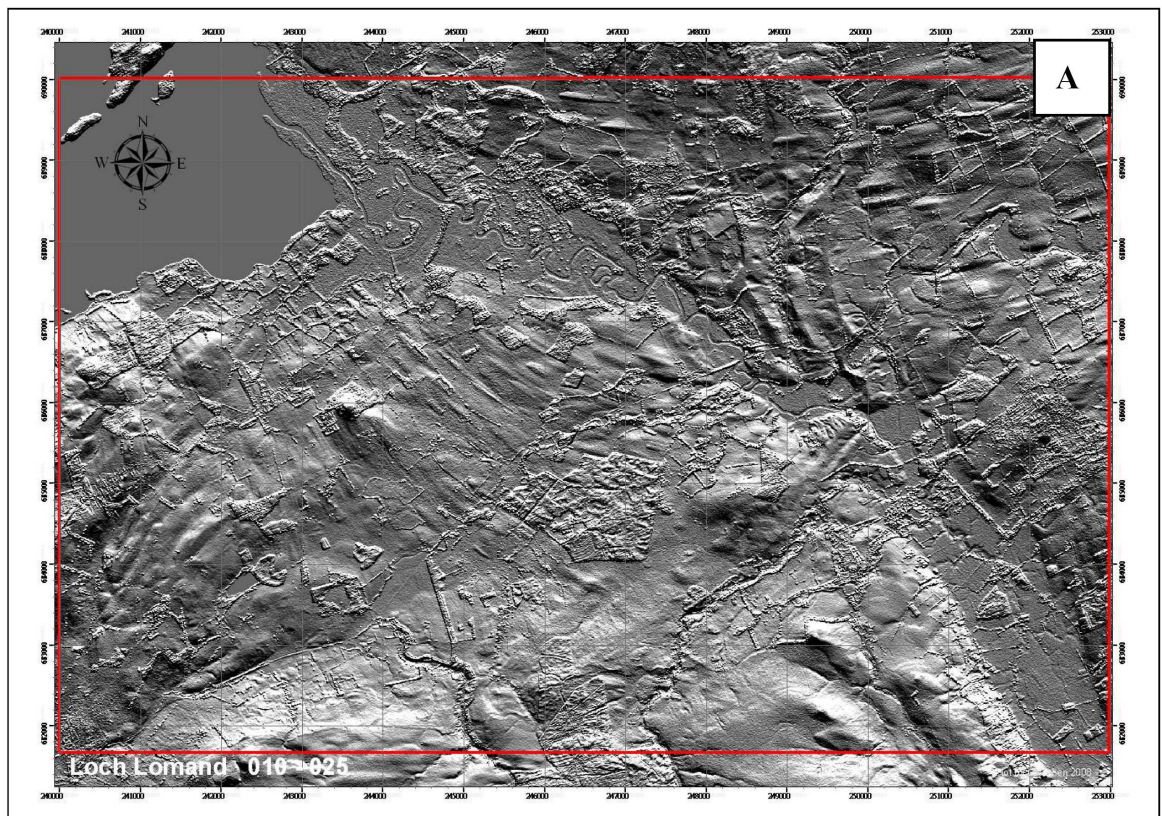


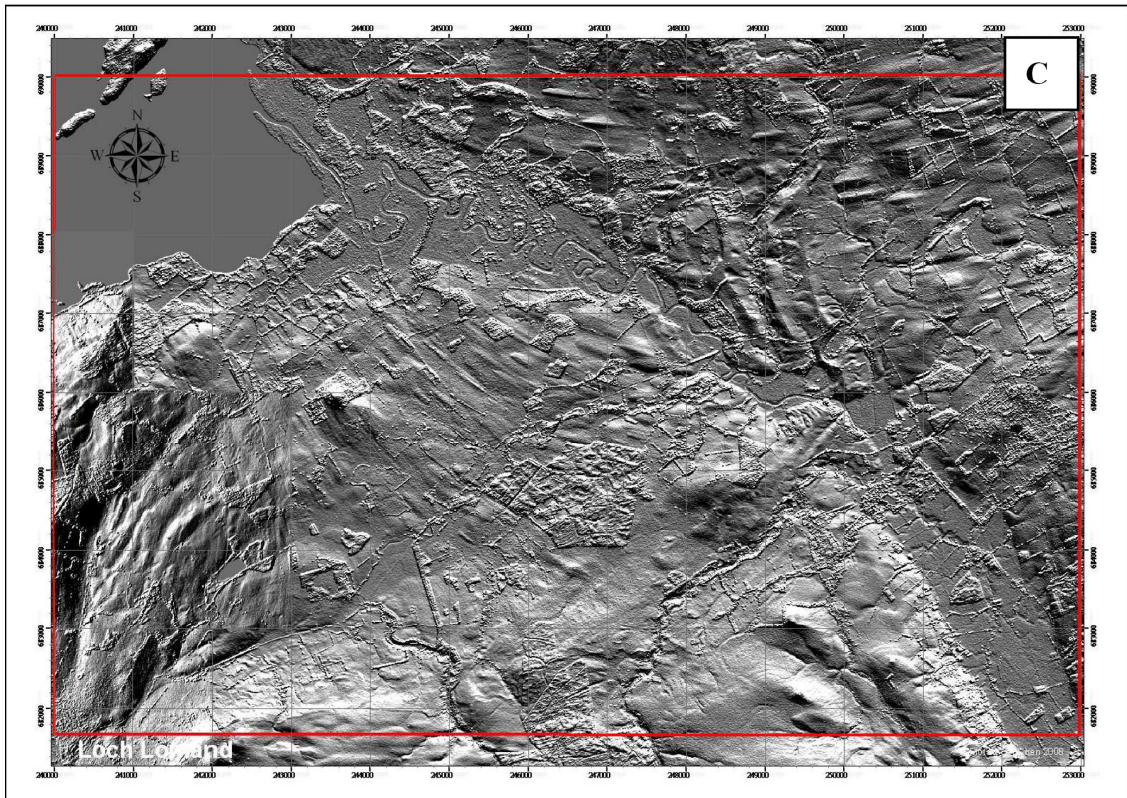
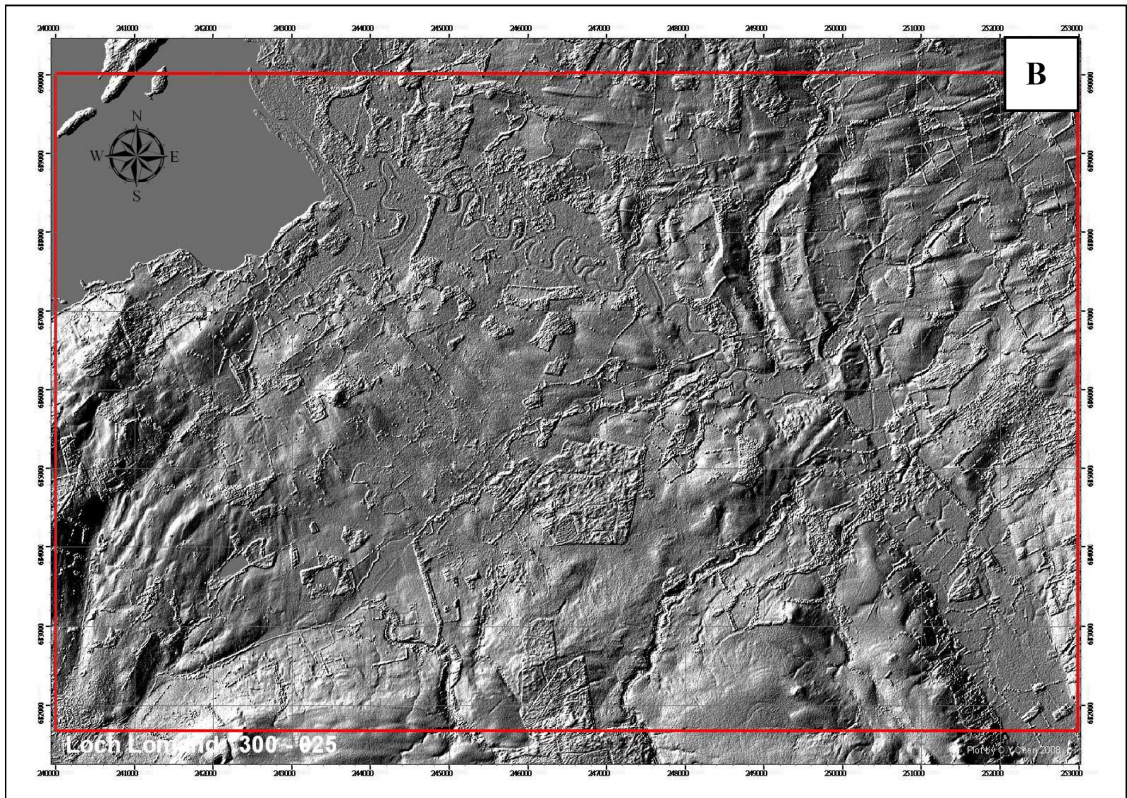
**Figure 4.38 Distribution of two main drumlin groups. (Blue group's azimuth:  $340^\circ\sim 40^\circ$ , Green group's azimuth:  $270^\circ\sim 330^\circ$ . The area represented is in the southeastern corner of the Loch Lomond basin in western central Scotland)**





**Figure 4.39** Illustration of merged part (hatched block). The area represented is in the southeastern corner of the Loch Lomond basin in western central Scotland.





**Figure 4.40 Comparison of the original imageries (A and B) with merged imagery C. Illumination setting are: A. Azimuth:10°, Altitude:25°, Contrast:60%; B. Azimuth:300°, Altitude:25°, Contrast:60%; and C. Azimuth: 10°+300°, Altitude: 25°, Contrast: 60%**

Part of 300° illumination imagery was taken (hatched parts, shown on Figure 4.39) and merged onto the base imagery. Figure 4.40 illustrates the mosaic imagery (C) in comparison with the original imagery. Obviously, the mosaic imagery can clearly represent more drumlins than imagery without this process. This method can be used without the rotating map and is suitable for use in a paper report.

#### **4.5 Conclusions and Recommendations**

- 1.** The rotating map with constantly changing illumination azimuth can not only provide a full, visual, depiction of landform information, but also be used as a mapping result testing platform to check the accuracy of the boundaries of mapped landform.
- 2.** The new mapping procedure and method proposed in this research has higher landform detecting ability relative to other methods that use orthogonal illumination, parallel illumination and intermediate illumination imagery for mapping. It is also more efficient and economic than ground survey mapping.
- 3.** The new NEXTMap rotating map, mapping system performs well with drumlins, kames and meltwater channels, but less satisfactory when applied to landforms that do not have distinct relief variation or clear boundaries (such as some kettle holes in the study area which are invisible on the rotating map). It is not recommended for mapping hummocky moraines directly from NEXTMap due to the image resolution, but NEXTMap can be used as a base map for detailed field survey.
- 4.** Mosaic imagery allows the user to improve the landform representation of a complex region where errors may be caused by illumination azimuth bias, and it is recommended that this method should be used to derive a base map for subsequent research.

## 5. Background to the Glen Roy area

---

### 5.1 Introduction

Glen Roy, located in the Lochaber region of Scotland (Figure 3.6, Figure 5.1), is a critical location for understanding Late Pleistocene environmental developments in the UK. Most scientific interest has focussed on the unique geomorphological and sedimentological evidence for cooling during the Loch Lomond Stadial (broadly comparable with the Younger Dryas/GS-1) found in records obtained from the area, which have led to a number of important conclusions. Firstly, both empirical and modelling evidence suggests the area occupied an important position with respect to maximal Loch Lomond Readvance ice limits (Sissons 1979b; Peacock and Cornish 1989; Hubbard 1999; Golledge 2008). Secondly, the region has three well-defined, ice-dammed lake shorelines associated with lakes impounded by the Loch Lomond Stadial ice advance, and when combined with sedimentological evidence allows the transient position of the ice margin and associated lake surface areas to be accurately defined (Palmer 2008b). Finally, varved lake sediments found in this valley and neighbouring Loch Laggan allow the duration of each lake system to be estimated more precisely than is the case for other former ice-dammed lakes in the Scottish Highlands (Palmer 2005, 2008b, 2010). These elements in combination allow Quaternary Scientists to calculate when the local ice margin position was attained, the duration of the lake systems, and by implication the rate of ice advance and retreat. This is a unique situation in the Scottish Late Pleistocene.

This chapter will introduce the location, topography and geological context of the Glen Roy area. Scientists have been drawn to this area for over 250 years, and because of its importance in the development of scientific ideas since the dawn of the Glacial Theory, a summary is provided of key researchers and developments, with specific reference to

the glacial evidence in the Glen Roy area. This leads in to a more detailed explanation of late 20<sup>th</sup> century thinking about the sequence of events in the area, which hinges on a model of landscape evolution proposed by Sissons in a series of papers published during the 1970's and 1980's, and referred to as the 'Sissons model' throughout this thesis (Sissons 1977, 1978, 1979a, 1979b, 1979c, 1981a, 1981b, 1983; Sissons and Cornish 1982a, 1982b). This model is widely recognised as the best available explanation of the detailed evidence, and underpins contemporary studies and interpretations. Outlining this model and its geomorphological context therefore provides key contextual information for the features and experiments reported in Chapters 6, 7, and 8 of this thesis, which test the applicability and reliability of the use of NEXTMap DEM data for geomorphological mapping. The details of the drainage catchments and the overall topography of the area are important for understanding glacier and lake changes discussed in later chapters.

## **5.2 Site location and bedrock geology**

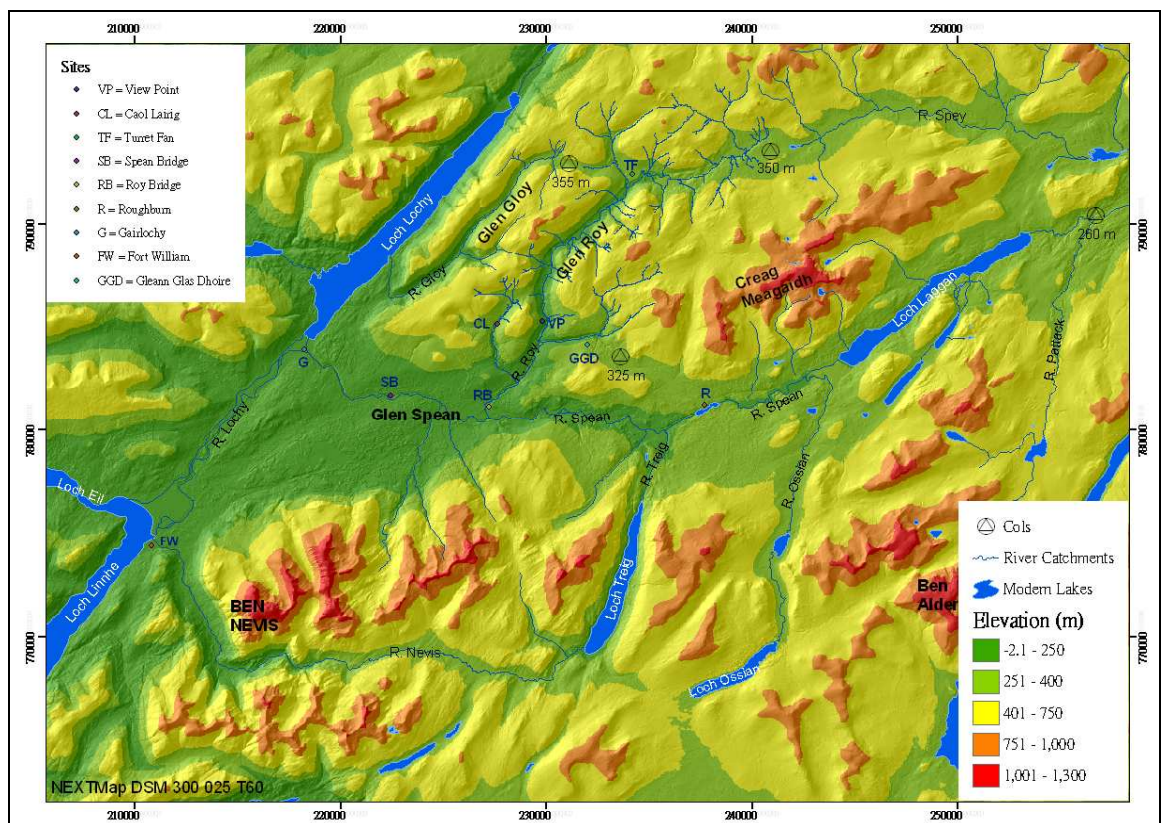
The sites studied are in the Lochaber region, Western Highlands of Scotland (Figure 3.6, Figure 5.1). Fort William and the mountain range of Ben Nevis lie 15 km to the southwest of the study area, which consists of Glen Roy, Glen Gloy and Glen Spean. The research presented in the following chapters concentrated on the Roy valley, but some elements also require knowledge of features in the Gloy and Spean valleys. Glen Roy itself is approximately 14 km in length, less than 1 km in width and trends in a NNE to SSW direction, parallel to the Glen Gloy valley. The Spean catchment is the dominant river system in the area, flowing broadly from east to west with headwaters rising on the northern flanks of Ben Alder coalescing to form the River Pattack which flows from north to south to enter Loch Laggan. The Spean river flows from the western end of Loch Laggan and eventually drains into Loch Lochy to the west. The

watershed to the Spey system lies to the east of Loch Laggan between the Pattack and Mashie rivers. The Roy is a north bank tributary of the Spean with the water rising at the head of the valley, which also forms the watershed to the Spey catchment. The River Gloy is the only main river in the Gloy discharge system; it flows south-westwards from the head of the Glen Gloy valley, turns abruptly north at the southern entrance of Glen Gloy to drain into Loch Lochy. Major south-bank tributaries of the River Spean include the rivers Ossian and Treig.

The bedrock geology of the Glen Roy area (Figure 5.2) predominantly consists of the appin and grampian groups of the precambrian (moinian) metamorphics, which trend in a SW-NE direction across the region. Psammite and semipelitic formations extend from the southern part of Caol Lairig to Allt Bhreac Achaidh and into the parts of the valley floor in Upper Glen Roy. Bounding Glen Roy to the NW is a quartzitic formation, which is found in areas around the Turret Fan and Glen Fintaig. To the east of Glen Roy, and including areas around the Viewpoint, Gleann Glas Dhoire, Canal Burn, Burn of Agie and to the north of Glen Roy, are the appin group of rocks dominated by pelites, calcsilicate rock and psammites. The rocks underlying the majority of the Glen Gloy valley are of the psammite and semipelite formation of the grampian group, but this is intruded by a 380~440 m wide quartzite formation (grampian group) branch that extends from the middle to the north of the valley.

A number of faults have been mapped on the *DiGMapGB-625-Bedrock geology v.5* map (Figure 5.2). However, these do not include faults, such as the Glen Gloy and Glen Fintaig Faults, identified by Key *et al.* (1997). They suggested that the Glen Gloy Fault contains at least three sections (No.1~3 in Figure 5.2), trending in a NNW-SSE direction. This fault is exposed in a stream on the north side of the glen and extends to dykes at the southern side of the glen (No. 2-3), although these are not precisely aligned

to one another. Ringrose (1987) and Sissons and Cornish (1982a and 1982b) identified a fault scarp in the middle of Glen Roy, which is suggested to be a further southern extension of this fault system (blue rectangle, Figure 5.2). However, Fenton and Ringrose (1992) and Key *et al.* (1997) argue that these dislocations are not true fault scarps but are due to block movements along pre-existing fractures above an active fault. The Glen Fintaig Fault is composed of two large ESE trending parallel faults (Nos. 4 and 5, Figure 5.2) on the south side of Glen Fintaig. These two faults are 130 m apart and dip to the NNE direction at  $70^{\circ}$ – $80^{\circ}$ .



**Figure 5.1** Topographic map of Glen Roy, Glen Gloy and the Glen Spean valley, constructed in the present project using NEXMap.

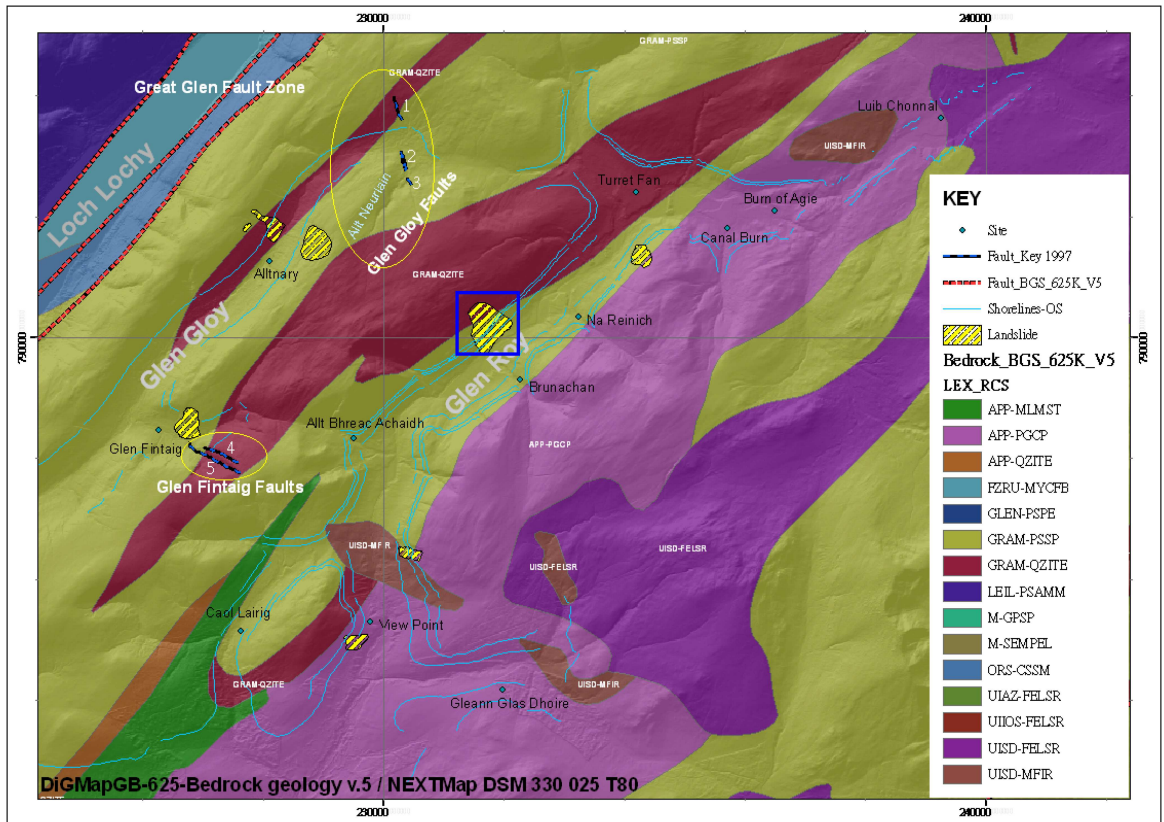


Figure 5.2 Geology map of the Glen Roy area based upon DiGMapGB-625-Bedrock geology v.5 (March 2010), with permission of the British Geological Survey. Ringrose (1987) and Sissons and Cornish (1982a and 1982b) claimed there is a fault scarp within the blue rectangle box, an observation doubted by Fenton and Ringrose (1992) and Key *et al.* (1997).

Table 5.1 Catalogue of the symbols used in Figure 5.2, extracted from the DiGMapGB-625-Bedrock geology v.5 (March 2010) table layer.

LEX_RCS	LEX_D	RCS_D
APP-MLMST	APPIN GROUP	METALIMESTONE
APP-PGCP	APPIN GROUP	GRAPHITIC PELITE, CALCAREOUS PELITE, CALCILICATE-ROCK AND PSAMMITE
APP-QZITE	APPIN GROUP	QUARTZITE
FZRU-MYCFB	FAULT ZONE ROCKS, UNASSIGNED	MYLONITIC-ROCK AND FAULT-BRECCIA
GLEN-PSPE	GLENFINNAN GROUP	PSAMMITE AND PELITE
GRAM-PSSP	GRAMPIAN GROUP	PSAMMITE AND SEMIPELITE
GRAM-QZITE	GRAMPIAN GROUP	QUARTZITE
LEIL-PSAMM	LOCH EIL GROUP	PSAMMITE
M-GPSP	MOINE SUPERGROUP	GNEISSOSE PSAMMITE AND GNEISSOSE SEMIPELITE
M-SEMPEL	MOINE SUPERGROUP	SEMIPELITE
ORS-CSSM	OLD RED SANDSTONE SUPERGROUP	CONGLOMERATE, SANDSTONE, SILTSTONE AND MUDSTONE
UIAZ-FELSR	UNNAMED IGNEOUS INTRUSION, NEOPROTEROZOIC	FELSIC-ROCK
UIIOS-FELSR	UNNAMED IGNEOUS INTRUSION, ORDOVICIAN TO SILURIAN	FELSIC-ROCK
UISD-FELSR	UNNAMED IGNEOUS INTRUSION, LATE SILURIAN TO EARLY DEVONIAN	FELSIC-ROCK
UISD-MFIR	UNNAMED IGNEOUS INTRUSION, LATE SILURIAN TO EARLY DEVONIAN	MAFIC IGNEOUS-ROCK



### **5.3 Early studies in the Glen Roy area**

Detailed study of the Glen Roy valley was initially aroused by the discovery of the phenomena of the Parallel Roads in the 18<sup>th</sup> Century by Thomas Pennant and has continued until the present day. Research over this time period can be divided into three main periods: 1) 1771-1840 with the early analysis and theories for the formation of the Parallel Roads; 2) 1840-1900 with the acceptance of the Glacial Theory and emerging ideas using the glacial theory paradigm; and 3) 1900- 2011 with considerable refinement of ideas within the context of the Loch Lomond Readvance. The key contributions of individual researchers are summarised in Table 5.2.




The first period is dominated by arguments concerning the formation of the parallel roads by marine or lacustrine processes. Those who favoured a lacustrine explanation could not explain the absence of obvious barriers to impound lake waters. Conversely, the marine theory, which was expounded by Darwin (1839), could not explain the lack of shorelines at the same altitude in other valleys of western Scotland that were open to marine incursion, nor the lack of marine fossils on any of the shorelines. It was not until Agassiz (1840) visited the area when examining other regions for evidence of glacial activity that the lost barriers could be explained by the former presence of glacier ice that created a glaciolacustrine system that led to the formation of the parallel roads. Darwin continued to hold onto his marine model, but was eventually persuaded of the more credible attributes of the ice-dammed lake theory by 1863.




The second period of research development in Glen Roy was from 1840-1900, with notable contributions from Thomas Jamieson (1863, 1892) and Joseph Prestwich (1879). Jamieson (1863) developed Agassiz's ideas and proposed that ice developed in the Nevis Range, flowed north and blocked the drainage of the River Roy. The resultant proglacial lake surface, identified by the distribution of the parallel roads, attained

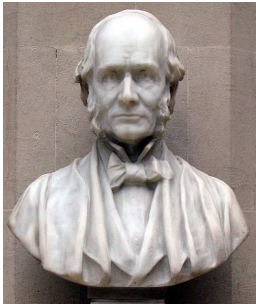

altitudes based on the height of overspill cols adjacent to the valley. Jamieson (1863) also observed that evidence for the former ice masses was concentrated on the western side of the highlands, and he therefore inferred that a strong precipitation gradient from west to east favoured ice sources in the Nevis Range, which were nourished by moisture delivered from the Atlantic Ocean.

Further developments were catalysed by the publication of the first Ordnance Survey 6-inch topographic maps of the Glen Roy area, which provided the first accurate survey of the Parallel Roads. Prestwich (1879) was the first to use the data to discover that the Parallel Roads apparently had uneven altitudes, with variances of up to 15 feet. He argued that the variability was caused by slippage of valley-side debris from either material brought down from above on to the Parallel Road surfaces, or by collapse of the debris of which the 'Roads' were formed. Jamieson (1892) re-evaluated Prestwich's claims using the same OS data and concluded that the variance in heights could be explained by a lack of consistency in the exact positions from which measurements of the shoreline surfaces had been taken, which are affected by different thicknesses of peat cover. Jamieson (1892) suggested that this could be resolved by a more detailed systematic survey of the shorelines that made allowance for such factors. This recommendation was not taken up until Sissons published a series of highly influential papers in the 1970's and 1980's, which established the basis of current ideas for this locality. The following section concentrates on these more recent ideas, which more directly relate to the aims and objectives of this PhD project.

**Table 5.2 Important field investigators and their contributions to the development of ideas on the formation of the Parallel Roads of Glen Roy**

Name	Time	Reference	Contribution
<p>Thomas Pennant</p> 	1771	<i>A Tour in Scotland 1769</i>	The oldest published record that mentions the “Parallel Roads of Glen Roy”, which drew other scientists’ attention to the phenomena in Glen Roy.
<p>Thomas Dick Lauder</p> 	1823	<i>On the parallel roads of Lochaber. Transactions of the Royal Society of Edinburgh v.9 p.1-64</i>	<ol style="list-style-type: none"> <li>1. Levelled the 355 m shoreline in Glen Gloy and found it to have exactly the same level as the Gloy/Roy col (355 m) at the head of Glen Gloy (Figure 5.3A).</li> <li>2. Found the 350 m shoreline in Glen Roy to be on a level with the Roy/Spey col (350 m) at the NE head of Glen Roy. He suggested that water of the former 350 m lake in Glen Roy overflowed the Roy/Spey col into Glen Spey to the east.</li> <li>3. He identified the 260 m Pattack/Mashie col and suggested it was the overflow route of the former 260 m lake in Glens Spean and Roy.</li> </ol>
<p>Charles Darwin</p> 	1839	<i>Philosophical Transactions of the Royal Society of London, Vol.129, 39-81.</i>	Observed the Parallel Roads of Glen Roy, and other parts of Lochaber. He initially suggested that the roads were formed by marine processes (Figure 5.3B), but subsequently became persuaded by the glacial theory of Agassiz and a glacial explanation for the parallel roads.

<p>Louis Agassiz</p> 	<p>1840</p>	<p><i>Proceedings of The Geological Society of London v.III (Nov. 1838 to June 1842), Part II (1840-1841), no.72 p.327-332</i></p>	<ol style="list-style-type: none"> <li>1. Used evidence in Scotland to support his glacial theory, which included observations of landforms in the Glen Roy-Loch Treig area (Figure 5.3C). Made comparisons with similar features associated with ice-dammed lakes in Switzerland.</li> <li>2. Crucially, was the first proponent of the theory that the parallel roads recorded the former existence of ice-dammed lakes.</li> </ol>
<p>David Milne</p> 	<p>1847</p>	<p><i>On polished and striated rocks, lately discovered on Arthur Seat, and other places near Edinburgh. Edinburgh New Philosophical Journal 42: 154-72</i></p>	<p>Discovered the 325 m Roy/Laggan col in Glen Roy which went unnoticed in Lauder's (1823) work. He concluded that the water of the former 325 m lake in Glen Roy overflowed this col into Glen Spean (Figure 5.3A)</p>
<p>Thomas Jamieson</p> 	<p>1863</p>	<p><i>Quarterly Journal of the Geological Society, V. 19, 235-259</i></p>	<ol style="list-style-type: none"> <li>1. The first scientist to propose a sequence of events that accounted for the formation of the roads and which integrated the presence of the overspill cols into the theory (Figure 5.3D).</li> <li>2. He claimed that the lakes formed during the last time that ice occupied the Scottish Highlands.</li> <li>3. He noted that a precipitation gradient from west to east could explain the configuration of ice growth, which left the contemporaneous Upper Roy and Spean valleys ice-free.</li> <li>4. He suggested that</li> </ol>

			<p>moisture-bearing winds from the Atlantic nourished ice that developed in the Ben Nevis Range and which was the source of ice entering the Spean valley from the west. He also noted that the surface altitude of the ice declined eastwards from that range.</p>
<p>Joseph Prestwich</p> 	1879	<p><i>Philosophical Transactions of the Royal Society of London</i> 170, 663-726.</p>	<ol style="list-style-type: none"> <li>1. The first to focus on the detailed characteristics of the ‘Roads’ and the nature of the barriers that impounded the lakes.</li> <li>2. He observed, using recently released OS maps, that the ‘Roads’ were not precisely parallel, but are uneven with a vertical variance of up to 15 feet. He suggested that the unevenness was caused by shoreline collapse or by material falling onto the road surface from the valley sides.</li> <li>3. He described exposures of very finely laminated “yellow” and “grey” clays in Glen Roy valley.</li> </ol>
<p>Thomas Jamieson</p> 	1892	<p><i>Quarterly Journal of the Geological Society</i>; 1892; v. 48; issue.1-4; p. 5-28</p>	<p>He argued against Prestwich’s ideas, and concluded that the vertical variation reflected a poor strategy by the OS for selecting survey points on the parallel roads. He argued for a more rigorous, systematic survey of the roads to overcome this problem.</p>
<p>J.B. Sissons</p>	1977 to 1983	<p>See <i>Bibliography</i>.</p>	<p>Used geomorphological mapping at either the 1:10,000 or 1:25,000 scales coupled with instrumental levelling of points along the Parallel Roads and fluvial terraces occupying lower Glen Roy and Glen Spean.</p> <ol style="list-style-type: none"> <li>1. Concurred with Jamieson’s ideas concerning the source of glacial ice and the sequence of events</li> </ol>

			<p>that led to the formation of the roads.</p> <ol style="list-style-type: none"> <li>2. Concluded that the lakes formed during the Loch Lomond Readvance.</li> <li>3. Proposed the final lake stages were drained by a 'jökulhlaup' from Glen Roy.</li> <li>4. Suggested that the shoreline widths were highly correlated with length of fetch from the south-west.</li> <li>5. Suggested that shoreline fragments were uplifted by up to 3m above normal shoreline altitudes in specific sections of Glen Roy, probably associated with a major fault that was activated by crustal deformation triggered by catastrophic lake drainage in the falling sequence (see section 5.4).</li> </ol>
J.D. Peacock	1986	<i>Scottish Journal of Geology</i> 22: 347–366.	<ol style="list-style-type: none"> <li>1. Examined sedimentary exposures of major fans developed along the flanks of Glen Roy valley and concluded that the Turret Fan, Allt na Reinich Fan and Allt Brunachan Fan were deposited subaerially.</li> </ol>
J.D. Peacock and R. Cornish	1989	<i>Glen Roy Area: Field Guide. Quaternary Research Association</i>	<ol style="list-style-type: none"> <li>2. This required Glen Roy to be free-draining during their formation which was most likely to have occurred during the retreat of ice from the Late Devensian ice sheet maximum. By contrast. Sissons assumed that the Fans developed subaqueously during the LLR.</li> </ol>
P.S. Ringrose	1987	<i>PhD thesis, University of</i>	Identified two episodes of formation of sediment deformation structures in

		<i>Strathclyde</i>	Glen Roy, the first attributed to an earthquake caused by reactivation of the fault which runs through Roy and Gloy (Figure 5.2; blue rectangle) prior to the falling sequence of the 260 m lake in Glen Roy and the 355 m lake in Glen Gloy, and the second to a second earthquake or to sudden isostatic adjustment after catastrophic lake drainage, as proposed by Sissons (1982b).
A.H. Dawson <i>et al.</i>	2002	<i>Journal of Quaternary Science</i> , 17, 527-533.	Carried out an independent instrumental levelling exercise on the Glen Roy shorelines and concluded that they show consistent along-valley tilts of about 0.11 to 0.14 m km <sup>-1</sup> , similar to the gradient of the glacio-isostatically tilted Main Rock Platform in western coastal Scotland. This differed from Sissons and Cornish's (1982b, 1983) conclusion that the shorelines are distorted by complex dislocation and block tilting effects, not all blocks being tilted in the same direction.
D.I. Benn and D. Evans	2008	<i>The Quaternary of Glen Roy and Vicinity: Field Guide; Quaternary Research Association, London; 158–161.</i>	First to present geomorphological evidence that suggests the formation of Loch Lomond Readvance ice in the mountains to the north of Glen Roy. They proposed that a local ice cap developed on the Carn Dearg plateau, with ice flowing down Glen Turret to terminate at the Glen Turret Fan.
N.R. Golledge <i>et al.</i>	2008	<i>Quaternary Science Reviews</i> , 27, 888-904	Applied numerical modeling of ice growth to simulate the maximum Loch Lomond Stadial ice cover in Scotland. The model suggests that glacial ice extended beyond the mapped empirical limits and that the

			mountains adjacent to Glen Roy would have supported cold-based or slow moving temperate ice.
D. Jarman	2008	<i>The Quaternary of Glen Roy and Vicinity: Field Guide; Quaternary Research Association, London; 2008; 98– 104.</i>	Mapped rock slope failure phenomena in Glen Roy area and argued against Sissons and Cornish's (1982b) view, proposing that the parallel roads were not dislocated after their formation by faulting processes but by post-glacial differential tectonic rebound effects.
A. Palmer <i>et al.</i>	2010	<i>Journal of Quaternary Science, ISSN 0267-8179.</i>	Published the results of micromorphological analysis and counting of laminated (varved) sediments and concluded that the lake system in Glen Roy existed for a total of 515 years. During a rise in lake levels, the 260 m, 325 m and 350 m lakes existed for minimal periods of 191, 112 and 116 years in the rising sequence, and it took 95 years for the lake levels to fall from 350 m to 260 m. Calculated ice advance rates of between 13.4 and 41.9 m/year, and ice retreat of around 38.5 m/year.
D. Fabel <i>et al.</i>	2010	<i>Journal of Quaternary Science, 25(4) 597–603</i>	Used surface exposure dating (cosmic-ray generated <sup>10</sup> Be in quartz) to date four bedrock samples from the surface of the 325 m shoreline, which yielded a mean formation age of ca. 11.5–11.9 ka BP. Other dates suggested that the 260 m lake drained before ca. 10.7–11.0 ka and that some subaerial sedimentation occurred on the Brunachan fan after ca. 9.7–9.9 ka BP.



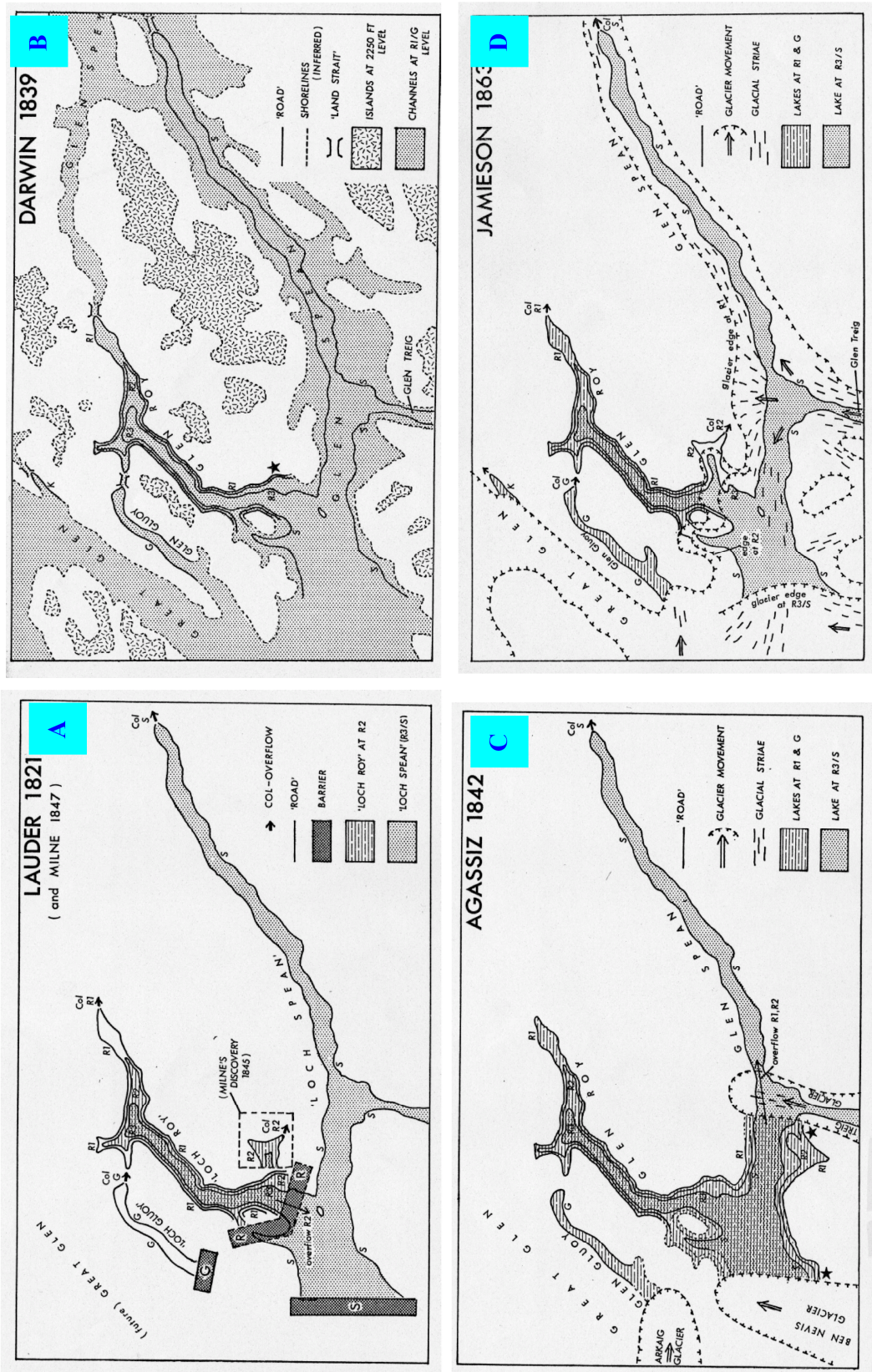


Figure 5.3 Reconstructions of the former lakes in Glen Roy based on interpretations of the ‘parallel roads’ and associated geomorphological features: A. Lake overflow controls by Lauder-1821 and Milne, 1847); B. Marine interpretation by Darwin (1839); C. Glacial interpretation by Agassiz (1842); D. Glacial interpretation by Jamieson (1863) (figure taken from Rudwick 2009)

## **5.4 Interpretations of the Glen Roy evidence by J.B. Sissons**

J.B. Sissons conducted detailed geomorphological mapping of the Glen Roy area using 1:10,000 and 1:25,000 O.S. maps and instrumental levelling of selected landforms, including systematic measurement of the altitudes of the parallel roads and river terraces. His main contributions published between 1977 and 1983 addressed four main topics: (1) defining the Loch Lomond Readvance ice limits in the Glen Roy-Glen Spean area (Sissons 1979b, 1982b); (2) accurate measurement of the shorelines in Glen Roy to establish the processes of their formation (Sissons 1977, 1978; Sissons and Cornish 1982b); (3) assessment of the rate of shoreline formation (Sissons 1978); and (4) examination of the evidence for neotectonic activity in the Glen Roy valley (Sissons 1982a; Sissons and Cornish 1982b). The results of this research led to the formulation of the 'Sissons model' of the sequence of glacier margin and lake-level changes in Glen Roy. The remainder of this chapter summarises the key elements of the Sissons model and the data upon which it is based. Subsequent chapters (6, 7 and 8) include independent examination of the landforms in the same area using NEXTMap, and the results of some tests of the Sissons model.

### **5.4.1 The sequence of lake changes in Glen Roy**

The Sissons model suggests that glacier ice, during the LLR, was sourced in the mountains to the west of the Great Glen and flowed to the east across the Great Glen. This ice became confluent with glaciers flowing northwards from the Ben Nevis range, the combined ice mass pushing eastwards into Glen Spean and then entering the lower parts of both Glen Gloy and Roy. This ice blocked the natural drainage of the Rivers Gloy, Spean and Roy, causing the lakes to form and rise. Further advance of the ice isolated the Roy valley from the Spean valley and allowed lake waters to rise to two higher levels controlled by independent cols. Water levels in the Gloy were always controlled by a single col at 355 m at the watershed between the Gloy and the Roy. In

the Sissons model, the different lake levels were attained by progressive abandonment of lower cols as the ice margins migrated and grew in thickness. The lowest lake was controlled by the 260 m Pattack/Mashie col, the next highest by the 325 m Roy/Laggan col, and the highest, the 350 m lake surface, by the Roy/Spey col (Figures 5.1, 5.4 and 5.5). As the ice advanced, the lake waters in Glen Roy were progressively cut off from the lower cols, and this Sissons referred to as the *rising sequence* of lake surface altitudes and lake shoreline formation. When the ice melted and receded, the lake waters could escape to the lower cols, and this is referred to as the *falling sequence* of lake surface altitudes and lake shoreline formation. The rising and falling sequences of lake levels in the Glen Roy area can be divided into eight stages, described in the following sections. Details of the corresponding ice margin positions and of lake water dynamics at each lake stage are also summarised below, with the positions of the cols, ice margin positions and shoreline distributions illustrated in Figure 5.4.

#### **5.4.1.1 Stages 1-5: The Rising Sequence**

**Stage 1** is the inception of the lowest lake system at 260 m. When the glacial ice from the west of Great Glen and the Ben Nevis mountain range blocked the westward-flowing drainage in the lower part of Glen Spean (Figure 5.4 A; Figure 5.5 A), it created a 260 m lake which occupied the Spean-Laggan valley. This lake extended east to, and its altitude was maintained by, the 260 m Pattack/Mashie watershed col (Figure 5.1 and 5.5). This lake water submerged Glen Spean and the lower part of Caol Lairig and extended into Upper Glen Roy as far as the confluence of Glen Turret and Roy. At this time, the position of the ice front in the Gloy valley is a controversial and an unresolved issue. Initially it was generally believed that the ice front only reached as far as somewhere in lower to mid Glen Gloy, leaving the north-eastern part of the Gloy ice-free, and hence filled with a lake that overflowed the 355 m col between Gloy and Turret drainage networks. Sissons (1982b) subsequently changed his view on this

matter, as a result of mapping in the area around Glen Turret, and came to the conclusion that LLR ice advanced all the way up Glen Gloy to overtop the 355 m col, and indeed descended into the Turret valley, to reach its maximum position at the Turret Fan (Figure 5.5, I). The fact that the 355 m lake shoreline exists in upper Glen Gloy would mean, under Sissons' explanation, that the ice subsequently retreated in Glen Gloy to allow the lake to form. Peacock (1986) argued that the Turret Fan could not have been formed during the rising sequence of the 260 m lake because sedimentological structures in the Turret Fan were indicative of subaerial sedimentation (discussed in more detail in Chapter 6). He took the view that this implied that the Turret Fan was formed prior to the LLR, and that therefore LLR ice was restricted to Glen Gloy during this time.

**Stage 2** is associated with advance of the ice into Lower Glen Roy and into the lower parts of Caol Lairig (Figure 5.5, B), which forced the water level to rise in Caol Lairig until it escaped over the lowest point on the watershed between Caol Lairig and Glen Roy, close to Achavady, which has an altitude of 297m. Lake shorelines are found within Caol Lairig at this altitude. The lake in Glen Roy was still at 260 m at this time, as the ice had not advanced sufficiently into Glen Roy, or grown sufficiently thick at the ice front, to prevent water flowing out of lower Glen Roy into the Spean-Laggan valley.

**Stage 3** occurred after the ice advanced sufficiently into Glen Roy, and was thick enough, to prevent water from Glen Roy (Figure 5.5., C1) and overflow water from Caol Lairig (Figure 5.5, C3) flowing directly out of lower Glen Roy into the Spean-Laggan system. The lake waters rose at this stage to 325 m, controlled by a col on the watershed between the Roy and Laggan catchments within Gleann Glas Dhoire (Figure 5.4; Palmer 2008b). The upper part of Caol Lairig was also flooded to this level at this time. The lake in Glen Roy extended further up the valley than the 260 m lake,

beyond the confluence of the Burn of Agie and the River Roy (end point of the 325 m shoreline; Figure 5.5). The 325 m lake waters joined the lake in Loch Laggan in the vicinity of Roughburn; note that the lake in Loch Laggan remained at the 260 m level at this time, as the waters here could still escape over the Pattack/Mashie col. Sissons (1982b) suggested that the ice in Glen Gloy at this time retreated to Altnary (Figure 5.5, H), with a lake occupying upper Glen Gloy at the altitude of the Gloy-Turret col at 355 m OD. (Figure 5.4 B).

**Stage 4** is defined by the ice advancing to position D1 (Figure 5.5) to block the drainage path of lake water from Glen Roy through to Gleann Glas Dhoire. This ice advance in caused the lake waters in Glen Roy to rise to the level of the 350 m Roy/Spey col at the head of Glen Roy, and the lake waters extended to the head of Glen Turret. Also a small lake was impounded by ice within Gleann Glas Dhoire at this time, which remained at 325 m, as it continued to have access to the 325 m col. The ice eastwards along Glen Spean reached its maximum position at around Roughburn at this time, where it entered the 260 m lake in Loch Laggan – still maintained at that level by the Pattack/Mashie col. There is a lack of firm evidence for ice movements and position in Glen Gloy during this time, with Sissons (1982b) suggesting that the ice had receded to Altnary (Figure 5.5; H), although it seems difficult to reconcile such a degree of ice retreat in Glen Gloy with ice fronts still advancing in Glen Roy and Glen Spean at the same time (Figure 5.4 C), and presumably under the same general climatic conditions.

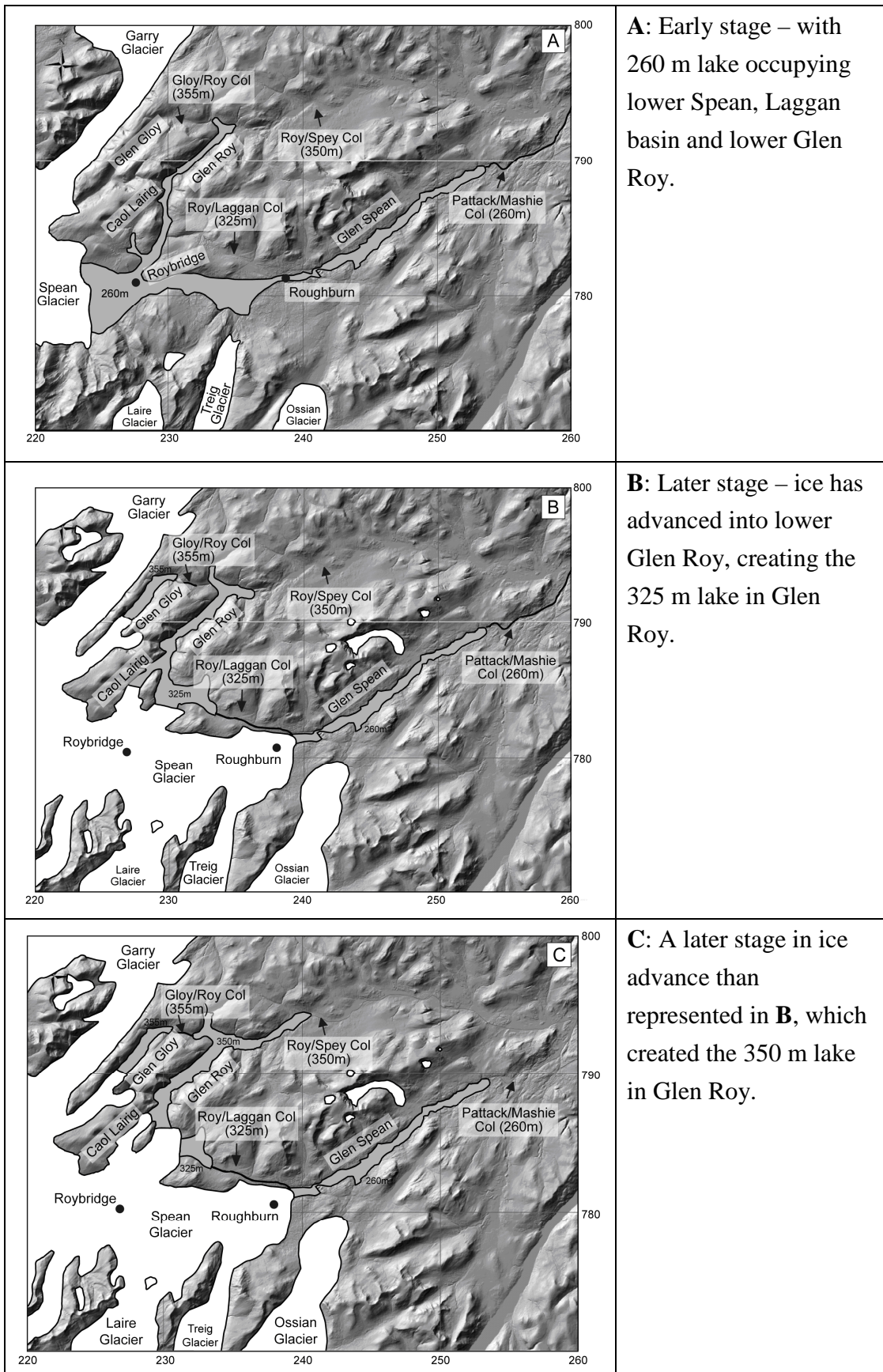
**Stage 5** is marked in Glen Roy and Caol Lairig by evidence for the ice front moving further forward to reach its maximum extent in the vicinity of the Viewpoint in Glen Roy, where Sissons has mapped a large mass of glacial deposits (referred to as the '*Massive Drift Accumulation*'), while the ice in Caol Lairig advanced to a well marked terminal moraine located close to the col between Glen Roy and Caol Lairig (Figure 5.5;

Figure 6.3; Sissons 1979). The lake water in Glen Roy remained at 350 m, as it continued to be controlled by the 350 m Roy/Spey col. The position of the ice in Glen Gloy at that time is still unresolved.

#### **5.4.1.2 Stages 6-8: The Falling Sequence**

In the Sissons model it is assumed that the lake levels fell in the reverse order to that described above, when the ice melted and receded back into the lower parts of Glen Spean. In **Stage 6**, the ice front retreated from position C1 to C3 (Figure 5.5), unblocking Gleann Glas Dhoire and hence enabling the lake waters to escape over the Roy-Laggan col, thereby allowing the lake surface to fall to 325 m OD. Continued ice recession led to **Stage 7**, when the ice in lower Glen Roy receded and thinned sufficiently to allow the 325 m lake waters to escape into the Spean Valley and thus to fall to the 260 m lake surface level. The exact position of the ice front at this point is difficult to determine, for it could be that lowering of the ice surface allowed the lake waters to drain over rather than around the ice margin. It is also not clear how the Gloy glacier system was responding at this time, although it seems likely that the ice would not have extended beyond the southerly limits of the 355 m shoreline in Glen Gloy, which tapers out in the vicinity of Alltnaray (Figure 5.5, G).

**Stage 8** is associated with the final drainage of the 260 m lake system, which Sissons (1979c; 1981b) attributed to a catastrophic flood or 'jökulhlaup' and to several subsequent lower magnitude flood events as the ice mass reduced in size more gradually and the Spean-Roy lake intermittently emptied. According to Sissons, when the 'jökulhlaup' took place, about 5 km<sup>3</sup> of lake water escaped through a subglacial tunnel valley in Glen Spean and flowed north to Fort Augustus, then north-eastwards along the Great Glen to pour into Loch Ness, finally entering the Moray Firth at Inverness.



**Figure 5.4** The ice limits and lake surfaces during the rising sequence of lake formation, based on the *Sissons (1979)* model (adopted from *Lowe et al. 2008b*, pp.18-19)

Sissons (1979c) and Sissons and Cornish (1983) levelled the heights of terrace fragments in the Glen Roy and Glen Spean valleys and found a series of terraces with surface altitudes at 113, 99, 96.5 and 90.5 m in lower Glen Roy and the Glen Spean valley. The evidence suggested that those terraces were formed after the catastrophic 'jokulhlaup' drainage, when the ice mass was gradually diminished in its size and the lake level intermittently halted, allowing small lakes to occupy parts of Glen Spean. A 2 km long sector of Glen Spean contains a mass of kames and other dead-ice features that suggest stagnation of the ice mass.

The Sissons model cannot, however, explain the presence of poorly-developed, discontinuous shorelines in Glen Roy at 334 m (Sissons 1978; Peacock and Cornish 1989) and 344 m (Peacock and Cornish 1989) and at least three shorelines in Glen Fintaig, a tributary valley of Glen Gloy, at 295 m, 416 m and 426 m (Peacock and Cornish 1989; Key *et al.*, 1997). These minor shorelines do not have altitudinally-comparable overspill cols, as is the case with the major shorelines, and are not well mapped. Their presence would suggest a more complicated response to ice-lake dynamics than has been accounted for so far.

Whilst the Sissons model places all of the above stages within the Loch Lomond Stadial, with perhaps some of the later terraces and stagnation features dating to the early Holocene, the exact duration of the lake systems remained uncertain. Palmer *et al.* (2010) have presented detailed micromorphological evidence for the presence of sequences of glaciolacustrine annually-laminated (varved) sediments within Glen Roy and Loch Laggan, all associated with the LLR. Variations in varve thickness are considered to reflect changes in the position of the LLR ice margin and stratigraphical marker events enable the varve sequences to be related both to variations in the positions of the ice margin and corresponding changes in lake level. This evidence



indicates that the lake sequence (260, 325 and 350 m lake levels) existed for a minimum of 515 years overall, while the durations of each lake stand in the rising sequence could also be estimated from the varve evidence. The results suggest that the 260 m, 325 m and 350 m lakes in the rising lake sequence existed for minimum periods of 191, 112 and 116 years respectively. Palmer *et al.* (2010) also concluded that the lake level fell from 350 m to 325 m over a 95 year period, although it was not possible to identify a fall to the 260 m level within the varve records.

Fabel *et al.* (2010) have introduced a new approach to the study of the Glen Roy area by using the surface exposure dating method (cosmic ray-produced  $^{10}\text{Be}$ ) on four bedrock samples obtained from the surface of the 325 m shoreline in order to date its formation. The results provide a mean age of  $11.5 \pm 1.1$  (0.5) to  $11.9 \pm 1.5$  (0.5) ka BP, confirming the long-held view that the parallel roads are of Loch Lomond Stadial age. They also applied the same methodology to boulders on the surfaces of the Glen Turret and Brunachan fans. Those from the Brunachan fan surface yielded ages of  $9.7 \pm 1.0$  (0.6) to  $9.9 \pm 1.3$  (0.6) ka BP, indicating that subaerial sedimentation on the fan surface continued beyond the close of the Loch Lomond Stadial.

The above summary of the sequence of events was the established position at the commencement of this PhD project, with the exception of the data and views published by Palmer *et al.* (2010) and Fabel *et al.* (2010), which became available during the PhD programme. Other relevant assessments of the features in Glen Roy, available at the start of the project, concerned the physical attributes of the shorelines themselves, which are summarised next.

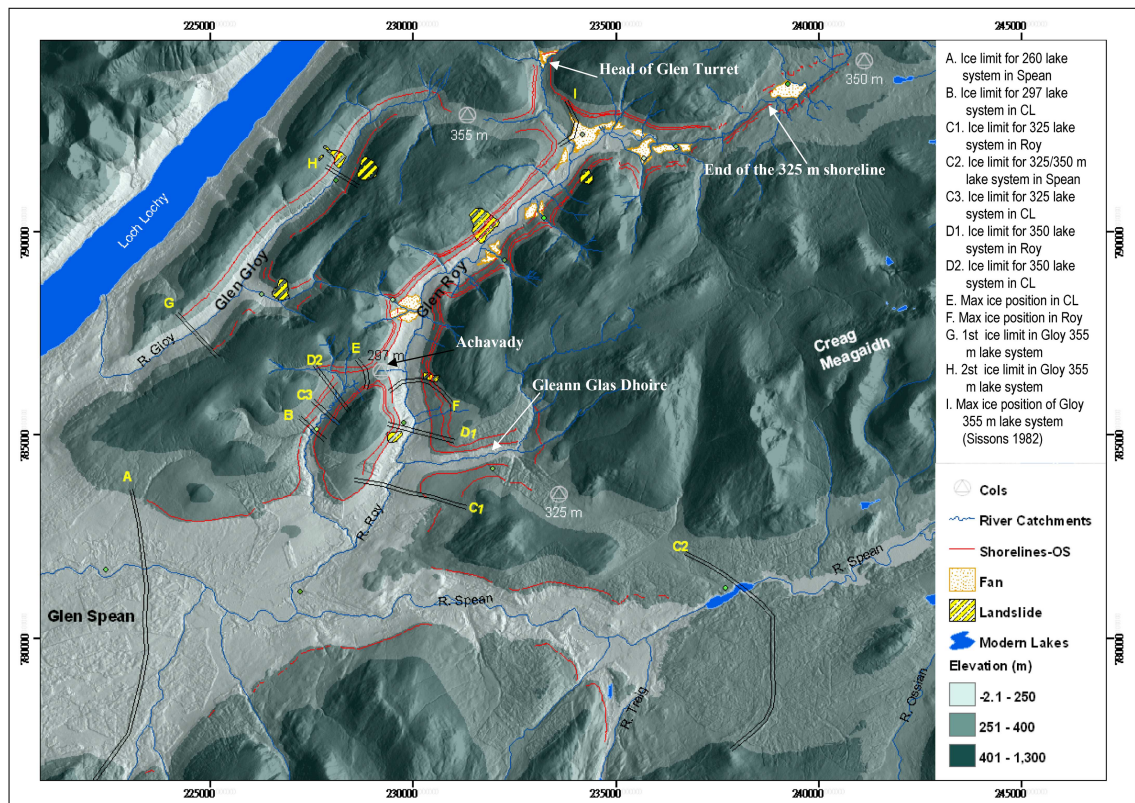


Figure 5.5 Ice-marginal positions and the key catchment controlling cols in Glen Roy area. Also see Figure 5.1 for the wider geographical context.

#### 5.4.2 Nature and formation of shorelines

In Glens Roy, Spean and Gloy, Sissons (1978) instrumentally measured the widths, aspects and notch positions of the backwalls of the shorelines at 787 points with an average horizontal interval of 115m. From this work Sissons drew the following conclusions:

1. The average widths of the shorelines (distance between the shoreline backwall and the front edge) in Glen Roy for the 350 m, 325 m and 260 m levels are 15.2 m, 10.5 m and 10.4 m respectively. In Glen Gloy the 355 m shoreline is 7.3 m wide.
2. There are consistent shoreline widths between areas inside and outside of the limits of the LLR ice. In Glen Roy, the 350 m, 325 m and 260 m shorelines inside the limit are, 9.4 m, 9.4 m, and 11.7 m wide respectively and in Glen Gloy are 9.8m. Outside of the limits, the 350 m, 325 m and 260 m shorelines are 11.3,

10.6 and 10.1 m wide respectively and in Glen Gloy are 10.0 m wide. He assumed that glacial ice advance was sufficient to erode previously-cut shorelines inside the ice limits, which generated fresh bedrock surfaces to be eroded on retreat of the ice. His evidence suggested that the shorelines were formed quickly and subsequently stabilised at a uniform width.

3. Shoreline widths are strongly influenced by aspect and length of fetch (the lake span at right-angles to the direction in which the backwall faces) with the platforms being better developed on valley sides facing SW with the longest fetch. The widest shorelines were also found to be associated with streams depositing fluvial sediments on the shoreline platforms.

Detailed discussion and comparison of these datasets with NEXTMap information are developed in Sections 7.3 and 7.4.

#### **5.4.3 Differential glacio-isostatic uplift of crustal blocks at Glen Roy**

Sissons and Cornish (1982b) re-levelled the shorelines at intervals of 25 to 30 m on the basis of Sissons' (1978) paper. The results identified that the shorelines did not have consistent altitudes or along-valley gradients, but are dissected into a series of blocks that show varying degrees of tilt: some blocks are horizontal, while others record varying gradients of up to  $4.6 \text{ m km}^{-1}$ . This suggested that there were a series of shoreline dislocations in Glen Roy. One particular dislocation site is possibly the southern extension of the Glen Gloy fault (Figure 5.2), where the shoreline fragments have been uplifted by up to 3m above average shoreline altitudes. Sissons and Cornish (1982b) inferred that these crustal dislocation patterns were fault scarps caused by palaeoseismic activity, possibly triggered by catastrophic lake drainage ('jökulhlaup') occurring immediately after the final drainage of the 260 m lake during the late LLS.

These dislocation features were also re-examined in the current project, using NEXTMap DEM data, and the results are examined and discussed in sections 7.7 ~7.10.

## **5.5 Synopsis**

This review of previous studies in the Glen Roy area has established that the ‘Sissons model’ (developed in the 1970’s to early 1980’s) is the most widely accepted version of events concerning the evolution of the ‘Parallel Roads’ of Glen Roy and their association with glaciation – or at least that was the case when this PhD programme of research was commenced. This was therefore the adopted starting point for the present study, and in the chapters that follow the ‘Sissons model’, and the geomorphological evidence on which it is based, will be re-examined and tested by the application of NEXTMap technology. This will begin in Chapter 6 with a comparison between key geomorphological features identified in NEXTMap imagery with features previously mapped in the field by Sissons and contemporary researchers. Chapter 7 will then focus on a detailed examination of the shorelines themselves, and compare results obtained using NEXTMap technology with the instrumentally-levelled results published by Sissons. The overall results are combined in Chapter 8, to re-assess the sequence of events hypothesised for the Glen Roy area during the Loch Lomond Readvance/Stadial.

## 6. Glaciation effects in Glen Roy and vicinity

### 6.1 Introduction

In this chapter, glacial landforms in the Glen Roy area will be examined through the use of NEXTMap DEM data. Vertical and 3-D perspective imagery with different illumination sources generated from NEXTMap (see Chapter 3) were used to evaluate evidence in locations formerly occupied by glacier ice and by glacier ice-dammed lakes; the main focus was on (a) fluctuations in lake level that were a consequence of ice-lake interactions, and (b) ice-wastage, ice-movement and ice-marginal landforms (see Chapter 5). For ease of communication in this chapter, Glen Roy is divided into three parts: i) a lower section that includes the Viewpoint and Caol Lairig; ii) a middle section that includes the Allt Bhreac Achaidh Fan, the Brunachan Fan and the Reinich Fan; and iii) an upper section that encompasses the Turret Fan, Allt a' Chomhlain, Coire Dubh, the Allt Dearg Fan, the Canal Burn Fan and the Burn of Agie Fan (Figure 6.1).

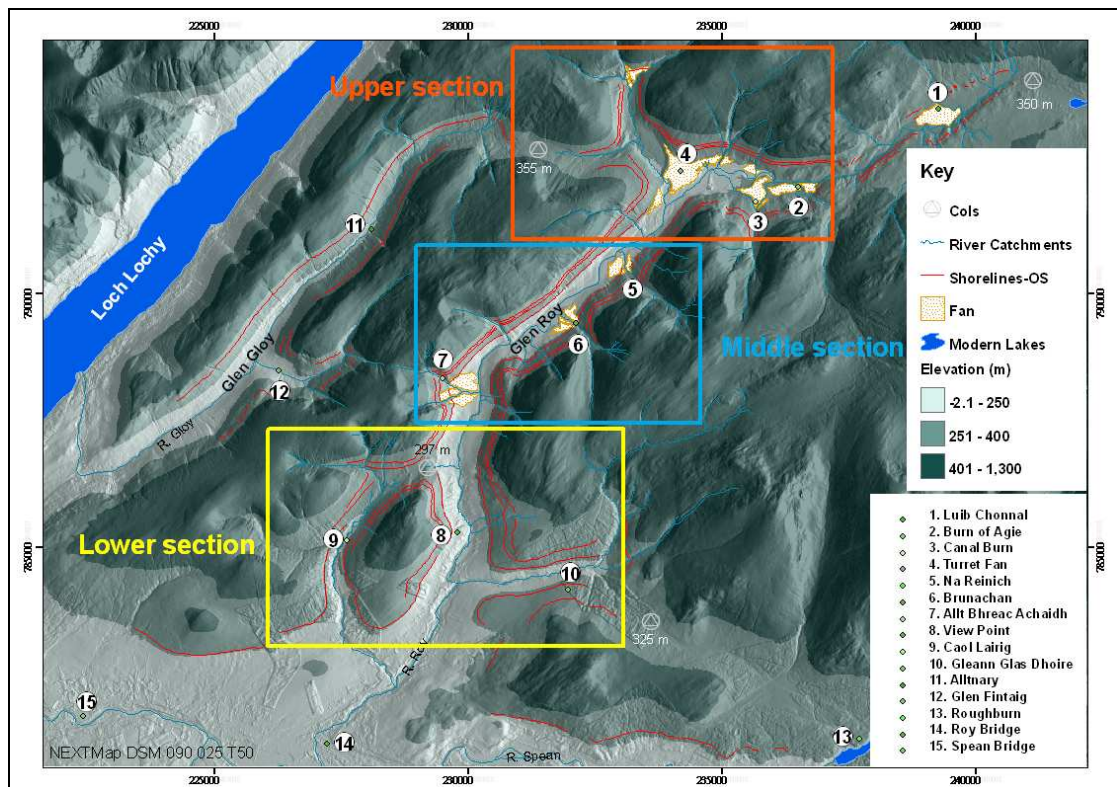


Figure 6.1 Site locations and section boundaries in Glen Roy referred to in text.

Critical features mapped by the author using NEXTMap DEM data are compared with mapped features reported in previous works. Finally, a NEXTMap-based experiment was carried out to reconstruct the precise areal extent of ice-dammed lakes at different lake water levels. Part of the text and some of the figures in this chapter have been published in Chen and Rose (2008b and 2008c), but some details and interpretations herein have subsequently been revised.

## 6.2 Lower section of Glen Roy

### 6.2.1 Introduction

The lower section of Glen Roy contains the Viewpoint and the Caol Lairig valley (Figure 6.2).

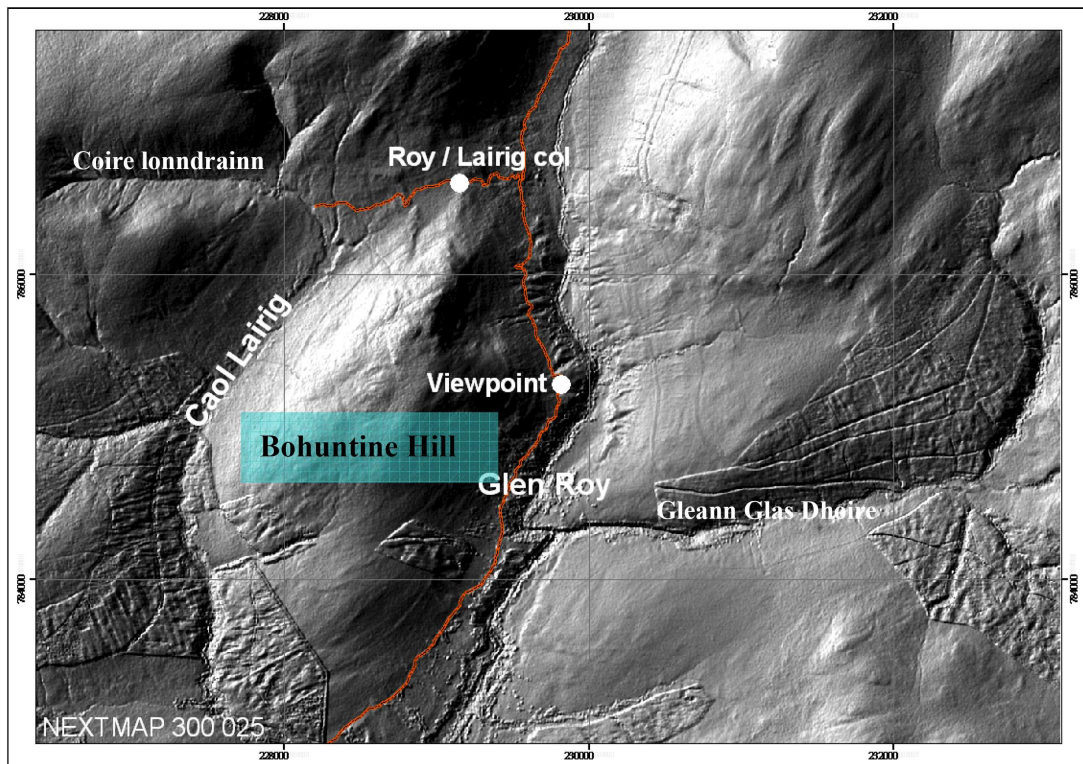


Figure 6.2 Locations of the Viewpoint and Caol Lairig (scale of 1:33,000). The red line shows the track of the main public roadway in Glen Roy.

This part of the Glen Roy drainage system is significant because the glacier that extended up Glen Roy divided into two lobes, one extending up-valley into the lower

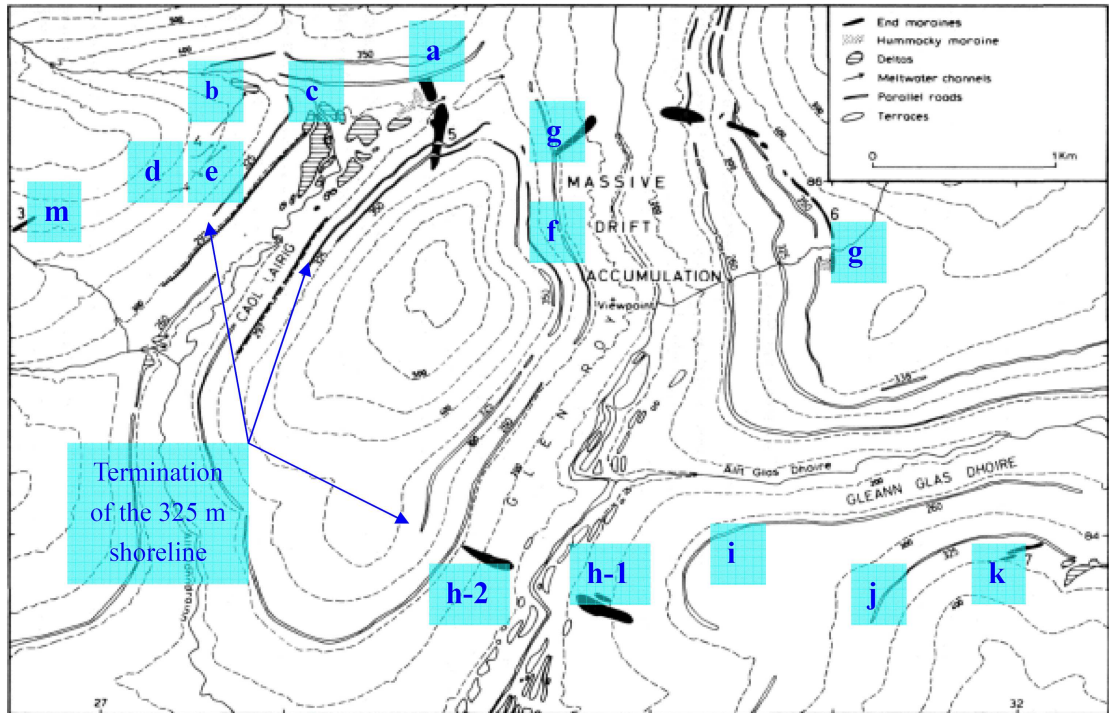
Roy on the east flank of Bohuntine Hill, and the other (the Lairig lobe) extending up Caol Lairig on the west flank of Bohuntine Hill. Interaction between the ice and shoreline limits can be mapped in detail within a tightly constrained area, and it will be shown how NEXTMap DEM data reveal subtle changes in (a) the timing of glacier advance and retreat during the maximum extension of the LLR glacier margins, (b) ice-marginal behaviour and (c) the relationships between glacier margins and proglacial lake shoreline development.

### **6.2.2 Previous studies in the lower section of Glen Roy**

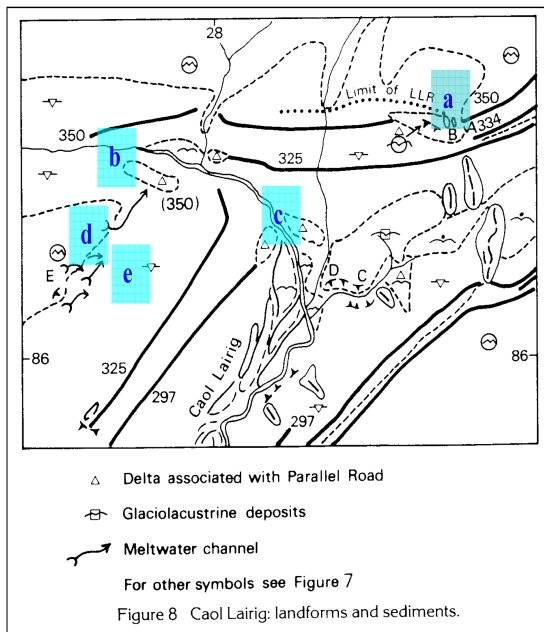
This part of the Glen Roy catchment has been described by Sissons (1979b) and Peacock and Cornish (1989) using predominantly geomorphological evidence to understand the interplay between shorelines, limits of the LLR and ice-marginal landforms (Figure 6.3; notation for the landforms specifically referred to in the text are given in Figure 6.3 – A). The maps of Sissons (1979b) and Peacock and Cornish (1989) are essentially schematic in their presentation and provide only limited detail on the dimensions and relative positions of the mapped landforms, while the generalised areas of sediment accumulation are of only limited use when trying to understand the complex interrelationships between landforms. Thus it was considered worthwhile to evaluate the use of NEXTMap technology to establish whether greater detail could be deciphered from the LLR deposits preserved in this part of the valley.

Sissons (1979b) suggested that there are three critical landforms in Caol Lairig that can be used to delimit the LLR ice limits: i) a 2-3 m high lateral moraine found at an altitude of 460 m on the high western flank of the valley (feature m, Figure 6.3A); ii) four small but well formed meltwater channels that trend parallel to the valley side but slope north-eastwards (feature d, Figure 6.3B) and which represent the down-valley continuation of the upper limit of LLR ice; and iii) a 5 m high end moraine that runs

A.



B.



C.

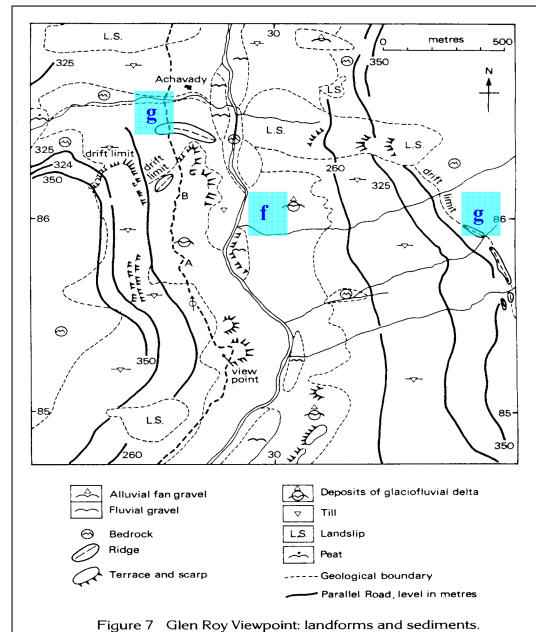


Figure 6.3 A. Geomorphological map of lower Glen Roy, including Caol Lairig, from Sissons (1979b); B. and C. Geomorphological maps of lower Glen Roy from Peacock and Cornish (1989). Critical landforms referred to in the text are highlighted in blue and labelled alphabetically. Landforms common to both the Sissons (1979b) and Peacock and Cornish (1989) maps are given the same alphabetical label.



transverse to the axis of the Caol Lairig valley (feature a, Figure 6.3A; see also Figure 6.4). In addition, Peacock and Cornish (1989) identified a kame terrace at an altitude of 350 m (feature a, Figure 6.3B), the surface of which is associated with the 350 m shoreline, a feature not reported by Sissons (1979b). Other (non-glacigenic) landforms represented in both the Sissons and Peacock and Cornish maps include a small delta associated with the 350 m shoreline (feature b, Figure 6.3A and 6.3B), and fragments of a deltaic spread near the confluence of the Iondrainn and Lairig, which has been dissected by the stream flowing down through Coire Iondrainn (feature c, Figure 6.3A and 6.3B). The apex of this delta-complex lies at an altitude of around 297 m, the significance of which is explained below, while the deltaic formations in this part of the Caol Lairig valley inter-finger with lacustrine sediments (laminated silts and clays).

The former LLR ice limits in lower Glen Roy reported by Sissons (1979b) were based in the main on the following important features: i) a ca. 80 m thick massive drift accumulation composed of lacustrine, fluvioglacial and till deposits (feature f, Figure 6.3C); ii) a low ridge on the eastern side of Glen Roy that forms the northern boundary to the massive drift accumulation and that extends up the valley side, beyond the 350 m shoreline, as a series of 2-3 m high lateral moraines (feature g, Figure 6.3C); . iii) several 2-3 m high moraine ridges most clearly developed on the southern flank of Gleann Glas Dhoire (feature k, Figure 6.3A); and iv) two prominent moraine ridges to the south of the confluence between Allt Glas Dhoire and the Roy (feature h-1 and h-2, Figure 6.3A), that lie adjacent to the southern terminations of the 325 m shoreline on both sides of the Roy Valley (the easternmost of these is feature i in Figure 6.3A).

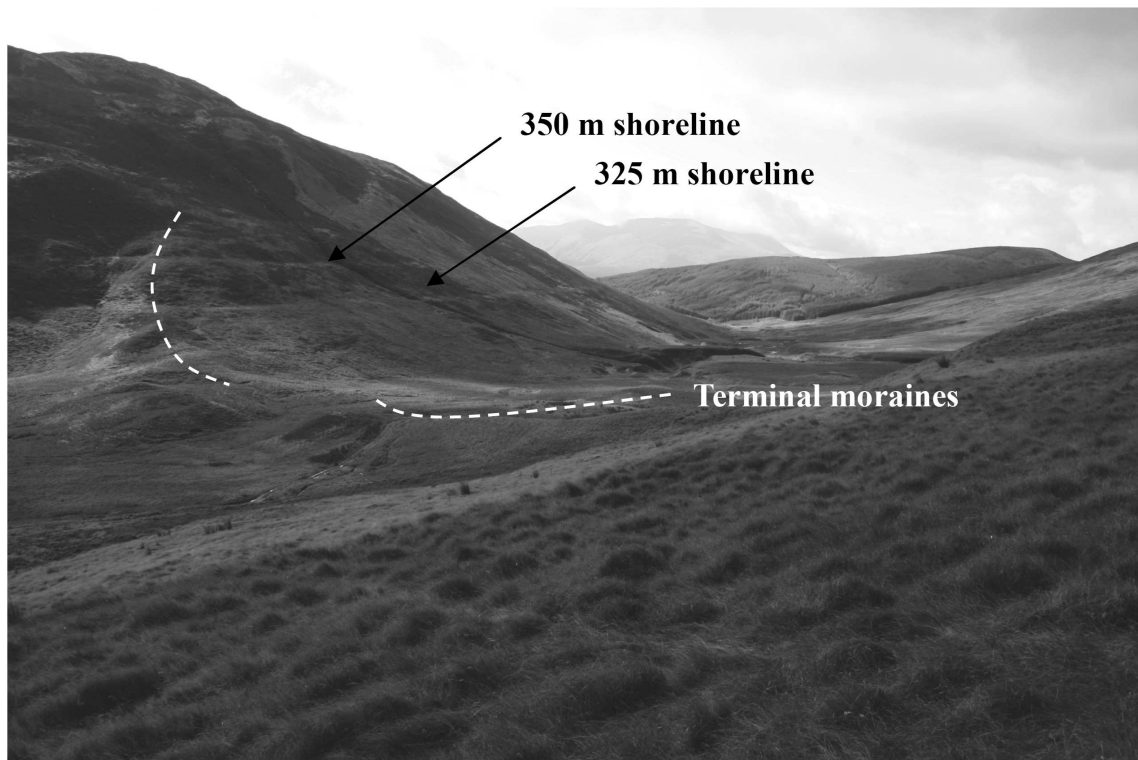


Figure 6.4 View of the pronounced terminal moraine (feature a, Figure 6.3 A) and the 325 and 350 m shorelines taken from the head of Caol Lairig, looking south-west. (Photo taken by A. P. Palmer)

### 6.2.3 NEXTMap interpretation of ice limits and marginal features in lower Glen

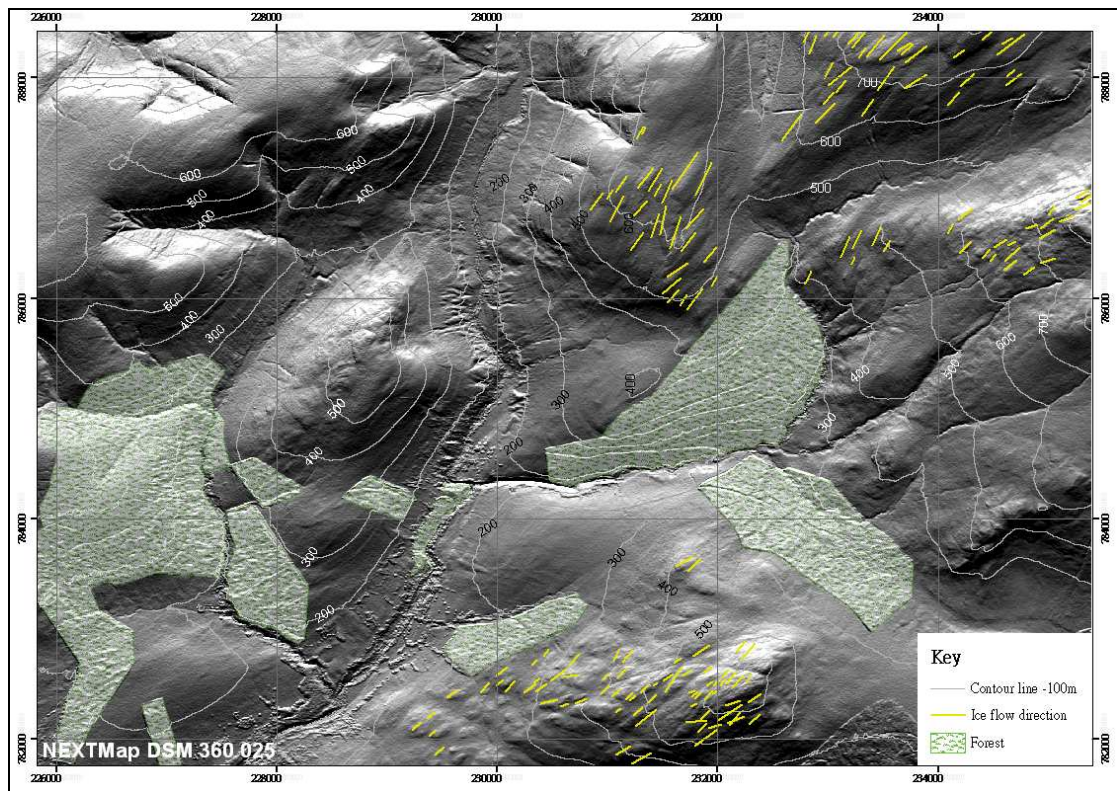
#### Roy

This section reports the use of NEXTMap DEM data to re-map and re-evaluate the extent of the LLR ice limits in the lower section of Glen Roy and compares the results to the published maps of Sissons (1979b) and Peacock and Cornish (1989), as summarised above.

#### 6.2.3.1 The potential ice-flow direction in lower Glen Roy

Figure 6.5 and 6.6 illustrate the SW-NE trending lineaments on hill tops to the east of Lower Glen Roy that are clearly reflected in NEXTMap DEM data. The lengths of individual features range from 47 m to 410 m, and they occur throughout an altitudinal range of 232 m to 780 m OD. The great majority of these features occur outside of the LLR ice maximum limit (feature g, Figure 6.3A) and lie above 460 m OD. They are interpreted as subglacially-moulded bedrock lineations for two reasons. Firstly,

although the grain of the bedrock geology is from SW-NE in this locality, it is clear that the crests of ice-moulded surfaces maintain the same trend across the whole region, independent of underlying geological structure. For example, while the local psammite and mica-schist show a consistent SW-NE grain, the ice-moulded features shown in Figure 6.5 diverge from NNE to ENE. Secondly, evidence for local ice movement is constrained to the valley bottoms below a maximum altitude of 460 m (feature m, Figure 6.3A) in both Caol Lairig and around the Viewpoint, which suggests that these lineaments on the hilltops relate to a period of glacial activity that precedes the LLR.



**Figure 6.5** Vertical NEXMap DEM plots of the Caol Lairig and Viewpoint area. The light source is set to azimuth 360° and elevation 25°. Yellow lines denote the lineation of crest-lines of glacially moulded bedrock surfaces.

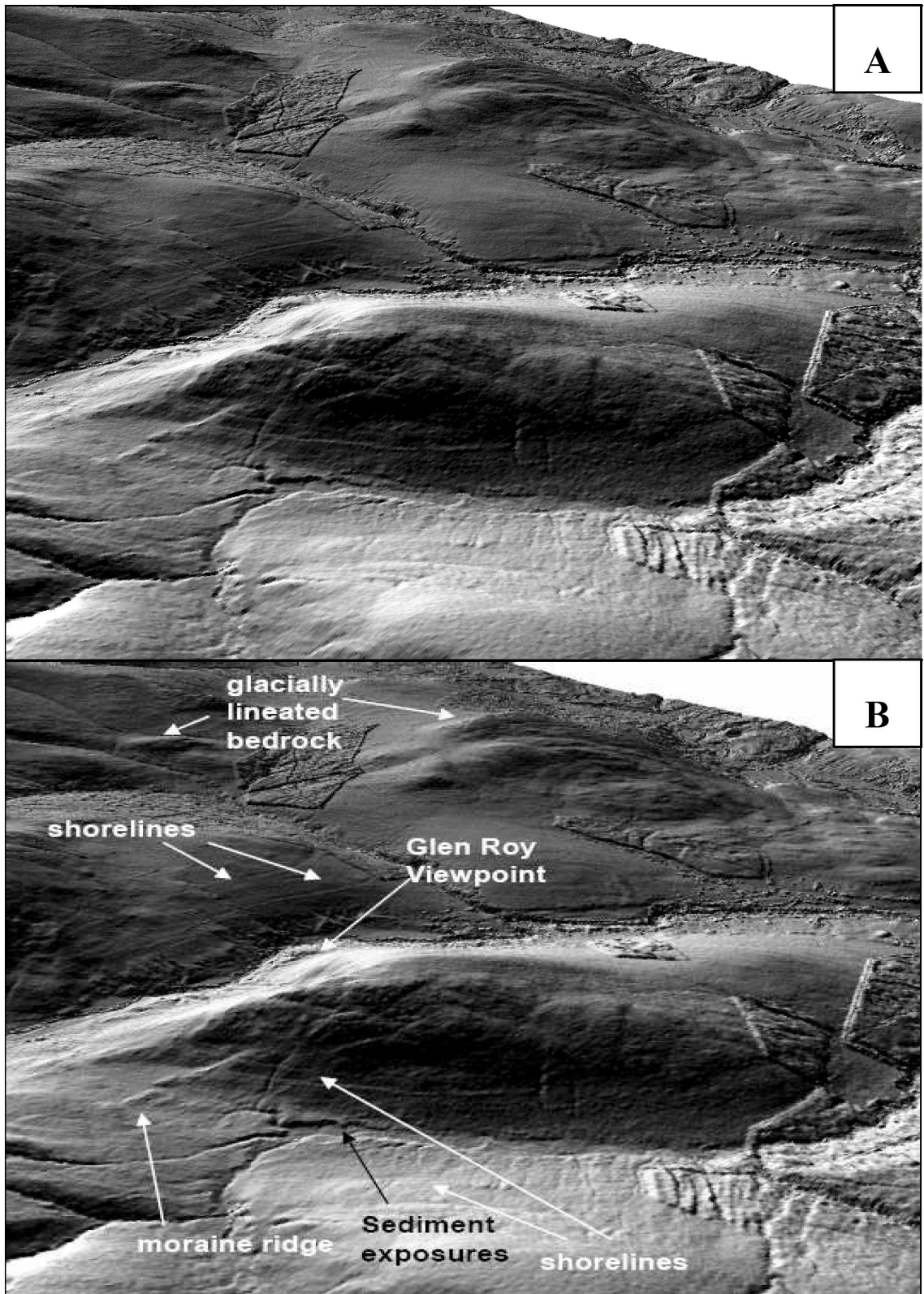


Figure 6.6 3D perspective of the Caol Lairig area viewed from the NW (Illumination set to Azimuth 90° and Altitude 30°). A is the original image, while critical landforms and the location of sediment exposures are identified on B. Also see Figure 6.4 for a different perspective and closer view of the arcuate moraine in Caol Lairig.

### **6.2.3.2 Ice-marginal features and lake shorelines**

Figure 6.7 allows a comparison to be made between (A) the distribution of the Parallel Roads of Glen Roy mapped by officers of the Ordnance Survey at a scale of 1:25000 with (B) details observed by the present author from NEXTMap DEM data. Note, however, that the NEXTMap evidence for the 260 m shoreline is obscured on the southern flanks of Bohuntine Hill and in Gleann Glas Dhoire by forestry plantations. Where the shorelines are in full view, however, it can clearly be seen that they are not continuous features, as represented on OS maps and implied for large tracts represented on the geomorphological maps of Sissons (1979b) and Peacock and Cornish (1989). Instead, the shorelines are commonly very fragmentary, which is particularly noticeable in Caol Lairig and on parts of the western flank of Glen Roy. A shoreline that is confined to Caol Lairig and which occurs at 297 m (controlled by the height of the col between Caol Lairig and Glen Roy, to the immediate north of Bohuntine Hill), also appears as fragmentary on NEXTMap DEM data. The surface appearance of the shorelines is examined in more detail in Chapter 7.

The NEXTMap DEM data also pick out the moraines identified by Sissons (1979b) and Peacock and Cornish (1989) that are marked in Figure 6.3, but with additional subtle detail that is not represented in those maps, while they also provide a clearer perspective on how the features are linked spatially (Figure 6.6, 6.8 and 6.9). The prominent moraine on the floor of Caol Lairig, close to the 297 m col to the north of Bohuntine Hill, that marks the LLR maximum advance in Caol Lairig, is very distinctive on the NEXTMap DEM data, but it appears to extend further up the western flank of Bohuntine Hill than mapped by Sissons (1979b) (see Figure 6.9B). There may also be a second arcuate ridge on the western flank of Bohuntine Hill, that demarks a temporary halt of the glacier during recession (Figure 6.9B).

The NEXTMap DEM data also show that the arcuate moraine at the head of Caol Lairig (Figure 6.4) is fragmented, with three fragments on the northern flank and seven on the southern flank of the col, as identified by closer examination of the features at location a, on Figure 6.10B. The highest of them reaches an altitude of 331 m OD on the northern flank and 327 m on the southern valley flank of the col. The lowest moraine crest is at an altitude of 297 m OD on the valley floor. The 325 m shoreline is cut into the upper part of the moraines on both sides of the valley, which suggests that the 325 m shoreline was formed after the deposition of the moraines.

On the western side of Caol Lairig, the lateral meltwater channels are also clear, but these appear on NEXTMap to be associated with drift benches that are inclined down valley at similar gradients to the meltwater channels, and hence appear to represent trim-lines (Figure 6.8B). These have a similar gradient to the meltwater channels, and when projected southwestwards (down valley) also link to a short drift ridge, which is interpreted as a fragment of lateral moraine. An upper trim line is approximately 590 m in length and dips from an altitude of 375 m at its southwestern extent to 357 m at the eastern end. This appears to be associated with the arcuate moraine ridge previously described. In addition at this locality, a bench that dips from 356 m OD to 350 m OD with dimensions of 150 m x 55 m merges with the 350 m shoreline at its eastern extremity. Delta fragments on the floor of the Ionrainn outlet are heavily dissected but clearly have an overall apex that coincides with the 325 m shoreline (Figure 6.8B). NEXTMap DEM data indicate that a total of six sharply-incised, steep-sided channels run sub-horizontally from SW to NE between altitudes of 475 m and 360 m OD at locality d in Figure 6.10B (see also d in Figure 6.3). The largest channel is 144 m in length and 71 m wide. Their configuration, lack of obvious interconnection and disconnection from any in-feeding higher drainage system suggests that these are ice-marginal meltwater channels. The gradient on these channels suggests that they may

be associated with trim-lines detected further to the SW, at locality m in Figure 6.10B. At this locality, Sissons (1979b) mapped a lateral moraine ridge. Close inspection of the NEXTMap DEM data in this vicinity shows that a bench does indeed exist on this flank of Caol Lairig, which can be traced for up to 500m in length, and which in places is 20 to 37 m in width. However, what can also be detected on the DEM plots are two subtle linear features that extend between this bench and the southern termination of the 325 m lake shoreline. These trim-lines trend towards the meltwater channels, and may have been formed at the same time as the channels were incised. It seems highly likely that the channels, trim-line and lateral bench all trace the upper limit of an ice mass that probably occupied Caol Lairig during the time the 350 m and 325 m lakes extended into Caol Lairig. The collective evidence in this vicinity therefore suggests the upper ice margin and gradient for the glacier delimited in Figure 6.8B.

Figure 6.10 A and B shows a number of features in the lower Glen Roy area mapped directly from NEXTMap, with the area around the confluence between Glas Doire and the Roy expanded in Figure 6.10 C and D. Some subtle features can be noted that have not been reported in the published literature. For example, a small delta, approximately 141 m long and 30 m wide occurs on the southern flank of Coire Ionndrainn, with a surface elevation between 357 m and 351 m OD (feature b, Figure 6.10B). Its exact relationship to the 350 m shoreline is, however, not clear, for this shoreline is poorly developed here, compared with the northern side of the valley. Another better developed delta-shaped fan that lies at the confluence of the Ionndrainn and Caol Lairig streams (feature c, Figure 6.10B) was noted by Peacock and Cornish (1989). It has an apex at 304 m and distal edge at 258 m OD, as it spreads southwards into Caol Lairig. It is 960 m long along its main axis and 434 m wide at its lower limit. Peacock and Cornish (1989) noted that parts of these delta surfaces were covered by lake deposits, and concluded that the delta deposits were formed during the rising and falling sequence of

the 297 m lake in Caol Lairig. The present author considers that these deltas were formed mainly in the falling sequence of the 297 m lake, as glacier advance to the arcuate moraine ridge near the Caol Lairig-Roy col would have destroyed features laid down during the rising sequence.

In the area around the Viewpoint in lower Glen Roy, the shorelines observed in NEXTMap DEM data generally accord with the mapping of Sissons, Peacock and Cornish, and with their representation on the OS map (Figure 6.7), except that the shorelines are more fragmentary in the images than depicted in published maps. There is also general accordance in the form and interpretation of the ‘massive drift accumulation’, the dissected mass of deposits that marks the LLR ice limit in the vicinity of the Viewpoint (feature f, Figure 6.10B). In NEXTMap this feature can be traced over 1.7 km along the valley floor, and is up to 0.85 km wide, with the majority of the accumulation occurring below the 260 m shoreline on both sides of the valley floor. The drift accumulation is heavily dissected by gullies running down slope. North of the massive drift accumulation, the floor of the Roy valley is characterised by more subdued landforms, and this contrast is very clear on the NEXTMap plots, which supports previous interpretations that the northward margin of the massive drift accumulation represents the LLR ice limit. However, whereas Sissons (1979b) described the limit as being marked only by “moraines”, Peacock and Cornish (1989) interpreted it as part “moraine” and part “drift limit”, though the precise nature of the ‘drift’ is not specified. Sissons’ assessment is preferred, because the limit of the massive drift accumulation clearly coincides with terminal moraine ridges that extend on both sides of the valley (features g in Figure 6.10B and 6.3). On the east flank of Glen Roy, these extend from just below the 260 m lake shoreline up to 376 m OD on the higher valley flank. These terminal moraine ridges are cut into by all three of the lake shorelines, a point returned to in a later section of this chapter.



To the south of the Viewpoint another series of cross-valley ridges, mapped by Sissons (1979b) but not by Peacock and Cornish (1989), occur at locality h in Figure 6.10B and 6.3. Sissons, however, only records them as extending across the valley below the level of the 260 m shoreline (see Figure 6.3A), whereas the NEXTMap plots clearly show a series of ridges running up the valley flanks, in line with the lower moraine ridges mapped by Sissons. On the western flank of the Roy, seven separate ridge fragments can be observed, extending up to an altitude of c. 370 m, while on the eastern flank 13 fragments extend up to an altitude of 361 m. These observations suggest a broad terminal ice front occupied this locality, probably around the time that the 325 m lake existed, since this moraine limit lies close to the southerly limits of the 325 m shorelines. Another terminal moraine was identified by Sissons (1979b) at locality k in Figure 6.10D and 6.3, in the upper part of Gleann Glas Dhoire, but this proved difficult to corroborate using NEXTMap plots as a result of masking by woodland cover.

Inspection of NEXTMap DEM data suggests that three faint trim-lines occur on the southern flanks of Bohuntine Hill, marked as n, o and p on Figure 6.10B. The lowest (feature n) lies at an altitude of 372 m, the middle one (o) at 460 m and the highest (p) at 492 m. The middle feature (o) bears a resemblance to, and lies at a similar altitude to, feature m (altitude 461 m) in Caol Lairig, previously described. It is speculated that the uppermost marks the maximum LLR ice limit, and the others reflect temporary positions of the lateral ice margin during retreat. The features are very faint, and are best observed on screen, under magnification, but an attempt is made to depict them on false colour images in Figure 6.11 and 6.12, with the latter showing the features better. The eastern end of feature n lies close to the end moraines at locality h (see above) and the gradients of all three trim-lines are similar to that inferred for feature m the west bank of Coal Lairig. Hence it is further speculated that the middle trim-line line (feature o) is

related to the 350 m falling lake and the lower line (feature n) to the 325 m lake in the falling sequence.

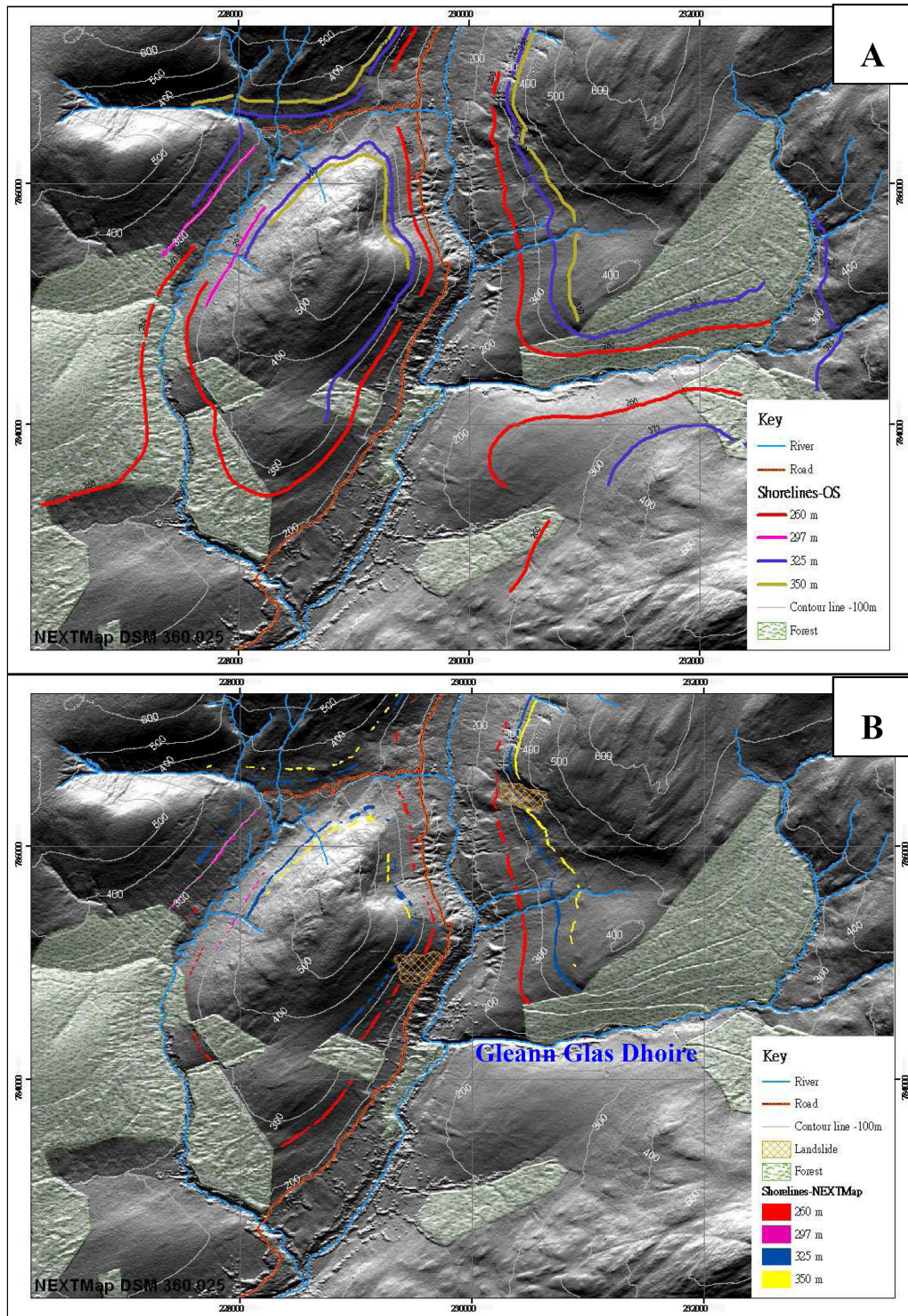


Figure 6.7 Ice-dammed lake shorelines in lower Glen Roy: A is digitized from the 1:25,000 scale Ordnance Survey map, B has been mapped from NEXTMap DEM data where not obscured by recent forestry plantation. The NEXTMap plots show in much greater detail how the shorelines vary in surface detail and are more fragmented than depicted in published maps.

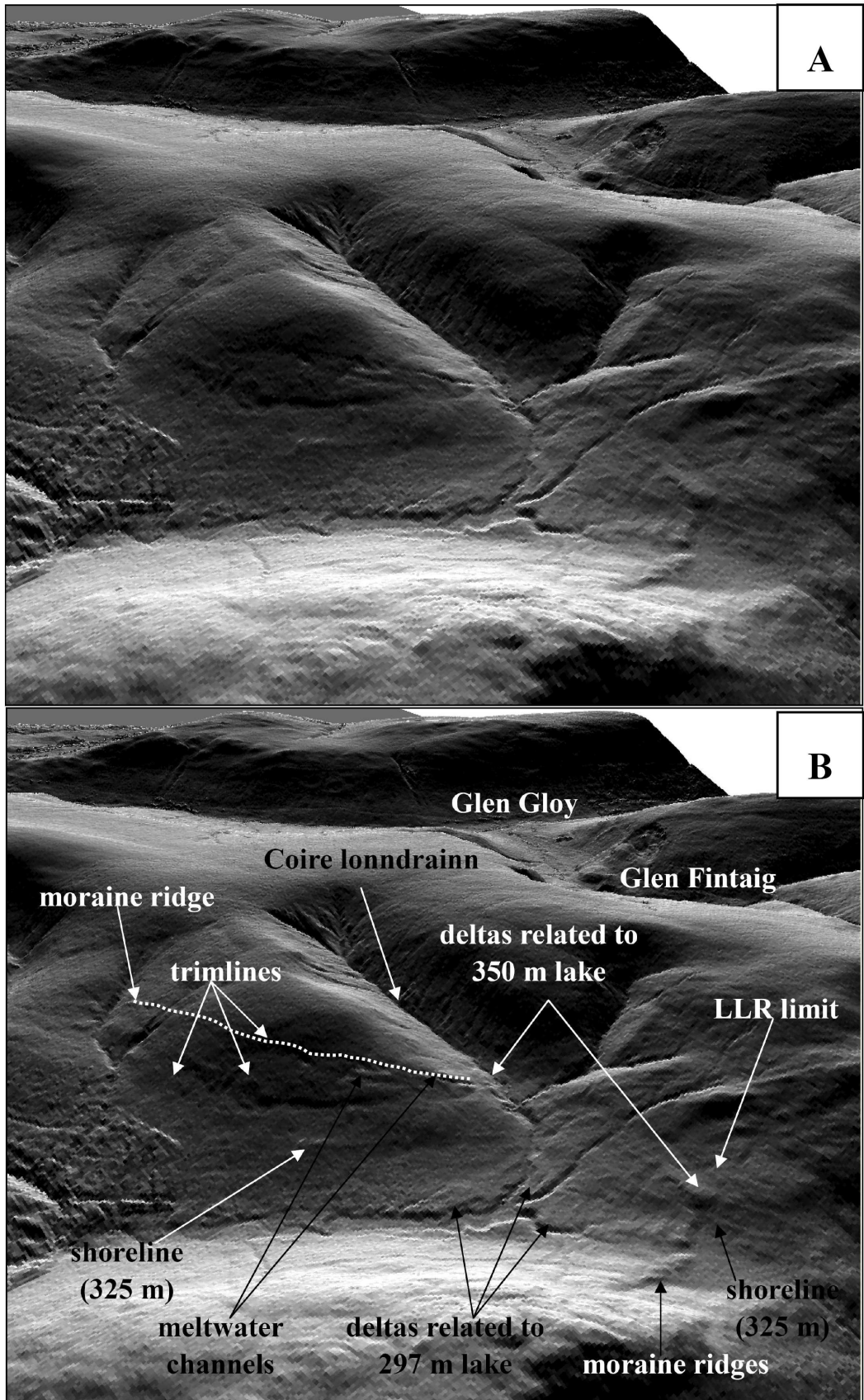


Figure 6.8 3D perspective of the Caol Lairig area from the SE direction (Illumination setting: Azimuth – 310°, Altitude – 30°). A is the unmarked image, while B indicates the positions of critical features.

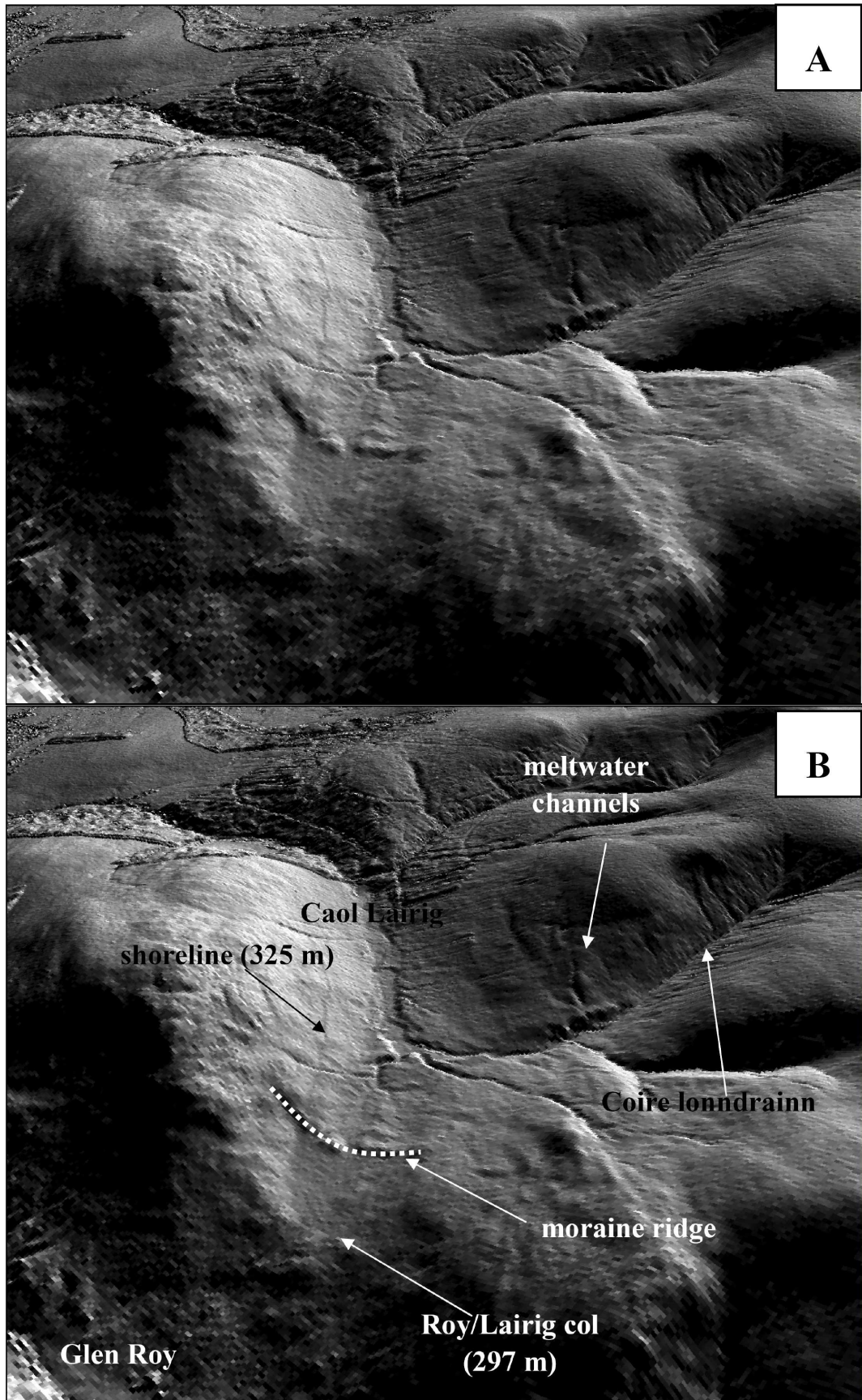
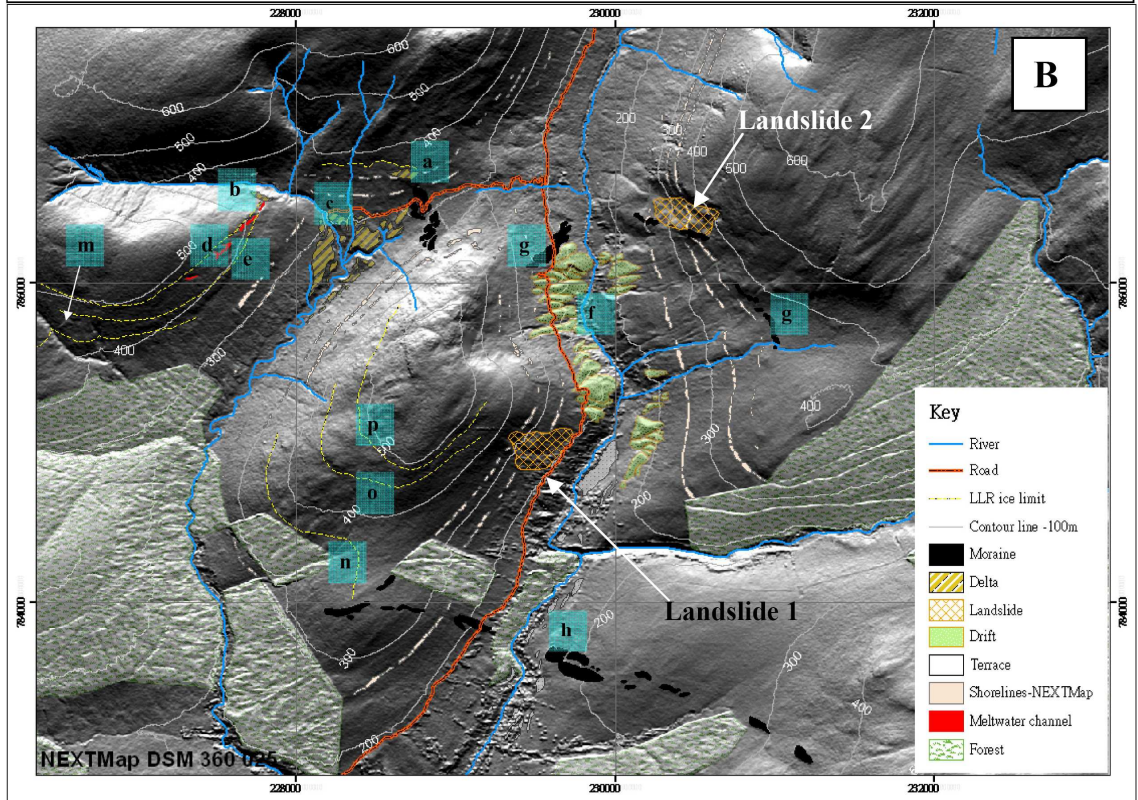
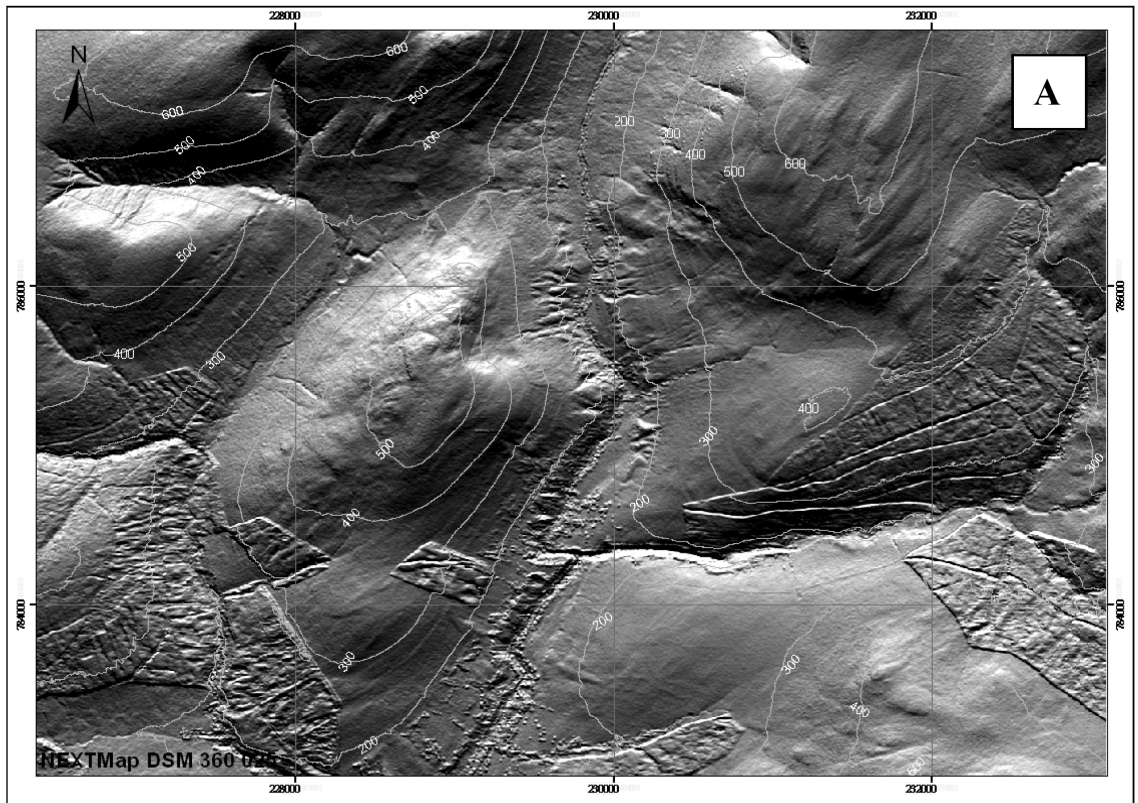


Figure 6.9 3D perspective of the Caol Lairig area from the NW direction (Illumination setting: Azimuth – 260°, Altitude – 30°). A is the original unmarked image, while B indicates the positions of critical features.



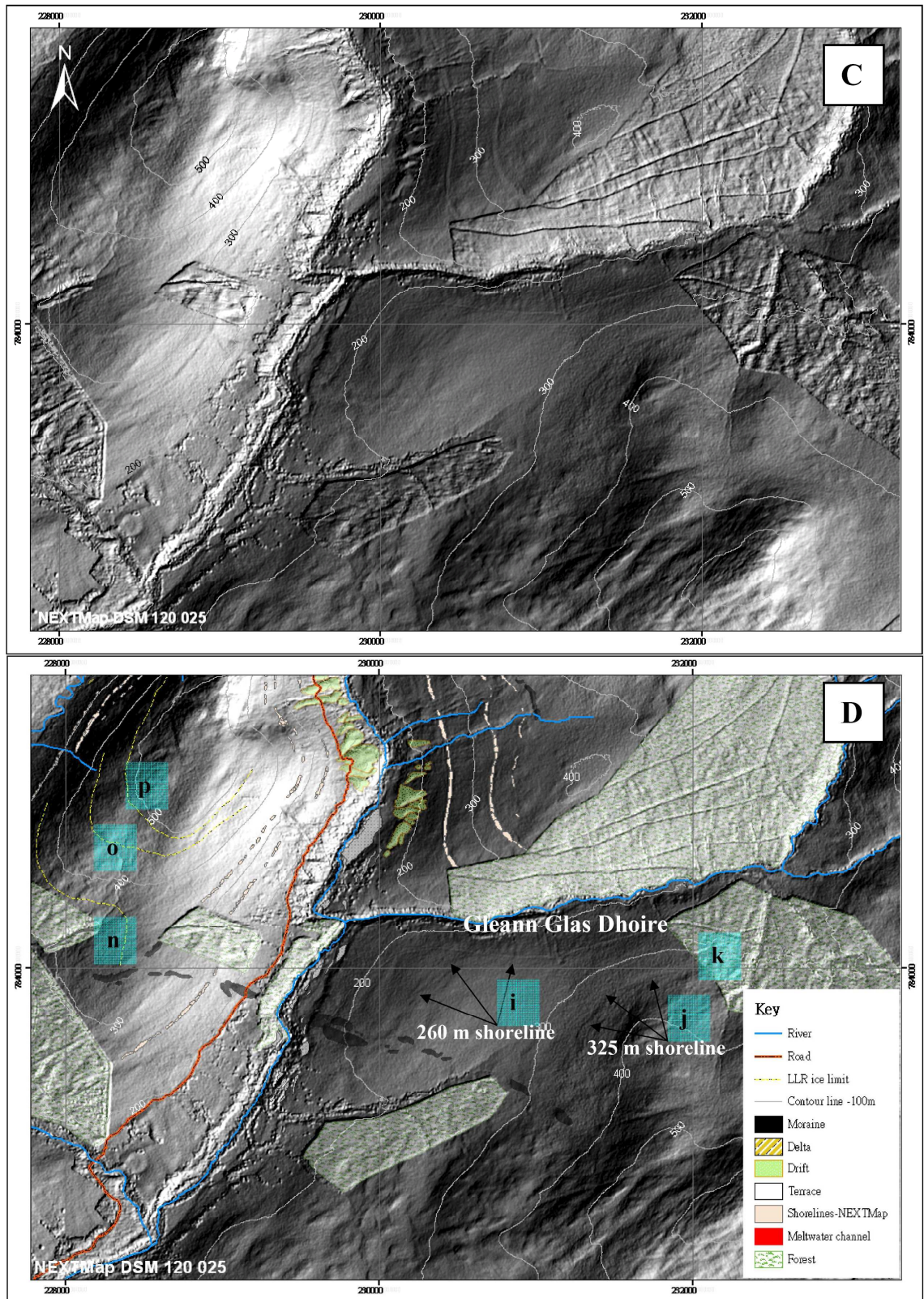


Figure 6.10 Digitised map of the distribution of landforms in lower Glen Roy as depicted on Hillshade NEXMap DEM data. A and C are the unmarked images, B shows landforms identified from the NEXMap plots, and D shows some features in larger scale and the distribution of the 325 m and 260 m shorelines that have not been examined in detail in the present research. (See Figure 6.3 for comparison.)

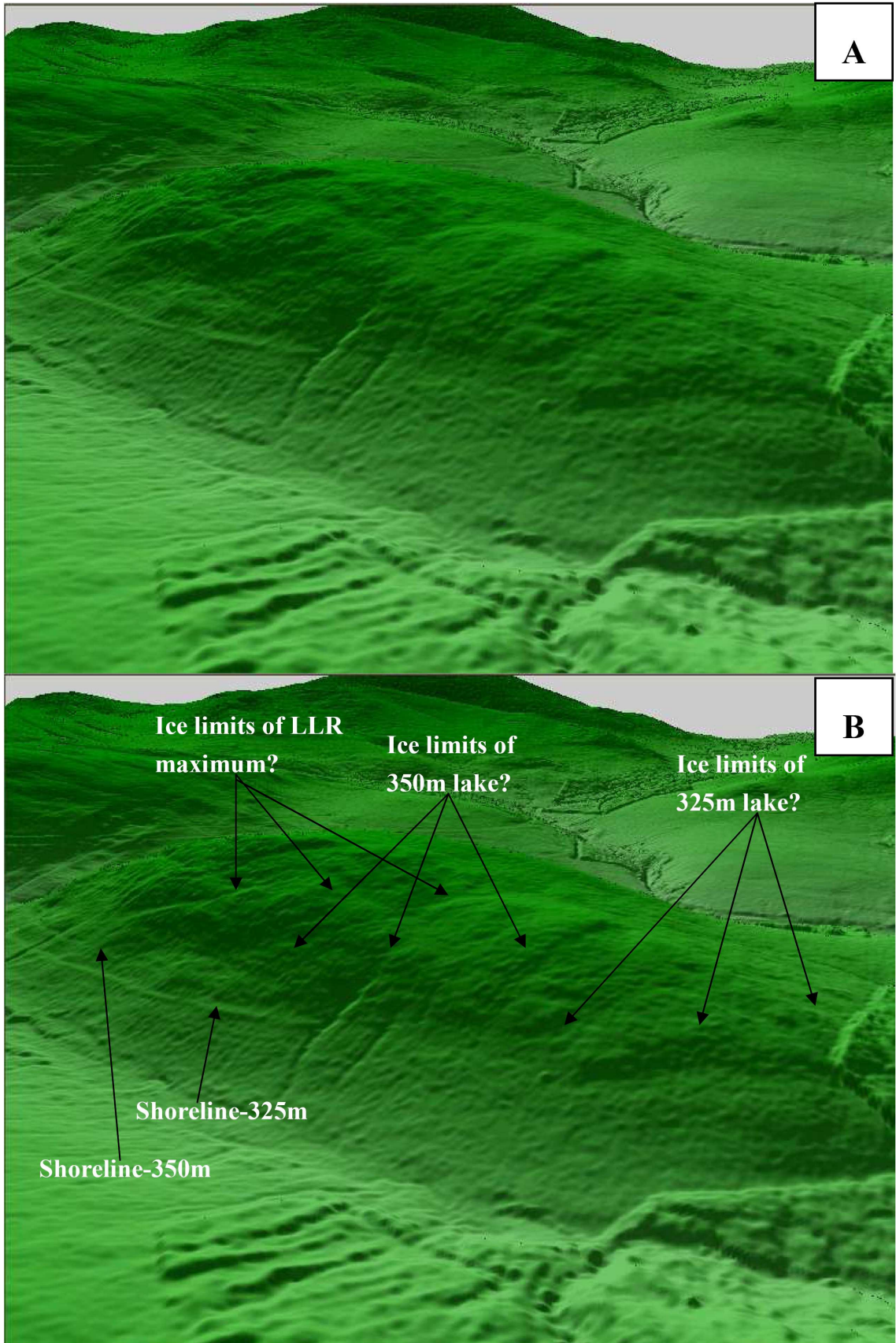


Figure 6.11 3D perspective of southern flank of Bohuntine Hill viewed from SW direction (Illumination azimuth  $75^\circ$  from altitude  $25^\circ$ ; image contrast ratio 75%). A is unmarked image while B shows mapped features. (See Figure 6.10 for comparison).

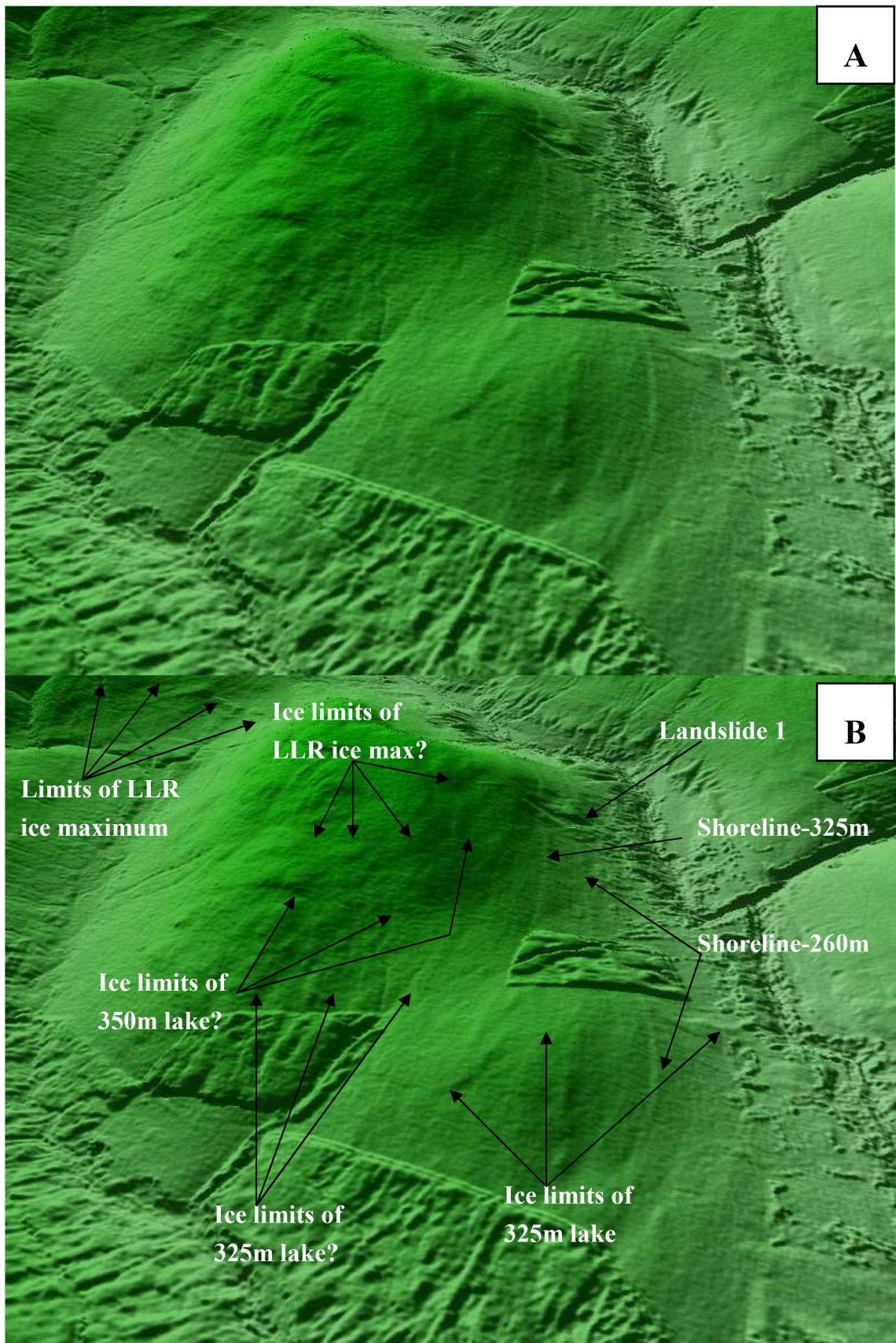


Figure 6.12 3D perspective of southern flank of Bohuntine Hill viewed from S direction (Illumination azimuth  $7^\circ$  from altitude  $25^\circ$ ; image contrast ratio 90%). A is unmarked image while B shows mapped features. (See Figure 6.10 for comparison).



### 6.2.3.3 Evaluation

Most of the landforms associated with glacier activity in lower Glen Roy during the Loch Lomond Stadial discussed above were identified in previous studies and included in maps published in Sissons (1979b) and Peacock and Cornish (1989). There is general accordance, therefore, between the evidence examined in the present study and that of previous research, concerning the former ice limits and how they relate to the lake shorelines. However, some differences in detail have been noted, which add some finesse to the established Sissons model. In particular, the possible trim-lines identified on the southern flanks of Bohuntine Hill and in Caol Lairig may provide additional guidance as to the dimensions of the LLR ice body at different stages in ice retreat. In Caol Lairig, the maximum position of the LLR ice position is demarcated by a prominent terminal moraine (feature a in Figure 6.3 and 6.10), by ice-marginal meltwater channels (feature d in Figure 6.3 and 6.10) and by an ice-marginal delta (feature b, Figure 6.3 and 6.10), all showing that ice occupied almost the whole of Caol Lairig at the LLR maximum. Yet mapping of former lake shorelines indicates that a lake with a surface altitude of 297 m occupied much of the northern part of Caol Lairig during deglaciation, because the shorelines are found down-valley of the terminal moraine. This lake could only have existed after the lake levels in Glen Roy had declined to the 260 m level, otherwise the water of the 325 m lake would have flooded into Caol Lairig. This in turn means that the Spean-Roy Glacier ice front must have receded beyond the Gleann Glas Dhoire tributary valley and 325 m overflow col into Glen Spean during the time that the Caol Lairig Glacier ice was maintained relatively close to its maximum position. The Spean-Roy Glacier therefore appears to have receded much more quickly than the glacier front in Caol Lairig. This is important evidence for non-contemporaneous adjustments of the ice fronts during ice decay. This point will be returned to later in this chapter, while a detailed analysis of the lake shorelines themselves is provided in Chapter 7.

## 6.3 Middle section of Glen Roy

### 6.3.1 Introduction

The most conspicuous landforms of middle Glen Roy are three large fans: the Allt Bhreac Achaidh Fan, the Brunachan Fan and the Reinich Fan (Figure 6.13). There is also evidence for crustal block deformation, as indicated by dislocation of the Parallel Roads, reported by Sissons and Cornish (1982b) and discussed in detail in Chapter 7. In this section, the author will restrict attention to a review of published interpretations of the three major fans and a re-evaluation of the evidence in the light of observations made using NEXTMap DEM data.

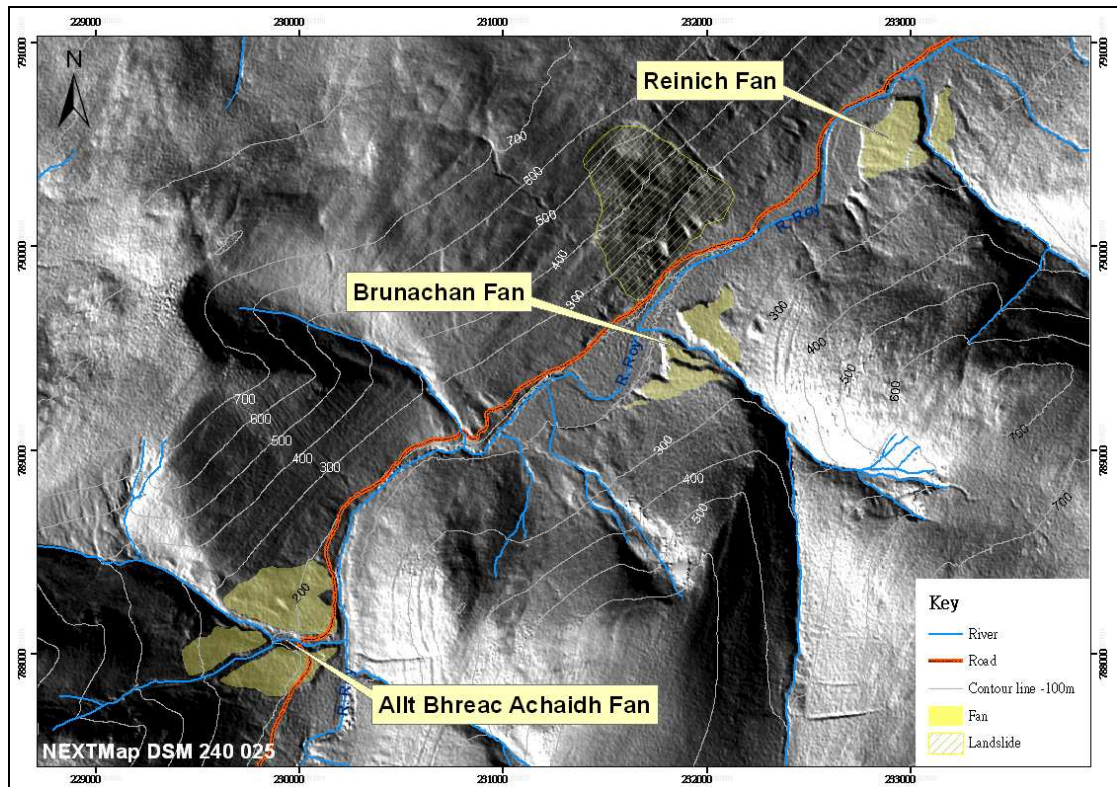
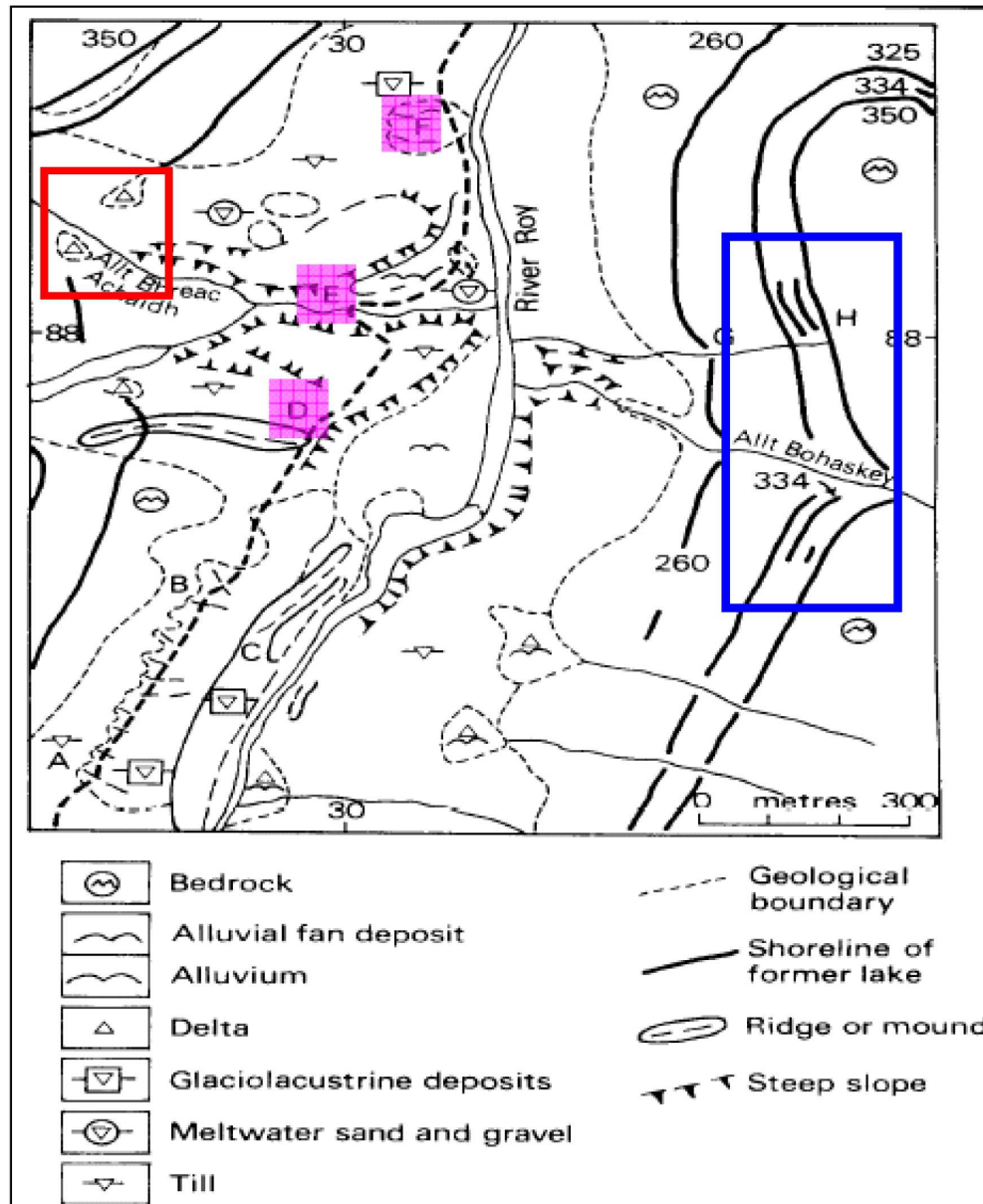


Figure 6.13 Location of the Allt Bhreac Achaidh Fan, the Brunachan Fan and the Reinich Fan in the middle section of Glen Roy. The boundaries of the fans were mapped using NEXTMap Slope images that best depict the fan surfaces.

### 6.3.2 Allt Bhreac Achaidh Fan

There is little published detail on the Allt Bhreac Achaidh Fan (ABAF), which is composed of sediment sourced from the Allt Bhreac Achaidh stream that is currently

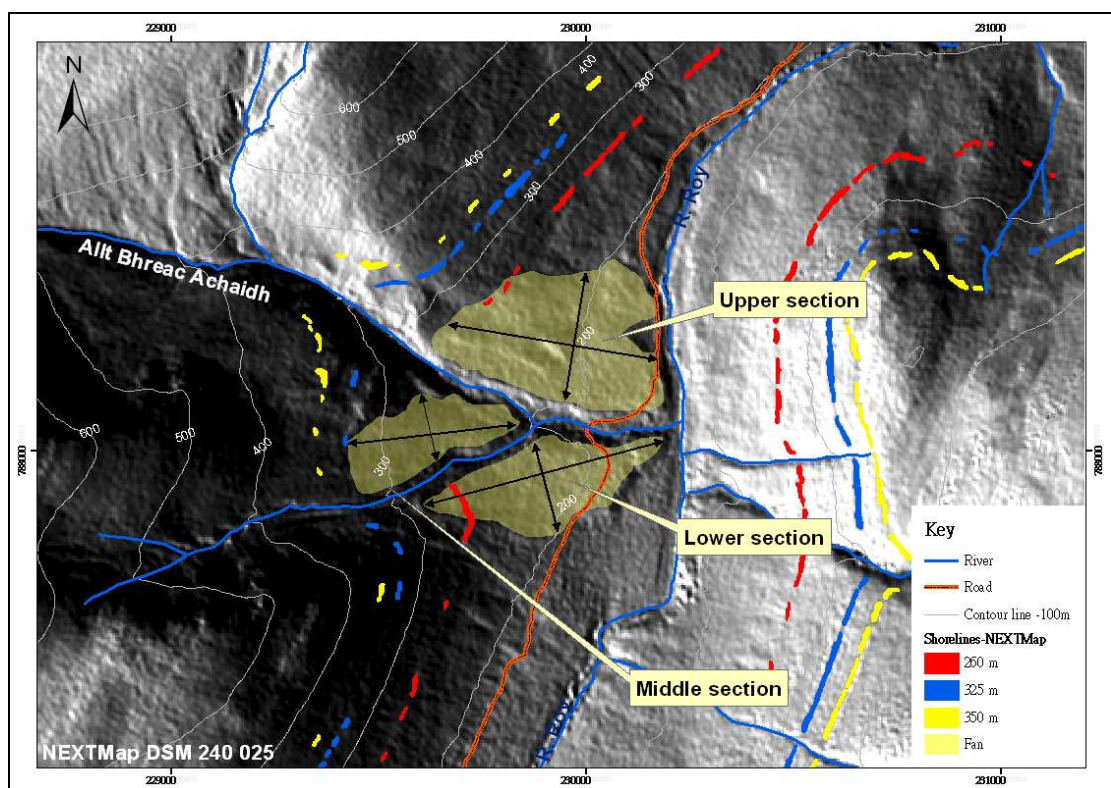
incised into the fan surface and adjacent lake shorelines. Peacock and Cornish (1989) provide the only published geomorphological map of the ABAF (Figure 6.14).



**Figure 6.14** The Allt Bhreac Achaidh Fan and adjacent landforms (from Peacock and Cornish 1989, Figure 9). The blue rectangle highlights the area where the 334 and 344 m minor shorelines are located. For further explanation, see text.

In addition to generating the map shown in Figure 6.14, Peacock and Cornish (1989) also examined the nature of the sediments exposed at several localities. Sediments exposed in the fan at locality E consist of 4 m of silty till overlain by 0.3 – 1.5 m of laminated clayey silt. Other parts of the fan are composed of a complex of undulating

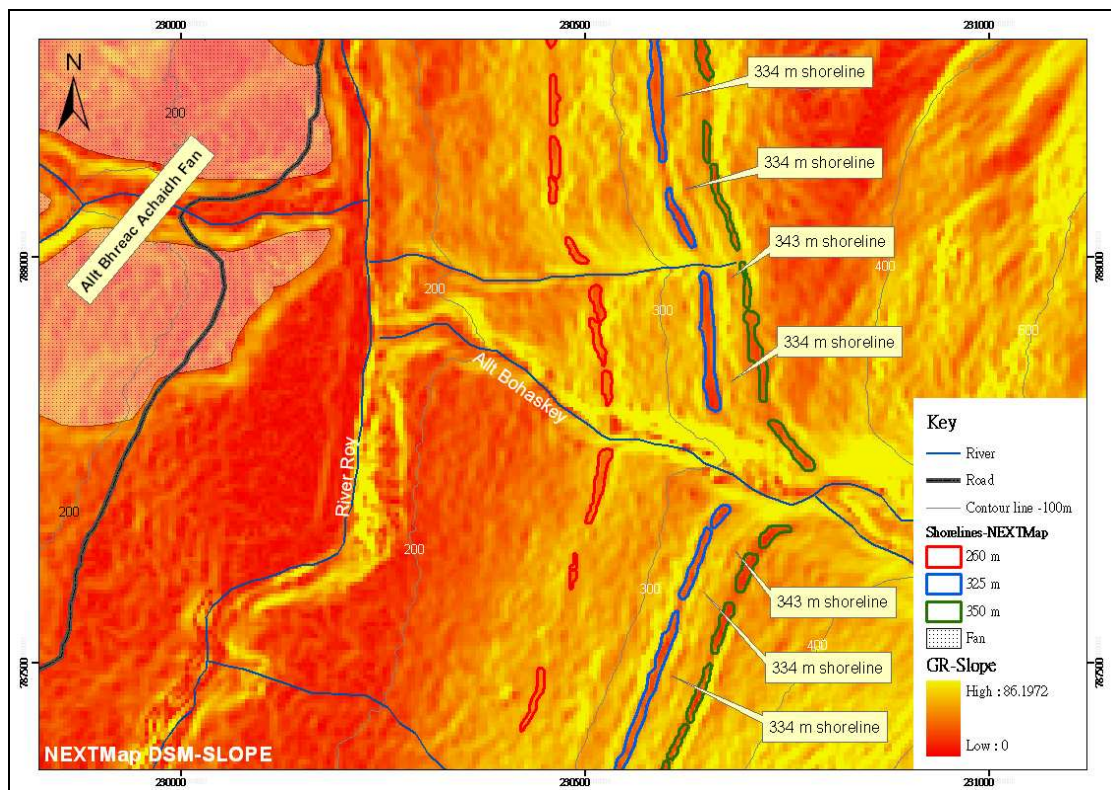
till, sand and gravel mounds, lake sediments and erosional terraces, but there are also ridges or mounds on the fan surface (D+F). In addition, landforms coincident with the 260 m shoreline are interpreted as deltas (the features within the red square in Figure 6.14). On the eastern side of the valley, adjacent to Allt Bohaskey, two rock-cut benches were observed at 334 and 344 m, and are interpreted as shorelines cut prior to the LLR (within the blue rectangle). From these descriptions, it is difficult to establish the origin of the fan.



**Figure 6.15** The surface and margins of the Allt Bhreac Achaidh Fan and preserved parts of the Parallel Roads on adjacent slopes, mapped using NEXTMap DEM data.

Examination of the fan and the adjacent parts of the valley using NEXTmap DEM data (Figure 6.15) adds very little to the picture, except that it demonstrates that the feature does not have a simple form. The streams have dissected the fan into three blocks, termed the lower, middle and upper sections for descriptive purposes. The longest axis of the upper section runs down-slope over 514 m and is at maximum 314 m wide, with

the apex meeting the 260 m shoreline. The middle section is 410 m long and 165 m wide, with the apex at 325 m, and hence may be associated with the 325 m lake. The lower section is 593 m long and 231 m wide, with apex lying above the 260 m shoreline, which cuts into the fan surface. The fan may be a complex feature, with some or all of the deposits pre-dating the formation of the 260 m lake in the falling lake sequence. The association of the highest part of the fan with the 325 m lake shoreline might indicate an association with the lake, but this is not clear. Ultimately it is only possible from NEXTMap DEM data to describe the general form of the fan deposits, and any direct association between fan deposition and lake formation remains speculative.



**Figure 6.16** The 334 m and 343 m minor shorelines at Allt Bohaskey as depicted on NEXTMap DEM data. This figure is a slope map which represents changes in slope relief (reddish orange for gentle slopes; yellow for steeper slopes).

What the NEXTMap plots do support, however, is the presence of feint steps at 334 m and 343 m that continue for some distance along the eastern flank of the Roy Valley in the vicinity of Bohaskey (Figure 6.16), in the place in which Peacock and Cornish

(1989) reported the presence of 'minor shorelines'. NEXTMap measurements suggest the higher feature to lie at 343m and not 334 m, but for ease of communication this is marked on Figure 6.16, and will continue to be termed, as the 344 m minor shoreline. The origin of these shorelines is unclear, but they might represent faint remnants of older (pre-Loch Lomond Readvance) shorelines that have survived glaciation during the LLR. An alternative possibility is that lake water could have escaped over the margins of the ice as it advanced into Glen Roy and before it completely blocked Gleann Glass Dhoire to form the 350 m lake. Neither of these explanations are testable, however, with present information.

### **6.3.3 The Brunachan Fan**

Peacock (1986) has published a generalised map of the form of the Brunachan Fan, which is located to the north of the ABAF (Figure 6.17). The fan has been deeply incised by the Allt Brunachan stream, to form two main sections. According to Peacock (1986), the fan surface changes abruptly in altitude by approximately 60 m (from below 210 m OD to 270 m OD) and is cut into by the 260 m shoreline in its upper part. He also reported exposures on the north side of the fan, near a 245 m OD bluff, which reveal very poorly sorted and well imbricated boulder gravel overlain by laminated silt. On the south side of the fan, he found a 10 to 20 mm-thick bed of sheared yellow-brown laminated clay resting on, and penetrating into cracks in the local bedrock, and which were overlain by slumped gravel. Furthermore, at locality J (Figure 6.17) he described an exposure of sediments, 8.5 m in thickness, composed of clast-supported, matrix-rich cobbly gravel, interbedded with open-work gravel and sand, capped by a further 1m of laminated silt.

There are two main schools of thought regarding the possible formation of the Brunachan Fan. Sissons and Cornish (1983) favour a subaqueous origin, with the

sediment in the main body of the fan transported during high discharge events, probably caused by rapid snow melt in the fan's catchment during spring thaws. Because the 260 m shoreline cuts into the fan surface, they see the main period of fan aggradation to have likely occurred prior to and during the rising 260 m lake level. Peacock (1986) on the other hand suggested that the basal laminated silt found on the southern side of the fan may indicate a lacustrine phase prior to fan deposition, and was of the view that the overlying gravels were reworked from glacial drift by the Allt Brunachan stream. Another possibility, in the present author's view, is that the gravels and thin laminated silts in this part of the fan were derived entirely by paraglacial processes, deposited following the wasting of glacier ice in Glen Roy during the Dimlington Stade.

NEXMap DEM data clearly show that the Brunachan Fan has been dissected by streams into 4 main sections (Figure 6.18) rather than the two suggested by Peacock and Cornish (1989), and that in part this has resulted from avulsion of the Allt Brunachan stream. Section one is 366 m long and 255 m wide with an apparent maximum thickness of 17 m, while the corresponding values for the other three sectors are 197 m, 56 m and 13 m for section 2, 401 m, 166 m and 23 m for section 3, and 114 m, 19 m and 20 m for section 4, respectively. Sections 1 and 2 are separated by the Allt Brunachan, and it is possible to identify a 12m high bluff that separates sections two and three, with section 2 at the lower altitude. This step was also identified by Peacock (1986). The elevation of the fan changes from 265 m OD to 210 m OD at its distal edge with a change in relief of 55 m. The boundary of section 4 is difficult to resolve and only the flat surface has been mapped in this research. Nonetheless it is still possible to identify that the 260 m shoreline is cut into the fan surface close to its apex, implying that the fan formed prior to the falling sequence of the lake systems, though its formation could pre-date the 260 m lake by a considerable period.

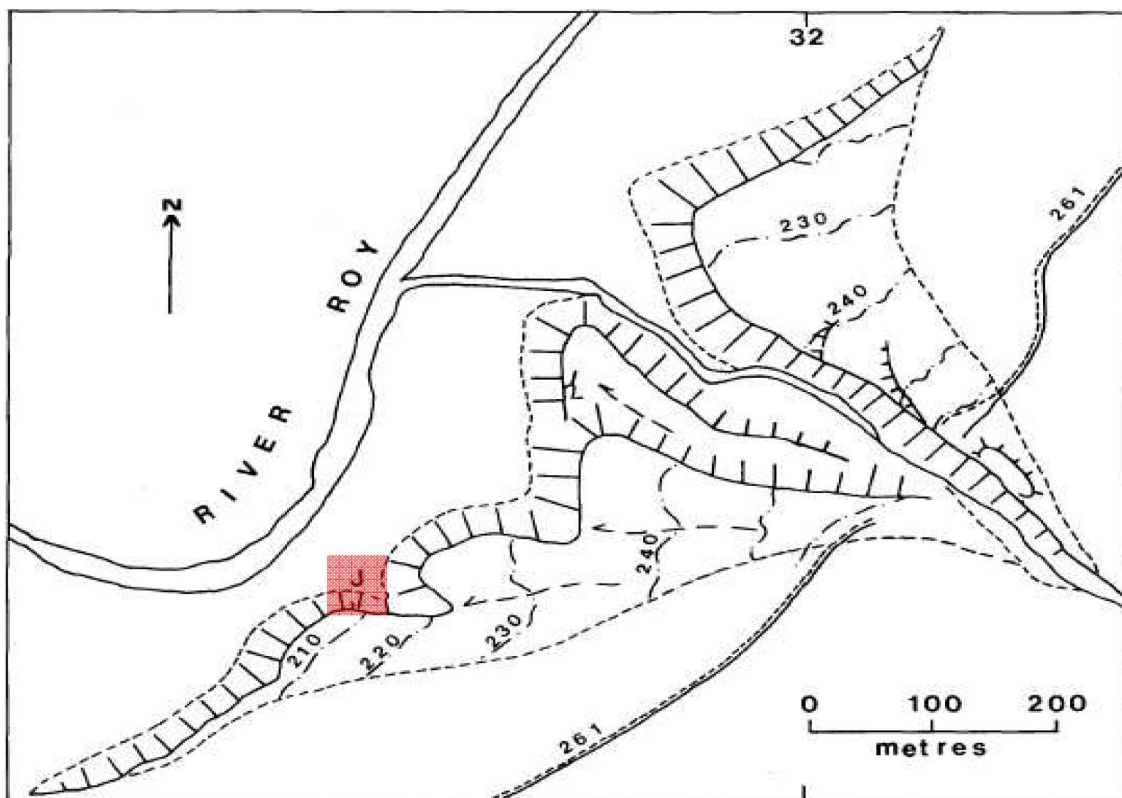


Figure 6.17 Geomorphological map of the Brunachan Fan (from Peacock, 1986).

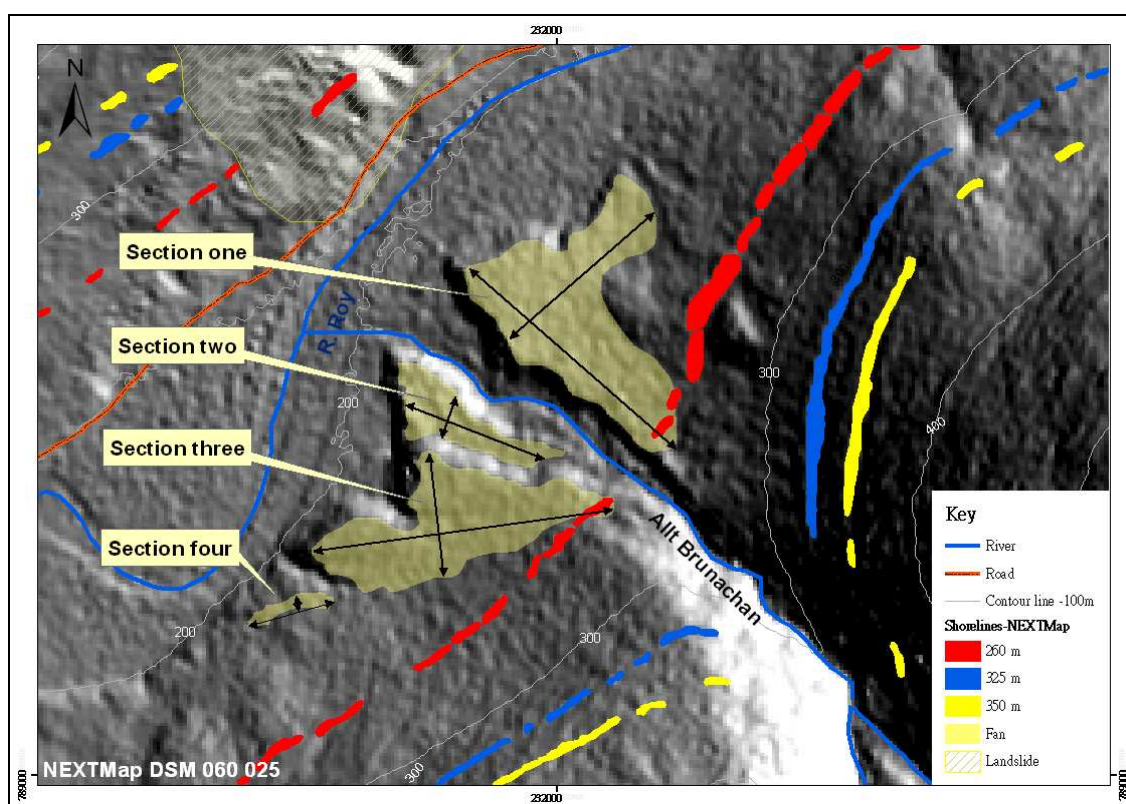


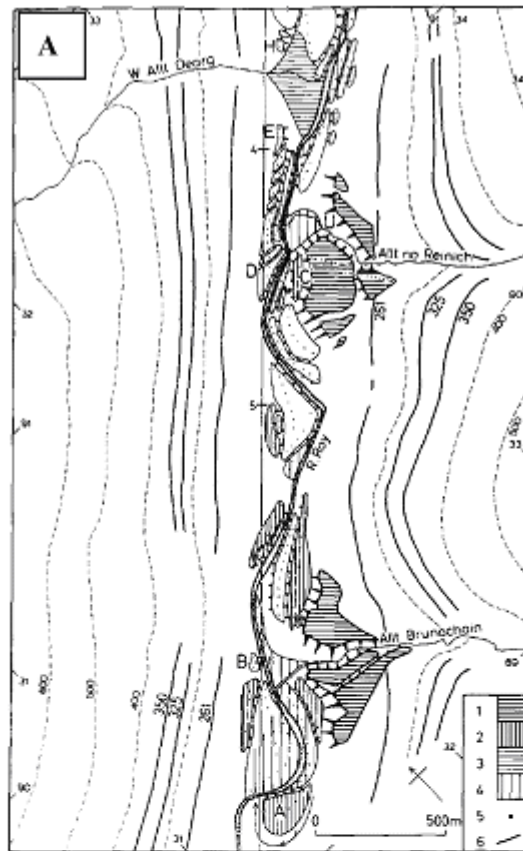
Figure 6.18 Surface form and margins of the Brunachan Fan and distribution of preserved parts of the Parallel Roads on adjacent slopes, mapped using NEXTMap DEM data. The fan has been dissected into four parts (sections), as described in the text.



#### **6.3.4 The Reinich Fan**

The Reinich Fan, located to the north of the Allt Brunachan Fan, has been mapped by both Sissons and Cornish (1983) and Peacock (1986), who recognised two main parts, separated by the Allt na Reinich stream which has dissected the main body of the fan (Figure 6.19). There are differences in detail between the two interpretations, however: the fan is shown to be fragmented in the Sissons and Cornish (1983) map by comparison with the Peacock (1986) map, while the latter shows more extensive deposits to the north of the Allt na Reinich than the former. Both, however, recognise a distinct 5m high bluff in the southern part of the fan, the top of which coincides in altitude with the 260 m shoreline (Figure 6.19 and 6.20). Below this bluff, Peacock suggests that shallow longitudinal depressions and ridges (up to 3 or 4m in height) traverse the surface of the lower parts of the fan, but these are not represented in the Sissons and Cornish (1983) map. Peacock (1986) also examined sediments exposed in the fan and observed a cover of laminated silts up to 2 m in thickness on the fan surface, as well as about 0.5 m of laminated silts with convolutions near the base of the fan at locality H (Figure 6.19B). Below this, Sissons and Cornish (1983) suggest that a fluvial terrace cuts into the toe of the fan, where gravels are exposed. However, Peacock (1986) regards this as a thin veneer of gravel that overlies (probably) till and bedrock. On the northern part of the fan at locality I (Figure 6.19B), Peacock (1986) observed a section with compact, clast-supported, bouldery gravel in the lower bluff: he interpreted the upper, gently inclined part of the fan as a delta associated with the 260 m lake, and the lower part as an alluvial fan which could have been formed either subaerially or subaqueously. Sissons and Cornish (1983) suggested a subaqueous mode of formation for the Reinich Fan, as they had also concluded for the Brunachan Fan, with sediment transported from the relatively small Reinich catchment during periods of high discharge, probably by melting snows in spring. They also concluded that the fan

sediments accumulated during the rising sequence of the 260 m lake system, because that shoreline is etched into the fan surface.



- Key: (according to original descriptions)**
1. Fans associated with the 26 1m lake.
  2. Terrace AC of Fig. 4.
  3. Fan post-dating the 26 1m lake.
  4. Floodplain.
  5. Levelled points.
  6. Parallel roads.

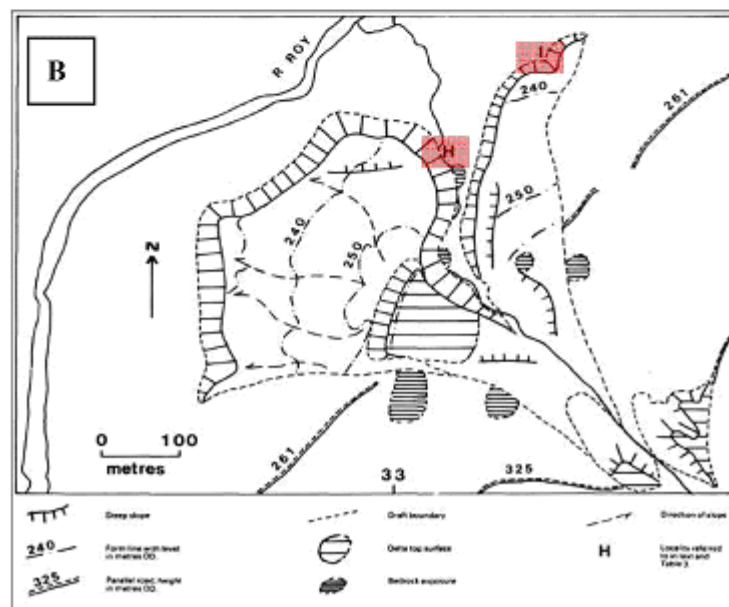
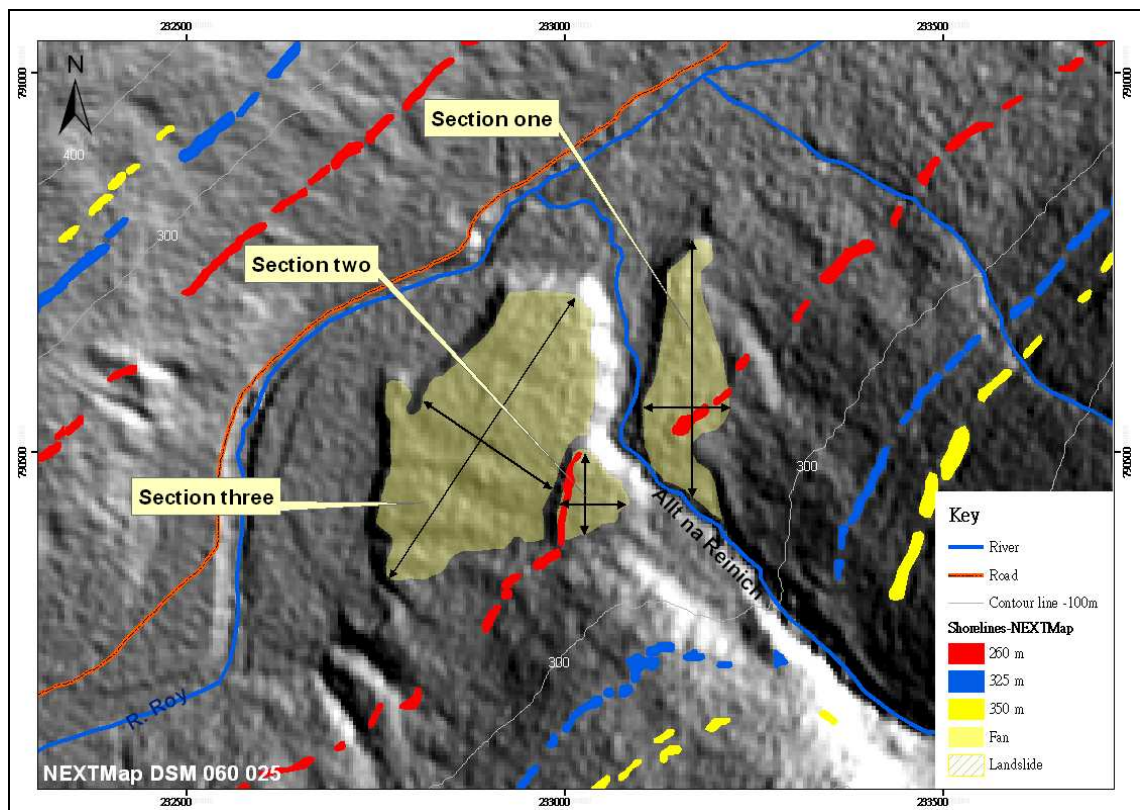


Figure 6.19 Geomorphological maps of the Reich Fan: A from Sissons and Cornish (1983) and B from Peacock (1986).



**Figure 6.20** The form and margins of the Reinich Fan mapped using NEXTMap DEM data. The 260 m shoreline passes through the upper part of section one and the western edge of section two.

The NEXTmap DEM data of the Reinich Fan show some similarities and dissimilarities with both published maps (Figure 6.20). The fan appears not to be as heavily dissected as indicated in the Sissons and Cornish (1983) map, not to be as extensive to the north of the Allt na Reinich as indicated in the Peacock (1986) map, and to show minor ridges and depressions over the fan's inclined surface, but they are not nearly as pronounced as suggested by Peacock (1986). The most significant feature, however, is the clear etching of the fan surface by the 260 m shoreline, in both the northern and southern parts of the fan (Figure 6.20). Above this, the apex of the fan appears as a small delta superimposed on the larger fan body below, though this could not be confirmed by sedimentological observations, as no significant exposures could be found on the fan, either in the field or on the NEXTMap plots. It should also be noted that Peacock (1986) identified two delta fragments with surfaces at 325 m on the steep valley sides of the Allt na Reinich (lower

right corner of Figure 6.19B), but these are not evident in the NEXTMap plots obtained for this locality.

### **6.3.5 Evaluation of landforms in Middle Glen Roy**

The origin of the massive fans that dominate the middle part of Glen Roy have long been disputed, with Sissons and co-workers favouring rapid deposition of the fans during the Loch Lomond Readvance, while Peacock favours an origin during an earlier glacial interlude, with the possibility of some minor deposition superimposed on pre-existing fans during the LLR. There are only three lines of evidence that can currently be brought to bear on this problem: morphology of the features, sedimentological observations (where possible) and the relationship between the lake shorelines and the fans. Sedimentological studies were not undertaken as part of this PhD project, and hence the only perspective that can be examined here is the precise relationships between the fans and the lake shorelines.

In the field the three main shorelines appear well developed and preserved on both sides of the valley. This is also the case on NEXTMap plots, though the shorelines are not as continuous as suggested by O.S. maps, especially with respect to the 350 m shoreline on the western flank of the Roy Valley and in the cases of all three shorelines on the slopes adjacent to the Allt Bhreac Achaidh Fan (Figure 6.21, white rectangle). All three shorelines are, however, particularly well developed on the eastern flank of the valley, in the vicinity of the Brunachan and Reinich fans (Figure 6.22). From Figure 6.22 it can be seen that all three fans considered above have apexes at or close to the 260 m shoreline, and, perhaps just as significantly, there are no major fan developments associated with either the 325 or 350 m shorelines. The origins of the fans will be discussed again in the final section of this chapter, after consideration of the additional evidence available for major debris fans in Upper Glen Roy.

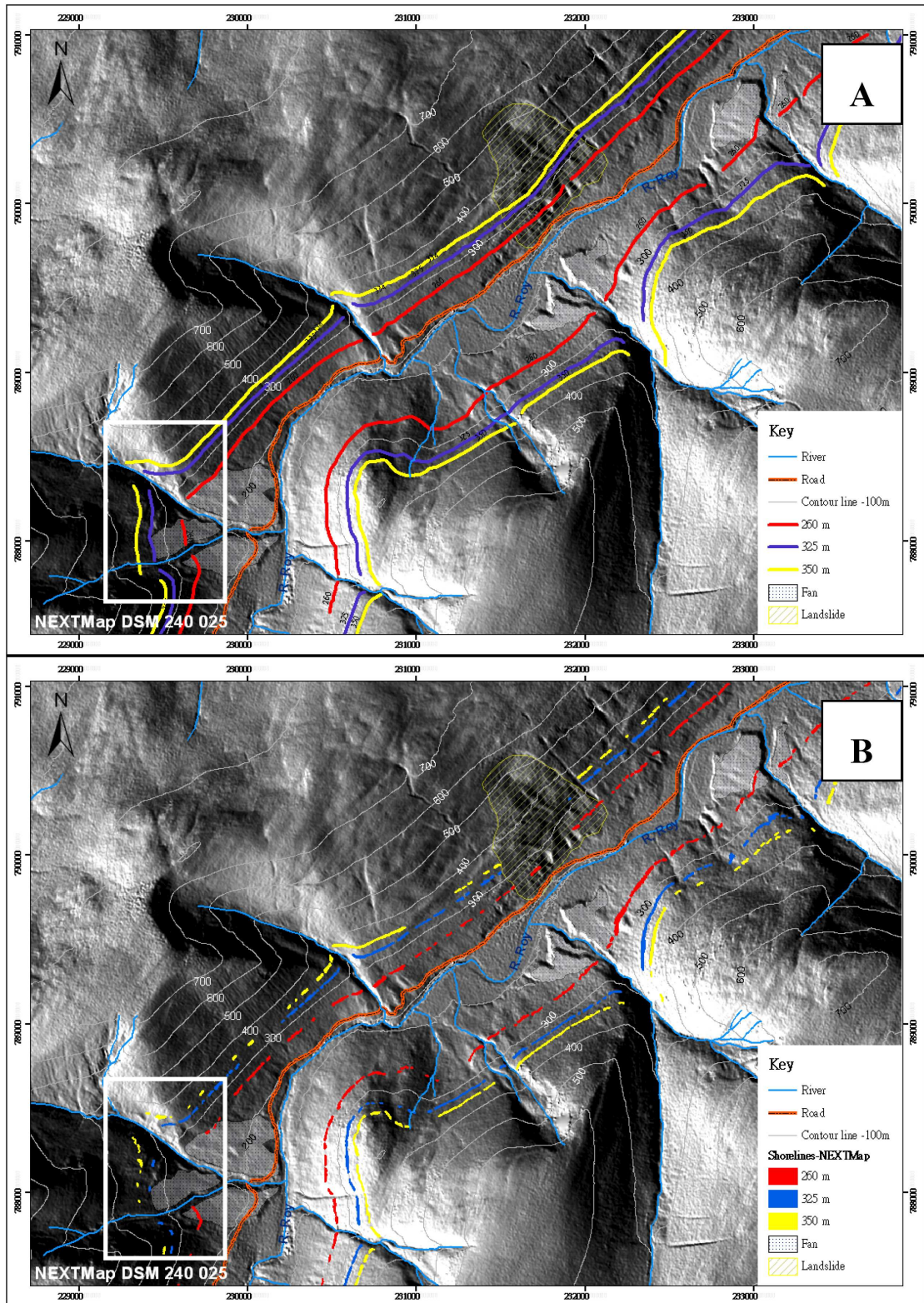


Figure 6.21 Comparison between the mapped distributions of the Parallel Roads in the middle part of Glen Roy: A -- digitalized from the Ordnance Survey 1:25,000 scale map; B -- as mapped by the author using NEXTMap DEM data. For further explanation see text.

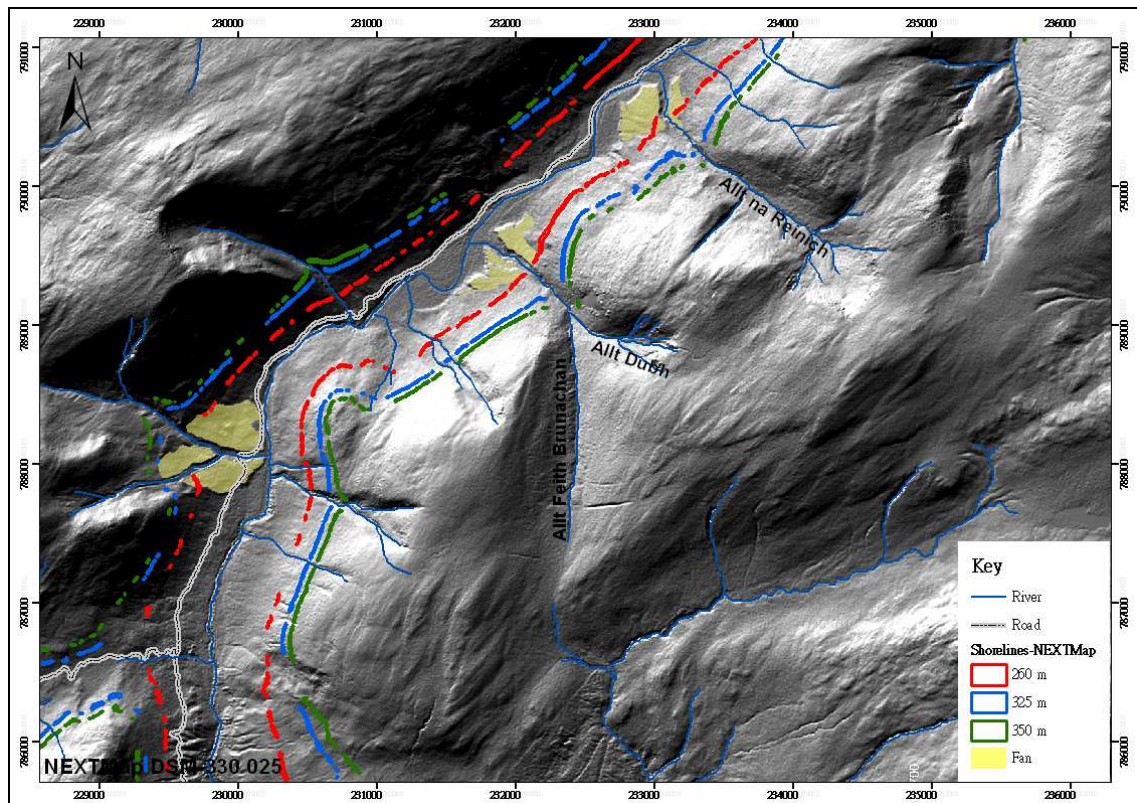


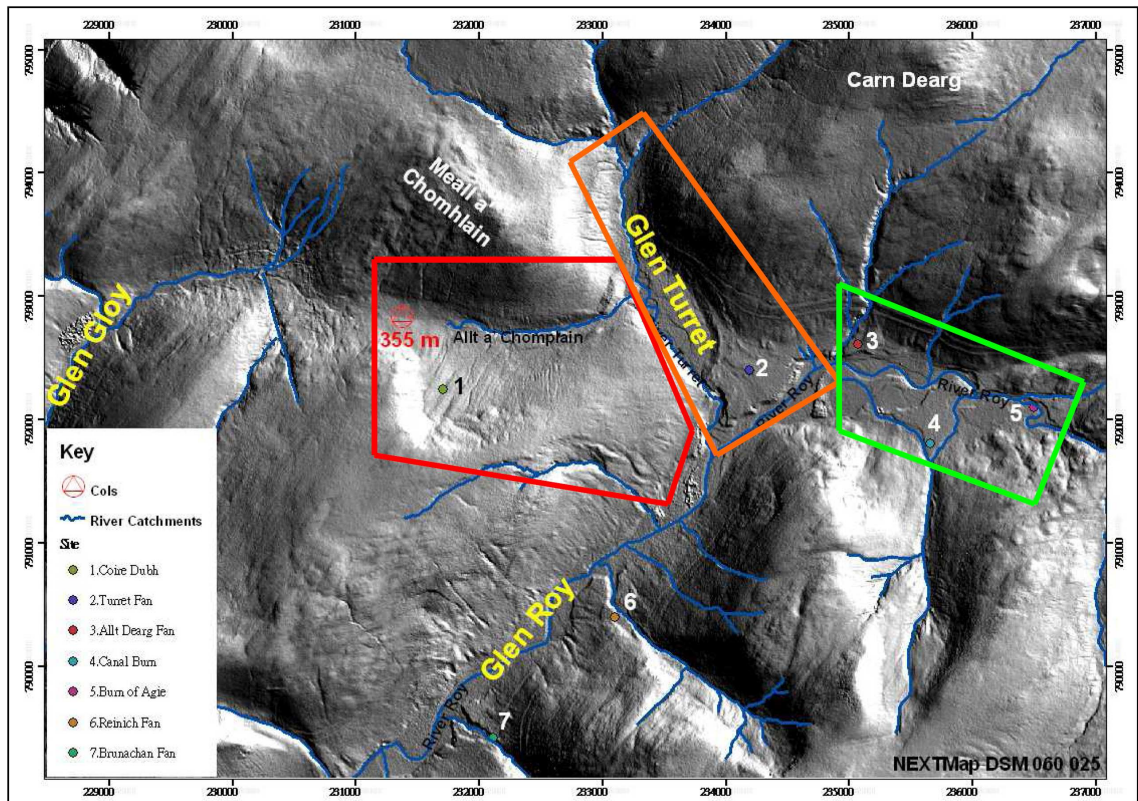
Figure 6.22 The three prominent fans of the middle sector of Glen Roy and the distribution of well preserved parts of the Parallel Roads, mapped using NEXMap DEM data.

## 6.4 Upper section of Glen Roy and Glen Turret

### 6.4.1 Introduction

In this section, a review of previous work in Upper Glen Roy will be undertaken, allied to new descriptions of the landforms based on the analysis of NEXMap DEM data. Upper Glen Roy covers a wide area and is therefore considered in three blocks (Figure 6.23). Block I (orange trapezium) encompasses the Glen Turret valley and includes the Turret Fan, a major fan that extends across the Turret-Roy confluence. Block II (red trapezium) covers the valley of the Allt a' Chomhlain stream, a tributary of the Turret, and Coire Dubh on the southern flank of this valley, which extends southwards from the Allt a' Chomhlain to the watershed that separates its catchment from the Roy. This tributary valley extends from the 355 m Gloy/Roy overflow col to Glen Turret, and contains landform evidence critical to understanding the origin of the Turret Fan. Block III (green trapezium) extends to the east of the Turret Fan, and includes three other

prominent fans: the Allt Dearg Fan, the Canal Burn Fan and the Burn of Agie Fan. Little detailed geomorphological evidence has been published for this part of Glen Roy, and hence particular attention has been paid to the NEXTMap DEM representation of key features in this area.



**Figure 6.23** A vertical NEXTMap plot of parts of Glens Gloy, Turret and upper Roy (azimuth of light source from 60° with an elevation angle of 25°). Critical sites are labelled by number. The coloured trapezia are referred to in the text.

## 6.4.2 Published information on the glacialic landforms in Upper Glen Roy

### 6.4.2.1 Block I: the Glen Turret area

The Turret Fan dominates the landscape at the confluence of Glen Turret and Glen Roy, immediately north of Braeroy (feature 2, Figure 6.23). The surface of this feature lies approximately 20 m above the Glen Roy valley floor and is composed predominantly of sub-horizontally bedded gravels (Peacock 1989). In depressions on the surface of the

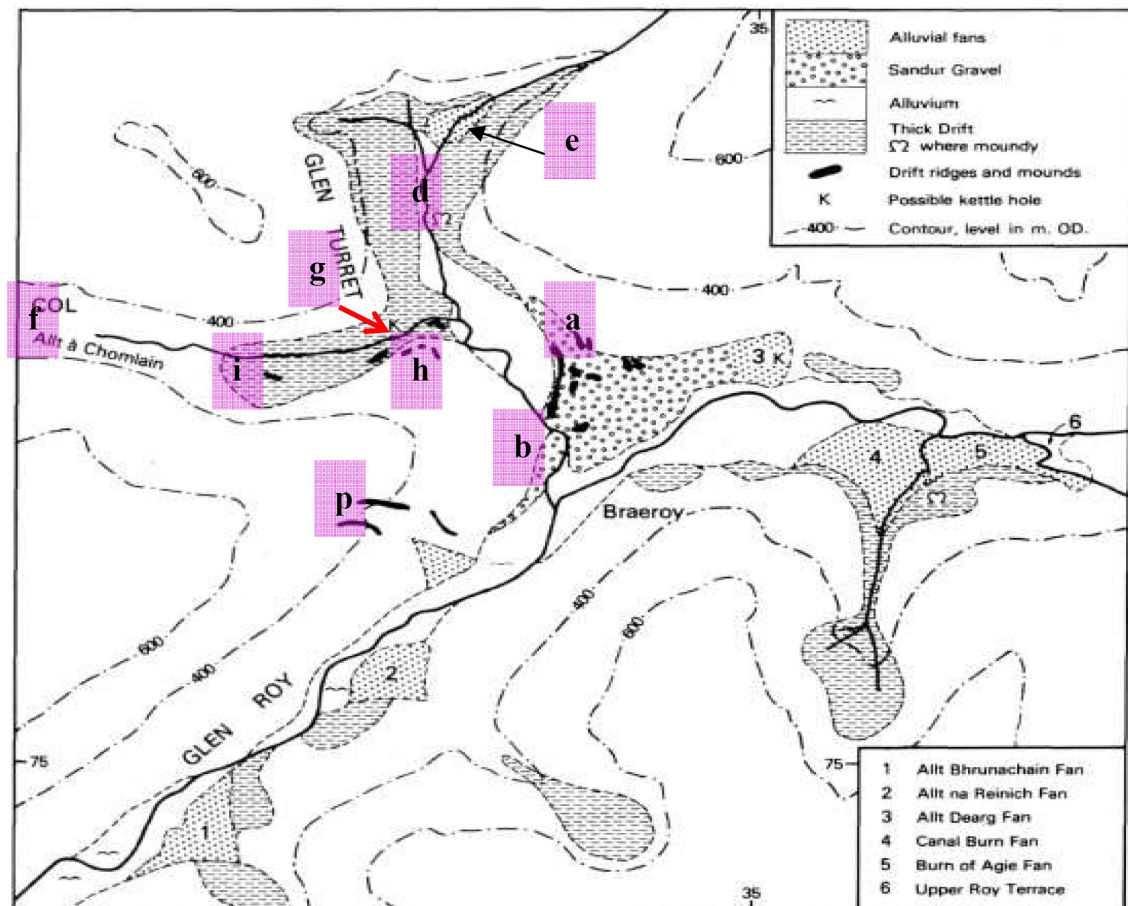
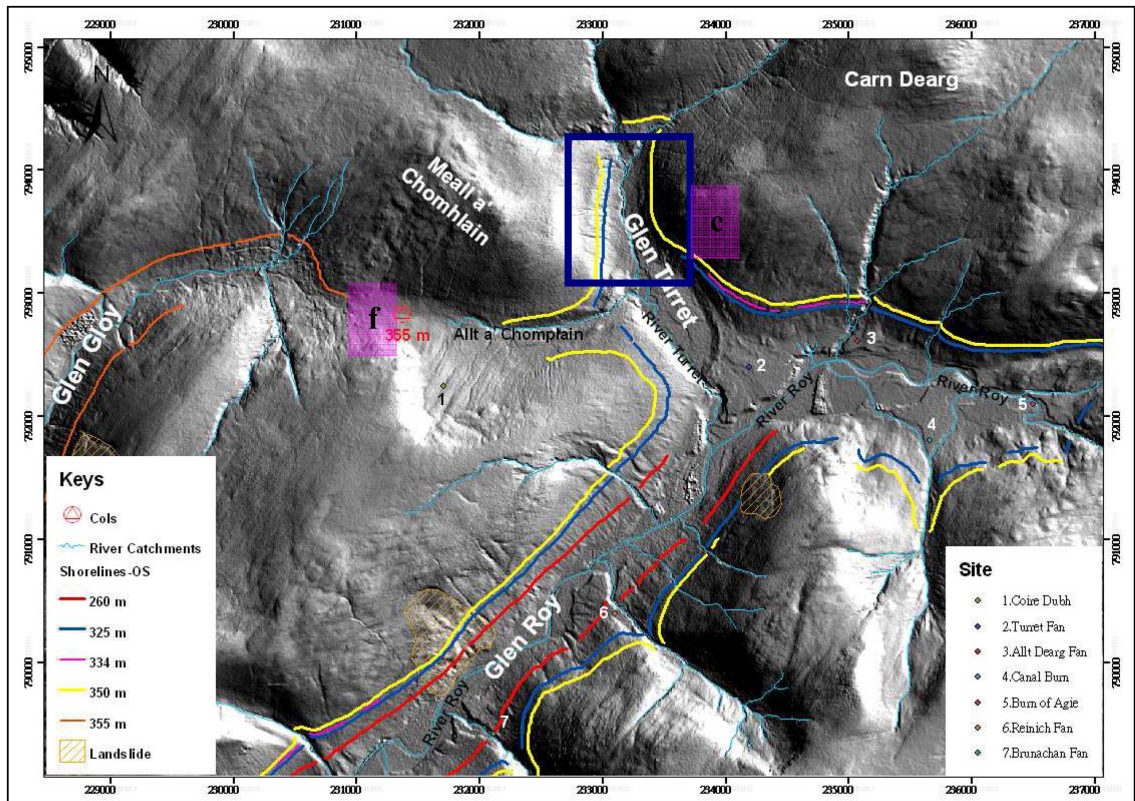


Figure 6.24 Glacial landforms and sediments in upper part of Glen Roy (from Peacock 1986).

fan, particularly in distal locations, are laminated silts and clays up to 1.5 m thick. The fan surface dips from an apex at the NW edge of the land mass, towards SE, from 270 m OD at the up-valley apex (feature a, Figure 6.24) to the lower distal edge at 246 m OD, adjacent to the present course of the Roy. There is a steep slope on the proximal edge of the fan dipping up-valley (Glen Turret). A series of ridges are located on the proximal part of the fan surface (drift ridges shown near a, in Figure 6.24). Similarly two ridges exist on the hillside to the SW of the fan at an altitude of 460 m OD (features at b, Figures 6.24 and 6.26). Overlooking the fan surface on the hillsides are the 325 m, 334 m (minor shoreline) and 350 m shorelines cut into bedrock, while the 260 m shoreline extends only as far as the southerly margin of the GTF on the eastern side of Glen Roy (Figure 6.24), terminating near Brae Roy.





**Figure 6.25** The distribution of the Parallel Roads in upper Glen Roy, digitalized from the 1:25,000 scale Ordnance Survey Map. The 325 m shoreline within the blue rectangle was absent from the east flank but preserved on the west flank of the valley.

Further up the Turret valley, it should be noted that the 325 m shoreline is not represented on the eastern flank of the valley but is eroded on the western flank (in the vicinity of c in Figure 6.25). Although this had been noted by Sissons (1978), who suggested that this was a ‘terrace associated with the 325 m lake’, while Peacock (1986) concluded that this part of the valley was “*partly floored by glacial deposit, chiefly silty sandy diamicton, overlain in places by laminated silt*” (areas d and e in Figure 6.24), the exact reason for this anomalous gap in representation of the 325 m shoreline has yet to be satisfactorily explained.

The formation and age of the Quaternary landforms in Glen Turret have been a matter of debate since the 19th century and remain contentious. Jamieson (1892, p. 24-25) interpreted the Turret Fan as a delta with sediment supplied by water from an ice-dammed lake in Glen Gloy that overflowed the Gloy-Chomhlain col (f in Figure

6.25) to enter the Turret catchment, though this did not explain why the fan was confined to the confluence of the Turret and the Roy. Sissons and Cornish (1983) interpreted the Turret Fan as a glacial outwash feature, and the arcuate ridges that delimit the fan's apex (best represented in Figure 6.26) as a terminal moraine. The source of the ice they presumed to be from the Gloy, which represented a radical change in perspective at that time. Prior to this suggestion, it had generally been assumed that the LLR advance glacier limit in Glen Gloy was within the Gloy valley, forming the lake that etched the 355m shoreline into the flanks of upper Glen Gloy (Agassiz 1842; Jamieson 1863; Sissons 1979b). Sissons and Cornish's (1983) interpretation entailed the advance of LLR up the entire length of Glen Gloy, over the col into the Turret catchment and down the Chomhlain and Turret as far as the GTF. They also envisaged that this was contemporaneous with the 260 m Glen Roy lake of the rising sequence. Because a large part of the fan deposits lie below 260 m OD, this could imply that most of the fan body should have been deposited subaqueously and that the glacier margin would have calved back as the lake water in Glen Roy rose to the 325 m and subsequently 350 m levels. They also observed that the fan extends a considerable distance southwestwards down Glen Roy, across the area presently occupied by floodplain and river terraces, the latter being formed by erosion and reworking of parts of the eastern extremities of the fan.

Peacock (1986) favoured a different origin for the fan, because he had observed major exposures of the internal deposits of the fan, which consisted of sub-horizontal beds of gravel and sand typical of subaerial deposition, and not the steeply-dipping clinofolds expected in a lacustrine delta. Peacock (1986) argued that since the Glen Gloy and Glen Roy ice lobes were both outlets of the West Highland Icefield during the LLR, the Gloy glacier could not have existed before Glen Spean became ice-dammed. Therefore Glen Roy could not have been free-draining to the Great Glen at that time. Peacock (1986)

therefore concluded that the GTF must have formed prior to the LLS, probably during the Dimlington Stade, possibly during a still-stand phase during the general retreat of the Main Ice sheet.

Benn and Evans (2008) have subsequently proposed a new hypothesis for the formation of the Turret Fan. They have proposed, from mapping of glacial landforms, that a small ice cap existed on the plateau between Glen Turret and the Great Glen on Carn Dearg (Figure 6.25) during the LLR, and that the ice flowed down Glen Turret as far as the GTF, forming the terminal ridges at locality a in Figure 6.24. This glacier then calved back towards the head of Glen Turret when the lake water rose in Glen Roy to the 325 m and 350 m levels.

#### **6.4.2.2 Block II: Allt a' Chomhlain and Coire Dubh**

A series of landforms in this area may provide important evidence for understanding the sequence of events in the Turret valley at the end of the last glacial stage. They may also have important implications for establishing the extent of glaciation in Glen Gloy during the LLR. A mass of sediment mounds occurs at the mouth of the Allt a' Chomhlain valley, where it joins the Turret (locality g in Figure 6.24). Within these deposits is a deep, rounded basin, surrounded by ridges that were interpreted by Peacock and Cornish (1986) as having a level (topset) surface and steep (foreset) slopes, suggesting deposition in standing water; the depression was interpreted as a kettle hole. Chen and Rose (2008b) also interpreted this small basin as a kettle hole and the steep slope on the bounding sediment ridge as an ice-contact delta. The top of this ridge lies at 325 m and hence they considered this mass of deposits to have accumulated in the 325 m lake. In association with the inferred delta feature is a moraine ridge (h in Figure 6.24) and a probable kame terrace ( i in Figure 6.24: Note that this feature was not mapped in the original figure but was described in the 1989 field guide book, p.41), also associated

with the 325 m lake. Sediments exposed in the latter led Peacock and Cornish (1989) to report that the terrace is “*underlain by interbedded gravel, including matrix- rich and openwork gravel, and silt/fine-grained sand which is partly laminated and partly cross-bedded*”.

#### **6.4.2.3 Block III: The upper Roy, upstream from the Turret Fan**

##### *The Allt Dearg Fan*

This large debris fan occurs on the northern flank of upper Glen Roy, about 1.5 km upstream from the confluence of the Rivers Roy and Turret (feature no. 3 in Figure 6.23.). The main stream, the Allt Dearg, flows from the high ground to the north and cuts the fan body into two parts. Virtually all of the fan’s surface lies below 255 m OD and merges with the Turret Fan on its western margin. Peacock (1986) suggested that the fan could be separated into an upper and lower part, the apex of the upper part being immediately below a small dissected delta which he associated with the 325 m shoreline, and the lower (main) body of the fan. However, there is no figure giving evidence to support this idea. Sissons and Cornish (1983) have also mapped the features in this area (Figure 6.26), but their map gives no hint of the upper fan suggested by Peacock (1986), only the lower fan below 260 m (Figure 6.26). Examination of NEXTMap DEM data (discussed below) supports Sissons and Cornish’s (1983) interpretation.

During the 1980’s, exposures could be observed in the lower parts of the Allt Dearg fan, that are now obscured. Sissons and Cornish (1983) reported evidence of laminated sediments that were overlain by the fan gravels, and presumed that the former had accumulated in a lake. However, Peacock (1986) subsequently observed that the main body of the fan was composed of clast-supported, sandy, boulder gravel with sub-horizontal beds, and concluded that the greater part of the fan was therefore formed by fluvial processes.

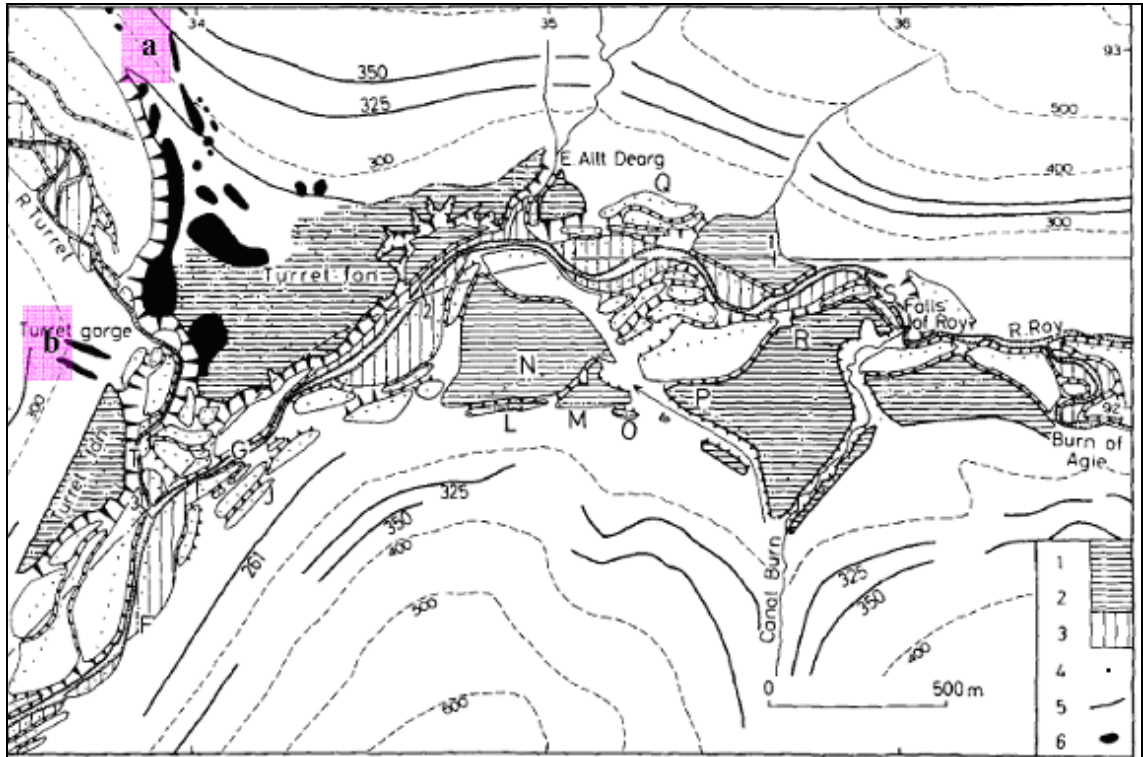


Figure 6.26 Geomorphological map of the fans and river terraces of the northern part of upper Glen Roy. 1. Highest Roy terrace and fans associated with the 260 m lake. 2. Fans post-dating the 260 m lake. 3. Floodplain. 4. Levelled points. 5. Parallel roads. 6. Drift mounds (from Sissons and Cornish, 1983).

### The Canal Burn Fan

The Canal Burn is a tributary stream that enters the upper Roy from the south and where it joins the Roy, a large debris fan splays out over the floor of the Roy with an apex in the lower part of the Canal Burn's channel (Figure 6.26). The surface altitude of this Canal Burn Fan decreases from 285 m OD at the apex to 260 m OD at its northern edge. The fan has been dissected near its eastern margin, with the larger fan body preserved to the west of the Canal Burn (measuring 651 m long, 497 m wide, with an estimated thickness of 11m), while a much smaller remnant occurs on the eastern side of the stream (275 m long, 35 m wide and c. 4 m thick). An exposure discovered by Peacock (1989) in the eastern part of the Canal Burn fan (about 200 m NE of the apex) showed imbricated cobble gravels up to 2.5 m thick resting either on matrix-rich gravel or

laminated silt. The upper part of the gravels appears to have been deposited during the postglacial period, as buried soils occur within them; these are presumed to indicate reworking of the fan gravels during the Holocene. The matrix-rich gravel below the imbricated gravel layer was deposited under quite different conditions and is assumed to be a paraglacial or ice-contact deposit. Based on the altitudinal relationships between the fan surface and the lake shorelines, this site was not submerged by the 260 m lake level but was inundated by the 325 m and 350 m lakes.

### *Burn of Agie Fan*

The Burn of Agie, situated at minimum c.70 m east of the Canal Burn (Figure 6.26), is also a tributary stream that enters the upper Roy from the south, through a gorge, from which a large fan has been fed on to the floor of the Roy. The surface gradient of this Burn of Agie Fan trends from East to West, from an easterly apex near the gorge at 290 m OD to a lower margin in the centre of the Roy valley at 265 m OD. Lake sediments in the form of laminated silts have been deposited on the fan surface, downstream of the gorge; they lie at an altitude of 272 m OD and are therefore considered to have been laid down within the 325 m and 350 m lakes during the rising lake sequence (Peacock and Cornish, 1989; Palmer *et al.*, 2010).

## **6.4.3 Analysis of landforms in upper Glen Roy based on NEXTMap DEM data**

### **6.4.3.1 Introduction**

The landform assemblages in upper Glen Roy described above were examined in the present investigation using NEXTMap DEM data, with two objectives: first to determine how well the various features reported in the published literature are represented on DEM data plots, and second, to establish whether new information might be brought to light that advances knowledge of the sequence of events in Glen Roy. The new data are presented in the same order as before, using the three spatial blocks

outlined in Figure 6.23. Before proceeding with the details of the depositional features in these selected areas, however, a wider perspective is provided of the general physiographical architecture of the area, in order to draw attention to some general but important features.

Figure 6.27A is a vertical view of the study area compiled using a mosaic of NEXTMap tiles. What is striking from this plot is the volume of thick deposits that seemingly chokes the upper Roy Valley, from Brae Roy northwards and eastwards, and to a certain extent within the Turret valley and its tributaries. South-west of Brae Roy, the middle Roy valley has a much less smooth appearance, and is heavily gullied. There are no clear glacial landforms, with the most marked features being the major fans (Breach Achaidh, Brunachan, Reinich) fed from tributaries. This holds true for much, if not all, of the Roy valley between the GTF and the massive drift accumulation at the Viewpoint. So the deposits around the Viewpoint, generally accepted to be of LLR age, and the deposits around the Turret-Roy confluence, the ages of which are debated, stand out as being exceptional focal points of sediment accumulation, with clear glacial landforms, in stark contrast to the middle reaches of the Roy valley.

The second point to note is that the whole area has clearly been glacially moulded from SW to NE, with this dominant grain most noticeable on the upper slopes and hill-tops, which show classic roches moutonnées streamlined forms. Although their dominant lineation is coincident with the orientation of the strike of much of the local schistose bedrock, the dominant SW-NE 'grain' in the landscape is maintained across geological boundaries and over significant topographic undulations, and is therefore independent of their influences. The position of the landforms on the high slopes and the fact that evidence for local ice movement is predominantly restricted to the lower slopes and

valleys suggests that these ice-moulded landforms are the product of ice cover during the Late Devensian ice sheet advance, possibly generated at the Last Glacial Maximum.

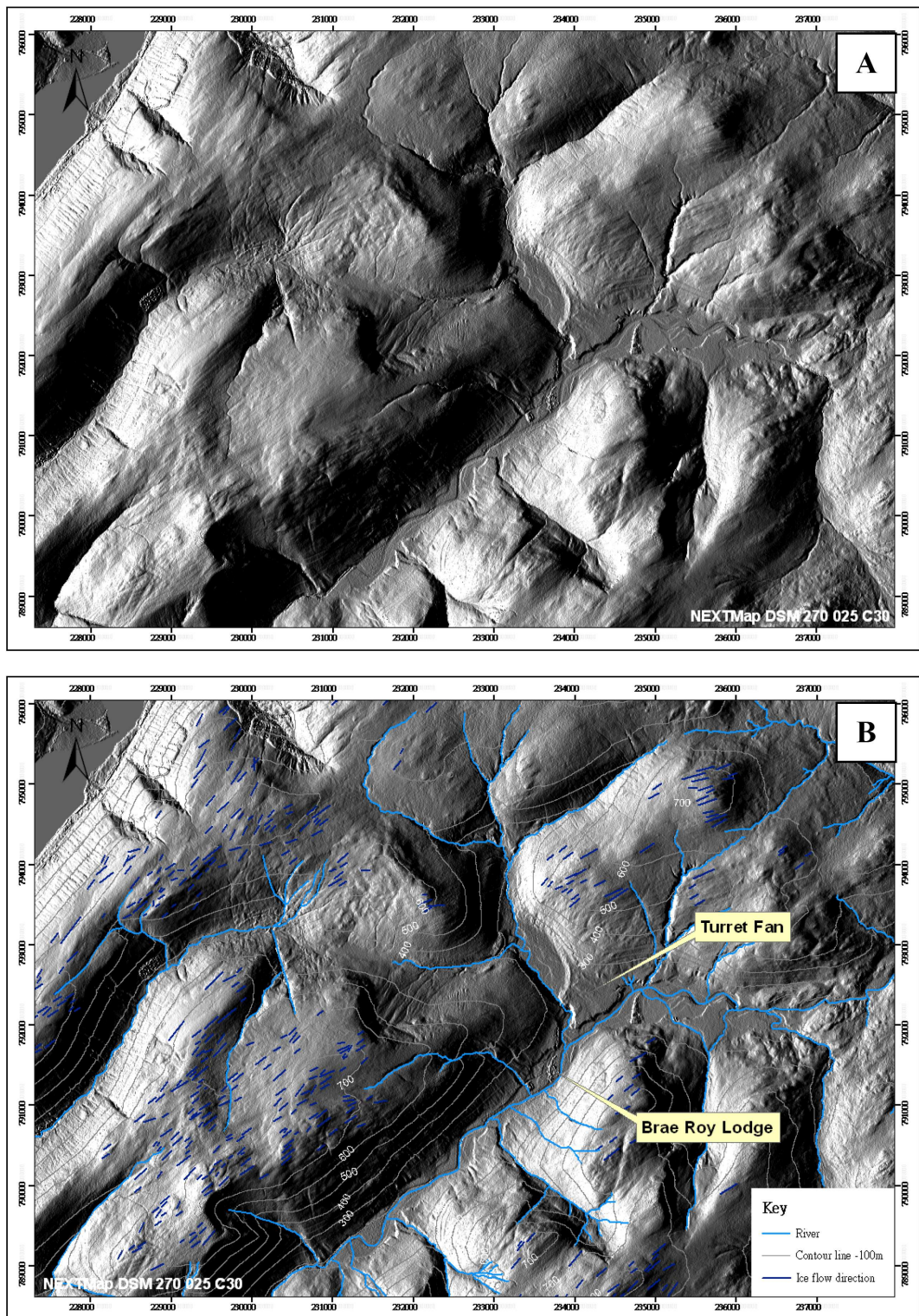


Figure 6.27 Vertical NEXTMap plots of the upper Glen Roy area, with light source set to azimuth 270° and elevation 25°. A is the unmarked image; the blue lines on B denote the axial trends of glacially-lineated features.



It seems quite clear, therefore, that the whole area was inundated with ice from the SW during the Dimlington Stade. Presumably the ice built up in earlier (pre-LLR) glacial episodes in much the same way as it did during the LLR, invading the Spean Valley from the west and SW, then penetrating Glen Gloy, Glen Roy and Caol Lairig from the south, and spreading ever further northwards to engulf the Gloy, Turret and Roy valleys and overflow into the upper Spey catchment. This raises the question of why, if the whole of the Roy catchment was filled with ice during the Dimlington Stade, no obvious glacigenic landforms can presently be observed in the middle sector of Glen Roy? One possibility is that any such landforms generated during the wastage of the Late Devensian ice sheet became heavily modified by paraglacial and periglacial processes, especially during the harsh climatic conditions of the LLR. If that is the case, then why are the obvious glacigenic landforms and flat terraces/fans in the upper Roy not also significantly altered, or even destroyed? This question will be returned to in the final section of this chapter, following the presentation of the results of NEXTMap examination of the deposits on the lower slopes of the upper Roy.

#### **6.4.3.2 Landforms in Glen Turret (Block I)**

Figure 6.28A shows a 'raw' NEXTMap compilation plot for the area around the Turret-Roy; the principal landforms identified by the author and considered to be relevant to the glacial history of the area are added in Figure 6.28B. Key features are the Turret Fan (k, Figure 6.28B) and the pronounced arcuate moraine ridges that coincide with the highest margin (apex) of the Turret Fan (j and p, Figure 6.28B). The northern margin of the GTF, which is sharply bounded by a very steep bluff running roughly parallel to the moraine ridges for some 750 m, is considered an ice-contact slope. The moraine ridges on the fan surface can also be traced onto the adjacent valley sides, those on the southern side extending up to an altitude of 450m (near o on Figure 6.28B) and

those on the northern side up to 340 m OD (near a on Figure 6.28B). Other significant features identified on Figure 6.28B are as follows:

1. Feature c on the eastern valley flank in the middle of Glen Turret is a possible fragment of the 325 m shoreline, approximately 222 m in length and 35m wide; its upper surface has an altitude of exactly 325 m.
2. Feature d marks the position of the heavily dissected massive drift described by Peacock (1986) and verified as such in the present research.
3. Feature e is a mass of sediment that appears to be a dissected fan of some kind. Exposures in this fan reveal thick deposits of laminated silts, interbedded with sands, gravels and diamicts, which Benn and Evans (2008) have interpreted as mass flows, turbidites and rain-out deposits laid down in standing water in close proximity to a glacier margin. In support of this interpretation, the finer-grained units contain large angular clasts considered to represent drop-stones, while the upper 3 m of the succession consists of a massive, boulder diamict, thought to derive from a subaerially-deposited moraine.
4. Feature k refers to a series of channels that run down-slope across the surface of the GTF; 17 separate channels were identified on the NEXTMap plot, the longest of which almost reaches the distal edge of the fan; in nearly all cases the channels, which extend down to an altitude of c. 276 m OD, have no links with local drainage networks developed on the valley sides, and thus are interpreted as features eroded by glacial meltwater.
5. Feature m marks the position of the valley floor of Glen Turret but when viewed in conjunction with the ice-contact slope on the northern margin of the GTF and terminal moraine ridges has the form of an ice tongue basin that extends up valley for 1.1 km and is approximately 380 m wide.

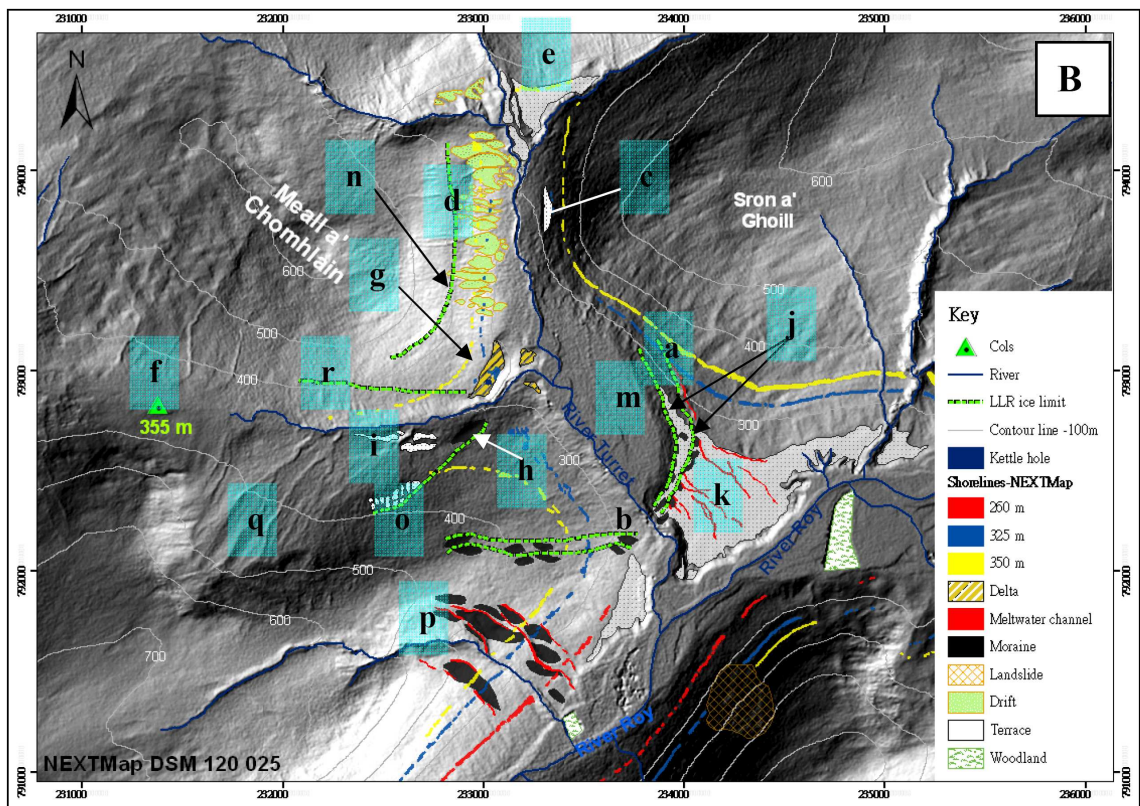
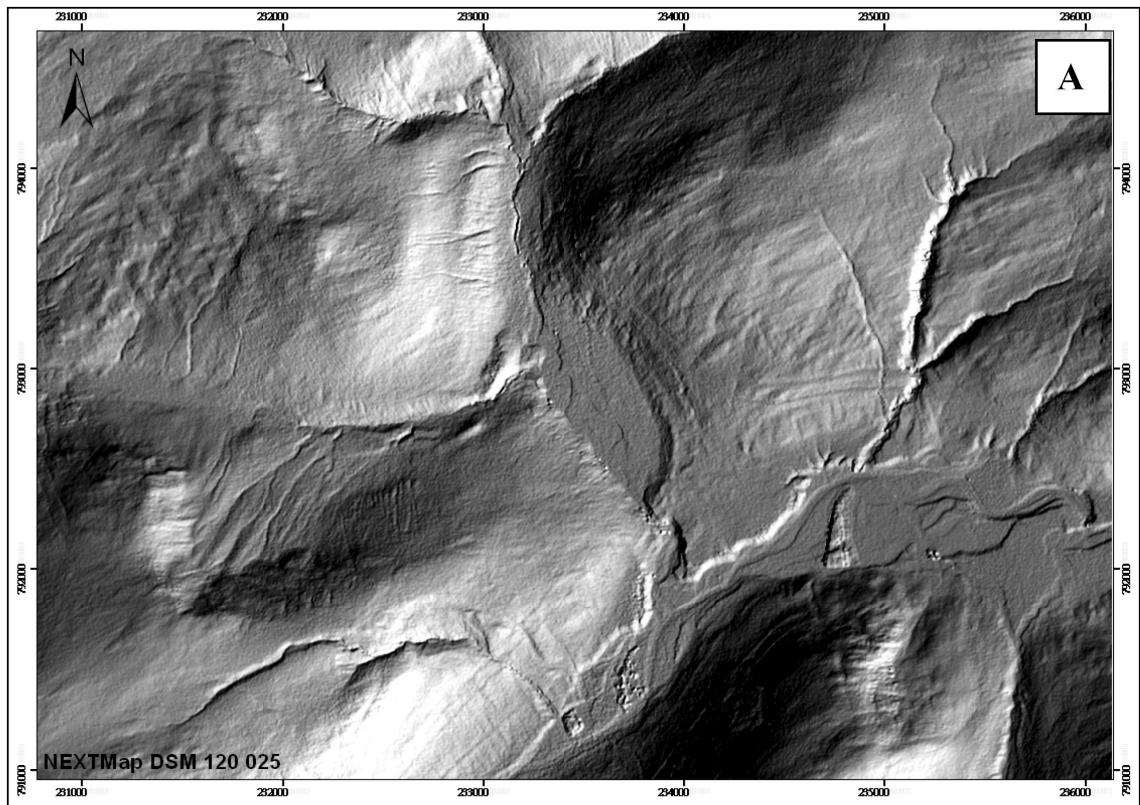


Figure 6.28 Geomorphological map of the area around the Turret-Roy confluence based on NEXTMap DEM data. A is the raw image and B shows key landforms identified by the author. Also see Figure 6.23, 6.29, 6.30 and 6.31 for comparison.

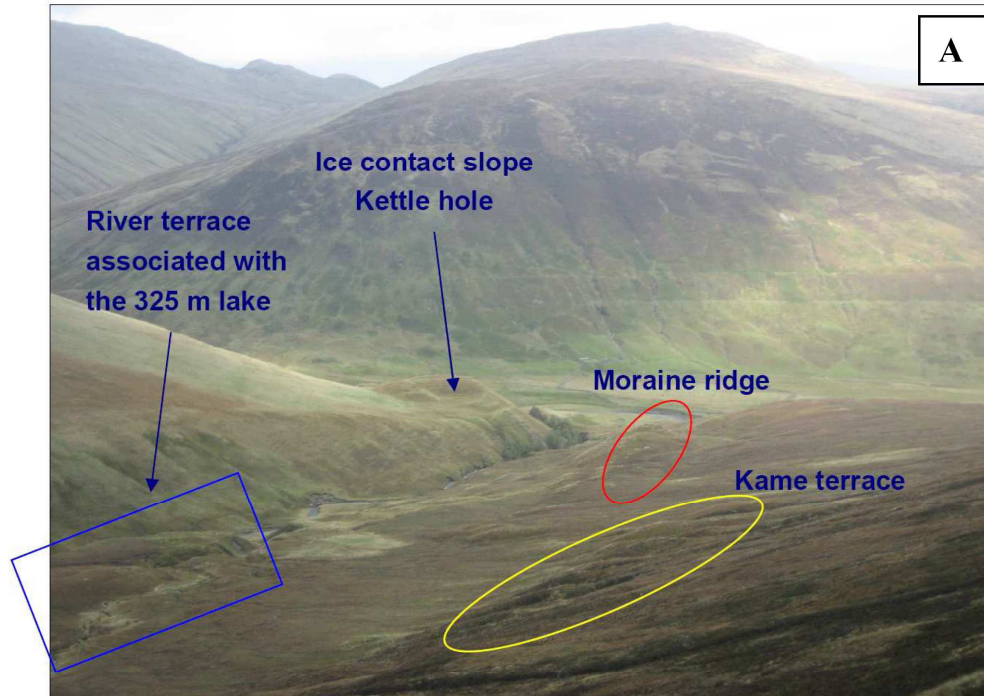
Other features identified in Figure 6.28B are referred to in the following sub-section, before an overall interpretation is drawn. Note, however, that the distribution of the Parallel Roads is also significant in upper Glen Roy. The 260 m shoreline extends to the southern margin of the GTF, just to the north of Brae Roy Lodge, but does not extend into Glen Turret, which is highly significant, since parts of the floor of the Turret Valley, north of the GTF, lie below 250 m in altitude. The 325 m shoreline appears to be fragmented in much of the Turret valley on NEXTMap DEM data and is not clearly expressed on the eastern flank of Glen Turret in the vicinity of locality c on Figure 6.28B. Some fragments of the 325 m shoreline were observed on the southern flank of the Turret valley, close to the Turret Fan. The 350 m shoreline, by comparison, extends further to the north in Glen Turret and appears well defined on the northwestern and southern flanks of the Turret valley. The significance of these observations is also addressed below.

#### **6.4.3.3 Landforms in Allt a' Chomhlain and Coire Dubh (Block II)**

The glacial landforms identified by previous researchers in this small tributary valley are clearly identifiable on NEXTMap DEM data. This includes the remnants of what is presumed to be an ice-contact delta with a kettle hole formed within it (feature f on Figure 6.28B, and illustrated in Figure 6.29B, with its location shown in Figure 6.29A). The upper delta surface is at 325 m and extends down to the valley floor, with a steeply dipping slope to 270 m OD. Other significant features identified on NEXTMap in the Allt a' Chomhlain tributary valley, and itemised on Figure 6.28B, include:

1. At locality h, a distinct linear ridge that runs along the valley for 205 m, is 69 m wide and up to 10 m high (see Figure 6.29A); this may have been connected

with a smaller ridge, further to the west on the same side of the valley; these are considered features that formed on the lateral margin of a glacier.



**Figure 6.29** A. View of the landforms in the Allt a' Chomhlain-Coire Dubh tributary valley taken from the SW looking toward the NE. B. The kettle hole (diameter 28 m) in the ice-contact delta deposits at the mouth of the Chomhlain.

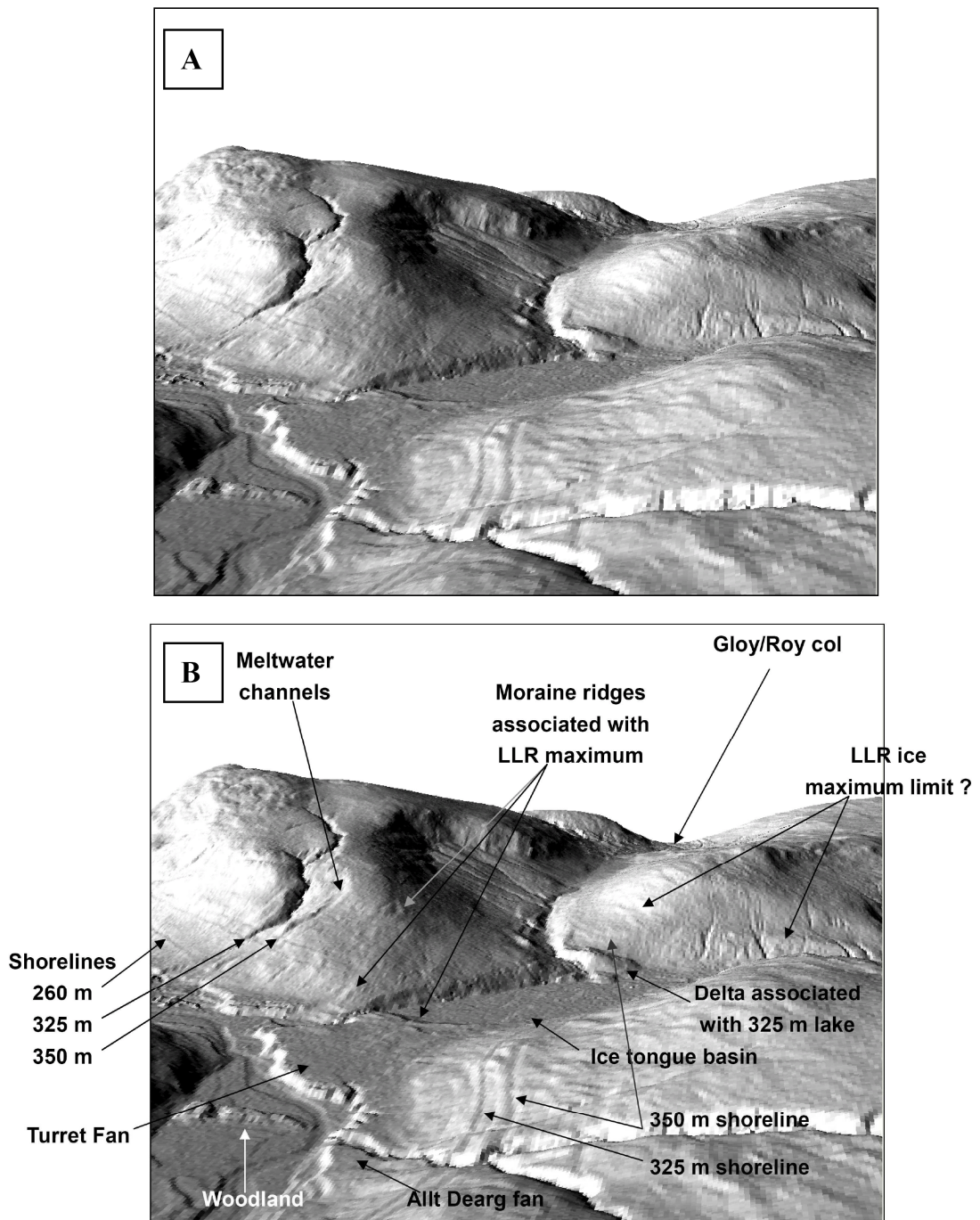


Figure 6.30 A. 3D perspective of the Glen Turret area from the NE direction (Illumination azimuth 150°, Altitude 30°) with significant landforms identified in B.

2. At locality o on the southern flank of the Chomhlain are a series of dissected terraces, running for 414 m along the valley, which are up to 92 m wide, and the flat surfaces of which are between 355 and 390 m OD; there are no exposures in this extensive feature but its position on the valley side and flat upper surface

suggest some kind of lateral glacial feature – possibly a kame terrace (see Figure 6.29A).

3. In Coire Dubh, in the area around locality q, a notably thick spread of ‘drift’ is deeply incised by a series of gullies that flow directly down-slope to the Allt a’ Chomhlain.; the linear ridges between the gullies were originally interpreted as ‘flutes’ by Chen and Rose (2008b), but the present author now considers this to have been a mass of drift that was laid down by ice, because lineation parallel to the valley sides is discernible on NEXTMap, while the dense gullies give a false initial impression of ridges running at right-angles to this original grain.
4. On the northern flank of the Chomhlain, at locality r, is a linear ridge that reaches an altitude of 400 m at its western end but whose long-axis surface slopes down towards the Turret valley; its altitude is comparable with features o and h on the opposite side of the valley.
5. A series of large and pronounced moraine ridges that are dissected by meltwater channels occurs at locality p; they descend the hill-side from 466 m to 234 m OD; an important observation to note is that these moraine ridges are incised by all three of the Parallel Roads, implying that they were formed before the lakes were formed.

These observations are considered in association with those already reported for the Turret valley and Turret-Roy confluence in the synthesis section below (section 6.4.3.5). For further illustration of the features referred to above, and of their overall relative positions in the landscape, three sets of oblique 3-D images of the area are provided (Figure 6.30, 6.31 and 6.32), which will be important for following the details of the explanations provided in the synthesis section.

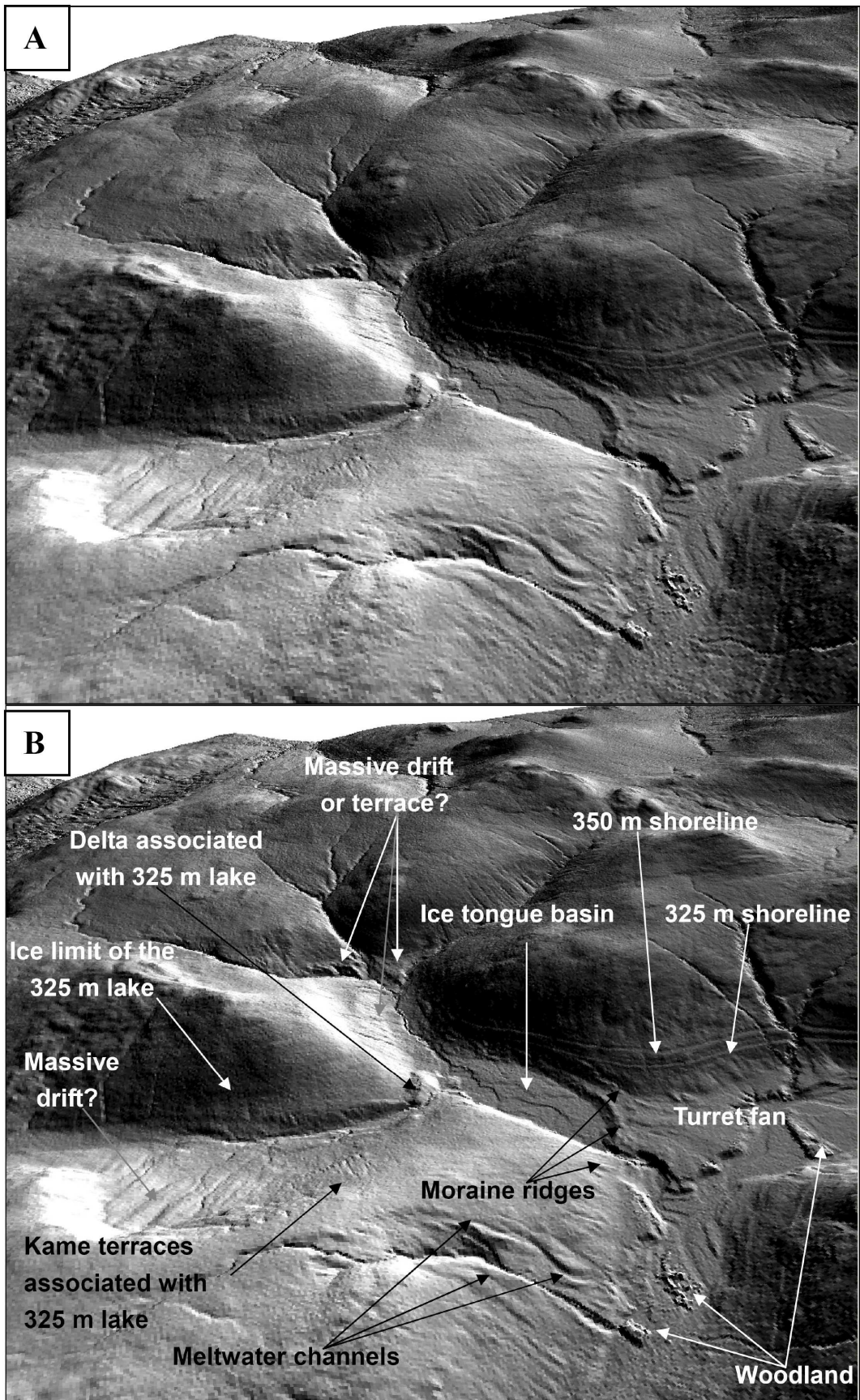


Figure 6.31 A. 3D perspective of the Glen Turret area from the SSW direction (Illumination azimuth: 60°, altitude 30°) with significant features identified in B.



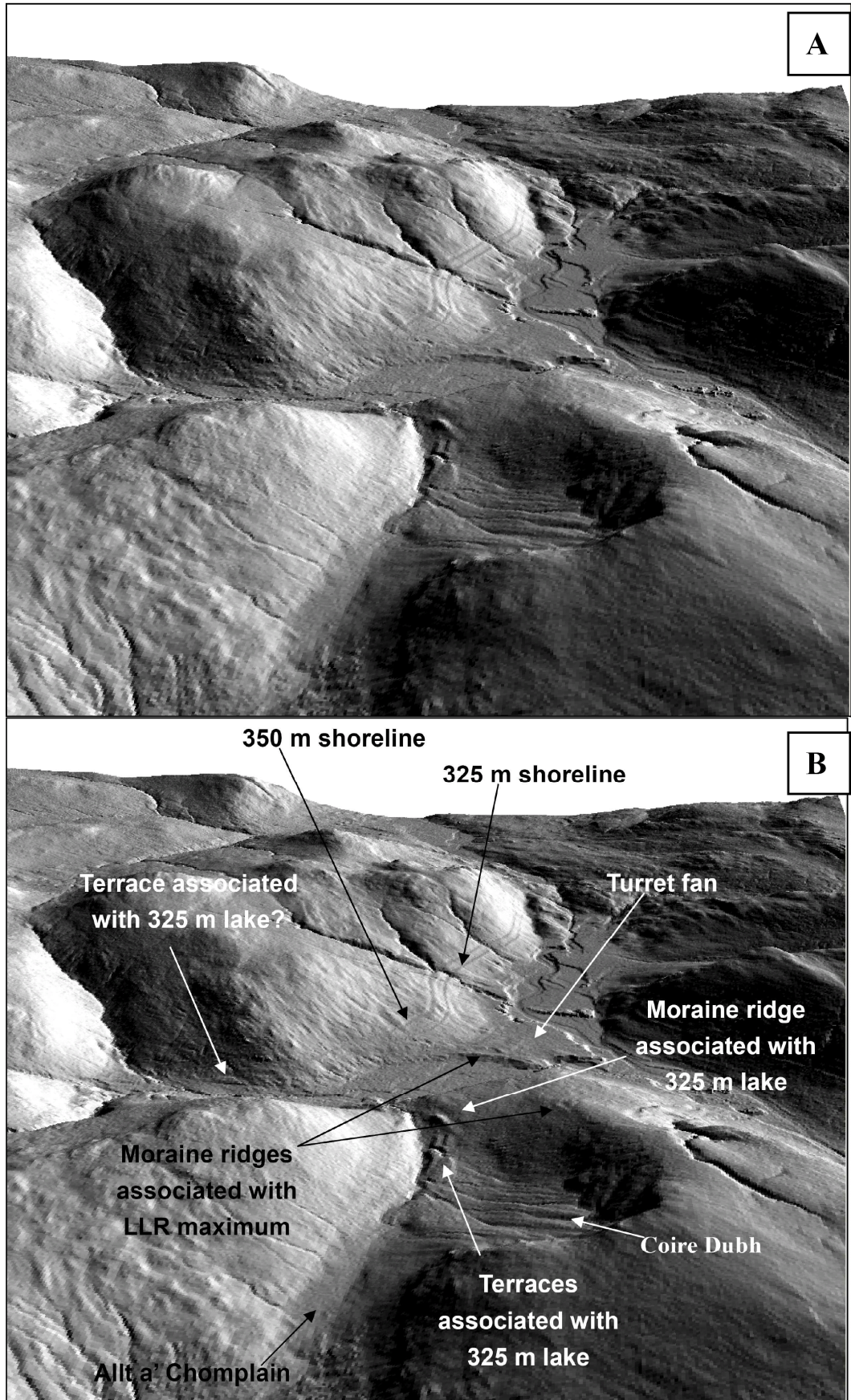
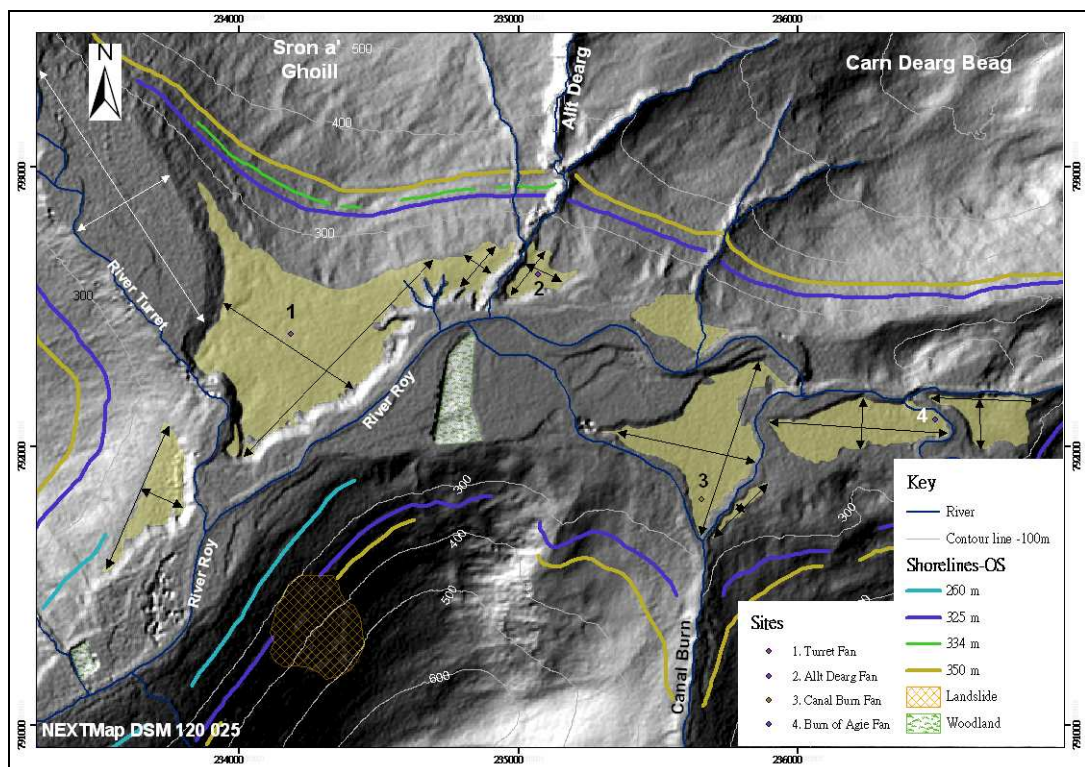


Figure 6.32 A. 3D perspective of the Glen Turret area from the W (Illumination azimuth 150°, altitude 30°) with significant features identified in B.

#### 6.4.3.4 Upper Glen Roy, east of the GTF (Block III)

Figure 6.33 shows the key features identified from NEXTMap DEM data for the upper Roy. East of the Turret Fan, no clear glacial forms are evident, except for much further east, where a glacier tongue appears to have descended from the Carn Dearg plateau onto the head of Glen Roy (discussed in Chapter 7). In this part of the valley, large fans dominate. These have clearly been heavily dissected by the River Roy and its tributary streams, but four clear sources for the original fan gravels can be identified, for their surfaces decline from apices situated in lower Glen Turret and at the mouths of the Allt Dearg, Canal Burn and Burn of Agie. Collectively, these represent an enormous volume of gravels, which prior to dissection must have covered the whole floor of the Roy Valley. An idea of the mass of gravel represented can be gleaned from Table 6.1., but their original dimensions must have been significantly greater.



**Figure 6.33 Preserved remnants of major fans and distribution of the Parallel Roads in upper Glen Roy mapped using NEXTMap DEM data. The dimensions of the fan surfaces are provided in Table 6.1. 1 = Glen Turret Fan (GTF); 2 = the Allt Dearg Fan (ADF); 3 = the Canal Burn Fan (CBF) and 4 = the Burn of Agie Fan (BAF).**

**Table 6.1 Estimated dimensions of the preserved fragments of the major fans in upper Glen Roy. 1 = Glen Turret Fan (GTF); 2 = the Allt Dearg Fan (ADF); 3 = the Canal Burn Fan (CBF) and 4 = the Burn of Agie Fan (BAF).**

Fan remnant	Long axis (m)	Tangential axis (m)	Estimated area (m <sup>2</sup> )	Est. mean thickness (m)	Estimated volume (m <sup>3</sup> )
GTF main	976	558	330,621	21	6,943,041
GTF west	565	162	47,069	18	847,242
ADF west	190	111	27,661	21	580,881
ADF east	201	135	20,946	14	293,244
CBF main	651	497	134,130	11	1,475,430
CBF small	275	35	6,512	4	26,048
BAF west	633	180	85,303	8	682,424
BAF east	389	174	40,316	8	322,528

The altitude of the apices of the fans are 270 m OD for the GTF and ADF, 285 m OD for the CBF and 291 m OD for the BAF. Unlike the fans in middle Glen Roy, these apices do not coincide precisely with any of the lake shorelines, though they accord most closely with the 260 m lake level. There is no evidence for any gravel input in association with the 325 or 350 m shorelines. A parsimonious proposal would be that the fans are contemporaneous, as there is no evidence to the contrary, but this cannot be established on the basis of available information. Attempts have been made to date the fans in Glen Roy using the OSL method, but this has proved unsuccessful due to very weak luminescence signals and ‘anomalous fading’ (Lowick and Bailey, 2008). Fabel *et al.* (2010) have attempted to date boulders on the GTF using surface exposure (cosmogenic nuclide) dating, which gave ages of  $11.0 \pm 1.7$  and  $10.2 \pm 1.0$  ka BP, and which therefore might suggest an LLS age for fan deposition, though the results could be affected by deposition of younger sediments on the fan surfaces.

#### **6.4.3.5 Synthesis of evidence in upper Glen Roy**

The collective landform evidence from the Allt a’Chomhlain and Glen Turret valleys suggests that a glacier tongue occupied Glen Turret and terminated at the arcuate

moraines that delineate the northern margin of the GTF (features a and b, Figure 6.28B). This ice lobe appears to have filled Glen Turret up to its head, for a thick bench of drift occupies the western flank of upper Glen Turret, which has an upper limit (d, Figure 6.28B) that declines towards the dissected delta-form deposits (e, Figure 6.28A) at the head of the valley. Several lines of evidence suggest that this occurred during the LLS, and to help make this point, as well as to visualise the situation, NEXTMap software was employed to superimpose the 260 m lake surface on the DTM image of the area (Figure 6.34). Note that this reconstruction colours in blue all parts of the area that lie below 260 m OD, which would be the surface area of a lake that occupied the area today which had a surface at 260 m OD. The evidence that supports the proposal that a glacier lobe occupied Glen Turret during the LLS is four-fold:

1. The ice-marginal landforms described from the NEXTMap plots not only make a coherent pattern that fits with an ice-tongue hypothesis, but the landforms are conspicuous – especially the arcuate moraines – and appear undegraded, suggesting they have not been affected by periglacial processes during the LLS.
2. There is no evidence for 260 m lake shorelines ‘inside’ (i.e. up-valley of) the GTF in Glen Turret, yet Figure 6.34 shows that the waters of the lake would have flooded into the valley if the GTF and associated landforms pre-dated the LLS.
3. Lowe and Cairns (1991) have cored the infilled sediments in Glen Turret to the north of the arcuate moraine and found only Holocene sediments, with pollen evidence at the base of the sequence for an early Holocene invasion plant sequence (*Rumex*, *Empetrum*, *Juniperus*, *Betula*) typical of the LLS-Holocene transition, and they therefore conclude that the most likely explanation is that the terminal moraine at the GTF was formed during the LLS.

4. The evidence of cosmogenic dates obtained from boulders on the surface of the GTF, which are no older than the LLS, has already been alluded to above.

While each of these criteria is individually inconclusive, taken together they would tilt the balance of argument in favour of the inferred ice-lobe in Glen Turret having formed during the LLS. This conclusion was also reached by Sissons and Cornish (1983) and by Benn and Evans (2008), but the present author's interpretation differs in detail from these previous proposals. Sissons and Cornish (1983) make no mention of the lobe extending up to the head of the Turret, so the interpretation presented here adds to their proposal. Benn and Evans (2008) suggested that the source of the ice that terminated at the GTF was the Carn Dearg plateau, high above the eastern flank of the Turret Valley, and that the ice came not from Glen Gloy, but from the small valley that drains from the Carn Dearg plateau into the head of the Turret. Inspection of NEXTMap DEM data by the author in that valley and the adjacent parts of the Carn Dearg plateau failed to detect any evidence in support of this hypothesis; that valley is devoid of any clear glacialic landforms.

A second simulation was constructed for the lake at the 325 m level, to assist in visualising events associated with it (Figure 6.35). This shows that this lake would have extended throughout the lower part of upper Glen Roy and most of Glen Turret. It is necessary to note that both the delta and terrace associated with the 325 m lake that were highlighted in preceding sections (Figure 6.28B, and 6.29) would have been submerged by the 325 m lake. The landform evidence in the lower Allt a'Chomhlain suggests an ice margin delimited by the delta landforms and the marginal features described earlier, with the margins shown on Figure 6.35. It can be seen that these

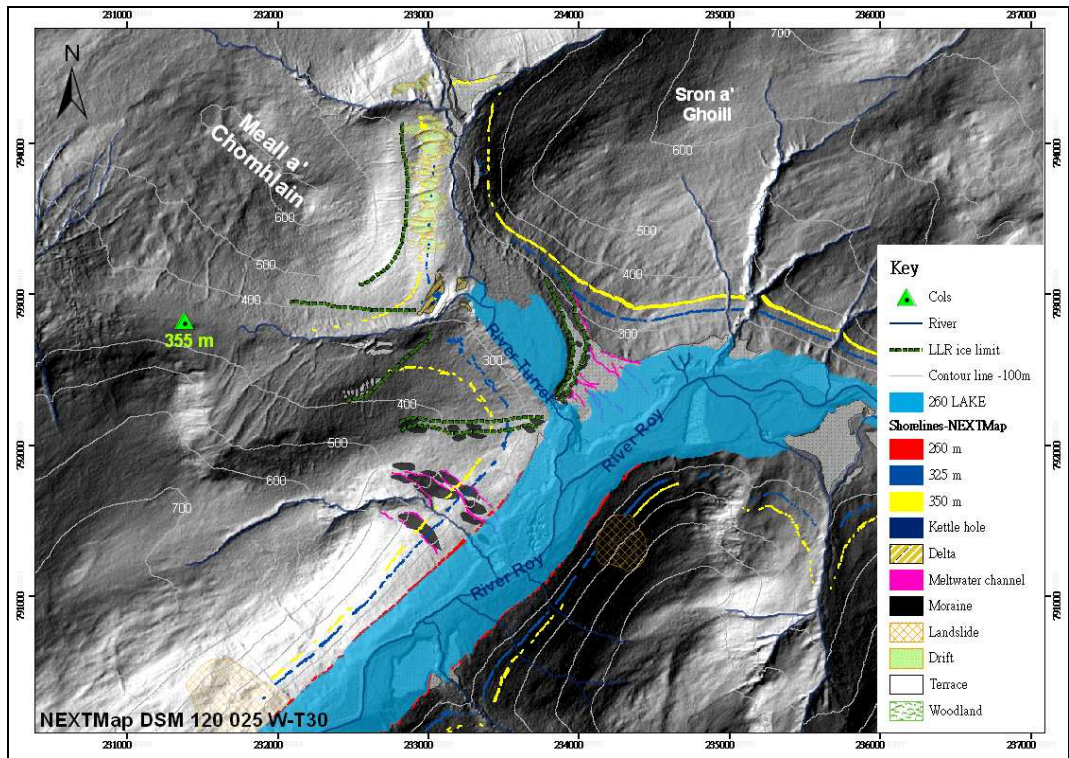


Figure 6.34 A simulation of the 260 m lake in upper Glen Roy based on GIS software, superimposed on composite NEXTMap plot. Also shown are the principal ice limits in the Turret and Allt a'Chomhlain valleys and the distribution of preserved fragments of the Parallel Roads inferred from NEXTMap DEM data.

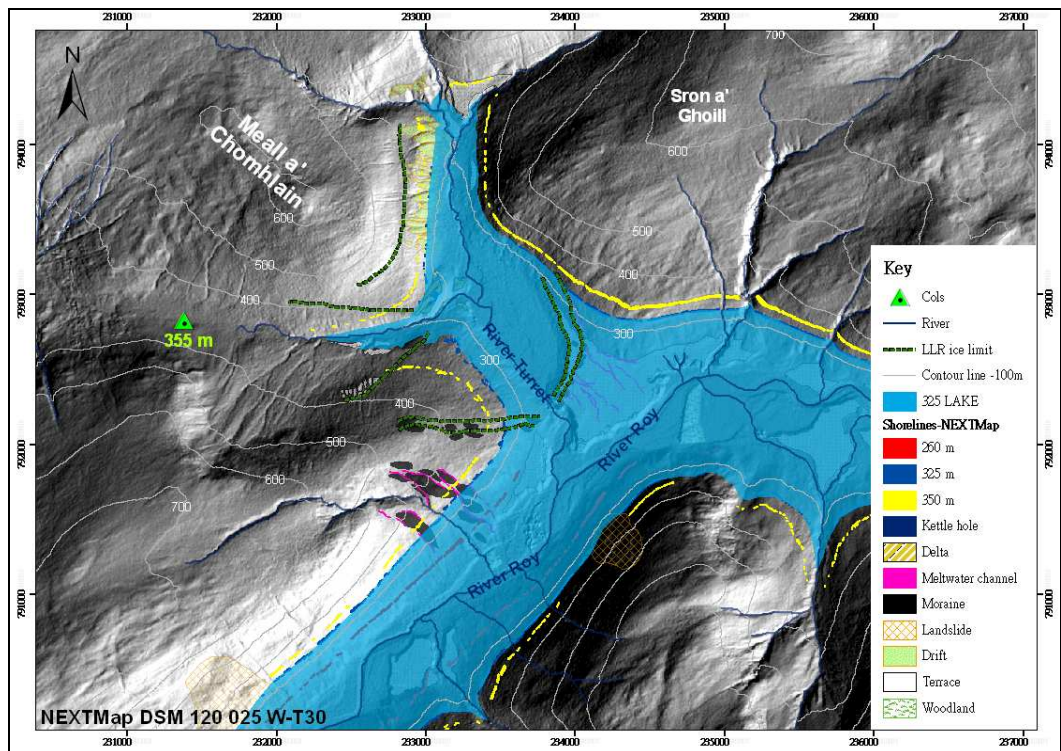


Figure 6.35 A simulation of the 325 m lake in upper Glen Roy based on GIS software, superimposed on composite NEXTMap plot.

marginal limits lie close to where the 325 m shoreline peters out in the Allt a'Chomhlain valley. The absence of the 325 m shoreline westwards of the inferred limits was verified in the field. It seems reasonable to conclude, therefore, that the delta deposits formed in the 325 m lake in the rising lake sequence. This rise in lake level may have been sufficient to destabilise the ice lobe that occupied the Turret at the time of the 260 m lake, causing it to retreat and become stabilised on land or in very shallow water, near the margin of the 325 m lake. The fluvial terrace on the northern flank of the Chomhlain (feature r, Figure 6.28; see also Figure 6.29) may have formed in the 325 m lake of the falling lake sequence, after the ice had retreated further.

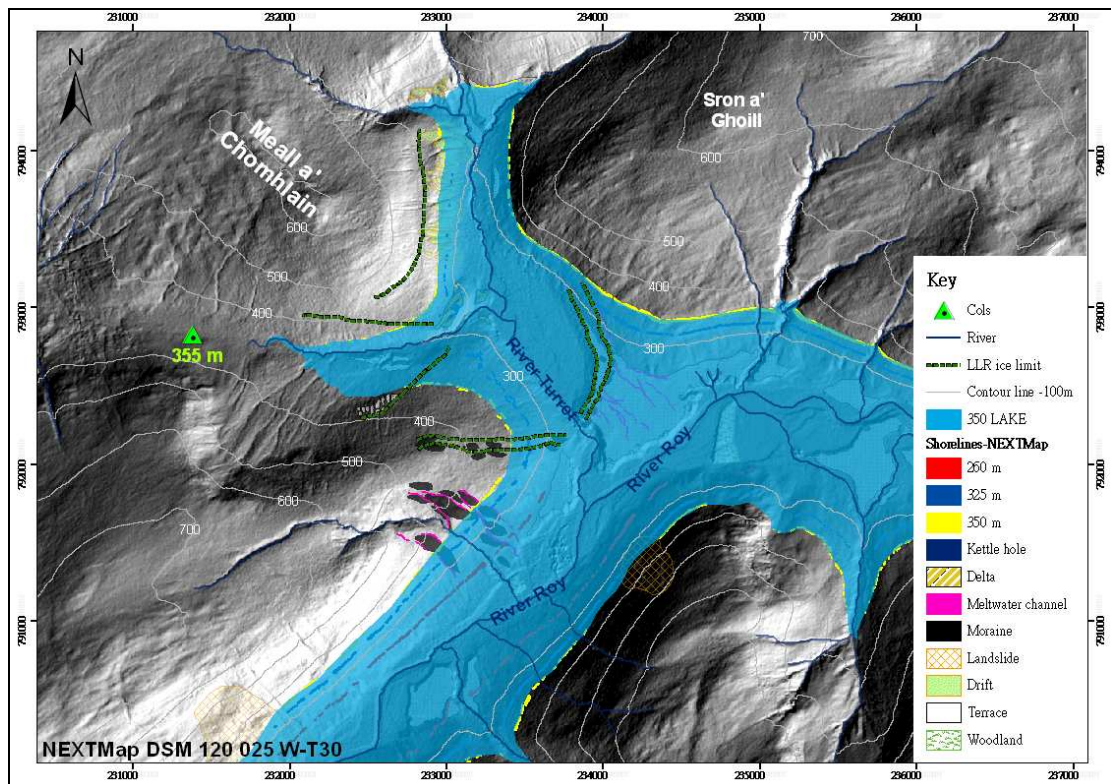


Figure 6.36 A simulation of the 350 m lake in upper Glen Roy based on GIS software, superimposed on composite NEXTMap plot.

A simulation of the 350 m OD lake level based on NEXTMap and GIS software (Figure 6.36) shows that that lake would have extended throughout the lower part of upper Glen Roy and Glen Turret and into the tributary valleys of Glen Turret. In the light of

arguments presented above, it is presumed that the glacier would have receded further, under increased water depth, and the fact that the 350 m shoreline tapers out on both sides of the Chomhlain valley might indicate that the ice margin retreated only a minimal distance to this part of the valley, preventing formation of the shoreline. This remains speculative, however, as no landform evidence could be found in the NEXTMap plots to support this suggestion. The matter is discussed further in the final section of this chapter.

A final point to note, with respect to Figure 6.36, is that all of the fans in upper Glen Roy were completely submerged by both the 325 m and 350 m lakes, and it is surprising that no significant sediment bodies developed where streams entered the lakes, a point which is also returned to in the final section.

## **6.5 Conclusions**

Glen Roy and vicinity was selected as a study area for testing the potential of NEXTMap DEM data for landform mapping and analysis because of the variety and complexity of the landforms in the area, while the presence of the lake shorelines ('Parallel Roads') provide unique 'isochrons' that help to establish the temporal relationships of some of the landforms. The results presented here have shown that the landforms identified by previous researchers, based mostly on detailed field mapping and aerial photography, are faithfully represented in the NEXTMap DEM plots. Indeed, because of the ability to change illumination direction, the landforms can be viewed in 3D from a variety of angles, providing a level of scrutiny that may not always be possible in the field. Furthermore, the whole field area can be examined, including inaccessible parts. NEXTMap plots also provide a perspective that is difficult to achieve using other media. Aerial photographs, for example, frequently have parts obscured by



cloud cover or distortions of light, and can usually only be examined under one mode of illumination. NEXTMap data offer much more flexibility in this respect, as well as the ability to enlarge features, almost instantaneously. It also shows up detail that may be difficult to observe in the field or on other media, such as the faint ‘minor’ shorelines in the Bohaskey area of Glen Roy (section 6.2.2) and the possible trim-lines on Bohuntine Hill and the flanks of Caol Lairig (section 6.2.3.2).

Another advantage of NEXTMap data demonstrated here is that the application of the visual optimisation method, explained in Chapter 3 and 4, generates a level playing field for comparing features between localities. A striking feature of the images prepared for this study of the Glen Roy area, presented in earlier sections of this chapter, is the difference in ‘freshness’ of the landscape that can be detected: compare, for example, the appearance of the features on the floor of the upper Glen Roy, the Roy-Turret confluence, Caol Lairig and the Viewpoint on the one hand, with the appearance of the middle Roy Valley on the other. The former appear far fresher and smoother than the latter, which, in retrospect, reflects the interpretations made (independently) on the basis of the landform assemblages. In other words, the areas and features identified as of LLS age appear very different to those interpreted as older in age. Of course this may prove a simplification, when comparable studies are undertaken in other areas, but the matter that needs to be examined in future research is *whether this will hold true providing that the images can be compared under optimal illumination constraints.*

A further advantage of NEXTMap DEM data is the ability to manipulate the plots or compilations of images to test ideas about landscape evolution. This has been illustrated here through the importation of the lake simulation experiments (Figure 6.34, 6.35 and 6.36) which were used to examine the interactions between glaciers and lakes, the results of which have enhanced understanding of the sequence of events in the area.

NEXTMap data seem to offer considerable scope for further experimentation of this type. It also offers the capacity for rapid measurement of landscape properties, a feature which will be illustrated in Chapter 7, where this facility is exploited to undertake a detailed examination of the surface form of the Parallel Roads.

Although not the primary objective of this research project, the observations presented in this chapter have led to a re-assessment of the age and sequence of events in Caol Lairig and Glen Turret, and added some intriguing new information to the inventory previously available for the Glen Roy area. However, some mysteries remain. The conclusions about the sequence of glacial-lake interactions presented above, and the conundrums that remain to be resolved, will be summarised in chapter 8, the final chapter of this thesis, which synthesises the key outcomes of the research.

## **7. Shoreline analysis: distribution, form and architecture**

---

### **7.1 Introduction**

The Parallel Roads of Glen Roy were levelled instrumentally and comprehensively for the first time by the Ordnance Survey (OS) in the mid 19<sup>th</sup> Century. However, Jamieson (1892) noted some limitations with the measurements obtained by the OS officers. First, they selected the mid-points between the shoreline notch and the outer edge of the platforms, with little explanation of how representative these points might be or how precisely the mid-points could be determined. Second, some measurements were obtained from sections of the roads that are very poorly developed, and in some instances where they are not observable in the field. Third, no allowance had been made for the patchy occurrence of peat development or of varying amounts of scree and colluvial material draped over the road surfaces. In combination, these factors introduced an unquantified degree of noise to the data, which led Jamieson (1892) to recommend that a more careful, systematic survey of the roads be undertaken, a challenge not met until J.B.Sissons initiated new surveys in the area in 1978.

Sissons (1978) initially measured the widths, aspects and notch altitudes of the shorelines at 787 different points and at an average horizontal interval of 115 m. He took into account peat depths and avoided locations with scree/colluvial cover. He subsequently re-leveled the shorelines at intervals of 25 to 30 m (Sissons and Cornish, 1982b). On the basis of these results, he was able to make a number of important observations about the Parallel Roads. First, they appeared to have consistent widths throughout Glens Roy, Gloy and Spean, both within and outside the mapped Loch Lomond Readvance (LLR) ice limits. The average widths of the top (350 m), middle (325 m) and lowest (260 m) shorelines in Glens Roy, and of the single (355 m) shoreline in Glen Gloy, were found to be 15.2, 10.5, 10.4 and 7.3 m respectively, but he

did not detect a significant difference in the mean widths of the roads inside and outside the LLR ice limits. The road widths were also influenced strongly by aspect (direction in which the backing cliff faced) and by streams delivering fluviially-transported load on to the platforms. Away from these influences, however, he found the shorelines to be remarkably uniform in width, from which he deduced that the Roads must have been formed exceedingly quickly and subsequently stabilised at a uniform width (Sissons, 1978).

Second, he found that the Roads do not have consistent altitudes or along-valley gradients, but are dissected into a series of blocks that show varying degrees of tilt: some blocks are horizontal, while others record varying gradients of up to  $4.6 \text{ m km}^{-1}$  (Sissons and Cornish, 1982b). Third, significant dislocations of adjacent segments of the road surfaces are apparent, with vertical throws of up to 3 m or so, usually found in association with faults or landslips/rockfalls. From these observations, Sissons concluded that the roads had been differentially dislocated at numerous points caused by loading or unloading of the ground by glacial ice and/or the associated ice-dammed lakes. He therefore also concluded that this degree of deformation precluded the possibility of measuring overall shoreline gradients for the Parallel Roads.

By contrast, Dawson *et al.* (2002) conducted independent measurements of the Roads in Glen Roy and on the basis of 104 altitudinal values concluded that they show consistent along-valley tilts of about  $0.11$  to  $0.14 \text{ m km}^{-1}$ , which they attributed to a regional trend in glacio-isostatic uplift. On the basis of this evidence, they suggested some minor modifications to previously published uplift isobase patterns for Scotland, as proposed by Smith *et al.* (2000). This conclusion was subsequently vigorously contested by Sissons, on the basis of his published evidence for complex and pronounced dislocation of the Roads (J.B. Sissons, oral presentation, QRA field meeting, September 2008).

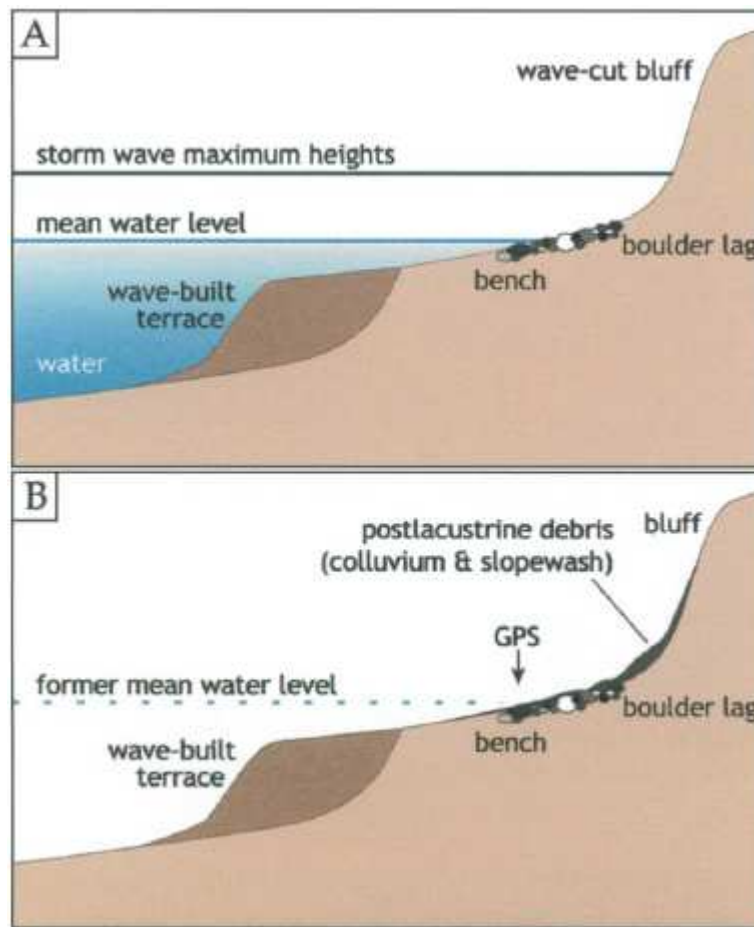
The availability of NEXTMap coverage for the Glen Roy area offered the opportunity to re-visit this matter, and to test Sissons' survey results and conclusions as well as the validity of Dawson *et al.*'s claims. The main purpose of this chapter, therefore, is to generate more comprehensive data on the distribution, altitudes, widths and surface architecture of the Parallel Roads using the facilities offered by NEXTMap DEM compilations. Altogether almost 32,000 spot-height measurements have been obtained from mapped shoreline surfaces, the results of which are presented below. These data are used to establish (a) the degree of vertical precision with which the shorelines can be measured using NEXTMap-generated data; (b) the degree to which the shorelines are deformed or dislocated; and (c) whether, despite the local effects of dislocation, regional glacio-isostatic trends can be discriminated using this much larger data-set of surface measurements. One possible future application of the results of this investigation could be the reconstruction of the original architecture of the shorelines, prior to deformation.

## **7.2 Methodology**

### **7.2.1 Assumptions concerning the mode of formation of the Roads**

Sissons (1978) concluded that the Parallel Roads were not formed by wave action alone, in the manner generally proposed for wave-cut platforms (e.g. by Schaetzl *et al.*, 2002; see Figure 7.1), but in an accelerated process involving frequent wetting and drying at the lake margin under arctic conditions. The assumption he made was that the Roads were excavated entirely during the interval of the Loch Lomond Readvance, which he assumed to have lasted approximately 1,000 years, the then-accepted duration of the Loch Lomond Stadial. Subsequently Palmer *et al.* (2010) have developed a chronology for the formation of the Roads based on varve analysis, and concluded that the ice-dammed lakes existed for a maximum of around 515 years, which therefore also limits the time available for formation of the Roads, a point returned to in later sections

of the thesis.



**Figure 7.1** A. Generalised model of wave-cut platform and bluff formation, showing the position of mean water-level and boulder lag. B. Surviving features after lake recession, with assumed level of former mean water-level (from Schaetzl *et al.*, 2002)

Under an arctic climatic régime, lake-marginal ice removes material progressively during thaw periods, constantly exposing fresh surfaces to freeze-thaw processes (Matthews *et al.*, 1986; Aarseth and Fossen, 2004). The excavation process envisaged for the formation of the Roads is therefore significantly different to that for normal wave-cut bench formation under temperate conditions. For the latter, the lake water erodes the bluff and transports debris from the storm-wave maximum height position, either downwards or by wind drift along the platform edge, to form a wave-built terrace (Figure 7.1). The shoreline can be defined at any position between the storm wave maximum height and the top of the wave-built terrace, though some have argued that the best indicator of mean water level is the foot of the wave-cut bluff or of any

associated boulder lag (Johnson, 1933; Miller, 1939). However, melting blocks of ice can carry material out into the deeper parts of the lake, beyond any wave-built terrace, and could in theory also extract material from the back wall that lies above the mean level of the lake, where the lake ice is sufficiently thick. These factors therefore lead to more efficient excavation of debris from the platform, but may limit the development of a wave-built terrace. Indeed, evidence of a wave-built terrace was rarely observed by the author during field surveys, while the lowest points of observed boulder lags were frequently difficult to define in the field, as a result of peat cover. For these reasons, consistent definition of a particular profile marker (e.g. bluff foot; boulder lag edge; platform mid-point; etc.) is difficult to apply in the field, and is even more problematic when attempting to identify such features using NEXTMap DEM data. In any case, the significance of such features may be equivocal when considering platforms excavated by prolonged freeze-thaw processes, for the reasons given above. To avoid subjective selection, therefore, an alternative approach was adopted, which was to measure as many random measurements as possible from pre-defined small plots set out at regular intervals along the Road surfaces. One great advantage of using NEXTMap technology is that it enables the rapid measurement of numerous spot heights. In this approach, it is assumed that the mean measurement for each plot approximates the altitude of mean lake water level.

### **7.2.2 Mapping shoreline fragments using NEXTMap DEM data**

Ice-dammed lake shorelines have characteristics that are quite different to other landforms examined in earlier chapters. Firstly, they are relatively “flat” in comparison with the general relief in the immediate vicinity, though for the most part they have a gentle gradient from the back-wall to the front edge, hereafter termed the ‘platform slope’ to distinguish it from the along-valley longitudinal gradient of the shorelines; the latter are the main focus of the current study. Their second important characteristic,

from the point of view of digital mapping, is that they form continuously linear features at predictable elevations within the valleys, and hence can be easily distinguished from other linear features, even where displaced by post-glacial tectonic rebound or local seismic activities.

In Chapter 4, the mapping of glacial landforms such as drumlins relied on the use of hill-shaded imagery and examination of the form and boundaries of features using the rotating (incident) light method. This approach was, however, not found to be helpful for the identification and mapping of shoreline fragments. Changing the altitude and azimuth angle of incident light was frequently found to be unproductive, because the very narrow shoreline features become quickly obscured by shadows projected by adjacent valley walls, especially where shoreline fragments are located in the middle part of a steep hill (as illustrated in Figure 7.2 A). An attempt to improve the clarity of the shorelines on the DEMs was made using hillshade plots with a vertical illumination angle, but the results provided poor visualisation of the relative relief on the shoreline surfaces. This caused difficulties for defining the boundaries of shoreline fragments. To avoid this shortcoming, the slope map approach was employed (Figure 7.2 B); this has advantages over hill-shade plots. (1) It is not affected by azimuth bias (see Chapter 4). (2) There is no requirement to pre-set the azimuth and altitude angle, which means that a single image setting can be employed for the whole mapping process. (3) Abrupt changes in relief and flat features are easier to detect and map. The hill-shade transformations can also be used in tandem with slope map transformations to provide additional detail, but only where free of the shadow effects illustrated in Figure 7.2A. However, hill-shade transformed plots generally aid the human eye better, and hence are employed where possible for assessing geo-spatial relationships between the Roads and other features.



The generation of slope maps for the mapping of shoreline fragments is quite straightforward. It consists of delineating ground that is relatively flat and continuous over a fixed altitude, initially at a scale of 1:10,000 (Figure 7.3A). In order to increase the accuracy of the mapping, however, the image scale used in the present research for mapping shoreline fragments was usually larger than 1:2,000: an example is provided in Figure 7.3B, which shows the mapped boundaries of shoreline fragments identified using an image scale of 1:1,000. The shoreline fragment boundaries were delineated carefully along the junction between flat and steep ground.

### **7.2.3 Measurement of shoreline altitudes**

Sissons (1978, 1982b) employed a surveyor's level and Sopwith staff to obtain his measurements of the altitudes of the Parallel Roads. The target measurement accuracy maintained was 0.01 m with a closing error on survey traverses of less than 0.15 m. Traverses with larger errors were repeated until the closing error was achieved. This method requires frequent temporary benchmarks to be established, especially in stretches that are distant from fixed OS benchmarks. The precise positions of the measured points on aerial photographs and maps are likely to have been difficult to determine exactly: Sissons' work was conducted before the development of good quality GPS equipment. A further difficulty with the Sissons (1982b) data-set is that single measurements were obtained from selected parts of the platforms at each survey point; these were assumed to be representative of mean water level, the verification of which is difficult to judge.

Digital elevation data derived from NEXTMap, on the other hand, have potential horizontal errors of up to 5 m and potential vertical resolution uncertainties of ca. 0.5 to 1.0 m (Chapter 3; but see section 7.6, below). The horizontal error is not regarded as a problem for the interpretation of the data presented below, as it is tiny compared with

the overall Road lengths analysed (ca. 20 km in total). On the other hand, the operating error for altitudinal measurements is relatively large compared with the altitudinal range of each Road surface. The key question, therefore, is whether reliable statistical trends in shoreline altitudes can be obtained using NEXTMap data.

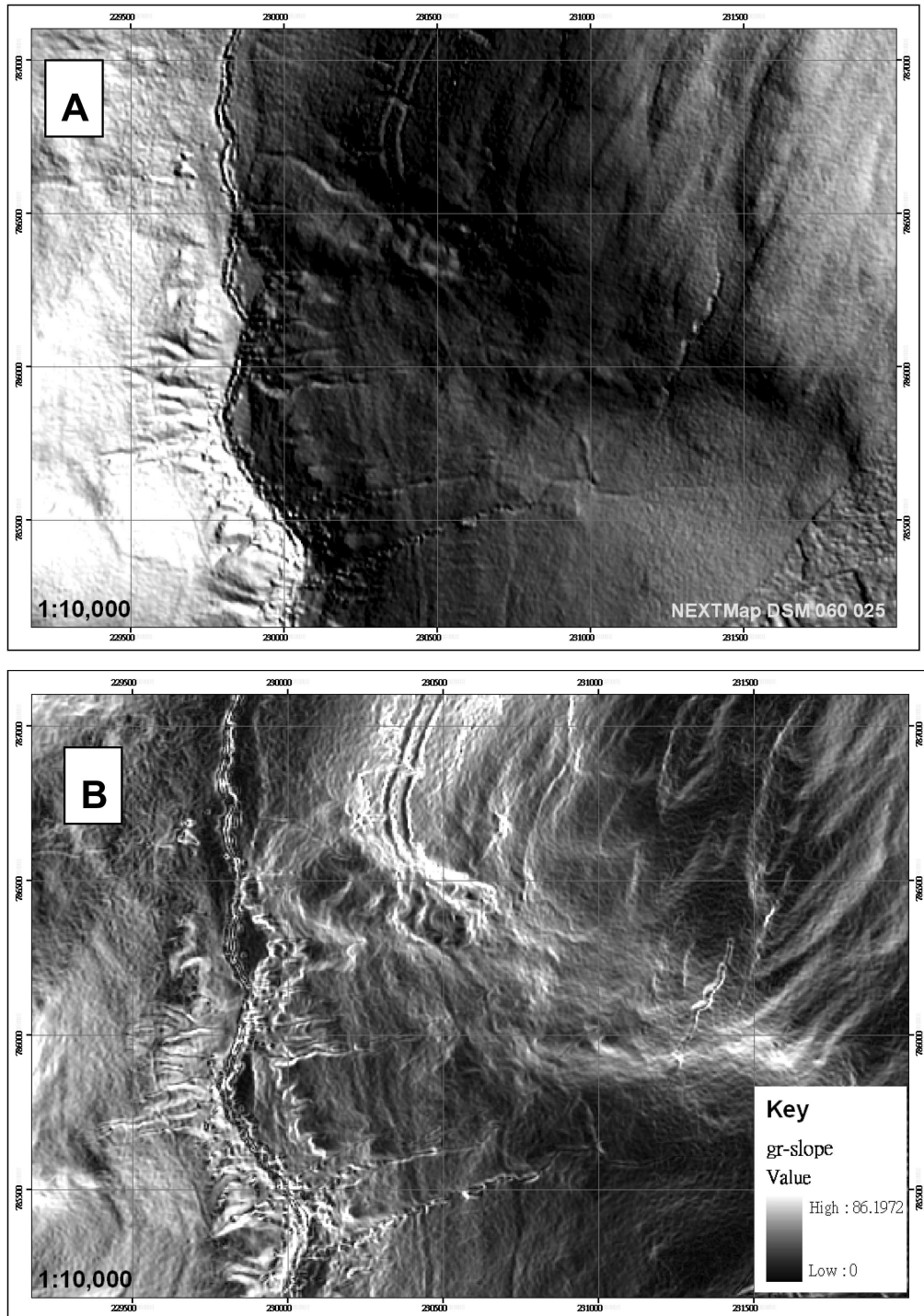
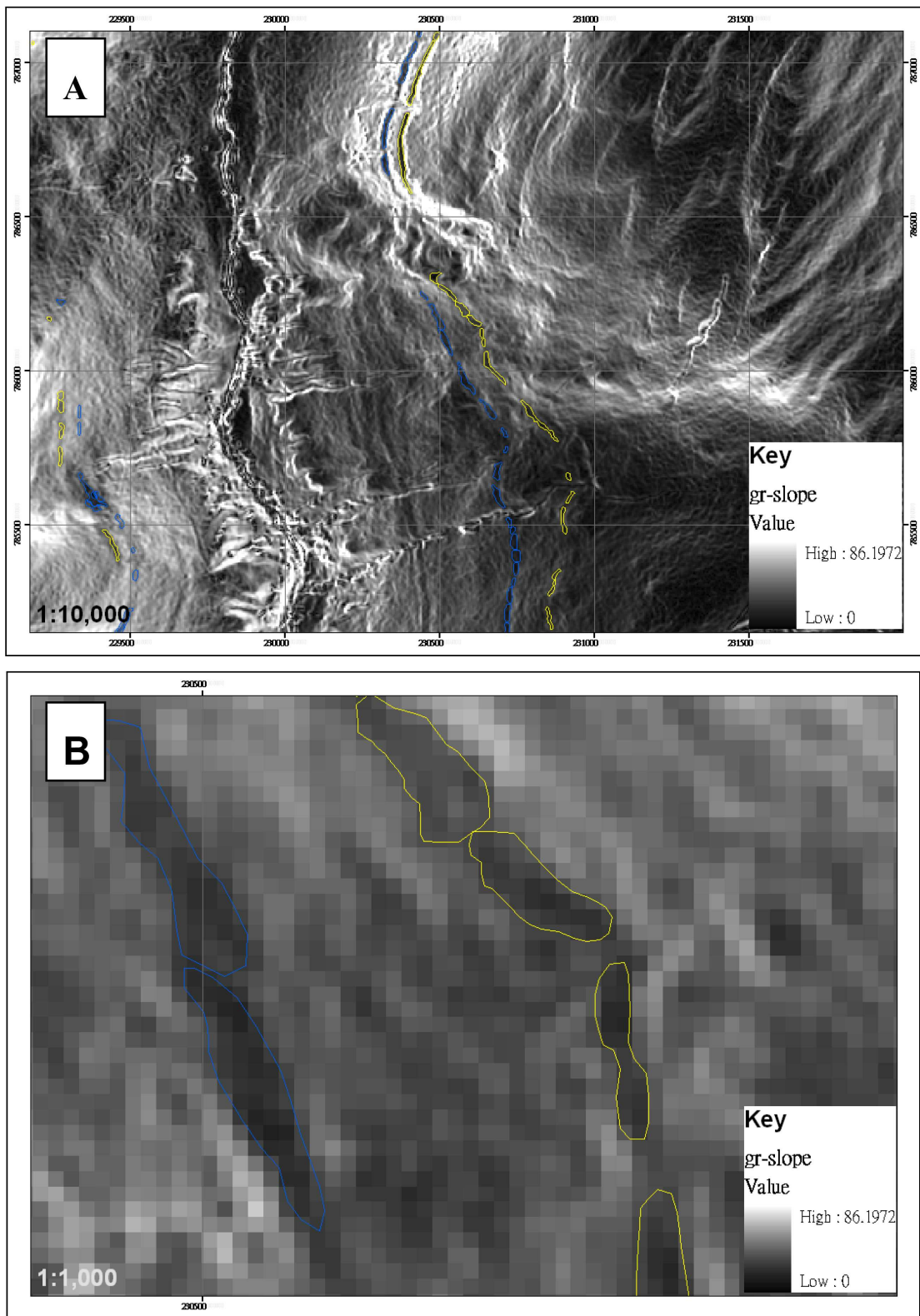


Figure 7.2 A. Hill-shaded plot of the area close to the Viewpoint in Glen Roy. B. Slope gradient plot of the same area. Note that the roads are obscured on the western side of the valley in Figure 7.2A



**Figure 7.3 A: Mapping of shoreline fragments at the 1:10,000 scale, used for initial delineation of shoreline fragments. B: Fragments of the 350 m (yellow) and 325 m (blue) shorelines mapped at a scale of 1:1,000.**

Altitudinal variations along the Parallel Roads were statistically tested using (a) regression analysis, (b) comparisons of means and standard deviations of selected

fragments or blocks, and (c) trend-surface analysis. The first two approaches provide information on localised patterns and discrepancies in the data, while (c) provides the best test for discriminating the overall three-dimensional architecture of the platforms. Trend-surface analysis is an established tool for detecting spatial trends in three-dimensional surface data, and has been most widely applied in the British Isles for the measurement of the surface architecture of raised marine terraces (raised beaches, rock platforms) and for determining their regional isobase patterns (e.g. Gray, 1974, 1978; Smith *et al.*, 1969, 2000, 2006; Dawson, 1989; Fretwell *et al.*, 2004). It was also employed by Dawson *et al.* (2002) to construct isobase trends for the Parallel Roads of Glen Roy, the results of which are assessed in section 7.10. Trend surface analysis was undertaken in this research primarily to test the results of Dawson *et al.* (2002), using software supplied by *ET Geo Wizards* (version number 9.9), a plug-in tool designed for operation with Arc GIS.

The data-set for statistical testing of the surface architecture of the Roads was generated as follows. First, well developed ‘*stretches*’ or ‘*reaches*’ of each of the Roads were mapped using a combination of NEXTMap DEM data, 1:25,000 scale O.S. maps, and field mapping. Each stretch or reach was usually bounded by deep ravines, gullies, landslips or other physical features responsible for localised destruction or obscurity of the Roads. The stretches identified by this procedure are defined in Figures 7.4 to 7.6. Each stretch was subsequently subdivided into smaller *segments*: these are constituent fragments of each road stretch that could be mapped continuously at a high spatial scale (1:2,000 to 1:1000), as illustrated in Figure 7.3B. For each segment, a fixed number of random measurements were obtained using the random sampling protocol included in *GIS-ET Geo Wizards* software, but with an arbitrary, minimum sample-point separation of 2.5 m, as illustrated in Figure 7.7. The GIS program employed automatically provided X and Y co-ordinates to define each sample point in space, as well as Z

co-ordinates defining the altitude of each point relative to OD. The total number of measured points generated was 31,952, of which 7,991 were obtained for fragments of the 260 m shoreline, 11,917 for the 325 m shoreline, and 12,044 for the 350 m shoreline. This compares with the total of 1029 points used by Sissons (1982b) in his analysis. Note that this study is limited to Glen Roy north of the Viewpoint, as this was primarily the focus of both the Sissons (1978) and Dawson *et al.*, (2002) studies. The **trend analysis** facility provided in the *GeoWizards* statistical tool box for use with Arc GIS was employed to generate trend surface models from these data (section 7.10).

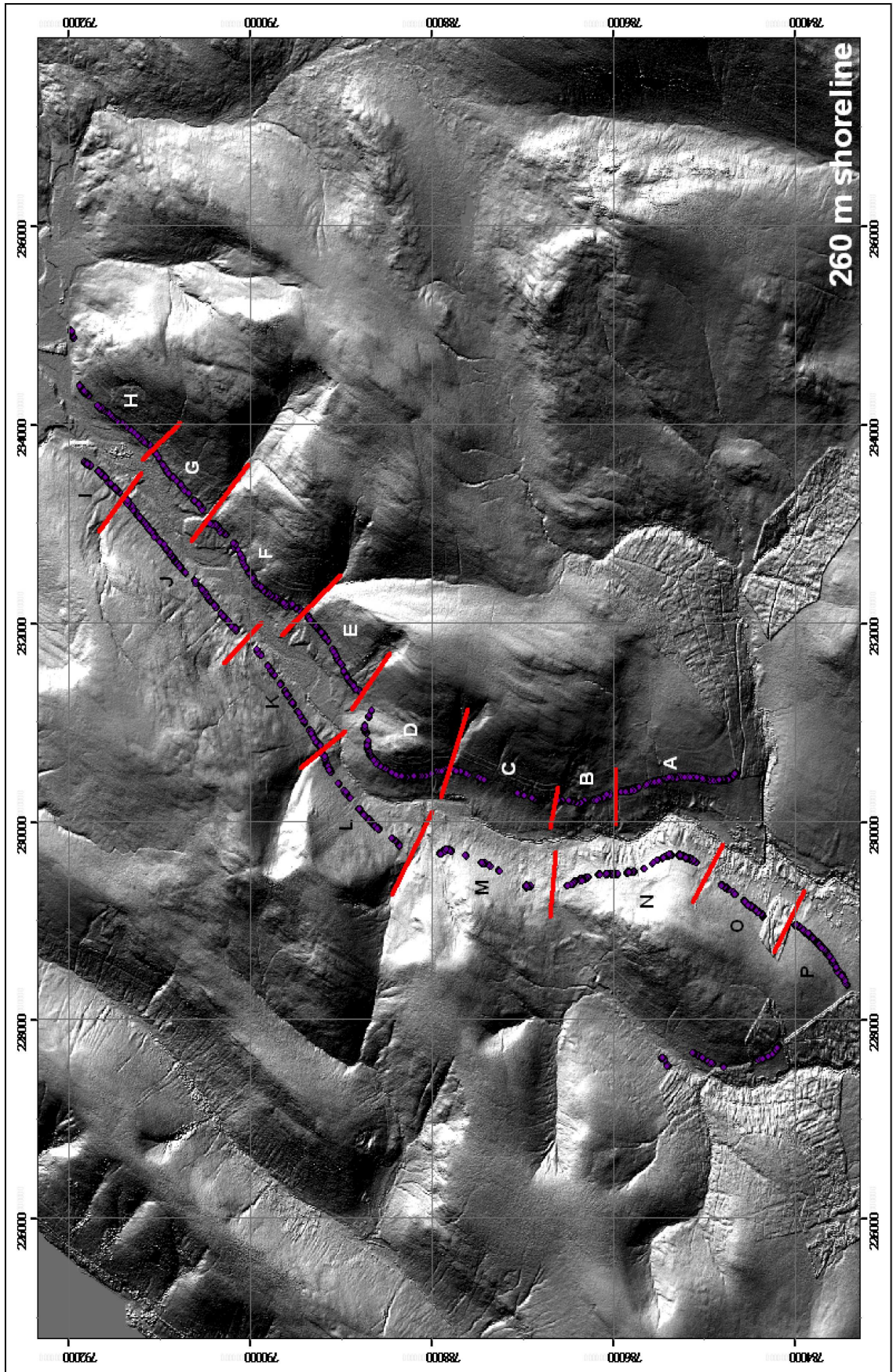


Figure 7.4 Continuous stretches of fragments recognised for the 260 m shoreline, labeled by alphabetical letter

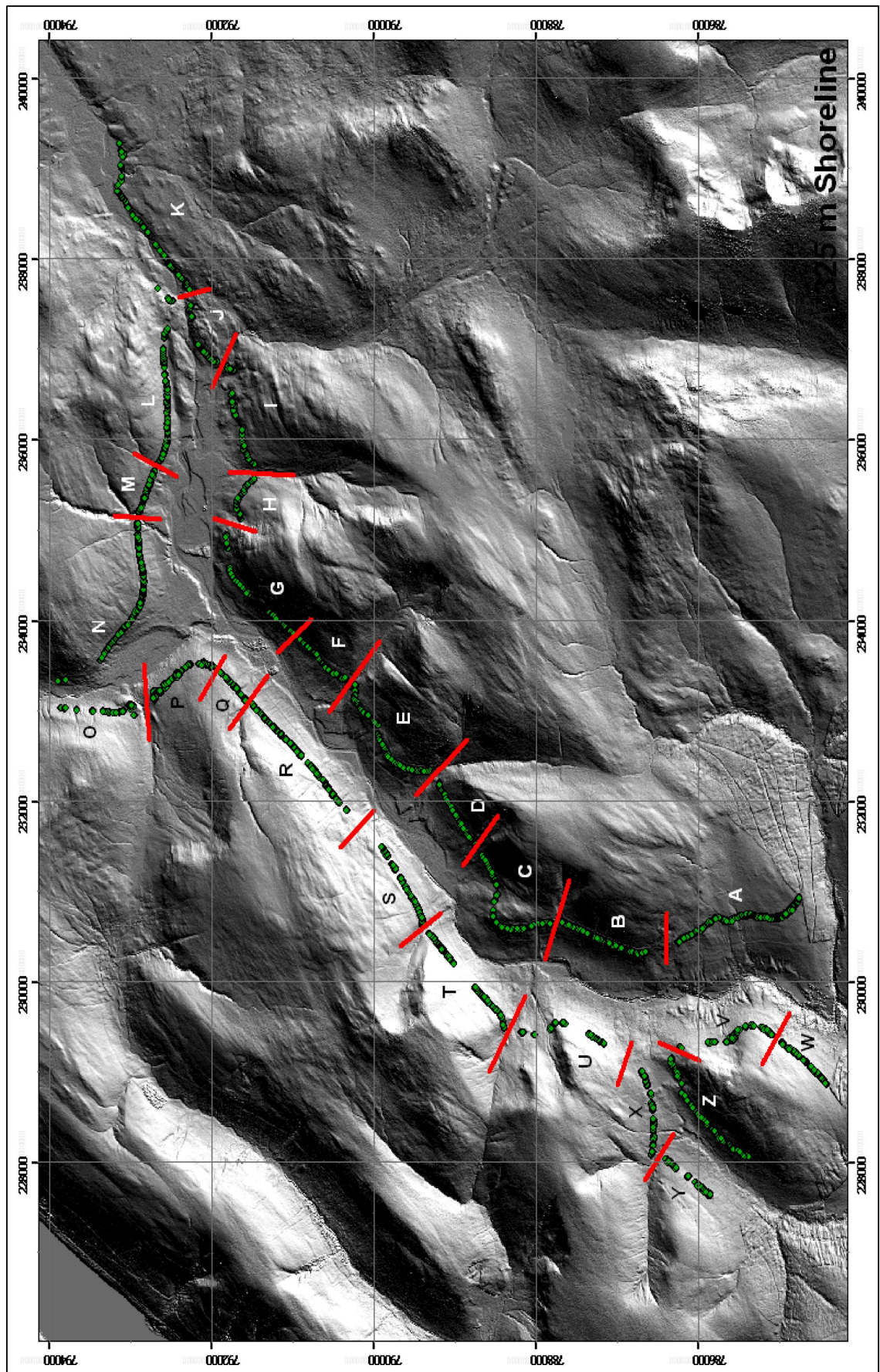


Figure 7.5 Continuous stretches of fragments recognised for the 325 m shoreline, labeled by alphabetical letter.

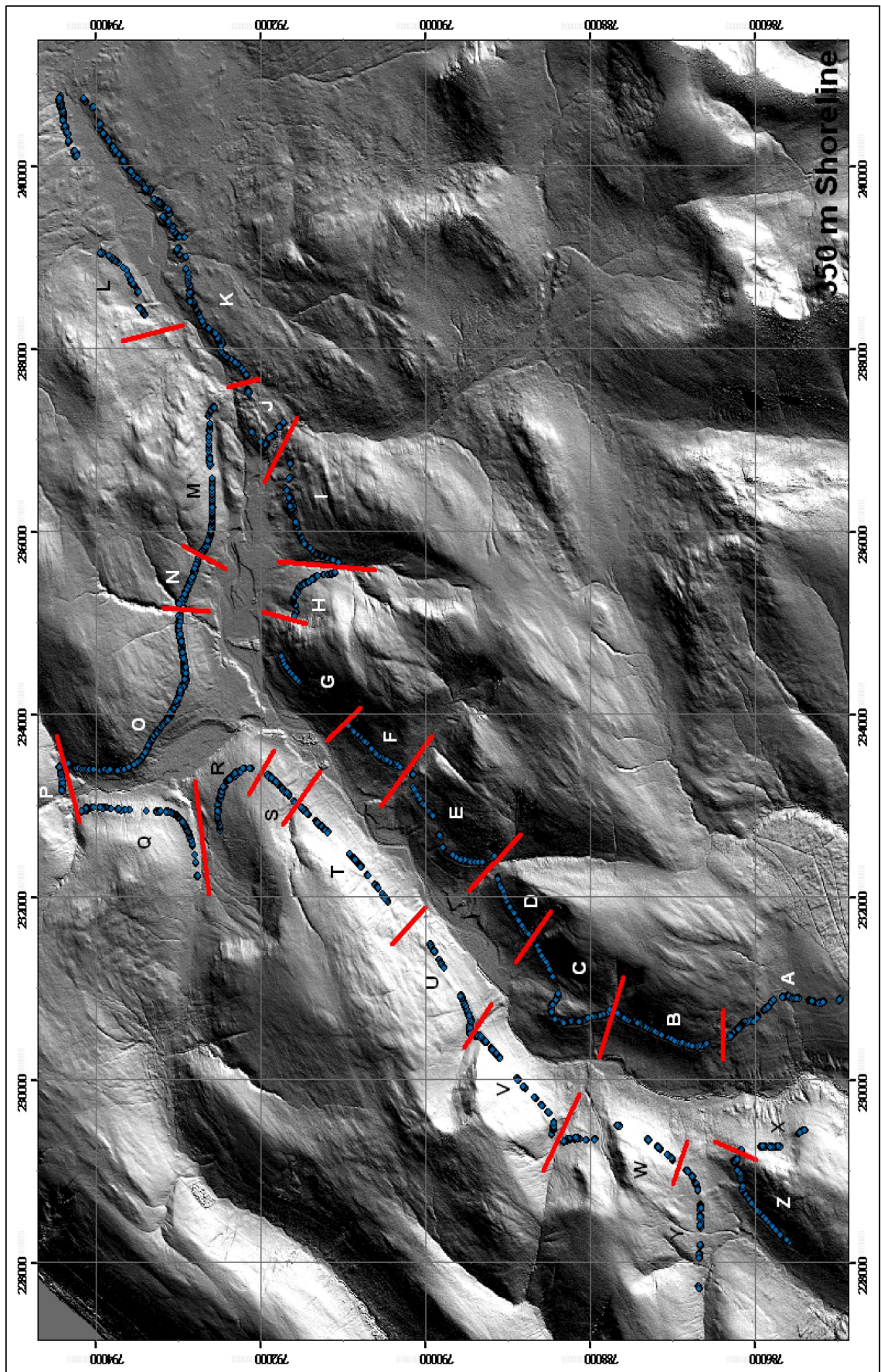


Figure 7.6 Continuous stretches of fragments recognised for the 350 m shoreline, labeled by alphabetical letter.



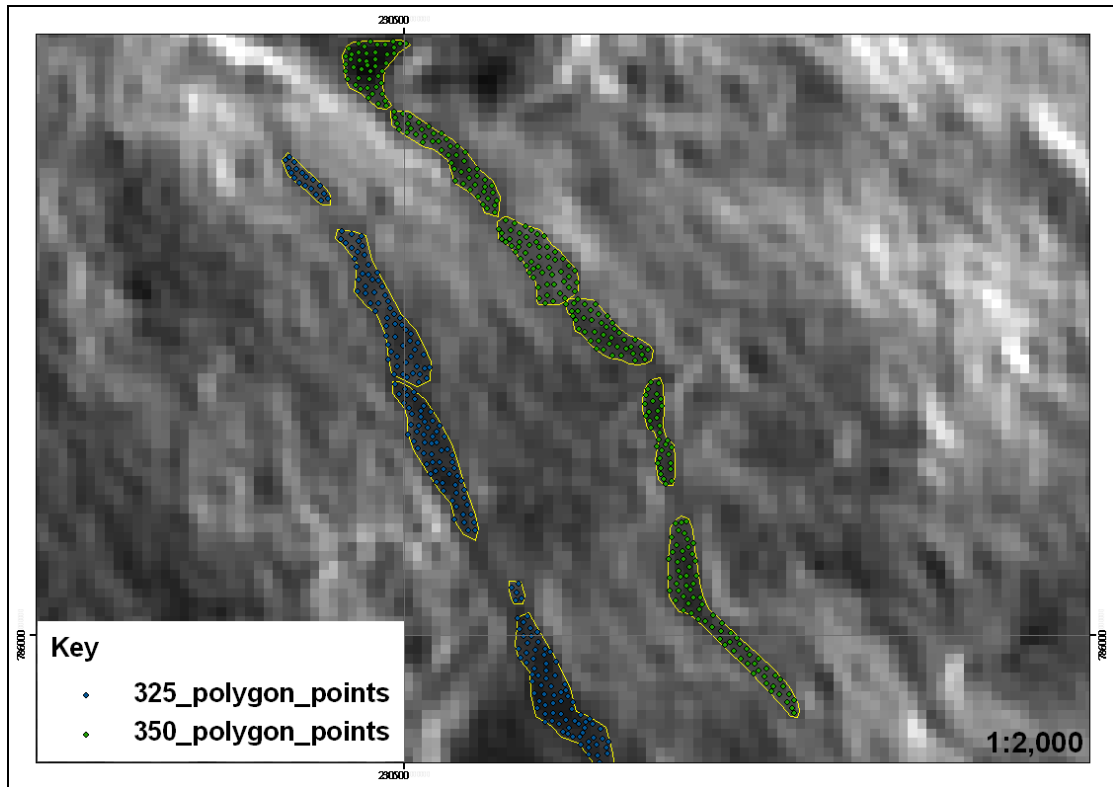


Figure 7.7 Illustration of typical density of randomly distributed measured points on stretches of the 325 m (blue points) and 350 m (green) Parallel Roads. These features are located close to the Viewpoint in Glen Roy on the eastern side of the valley (stretches labeled A in both Figure 7.5 and 7.6).

### 7.3 Distribution of the Parallel Roads

Ordnance Survey maps show the distribution of the Parallel Roads in Glen Roy based on field surveys conducted by O.S. officers in the mid-19<sup>th</sup> century. The depiction of the Roads on the 1:25,000 O.S. maps were digitised, and the results (Figure 7.8) compared with the results of mapping undertaken in the present research using NEXTMap DEM data at a scale of 1:10,000 (Figure 7.9). Both maps are compared with the results of mapping and survey of the Roads published by Sissons in 1978 (Figure 7.10). In general terms, the shoreline distributions mapped by the Ordnance Survey and by Sissons (1978) are similar to those derived from NEXTMap mapping, but there are notable differences, with examples highlighted by the boxed areas (marked A, B and C) in Figure 7.8 to 7.10, and shown in greater detail in Figure 7.11 to 7.16.

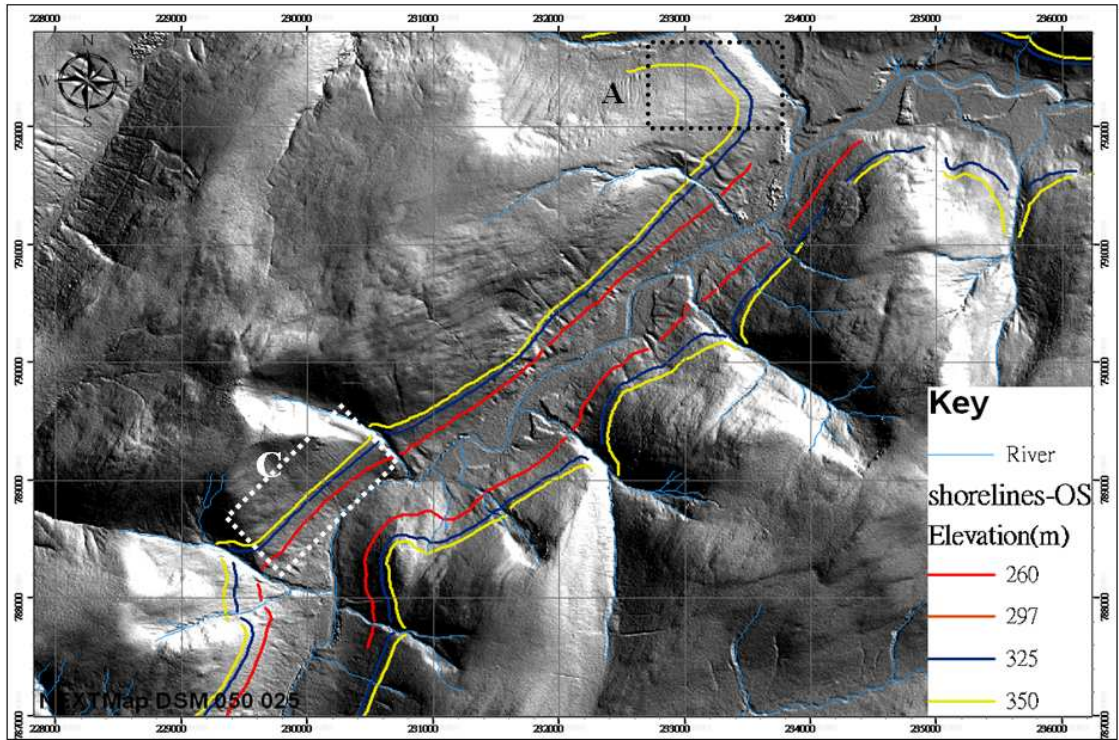


Figure 7.8 Digitised map of the distribution of the Parallel Roads of Glen Roy as depicted on 1:25,000 O.S. maps. For explanation of boxed areas, see text.

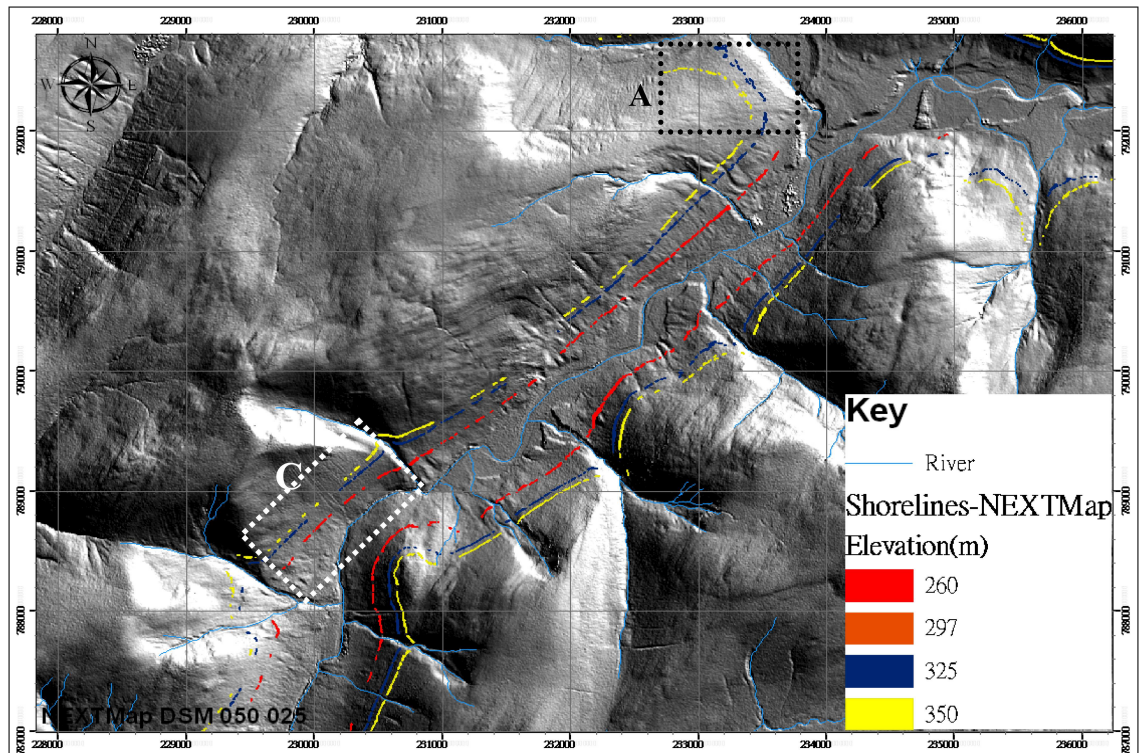


Figure 7.9 Distribution of Parallel Roads in Glen Roy using NEXTMap DEM data at a scale of 1:45,000. For explanation of boxed areas see text

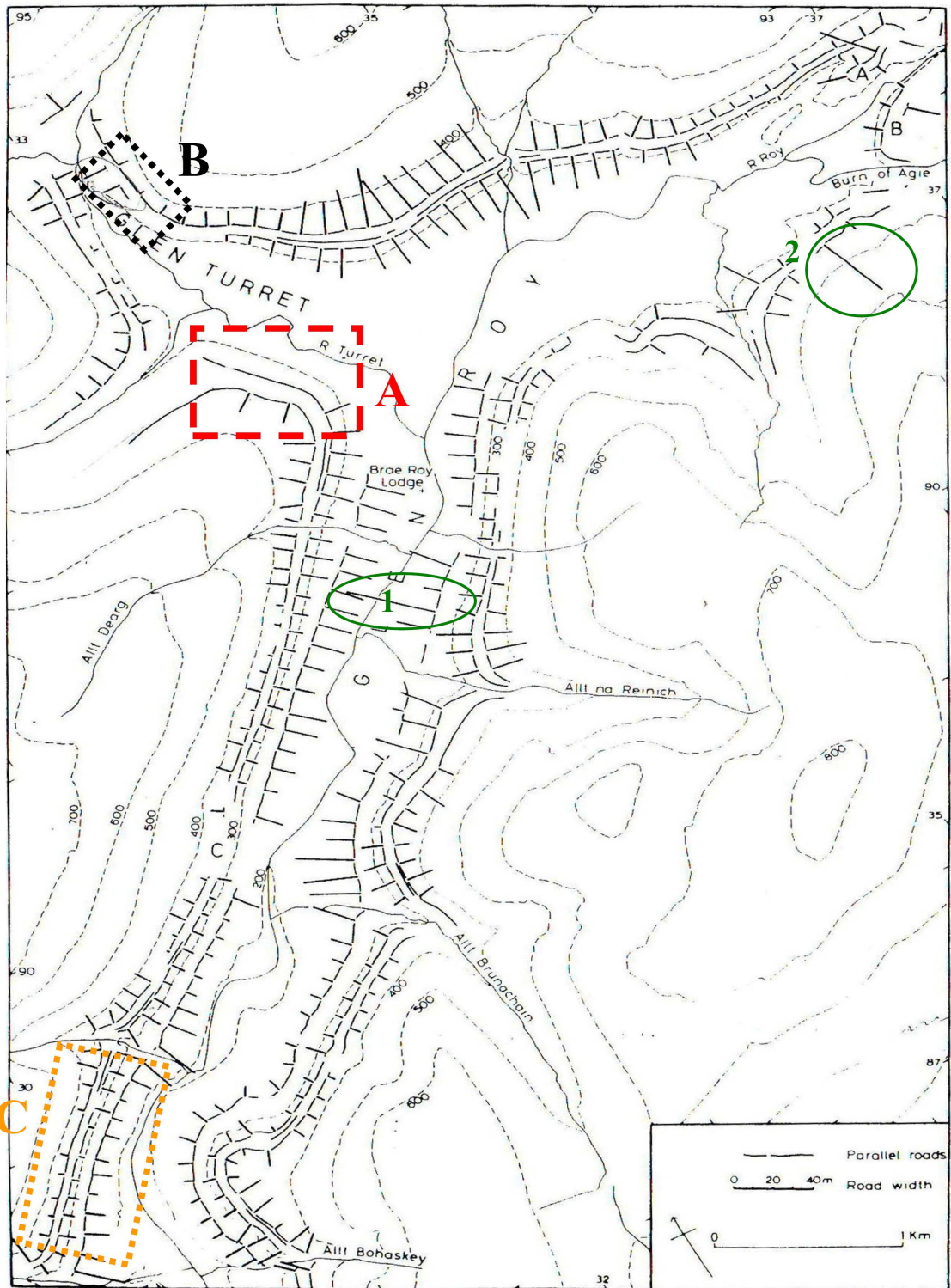


Figure 7.10 Distribution and widths of Parallel Roads of Glen Roy as surveyed by Sissons (1978).

Box A encompasses the west (right) bank of the River Turret, between the Allt a'Chomlaich and the Roy Valley. Sissons (1978) did not make measurements of the 325 m shoreline widths in this sector, and obtained only two width measurements from the

350 m shoreline (Figure 7.10), which means that he considered them to be poorly developed and discontinuous. Yet the shorelines appear continuous on the OS maps (Figure 7.11 and 7.12) and are clearly represented on NEXTMap DEM plots (Figure 7.13 and 7.14). Indeed, both the 350 and 325 m shorelines in this stretch appear to be ‘double-lined’ (each marked by two linear markings aligned in very close proximity – less than 1.0m apart). The reason for this is not clear, but it could indicate a slight shift in position of the land surface in this vicinity over the time that the 325 m lake existed, perhaps in response to isostatic adjustments. The adjustment could have taken place between the times that the 325 m lake occupied the valley in both the rising and falling lake sequences. A further possibility is seasonal changes in lake level, perhaps as a result of the overflow cols being choked with ice during winters. It is strange, however, that this phenomenon is confined to this small area, for similar features have not been detected on the images that cover other parts of the Roy and Turret valleys.

The head of Glen Turret (*Box B*) may hold important evidence for testing the origin of the Turret Fan (see section 6.4) and therefore the distribution and form of shorelines in this area could be critical. The O.S. maps do not show the 325 m shoreline on the east side of the upper Turret (*Box B*, Figure 7.11), but NEXTMap DEM data support the interpretations of Sissons (1978), who mapped small remnants of the 325 m shoreline that are discernible in this vicinity (Figure 7.10, 7.13, 7.14), though they appear more discontinuous on the NEXTMap plots than in the Sissons map. Field observations by the present author suggests that these 325 m shoreline remnants are closely associated with a mass of glacial sediments that occupy the head of the Turret, and indeed may be associated with a terrace, possibly a kame terrace, a point illustrated in section 6.4 where the origin and age of the Turret Fan are discussed. Also in this area, the 350 and 325 m shorelines on the opposite side of the valley are shown as continuous features (Figure 7.11 and 7.12). Sissons shows the 350 m shoreline to be almost wholly

continuous in this area, but the 325 m shoreline to be discontinuous (Figure 7.10). The NEXTMap plots suggest both shorelines to be markedly discontinuous (Figures 7.13 and 7.14).

Within *Box C* are shorelines developed on the NW side of the middle section of the Roy Valley, ca. 1.5 km north of Achavady ruin and of the col separating the Roy from Caol Lairig.

All three shorelines are cut into bedrock and have a steep outward (platform) slope. Both the O.S. maps (Figure 7.15) and Sissons' map (Figure 7.10) show all three shorelines as continuous features, but they appear distinctly discontinuous on the NEXTMap plots (Figure 7.16). From personal field observations, the shorelines look continuous from the valley bottom, but on closer inspection it is difficult to trace them continuously on foot, as they are often exceedingly narrow, have very steep backing slopes, and hence disappear beneath scree and slope wash debris. These properties make it exceedingly difficult to trace the shorelines using NEXTMap plots with a 5 m horizontal resolution.

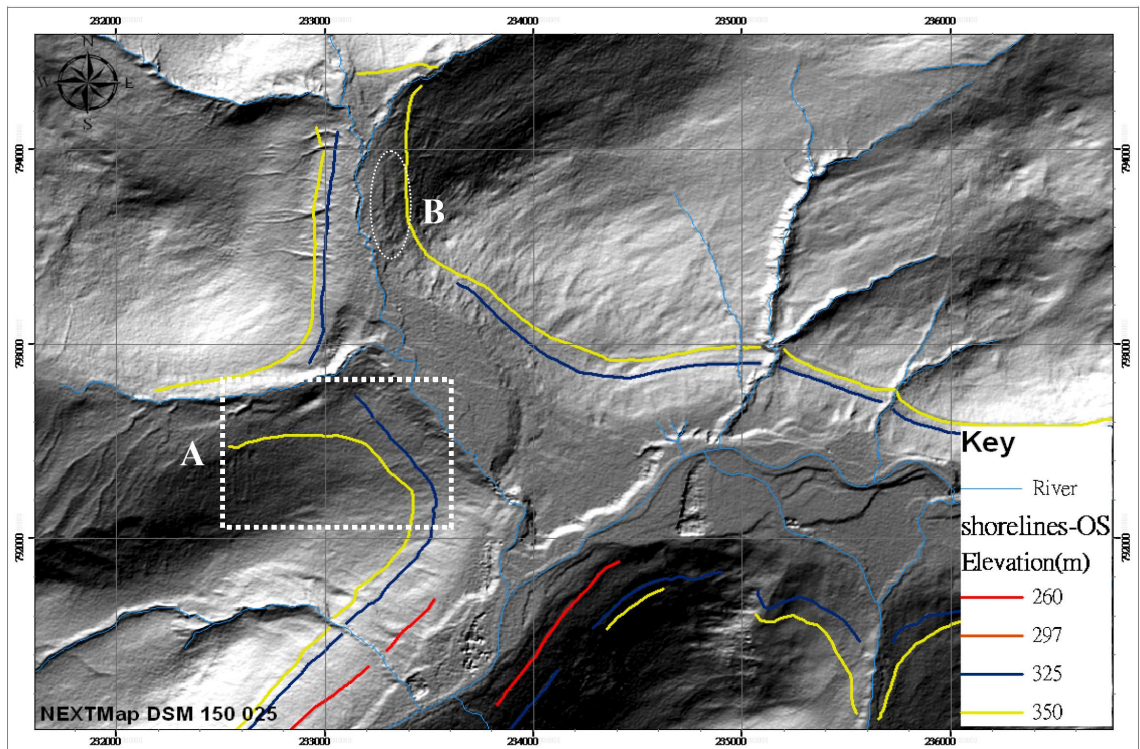


Figure 7.11 Digitised transform, based on 1:25,000 O.S. maps, of the shorelines mapped by the O.S. in the vicinity of the Turret-Roy confluence, shown on DEM plot.

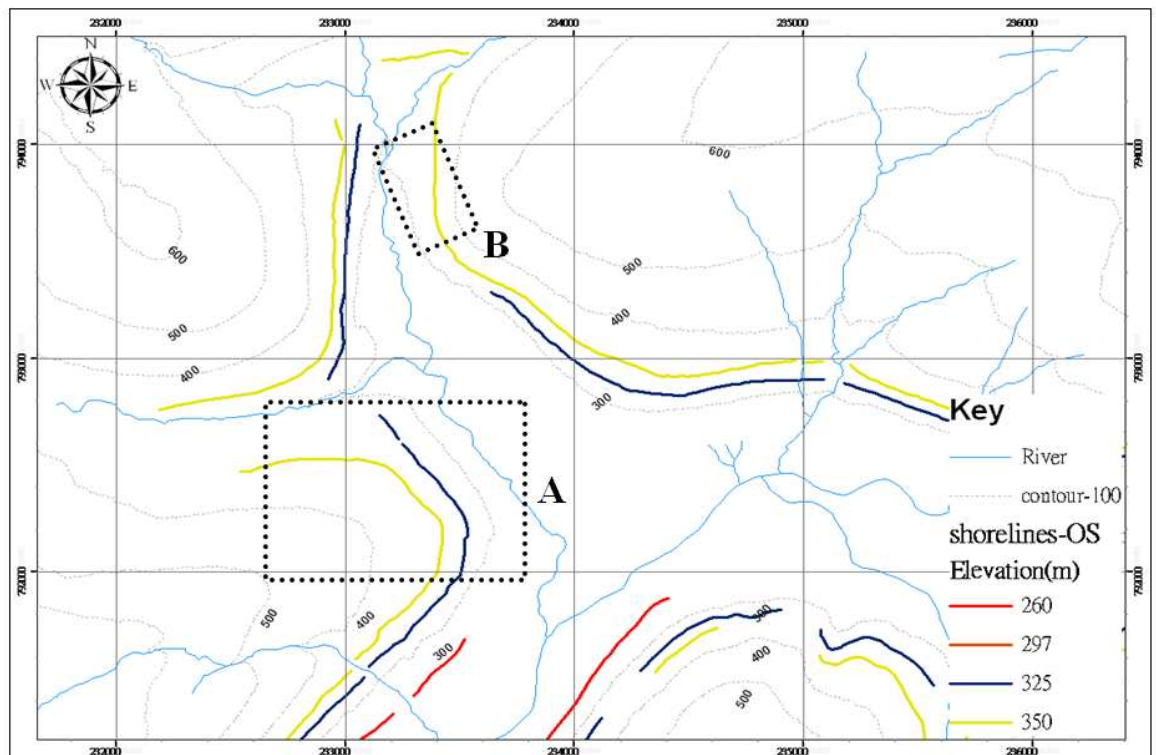


Figure 7.12 Simplified map version of the digitised O.S. shoreline distributions shown in Figure 7.11.

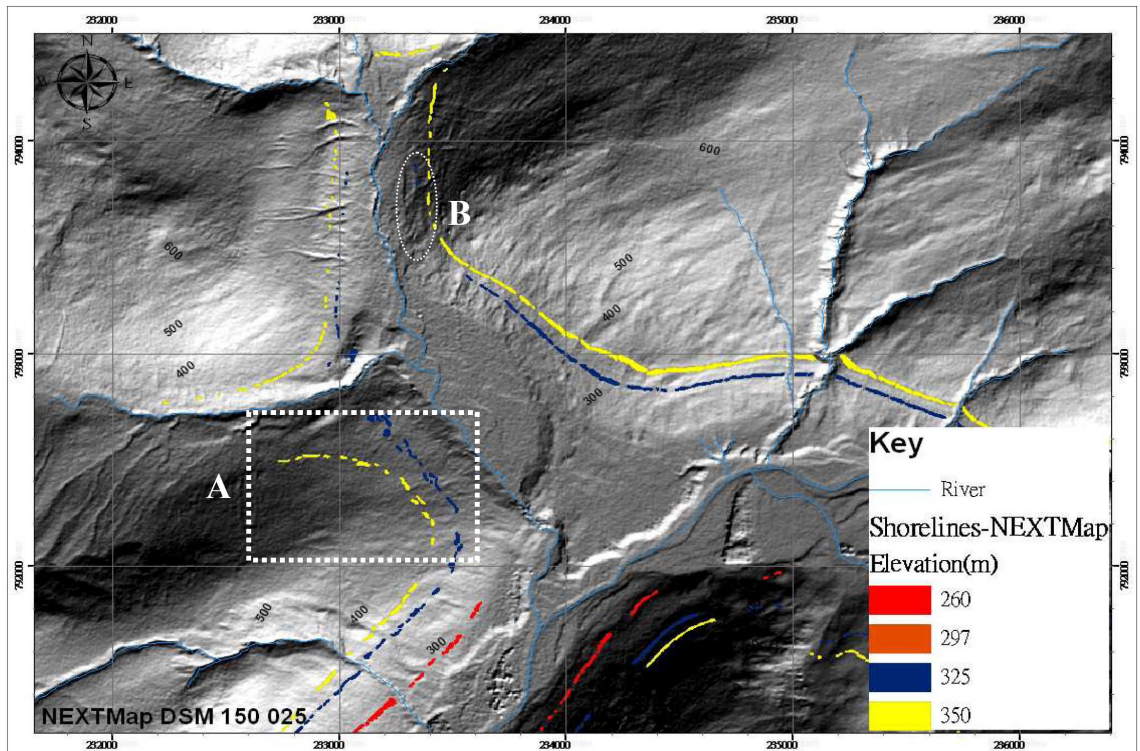


Figure 7.13 Shorelines in the vicinity of the Turret-Roy confluence mapped from NEXTMap plots at a scale of 1:25,000.

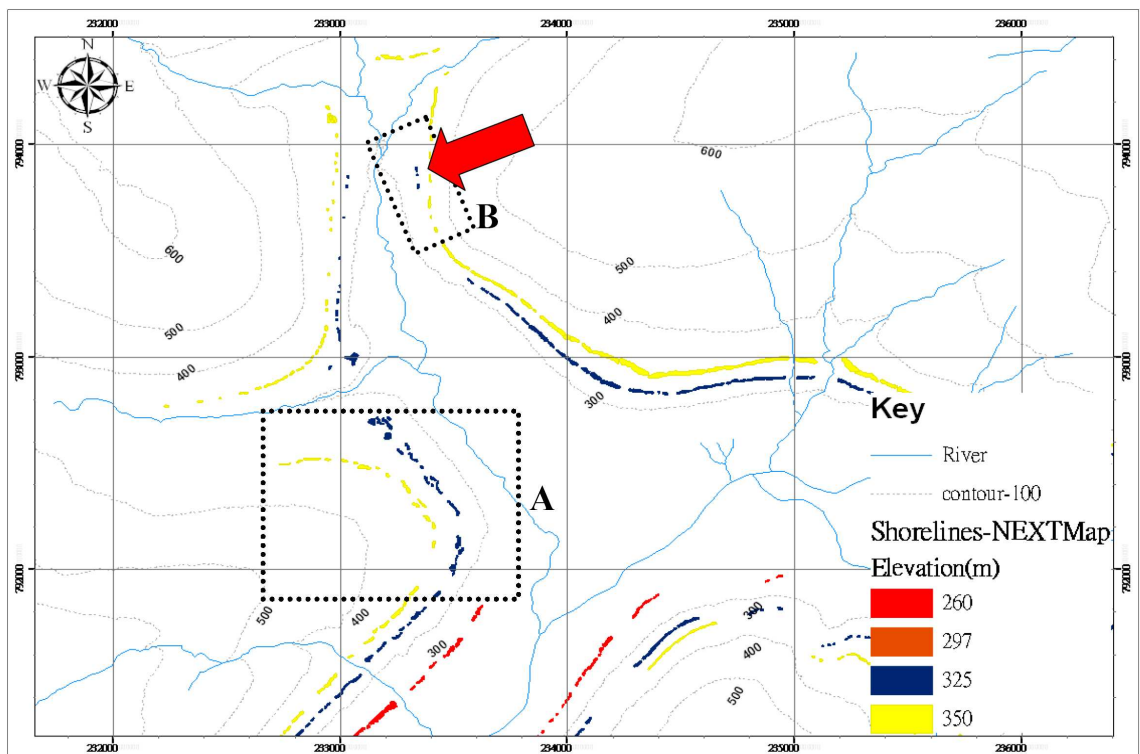


Figure 7.14 Simplified map of the shoreline distributions shown in Figure 7.13. The red arrow points to small patches of 325 m shoreline identified.

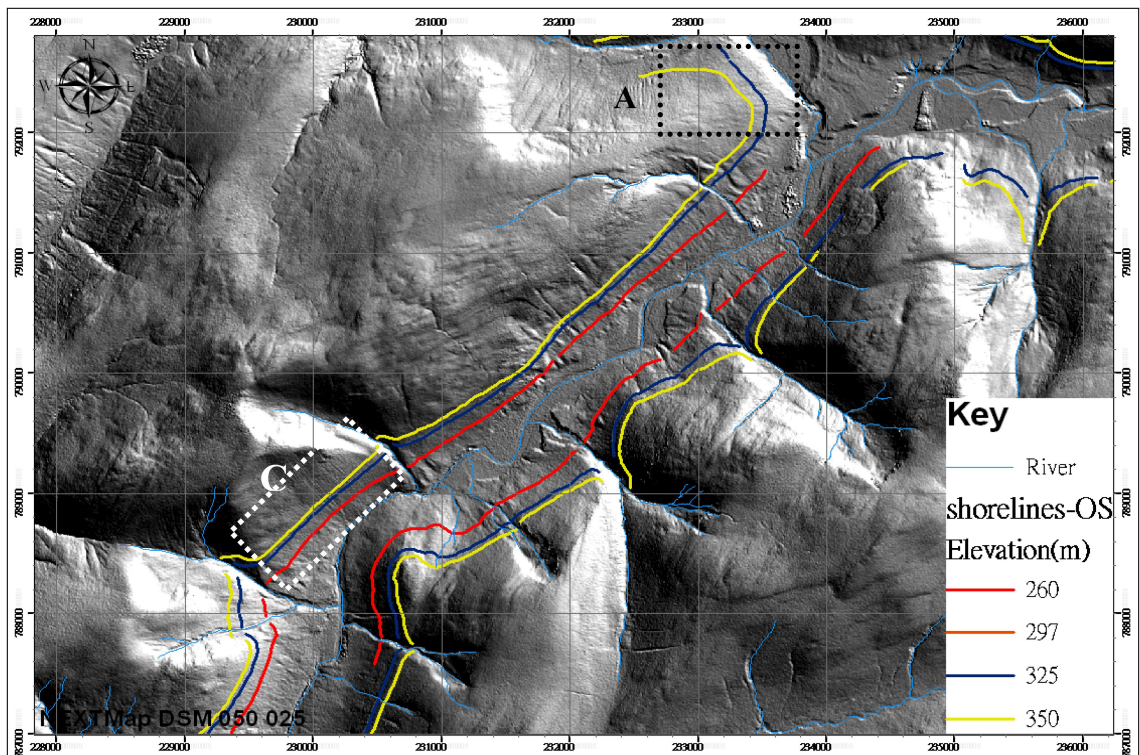


Figure 7.15 Shorelines in the middle reach of Glen Roy digitised from 1:25,000 O.S. maps.

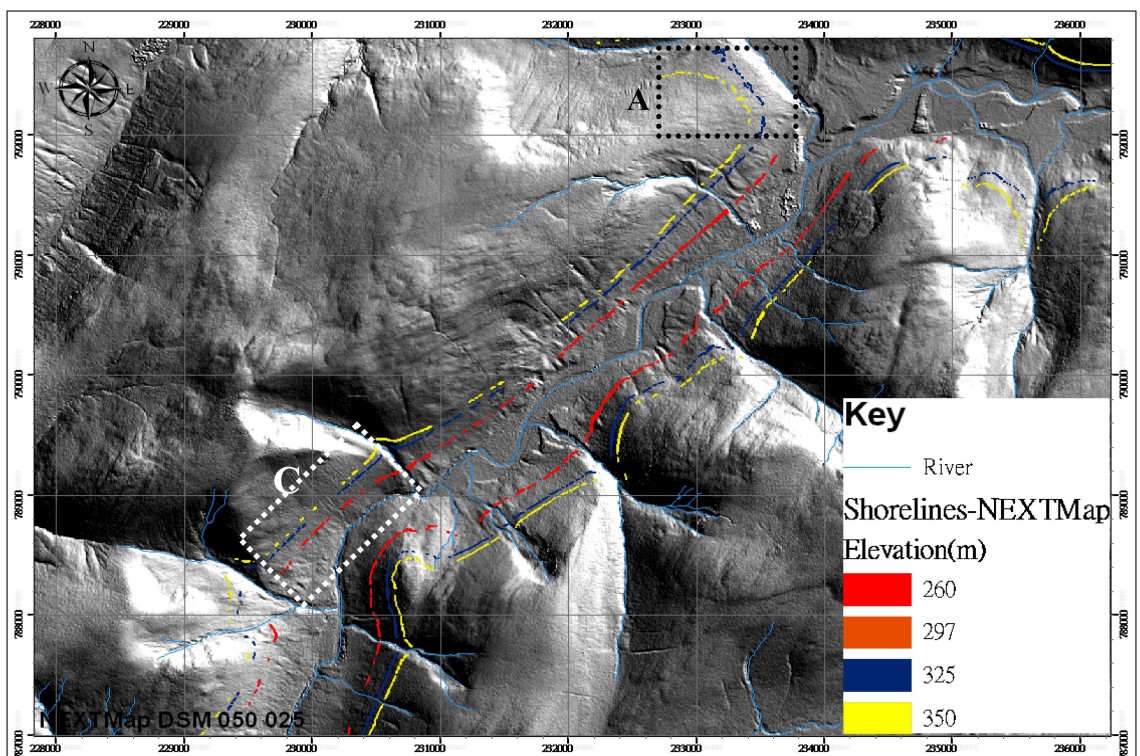


Figure 7.16 Shorelines in the middle reach of Glen Roy mapped using NEXTMap DEM plots.

A further example of the degree of discrepancy between mapped distributions of shoreline fragments based on NEXTMap plots and those based on field surveys relates to the northern extremity of Glen Roy, near the confluence with the Allt Chonnal, which



drains the Carn Dearg plateau (Figure 7.17). Benn and Evans (2008) suggested that irregular, small moraines on this plateau surface and more prominent moraines and fans in the lower reaches of the Allt Chonnal could be the product of a cold-based ice cap. They also suggested that this plateau ice fed a glacier that descended the Allt Chonnal on to the floor of the Roy, where prominent terminal features have been mapped (within area D in Figure 7.17). Sissons did not investigate this area, but the O.S. maps show the 350 m shoreline cutting into these terminal features on their southern sides (Figure 7.17). This evidence would suggest that these terminal deposits pre-date the formation of the 350 m lake. This interpretation is not supported, however, by more recent mapping or by NEXTMap DEM plots.

Eaves (2009) has re-mapped the Carn Dearg plateau and came to similar conclusions to those of Benn and Evans (2008), though he has supplied fuller details on the distribution and form of the glacial landforms in the area. He supports the interpretation of the deposits enclosed by area D, Figure 7.17, as marking the terminus of an outlet glacier descending the Allt Chonnal, but finds no evidence for the 325 m shoreline associated with these landforms. The NEXTMap DEM plots support the views of Eaves, as no shoreline features could be detected in this vicinity (Figure 7.18). This places a different possible interpretation on the age of the glacier terminus: either it occupied the area during the time the 350 m lake existed, or it post-dates the 350 m lake. Either interpretation would imply that the glacier reached its terminus during the Loch Lomond Stadial. This demonstrates the importance of establishing the true distribution of the shorelines, and their association with other landforms, as they can provide key information on the age of associated features. An alternative possibility, however, is that the shorelines, which tend to be best developed on bedrock, were poorly developed or have not survived on the unconsolidated material of which the Allt Chonnal terminal landforms are composed. This interpretation is not favoured, however, because Figure

7.18 shows that the 350 m shoreline is present both to the NE and SW of the Allt Chonnal mouth, and is only missing from the area where the terminal landforms have been mapped. For this reason, the preferred interpretation is that of Benn and Evans (2008) and Eaves (2009), that a glacier occupied the Allt Chonnal valley during the Loch Lomond Stadial.

In conclusion, identification of the shorelines using NEXTMap DEM data generates distributions for the three Parallel Roads that are, in overall pattern, reasonably compatible with results based on instrumental surveys. Discrepancies between the NEXTMap results and those of the O.S. survey were checked in the field, and in all cases the former proved the more reliable and to provide more realistic detail of the variation in form of the Roads and of their 'patchy' nature. Discrepancies between NEXTMap results and the published data of Sissons (1978) are more minor, but the NEXTMap distributions again show more variation and detail; in some instances this may be false detail, where a combination of steep relief and angle of light incidence obscures features that can be more readily assessed by field examination. In most cases checked in the field, however, the level of detail represented in the NEXTMap DEM plots was found to be real. It is concluded, therefore, that the distribution maps of the Parallel Roads based on NEXTMap DEM data are currently the most detailed and reliable representations of the distribution and continuity of the Parallel Roads.

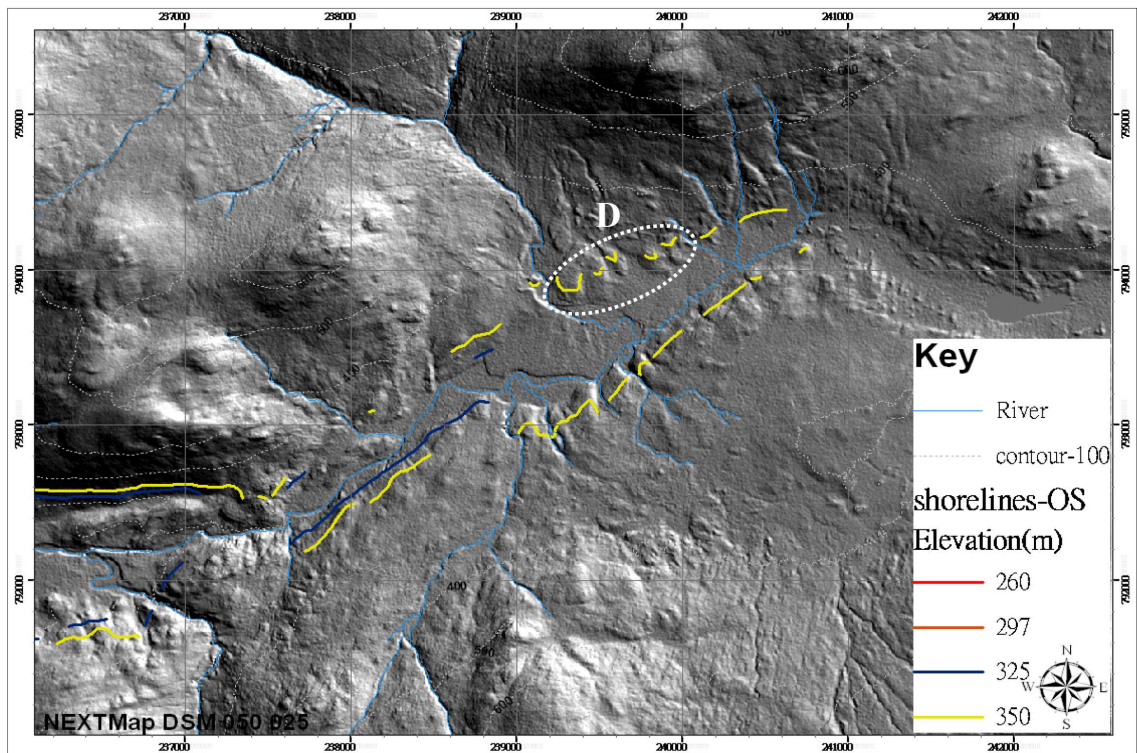


Figure 7.17 Shorelines in the vicinity of the Allt Chonnal-Roy confluence digitised from 1:25,000 O.S. maps.

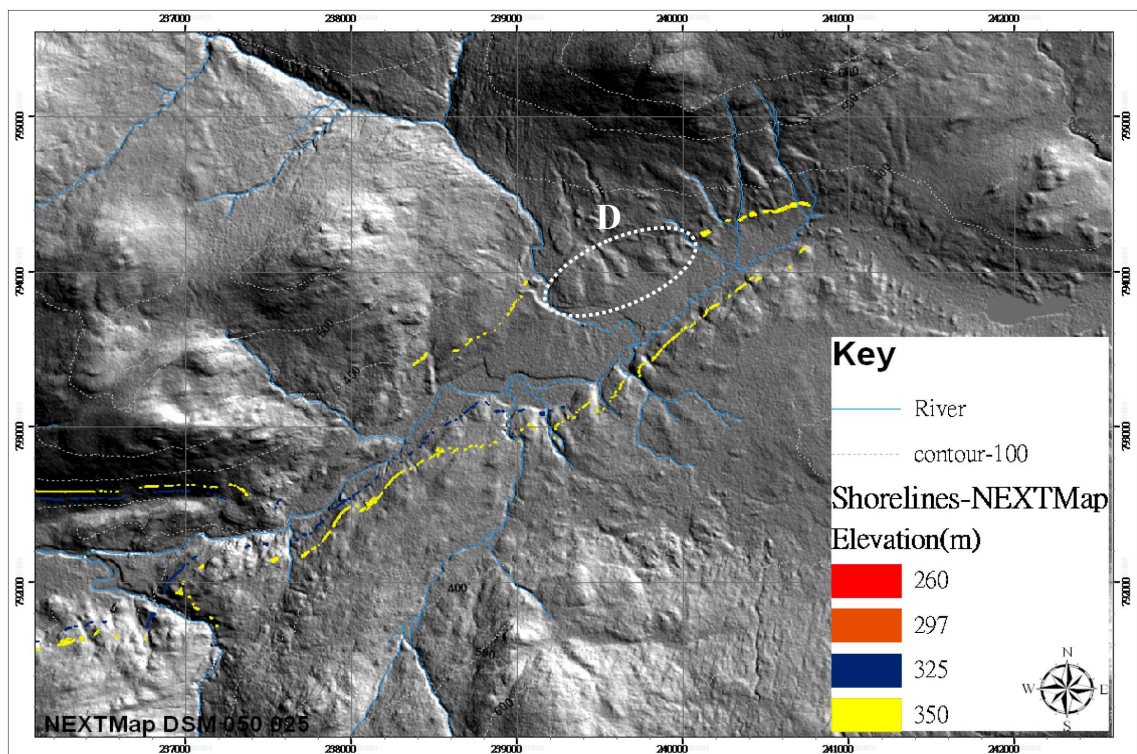


Figure 7.18 Shorelines in the vicinity of the Allt Chonnal-Roy confluence based on NEXTMap DEM plots.

#### **7.4 Variations in platform width, aspect and slope**

Sissons (1978) measured the widths of the shorelines from the foot of the wave-cut 'bluff' or cliff to the outer edge of the Road platform at a total of 787 locations (Table 7.1). The measurements were of horizontal widths, not the length of the inclined platform slope. He observed that the Roads and backing cliffs tend to be best developed on slopes facing towards the SW – towards the direction of the present-day dominant wind direction. Assuming this was also the dominant wind direction at the time the ice-dammed lakes existed, this suggests that the process of shoreline formation was wind-assisted. He also found that they were influenced by inflowing streams, which appear to have delivered fluvial deposits to the lake edge; his observations showed that this influence could extend a long way along the shorelines, presumably as a result of wind-drift. Finally, and perhaps surprisingly, he found that the shorelines were wider where they occurred within the maximum limits of the Loch Lomond Readvance than they are outside those limits. Clearly the shoreline widths are influenced by a number of factors, which Sissons (1978) was able to note in the field and subsequently analyse in detail. He also measured the angle of platform surface inclination from backing cliff to outer edge (platform slope), and noted a number of factors that influenced this property also.

It is not possible to distinguish stream influence from NEXTMap data directly, as it is usually extremely difficult to make a distinction between uncovered rock platforms and debris-covered platforms from examination of the DEM plots. Data generated in this thesis therefore focus on the overall variation in platform widths and slope, and are compared directly with Sissons' total data-set and averages for the total set of measurements he obtained for each platform. To make the comparisons valid, the new data will be compared with Sissons' results for outside the Loch Lomond Readvance limits only (i.e. measurements obtained beyond the Viewpoint, which is the area

examined in the present study). In this study, a total of 5203 measurements were obtained for both platform horizontal widths and slope gradient by random selection, for comparison with Sissons' (1978) data. 1111 measurements were obtained from the 260 m, 1931 from the 325 m and 2054 from the 350 m shorelines in Glen Roy, and 107 from the 297 m shoreline in Caol Lairig; Table 7.2)(data also provided in the CD, Appendix 3.1). No measurements were obtained from Glen Gloy.

**Table 7.1 Summary of measurements made by Sissons (1978) on the horizontal widths of the Parallel Roads of Glen Roy outside the Loch Lomond Readvance ice limits**

	260m	325m	350m	Gloy	All
No. of measurements	90	182	158	49	479
Average width (m)	12.4	9.9	9.8	8.6	10.2
Standard deviation (1 $\delta$ )	7	5.4	6.2	4	6
Greatest width (m)	63.6	31.2	55.3	23.8	63.6
Smallest width (m)	3.4	2	1.6	2.6	1.6

**Table 7.2 Summary of measurements of the horizontal widths of the Parallel Roads made in this research using NEXTMap DEM plots.**

	260m	325m	350m	297m	All
No. of measurements	1111	1931	2054	107	5203
Average width (m)	10.51	10.35	9.76	9.04	10.12
Standard deviation (1 $\delta$ )	3.86	3.81	3.43	1.99	3.66
Greatest width (m)	26.24	26.98	28.03	14.38	28.03
Smallest width (m)	4.61	4.39	3.47	4.76	3.47

Before comparing results, it is important to point out anomalous values in the Sissons (1978) data. In two places, Sissons recorded unusually wide platform widths, circled green on Figure 7.10. Point 1 is considered by Sissons to be a kame terrace that is associated with the 350 m shoreline, measuring 55.3 m in width. Sissons noted that this was responsible for increasing the standard deviation calculated for his 350 m shoreline width measurements. There also appear to have been some extreme values encountered in association with the 260 m shoreline, the maximum width value of which Sissons measured to 63.6 m (Table 7.1). Sissons explained these as measurements taken from

outwash fans and kames terraces that coincided with shoreline altitudes, and are probably mostly encountered in the lower Roy (south of the Viewpoint), though at least one anomalous value for the 260 m shoreline is marked on Figure 7.10 at point 2. No extreme values of this nature were obtained from the NEXTMap data, and indeed field examination failed to uncover the kame terrace referred to by Sissons. In any case, it appears that these extreme values relate to special depositional circumstances, and are not representative of the platforms.

Since the original data generated by Sissons were not supplied in the 1978 paper and are now no longer available, direct comparisons between the Sissons and NEXTMap data (Tables 7.1 and 7.2) are not straightforward. Nevertheless, the following observations can be made. There is a reasonably close correspondence in the measurements for the widths of the 325 m shoreline, with a mean of  $9.9 \pm 5.4$  m obtained by Sissons, compared with  $10.35 \pm 3.81$  m from the NEXTMap study. There is much closer correspondence in calculated mean widths for the 350 m shoreline ( $9.8 \pm 6.2$  m Sissons, cf.  $9.76 \pm 3.43$  m NEXTMap), despite the extreme value influencing the Sissons data. The biggest difference between the two data-sets concerns the measurements for the 260 m shoreline:  $12.4 \pm 7.0$  m (Sissons) cf.  $10.51 \pm 3.86$  m (NEXTMap). Although the standard deviation ranges ( $1\sigma$ ) overlap considerably, the difference in mean values is marked, and suggests a systematic difference between the two sets of measurements. It may reflect the much greater number of measurements made using the NEXTMap software – almost 8 times the number of measurements generated by Sissons’ study for the whole of the Roy-Gloy-Spean system. With such a large number, the locations of which were generated randomly, extreme values in unusual locations are less likely to skew the overall results. The benefit of a much larger number of measurements may also be reflected in comparisons of the standard deviation values obtained in the two studies. Sissons’ calculated SD values for the Roy platform width measurements of 7.0,

5.4 and 6.2 (m) for the 260, 325 and 350 m shorelines respectively, compare with 3.86, 3.81 and 3.43 (m) for the NEXTMap results respectively. The tighter SD values obtained from the NEXTMap data suggests that extreme values have less influence on the overall averages: it appears that the 5m horizontal resolution limitation of NEXTMap data has not seriously distorted these results.

An interesting outcome of the NEXTMap results is that the highest mean value is obtained for the 260 m shoreline, the next highest for the 325 m shoreline and the lowest for the 350 m shoreline. This is commensurate with the relative length of time each lake is thought to have been in existence – the 260 m lake for longest, and the 350 m lake for the shortest amount of time (Palmer *et al.*, 2010). The 297 m lake in Caol Lairig probably existed for an even shorter time than the 350 m Roy lake (Tye, 2007), and hence the mean value obtained for this shoreline is in line with the Roy data. However, the differences between the four mean widths are remarkably small, which supports Sissons' (1978) conclusion that the Parallel Roads were formed quickly, attained a near-uniform average width, and thereafter developed much more slowly.

Sissons also analysed the influence of shoreline aspect on platform widths, the aspect being the compass direction that the backing-cliff faces towards. For example, a line projecting at right-angles from the backing cliff towards the outside edge of a platform that points towards the NE is classified as having a NE aspect. His results are summarised in Table 7.3. A similar exercise was conducted in the current project, but two things limit direct comparisons between the two data-sets. First, measurements of the 297 m shoreline from Caol Lairig were included in the current work (Table 7.4) and not the 255 m shoreline in Glen Gloy included by Sissons. This by itself would not be a major problem, since these data form a very minor proportion of the totals in each study. The second is a more insurmountable problem: Sissons provided summary data for the

total of 713 measurements he made in his overall study, combining the results obtained from locations outside and inside the Loch Lomond Readvance ice limits. Since the primary data are not supplied, and are no longer accessible, is it not possible to discriminate the measurements for shoreline remnants lying outside the ice limits. Furthermore, Sissons does not supply standard deviation values for these calculations. Care needs to be exercised, therefore, when making comparisons between the two data-sets.

Nevertheless, in both studies the widest average platform measurements, 15.3 m in the Sissons data compared with 12.45 m in the current study, are found on SW-facing slopes (Tables 7.3 and 7.4). The rank order of average platform width measurements show two marked differences: (1) south-facing shorelines are ranked second in the Sissons data, but 6<sup>th</sup> in the current study. (2) NE-facing shorelines 3<sup>rd</sup> equal in the Sissons study, but 8<sup>th</sup> in the current study. The differences may in part reflect the influence of measurements obtained by Sissons from Glen Spean, which generally runs W-E, with little variation in hillslope aspect. Similarly, Glen Roy runs predominantly either N-S or SW-NE, and hence there is not an equal opportunity for shoreline development in each sector. This is reflected by the very low numbers of measurements obtained by Sissons for the NE, N and SW sectors; these sectors are better represented in the current study.



**Table 7.3 Width of the Glen Roy and Gloy shorelines related to aspect as reported by Sissons (1978).**

**Column 3 gives average platforms widths and run order (R.O.)**

<b>Aspect</b>	<b>Frequency</b>	<b>AVE_WIDTH &amp; R.O.</b>
<b>N</b>	36	9.5 (6)
<b>NE</b>	9	11.2 (3=)
<b>E</b>	60	8.8 (7)
<b>SE</b>	188	8.7 (8)
<b>S</b>	133	14.1 (2)
<b>SW</b>	52	15.3 (1)
<b>W</b>	90	11.2 (3=)
<b>NW</b>	145	9.8 (5)
<b>All</b>	713	11.1

**Table 7.4 Widths of the Glen Roy and Caol Lairig shorelines related to aspect from the results obtained in this thesis. Column 3 – average platform width and rank order; column 4 – standard deviation of width measurements; column 5 – average platform slope from horizontal in degrees; column 6 – standard deviation of angle of slope.**

<b>Aspect</b>	<b>Frequency</b>	<b>AVE-PLAN_WIDTH &amp; R.O.</b>	<b>STD-WIDTH</b>	<b>AVE_SLO-DEG</b>	<b>STD-SLOPE</b>
<b>N</b>	404	9.38 (7)	3.57	9.83	3.6
<b>NE</b>	193	8.58 (8)	2.25	10.15	5.31
<b>E</b>	425	9.68 (5)	4.06	13.67	3.79
<b>SE</b>	953	10.83 (3)	3.31	16.11	6.12
<b>S</b>	706	9.49 (6)	2.8	14.36	6.5
<b>SW</b>	345	12.45 (1)	4.42	11.33	4.22
<b>W</b>	922	10.76 (2)	4.31	11.29	6.51
<b>NW</b>	1255	9.72 (4)	3.01	11.3	5.81
<b>All</b>	5203	10.11	3.58	12.26	5.83

The difference in results obtained for NE-facing platforms is the biggest single difference between the two studies. In theory, if Sissons' explanation is correct, this should show one of the lowest average width measurements, since NE-facing slopes should be protected from a south-westerly air stream. The highest width measurements should be expected on SW-, SE- and NW-facing slopes, since the first faces directly into the wind, and the other two funnel the wind along a SW-NE axis. The NW aspect is ranked in the middle of the series in both studies, but SE is ranked lowest in the Sissons study and second highest in this study. On face value, therefore, the results from the

present study better fit the expected pattern if exposure to wind direction and fetch had a dominant influence on platform development.

Sissons (1978) measured the angle of inclination of platform slopes in Glen Roy, from back-wall to outside edge, and found the 260 m shoreline to have the highest inclination (12.0 degrees) and the 325 m platform to be shallowest in inclination (10.6 degrees) for locations lying outside the Loch Lomond Readvance limits (Table 7.5). His study was based on a total of 479 measurements.

**Table 7.5 Inclination of platform slopes of Parallel Roads lying outside the Loch Lomond Readvance limits measured by Sissons (1978).**

	260m	325m	350m	Gloy	All
No. of measurements	90	182	158	49	479
Average slope(degree)	12	10.6	11.8	10.6	11.3
Standard deviation(degree)	2.9	3.3	3.6	2.3	3.3
Maximum slope(degree)	23.5	19	19.5	21.5	23.5
Minimum slope(degree)	5	3	2	5	2

An attempt was also made in the present study to measure the slope values of platforms lying beyond the Loch Lomond Readvance limits using NEXTMap measurements obtained from 5203 locations (Table 7.6). The results obtained give steeper inclinations for all three shorelines in Glen Roy than calculated by Sissons, with the results for the 325 m shoreline showing the largest difference (10.6 degrees in Sissons study compared with 13.55 m in the current study). Furthermore, the NEXTMap results show the highest variance, with standard deviation values significantly higher than those calculated by Sissons.

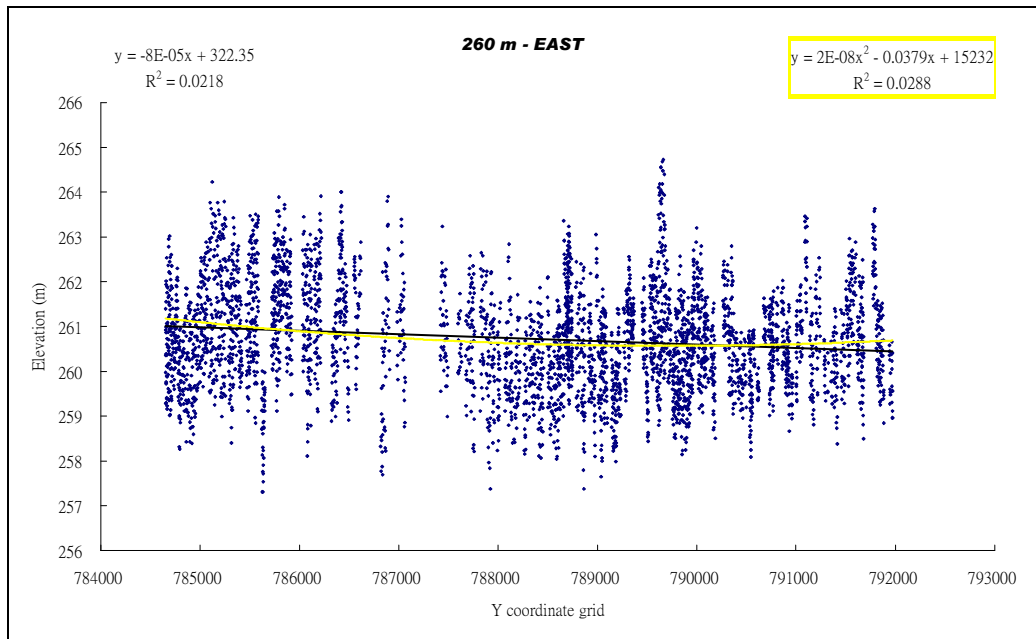
**Table 7.6 Inclination of platform slopes of Parallel Roads lying outside the Loch Lomond Readvance limits measured in current study.**

	260m	325m	350m	297m	All
No. of measurements	1111	1931	2054	107	5203
Average slope(degree)	12.56	13.55	12.24	12.07	12.79
Standard deviation(degree)	4.68	6.33	6.3	3.47	5.98
Maximum slope(degree)	27.94	29.58	29.96	20.08	29.96
Minimum slope(degree)	1.99	0.8	0.74	4.94	0.74

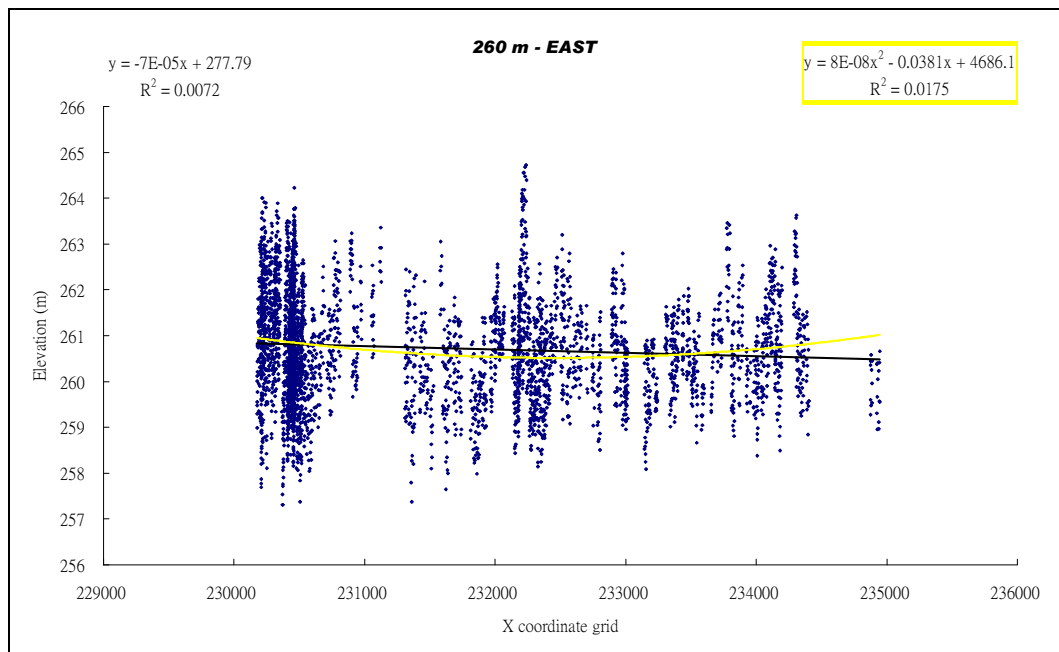
It appears, therefore, that NEXTMap performs least well when assessing parameters that require both spatial and vertical definition, as their computation entails the combination of horizontal (5 m) and vertical (0.5 – 1.0 m) measurement errors. Furthermore, the results are based on a DSM (digital surface model) which has not been corrected for peat, scree or colluvial cover, whereas Sissons was able to take this into account in his calculations. Hence little significance is attached to the NEXTMap-generated platform slope data.

### **7.5 Measurement of longitudinal shoreline gradients**

Nearly 32,000 altitude values have been obtained for mapped stretches of the Parallel Roads of Glen Roy located north of the Viewpoint (section 7.2.3), primarily to test for systematic altitudinal trends in the data. Analysis of the results is far from straightforward, however, due to the discontinuous and complex architecture of the Roads. The problems are exemplified in this section by reference to a sub-set of the data, plotted in Figures 7.19 and 7.20. These figures show all altitude measurements obtained from NEXTMap for the surface of the 260 m shoreline extending along the eastern side of Glen Roy between geographical co-ordinates NN3084 and NN3592. Each datum point is defined in NEXTMap by X and Y co-ordinates which determine geographical location and a Z co-ordinate which measures altitude in m OD.



**Figure 7.19** Altitude data for the 260 m shoreline on the eastern side of Glen Roy plotted orthogonally on to a northing axis extending between NN840000 and NN920000. Regression equations and  $R^2$  values are given for linear (top left) regression analysis (black line) and 2<sup>nd</sup> order polynomial (top right) regression analysis (yellow line) of the data. For further explanation see text.



**Figure 7.20** Altitude data for the 260 m shoreline on the eastern side of Glen Roy plotted orthogonally on to an easting axis extending between NN300000 and NN360000. Regression equations and  $R^2$  values are given for linear (top left) regression analysis (black line) and 2<sup>nd</sup> order polynomial (top right) regression analysis (yellow line) of the data. For further explanation see text.

Figure 7.19 shows the data orthogonally projected on to a S-N (northing) axis, and Figure 7.20 shows the same data projected on to a W-E (easting) axis. The shoreline is not a continuous feature, however, but consists of the 'stretches' labelled A to H in Figure 7.4, which are composed of closely-spaced shoreline fragments that run between major interruptions in shoreline development caused by, for example, wide gullies or landslip scars. Each stretch in turn comprises a number of disjunct fragments or segments (see Figure 7.3) from which random altitude measurements have been obtained. The data obtained from each fragment have typical vertical ranges of 3 to 5 m, which explains the vertical lineation of the data in Figures 7.19 and 7.20: each series of vertically-aligned data were obtained from an individual fragment of the 260 m shoreline (for further explanation see section 7.7). Linear regression of these data suggests a slight declination towards both the north (Figure 7.19) and to the east (Figure 7.20), while 2<sup>nd</sup> order polynomial plots suggest gentle concave curvature of this part of the shoreline. The problem, however, is that the R<sup>2</sup> values are very small, and although significance tables/tests suggest them to be significant, this could be spurious because of the very high numbers of data-points included in the test. A key matter to resolve, therefore, is whether these longitudinal trends are real, given such exceedingly low R<sup>2</sup> values, and in view of the conclusions of Sissons and Cornish (1982b) that differential displacement of crustal blocks in Glen Roy causes segments of the shorelines to be tilted in different directions.

**The main hypothesis to be tested in this component of the research project, therefore, is: that a systematic longitudinal gradient can be detected within altitudinal data obtained from the surfaces of the Parallel Roads of Glen Roy when a sufficiently large number of measurements have been generated.** The thinking behind this assumption is that the shorelines may have been deformed by both regional and local influences. The regional pattern may conform to a gentle flexure of the Roads

imposed by wide-scale isostatic adjustment following loading and unloading by the lakes and glacier ice. Superimposed on this regional pattern may be more abrupt dislocations or deformations caused by localised fault movements, landslips or other impacts, while natural variations in rock platform surface development caused by ice-push, rock structural and other natural factors (e.g. Matthews *et al.*, 1986; Aarseth and Fossen, 2004) may complicate matters further, a point returned to in section 8.2.4. In order to test this idea, the full data-base of altitudinal information generated for Glen Roy will first be analysed at the local or 'stretch' scale, using regression and other statistical comparative methods (sections 7.7 and 7.8). This will be followed by a test for any underlying regional-scale trend using trend-surface analysis (section 7.9). First, however, a test of the degree of accuracy of the NEXTMap altitudinal data was considered necessary, a matter addressed in the next section.

### **7.6 Test of accuracy of NEXTMap altitudinal measurements**

The source information supplied with NEXTMap DEM data suggests that altitudinal measurements derived direct from the images are subject to uncertainties of between 0.5 and 1.0 m, which could potentially limit their use for establishing coherent and accurate trends, such as surface gradients, especially where the number of measurements is low. It was therefore important to test for accuracy and precision and this was conducted using four small experiments. Runways at Heathrow airport, London; near-horizontal surfaces at Loch Laggan, Scotland; and the surface of the Alcan hydroelectric scheme pipes at the northern flanks of Ben Nevis, Scotland; were selected to test how well measurements could replicate either a known horizontal or near-horizontal surface or artificial surfaces with constant inclinations (Figure 7.21). The fourth experiment compared analyses of the same landscape features obtained by both instrumental leveling and NEXTMap measurements.

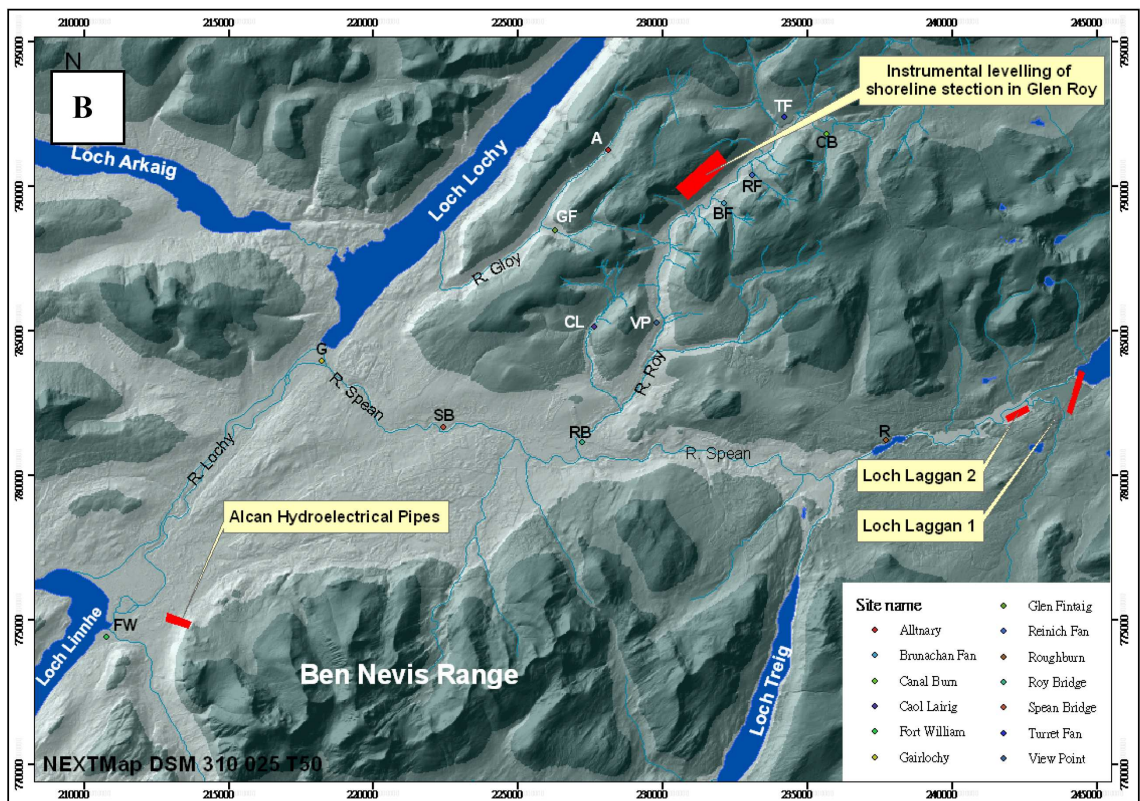
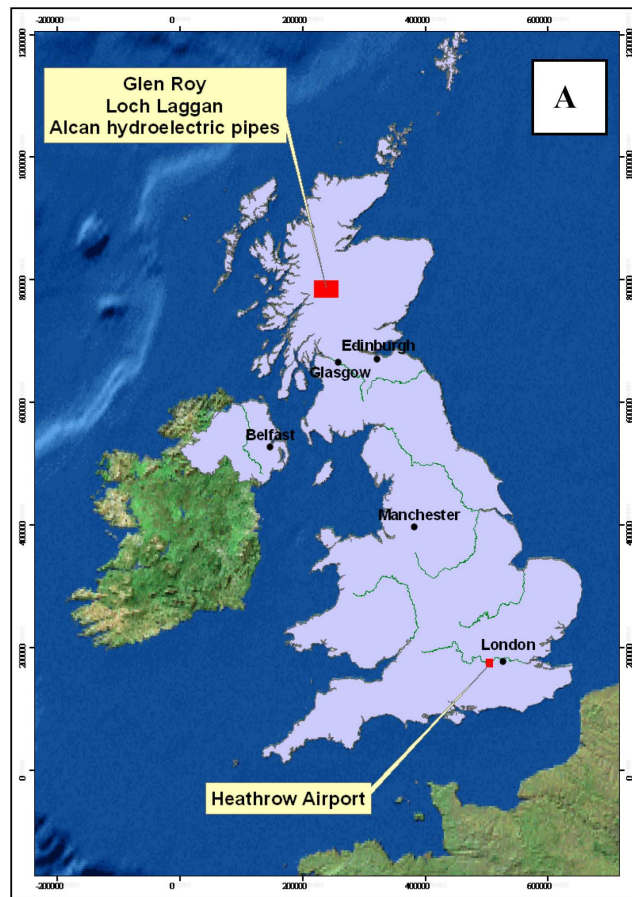


Figure 7.21 Location of sites for test the accuracy of NEXTMap altitudinal measurements. Glen Roy, Loch Laggan and the Alcan hydroelectric scheme pipes are in NW Scotland while Heathrow airport is located on the west side of London (A). The detailed locations of test sites in Scotland are represented in (B).

### 7.6.1 Testing for horizontality: runways at Heathrow airport

Two of the runways at Heathrow were selected for this test, runways 27R and 27L, as depicted on NEXTMap DEM plots (Figure 7.22). Presumed to be horizontal within a decimeter scale, these two runways lie at altitudes of c. 23.77 and 23.47 m OD, respectively, and both extend over c. 3 km in length. Altogether 4998 altitudinal measurements were obtained from NEXTMap data for these two surfaces, 2360 from runway 27R, and 2638 measurements from 27L (Figure 7.23)( the data are also provided in the CD, Appendix 3.2). The results, shown in Figures 7.24 and 7.25, show perfectly horizontal stretches, separated by small ramps (consistent slopes). Runway 27R appears to rise c. 80 cm over a distance of 350 m (co-ordinates 507750 to 505100), while a second slope of about 20 cm is discernible at around co-ordinate 506500 (Figure 7.24). Runway 27L shows a two-step slope of a 30 cm total vertical interval over a distance of c. 200 m (Figure 7.25A). The data pick out a scatter of points below the horizontal runway surface (red box in Figure 7.25A) that are thought to represent damage effects, which can be observed along the runway edge (Figure 7.25B and C).

The data suggest remarkable internal coherency, as the horizontal and ramped surfaces show little scatter in data, and those data that are scattered can be linked to damage effects. This suggests that the error term quoted with NEXTMap DEM data is not a constant that should be applied to individual height measurements, but is the error of relating the data as a whole to some geodetic reference datum. In other words, all of the data collected for a single flight or tile seem to be internally consistent and precise with respect to relative height differences, but the data-set as a whole has a 0.5 to 1.0 m error with respect to absolute height.



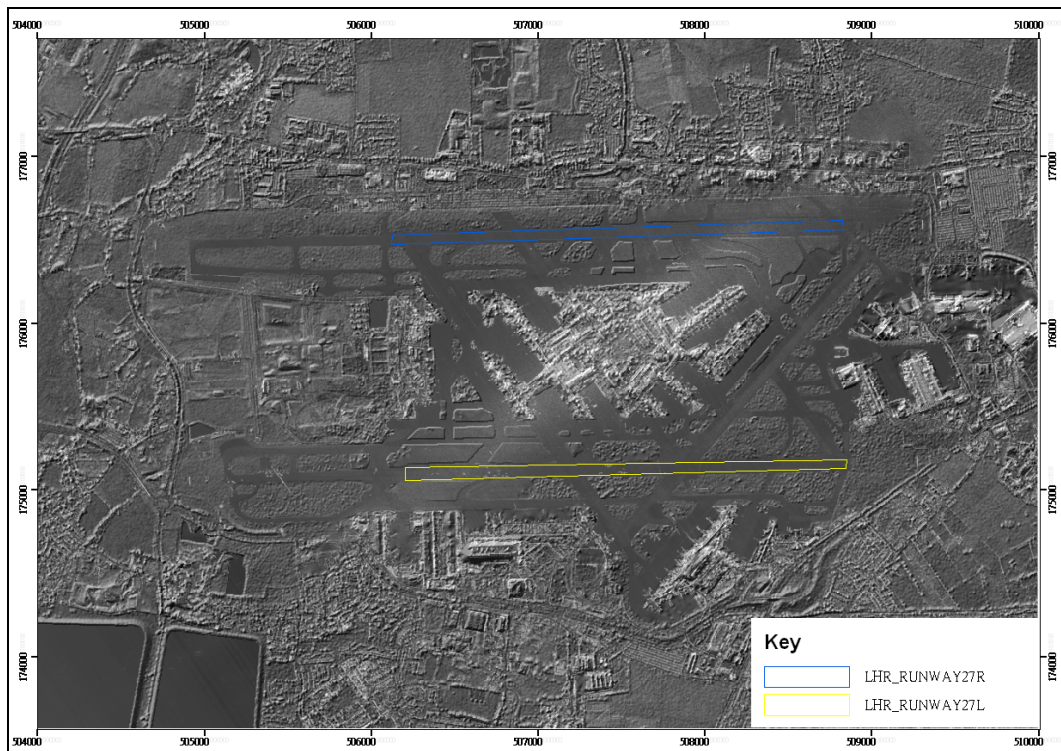


Figure 7.22 NEXTMap DEM plots of runways at Heathrow Airport selected for measurement for a test of NEXTMap depiction of a horizontal surface.

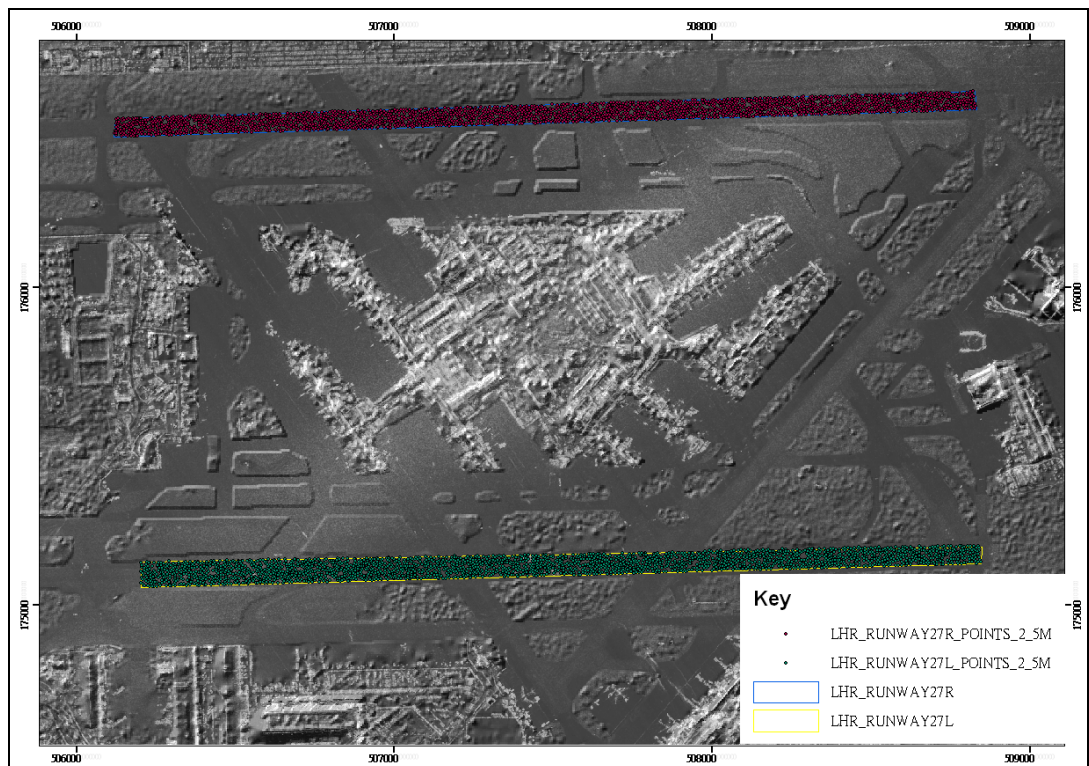
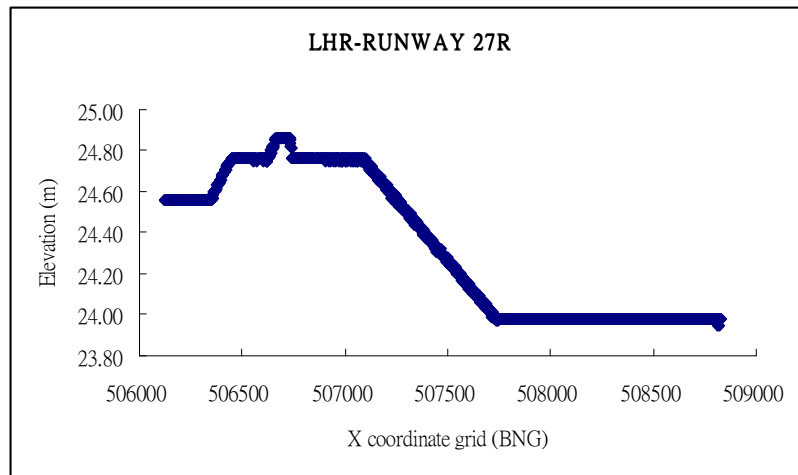
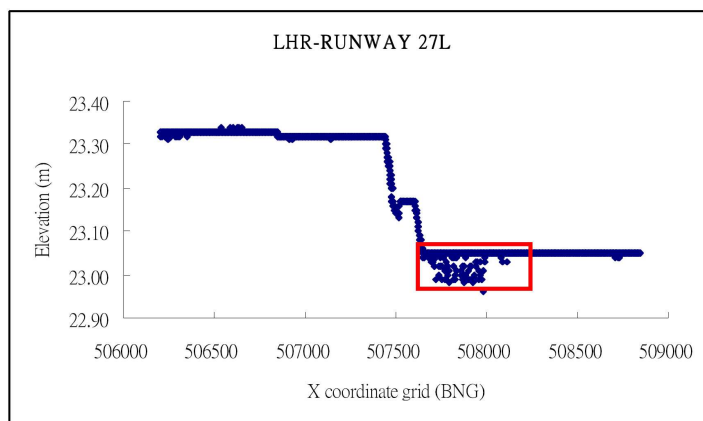


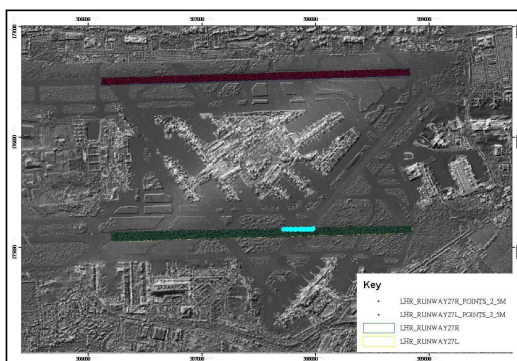
Figure 7.23 Location of points selected for altitudinal measurement on Heathrow runways 27R and 27L.



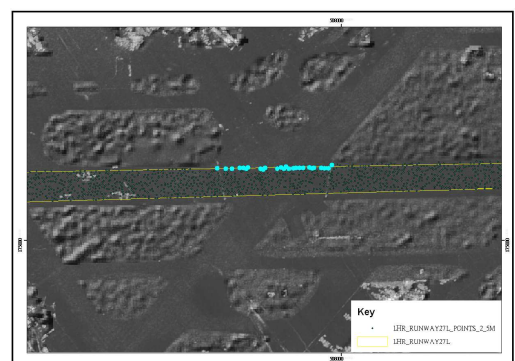
**Figure 7.24** Plot of altitudinal measurement of Heathrow airport runway 27R, derived using 2360 NEXTMap data-points. The X co-ordinate scale represents divisions of 500 m distance.



**A.**



**B.**



**C.**

**Figure 7.25 A:** Plot of altitudinal measurement of Heathrow airport runway 27L, derived using 2638 NEXTMap data-points. The X-co-ordinate scale represents divisions of 500 m distance. The scattered points in the red box are considered to reflect damage associated with a drain close to the runway edge; the location of these points are shown (in turquoise) on figures B and C

### 7.6.2 Testing horizontal and near-horizontal surfaces at Loch Laggan

NEXTMap measurements of altitude variation were obtained from fan surfaces situated close to the western extremity of Loch Laggan as well as from the surface of Loch Laggan itself (Figure 7.26). Two fan surfaces were examined: the Moy Fan, which enters Loch Laggan from the Ossian drainage catchment to the south, and which is considered to have been formed during the Loch Lomond Stadial (Sissons 1967) (Loch Laggan 1, Figure 7.26) and the modern river terrace surface located west of the Moy Fan (Loch Laggan 2), formed by westwards drainage of the rivers Spean and Abhainn Ghuilbinn and exposed during times of low lake stand.

A transect of 3054 altitudinal measurements were obtained from Loch Laggan 1, the results provided in Figure 7.27 (the data are also provided in the CD, Appendix 3.3). These clearly pick out the northward-dipping surface of the Moy Fan, the steeply inclined eroded bluff at the lake edge, and the lake surface. The measurements around the lake edge are complicated by trees, but a consistent gradient is reflected in the measurements obtained from the fan surface. There is a scatter of around 0.82 m ( $1 \sigma$ ) in the altitudinal values obtained from the fan surface over a horizontal distance of 50m, which could reflect measurement inaccuracies. However, the measurements obtained from the surface of Loch Laggan are absolutely horizontal, with no measurable variation. Altogether a total of 345 measurements were obtained from a transect across the loch surface, all of which measured 245 m altitude precisely. These data suggest that the variation of c.1m in the heights obtained from the fan surface are more likely due to real ground variation, caused by small mounds and depressions which form naturally on terrace surfaces. This may be supported by the 2523 altitudinal measurements obtained from Loch Laggan 2 (Figure 7.28) (the data are also provided in the CD, Appendix 3.3), which clearly reflect the westward dipping surface of the terrace, but with a scatter in altitudinal values over a range of up to 2m. This most likely reflects the undulations on

the terrace surface that are discernible in Figure 7.28A.

Both the sets of altitudinal measurements obtained from the runways at Heathrow and from the surface of Loch Laggan indicate that NEXTMap faithfully represents true horizontal or near-horizontal surfaces. The question that now arises is whether the scatter of points obtained from natural inclined surfaces, such as the fan surfaces considered here, is caused by natural surface variations or by increased ortho-rectification errors on inclined surfaces. An attempt to test this is provided in the following section.

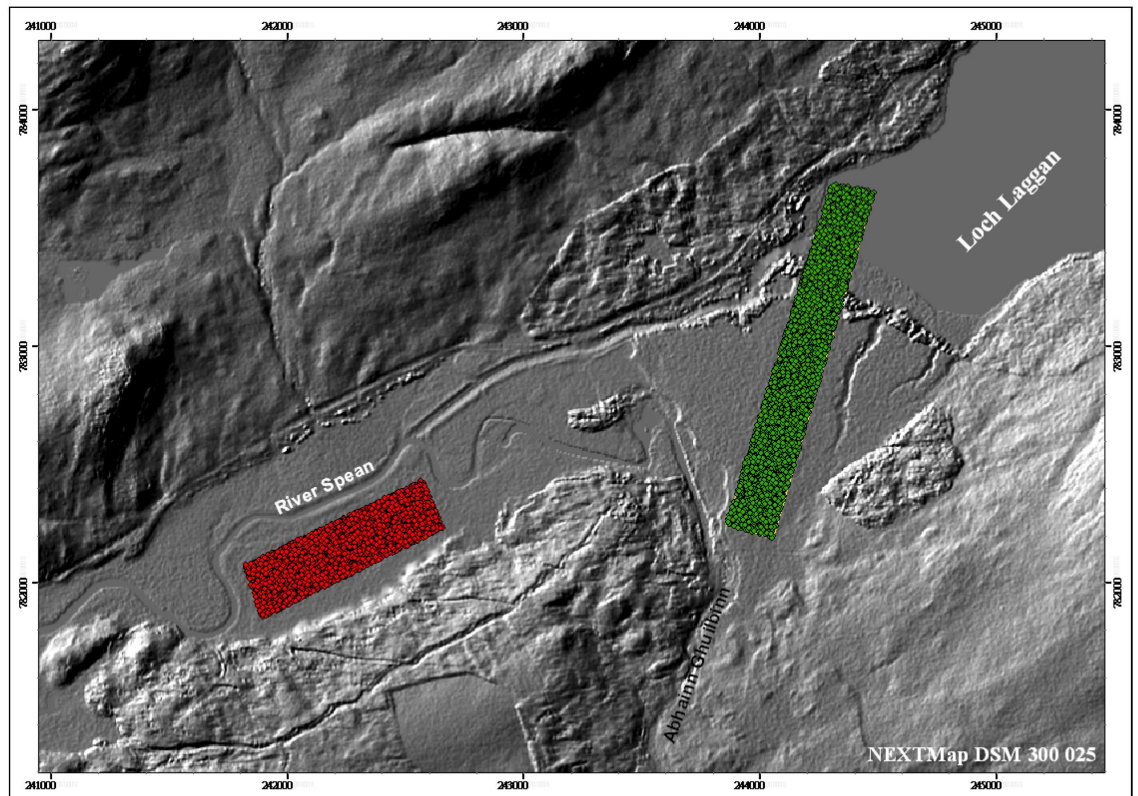
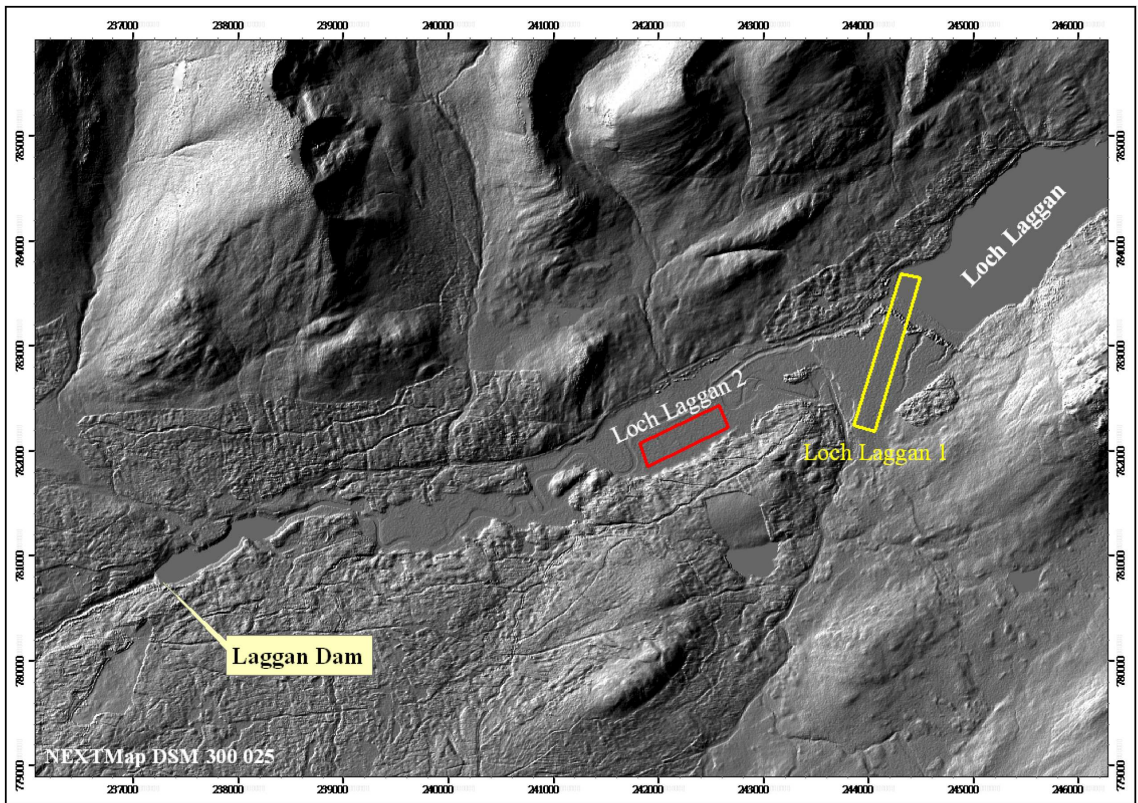
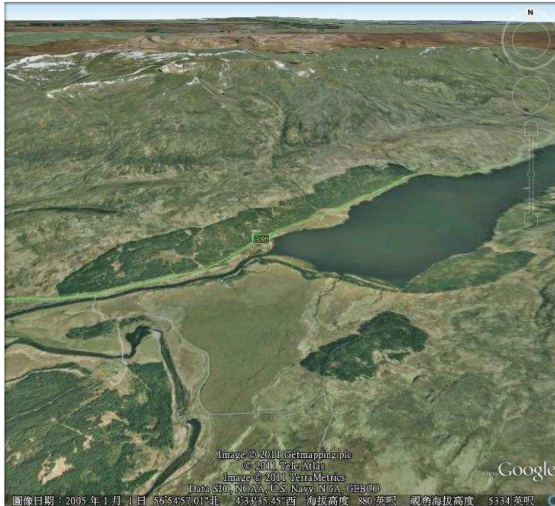


Figure 7.26 Location of transects of altitudinal measurements on terrace features at the western end of Loch Laggan; for further explanation see text. The lower diagram shows the number of 'spot-height' measurements obtained for each transect.

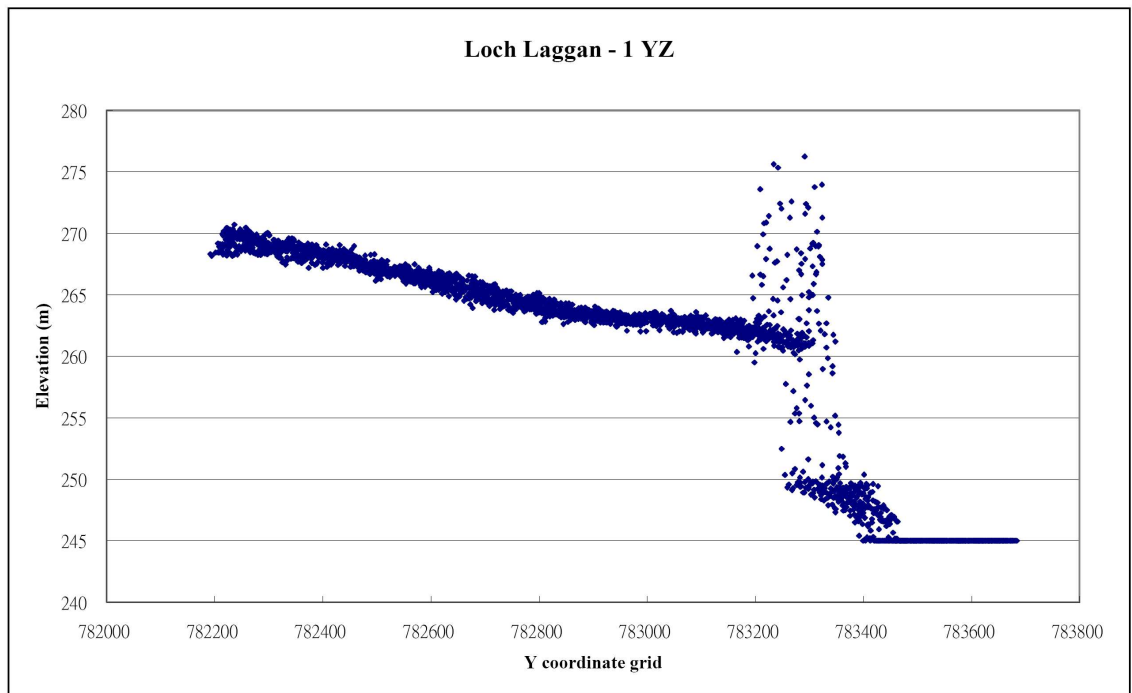
A.



B.

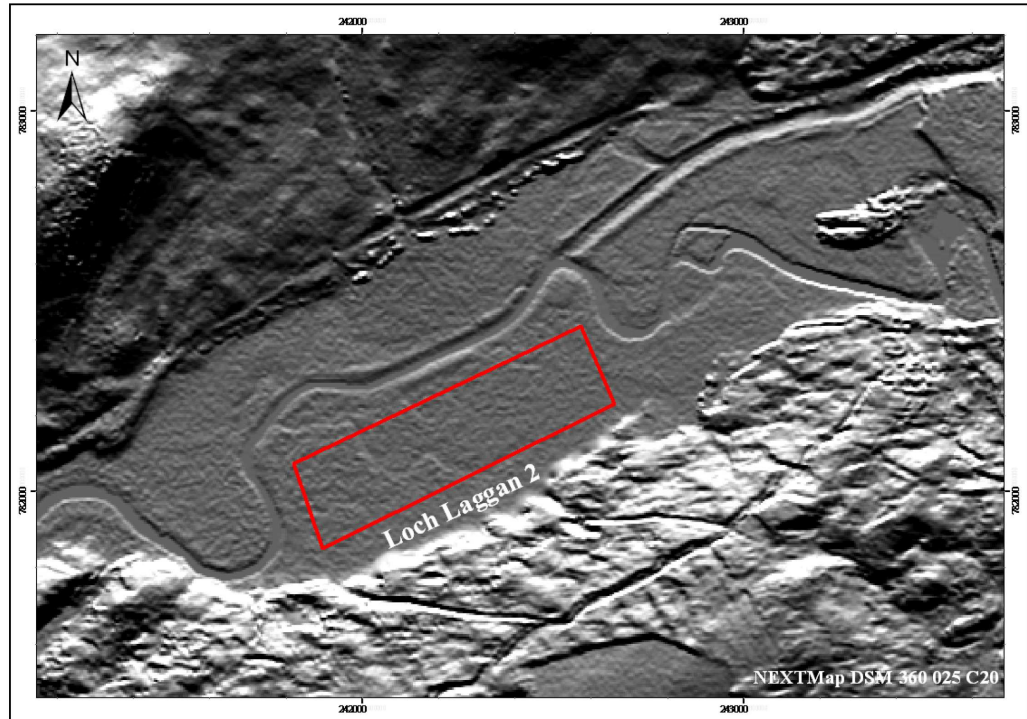


C.



**Figure 7.27 A:** Google-Earth image of the southwestern margin of Loch Laggan, viewed from the south over the Moy Fan. **B:** Google-Earth image of the Moy Fan, viewed from north, showing the outline of the Loch Laggan 1 transect from which altitudinal measurements were obtained. The transect is 1515 m long and 188 m wide. **C:** Plot of altitudes obtained from 3054 measured points along the Loch Laggan 1 transect.

A.



B.

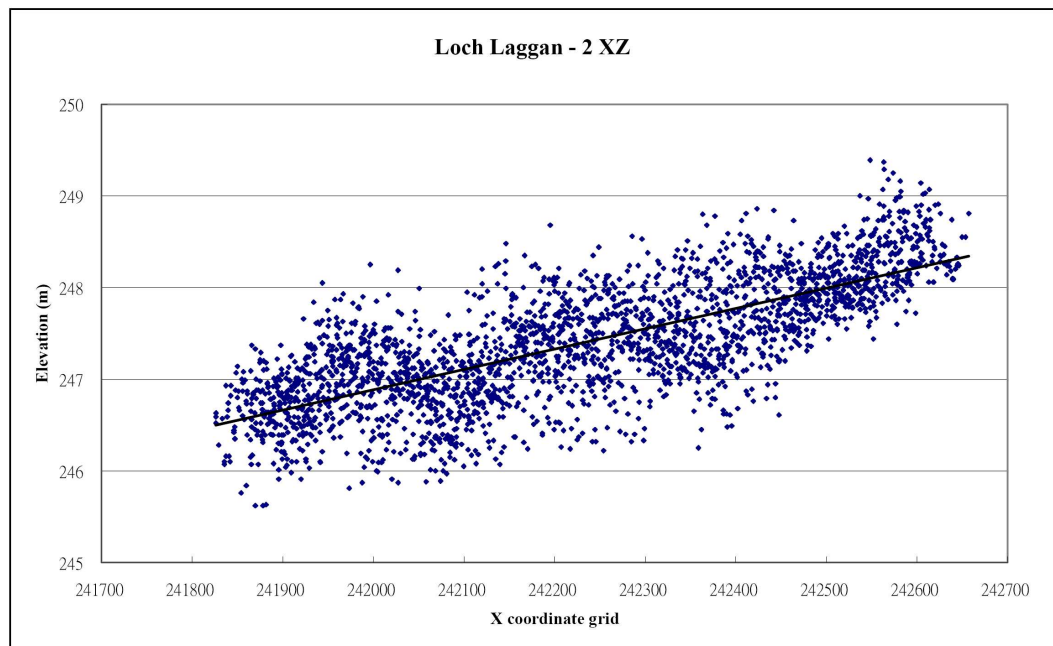


Figure 7.28 A: NEXTMap DEM plot of ground surface of fluvial terraces formed at the western margin of Loch Laggan, immediately down-stream from the Moy Fan (Figure 7.27) and showing the outline of transect Loch Laggan 2. The transect is 855 m long and 207 m wide. B: Plot of altitudes obtained from 2523 measured points along Loch Laggan 2 transect.

### **7.6.3 NEXMap altitude measurements obtained from controlled inclined surface**

The objective in this experiment was to assess the scatter of altitudinal measurements obtained using NEXMap DEM data from an inclined surface, not affected by natural ground surface variation. Since it is difficult to distinguish instrumental errors from small-scale ground surface variations on natural surfaces, an artificial structure was considered to provide more control. For this experiment, the surface of the Alcan hydroelectric scheme pipes which run down the northern flanks of Ben Nevis towards Fort William were selected (Figure 7.29), as they descend over an altitudinal interval of nearly 200 m. A total of 1000 NEXMap altitudinal measurements (yellow dots, Figure 7.29C) (the data are also provided in the CD, Appendix 3.4) were obtained from the surface of one of the pipes, over the full length of 830 m of exposed pipe, which is 4.4 m in diameter. A further 1000 NEXMap altitudinal measurements were obtained from the bare ground surface adjacent to the selected pipe (red dots, Figure 7.29C) (the data are also provided in the CD, Appendix 3.4), to establish whether there was greater measurement variation on a natural, compared with an artificial, inclined surface. The letters X, Y and Z added to each image denote the lowest end of the pipe, a marked change in gradient and the highest end of the pipe respectively, to facilitate comparison between the diagrams.

The results are shown in Figure 7.30. At the broad scale the overall result (Figure 7.30 A and B) show close parallel trends between the pipe and ground surface data, reflecting broad changes in surface gradient. Closer inspection of the measurements obtained between locations X and Y, however, show a more complex picture when viewed at a bigger scale (Figure 7.30C): both sets of data reveal a series of undulations and steps, suggesting that the pipe has been made to accommodate small-scale undulations or steps in the rock surface. The undulations in the ground surface data are larger than those associated with the pipe surface data, suggesting that some ground surface



smoothing was possible in some places. Linear trend lines are shown for the data, but these are rather spurious, because the data actually show very little scatter over short distances, from about 25 to at most 50 cm around mean values. Surprisingly, the scatter is less within the ground surface data than with the pipe surface data. It is thought that this reflects a combination of the curved (cylindrical) surface of the pipe and the fact that it is only 4.4 m in diameter, close to the horizontal resolution limit (5 m) of NEXTMap DEM data. Both sets of data suggest that NEXTMap is able to faithfully record ground surface altitudes on inclined surfaces with an error no greater than 0.5 m and most likely as low as 0.25 m, which is in line with the stated resolution limits in the NEXTMap Handbook V3.3 (2004). This level of precision is underlined by a final set of measurements taken along the surface of a section of the pipeline (Figure 7.31). The hydroelectric station kindly provided information on the original surveys associated with the pipelines, which were tied to the six anchor points shown in Figure 7.31A. Information was supplied on the instrumentally-levelled gradients of the pipelines between the anchor points. The measured gradient of NEXTMap altitudinal measurements obtained from the pipeline surface between anchor points 2 and 4 (Figure 7.31B) is  $18^{\circ}30'$ , which compares with the Alcan instrumentally-measured value of  $17^{\circ}03'50''$  (data provided by **Richard Wallis**, Alcan Aluminium UK Limited.). This result gives added confidence concerning the reliability of NEXTMap altitudinal measurements.

A.



B.



C.

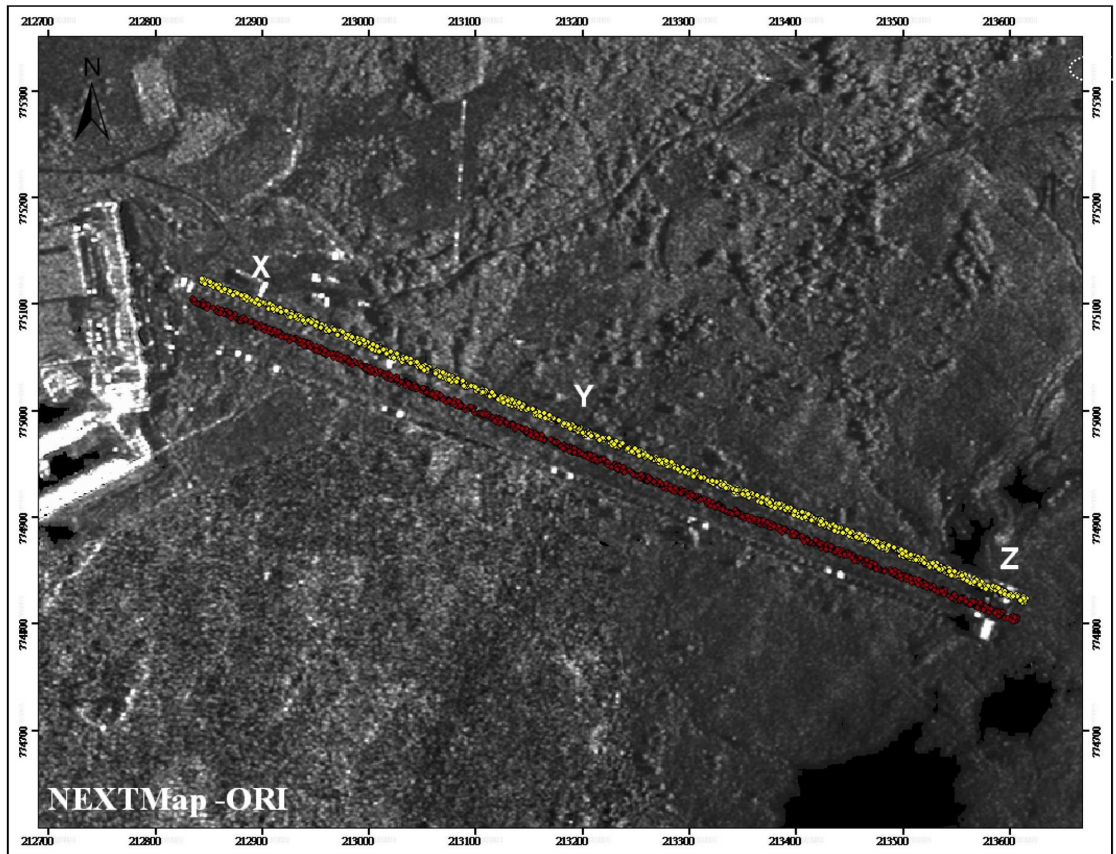
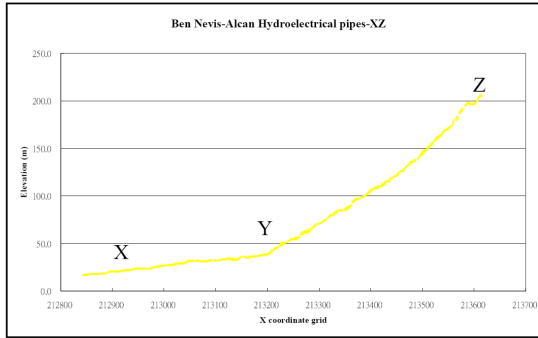
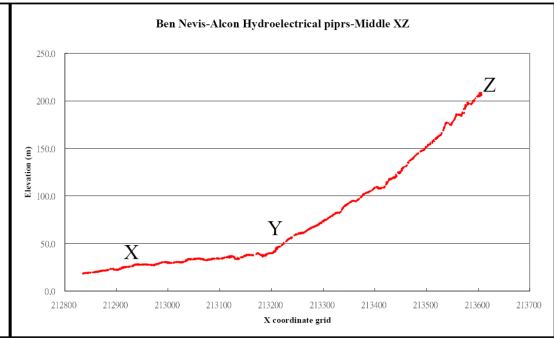


Figure 7.29 A. B. Images of the Alcan hydroelectric pipes on northern flank of Ben Nevis (A. from *Google-Earth*, downloaded May 2011; B. downloaded in May 2011 from <http://www.geograph.org.uk/photo/904685>. C. Scatter plot of measured spot-heights along one of the pipes and on the bare ground surface adjacent to the selected pipe, superimposed on *NEXTMap-ORI* plot. The horizontal distance represented between scale bars is 100 m.

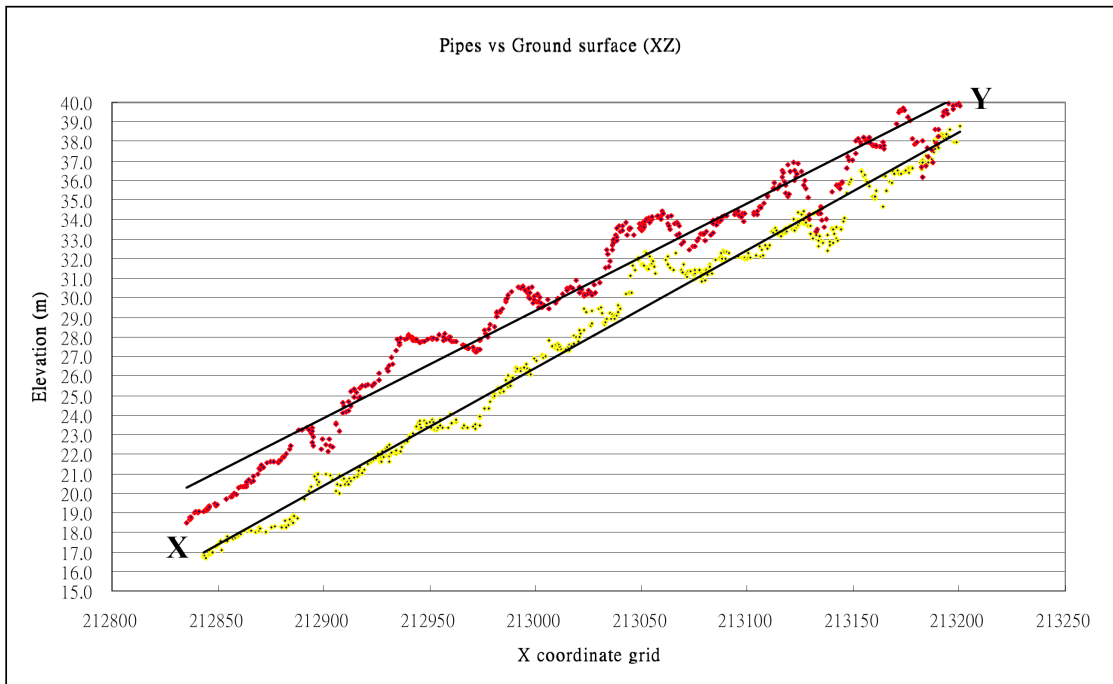
A.



B.

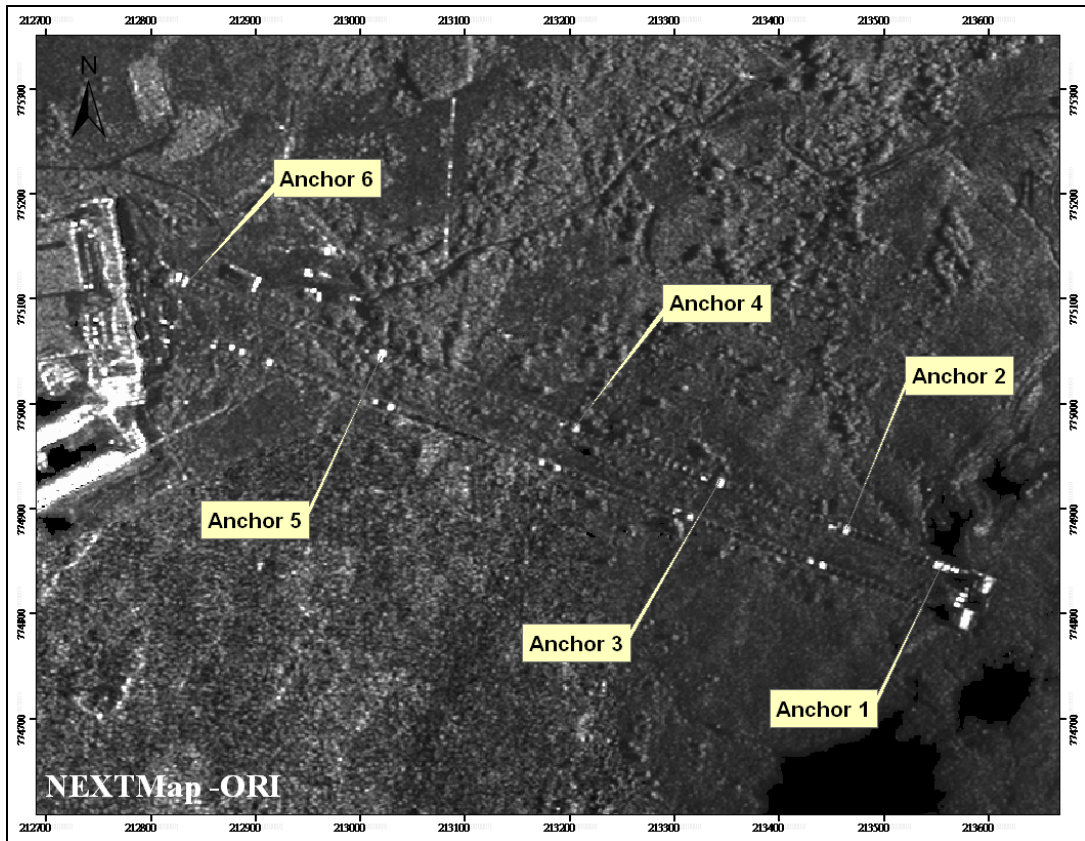


C.

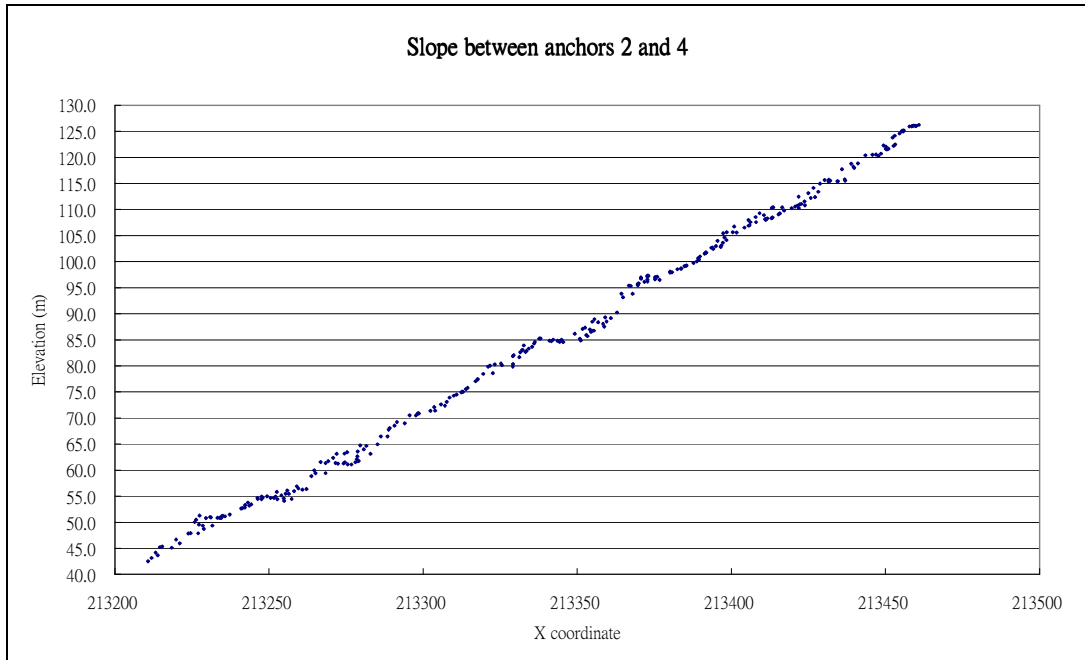


**Figure 7.30** NEXTMap altitudinal measurements obtained from the pipe surface (yellow dots) and adjacent ground surface (red dots) shown in Figure 7.29. Figures A and B show the data over the full measured length of each transect, and C shows the data for the sector between locations X and Z at a larger scale. The vertical scale between horizontal lines is 50 m in Figures A and B 1 m in C, and the horizontal distance between scale bars is 100 m in A and B and 50 m in C.

**A.**



**B.**



**Figure 7.31 A: Position of anchor points on the Alcan pipelines, Fort William; B: NEXTMap altitudinal measurements obtained on pipeline surface between anchor points 2 and 4 (shown in Figure 7.31A).**

#### 7.6.4 Instrumental levelling of shoreline stretches in Glen Roy

The stretches selected for this experiment were J and K of the 260 m shoreline, R and S of the 325 m shoreline, and T and U of the 350 m shoreline (Figure 7.32). All of these stretches lie on the western side of Glen Roy, between approximately NN305895 and NN330914 (between Allt nan Eun and the Allt Dearg, which descends to join the Roy Valley close to Brae Roy Lodge). These stretches were selected because (a) they were accessible from the vehicle road that runs along the western flank of Glen Roy, and (b) they are difficult and discontinuous stretches, and hence present a rigorous test of the capability of the NEXTMap measurements to represent the altitudinal variation along the Parallel Roads.

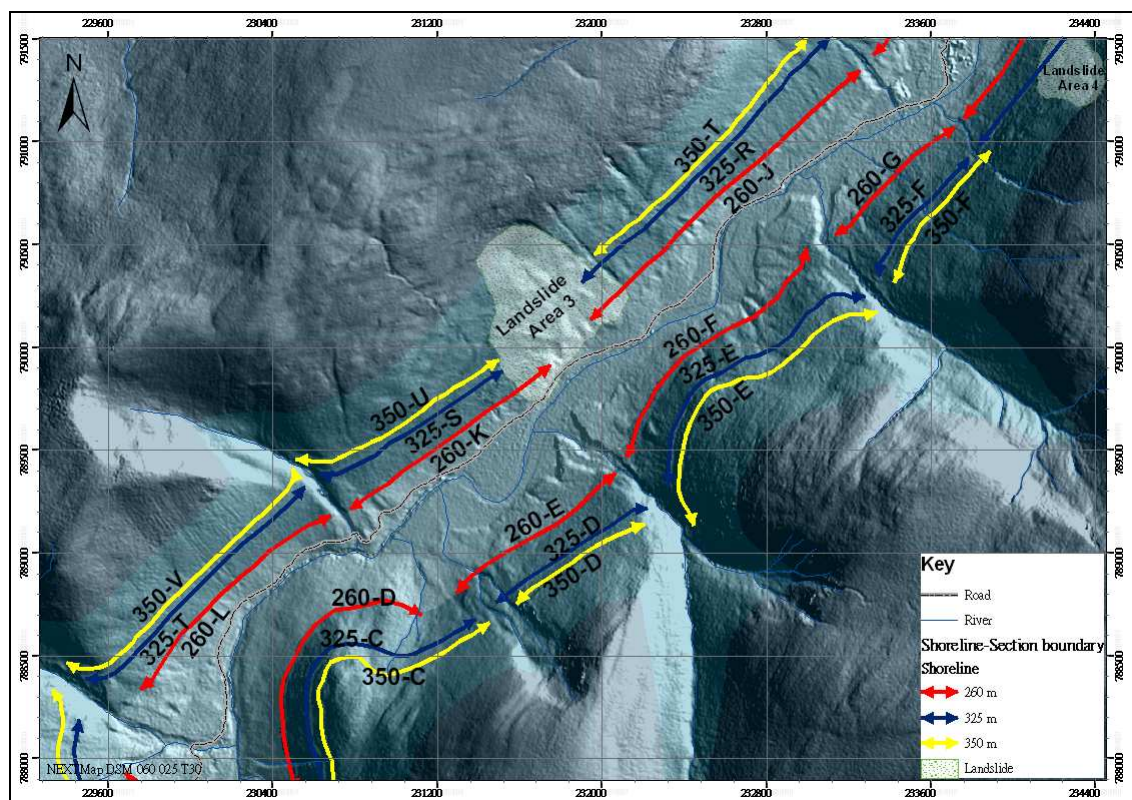


Figure 7.32 Location and ranges of shoreline stretches selected for instrumental levelling in Glen Roy. (260-J, 260-K of the 260 m shoreline, 325-R and 325-S of the 325 m shoreline, and 350-T and 350-U of the 350 m shoreline; also see Figure 7.4, 7.5, 7.6 and 7.21).

The instrumental levelling was conducted fully independently by a team of Royal Holloway Quaternary Science Masters students using a Topcon CTS-3000 Total Station under field instruction and guidance from Dr. Adrian Palmer and Professor John Lowe.

The students were not provided with the NEXTMap data that had been compiled for these stretches by the author until after the Total Station exercise was complete, and their own data compiled. They were then provided with the author's data-sets so that they could draw statistical comparisons between the instrumentally- and NEXTMap-derived data. The results are presented in full in Appendices 4 and 5 (See CD), for two of the individual reports submitted by the MSc students. While the results were obtained collectively by the team of seven students, each student interpreted the results individually, and sometimes with different statistical approaches. Overall, however, there was general consistency in the outcomes of this exercise. In particular, the instrumental data plot very closely to the NEXTMap results (Figure 7.33), and with a few exceptions show the same general horizontal trends (Figure 7.34). An essential difference between the two sets of data, however, were that the students were able to take account of peat accumulation on the shoreline surfaces, though this was usually under 30 cm in thickness.

In summary, the main conclusions drawn from this exercise are as follows. First, the altitudinal scatter in the NEXTMap data for each sector and shoreline is generally much wider than is the case for the instrumental data: the former can exceed 4 m in vertical range, whereas the latter are generally around 2 m at most. Second, the gradients/trend-lines based on the instrumental data tend to be similar in trend direction but sometimes vary in gradient value from the NEXTMap results.

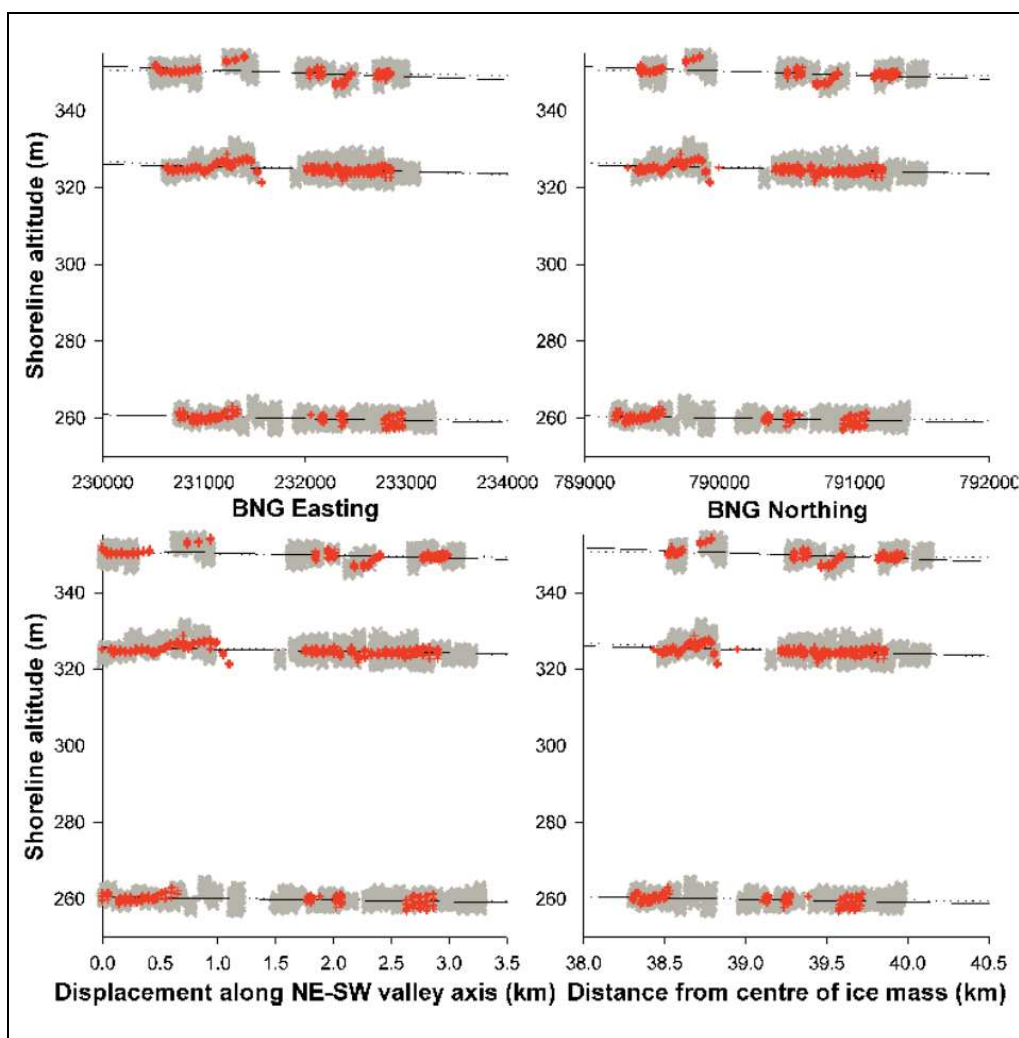
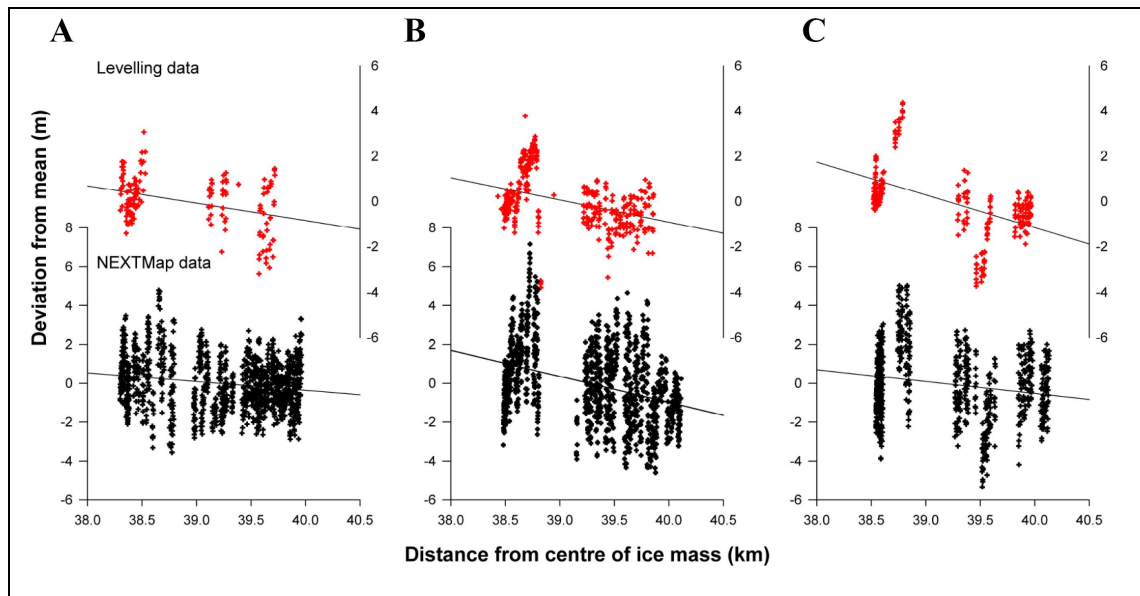


Figure 7.33 Plot of instrumentally-based altitudinal measurements (orange) and NEXTMap-generated data (grey) for stretches of the three Parallel Roads in the middle sector of Glen Roy (from Frings, 2010, Appendix 4). The trends are shown with an east-west (A), north-south (B) and SW-NE base-line (C), and (D) with distance from an origin in central Rannoch Moor.

This may reflect the lower number of instrumental measurements compared with the number of NEXTMap data-points. The instrumental measurements picked out the same short-distance differential tilting of blocks (see section 7.7) of the shorelines as are discernible in the NEXTMap data (Figure 7.34); individual blocks show the same trend direction and degree of differential displacement, but differ in computed



**Figure 7.34** Departures of altitudinal measurements from sector means based on instrumental measurement (red) and NEXTMap data (black) for stretches of the 260 m (A), 325 m (B) and 350 m (C) shorelines in the central Roy valley (from Frings 2010, Appendix 4).

**Table 7.7** Gradients and regression  $r^2$  values computed for shoreline stretches using instrumental (left) and NEXTMap-generated data (right).  $R^2$  values are low but highly significant for each plot ( $p < 0.001$ ). The data are shown for a north-south (North), east-west (East) and SW-NE trending base-lines, and for distance from an origin on Rannoch Moor (Rannoch) (from Frings 2010, Appendix 4).

	Shoreline	Levelling			NEXTMap		
		Gradient	Intercept	$r^2$	Gradient	Intercept	$r^2$
North	350	-0.00109		0.260	-0.00046		0.034
	325	-0.00073		0.130	-0.00102		0.121
	260	-0.00058		0.141	-0.00036		0.035
East	350	-0.00090		0.240	-0.00036		0.028
	325	-0.00060		0.118	-0.00086		0.107
	260	-0.00051		0.143	-0.00033		0.038
NE-SW	350	-0.00070		0.250	-0.00030		0.032
	325	-0.00047		0.124	-0.00066		0.114
	260	-0.00038		0.142	-0.00024		0.036
Rannoch	350	-0.00145	407	0.266	-0.00062	375	0.036
	325	-0.00098	363	0.134	-0.00134	379	0.126
	260	-0.00077	290	0.142	-0.00045	279	0.033

gradient value. Third, stochastic variation in altitudinal measurement on each shoreline is a major problem with the instrumental data, suggesting that more accurate measuring devices are not going to improve the trend data beyond the degree of scatter illustrated in Figure 7.34. Fourth, changes in base-line direction affect the computed gradients on the shoreline surfaces by a small amount; the steepest gradients determined using the



instrumental data are obtained for shorelines plotted by distance from an origin on Rannoch Moor (see Table 7.7). The gradients calculated for the instrumental data tend to be steeper than those based on NEXTMap data for the corresponding shoreline stretches, while the  $r^2$  values obtained for calculated gradients are usually significantly higher for the instrumental than for the NEXTMap gradient data.

### **7.6.5 Conclusions**

In general, the instrumental data from Glen Roy are considered concordant with the NEXTMap-generated data, though they clearly show lower variance and different (usually steeper) gradient calculations. It is not clear whether the differences in gradients reflect the much lower number of instrumental data-points available in the instrumental data, but the lower variance in these data and higher  $r^2$  values suggest the differences are real. A fairer test would be one in which (i) the number of measurements on each shoreline stretch are more equal between the two measurement approaches, (ii) both sets of measurements were obtained from exactly the same points or have approximately the same locational scatter, and (iii) all measuring points in both exercises were selected using the same criteria. A major difference is that the NEXTMap measurements were random, but some avoidance of atypical surfaces and an account of peat depths affected selection in the Total Station exercise. Figures 7.33 and 7.34 suggest, however, that the bulk of the NEXTMap data are capturing the essential gradient directions of both block tilts and along-valley general gradients of each shoreline; the data suggest that it may be valid to ignore the extreme altitudinal measurements in the NEXTMap data, by reducing the data to show only the  $1\sigma$  data range around the sector mean for each polygon data-set, a point returned to later in this chapter.

The four experimental tests appear to provide somewhat contradictory conclusions. The Heathrow runway, Loch Laggan surface and Ben Nevis pipeline data suggest that

there is little internal altitudinal error associated with height measurements obtained from ground and artificial surfaces using NEXTMap, providing the data are generated from the same flight tiles. The comparison of NEXTMap with Total Station data obtained from the same stretches of Parallel Road indicate much greater altitudinal scatter in the former, although both sets of data indicate the same surface gradients. This suggests that there is less internal consistency in the measurement of variable ground surfaces, which might be caused by attenuation of beam signals by different surface types, for example peat, soil, rubble and solid rock surfaces, and perhaps a dampening of true surface variation by selection of surfaces obtained from ground surveys. The data, however, also suggest that if very large numbers of altitudinal estimates are made, then statistical coherence may emerge from the data which reflect systematic trends. For example, where a large number of random NEXTMap altitude estimates are obtained from a deformed terrace or bench surface with variable surface cover, one might expect c. 65% of the estimates to lie within a narrow range ( $\pm 1$  standard deviation) of the average surface altitude or gradient, while the remainder reflect more extreme errors caused by attenuation or ground undulation effects. The capabilities of NEXTMap measurements in this regard are tested in sections 7.7 to 7.9, first by examining the evidence for large-scale deformation in the form of block dislocation and tilting, and ultimately by trend-surface analysis of the collective data to test for regional gradients.

## **7.7 Evidence for block-tilting of the Parallel Roads of Glen Roy**

### **7.7.1 Sissons and Cornish, 1982**

Sissons and Cornish (1982b) divided each of the Parallel Roads into a series of lengths or stretches, identified by alphabetical lettering in Figure 7.35 (A to C). They obtained and analysed altitude measurements for each stretch and also examined the collective evidence for each shoreline to assess overall trends in the data. Their statistical data are summarised in Tables 7.8 to 7.10. To test for accuracy in their results, with respect to representing the true tilts of the shorelines, they re-levelled several of the stretches without prior knowledge of the initial results, and found differences between the original and subsequent measurements of around 0.3 m and occasionally c. 0.5 m (Figure 7.36). However, this may have been because the measurements were not obtained from precisely the same survey points. For most stretches, this degree of variance in measured altitudes was not considered to invalidate the regression calculations derived from the data.

The most significant information to emerge from Sissons and Cornish's (1982b) investigations was that the Parallel Roads of Glen Roy are not uniformly tilted, but are severely dislocated by blocks that have been differentially displaced (Figure 7.37). Some stretches of shoreline are nearly horizontal, while others have varying tilts up to  $4.6 \text{ m km}^{-1}$ , but are tilted in different directions (Tables 7.8 to 7.10). Some are tilted in the opposite direction to that expected from regional isobase patterns (i.e. they tilt *downwards* from NE to SW or E to W). They also noted that particularly marked dislocations were associated with landslide scars, with some parts of the shorelines rising as much as 3 m above their expected altitudes (Figure 7.38). On the face of things, this evidence would appear to rule out the possibility of reconstructing more general isobase patterns. However, the data were collected from shoreline surfaces that extend over a distance of some 9 km; dislocations of c. 3 m or so therefore represent vertical movements of about 0.03% of total shoreline length or 0.2% of a stretch with length 1.5

km. Is such a scale of deformation sufficient to obscure more uniform trends within the data? Furthermore, some of the blocks may not have been tilted at all, and hence may preserve any original uniform isostatic tilting of the shorelines, a point examined in section 7.9.

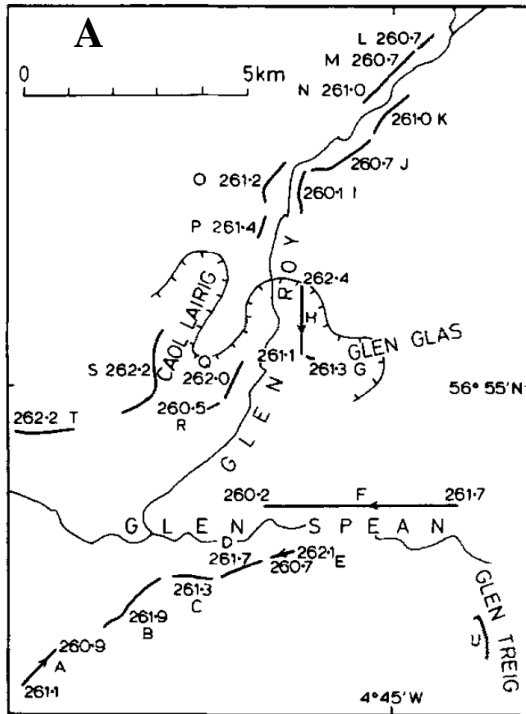
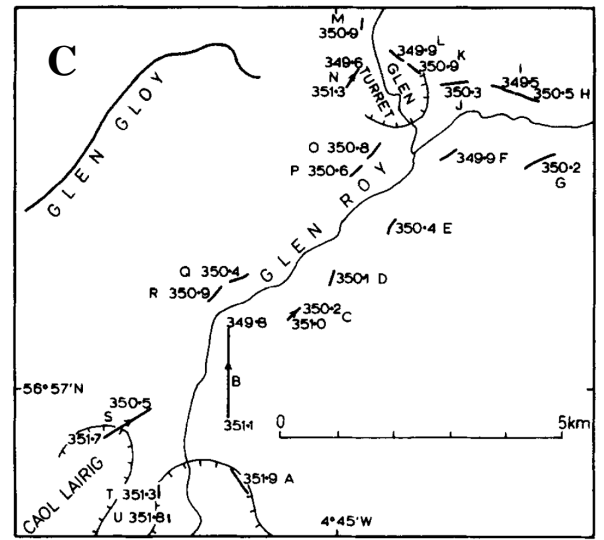
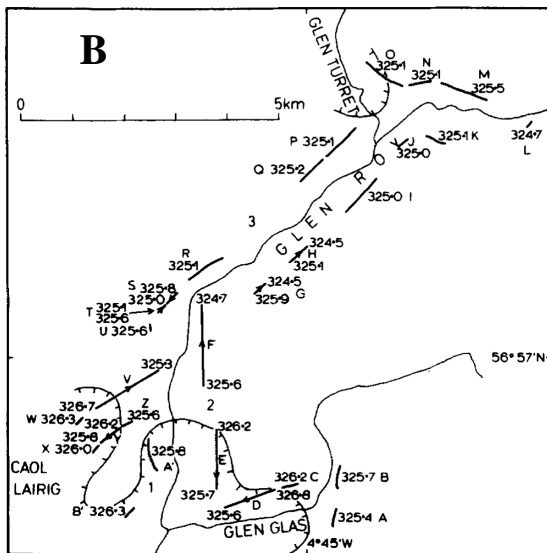


Figure 7.35 Altitude measurements obtained by Sissons and Cornish (1982b) for surveyed stretches of: A - the 260 m, B - the 325 m, and C - the 350 m shorelines in Glen Roy. The letters against each stretch correspond with those in Tables 7.8 to 7.10. A single value against a stretch indicates the mean altitude of that stretch; two values define the mean altitudes of each end of the stretch determined by regression analysis.



**Table 7.8 Statistical data for the 260 m shoreline from Sissons and Cornish (1982b). The alphabetical reference codes for each stretch accord with those in Figure 7.33A.**

Reference	Data points		Altitude (m)		Gradient (m/km)	<i>r</i>	Statistical significance
	Omitted	Used	Mean	Standard deviation			
A	1	22	261	0.22	0.19	0.29	NS
B	0	14	261.9	0.51			
C	0	16	261.3	0.69			
D	0	16	261.7	0.4			
E	3	15	261.5	0.18	2.47	0.93	0.001
F	19	73	261.1	0.45	0.33	0.73	0.001
G	0	9	261.3	0.22			
H	3	33	261.6	0.34	0.84	0.76	0.001
I	2	13	260.1	0.28			
J	4	7	260.7	0.4			
K	6	14	261	0.18			
L	0	15	260.7	0.18			
M	1	22	260.7	0.38			
N	4	14	261	0.22			
O	8	19	261.2	0.32			
P	1	11	261.4	0.24			
Q	0	11	262	0.27			
R	0	6	260.5	0.32			
S	1	11	262.2	0.24			
T	0	18	262.2	0.45			

**Table 7.9 Statistical data for the 325 m shoreline from Sissons and Cornish (1982b). The alphabetical reference codes for each stretch accord with those in Figure 7.33B**

Reference	Data points		Altitude (m)		Gradient (m/km)	<i>r</i>	Statistical significance
	Omitted	Used	Mean	Standard deviation			
A	1	9	325.4	0.35			
B	2	8	325.7	0.27			
C	0	9	326.2	0.09			
D	1	30	326.2	0.18	1.25	0.9	0.001
E	1	37	325.9	0.29	0.44	0.5	0.01
F	3	40	325.1	0.24	0.59	0.77	0.001
G	0	26	325.3	0.16	3.98	0.94	0.001
H	2	31	324.8	0.23	1.06	0.57	0.001
I	1	23	325	0.22			
J	0	7	325	0.22			
K	0	4	325.1	0.18			
L	0	6	324.7	0.33			
M	0	20	325.5	0.28			
N	1	16	325.1	0.38			
O	0	22	325.1	0.35			
P	0	12	325.1	0.18			
Q	0	20	325.2	0.18			
R	0	16	325.1	0.12			
S	0	10	325.4	0.17	2.72	0.84	0.01
T	0	9	325.3	0.1	2.17	0.89	0.01
U	0	4	325.6	0.19			
V	0	30	326	0.28	0.9	0.83	0.001
W	0	5	326.3	0.33			
X	0	6	326	0.18			
Y	1	13	326	0.05	0.72	0.94	0.001
Z	0	4	325.6	0.29			
A'	0	7	325.8	0.23			
B'	0	11	326.3	0.23			

Table 7.10 Statistical data for the 350 m shoreline from Sissons and Cornish (1982b). The alphabetical reference codes for each stretch accord with those in Figure 7.33C.

Reference	Data points		Altitude (m)		Gradient (m/km)	<i>r</i>	Statistical significance
	Omitted	Used	Mean	Standard deviation			
A	5	9	351.9	0.24			
B	0	29	350.4	0.22	0.89	0.9	0.001
C	4	18	350.6	0.08	2.49	0.96	0.001
D	2	9	350.1	0.26			
E	0	8	350.4	0.4			
F	0	11	349.9	0.62			
G	0	5	350.2	0.37			
H	1	12	350.5	0.22			
I	0	10	349.5	0.4			
J	0	11	350.3	0.41			
K	0	19	350.9	0.15			
L	0	14	349.9	0.34			
M	0	6	350.9	0.21			
N	0	14	350.4	0.14	4.59	0.97	0.001
O	0	10	350.8	0.36			
P	0	7	350.6	0.31			
Q	0	11	350.4	0.35			
R	0	10	350.9	0.24			
S	0	12	351.2	0.25	1.02	0.86	0.001
T	0	6	351.3	0.23			
U	0	4	351.8	0.33			

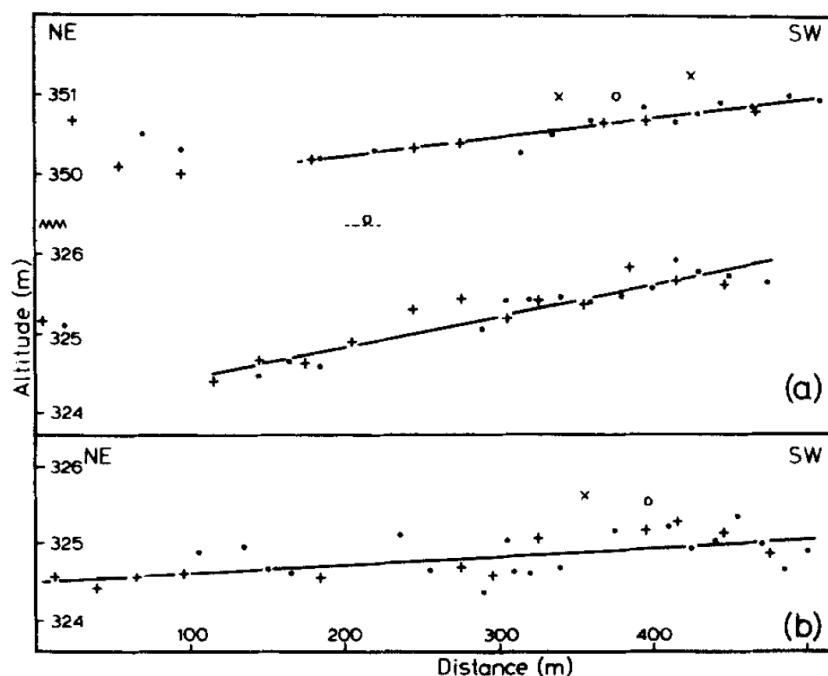


Figure 7.36 Results of instrumental levelling and re-levelling of three stretches of shoreline by Sissons & Cornish, 1982b). + sign indicates data obtained for the first survey and included in regression calculations; x indicates a survey point not included in regression calculations. Dots represent data obtained from the second survey and included in regression calculations; open circles data not included.

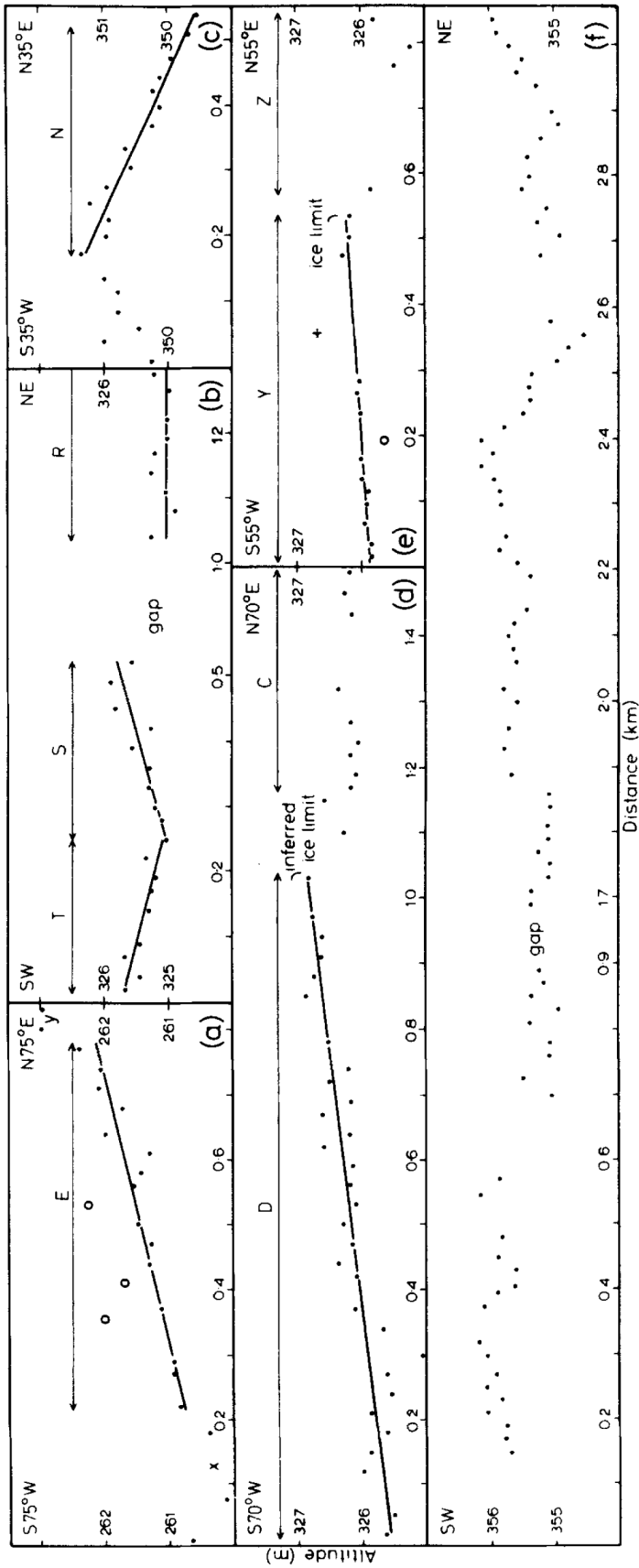


Figure 7.37 Evidence for differential block movement of the Parallel Roads of Glen Roy reported by Sissons and Cornish (1982b). Note the marked variation in tilt values, the fact that some stretches tilt in opposite directions, and the complex deformation of the 355 m shoreline in Glen Gloy (Figure 7.37 f).

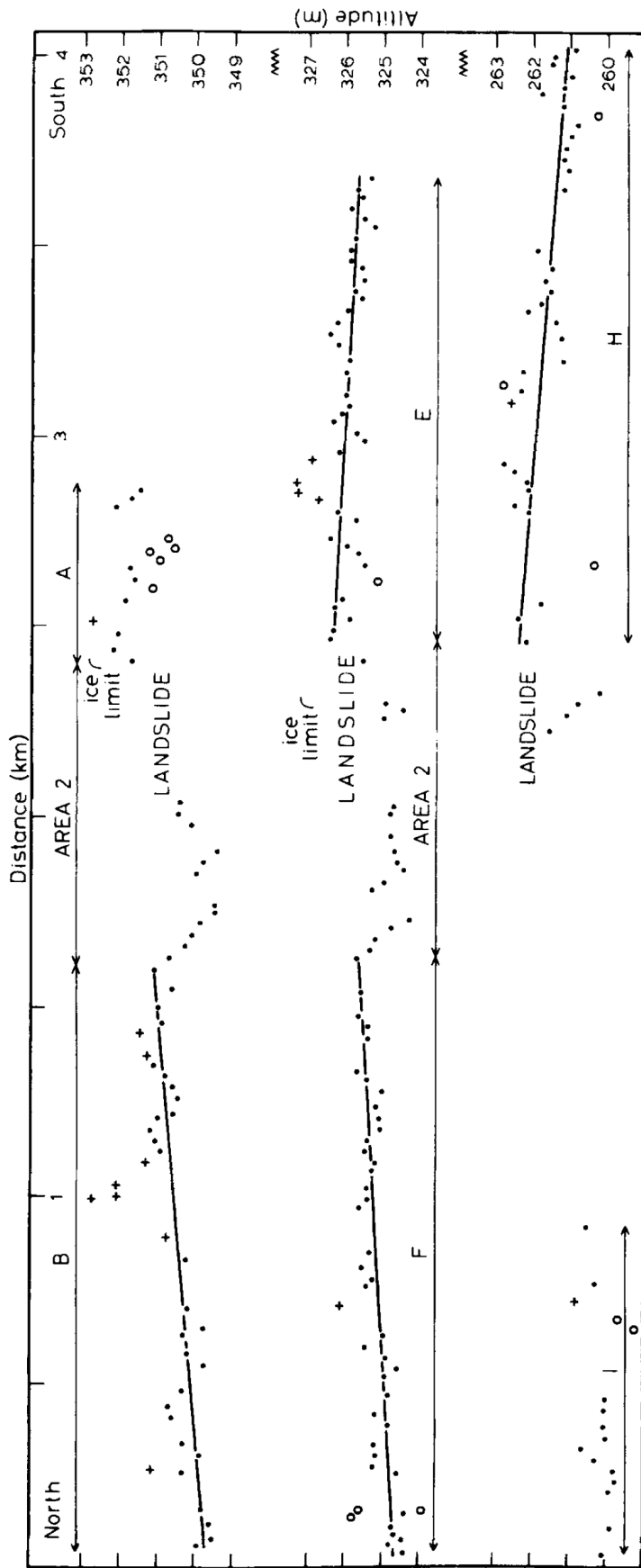


Figure 7.38 Altitudes of all three shorelines on either side of a major landslip scar located on the eastern side of the Glen, close to the Loch Lomond Readvance ice limit near the Viewpoint (from Sissons and Cornish, 1982b).



Sissons (1978) and Sissons and Cornish (1982b) concluded that the best preserved shoreline for altitude measurement is the 325 m Roy shoreline, because it is protected from slope debris by the 350 m shoreline which lies a short distance above it. Accordingly, Sissons and Cornish (1982b) found that the narrowest standard deviations of altitude variation were usually to be found associated with this shoreline: for example, the altitudes of stretches I, J, K, P, and Q of the 325 m shoreline (Figure 7.35B) vary by only 0.2 m, suggesting that these segments of the shoreline had not been subject to block dislocation, or at least not nearly to the same degree as some other parts. The stretches M, N and O (Figure 7.35B) were most affected by wave action, as they face SW and are likely to have experienced the longest fetch, and hence show wider variation in surface altitude. Stretch L was discounted because it has a large standard deviation. In the following section, some comparisons are made between the results reported by Sissons and Cornish (1982b) for the 325 m shoreline, and those generated in the current research.

### **7.7.2 NEXTMap measurements**

Tables 7.11 to 7.13 present the results of measurements of the altitudinal variations of the Parallel Roads in Glen Roy (outside the Loch Lomond Readvance limits) (data provided on the CD, Appendix 3.5), using the alphabetical sector references illustrated in Figures 7.4 to 7.6. Note that these alphabetical references are different to those identified and labelled by Sissons and Cornish (1982b). The tables show the number of randomly-generated altitudinal measurements available for each sector, the mean altitude and standard deviations per sector ( $1\sigma$ ), the computed linear gradients and their direction, and the  $R^2$  values of each gradient. These data are initially used to draw out some broad patterns within the data, as well as comparisons with the data published by Sissons and Cornish (1982b). Comparisons between the two data-sets are not straightforward, however, because Sissons and Cornish (1982b) achieved very low

standard deviation values, typically between 0.10 and 0.30, compared with  $1\sigma$  values frequently in excess of 1.0 in the current research. It should be noted, however, that the former were achieved by rejection of aberrant values and sometimes on the basis of very low numbers of altitudinal values per sector. In broad terms, the new data confirm a number of interpretations advanced by Sissons and Cornish (1982b). For example, there is no doubt that the shorelines have all been markedly deformed – short-distance displacements are evident in almost every sector studied, as illustrated in Figures 7.19 and 7.20, and in a number of diagrams below. Several sectors or blocks show varying tilts, some in opposing directions, suggesting localised causes rather than general regional isostatic influences. However, some sectors have near-horizontal shoreline gradients, which suggest they have been less prone to block-deformation. Some differences in detail were found with the interpretations of Sissons and Cornish (1982b). Following the presentation of some examples of this, attention is focused in section 7.8 on the description of selected major dislocations that drew particular note from Sissons and Cornish (1982b), and on their causes in section 7.9. Note that the gradients and data-plots in tables 7.11 to 7.13 and Figures 7.39 to 7.53 are aligned either on a W-E or S-N axis, according to the main trend of the valley in which the relevant sectors of the Parallel Roads are located.

**Table 7.11 NEXTMap-generated altitude measurements for the surface of the 260 m shoreline in Glen Roy. The reference codes (alphabetical letters) accord with those shown in Figure 7.4. Gradients have been calculated using linear regression of all data-points available for each stretch. A gradient of 0.4010(N-S) indicates that the shoreline surface is trending at 0.401 m km<sup>-1</sup> in a N to S direction. The data have been plotted using a S-N plane of projection except those marked by an asterisk (\*) which have been plotted with a W-E plane of projection.**

Reference	Data points used	Altitude (m)		Gradient (m/km)	R <sup>2</sup>
		Mean	Standard deviation		
A	1027	261.03	1.21	0.7328	0.054993
B	325	261.32	1.16	0.2900	0.00195216
C	207	260.76	1.23	0.0870	0.000634598
D	636	260.41	1.10	0.8577	0.0519632
E	433	260.29	1.03	0.8693	0.0211634
F	864	260.67	1.14	-0.6211	0.0229062
G	318	260.38	0.77	1.2188	0.0667092
H	425	260.82	1.07	-0.2313	0.00284555
I	234	260.80	1.20	-1.2343	0.0149528
J	889	260.91	1.19	0.1501	0.00215439
K	392	261.58	1.57	-0.0752	0.000123489
L	405	261.28	1.51	-0.4820	0.00641305
M	205	261.29	1.32	-0.1089	0.000891883
N	521	260.98	1.89	-1.5155	0.153869
O	293	262.25	1.70	0.2409	0.000422328
P	586	261.19	1.36	4.0567	0.234167

**Table 7.12 NEXMap-generated altitude measurements for the surface of the 325 m shoreline in Glen Roy. The reference codes (alphabetical letters) accord with those shown in Figure 7.5. Gradients have been calculated using linear regression of all data-points available for each stretch. A gradient of 0.4010(N-S) indicates that the shoreline surface is trending at 0.401 m km<sup>-1</sup> in a N to S direction. The data have been plotted using a S-N plane of projection except those marked by an asterisk (\*) which have been plotted with a W-E plane of projection.**

Reference	Data points used	Altitude (m)		Gradient (m/km)	R <sup>2</sup>
		Mean	Standard deviation		
A	1165	325.60	0.84	0.4010	0.0460023
B	548	324.80	1.01	0.3573	0.0119745
C	508	325.03	0.88	-0.1951	0.003276
D	336	325.33	1.19	-0.0300	1.21494E-005
E	573	325.19	1.28	0.1941	0.00189038
F	351	325.49	0.77	-0.2118	0.0020263
G	448	324.74	1.25	1.5019	0.134431
H*	125	325.55	0.77	1.2518	0.0384886
I*	355	325.15	0.77	0.4254	0.0500603
J*	182	324.50	0.88	1.7444	0.166374
K*	488	325.36	0.84	0.0807	0.00225468
L*	518	324.86	0.99	0.2111	0.0125339
M*	297	324.42	0.81	-0.6893	0.0144108
N*	908	324.67	0.89	-0.9558	0.225397
O	176	324.93	1.32	2.2511	0.187294
P	544	326.54	2.00	0.0980	0.000139993
Q	221	325.84	1.26	-1.0143	0.00637785
R	726	325.55	1.86	-1.2353	0.0474793
S	400	327.05	1.95	5.3899	0.211103
T	489	326.23	1.82	0.7521	0.0179473
U	190	327.09	1.54	-1.9675	0.196233
V	435	326.66	2.13	0.3465	0.00210459
W	356	326.53	1.71	-2.5782	0.0620744
X*	349	325.86	0.63	0.1016	0.00199768
Y	352	327.28	1.71	-3.3552	0.146266
Z	877	326.36	1.67	-0.3881	0.00478961

**Table 7.13 NEXMap-generated altitude measurements for the surface of the 350 m shoreline in Glen Roy. The reference codes (alphabetical letters) accord with those shown in Figure 7.6. Gradients have been calculated using linear regression of all data-points available for each stretch. A gradient of 0.4010(N-S) indicates that the shoreline surface is trending at 0.401 m km<sup>-1</sup> in a N to S direction. The data have been plotted using a S-N plane of projection except those marked by an asterisk (\*) which have been plotted with a W-E plane of projection.**

Reference	Data points used	Altitude (m)		Gradient (cm/km)	R <sup>2</sup>
		Mean	Standard deviation		
A	593	351.14	1.12	0.2627	0.00791626
B	560	350.26	1.07	1.8093	0.308677
C	607	349.95	1.05	-0.0410	0.000111317
D	265	350.09	1.18	0.1966	0.000360665
E	469	350.34	1.62	2.0261	0.147629
F	373	350.05	1.57	-3.4214	0.159977
G	124	349.47	0.73	1.9353	0.0289419
H*	244	350.26	0.88	1.3982	0.040189
I*	497	349.84	1.11	-1.5263	0.139227
J*	234	350.09	0.91	-0.0322	5.87386E-005
K*	1446	349.92	0.79	-0.0341	0.00160767
L*	754	350.00	0.96	-0.1936	0.0305735
M*	659	349.84	1.03	-0.1499	0.00559696
N*	434	348.69	1.12	1.1828	0.0246817
O*	1411	349.95	0.99	-0.2690	0.0200094
P*	136	350.16	0.92	3.4487	0.0988411
Q	442	350.16	1.37	0.4635	0.0309207
R*	350	349.35	2.50	-3.2378	0.0797734
S	216	350.33	1.02	0.2059	0.000312412
T	398	350.18	1.67	0.3385	0.00547272
U	394	351.20	1.84	5.1347	0.233837
V	363	350.83	2.41	2.1760	0.09871
W	217	351.57	1.97	-2.6113	0.397826
X	199	351.03	1.74	1.3147	0.0245815
Y*	245	350.30	0.81	-0.9104	0.156539
Z	414	349.90	1.50	2.3873	0.078565

Examples of detailed observations that conflict with those of Sissons and Cornish (1982b) include the following:

i) For the 325 m shoreline (Table 7.5), sectors F, G, H, Q and R in the present research equate with parts I, J, K, P, and Q in the Sissons and Cornish (1982b) study. This was the stretch of the 325 m shoreline that they identified with (on average) lowest altitudinal variation. This conclusion is not reached, however, with the NEXTMap measurements over the same stretch, for which a  $1\sigma$  range of 1.1 m is calculated, the highest in the NEXTMap data-set for the 325 m shoreline. Other stretches of the 325 m shoreline give narrower NEXTMap ranges, such as sectors A to E ( $1\sigma$  range of 0.8 m), S to W (0.86 m) and L to N (0.44 m). Indeed, the stretch with the lowest range in mean altitude value (0.3 m) calculated from NEXTMap is that between sectors C to E. For the 350 m shoreline, the lowest altitudinal variations obtained using NEXTMap measurements were for stretches C to D ( $1\sigma$  variation = 0.14 m) and K to L (0.08 m). For the 260 m shoreline, the lowest altitudinal variation ( $1\sigma = 0.12$  m) occurs in stretch D to E (equivalent to stretch C to D for the 325 m and 350 m shorelines). Hence several stretches were found associated with the three shorelines that have low altitudinal variance, and which may therefore reflect limited displacement or modification subsequent to formation, a point returned to in section 7.10 (trend-surface analysis). However, these did not always coincide with the sectors with the lowest gradients and variances computed by Sissons and Cornish (1982b).

ii) Sissons and Cornish (1982b) found their sector H of the 325 m shoreline to have an average gradient of  $1.1 \text{ m km}^{-1}$  over a horizontal distance of 0.5 km while their sector G of the same shoreline showed an independent tilt of  $4 \text{ m km}^{-1}$ . They also noted that the tilting of both their sectors G and H are from SW to NE, and associated with a general uplift of the shorelines to around 1 m above the expected level. The equivalent sectors

in the present research are D and E (Table 7.12), and these give quite different NEXTMap results: the average gradient of D is  $0.03 \text{ m km}^{-1}$ , tilting gently from southwest to northeast, while part E has an average gradient of  $0.194 \text{ m km}^{-1}$  and tilts from northeast to southwest (the opposite to that reported by Sissons and Cornish 1982b). The highest part of each of these two sections is also found by NEXTMap measurements to be raised about 3-4.5 m above each sector's average altitude, significantly more than computed by Sissons and Cornish (1982b).

**iii)** Another stretch of the 325 m shoreline that Sissons and Cornish (1982b) found to have experienced significant post-formational tectonic block movement are their sectors S and T, which they describe as distinctly above the near-horizontal parts of this shoreline. An attempt was made to compare their results directly with the NEXTMap results, but this proved difficult because of an absence of precise grid reference data in their paper; all that can be determined is that their sectors S and T fall within sectors T and S in the current research, but the deformation of the 325 m shoreline in this area as suggested by the latter appears to have been more complex than is described by Sissons and Cornish (1982b).

**iv)** Both the 325 m (X-Y) and 350 m (Y) shorelines increase in altitude from Glen Roy along both flanks of Caol Lairig, towards the limit of the Loch Lomond Advance. The rise continues till the terminations of both shorelines. On the south/east flank of Caol Lairig, the 350 m shoreline, according to the NEXTMap data, tilts northeastwards but the 325 m shoreline tilts slightly southwestwards; Sissons and Cornish (1982b) found that both the 325 m and 350 m shorelines tilt northeastwards inside the advance limit.

**v)** On the western flank of Glen Roy, marked tectonic uplift can be inferred from the surface altitude data for stretches S of the 325 m shoreline (Figure 7.5) and U of the 350 m shoreline (Figure 7.6). The mean surface altitudes of these stretches rise by c. 2 to 3

m above the local mean horizontal altitude, best represented by stretch S of the 325 m shoreline and stretch U of the 350 m shorelines. These record the steepest tilts of 325m and 350m shorelines. (Figure 7.39, Tables 7.12 and 7.13). For explanation of the symbols used in Figure 7.39, see below.

The NEXTMap data are clearly picking out localised deformation features, in line with the complex records reported by Sissons and Cornish (1982b). However, the magnitude and direction of surface deformation indicated by the NEXTMap measurements do not always accord with those reported by Sissons and Cornish (1982b), for reasons not understood. In the following section, six areas of localised deformation associated with landslides are analysed in more detail, to establish how well NEXTMap interpretations can constrain the magnitude and form of deformation.

### **Explanation of structure and symbols used in Figures 7.39 and subsequent figures of similar construction**

Altitudinal data are plotted in Figure 7.39 and a number of diagrams in section 7.8 that reveal deformed segments of the Parallel Roads. The data are grouped in blocks – these were parts of the roads that were traceable, sometimes continuously, on the NEXTMap DEM plots. Major blocks are usually separated by deep gullies, landslips or other major features where the roads have been destroyed or obscured. For each block or stretch on which the roads were detectable, the following features or symbols are used in diagrams presented below. In Figure 7.39 and part A of subsequent figures, linear regression (blue line) and 2<sup>nd</sup> order polynomial (yellow line) trendlines of the collective data in each major block are shown, with the corresponding regression equations at top of each diagram; thin coloured vertical lines show corresponding grid locations on each of the roads, to aid comparison between figures, as the grid positions vary between diagrams.



In parts B and C of subsequent figures, additional information is provided. B shows the same data as part A, but with small red dots added which bound what are considered to be separate deformational elements. Part C of subsequent diagrams shows mean and standard deviation ranges for the measured altitudes of each deformed crustal block.

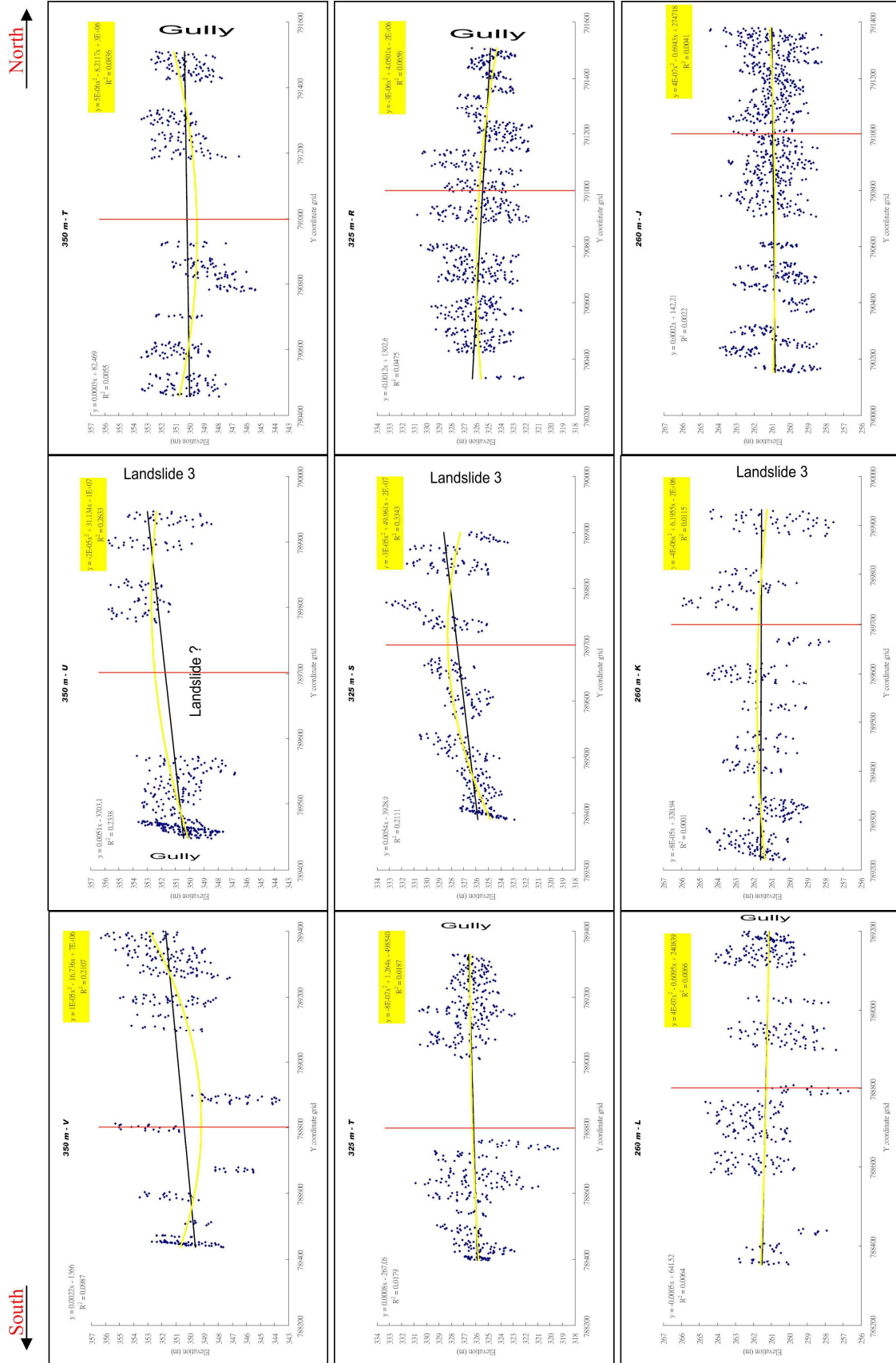


Figure 7.39 NEXTMap altitude measurements obtained for selected stretches of the Parallel Road of Glen Roy: for further explanation see text (p. 268).

## 7.8 Major localised dislocation of the Parallel Roads

The locations of six well marked landslides in the area are indicated in Figure 7.40 (numbered 1 to 6) as well as the approximate positions of glacier termini of Loch Lomond Stadial age in Glen Roy, Glen Gloy and Caol Lairig, the significance of which are discussed in Chapter 5 and 6. In this section, altitudinal measurements for landslides numbered 1, 2 and 3 are discussed, as well as deformed shoreline surfaces in the vicinity of the Turret Fan. Features 1 to 3 are selected for discussion because their shorelines have been markedly dislocated and tilted. By comparison, the shorelines beyond the Turret Fan in upper Glen Roy are much less deformed.

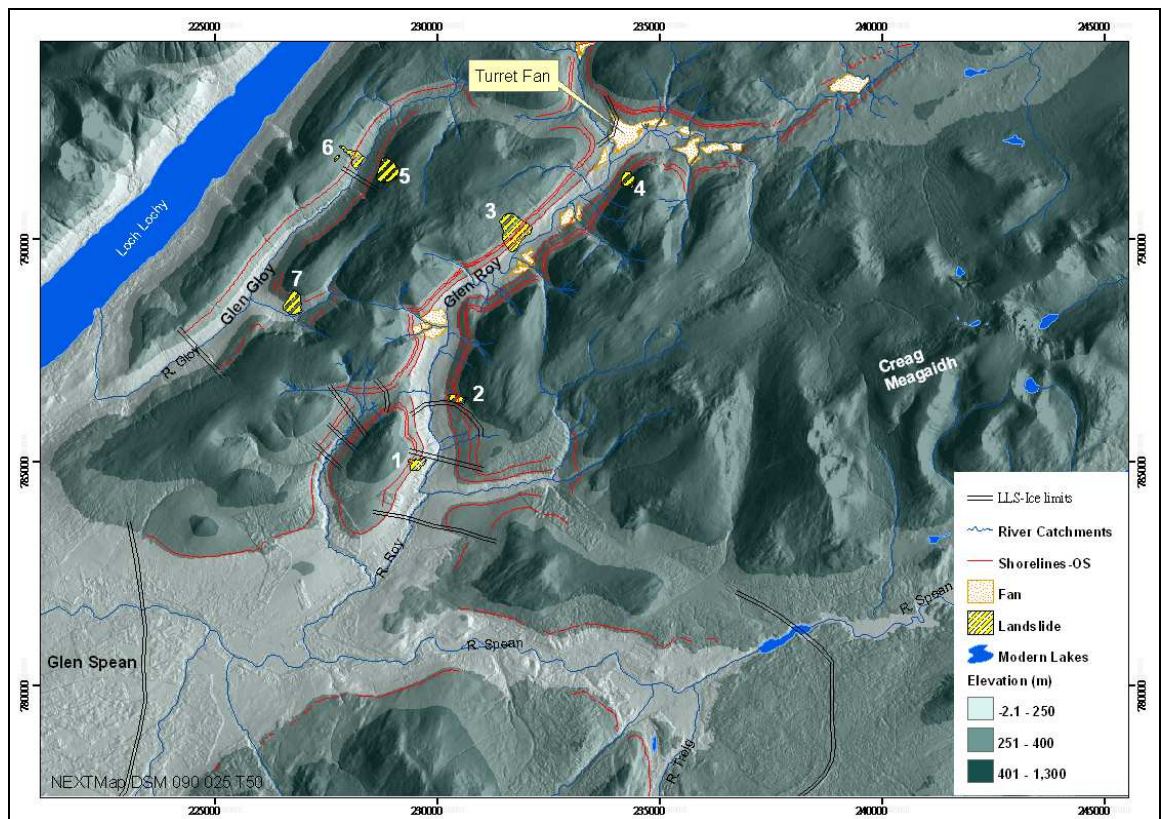
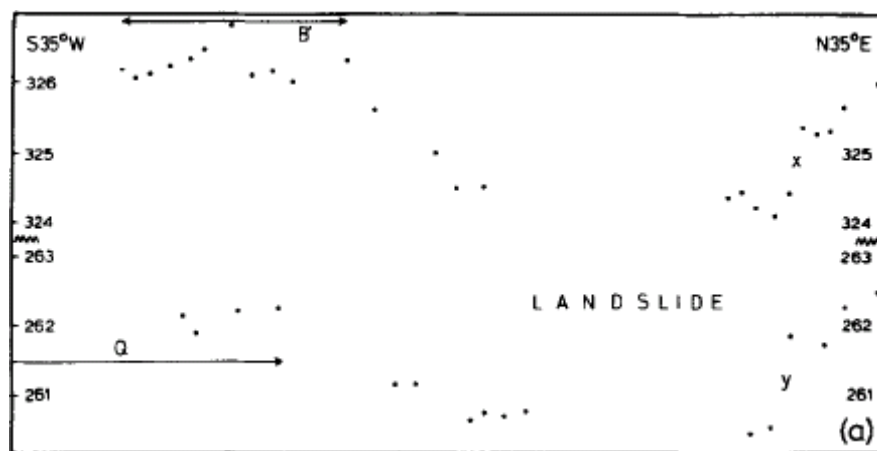


Figure 7.40 Location of 6 small landslides in glens Roy and Gloy (numbered) and of the positions of Loch Lomond Stadial glacier termini (shown schematically as black double-lined arcs).

### 7.8.1 Area around landslip 1, Lower Glen Roy

In the area located just to the south of the termination of the 350 m shoreline and of the confluence between Gleann Glas Dhoire and the River Roy, a landslide has obliterated a 300 m stretch of both the 260 m and 325 m shorelines (stretches W and V, 325 m

shoreline, and O and N, 260 m shoreline, Figures 7.5 and 7.4) (data provided in the CD, Appendix 3.5). Sissons and Cornish (1982b) reported an abrupt dislocation of the altitudes of the shorelines adjacent to the landslide (Figure 7.41). This area was re-measured using NEXTMap DEM data, the stretches of the roads that were measured shown in Figure 7.42, with the altitudinal data presented in Figure 7.43. Note that in the latter figure, and similar ones that follow, the blue stars denote the beginning and end of what are considered to be major deformational trends reflected in the data.



**Figure 7.41** The location of Landslide 1 and the measured altitudes of adjacent shorelines as reported by Sissons and Cornish (1982b).

Figure 7.43 shows that on each side of the landslide, both the 325 and 260 m shorelines are severely contorted along the full lengths of each stretch, with numerous dislocations and apparent tilted or deformed blocks (Figure 7.43B). The larger altitudinal scatter of the NEXTMap data (Figure 7.43A) makes it difficult to compare directly with the data of Sissons and Cornish (1982b), but is best achieved using the polygon mean and standard deviation values shown in Figure 7.43C. The mean values are in broadly the same altitudinal range as the values plotted in Figure 7.41, but show some notable differences with the Sissons and Cornish (1982b) data. A rise in the 325 m shoreline surface from c. 324 m to 326 m immediately to the NE of the landslide (Figure 7.41) is also shown in the mean values in Figure 7.43C, but this extends further to the NE and

reaches up to 328 m or possibly higher. The NEXTMap data extend further NE than the Sissons and Cornish (1982b) data and show a continued uplift of the 325 m shoreline until grid-point 785600, where there is a sharp reduction in altitude to c. 324 m. The rise in the level of the 260 m shoreline from c. 261 to 263 m immediately to the NE of the landslip (Figure 7.41) is also recorded in the NEXTMap data (Figure 7.43C) immediately adjacent to the landslip (grid-point 785100), but the new data show a complex pattern of warping of the shoreline, but with a long-gradient dip to 260 m at grid-point 786500. The data to the SW of the landslip for both the 325 and 260 m shorelines do not accord with those published by Sissons and Cornish (1982b). The 2 m drop in the altitude of the 325 m shoreline and 1.5 m drop of the 260 m shoreline that they found close to the landslide (Figure 7.41) are not shown by the NEXTMap data (Figure 7.43C); instead, complex block dislocation is indicated by the latter, with a long-gradient decrease in mean altitude towards the NE in the case of the 325 m shoreline, and a gradual increase in mean altitude values in the same direction in the case of the 260 m shoreline.

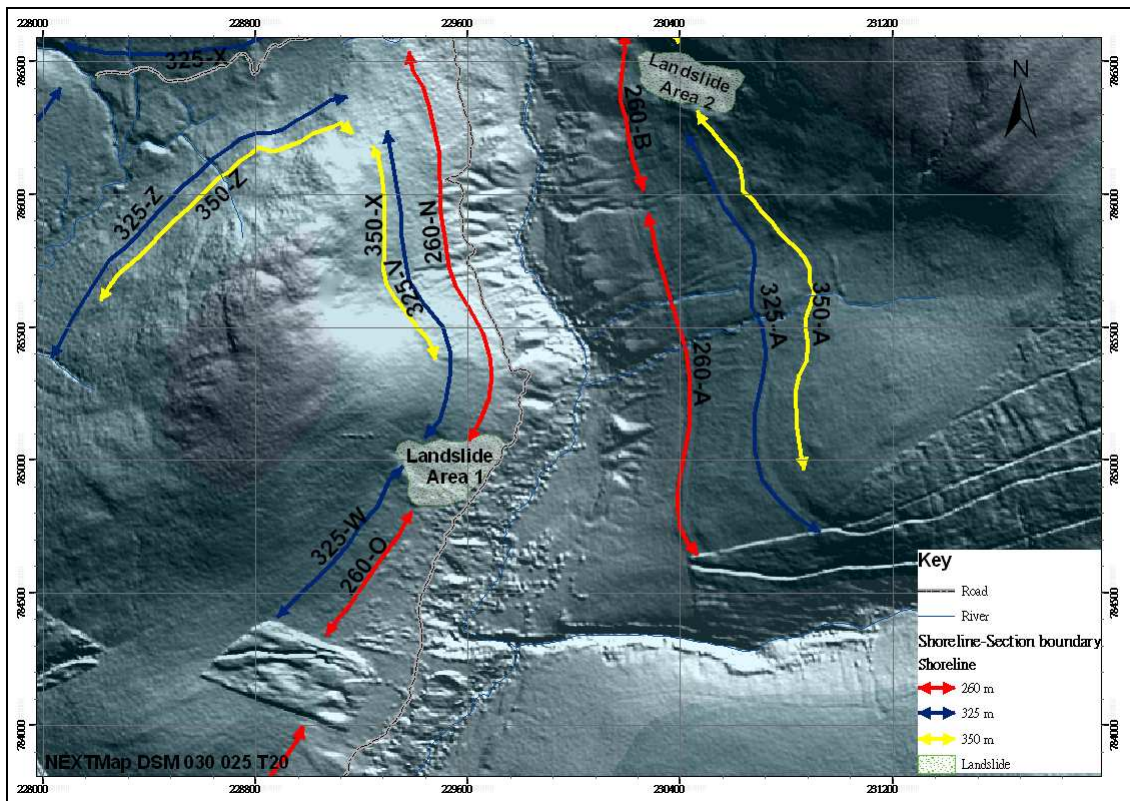


Figure 7.42 Stretches of the Parallel Roads from which NEXTMap altitude measurements were derived for Figure 7.43. Note that the Roads are not continuous, as depicted; the coloured lines show the geographical extent of each stretch and the arrow heads their terminations.

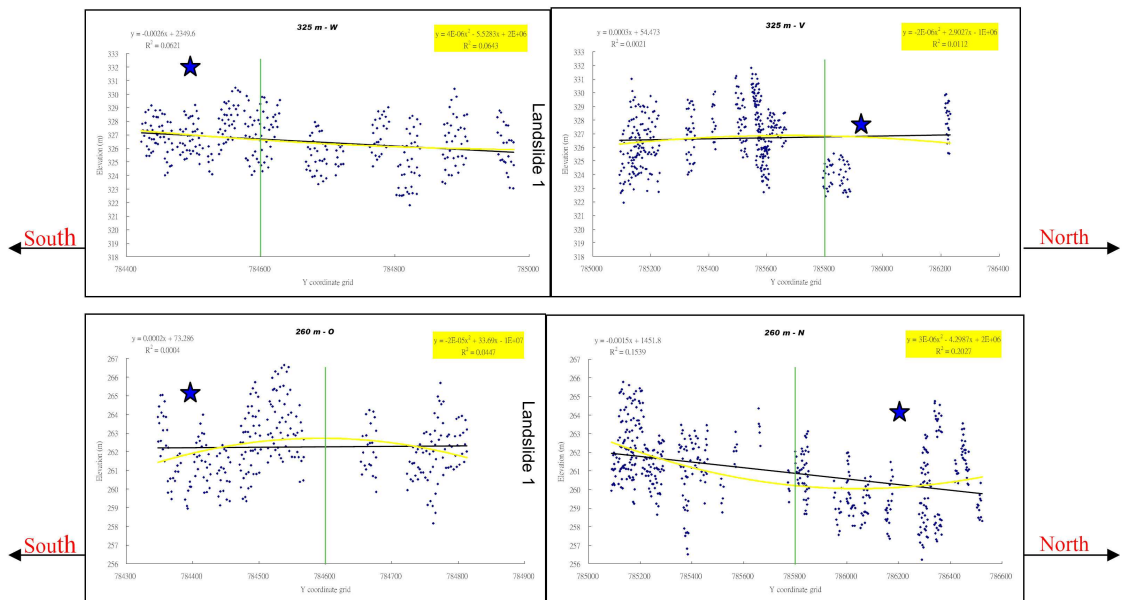


Figure 7.43A

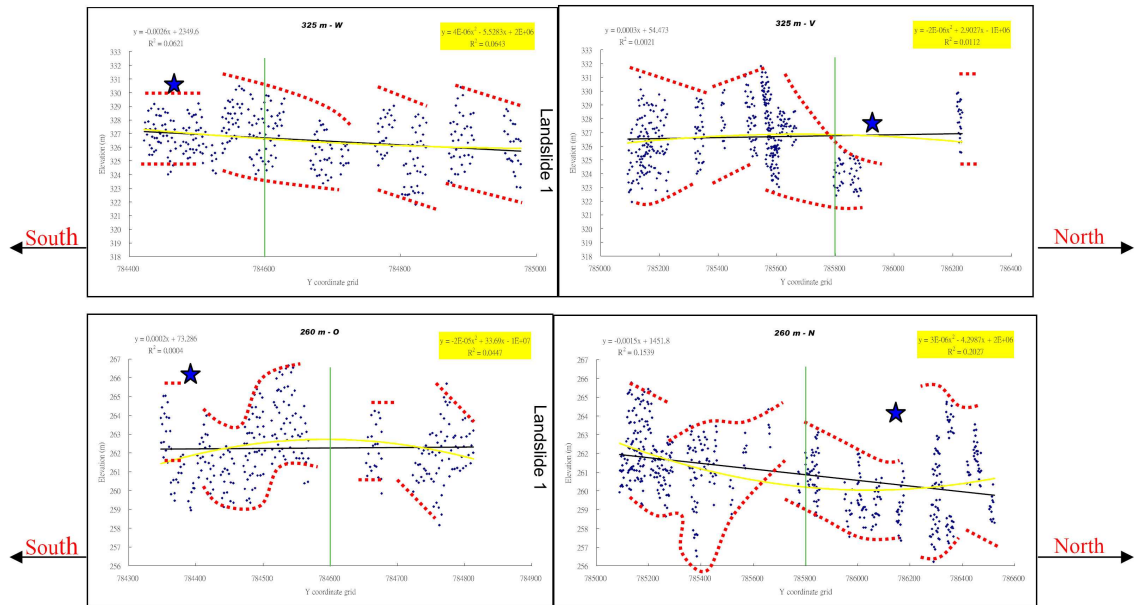


Figure 7.43B

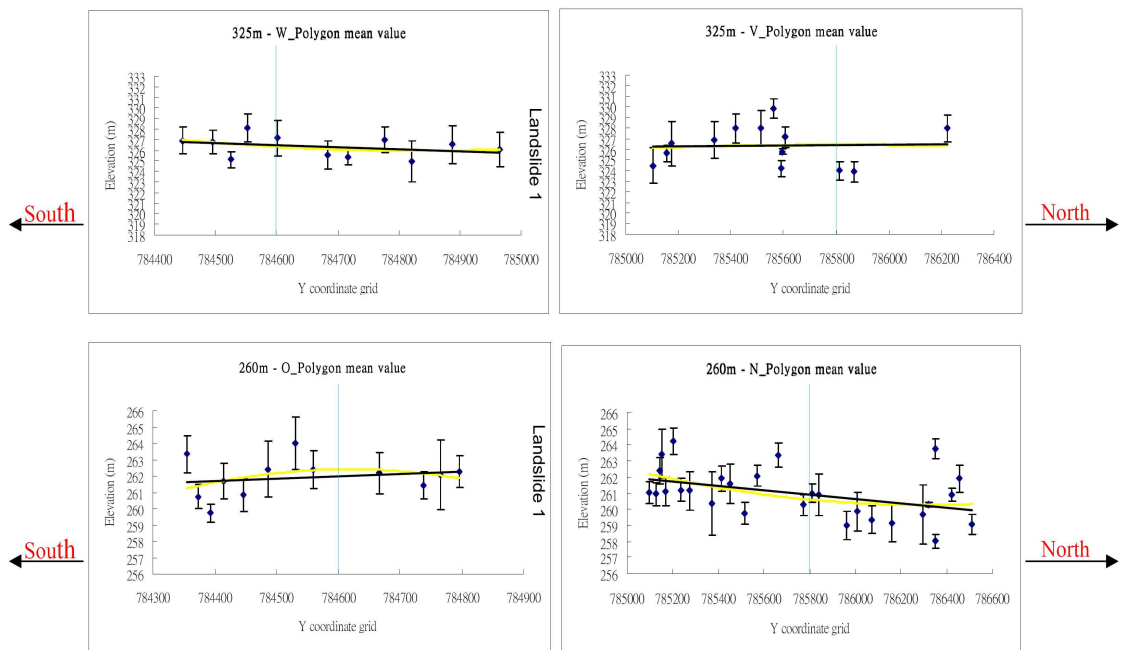


Figure 7.43C

Figure 7.43 Projected shoreline surface altitudes of the 325 and 260m Parallel Roads in the vicinity of landslide 1. Blue stars mark the ‘start’ and ‘end’ points of dislocation of each shoreline section. The X axis is the y value of the British National Grid Reference and the Y axis gives altitude in metres. Part A: scatter-plot of raw altitudinal values; Part B: suggested block dislocation pattern; Part C: Mean and standard values of the altitude scatter recorded for each polygon measurement set. For further explanation see p. 268.

### 7.8.2 Area around landslip 2, Lower Glen Roy

In this area (landslip number 2, Figure 7.40) the landslide scar is situated some 50-80 m above the 350 m shoreline. According to Sissons and Cornish (1982b), the 325 m and 350 m shorelines are well preserved on either side of a deep gulley (Figure 7.44) that runs straight down the valley side along the line of a narrow dyke. Sissons and Cornish's (1982b) measurements indicated that the most pronounced displacements of the 325 m and 350 m shoreline occurred some 200 to 400 m north of the landslide, where they are cut into bedrock. They therefore concluded it difficult to attribute the major displacements in the two shorelines to the landslide, instead suggesting the cause to be an ancient line of weakness (a dyke) found along the gulley which coincides with a change in shoreline altitudes and with the southern end of pronounced localized shoreline tilting.

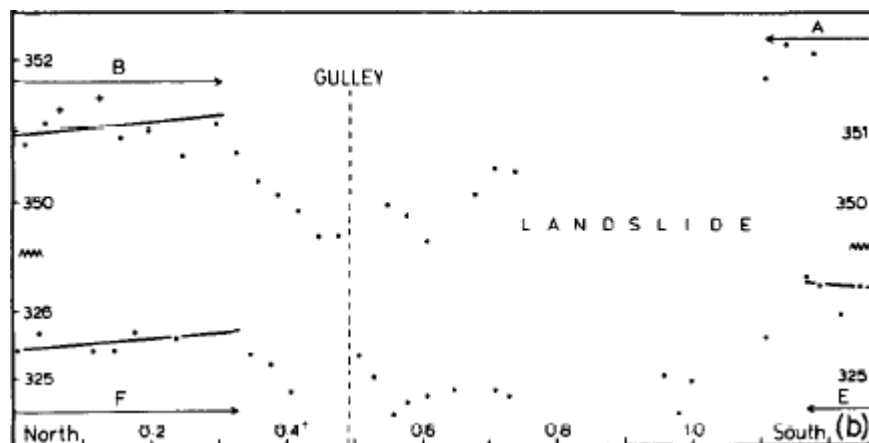


Figure 7.44 The location of Landslip 2 and the measured altitudes of adjacent shorelines as reported by Sissons and Cornish (1982b).

NEXTMap measurements were obtained from stretches of all three Parallel Roads on either side of landslip 2 on the eastern side of the Roy valley, but also from the western flank of the valley, directly opposite the landslip. The stretches measured were those labelled A, B and C (for all three shorelines) on the eastern flank, and stretches X, W,



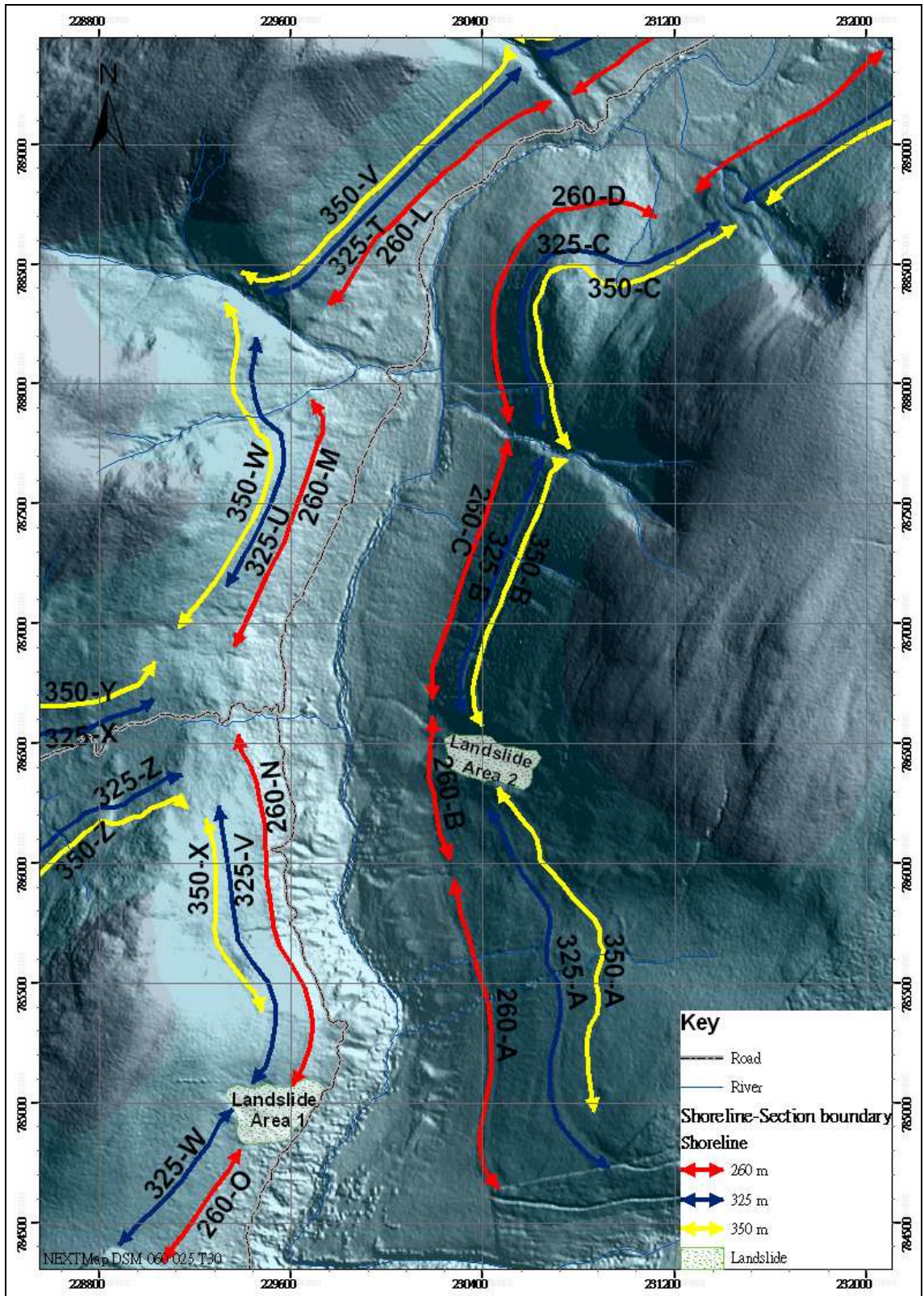


Figure 7.45 Stretches of the Parallel Roads from which NEXTMap altitude measurements were derived for Figures 7.46 and 7.47. Note that the Roads are not continuous, as depicted; the coloured lines show the geographical extent of each stretch and the arrow heads their terminations.

V for the 350, V, U, T for the 325, and N, M, L for the 260 m shorelines (respectively) on the western flank of the valley (Figure 7.45) (data provided in the CD, Appendix 3.5). On the east flank of Glen Roy, the largest shoreline dislocation occurs at close to Y:786200, adjacent to landslip 2, with a 3 m uplift as reflected in mean altitude values per measurement polygon (Figure 7.46C). Southwards of this point, the altitudes decline again to c. 351 m (Y:786000); this pattern is remarkably similar to that found by Sissons and Cornish (Figure 7.44). Indeed the mean polygon altitude values for all three shorelines are within the range measured by Sissons and Cornish (1982b) for these tracts of the shorelines. However, the NEXTMap data show a higher and more complex degree of dislocation over a longer measured stretch of each shoreline (Figure 7.46A and 7.46B). Also in line with Sissons and Cornish's (1982b) data, the vertical variation on the 325 and 260 m shorelines is much less than that for the 350 m shoreline, the former being more uniform, though small-scale dislocations are discernible. A more surprising result, however, emerges from the data for the western flank of the valley (Figure 7.47). Here the degree of vertical variation of block dislocation is greater in amplitude for all three shorelines on the western side of the valley, compared even with the degree of dislocation adjacent to landslip 2. Dislocations of up to 5 m vertical amplitude are inferred from the mean altitude values on the western flank, while the along-shoreline average gradients are generally steeper than those on the eastern flank of the valley (Figure 7.47C), though not always inclined in the same direction. The pattern of dislocation also appears more severe on the western than on the eastern flank (cf. Figure 7.46 A to C with Figure 7.37 A to C), with the greatest amount of deformation affecting the 260 m shoreline in stretch N. This indicates that the effects of landslip 2 were marginal and only additive to the overall disruption of the shorelines in this part of Glen Roy, the impacts of which were greater on the western than on the eastern flank.

North

South

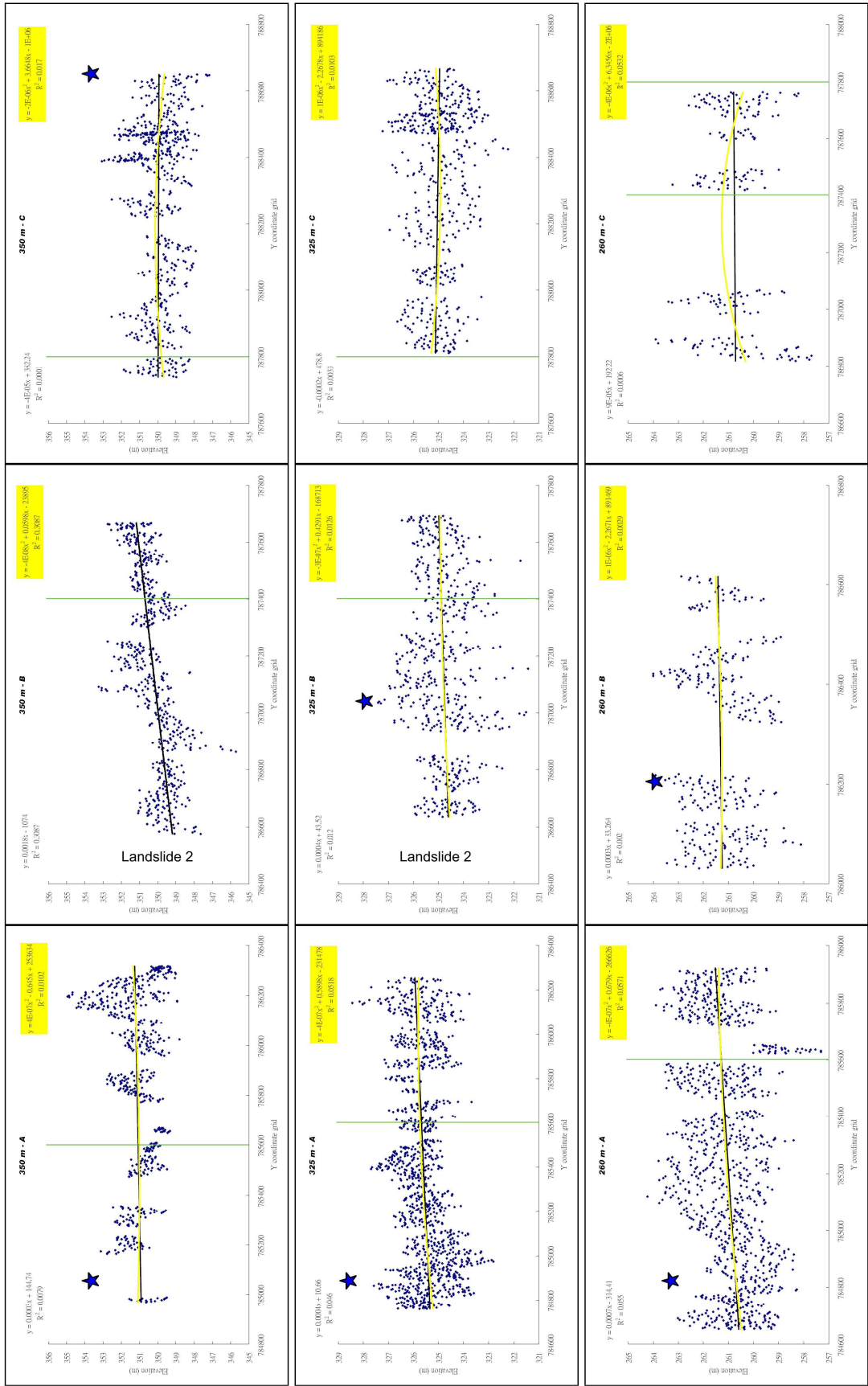


Figure 7.46A

North

South

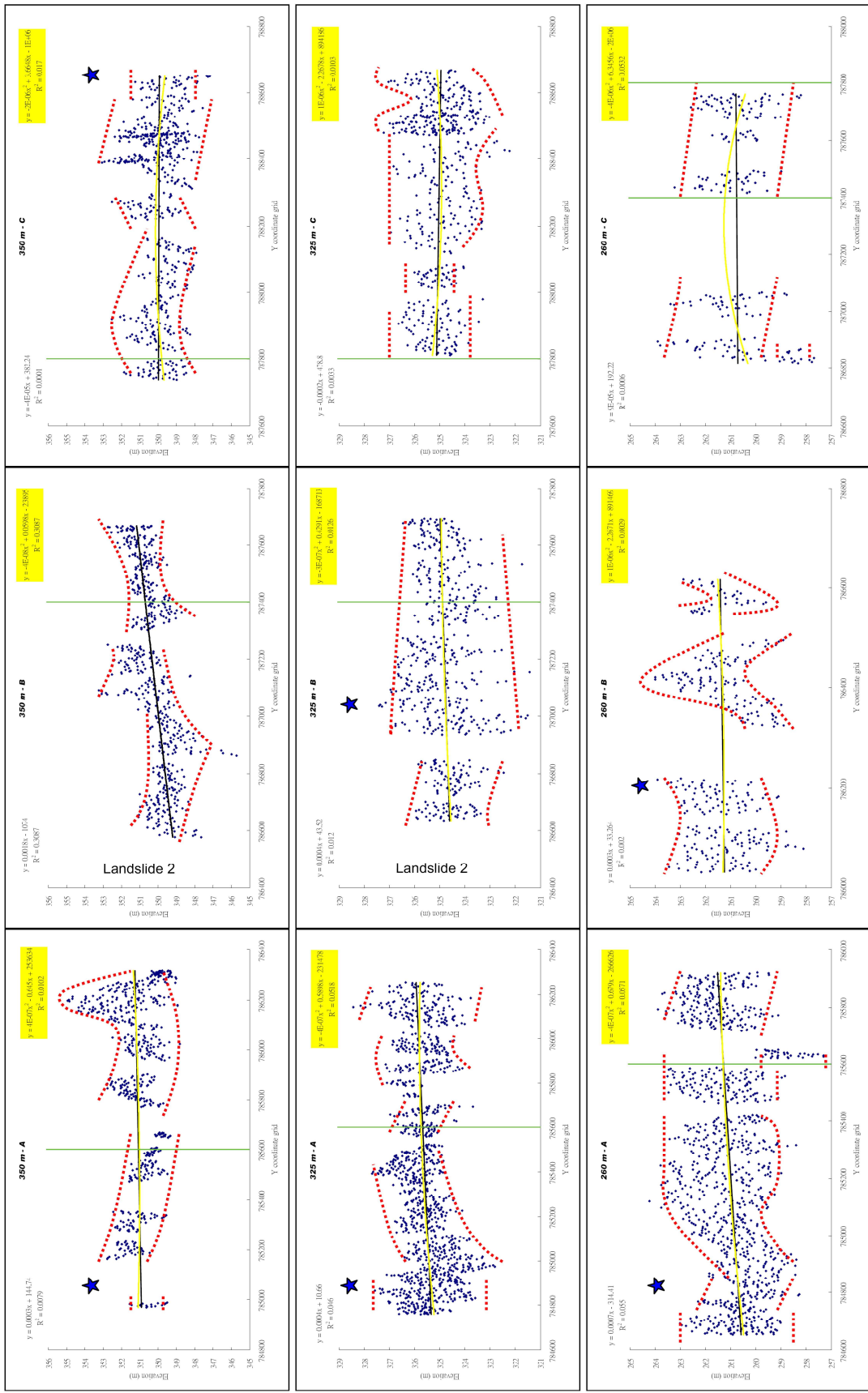


Figure 7.46B

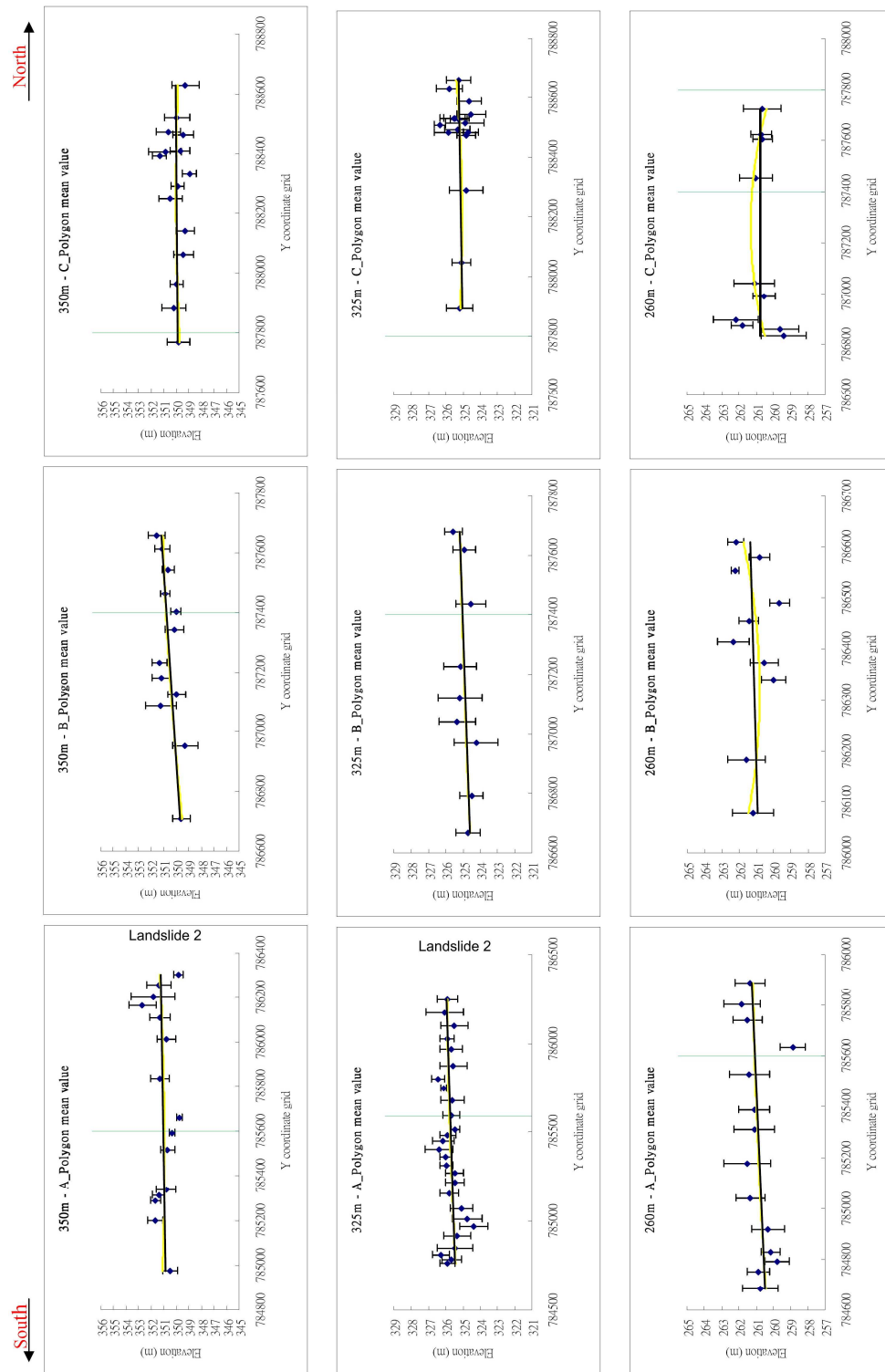


Figure 7.46C

Figure 7.46 Projected shoreline surface altitudes of the Parallel Roads in the vicinity of landslide 2 on the eastern flank of the valley. Blue stars mark the 'start' and 'end' points of dislocation of each shoreline section. The X axis is the y value of the British National Grid Reference and the Y axis gives altitude in metres. Part A: scatter-plot of raw altitudinal values; Part B: suggested block dislocation pattern; Part C: Mean and standard values of the altitude scatter recorded for each polygon. For further explanation of symbols see p. 268.

North

South

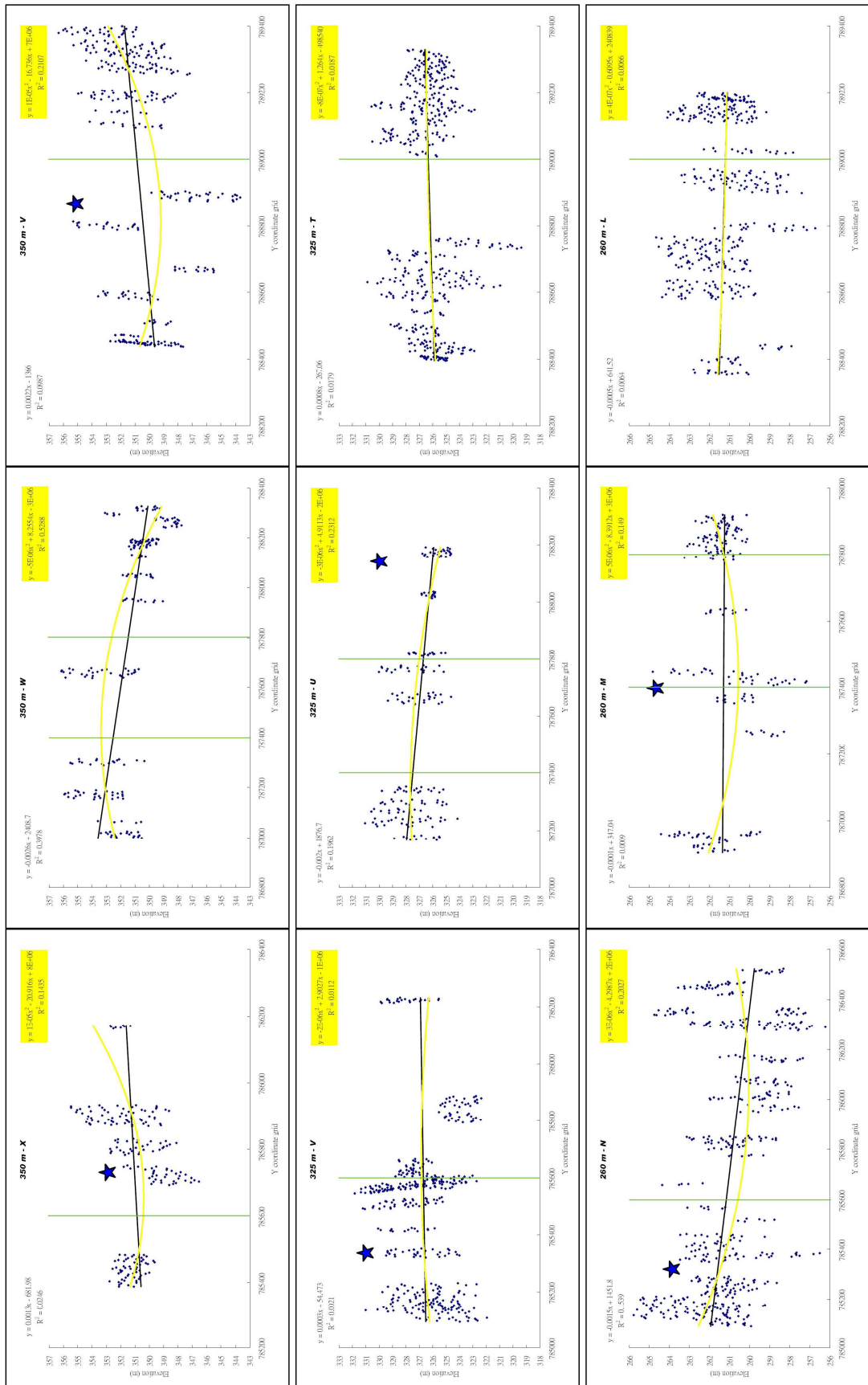


Figure 7.47A

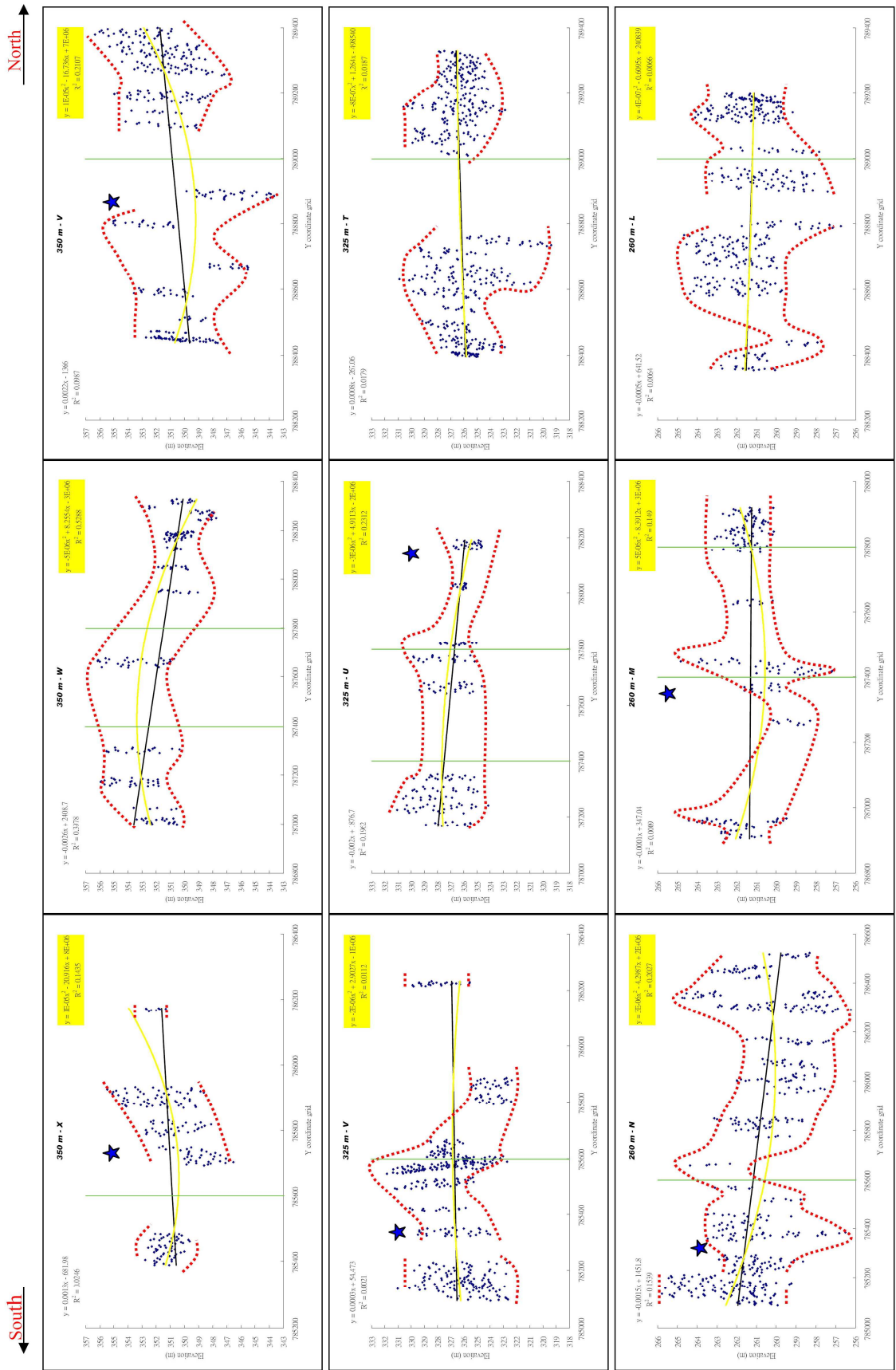


Figure 7.47B

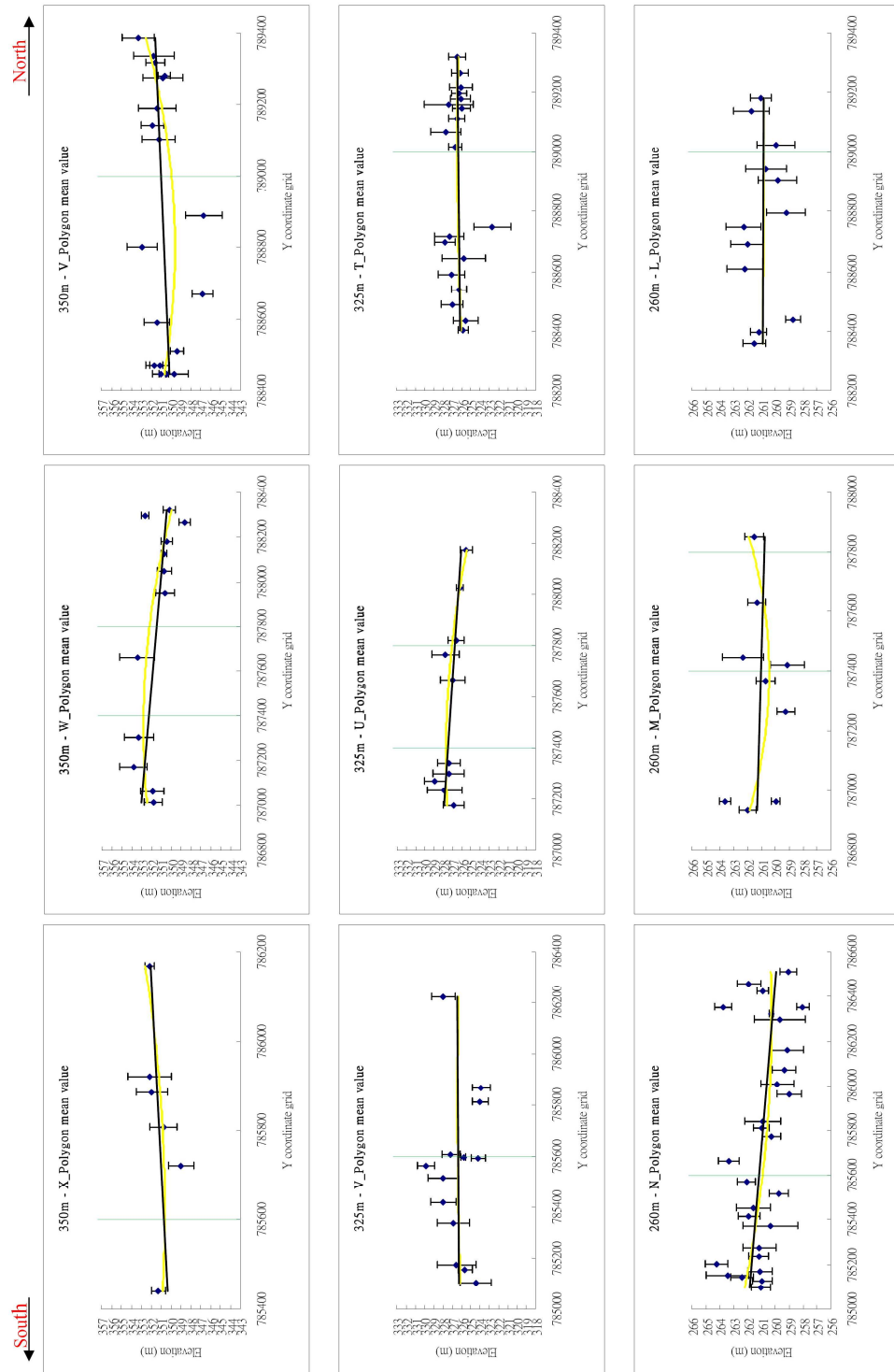


Figure 7.47C

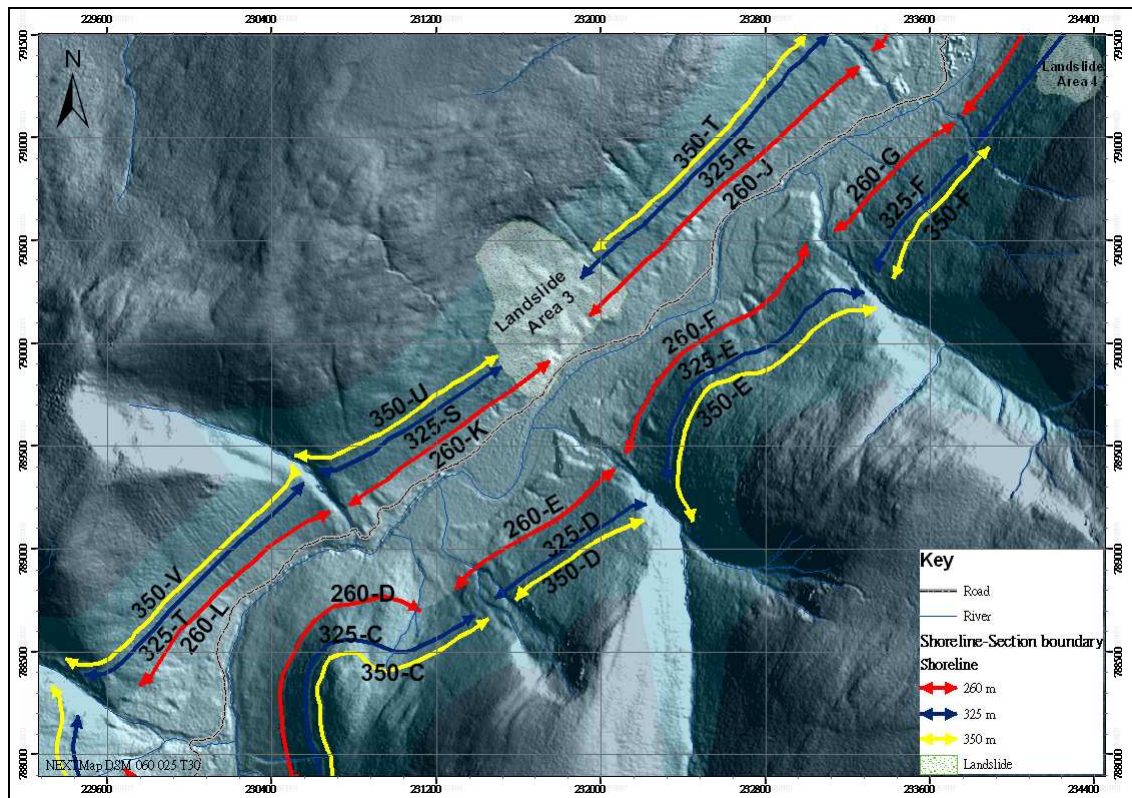
Figure 7.47 Projected shoreline surface altitudes of the Parallel Roads in the vicinity of landslide 2 on the western flank of the valley. Blue stars mark the ‘start’ and ‘end’ points of dislocation of each shoreline section. The X axis is the y value of the British National Grid Reference and the Y axis gives altitude in metres. Part A: scatter-plot of raw altitudinal values; Part B: suggested block dislocation pattern; Part C: Mean and standard values of the altitude scatter recorded for each polygon measurement set. For further explanation of symbols see p. 268



### **7.8.3 Area around landslip 3, Middle Glen Roy**

The landslide-affected area in area 3 (Figure 7.40) is about 500 m in length and 550 m in vertical height. Sissons and Cornish (1982b) described how both shorelines were severely dislocated adjacent to the landslip and concluded that this area was affected by glacio-isostatic uplift which compressed the crust and generated a reverse fault. The linear bedrock ridge they refer to is found above the 350 m shoreline, a few metres in width and extending 550 m in length, protruding above the adjacent ground. A narrow depression runs parallel to the ridge. All three shorelines were found to have been uplifted as much as 2.6~3.3 m above their normal altitudes in this vicinity. They proposed that the linear nature of the ridge and the depression combined with evidence of shoreline uplift indicated movement along a fault. Although no detailed geological map of this area is available to confirm this, the feature described by Sissons and Cornish (1982b) has a trend similar to a distinct fault mapped by Anderson (1956), situated c.10 km towards the north-west. The linear feature on the west bank of middle Glen Roy does not extend to the eastern flank of the valley, which Sissons and Cornish attributed to another fault, mapped by Anderson (1956), which runs along the axis of the Roy valley, and which confined local uplift to the western flank.

Landslide 3 is located within the K-J stretch of the 260 m shoreline, the S-R stretch of the 325 m shoreline and the T-U stretch of the 350 m shoreline (Figure 7.48) (Data were also provided in CD, Appendix 3.5). Altitudinal data obtained for stretches T, U, V on the 350 m, R, S, T on the 325 m, and J, K, L on the 260 m shoreline on the north-western side of the middle Roy valley are presented in Figure 7.49. The data for stretches D, E and F on both the 350 and 325 m shorelines, and for stretches E, F and G on the 260 m shoreline on the south-eastern side of the valley are presented in Figure 7.50.



**Figure 7.48 Stretches of the Parallel Roads from which NEXTMap altitude measurements were derived for Figures 7.49 and 7.50. Note that the Roads are not continuous, as depicted; the coloured lines show the geographical extent of each stretch and the arrow heads their terminations.**

Taking the north-western flank first, an interesting overall deformation pattern emerges from the data. The 350 m shoreline seems to be arched upwards in stretch U and bowed downwards in stretches V and T, with the blue stars marking the lateral limits of the upward arch (Figure 7.49A and C). This arch effect diminishes progressively in the corresponding stretches of the 325 m and 260 m shorelines (Figure 7.49A). The 2<sup>nd</sup> order polynomial regression calculations suggest a mean arching effect on the 350 m shoreline of up to 3.5 m extending over some 3.3 km, with the corresponding figures for the 325 m and 260 m shorelines being 2 m uplift over 1.1 km and 1-1.5 m uplift over 1.3 km, respectively. All three shorelines also show evidence of block dislocation, with the largest dislocation on each shoreline being close to the south-western margin of the landslip (Figure 7.49B).

On the exact opposite side of the valley, the amplitude of block dislocation is greater

than on the north-western flank, especially in the vicinity of the deep gully located at Y:790200 (Figure 7.50A and C). Here the 350 m shoreline rises along the length of stretch E towards the gully, but is severely dislocated close to the gully, first rising to a maximum of 354.5 m, before plunging to less than 348 m, a difference of 6.5 m over a distance of 200 m. The 325 m shoreline shows a similar pattern, with an amplitude of dislocation of c. 5 m over a distance of 100m or so. There is no evidence of such severe dislocation of the 260 m shoreline close to the gully, but this shoreline shows evidence for block dislocation along all three stretches, within a vertical range of up to 3 m (Figure 7.50C).

The data also suggest some arching of the shorelines, but this is of lower amplitude and is less distinct than on the north-western flank. Blue stars mark what are considered to be the lateral limits of warping affecting each shoreline (Figure 4.50A), and if this interpretation is correct, 2<sup>nd</sup> order polynomial data suggest an amplitude of warping of the 350 m shoreline of about 1.0 m over a distance of 1.95 km, with corresponding figures for the 325 m and 260 m shorelines being 0.5 m over 1.5 km and less than 0.5 m over 1.1 km for the 325 m and 260 m shorelines respectively.

The NEXTMap data for this part of the Roy valley show that the shorelines are severely disrupted on both sides of the valley with the largest dislocations being close to the landslip on the NW flank and to a major gully on the SE flank. The shorelines also appear to be arched or warped. Both the scales of dislocation and of warping are larger on the NW flank than on the SE flank. Clearly, the data indicate that localised faulting was not the only force acting on the shorelines: if the faulting effect was limited only to the NW flank, as suggested by Sissons and Cornish (1982b), then other factors have led to the deformation of the shorelines on the SE flank. This would be supported by the fact that the major dislocation of the shorelines has a lower amplitude on the SE flank

than on the NW flank. It is hard to understand why the fault does not continue across what is a very narrow part of the Roy valley, but this may well be the case. The NEXTMap data suggest, however, that similar deformational forces were affecting both sides of the valley, but diminished in magnitude from NW to SE, though a diminishing S to N trend can also be discerned in the data for the 325 m and 260 m shorelines on the SE flank (Figure 4.50 A and C).

North

South

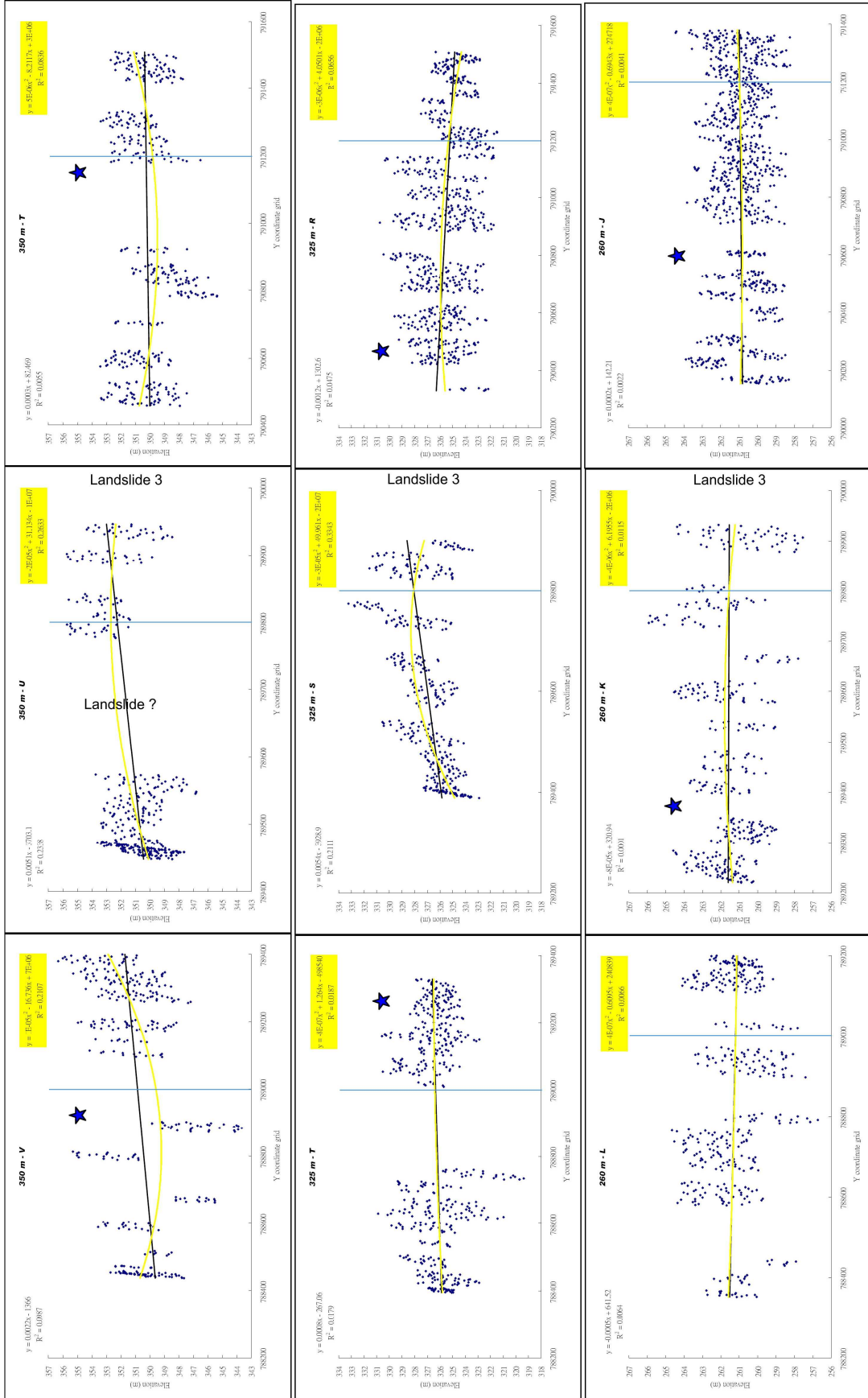


Figure 7.49A

North

South

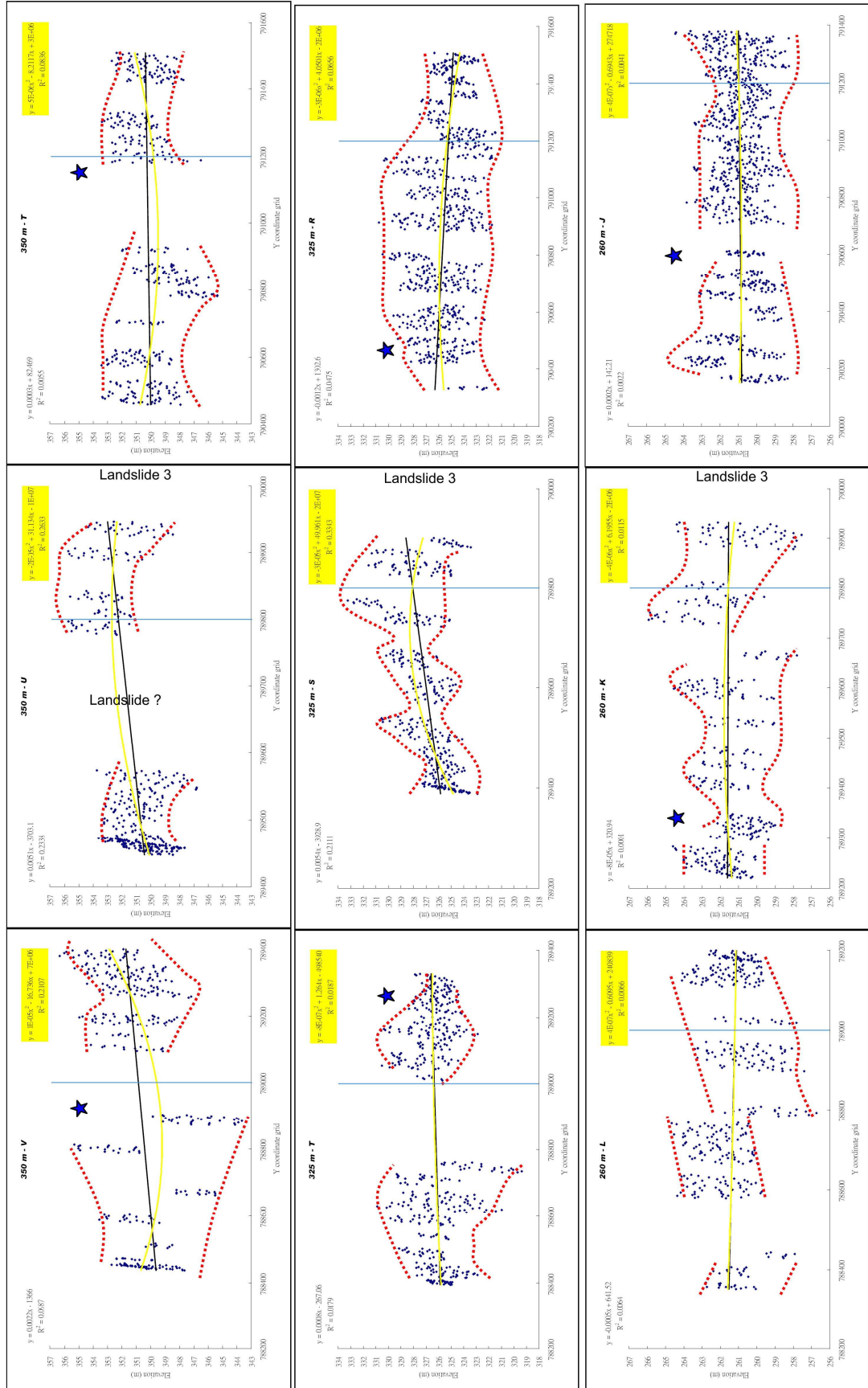


Figure 7.49B

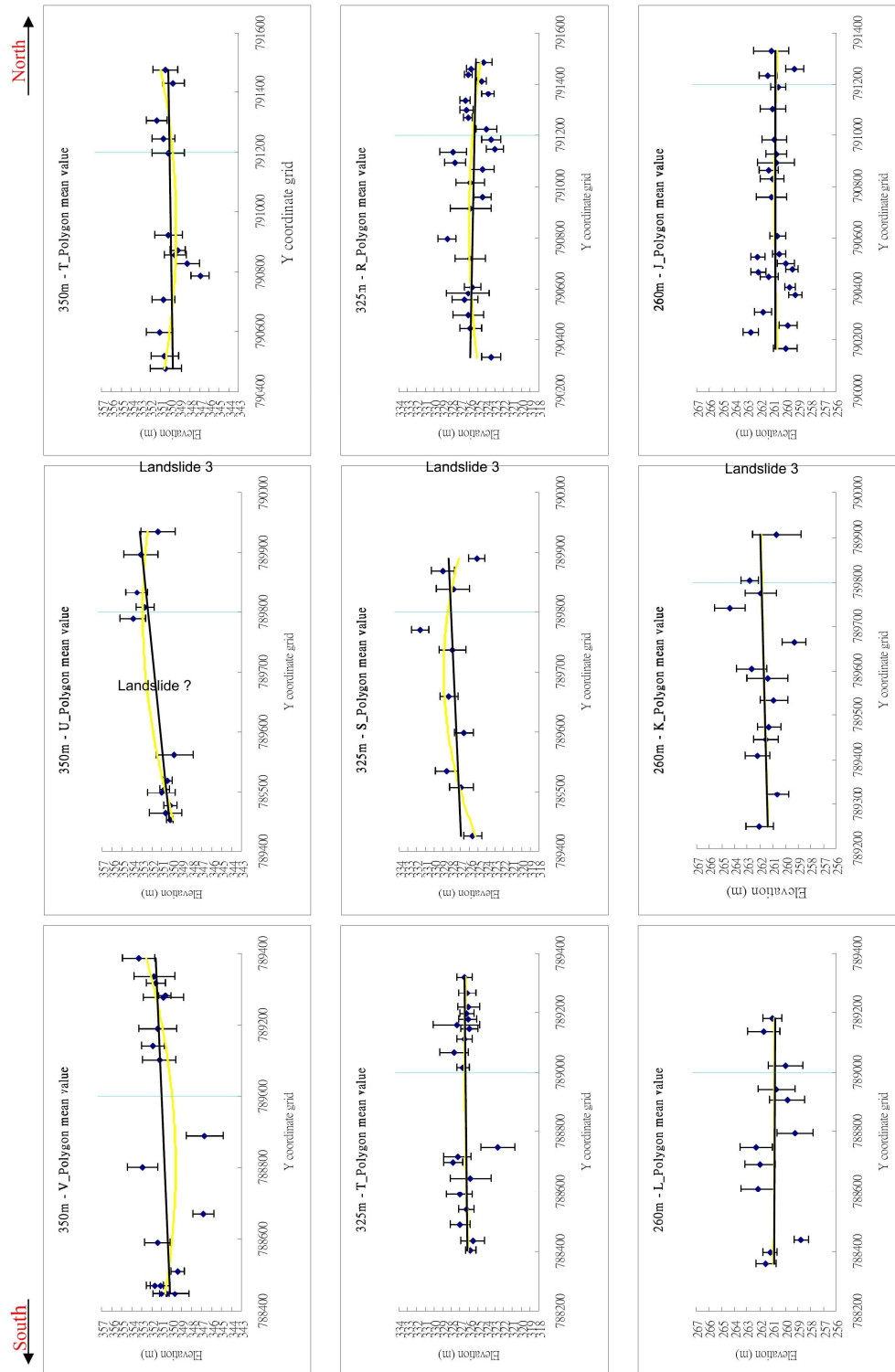


Figure 7.49C

Figure 7.49 Projected shoreline surface altitudes of the Parallel Roads in the vicinity of landslide 3 on the north-western flank of the Middle Roy valley. Blue stars mark the ‘start’ and ‘end’ points of dislocation of each shoreline section. The X axis is the y value of the British National Grid Reference and the Y axis gives altitude in metres. Part A: scatter-plot of raw altitudinal values; Part B: suggested block dislocation pattern; Part C: Mean and standard values of the altitude scatter recorded for each polygon measurement set. For further explanation of symbols see p. 268.

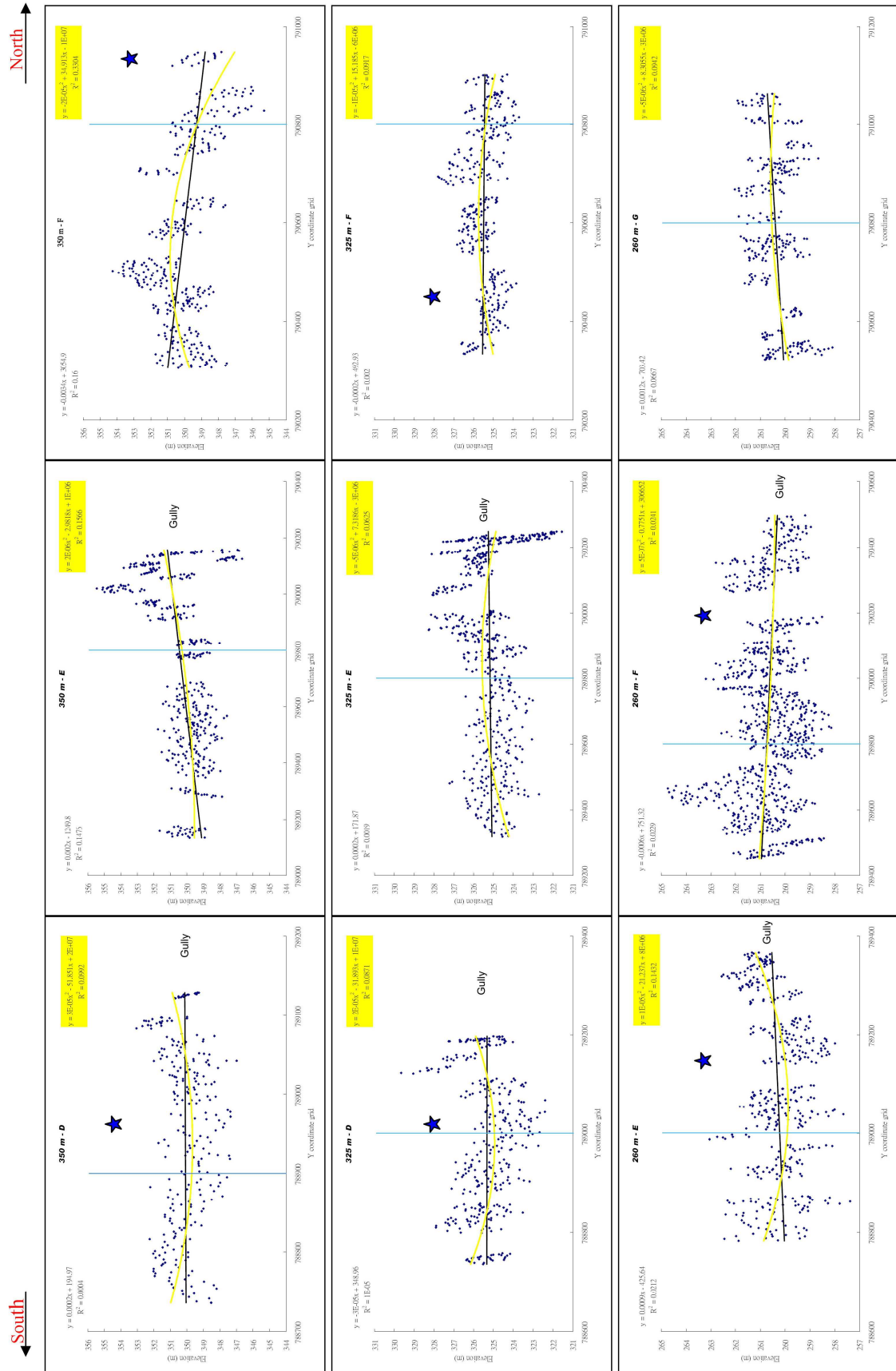


Figure 7.50A



North

South

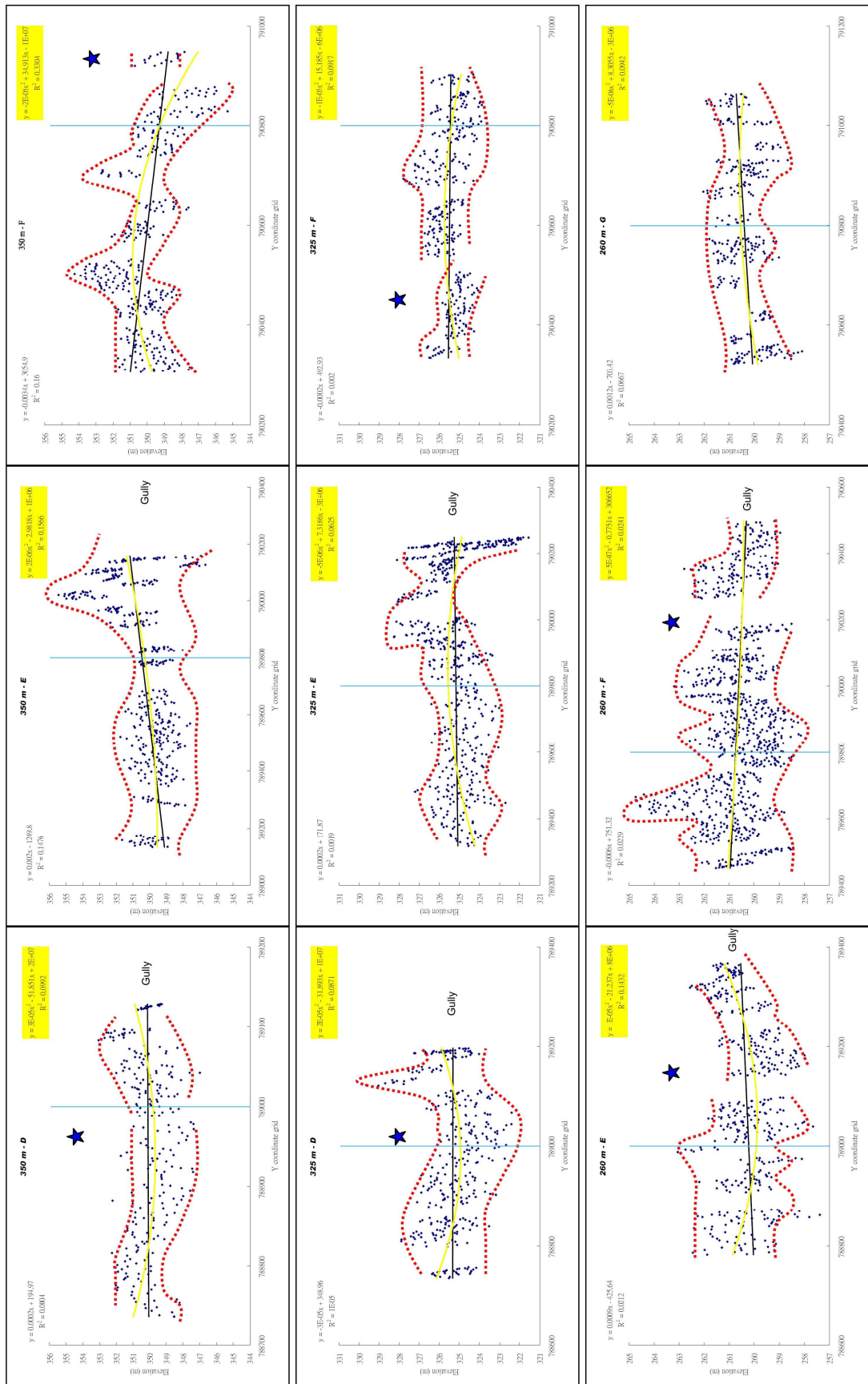


Figure 7.50B

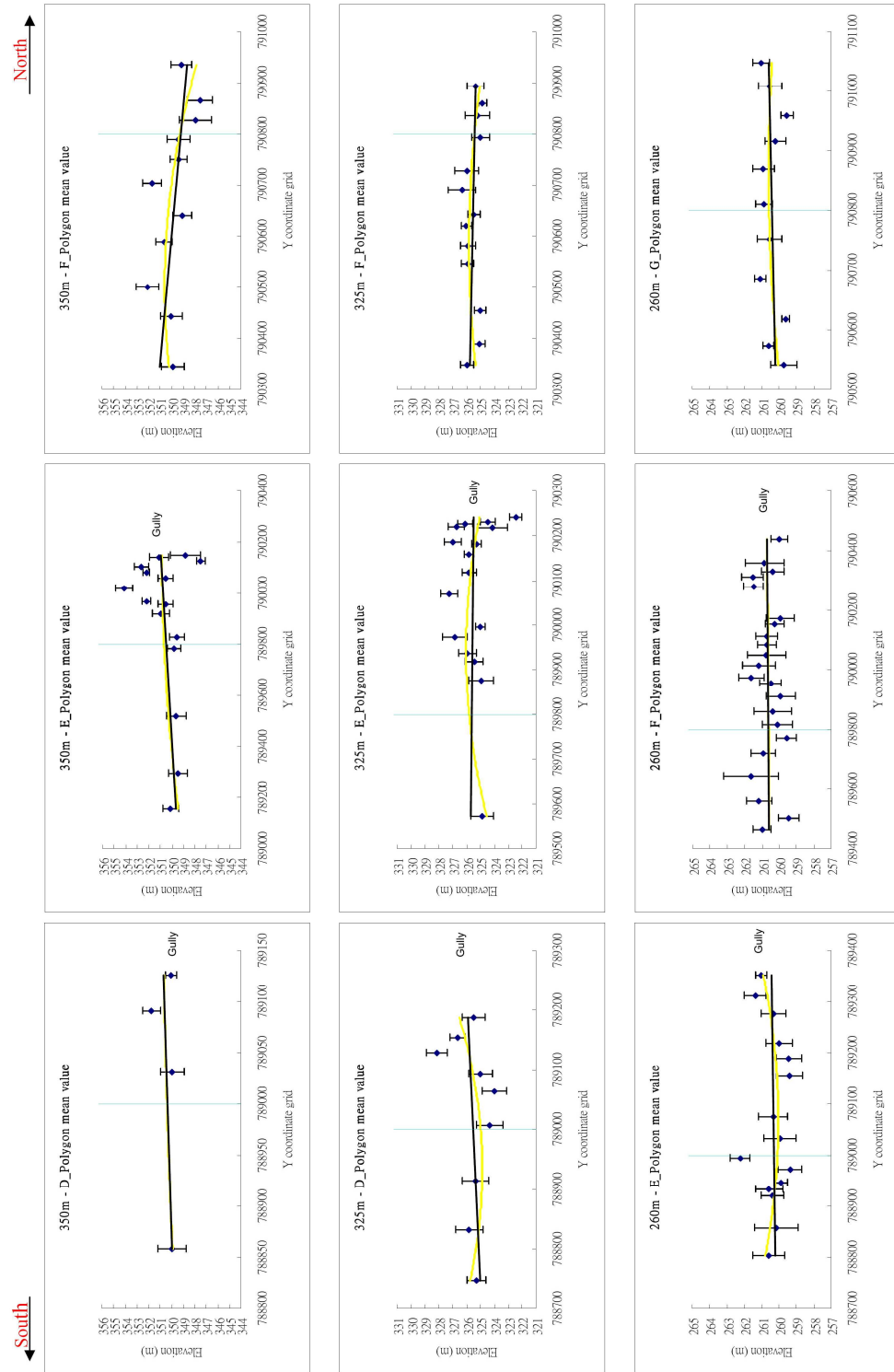


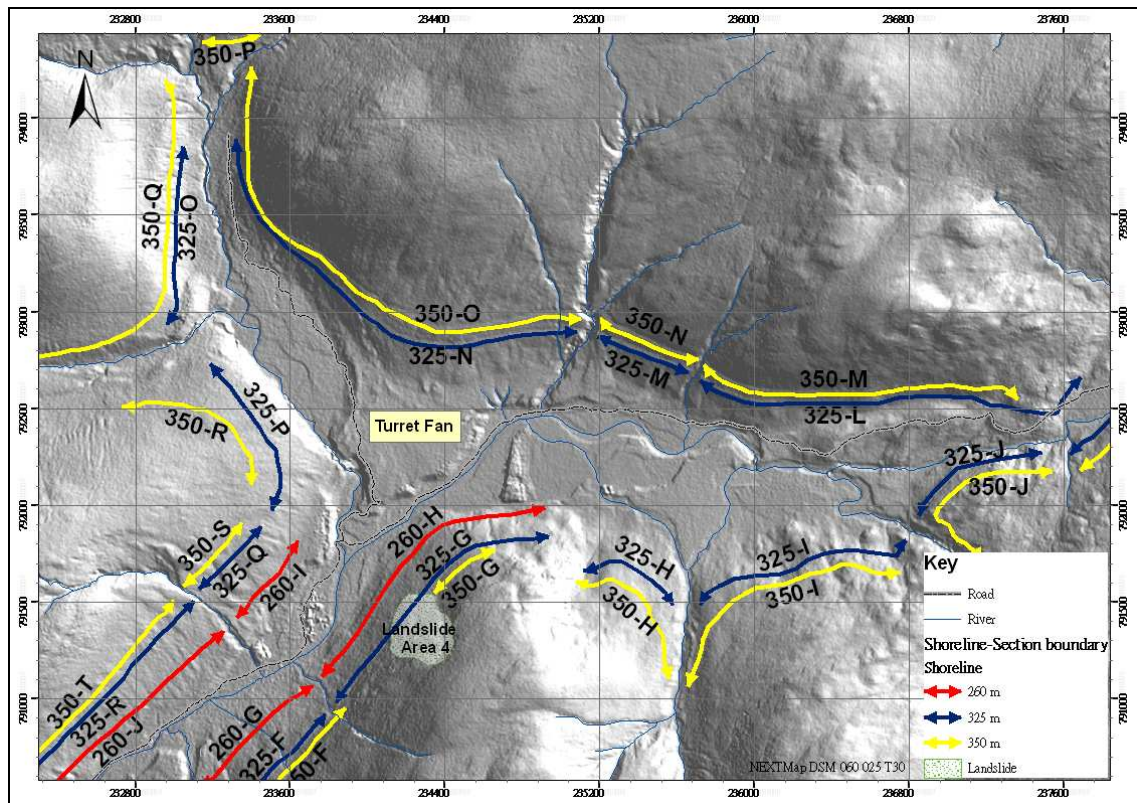
Figure 7.50C

Figure 7.50 Projected shoreline surface altitudes of the Parallel Roads in the vicinity of landslide 3 on the south-eastern flank of the Middle Roy valley. Blue stars mark the ‘start’ and ‘end’ points of dislocation of each shoreline section. The X axis is the y value of the British National Grid Reference and the Y axis gives altitude in metres. Part A: scatter-plot of raw altitudinal values; Part B: suggested block dislocation pattern; Part C: Mean and standard values of the altitude scatter recorded for each polygon measurement set. For further explanation of symbols see p. 268.

#### **7.8.4 Upper Roy, NE of the Turret fan**

The Turret fan, located near the confluence of Glen Turret and Glen Roy (Figure 7.51), has been regarded as an ice-marginal feature of Loch Lomond Stadial age (Sissons 1978, 1979b, 1983; Peacock and Cornish 1989). The 325 m and the 350 m shoreline are well developed and cut into bedrock for up to 12 metres in width in this vicinity. However, the 260m shoreline is weakly developed or absent, because the altitude of the valley floor is close to 260 m: the shoreline tapers out at the southern margins of the fan (Figure 7.51). Sissons and Cornish (1982b) found the base of the backwall of the 350 m shoreline to vary between 349.5 and 350.9 m on the northern bank of the River Roy and between 349.9 and 350.2m on the southern bank. The corresponding measurements for the 325 m were 325.1 to 325.5 m for the northern bank and 324.7 to 325.1 m for the southern bank. They concluded that these narrow ranges of altitudinal measurements indicated that no significant tectonic activities had disrupted the shorelines in the Upper Roy. In the present research, the 350 m shoreline stretches O to M and the 325 m shoreline stretches N to L on the northern bank of the Roy, and stretches H to J for both shorelines on the southern bank (Figure 7.51) were selected for NEXTMap measurement, to test this conclusion (data provided in the CD, Appendix 3.5).

The trend lines of stretch O of the 350m shoreline (Figure 7.52A and C) are nearly horizontal but show a gentle warp with an arch amplitude of about 1.0 to 1.5 m (Figure 7.52B). Stretches N and M do not show signs of warping but stretch N is lower than stretches O and M by about 1.0 to 1.5 m, and dips westwards. The 325 m shoreline also shows Regression lines have their lowest value around X:235200 and gradually rising up until point X:236000 in section M (marked with a blue star). The 325 m shoreline also shows evidence of downward displacement of the middle stretch (M) with respect to those stretches that flank it (N and L), the latter both dipping inwards towards stretch M, the eastward dip of stretch N being particularly pronounced. Both the 350 and 325 m



**Figure 7.51 Stretches of the Parallel Roads from which NEXTMap altitude measurements were derived for Figures 7.52 and 7.53. Note that the Roads are not continuous, as depicted; the coloured lines show the geographical extent of each stretch and the arrow heads their terminations**

shorelines, contrary to Sissons and Cornish's (1982b) conclusions, therefore do show evidence of dislocation with amplitude 0.5 to 1m over a tract of 2.3 km.

On the opposite side of the valley, there is also evidence of dislocation and block tilting of both shorelines (Figure 7.53). The 350 m shoreline appears to be arched across stretches H and I, with a marked dislocation (downward displacement of I relative to J) of about 1.0 m in scale (Figure 7.53A). Blue stars mark the limits of marked warping with overall amplitudes of about 1.0 m over a distance of 1.75 km for the 350 m shoreline and 1.3 km for the 325 m shoreline. Overall, the shorelines on both the northern and southern flanks of the upper Roy show evidence of deformation, and a degree of consistency, with downward displacement of the middle stretch on both flanks.

East

West

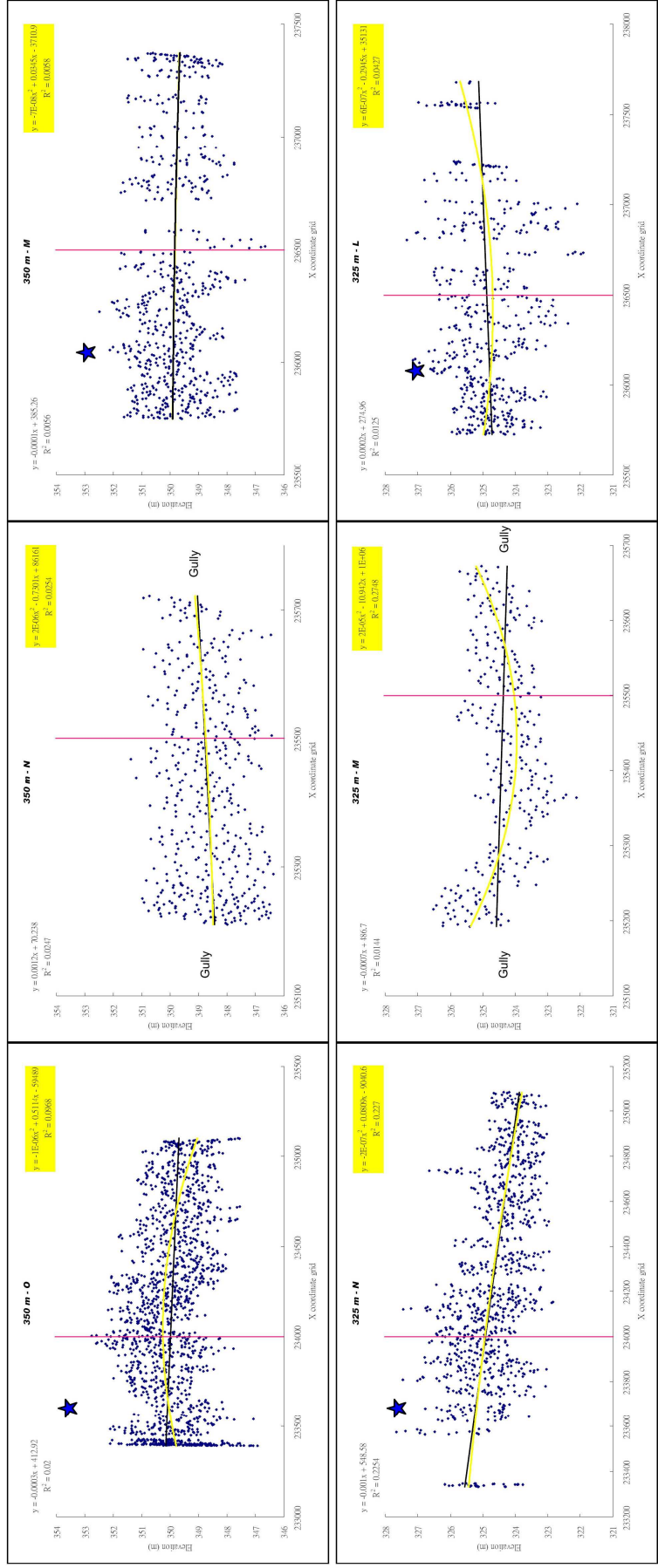


Figure 7.52A

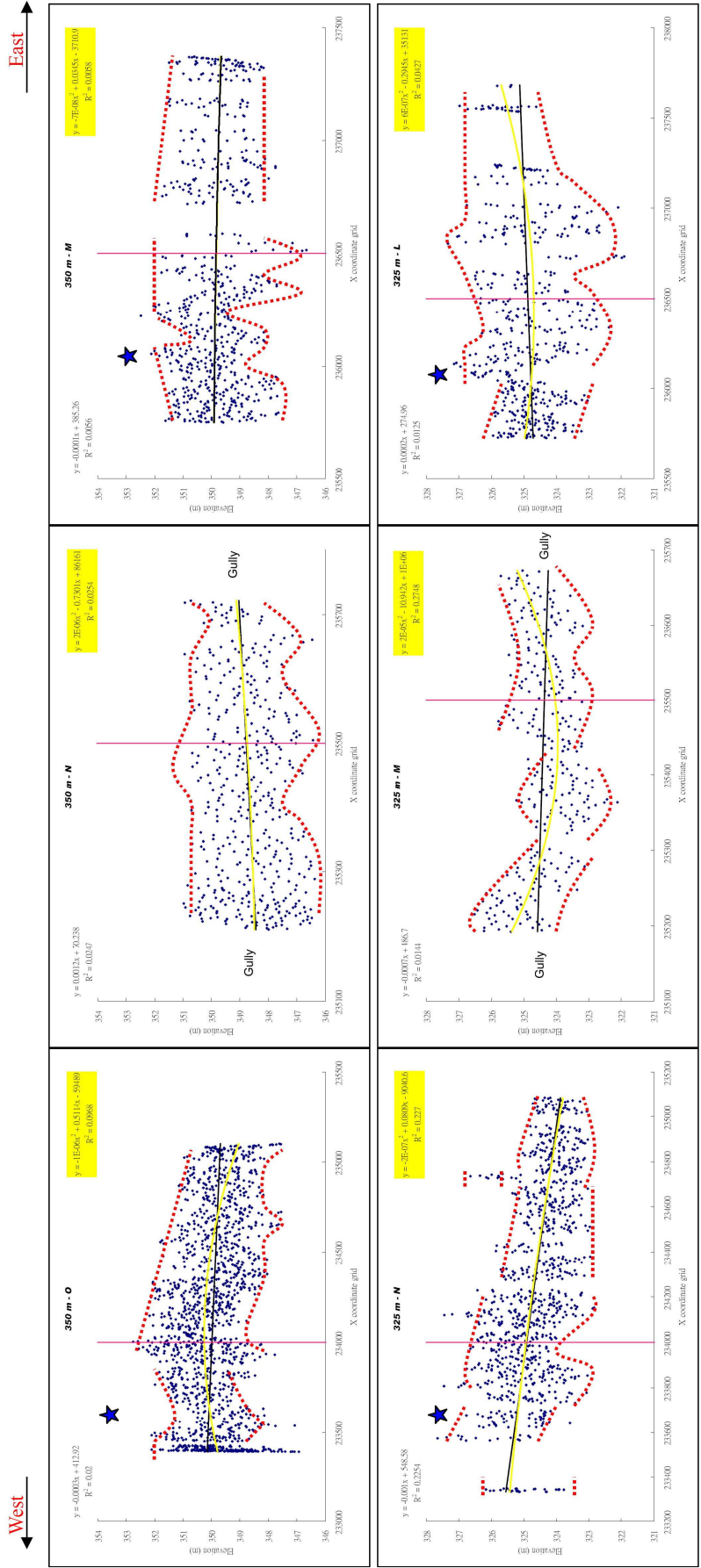
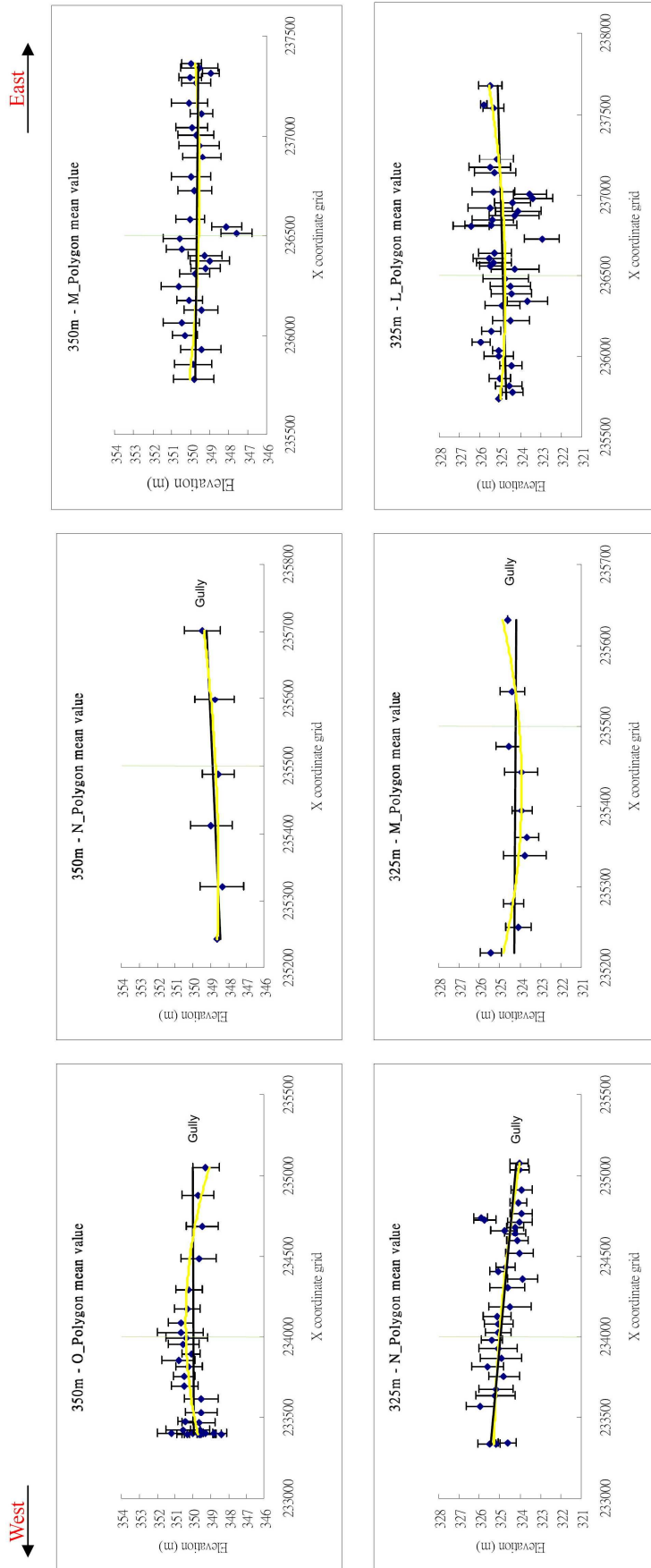


Figure 7.52B



**Figure 7.52 Projected shoreline surface altitudes of the Parallel Roads on the north flank of the Upper Roy, up-valley from the Turret fan. Blue stars mark the ‘start’ and ‘end’ points of dislocation of each shoreline section. The X axis is the y value of the British National Grid Reference and the Y axis gives altitude in metres. Part A: scatter-plot of raw altitudinal values; Part B: suggested block dislocation pattern; Part C: Mean and standard values of the altitude scatter recorded for each polygon measurement set. For further explanation of symbols see p. 268.**

**Figure 7.52C**

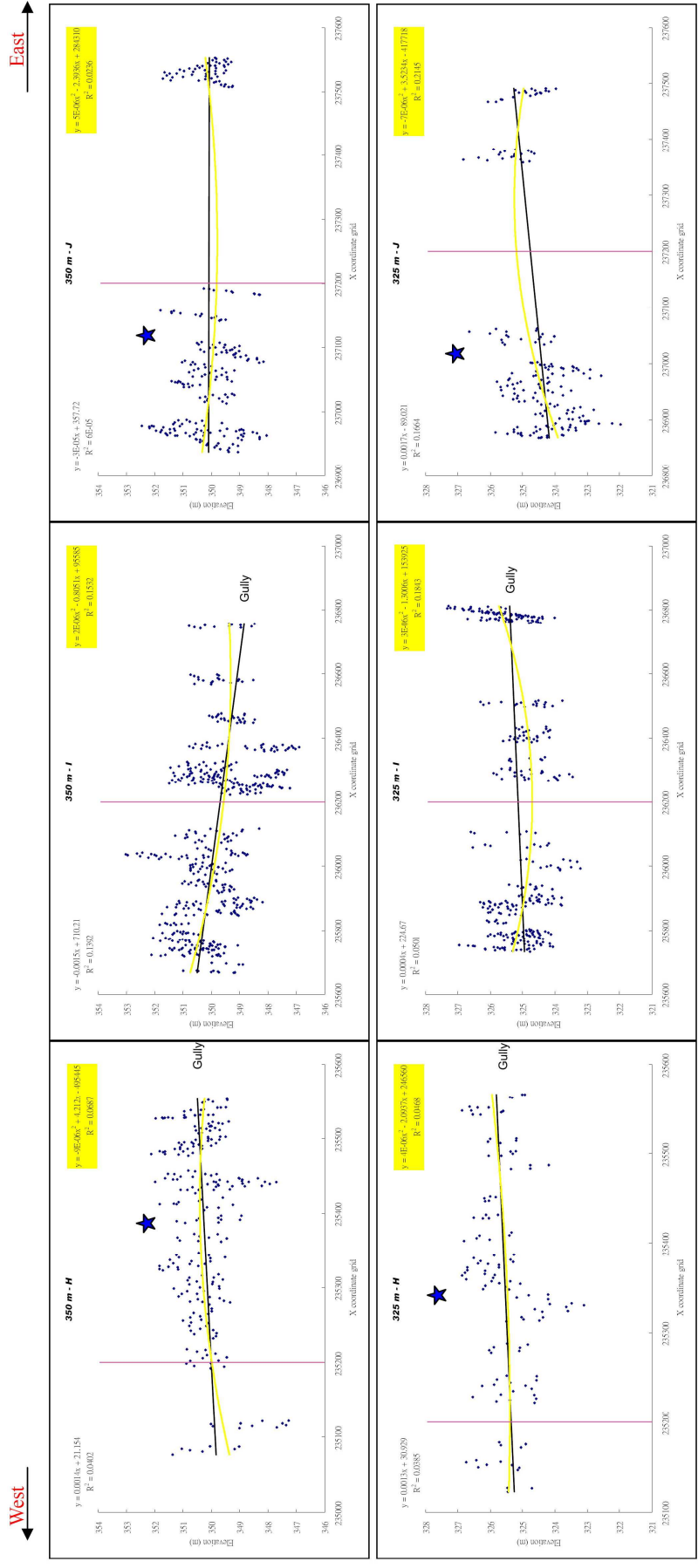


Figure 7.53A



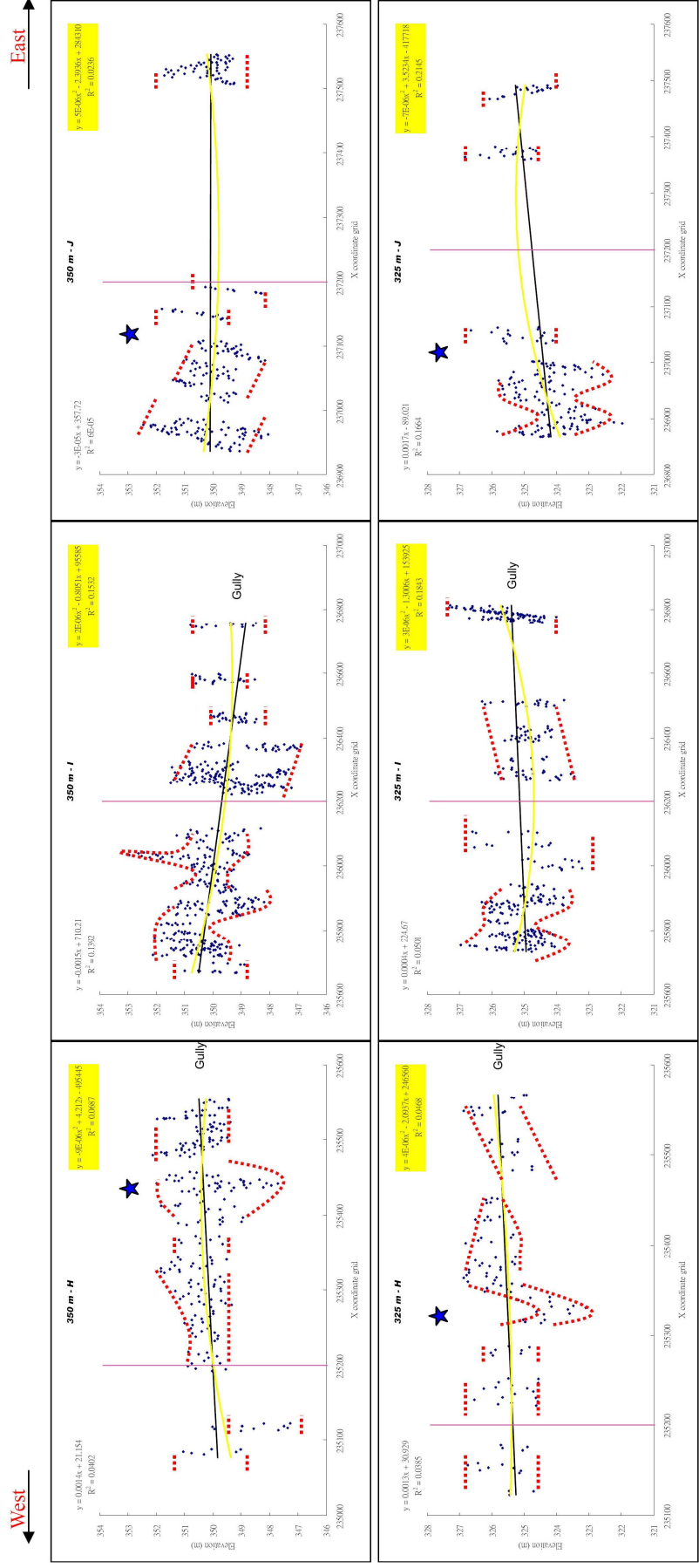
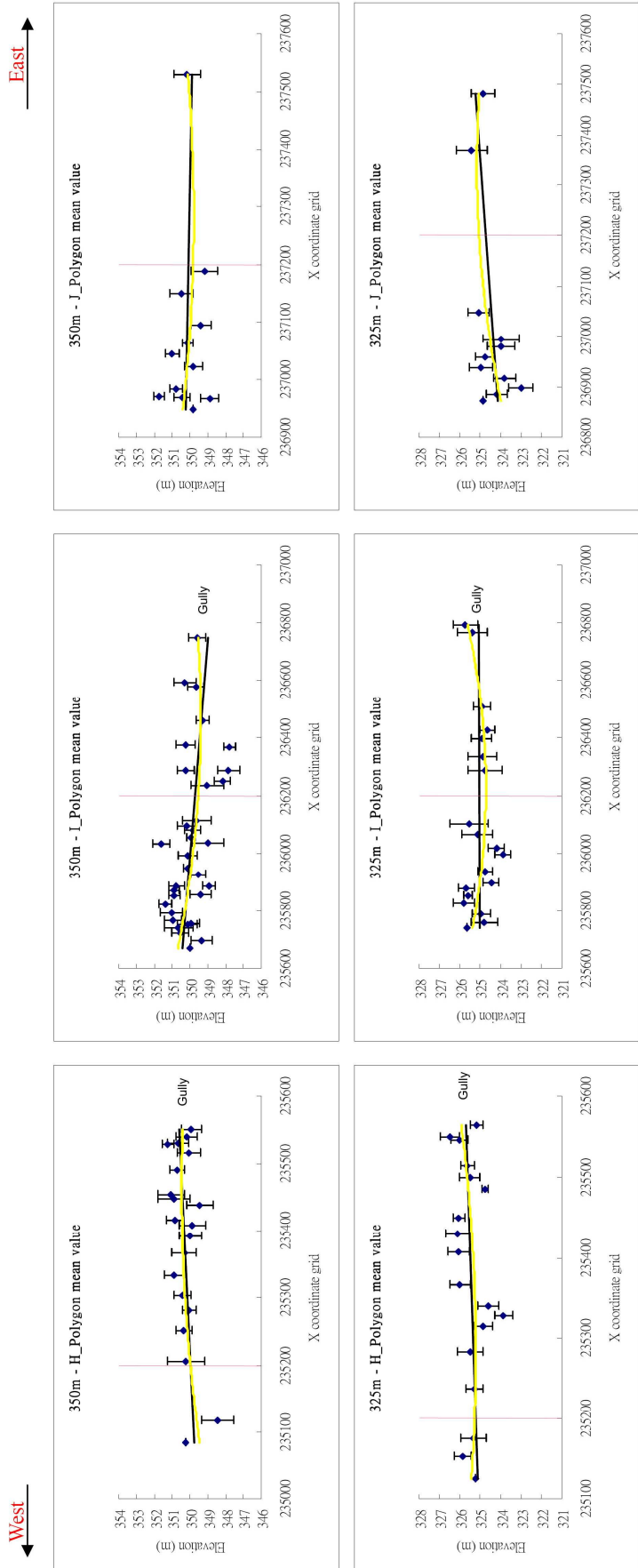


Figure 7.53B



**Figure 7.53 Projected shoreline surface altitudes of the Parallel Roads on the southern flank of the Upper Roy, up-valley from the Turret fan. Blue stars mark the ‘start’ and ‘end’ points of dislocation of each shoreline section. The X axis is the y value of the British National Grid Reference and the Y axis gives altitude in metres. Part A: scatter-plot of raw altitudinal values; Part B: suggested block dislocation pattern; Part C: Mean and standard values of the altitude scatter recorded for each polygon measurement set. For further explanation of symbols see p.268**

**Figure 7.53C**

## 7.9 Synopsis

A number of conclusions emerge from the information presented in section 7.8.

1. All stretches of the Parallel Roads examined in this thesis show some evidence of deformation, with the most marked dislocations often associated with landslips and major gullies, though severe dislocation can occur in other places too.
2. Some sections appear to be warped or arched, but this trend is usually disrupted by block tilting or displacement.
3. In general, the scale of deformation is greater in the lower and middle reaches of Glen Roy than in the upper reach, but the pattern of dislocation is so complex as to blur the overall picture.
4. The scale of deformation also seems to have a W-E gradient in some sectors, as for example in the middle reach of the Roy (section 7.8.3) where deformation is more pronounced on the NW than on the NE flank of the valley, or the shorelines on the northern flank of the upper Roy which shows more marked warping or tilting on the western than on the eastern stretches (section 7.8.4).
5. The scale of deformation tends to be greatest on the 350m shoreline, and diminishes successively on the 325 m and 260 m shorelines, but there can be localised exceptions which appear random, as for example the marked down-warping and block displacement of stretch N of the 260 m shoreline on the western flank of the lower Roy, near landslip 2 (Figure 7.47, section 7.8.2).
6. The pattern of displacement can be similar between two or all three of the shorelines, though different in scale, such as, for example on the northern flank of the upper Roy (Figure 7.52) or shown in sector E of both the 350 and 325 m shorelines on the south-eastern flank of the middle Roy (Figure 7.50). In the majority of cases, however, there is little accord in the scale and style of deformation affecting shoreline lengths lying immediately above or below each other. The direction of tilting can be the opposite in vertically aligned sections, or one road may appear

warped while another immediately above or below it may show block displacement. The pattern is exceedingly complex, and seems to indicate that each road was deformed independently, except where locally affected by a major landslide or fault.

The question arises as to what may be causing this complex pattern. It could simply be the result of the compound effects of the loading and unloading of the valley during ice growth and melting, associated with loading and unloading caused by lake volume change, which in turn may have activated the landslips and faults. However, one further possibility, or one further complication may be forebulge effects. As the ice advanced into the area, in the views of some to reach limits at the Viewpoint and the Turret Fan (Figure 8.1), a forebulge may have impacted the area, some distance ahead of the ice margins. The forebulge would, of course, be migratory, as would the maximum displacement it may have caused. Equally, migrational forebulge effects might have affected the valley during ice decay, as the local ice loads dissipated. This hypothesis will be returned to in the sections which follow, after an examination of the whole NEXTMap altitudinal data-set that is available for Glen Roy, using trend-surface analysis.

### 7.10 Analysis of longitudinal shoreline gradients: trend-surface analysis

The full altitudinal data-set for each of the three Glen Roy shorelines is shown on Figure 7.54 projected on to two orthogonal planes of projection and trendlines calculated using linear and second order polynomial regression. The data clearly demonstrate that all three shorelines have broadly similar trend directions when viewed either on a S-N or W-E projection plane. However, the projections in Figure 7.54, abstracted directly from NEXTMap measurements, do not retain information on the spatial referencing of measured points, but only their projected positions along the projection plane. Hence the data cannot be interrogated directly. This was resolved by transferring all of the data to MS Excel workbooks which enabled the data to be plotted at a higher resolution and the geo-referencing co-ordinates to be retained (e.g. the data for selected stretches of the 260m shoreline illustrated in Figure 7.55). Linear and 2nd order polynomial regression calculations for the resulting S-N and W-E trend-lines for each shoreline are provided in Table 7.14 (the data are provided in the CD, Appendix 3.5). The polynomial regression equations tend to have the higher  $R^2$  values and hence the better data interpretation capability, but the linear trends are retained for easier illustration purposes.

**Table 7.14 Calculated gradients for Glen Roy shorelines based on NEXTMap altitudinal measurements using linear and 2<sup>nd</sup> order polynomial regression.**

<u>Shoreline</u>	<u>S-N gradient</u>		<u>W-E gradient</u>	
	<u>(m km<sup>-1</sup>)</u>	<u>R<sup>2</sup> value</u>	<u>(m km<sup>-1</sup>)</u>	<u>R<sup>2</sup> value</u>
260 m (linear)	0.0731	0.0193504	0.113	0.0190854
260 m (polynomial)	0.072	0.0213814	0.1123	0.0191622
325 m (linear)	0.1378	0.0642915	0.1763	0.0969187
325 m (polynomial)	0.1402	0.0648677	0.1431	0.113868
350 m (linear)	0.107	0.0411956	0.0742	0.0313364
350 m (polynomial)	0.1081	0.0412356	0.0809	0.0389959

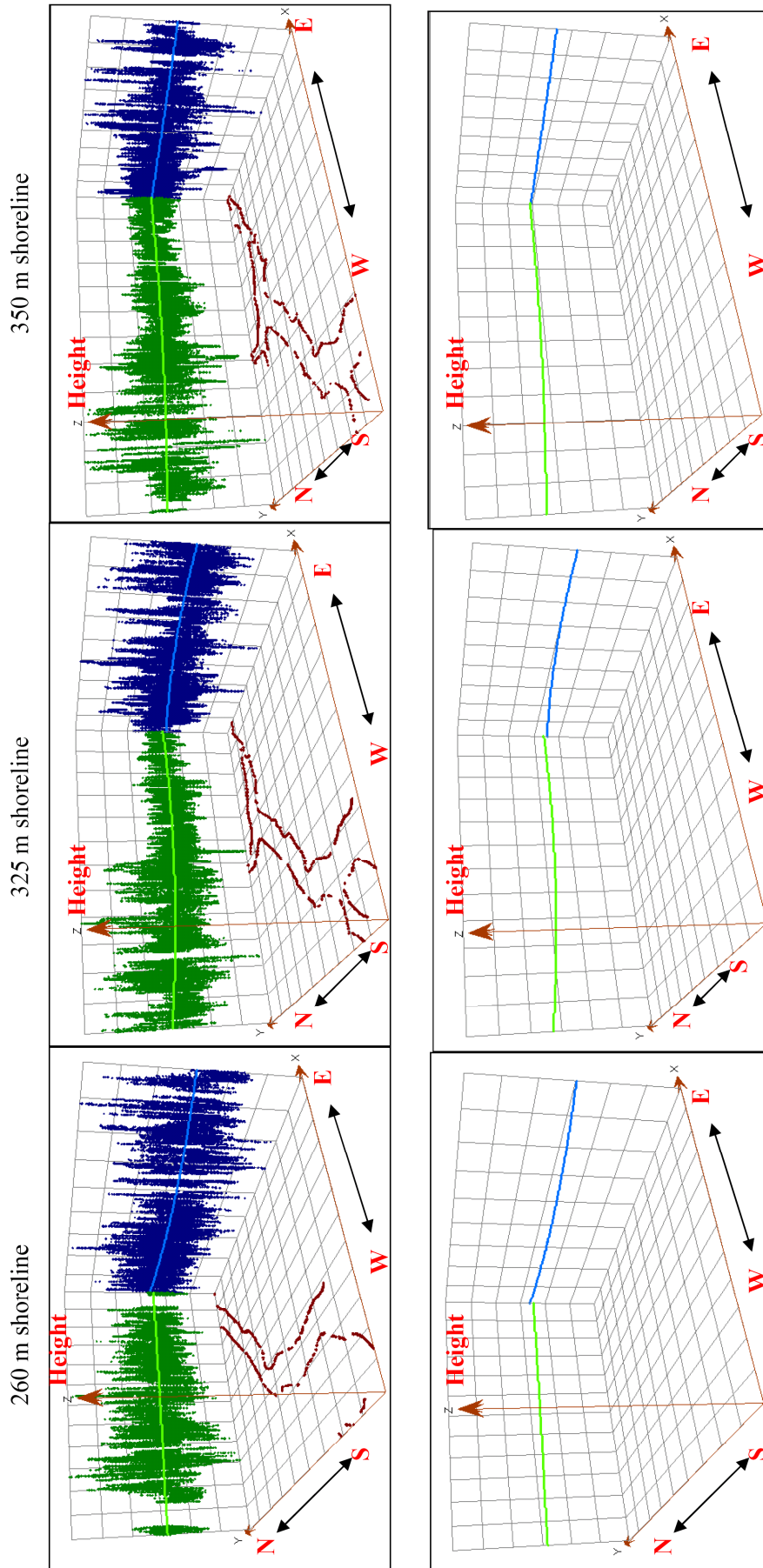
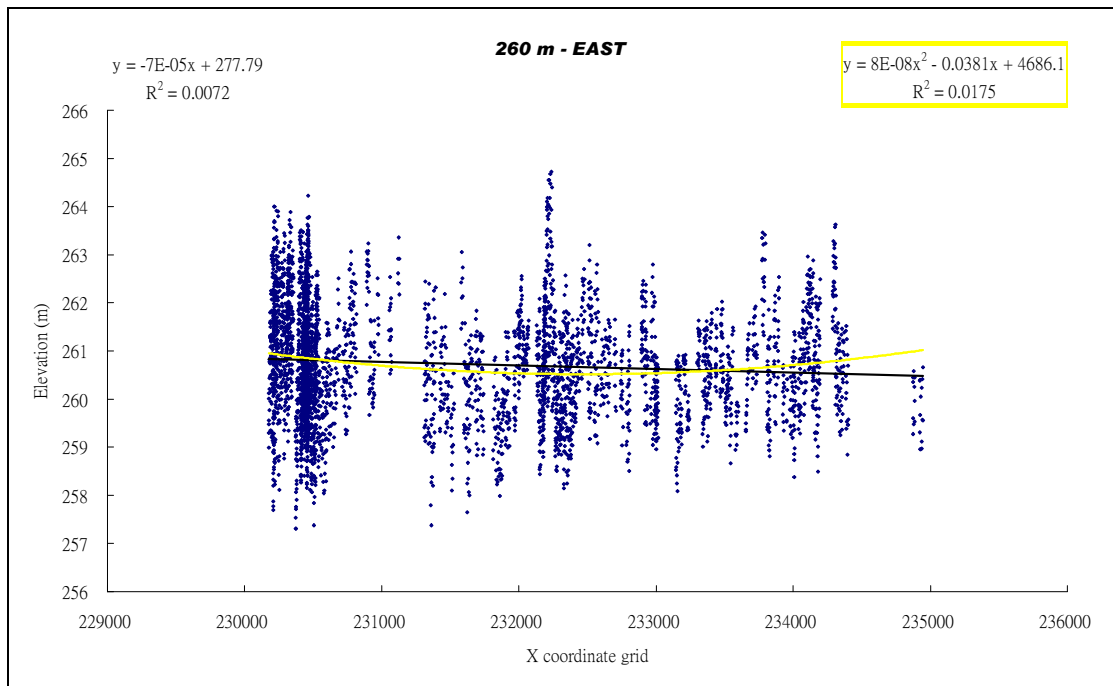
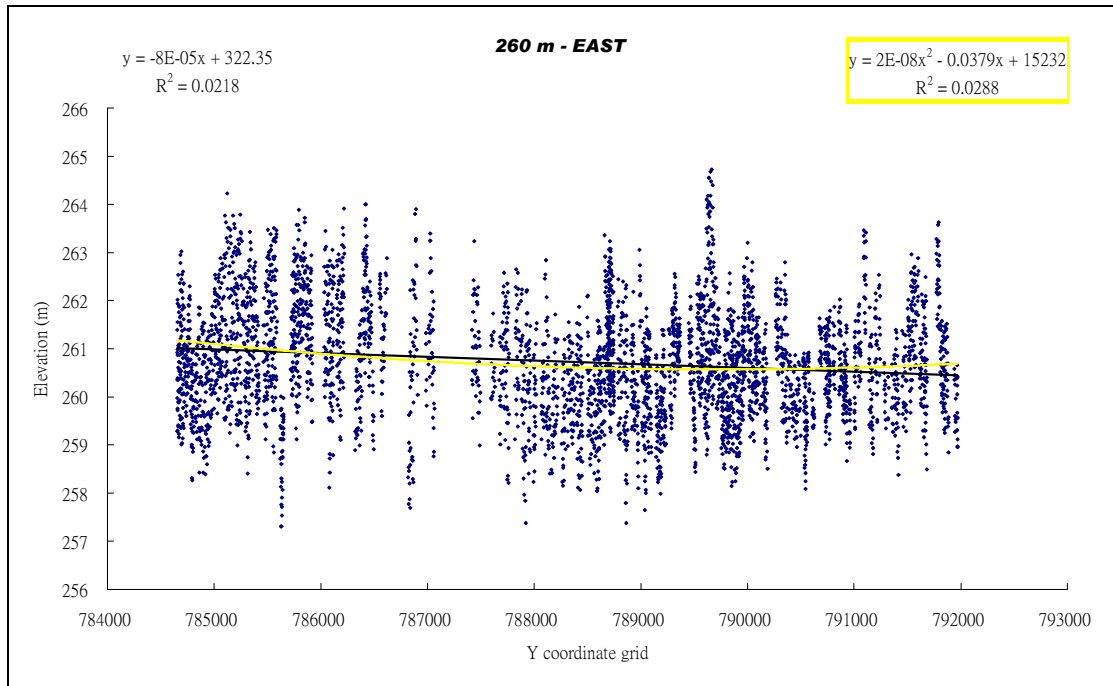


Figure 7.54 Trend surface data for the Glen Roy shoreline surfaces. The X axis is aligned on W-E grid coordinates and the Y axis on N-S grid co-ordinates. The Z axis is altitude (m) O.D. The spatial distribution of the co-ordinates of shoreline fragments, measured as XY co-ordinates on the OS grid, have been projected onto N-S and W-E axes to show overall two-dimensional gradient trends that are represented by 2<sup>nd</sup> order polynomial regression lines



**Figure 7.55 Example of the density of altitudinal information available for shoreline fragments. Here the data for a part of the 260 m shoreline are illustrated, using a S-N plane of projection (top diagram) and a W-E plane of projection (bottom). Linear (black) and 2<sup>nd</sup> order polynomial (yellow) regression lines are plotted through the data. Regression equations and R-square values are on the upper right and left side of the diagram**

**Table 7.15 Isobase contour parameters obtained by Dawson *et al.*, 2002 for the surfaces of the Parallel Roads of Glen Roy.**

Shoreline		Contour Plot		
		A	B	C
350 m shoreline	<i>f</i> ratio	0.749	0.906	0.67
	Bearing	N26°E	N16°E	N26°E
	Number of fragments	30	15	39
	Isostatic tilt (m km <sup>-1</sup> )	0.11	0.13	0.14
325 m shoreline	<i>f</i> ratio	0.898	0.960	0.841
	Bearing	N37°E	N25°E	N32°E
	Number of fragments	37	25	38
	Isostatic tilt (m km <sup>-1</sup> )	0.14	0.14	0.14
260 m shoreline	<i>f</i> ratio	0.887	0.966	0.664
	Bearing	N70°E	N63°E	N70°E
	Number of fragments	24	18	39
	Isostatic tilt (m km <sup>-1</sup> )	0.11	0.11	0.13

Dawson *et al.* (2002) used instrumental levelling to obtain measurements of the surfaces of the Parallel Roads in Glen Roy and from the results calculated their surface gradients (Table 7.15). According to their data, the tilts of the three shorelines along bearings of N26°E to N16°E are all between 0.11 and 0.14 m km<sup>-1</sup>. There is very little difference in gradient between the three shorelines, though the 325 m shoreline gives the consistently steeper value. These values compare with calculations of the long-shore gradient of the Main Rock Platform of 0.12 to 0.16 m km<sup>-1</sup> (Firth *et al.*, 1993). The data generated from NEXTMap (Table 7.14) generally suggest shallower gradient values, by about 2 to 3 cm km<sup>-1</sup>. Exceptions are the gradients of 0.1411 m km<sup>-1</sup> obtained for the W-E polynomial regression for the 325 m shoreline, which is very close to Dawson *et al.*'s estimate for the same feature, and 0.1729 m km<sup>-1</sup> for the calculated linear regression on the same feature – 3 cm per kilometre more steep than any other gradient calculation reported thus far. Dawson *et al.*, (2002) used trend surface analysis to reconstruct the three-dimensional form of the shorelines, and subsequently to construct isobases of shoreline uplift/deformation. This approach was also employed in the current research,



but based on a much higher number of altitudinal measurements.

In the present research, isobase maps for the three shorelines in Glen Roy were generated by the following procedures. First, each of the shorelines and their associated altitude measurements were separated into east, west and north sectors with respect to their position in the Roy Valley (data provided in the CD, Appendix 3.5). Second, trend surface analysis was computed for each shoreline group. The main purpose of this step was to obtain separate regression equations for each geographical sector. The regression method selected for this step was linear regression, for it is simpler for representing the overall surface trends. For each shoreline sector, regression equations were solved for both the YZ and XZ planes of projection. Third, a number of geo-referenced root points (obtained from YZ and XZ grid co-ordinates) were selected in order to display the resulting isobase contours (data provided in the CD, Appendix 3.6). The isobase values are calculated from the root points obtained in step 3 by the IDW interpolation tool (Inverse Distance Weighted) which is integral to the Spatial Analyst model of Arc GIS. This software can be used to predict altitudinal values for any unmeasured location. This method assumes that things that are close to one another are more alike than those that are farther apart, which means each measured point has a local influence that diminishes with distance. The IDW tool uses the measured values surrounding the prediction location and gives greater weight to points closer to the prediction location than those farther away. The results are presented for each of the three shorelines in Figures 7.56 to 7.58, and compared with Dawson *et al.*'s (2002) results in Figure 7.59.

Dawson *et al.* concluded that the surface of the 350 m shoreline declines towards between N16°E and N26°E, the 325 m towards N25°E and N37°E and the 260 m shoreline towards between N63°E and N70°E. Hence the highest shoreline has the more northerly dip, and the youngest the most easterly, implying a shift in the location of the

centre of glacio-isostatic depression and rebound (Figure 7.60). The new results presented here suggest the reverse order, with the gradient of the 260 m shoreline inclined towards between N39°E and N49°E, the 325 m shoreline towards between N48°E and N58°E and the 350 m shoreline towards between N65°E and N75°E. These results suggest a shift in the centre of glacio-isostatic depression and uplift from a position towards the west of Glen Roy at the time of formation of the 350 m shoreline, to a more south-westerly location at the time of formation of the 260 m shoreline. The differences between the two data-sets could reflect the very much higher density of measured points used in the NEXTMap-based experiment.

Dawson *et al.*, (2002), based on their isobase reconstructions, suggested that the tectonic uplift centre shifted from the south-west to the south when the lake water in Glen Roy and vicinity rose from the 260 m to the 350 m level. This appears plausible, because the ice initially built up in the mountains to the west of the Glen.

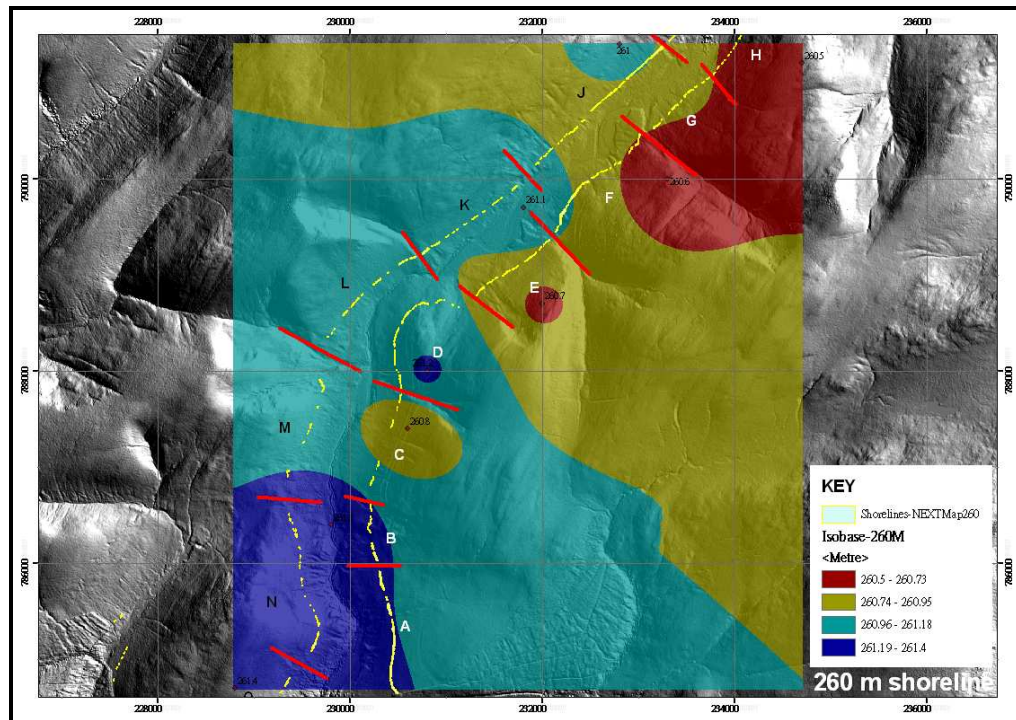


Figure 7.56 Isobase contours for the 260 m shoreline in Glen Roy generated using NEXTMap-based altitudinal measurements.

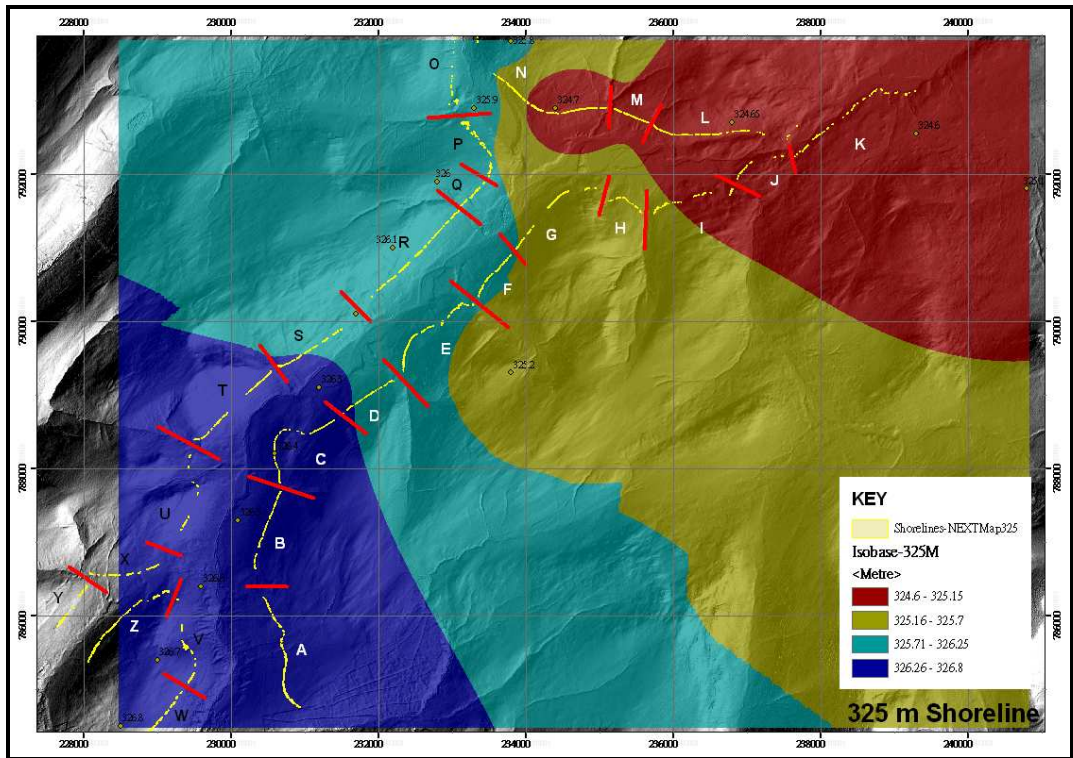


Figure 7.57 Isobase contours for the 325 m shoreline in Glen Roy generated using NEXTMap-based altitudinal measurements.

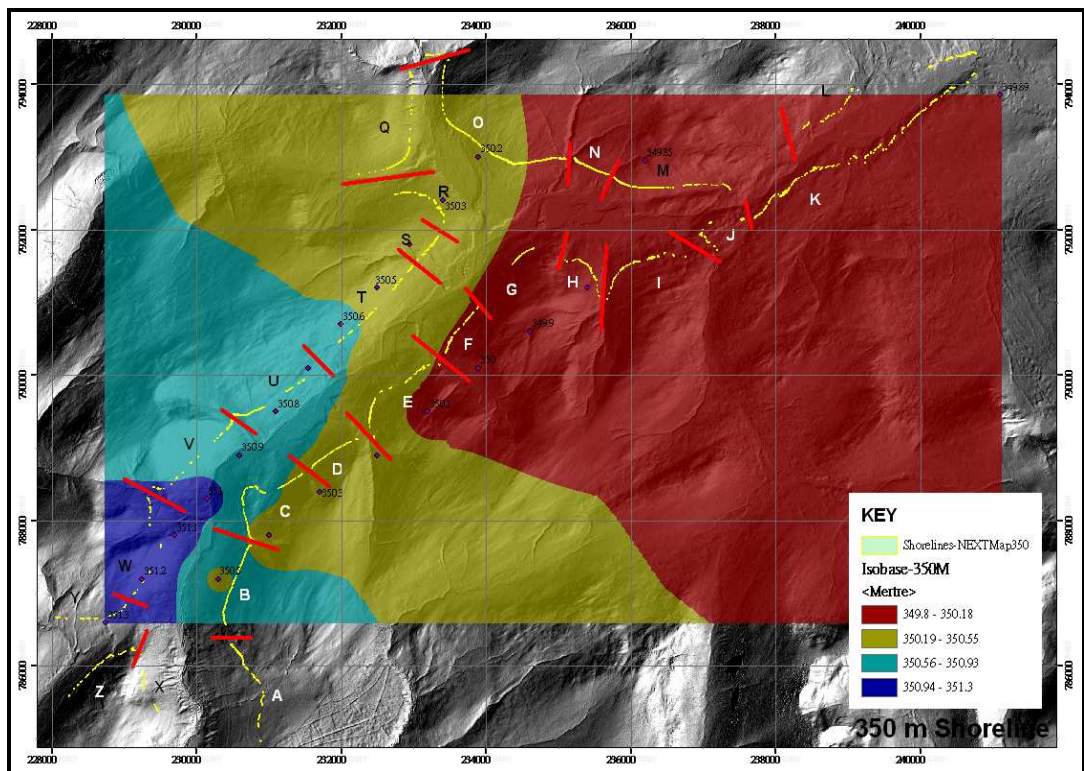
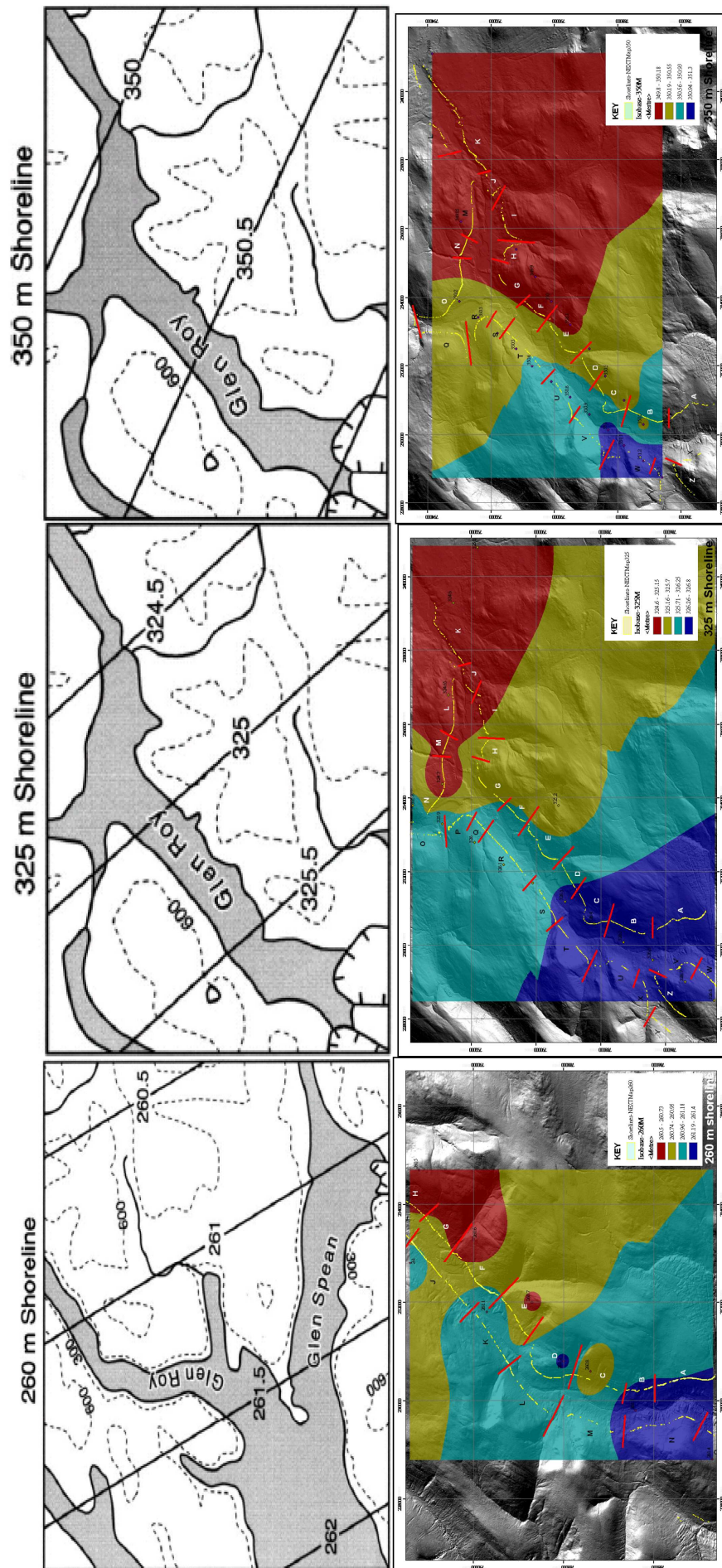


Figure 7.58 Isobase contours for the 350 m shoreline in Glen Roy generated using NEXTMap-based altitudinal measurements.



**Figure 7.59**  
**Comparison of the**  
**isobase maps**  
**generated (top) by**  
**Dawson *et al.*, (2002)**  
**and (bottom) in the**  
**present research.**

Hence local ice-loading might have affected the area during ice build-up. However, the new NEXTMap results perhaps suggest a different dynamic, possibly as a result of ice decay while the lakes were falling from the 350 m to the 260 m level (Figure 7.61). Under this scenario, local ice-loading has a more southerly impact at the start of the process, and drifts westwards during ice-decay, as a result of the ice diminishing in volume towards the source areas. The complication, of course, is that the 260 m and 325 m shorelines are thought to have formed during both the rising and falling lake sequences (Sissons, 1978; Palmer *et al.*, 2010), and differences in ice-mass distribution over that period could have led to different loading patterns and hence deformational stresses, perhaps accounting for some of the ‘noise’ in the altitudinal data. The 350 m lake, on the other hand, was formed during one phase only, and hence in theory this shoreline might be expected to be simpler in form. However, Sissons (1978) noted that the 350 m shoreline surface was the most susceptible to debris accumulation, while this shoreline appears to have been the most short-lived (Palmer *et al.*, 2010) and hence may not have been as well developed as the others.

Another complication might be glacier forebulge effects, as proposed in section 7.9, and based on an analysis of the deformation features throughout the Roy Valley in section 7.8. The glaciers in the region during the Loch Lomond Stadial were relatively small, by global standard, and there is little information in the literature concerning possible forebulge effects of the scale proposed for Glen Roy. The importance of these new data from Glen Roy, however, is that they appear to show evidence of shifting deformational isostatic effects during ice build up or ice decay at a temporal and spatial level of resolution that is relatively unique. This level of detail is only possible because of the three very distinct shoreline surfaces that were formed over a very short period of time – according to Palmer *et al.* (2010), within a total period of 515 years. Further research of this type, perhaps using NEXTMap but ‘ground-truthed’ more robustly at a number of

places, might reward the effort by providing a clearer picture of the pattern of ice-loading or unloading in this region during the latter stages of the Loch Lomond Readvance.

This concludes the examination of the distribution, form and gradients of the Parallel Roads, except that the causes of the deformation of the roads is further examined in the concluding chapter, Chapter 8, where the shoreline data are integrated with other lines of evidence examined using NEXTMap.

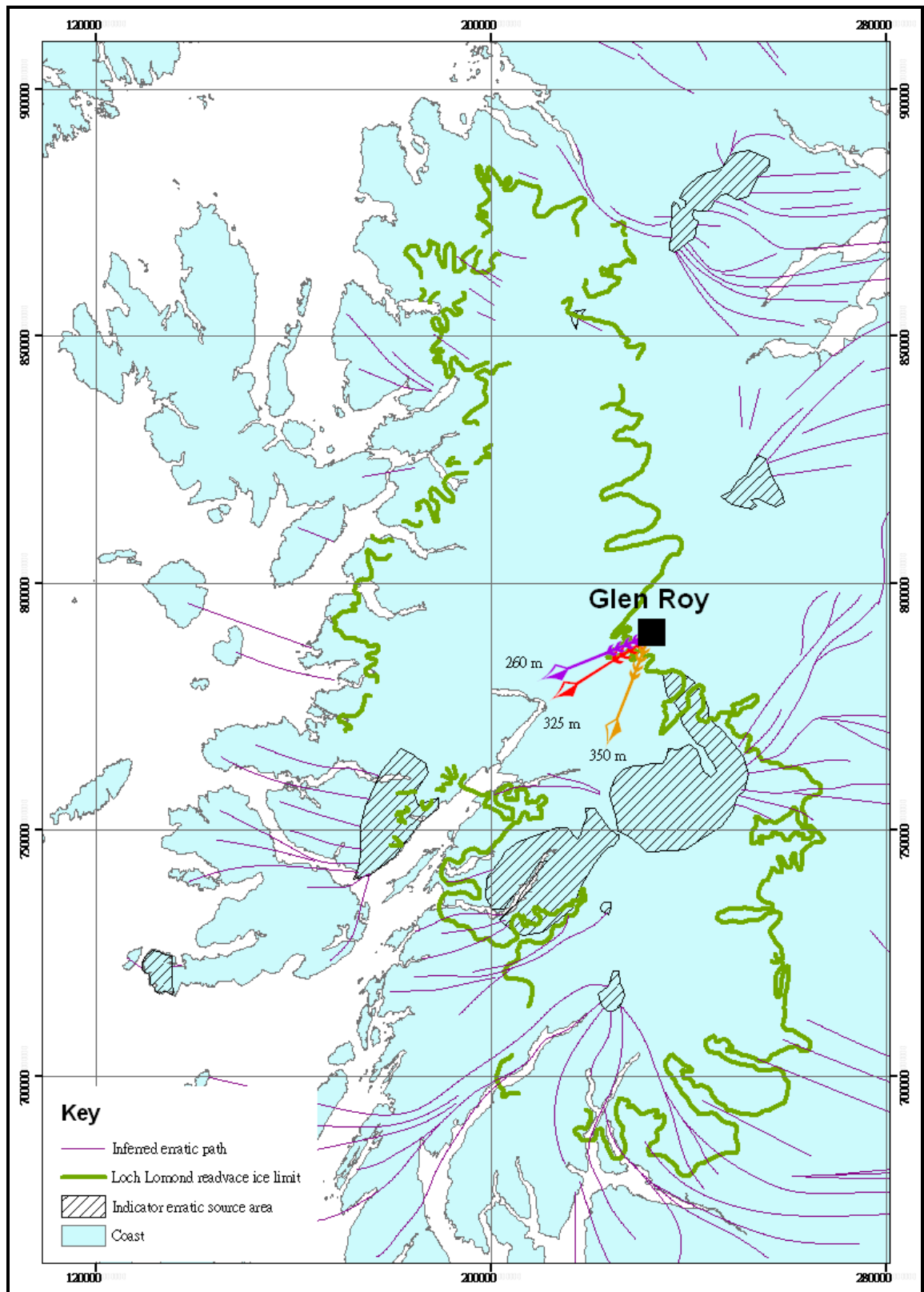


Figure 7.60 Arrows point towards the centre of glacio-isostatic load at the time of formation of each of the three Parallel Roads of Glen Roy, as concluded by Dawson *et al.*, (2002) based on trend-surface analysis. These are superimposed on the BRITICE map which shows the Loch Lomond Readvance ice limits and principal sources and directions of glacial erratic transport (from BRITICE GIS-files, [http://www.shef.ac.uk/geography/staff/clark\\_chris/britice](http://www.shef.ac.uk/geography/staff/clark_chris/britice). Accessed on 11th/August 2010).

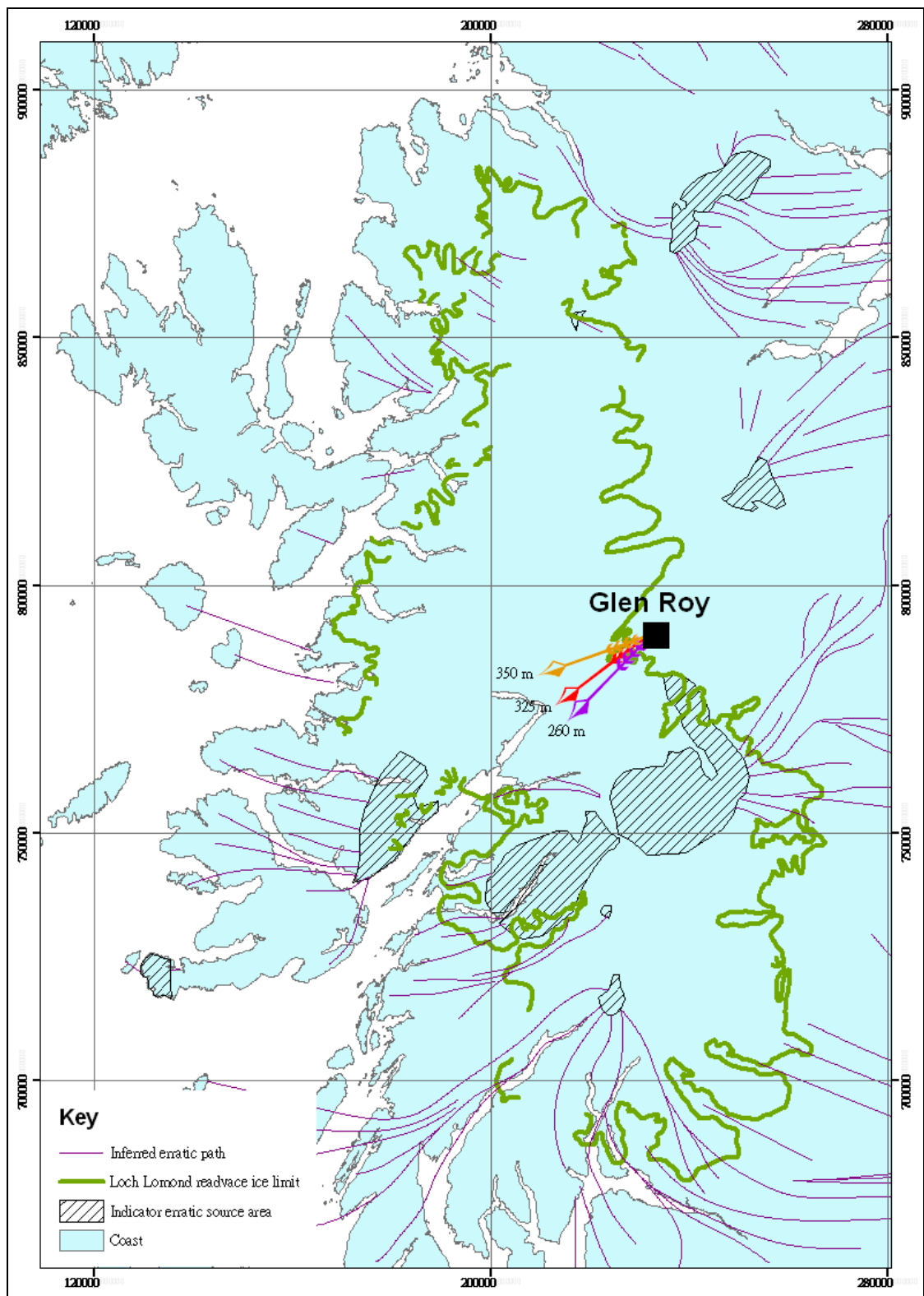


Figure 7.61 Arrows point towards the inferred centre of glacio-isostatic load at the time of formation of each of the three Parallel Roads of Glen Roy, based on trend-surface analysis of NEXTMap altitudinal data undertaken in the present research. These are superimposed on the BRITICE map which shows the Loch Lomond Readvance ice limits and principal sources and directions of glacial erratic transport (from BRITICE GIS-files, [http://www.shef.ac.uk/geography/staff/clark\\_chris/britice](http://www.shef.ac.uk/geography/staff/clark_chris/britice). Accessed on 11th/August 2010).



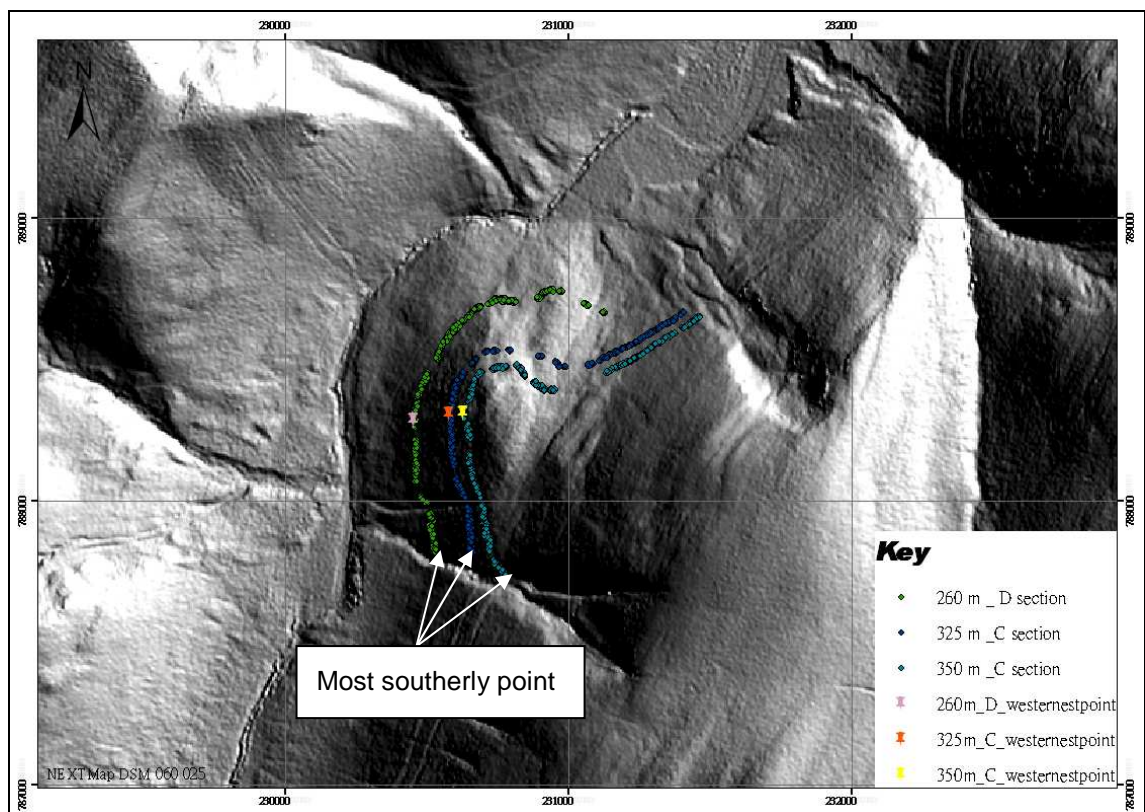
### **7.11 Deriving representative gradients for the Parallel Roads**

The results of trend surface analysis (TSA), referred to in section 7.10, highlight a number of uncertainties relating to the application of TSA to shoreline surfaces that are confined to a single valley, as attempted in this study for the analysis of the shoreline surfaces in Glen Roy. This case differs significantly from the more usual applications of TSA. For example, where TSA has been employed to reconstruct patterns of isostatic rebound and marine shoreline deformation, the surfaces of the former shorelines under study (raised beaches and platforms) are dispersed over a large area with along-shore gradients that trend in a range of compass directions (e.g. Smith *et al.* 1969, 2000; Andrews and Barnett, 1972; Gray, 1974, 1978). Any local anomalies in the data are therefore unlikely to distort the overall isobase patterns. The Parallel Roads in Glen Roy, by contrast, are not only confined to a single narrow valley, but the valley itself changes course quite markedly over short distances, with the more significant changes in course being between the lower and middle Roy and around the confluence of the Turret and upper Roy (Figure 7.4 to 7.6). It is therefore more likely that local deviations from any overall surface gradient trend could have a significant distorting influence on the TSA results.

These changes in the course of the Roy Valley, and in the trend directions of the former lake shorelines, raise the question of how much influence the choice of projection axis will have over the resulting gradients calculated for each of the three shorelines. In this study, the data have initially been projected (arbitrarily) on to W-E (easting) and south-north (northing) axes to create the two-dimensional projections presented and analyzed in sections 7.6 to 7.9. These axial directions cannot be optimal for establishing the maximal surface gradients of all sectors within Glen Roy, for a change in valley direction will shorten or stretch the data relative to the axial plane. The results of gradient analysis (both direction and magnitude) of the shorelines in Glen Roy are likely

therefore to be dependent on the selected axis of projection as well as on local ‘noise’.

The degree to which the gradient data have been influenced by these factors has been tested. First, a sector was selected for study where the valley changes course, where the orientation of the shorelines changes dramatically over a short distance. The sector chosen was the right flank of the Roy, at the junction between the lower and middle Roy, where the along-shore direction of the shorelines changes by around 90° (Figure 7.62).

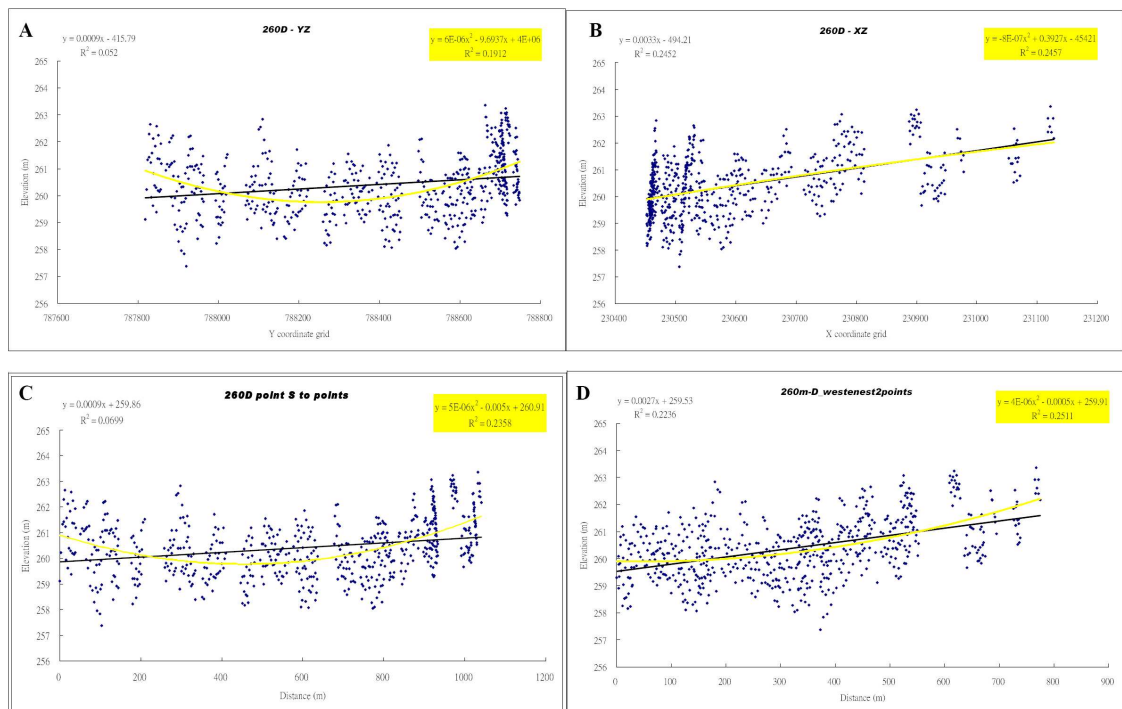


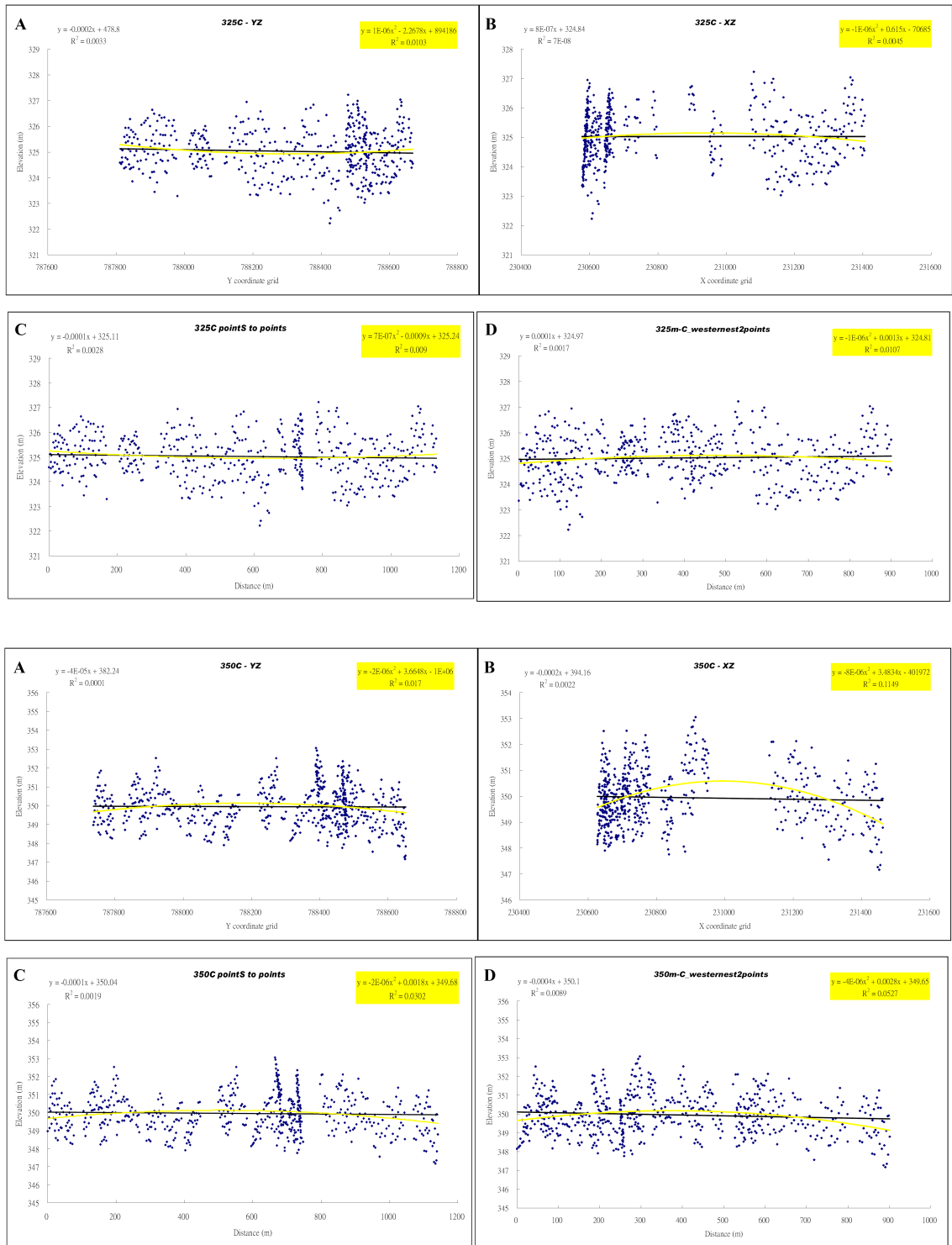
**Figure 7.62** Location of selected shoreline sections in Glen Roy for surface gradient experiment. A change in shoreline section course direction will shorten or stretch the data relative to the axial plane. The results of gradient analysis are dependent on the selected axis and method of projection.

A total of 1751 altitude measurements have been obtained for the shoreline surfaces in this sector, 607 from the 350 m, 508 from the 325 m, and 636 from the 260 m shorelines, respectively. Additional data and illustrations are provided in Appendix 6 on the CD. These altitudinal data were plotted using four different projections: (i) along a S-N projection axis, using orthogonal distance to the axis; (ii) along a W-E projection axis,

using orthogonal distance to the axis; (iii) along a S-N projection axis, using the shortest plan distance between points from an origin at the most southerly measured point on each shoreline; (iv) along a W-E projection axis, using the shortest plan distance between points from an origin at the most westerly measured point on each shoreline. The plots are illustrated in Figure 7.63 and the resulting calculated gradients are presented in Table 7.16.

The results for the 325 m and 350 m shoreline surfaces show minor differences in gradient but the gradient directions are mostly negative – i.e. sloping towards the points of origin, which is the opposite that would be expected from the overall isobase pattern (see section 7.10). This variance is probably explained by a localized effect of the sharp change in orientation of the shorelines combined with the data being geographically too condensed for the larger, regional trend to be evident. The biggest differences are found with the 260 m shoreline.





**Figure 7.63 Projected shoreline surface altitudes of the 260m\_D, 325m\_C and 350m\_C shoreline sections in Glen Roy ( see Figure 7.62) plotted (A) along a S-N projection axis, using orthogonal distance to the axis; (B) along a W-E projection axis, using orthogonal distance to the axis; (C) along a S-N projection axis, using the shortest plan distance between points from an origin at the most southerly measured point on each shoreline; (D) along a W-E projection axis, using the shortest plan distance between points from an origin at the most westerly measured point on each shoreline. Two regression lines were derived from each data-set (black line - linear regression; yellow line - 2<sup>nd</sup> order polynomial regression). Additional information is provided in Appendix 6 on the CD.**

**Table 7.16 Calculated shoreline surface gradients for the sector of Glen Roy shown in Figure 7.62, obtained using different projection axes.**

Shoreline –Method (Trending direction)	Gradient - m/km	Shoreline –Method (Trending direction)	Gradient - m/km	Shoreline –Method (Trending direction)	Gradient - m/km
260m-A (N-S)	0.857697239	325m-A (S-N)	-0.19506934	350m-A (S-N)	-0.040960573
260m-B (E-W)	3.27240135	325m-B (E-W)	0.000812407	350m-B (W-E)	-0.19148501
260m-C (N-S + NE-SW)	0.93501547	325m-C (S-N + SE-NW)	-0.141860316	350m-C (S-N + SW-NE)	-0.147694316
260m-D (E-W )	2.663632866	325m-D (E-W )	0.129129667	350m-D (W-E )	-0.407440829

These show steeper gradients than the 325 and 350 m shorelines, which again runs counter to the overall isobase patterns obtained from TSA, although all four projections for this shoreline have positive gradients. The differences between the A and C projections and the B and D projections are stark, however, and the author believes this may reflect local ‘noise’ (aberrant measurements) caused by debris that has accumulated on the back edge of the shoreline. This effect will be greater in some projections than on others, if the projection plane is orthogonal to the backwall of the platform, rather than running parallel to the backwall. Clearly, therefore, in localized areas where the shorelines change direction over short distances, the gradient calculations are dependent on the azimuth of the plane of projection, and the data in Table 7.16 suggest that no single plane of projection in such areas would be representative. It might perhaps be best to exclude data from such localities, when attempting to identify regional isobase patterns. This problem is not encountered in straight sections of the valley, however, as shown by Frings (2010; Appendix 4). He compared the resultant variations in calculated shoreline surface gradient for shorelines on the northern flank of the almost-uniformly straight middle Roy Valley, after progressively shifting the axial projection direction by 5° increments. Whether based on instrumentally-levelled data, or altitude measurements

obtained from NEXTMap, the resultant gradient values change by very small amounts (Table 7.17).

A second test focused on the effects on calculated shoreline surface gradient, throughout the Roy Valley as a whole, of changing the direction of the axial projection plane from S-N to SW-NE. The results are illustrated in Figure 7.64. The easiest practical procedure for changing the axial projection when using NEXTMap data was to reposition the original data-points by shifting them azimuthally by 45° (illustrated in top row in Figure 7.64) and using the S-N grid-line as the axis; this was computationally easier than, but is geometrically equivalent to, leaving the data-points in their original position and creating a SW-NE axis. The new gradients calculated for SW-NE projection axes for all three shorelines are shown in Table 7.18. The top line in the table gives the original gradients found when using an S-N projection, the middle line

**Table 7.17 Variation in gradient of the surfaces of the Glen Roy shorelines after incremental 5° angle changes in the direction of the plane of projection through the NE quadrant (from Frings, 2010; also see Appendix 4).**

Degrees from North	Levelling Data			NEXTMap Data		
	260m	325m	350m	260m	325m	350m
0	-0.00058	-0.00073	-0.00109	-0.00036	-0.00102	-0.00046
5	-0.00059	-0.00074	-0.00109	-0.00036	-0.00102	-0.00046
10	-0.00059	-0.00074	-0.00110	-0.00036	-0.00102	-0.00046
15	-0.00059	-0.00074	-0.00111	-0.00037	-0.00103	-0.00046
20	-0.00060	-0.00075	-0.00112	-0.00037	-0.00104	-0.00047
25	-0.00061	-0.00076	-0.00113	-0.00038	-0.00106	-0.00047
30	-0.00062	-0.00077	-0.00114	-0.00038	-0.00107	-0.00048
35	-0.00063	-0.00078	-0.00116	-0.00039	-0.00109	-0.00048
40	-0.00063	<b>-0.00079</b>	-0.00118	<b>-0.00040</b>	-0.00110	<b>-0.00049</b>
45	<b>-0.00064</b>	<b>-0.00080</b>	<b>-0.00119</b>	<b>-0.00040</b>	<b>-0.00112</b>	<b>-0.00049</b>
50	<b>-0.00065</b>	<b>-0.00081</b>	<b>-0.00120</b>	<b>-0.00041</b>	<b>-0.00113</b>	<b>-0.00049</b>
55	<b>-0.00065</b>	<b>-0.00081</b>	<b>-0.00120</b>	<b>-0.00041</b>	<b>-0.00113</b>	<b>-0.00049</b>
60	<b>-0.00065</b>	<b>-0.00080</b>	<b>-0.00119</b>	<b>-0.00041</b>	<b>-0.00112</b>	<b>-0.00049</b>
65	<b>-0.00064</b>	-0.00078	-0.00116	<b>-0.00041</b>	-0.00110	-0.00047
70	-0.00062	-0.00075	-0.00111	<b>-0.00040</b>	-0.00106	-0.00045
75	-0.00059	-0.00071	-0.00105	-0.00038	-0.00100	-0.00042
80	-0.00055	-0.00066	-0.00098	-0.00036	-0.00094	-0.00039
85	-0.00052	-0.00062	-0.00092	-0.00034	-0.00088	-0.00037
90	-0.00051	-0.00060	-0.00090	-0.00033	-0.00086	-0.00036

gives the new results based on a SW-NE projection axis, and the bottom line gives the percentage difference between them.

The main differences are that the SW-NE gradients are all lower than those calculated for the S-N gradients. This is because the data appear stretched over a greater axial distance. For the 260 and 325 m shorelines, the difference is relatively small, but significant (7% and 8.1% differences respectively). The biggest change, 37%, affects the 350 m data. This is because the 350 shoreline extends further into the Upper Roy Valley than the other shorelines, and the data are running W-E; the shift from an S-N to a SW-NE axis has a much bigger effect on the 350 m data than on the other two data-sets.

**Table 7.18 Comparison of shoreline surface gradients calculated for the three Parallel Roads using a N-S axial projection plane (top line) and a SW-NE axial projection plane (middle line). The bottom line shows the percentage change in gradient. The raw data are provided in Appendix 7 on CD.**

Shorelines	Gradient (m/km <sup>-1</sup> )	Shorelines	Gradient (m/km <sup>-1</sup> )	Shorelines	Gradient (m/km <sup>-1</sup> )
260 m-all data S-N projection	0.073128415	325 m-all data S-N projection	0.137800731	350 m-all data S-N projection	0.106999849
260 m-all data SW-NE projection	0.068014887	325 m-all data SW-NE projection	0.126602801	350 m-all data SW-NE projection	0.067649912
% difference	6.99	% difference	8.13	% difference	36.78

On the basis of the two experiments summarized in this section of the thesis, it can be seen clearly that the calculated shoreline gradients are dependent on the selected axial plane of projection as well as on local effects where the valley course is curved. This raises the question of what is the most valid procedure to adopt, in studies which focus on landforms confined to within a single narrow valley. A useful starting point is perhaps indicated by the initial results of TSA of the collective shoreline data, presented in Figures 7.56 to 7.58. Although the TSA results are compromised by the fact that the

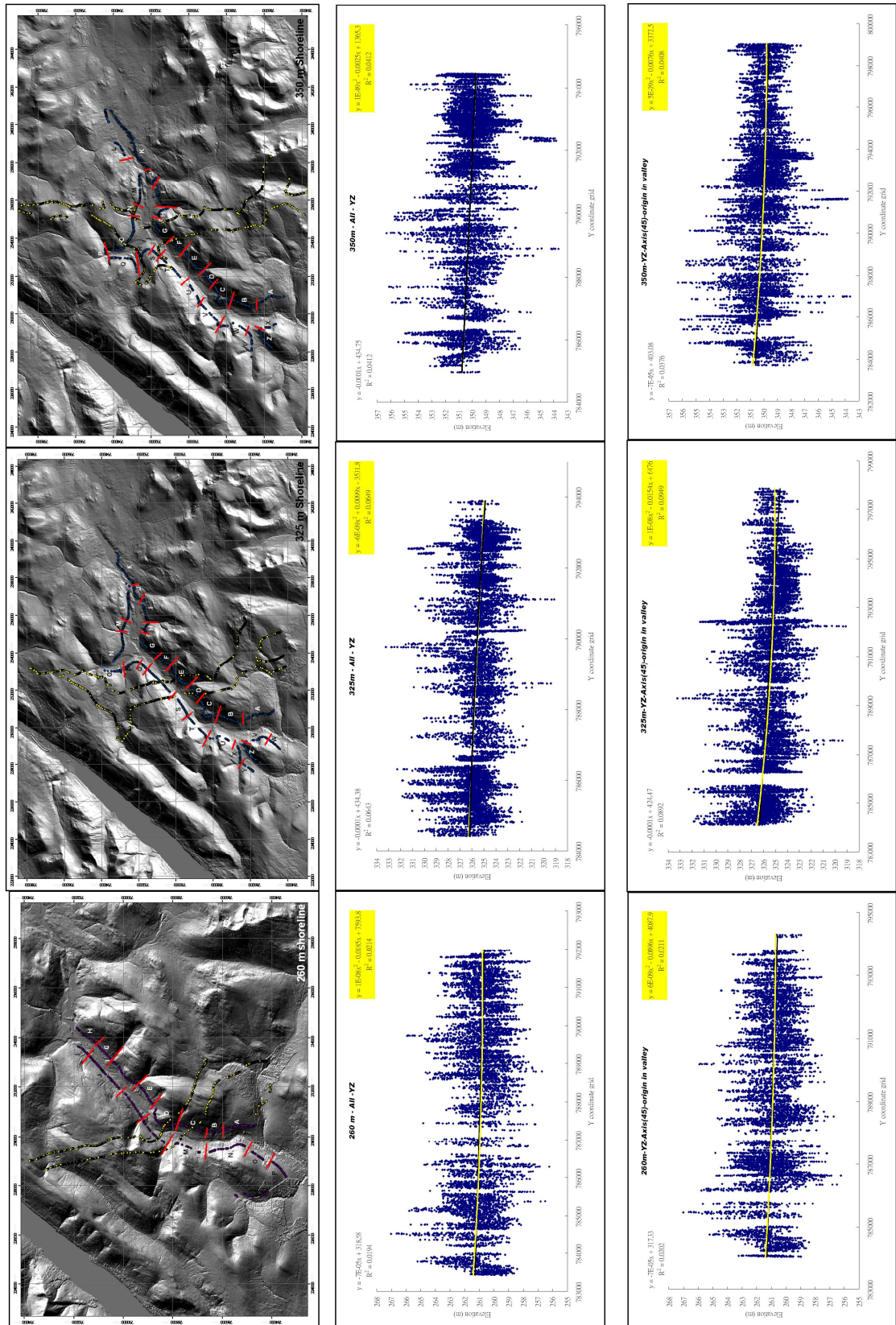


Figure 7.64 Comparison of the altitudinal data obtained using N-S and SW-NE projection planes. The top row shows the spatially transformed measurement points, shift azimuthally by 45°. The middle row shows the untransformed data, aligned on a N-S axial projection plane. The bottom row shows the transformed data, aligned on a SW-NE axial projection plane. For further explanation, see text. The raw data are provided in Appendix 7 on CD



data on which they are based are condensed into narrow bands, nevertheless all three shorelines show broadly similar patterns, with a general SW to NE decline in surface altitude. This would suggest that a SW-NE projection plane might be the most appropriate axial plane of projection. However, Figure 7.61 shows that the maximal gradient direction of each shoreline surface is slightly different; the arrow directions in Figure 7.61 are orthogonal to the smoothed isobase contour trends. In theory, therefore, a different axial projection plane should be chosen for each of the shorelines, in order to reveal the data plotted along the maximum plane of inclination. However, there remains the problem that the valley itself changes direction: the results of changing the axial plane of projection has different effects on each of the shorelines, as best illustrated by the 38% difference in gradient value on the 350 m shoreline, between a S-N and SW-NE plane of projection. Selecting the optimal projection plane for the Glen Roy shorelines is not a trivial exercise, therefore, and requires some judicious data selection. For example, perhaps the data for upper Glen Roy should be omitted, since that part of the valley is running W-E, parallel to the main isobases (Figure 7.61), rather than orthogonal to them. However, that would cut down the number of data-points available for the 350 m shoreline and, to a lesser extent, for the 325 m shoreline. Perhaps the analysis should be confined to the straight sections of the valley (the lower and middle courses), and avoid data from sectors where the valley changes direction abruptly. This might lead to a fairer set of comparisons between the architecture of the three shorelines, and provide the more reliable gradient figures.

In retrospect, and in the light of these considerations, the following procedure might prove optimal for establishing the representative maximal surface gradients of the ancient lake shorelines in Glen Roy:

- 1.** Run trend surface analysis experiments to establish the general architecture of the shoreline surfaces;

2. Identify the maximum gradient direction for each shoreline suggested by the TSA results;
3. Use the directions indicated by step 2 as the initial plane of projection for the shoreline altitude data;
4. Re-run step 3 for each shoreline in a series of experiments where (a) the axial projection plane is shifted progressively through 50 increments, and (b) data from curved sectors of the valley are omitted, and (c) data from upper Glen Roy are omitted;
5. Compare all results and select the data showing the maximum surface tilt.

Whether the gradient values identified in Step 5 define the ‘true’ isostatically-influenced surface gradients of the shorelines remains a debatable point, but this series of experiments would be worth running to establish the variance in the results obtained. Unfortunately, there was insufficient time to run these experiments in the time available for the PhD programme of study, but the author plans to undertake these further tests in the future.

This concludes the examination of the distribution, form and gradients of the Parallel Roads, except that the causes of the deformation of the roads are considered further in the concluding chapter, Chapter 8, where the shoreline data are integrated with other lines of evidence examined using NEXTMap DEM data.

## 8. Synthesis and Conclusions

---

### 8.1 Introduction

In this chapter the information presented in Chapters 6 and 7 will be synthesised to illuminate some new interpretations and key points that emerge from the data. The emphasis is on interpretations that diverge from those published by Sissons (1978, 1979a, 1981a and 1983), Sissons and Cornish (1982), Peacock (1986), Peacock and Cornish (1989) and Palmer *et al.*, (2010) concerning the sequence and timing of glacier margins and associated ice-dammed lakes during the Loch Lomond Stadial (Figure 8.1). In section 8.2, the material is focused around 6 key aspects of the landform evidence that have been the subject of considerable debate for several decades. These are: (i) the maximum extent of glacier advance in Glen Gloy; (ii) the origin of the Turret fan; (iii) the evidence for asynchronous ice-front changes in Glen Turret, Glen Gloy, Caol Lairig and Glen Roy; (iv) the causes of deformation of the Parallel Roads; (v) the time of formation of the Parallel Roads; and (vi) the locus and timing of a major jökulhlaup event during ice decay and lake level lowering. Figure 8.2 provides an overview of all of the main landforms and other features mapped and referred to in chapters 6 and 7, as a guide to the overall geographical perspective. Figure 8.3 shows the key morphological elements in the study area that more specifically relate to the 6 key questions listed above, bringing together the distribution and form of the Parallel Roads as well as the locations of various associated landforms, such as ice-terminal deposits, major landslips and debris fans. Reference will be made to additional landforms and contextual detail provided in Chapters 6 and 7, where necessary. Section 8.3 will integrate the information presented in section 8.2 into an overall scheme of the pattern and sequence of events in Glen Roy during the Loch Lomond Stadial, including some developments during ice decay. Section 8.4 summarises the key conclusions to emerge from the thesis as a whole.



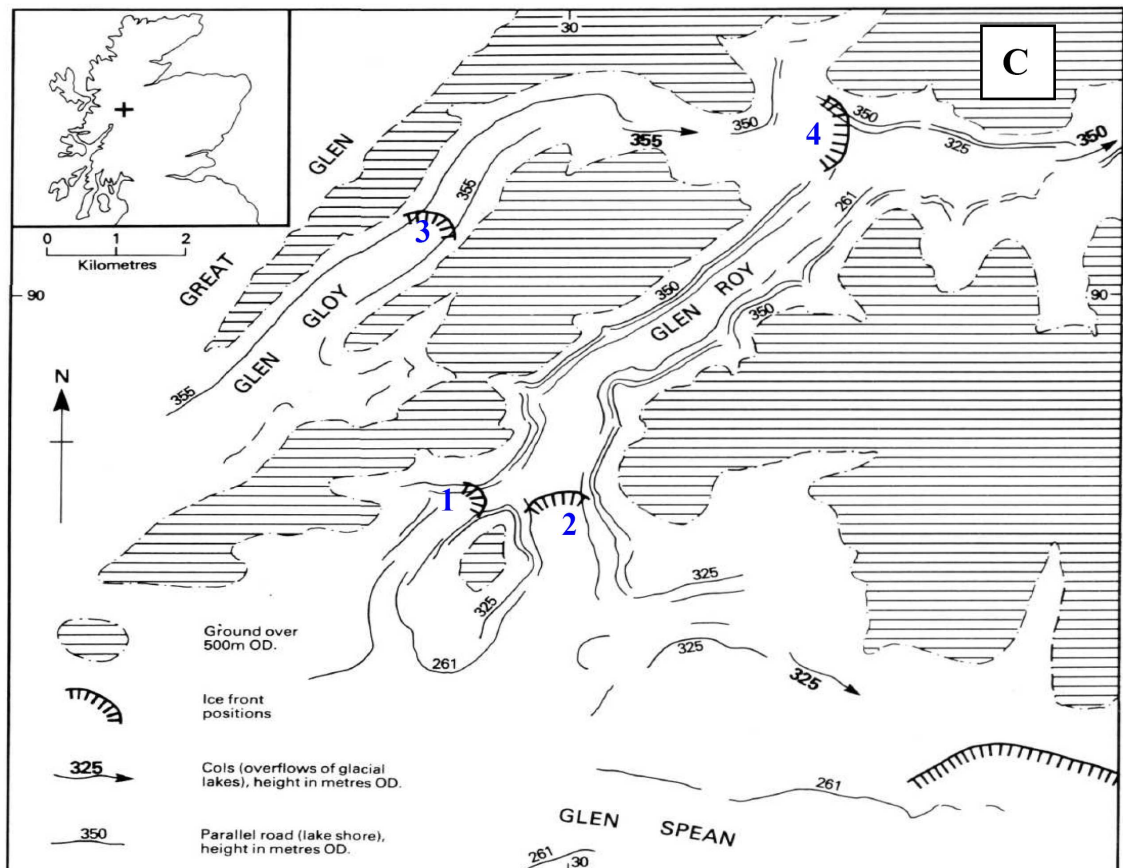


Figure 8.1 Different representations of the maximum ice stands in the Gloy-Roy area during the Loch Lomond Stadial. (A) The initial interpretation of Sissons (1979); (B) The revised assessment of Sissons and Cornish (1982), showing advancing ice margins in Glen Spean and lower Glen Roy (ice limits 1 to 5), the maximum position in Caol Lairig (6) and the maximum position of the Gloy Glacier, at the Turret fan (7); and (C) Postulated limits by Peacock (1986) in Caol Lairig (1), Glen Roy (2), and alternative interpretations for the Gloy glacier terminus (3 and 4), with position 3 being his preferred option.

## 8.2 Key issues concerning the sequence of events in the Glen Roy area during the Loch Lomond Stadial

### 8.2.1 Maximum extent of glacier advance in Glen Gloy

The position of the maximum extent of glacier advance in Glen Gloy during the Loch Lomond Stadial has been a matter of some uncertainty. Sissons (1979b) originally suggested the maximum position to be near Alltnaray (location 1, Figure 8.3), but later revised this interpretation considerably, when he concluded that the Gloy Glacier extended all the way up to the head of the Gloy valley, surmounted the Gloy-Turret col

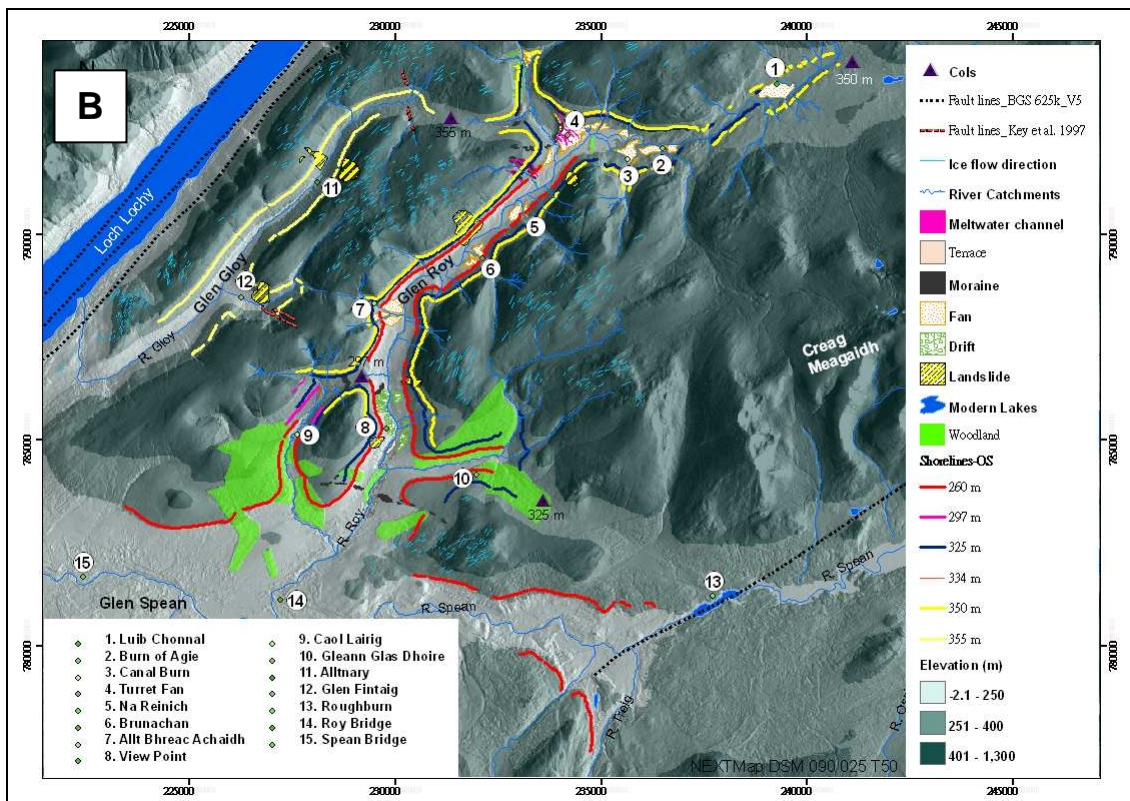
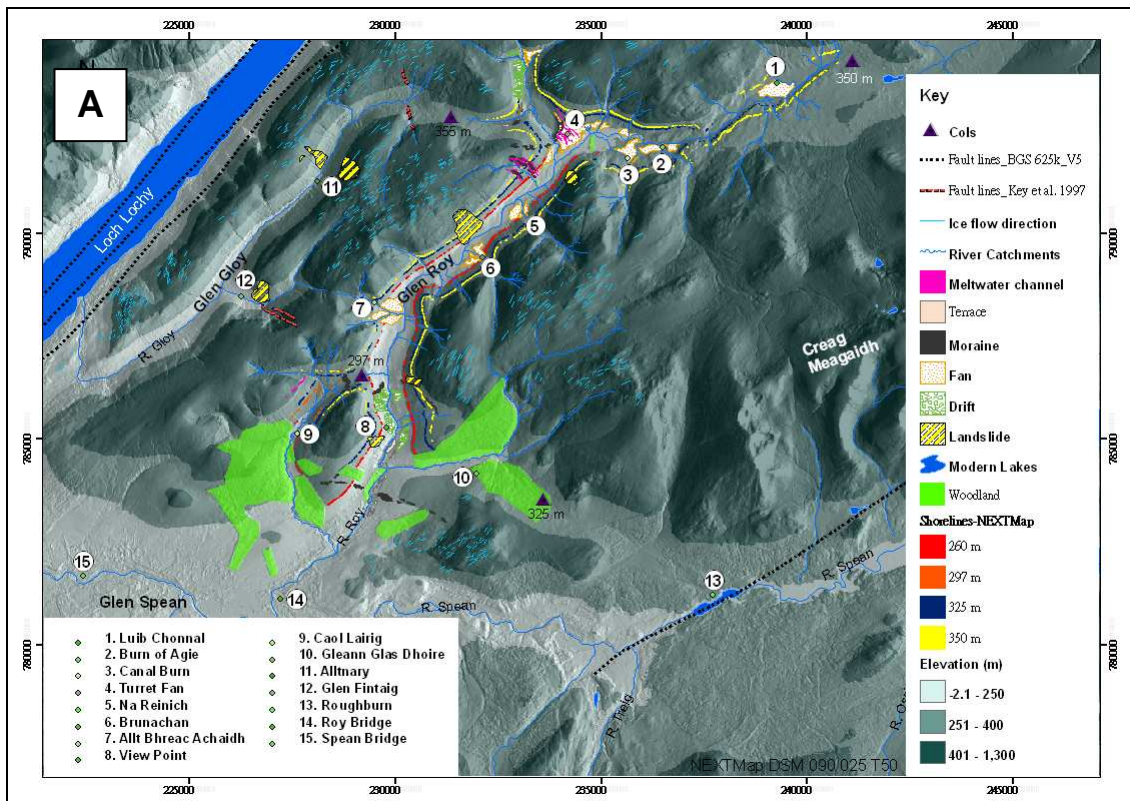
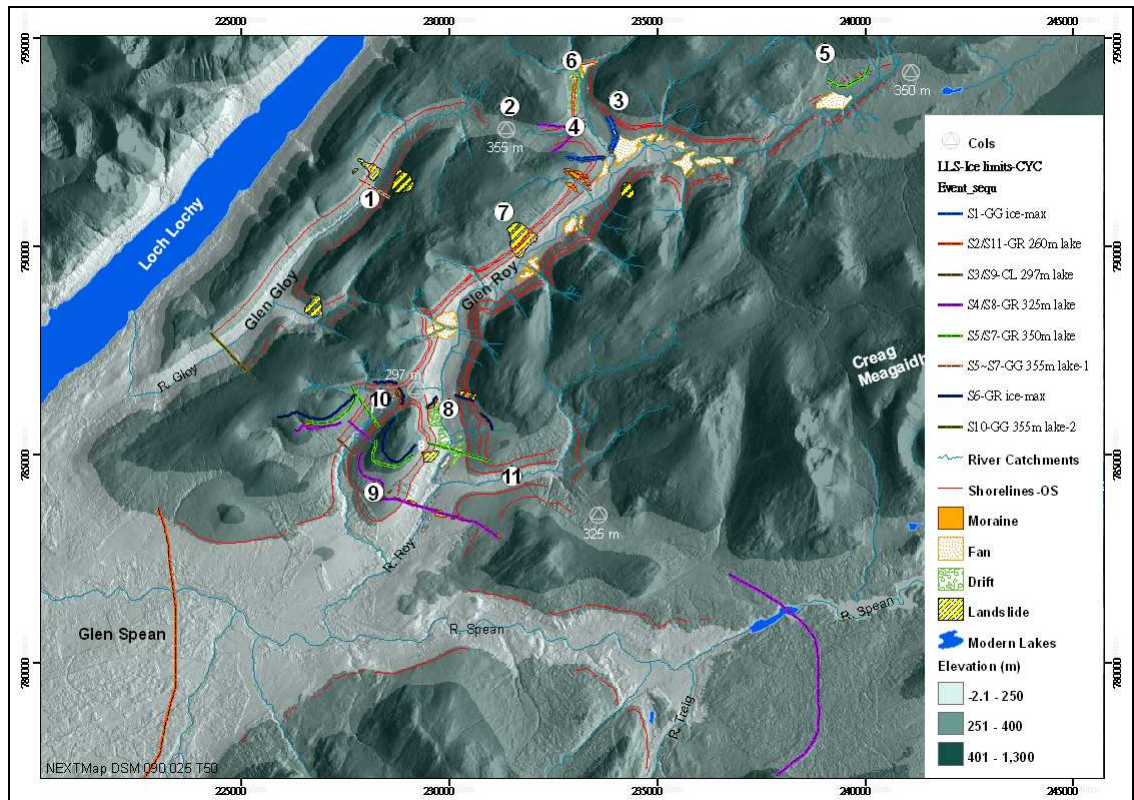


Figure 8.2 A general overview of the landforms and other features referred to in Chapters 6 and 7, including ice-moulded lineaments attributed to the Late Devensian ice sheet. Two digital versions of this figure are provided on the CD attached to this thesis: A with the distribution of the Parallel Roads according to the author's NEXTMap interpretations (Appendix 8), and B showing the original distributions according to the Ordnance Survey (Appendix 9).

(location 2, Figure 8.3), and eventually terminated at the Turret fan (location 3, Figure 8.3), near the confluence of the Turret and Roy valleys (Sissons and Cornish, 1982b).



**Figure 8.3** Locations referred to in text, where key geomorphological features occur that help to resolve the sequence of events in Glens Gloy and Roy during the Loch Lomond Stadal. For further explanation see text. The symbols in this figure are explained in Figure 8.10.

The basis for this significant change of interpretation, however, has not been explained in the published literature. Peacock (1986) considered the possibility of both of these maximal ice-marginal positions for the Gloy Glacier, but favoured the former for the following reasons: first, because the Glen Gloy and Glen Roy ice lobes were both outlets of the West Highland Icefield, and the Gloy Glacier could not have existed before Glen Spean became ice-dammed; and second, because analysis of the sediments in the Turret Fan indicated that it was formed largely under subaerial conditions. The first argument is perhaps equivocal, because it depends on the pattern of ice flow from the mountains to the west of the Great Glen, which is not yet clear. The second seems

more acute, because, according to Peacock, it is difficult to imagine that Gloy ice could extend all the way to the Turret Fan without the mouth of Glen Roy also being blocked by glacier ice, in which case an ice-dammed lake would exist in the vicinity of the Turret-Roy confluence. Under these circumstances, it would be difficult to explain how the fan sediments could have originated under subaerial conditions. Peacock therefore proposed that the Turret Fan was formed at a late stage in the retreat of the Late Devensian ice sheet, when meltwater could escape down the Roy Valley, and that it was not therefore formed during the Loch Lomond Stadial. He concluded that there was insufficient evidence to support the idea that the Gloy Glacier reached Glen Turret during the LLS.

A number of detailed observations made from NEXTMap DEM data, described in Chapter 6, have a bearing on this matter, and are summarised in Figure 6.28, and illustrated with oblique perspective in Figure 6.30 to 6.32. Collectively this evidence supports the view that the Loch Lomond Stadial ice surmounted the Gloy-Turret col and extended down to the Turret fan. In particular, key features include:

1. a distinct moraine ridge at Location h, Figure 6.28
2. a distinct terrace, interpreted as a kame terrace, at Location i, Figure 6.28
3. a kettle hole and ice-contact delta at Location g, Figure 6.28 (see also Figure 6.30 and 6.31)
4. a terrace feature interpreted as a marginal (kame?) terrace or delta at Location o, Figure 6.28 (see also Figure 6.31 and 6.32)
5. the absence of the 325 m shoreline in the vicinity of the confluence of Coire Dubh and Glen Turret (Location 4, Figure 8.1C).

The NEXTMap evidence therefore most closely accords with the interpretations of Sissons and Cornish (1982b), who observed most of these features from ground



mapping and analysis of aerial photographs. The notable absence of the 325 m shoreline around the mouth of the Allt a' Chomlainn and Coire Dubh suggests that glacier ice occupied this area at the time, an interpretation supported by the kettle-hole and delta features in this vicinity. This author therefore agrees with the suggestion of Sissons and Cornish (1982b) that Loch Lomond Stadial ice reached the western margin of the Turret fan, where it is marked by arcuate ridges, forming the ice-marginal arcuate moraines (Lines j, Figure 6.28) and mounds to be found in that vicinity. It is likely that this occurred at an early stage of the rising lake sequence before the 260 m lake extended to the Turret-Roy confluence (see section 8.2.2). The landform evidence also accords with the view that the Loch Lomond Stadial ice mass was destabilised when the lake level in Glen Roy rose to 325 m, causing rapid calving which led to ice retreat. The ice appears to have become stabilised under these new conditions at the confluence of the Allt a' Chomlainn and Glen Turret, just above the 325 m lake surface, its lateral margins represented by Lines r and o to h in Figure 6.28. What happened subsequently to this valley glacier is difficult to assess, because an analysis of the landforms in Glen Gloy did not form a major part of this PhD project. However, it seems likely that the ice was further destabilised by the rise of the Roy lake to 350 m, which forced the ice to retreat all the way to Alltnaray. This is suggested on two grounds. First, there are no obvious ice-marginal landforms between the mouth of the Allt na Chomlainn and Alltnaray (locations 4 and 1, Figure 8.1C). Second, maximum dislocation of the shorelines in Glen Roy occurred at a location due east of Alltnaray (Area 3, Figure 7.32; see also section 8.2.4), which suggests that ice and lake loading/unloading in Glen Gloy had impacts on the degree of ground deformation in Glen Roy. It is also likely to be at this stage that the 355 m lake shoreline in Glen Gloy was formed. The inter-connection of these different lines of evidence is examined further below.

### **8.2.2 Origin of the Turret fan**

The mode of formation and age of the Glen Turret fan have been the topic of discussion for more than 100 years. Jamieson (1892) suggested that the Turret Fan accumulated by the action of overflow water emanating from the ice-dammed lake in Glen Gloy during the Loch Lomond Readvance. Sissons and Cornish (1983) suggested it to be more likely an outwash fan formed when the Gloy Glacier over-flowed the 355 m Gloy/Turret col into Glen Turret at the time when the 260 m lake invaded upper Glen Roy. They drew attention to prominent arcuate ridges on the western edge of the fan that they interpreted as terminal moraines, marking the Loch Lomond Readvance terminus of the Gloy Glacier (Figure 6.28). They assumed that most of the fan body was deposited subaqueously, because a large part of the surface of the eastern flanks of the fan lie below 260 m OD, and would therefore have been submerged by the ice-dammed lakes. They also concluded that the fan would originally have extended across the Roy valley to block the drainage of the River Roy at some stage.

That interpretation is disputed, however, by Peacock (1986) and Peacock and Cornish (1989). They inspected the internal sedimentary structures of the fan and noted that they predominantly consist of poorly sorted, clast-supported sandy gravels showing distinct clast imbrication, forming parallel, sub-horizontally bedded layers that occasionally enclose thin lenticular bodies of finer sediment, the bedding assuming depositional slope values of about 1 in 40. They concluded that these properties reflect subaerial deposition, and not deposition of gravels in a subaqueous context where deltaic formations (clino-forms) would be more likely. They therefore proposed that the formation of the Turret Fan preceded the formation of the lakes associated with the Parallel Roads, and that the fan may have been deposited prior to the Loch Lomond Readvance, during a retreat phase of the Late Devensian ice sheet. A further argument used to support this interpretation is that subaerial deposition of the fan deposits would

require the free drainage of meltwater out of Glen Roy into Glen Spean, which he found impossible to imagine: if the Loch Lomond Readvance ice had invaded Glen Gloy and overtopped the Gloy-Roy col to reach the Turret Fan, then presumably there would be a contemporaneous advance of ice into lower Glen Roy, hence creating the 260 m lake. A counter-argument, however, might be that the position is also difficult to imagine for a Late Devensian ice sheet phase, with ice having been removed from lower Glen Roy and Glen Spean to enable free drainage, while maintaining an extensive glacier that occupied Glen Gloy and Glen Turret.

Benn and Evans (2008) added further evidence that is pertinent to the interpretation of the Turret Fan. Field mapping and analysis of NEXTMap DEM data in the area between upper Glen Roy and the great Glen (Johnson-Ferguson, 2004), occupied mainly by the Carn Dearg plateau (locality 5, Figure 8.3), led to the identification of a suite of glacial landforms that suggest that a local, cold-based ice-cap developed on the plateau surface. A tongue of this ice cap is thought to have extended into upper Glen Turret, to terminate at the Turret Fan. In their view, therefore, the source of sediment in the Turret fan was not related to the Gloy Glacier, but to this separate, locally-nourished ice cap, the deposits of which could be morpho-stratigraphically connected with the Glen Roy lake sequence, and which they therefore concluded to be of Loch Lomond Stadial age. They did not, however, comment on the nature of the fan sediments, and the problem of how they could be formed subaerially under this scenario.

A more recent study by Eaves (2009), also based on field mapping and analysis of NEXTMap DEM data, largely confirmed the interpretations of Benn and Evans (2008), finding evidence for an independent ice cap of Loch Lomond Stadial age on the Carn Dearg plateau. However, this study's conclusions differed from those of Benn and Evans (2008) in one important aspect: Eaves found no evidence for an ice tongue

descending from the plateau into upper Glen Turret. Eaves' conclusion for associating the plateau ice cap with the Loch Lomond Stadial rests on evidence for a glacier tongue descending from the plateau into the Allt Chonnal area of upper Glen Roy, and the absence of evidence of the 350 m lake shoreline from these landforms, suggesting their contemporaneity (see section 7.3, and Figure 7.17 and 7.18).

Two issues therefore have to be resolved, as far as the Turret Fan is concerned: the source of the material of which it is formed (i.e. from a glacier emanating from Glen Gloy, or alternatively from Carn Dearg), and how to account for the fact that the fan was deposited subaerially, when much of it lies below the altitude of the 260 m Glen Roy lake. The new evidence presented in this thesis may provide answers to these two questions.

First, as discussed in the preceding section, the geomorphological features in Allt a Chomlainn and Glen Turret suggest that ice did indeed flow over the Gloy-Turret col and into Glen Turret. This ice may have occupied the whole of Glen Turret at its maximum position, possibly forming ice-marginal deposits at the head of Glen Turret (location 6, Figure 8.3) as well as extending south-eastwards as far as the Turret fan (see Figure 6.28, locations a and b and line j). Furthermore, a simulation of the flooded area of the modern terrain at the time of the 260 m lake stand (Figure 6.34) shows that the 260 m lake should have entered further to the northeast in Glen Roy and further north into the southern part of Glen Turret than is indicated by the distribution of the 260 m shoreline in this vicinity. The absence of the 260 m shorelines in these localities therefore suggests occupation by ice at the time of shoreline formation.

The second issue is that of the mode of formation of the Turret Fan. The arcuate moraine ridges and associated mounds that flank the western margin of the Turret Fan

are prominent features that suggest formation under subaerial conditions, while the sedimentary evidence reported by Peacock (1986) and Peacock and Cornish (1989) seems convincing that the fan, at least initially, formed under subaerial conditions. Yet the evidence seems clear that a glacier terminated at the western margin of the fan during Loch Lomond Stadial times. The problem is how to reconcile this with the formation of the lakes in Glen Roy. One possibility is that the ice had spread from the Great Glen into Glen Gloy, extending as far as the Turret Fan before glacier ice in Glen Spean, originating from the Nevis Range, had accumulated to the thickness required to block the Spean sufficiently to create the 260 m lake. It is difficult to envisage water freely draining into Loch Linnhe at this time, as presumably ice would have built up in the vicinity of Fort William at an early stage during the Loch Lomond Readvance. One other possibility is that it took time for lake waters to build up to the 260 m level, with perhaps some seasonal sub-glacial drainage taking place before the ice tongues achieved a critical mass. If the outwash deposits of the Turret Fan could have built up very rapidly, within a matter of a few years, then this scenario would appear feasible, allowing subaerial drainage over sufficient time before the 260 m lake inundation changed the style of deposition at the Turret Fan, while further lake rise to the 325 m level forced the glacier margin to recede to the mouth of the Allt a Chomlainn.

### **8.2.3 Evidence for asynchronous ice-front changes in Glen Turret, Glen Gloy, Caol Lairig and Glen Roy**

As previously mentioned, it has long been assumed that the ice that occupied Glen Gloy came from different sources (Arkaig and Glen Garry basins, west of the Great Glen) to the ice that spread across Glen Spean into Glen Roy (the Nevis Range). It has also been assumed that the glaciers in Gloy and Roy reached their maximal positions at approximately the same time (e.g. Agassiz 1842; Jamieson 1863; Sissons 1979; Peacock and Cornish 1989; Palmer 2008) (Figure 5.3 C and D; Figure 5.4 and Figure 8.3). The

evidence based on NEXTMap imagery reported here provides no new perspective on the source regions of the Loch Lomond Readvance ice in the area, but does indicate asynchronous movements of the ice margins.

Reference has already been made to contrasting developments between the margins of the Gloy and Roy glaciers during the Loch Lomond Readvance. If the interpretations presented in sections 8.2.1 and 8.2.2 are correct, then the development of the 325 m lake forced the retreat of the Gloy Glacier from its maximum position at the Turret Fan, to where the Allt a Chomlainn joins the Turret (ice-marginal lines r and o to h in Figure 6.28). In turn, this would mean that the Gloy Glacier was forced into retreat before the Spean-Roy Glacier had reached its maximum position at the Viewpoint in Glen Roy. By the time the Spean-Roy Glacier achieved its maximum position, a further rise in lake level (to 350 m) forced the Gloy Glacier into further retreat, perhaps clearing the Allt a Chomlainn valley completely. This retreat of the Gloy Glacier margin back, perhaps, to the Gloy-Roy overflow col, appears to have proceeded without major interruption, for there are no obvious recessional features within Coire Dubh/Allt a Chomlainn. Indeed, there are no obvious ice-marginal features until Alltnaray (location 1, Figure 8.1C), where Jamieson (1896), Sissons (1979) and Peacock and Cornish (1989) report locally well-developed features interpreted as ice-marginal deposits. This part of the succession of events is difficult to understand, because if the Gloy Glacier was forced to retreat solely by the rising lake levels in Glen Roy, then the retreat should have halted at around the position of the Gloy-Roy col, which lies at 355 m altitude, 5 m above the highest lake level in Glen Roy and its tributaries. Instead, ice retreat appears to have continued progressively until it reached Alltnaray. That the ice then remained stationary at this position is perhaps supported by the local landslides (landslides 5 and 6, Figure 7.40) mapped in this vicinity. These landslides appear to parallel the zone of maximum shoreline dislocation and position of landslide 3 in Glen Roy (Location 7, Figure 8.3;

Figure 7.40). It is suggested that the dislocation of the shorelines and the triggering of the landslides may have had a common cause, one in which the position of an ice-terminus at Alltnaray played a significant role by contributing to localised crustal compression. However, this does not explain the pattern of retreat of the Gloy Glacier, which appears to have continued to recede down valley from the Gloy-Roy col without the influence of rising lake waters. This therefore appears to imply that the Gloy Glacier ice was already in decay because of ice-mass adjustments that were independent of the development of lakes, which suggests that the overall ice-mass dynamics had changed, probably as a result of regional climatic factors. If this is correct, then an explanation needs to be found for the apparent halt of the glacier in the vicinity of Alltnaray, which is difficult to understand at present.

The maximal position of the glacier margin of the Spean-Roy Glacier at the Viewpoint in Glen Roy (location 8, Figure 8.3) is widely recognised, and is clearly demarcated on NEXTMap DEM plots by terminal moraines (locations g in Figure 6.10B). Also clearly marked are trim lines on the southern flank of Bohuntine Hill (location 9, Figure 8.3; locations p, n and o, Figure 6.10B) and prominent cross-valley moraines in lower Glen Roy and adjacent Glen Spean (location h, Figure 6.10B). These reflect the decline in altitude of the ice surface and retreat of the Spean-Roy Glacier ice margin following its maximum stand. In Caol Lairig, a similar suite of landforms reflects the maximum position of the ice in this valley through the position of a prominent terminal moraine (location 10, Figure 8.3), ice-marginal meltwater channels (location d; Figure 6.10B) and an ice-marginal delta feature (location b, Figure 6.10B). Analysis of the landforms in Caol Lairig and lower Glen Roy also suggests non-contemporaneous adjustments of the ice fronts during ice decay. For example, the 297 m shoreline in Caol Lairig (section 6.2; Figure 6.7 and 6.8) indicates the presence of a lake in Caol Lairig and its state of preservation suggests that it must have existed while ice was receding within this

tributary valley. If so, then this lake could only exist after the lake levels in Glen Roy had declined to the 260 m level, otherwise the water of the 325 m lake would have flooded into Caol Lairig. This in turn means that the Spean-Roy Glacier ice front must have receded beyond the Gleann Glas Doire tributary valley and 325 m overflow col (location 11, Figure 8.3) into Glen Spean during the time that the Caol Lairig Glacier ice was maintained relatively close to its maximum position (Figure 6.3 and 6.10). The Spean-Roy Glacier therefore appears to have receded much more quickly than the glacier front in Caol Lairig.

#### **8.2.4 Causes of deformation of the Parallel Roads**

Sissons and Cornish (1982b) proposed that the lake shoreline dislocations in Glen Roy were caused by palaeoseismic activities that resulted from fault movements or the effects of jökulhlaup discharge. To support this hypothesis, Sissons and Cornish noted the close association between some major shoreline dislocations and lines of weakness identified on geological maps where dykes and fault lines are evident. This proposal was supported by Ringrose (1987, 1989a) who reported disturbed (liquefaction) features in what he termed laminated I type lake sediments, which he also attributed to seismic activity.

Jarman (2008) argues against the Sissons and Cornish (1982b) explanation of shoreline dislocation, preferring differential rebound effects to be the principal cause instead. His main arguments are as follows:

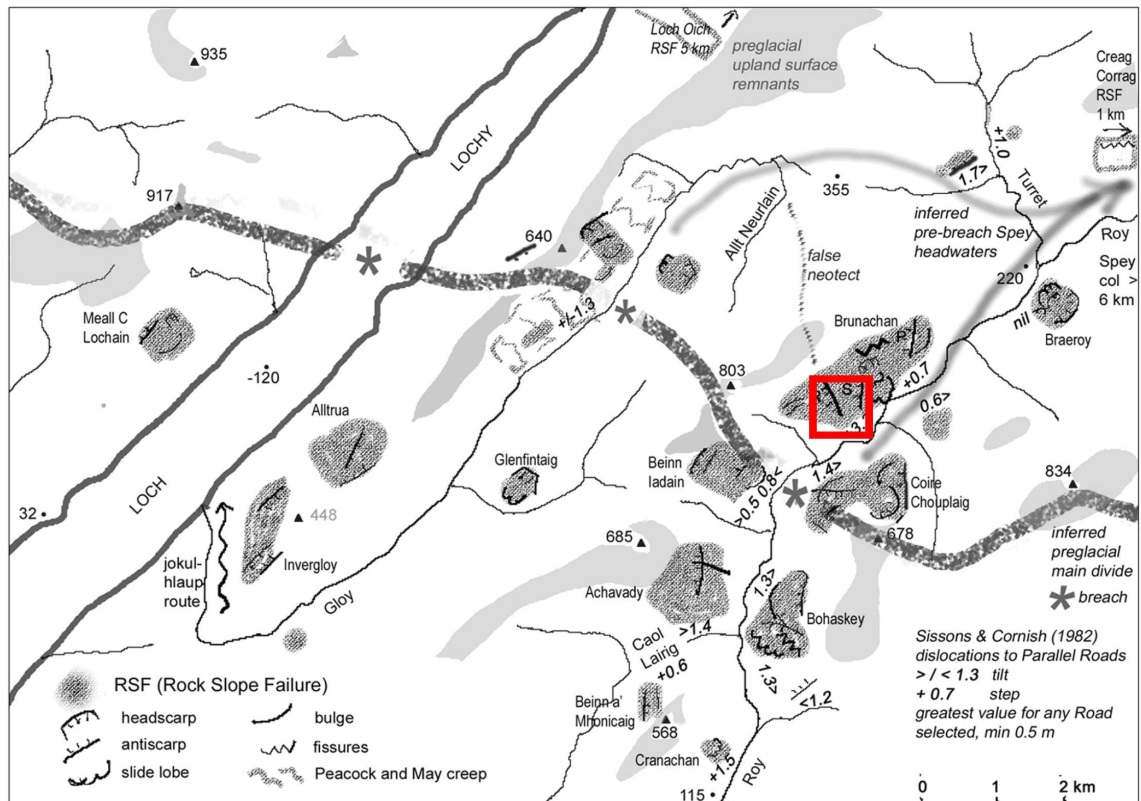
1. There is no evidence from the latest Geological Survey reports to suggest that major seismic events had occurred in Glen Roy (Key *et al.*, 1997; also see the BGS geology map and associated notes published in March 2010, and Figure 5.2).



2. The sites of marked dislocation of the Parallel Roads are all located within or adjacent to landslides (Sissons and Cornish, 1982b). The Glen Gloy Fault (Figure 5.2) has only a very short-length and there is no evidence that it extends across the Roy valley to link with a supposed fault scarp in the vicinity of Brunachan (red box in Figure 8.4), as claimed by Ringrose (1987).
3. Fenton (1991) and Key *et al.*, (1997) recognise that rock-slope failures (RSFs) in Glens Gloy and Roy variously cut and are cut by different Parallel Roads, and are therefore of several different ages.
4. The dislocations all consist of upward movements with respect to the 'normal' levels of the Roads, some as vertical steps, but others distinctly tilted. The tilted features are unlikely to represent dislocations that extend deeply into the crust, since lateral differential movement in such a complicated fashion would not be possible (i.e. could not be accommodated) at depth.

Peacock and May (1993) also investigated slope deformation features at various localities in Glen Roy and Glen Gloy, and concluded that slope deformations were caused by high cleft-water pressure combined with stress relief during glacial unloading. These combined processes, in their view, would have led to rock fracturing and the weakening of near-surface rock layers and surface slopes, so that localised deformation could take place.

In the present research, all stretches of the Parallel Roads examined in chapter 7 show shoreline sections that appear to have been warped or arched, with a number of sections that have been disrupted by block tilting or displacement. The greatest scale of deformation measured using NEXTMap DEM data clearly occurs in middle Glen Roy



**Figure 8.4** Diagram used by Jarman (2008) to illustrate the distribution of, and to explain the concept of, rock slope failures (RSFs) in the Glen Roy-Loch Lochy area. The red box surrounds the short fault scarp referred to in text, reported by Ringrose (1987).

(in the area adjacent to location 7, Figure 8.3, and to landslide 3 – see section 7.8.3) which tends to be greatest on the 350 m shoreline (stretches U and E; Figure 7.48), diminishing in scale successively on the 325 m and 260 m shorelines. In general, the scale of deformation is greater in the lower and middle reaches of Glen Roy than in the upper reach and it also seems to have a W-E gradient in some sectors, as for example in the middle reach of the Roy (section 7.8.3) where deformation is more pronounced on the NW than on the SE flank of the valley. Likewise, the shorelines on the northern flank of the upper Roy show more marked warping or tilting on the western than on the eastern stretches (section 7.8.4). The pattern of displacement is similar between two or all three of the shorelines, though different in scale. However, there is little accord in the scale and style of deformation affecting shoreline lengths lying immediately above or below each other.

Major dislocations in lower Glen Roy are close to landslides associated with former ice marginal positions; for example landslide 1 (Figure 7.40) is close to the terminal moraine ridges that confine the 325 m lake within Glen Roy, while landslide 2 is close to the LLR maximum ice limit at the Viewpoint. The greatest scale of deformation in middle Glen Roy lies beyond the ice maximum position in Glen Roy in a location that appears to align with landslides 5 and 6 (Figure 7.40) near Alltnaray in Glen Gloy, close to the recessional marginal position of the Gloy Glacier referred to in section 8.2.1. Distinct shoreline dislocations in upper Glen Roy, NE of the Turret Fan, also lie close to the maximum Loch Lomond Readvance limit of the Gloy Glacier. The most severe dislocation sites therefore appear to lie close or parallel to former Loch Lomond Readvance ice-marginal termini, and are not exclusively associated with faults. Also, the complex concavo-convex profiles of the deformed shorelines described in Chapter 7 of this thesis cannot all be explained by the presence of faults, for which there is little evidence.

The “fault theory” proposed by Sissons and Cornish (1982b) does not therefore adequately explain all of the shoreline deformation features derived from analysis of NEXTMap DEM data or described in other published accounts. It seems that the interpretations proposed by Jarman (2008) and Peacock and May (1993) provide more satisfactory explanations of the complexity of deformation that the Parallel Roads have been subjected to. In summary, the key characteristics of the manner and pattern of the deformation of the Parallel Roads, as outlined in Chapter 7, sections 7.7 to 7.9, are:

1. The style of deformation varies between arching or warping, block dislocation (vertical movements without tilting) and tilting over comparatively short distances.

2. The direction of tilting can have opposite gradients on the same measured stretch of shoreline.
3. Maximal scales of dislocation are associated with former ice-marginal positions and/or landslips.
4. The dislocation patterns on the three shorelines (350, 325 and 260 m) are not always consistent within vertically adjacent shoreline stretches; in other words, the pattern of deformation on adjacent stretches of the three shorelines appears to have responded independently to deformation forces, except in the close vicinity of major landslips where the three shorelines appear to have responded in similar fashion, but at different scales.
5. Despite the complexity of the deformation patterns and the precision limitations of altitude measurements derived from NEXTMap DEM data, the shorelines show regional-scale gradients, from SW to NE along the whole length of the shorelines, but with superimposed localised gradients across the Roy valley that also appear to reflect the influence of ice-marginal positions (section 7.10).

The evidence as a whole therefore points to a combination of two major forms of deformation: (a) regional effects of glacial loading and unloading, perhaps also complicated by the effects of associated lake-body loading and unloading; and (b) much smaller-scale effects that have led to more localised warping and dislocation, which tend to mask the larger-scale trends. The fact that the scale of deformation is at a maximum around and just beyond the mapped Loch Lomond Readvance glacier limits in Glens Gloy and Roy suggests localised ice-loading or ‘forebulge’ effects, although ‘forebulge effects’ are not considered to operate at such short-distance scales and under such relatively small ice bodies: they are usually considered to have effects at some hundreds of kilometres beyond an ice sheet margin, and to require the weight of continental-scale ice sheets to depress the lithosphere and displace the upper mantle

beneath (Walcott 1970, Fjeldskaar 1994, Lambeck, 1991, 1993a, 1993b, 1998; Shennan *et al.*, 2002; Smith *et al.*, 2006). While much smaller-scale deformations of the crust are known from seismic and tide-gauge studies (Firth and Stewart 2000, Stewart *et al.*, 2000, Aubrey *et al.* 1988, Van Dam *et al.*, 1997), whether glacial ice bodies can propagate minor ‘forebulge’ type effects is not presently considered likely by experts in this field.

Yet undoubtedly some form of small-scale dislocation has badly deformed the Parallel Roads, and some of the evidence points to the localised effects of ice advance and decay. Another possibility may be the upward deformation of near-surface rock layers, displaced by increased hydrostatic pressure in joints and clefts, as envisaged by Peacock and May (1993), but possibly exacerbated by freezing of the ground surface. The amount of displacement would be conditioned by joint spacing, the surface gradient, the angle of dip of joints and bedding planes, and other localised factors. Hydrostatic pressures under glacial or lake-body loading may have caused upward displacement of near-surface bedrock, either horizontally or in arched formations, which, when relaxed following unloading, may have re-settled in a complex manner. This could explain the short-distance dislocations evident in both arched and horizontally-displaced stretches of all three shorelines, and also the opposing gradients found in blocks within the same stretch on a shoreline, for collapse of the displaced layers of near-surface rock may have involved a stochastic element. One difficulty with this explanation, however, is that much of the bedrock in Glen Roy has high-angle bedding, which might not have allowed strong hydrostatic pressures to build up – unless severe freezing of the exposed and saturated clefts could have instigated such forces.

A major problem, mentioned in Chapter 7 but not developed, is that variations in the surface altitudes of the Parallel Roads cannot be attributed entirely to

isostatically-induced deformation, for lake shorelines in arctic regions commonly show surface undulations caused by a range of natural processes and factors. These may reflect lithological variations, for example in foliation architecture or fracture concentration (e.g. Trenhaile, 2002; Aarseth and Fossen, 2004), or in the intensity and depth of lake-ice freezing, which can lead to ice-pushed ridges on shoreline platforms, and variations in the level of interface between lake ice and bedrock (e.g. Matthews *et al.*, 1986; Shakesby and Matthews, 1987). It is difficult, however, to distinguish between, and hence to quantify the effects of, such ‘natural’ factors from those of isostatically-induced deformation of shoreline surfaces in arctic regions; in order to be able to achieve this, studies are needed of platforms currently forming in modern arctic lakes in regions that have never been subjected to glacio-isostatic influences. The author is not aware of any studies of arctic lakes that qualify in this respect, for most detailed studies reported in the literature are from areas that were formerly glaciated, or that were close to former ice margins. Clearly, however, the undulating surfaces of the Parallel Roads of Glen Roy must reflect both ‘natural’ and isostatically-induced processes. However, the scale of the deformation reported here, as well as the arched form and step-like nature of most of the dislocations, suggests that isostatic warping of the shorelines has been the predominant deforming process, but this is an assumption in need of testing by future research.

#### **8.2.5 The time of formation of dislocations of the Parallel Roads**

The NEXTMap data suggest that deformational forces affected both sides of Glen Roy, but diminished in magnitude locally from NW to SE, disrupting the general (underlying) tilts of the shoreline surfaces, which decline from S/SW to N/NE. The scale of deformation tends to be greatest on the 350 m shoreline, and diminishes successively on the 325 m and 260 m shorelines. Those trend patterns can be discerned in shoreline stretches around landslide 1, 2 and 3 for all three shorelines.

The greatest scale of deformation is to be found in the area around landslide 3 in middle Glen Roy (section 7.8.3). Here the 350 m shoreline (stretch E) is severely dislocated with a displacement of up to 6.5 m over a distance of 200 m. The 325 m shoreline shows a similar pattern, with a dislocation of up to c. 5 m over a distance of 100 m, but there is no evidence of such severe dislocation of the 260 m shoreline here. The second largest scale of deformation is evident adjacent to landslide 2 in lower Glen Roy. On the east flank of the valley in this locality, the largest shoreline dislocation occurs at location Y:786200 (stretch A of three shorelines; see Figure 7.45 and 7.46), adjacent to landslide 2, with a 3 m uplift, as reflected in mean altitude values (Figure 7.46C). The scale of deformation adjacent to landslide 1 is much smaller than those in landslide 2 and 3, but shows similar patterns.

Because all three shorelines are affected by dislocation differentially, this means that at least some of the dislocation took place during the Loch Lomond Stadial. If the displacements had occurred during Holocene ('postglacial') time, then all three shorelines should have been affected to approximately the same degree. The greatest scale of deformation is in middle Glen Roy, and is associated with landslide 3 (see Figure 7.40), some 5 km beyond (north of) the maximum advance of LLR ice into Glen Roy. However, landslide 3 aligns with landslides 5 and 6, located near Alltnaray in Glen Gloy, and hence all three landslides (3, 5 and 6) may reflect differential loading effects in association with the retreat of ice in Glen Gloy to its temporary deglacial limit at Alltnaray. Landslide 2 (Figure 7.40) is adjacent to the maximum LLR ice limit in Glen Roy; landslide 1 is closely associated with an ice retreat limit in Glen Roy; and the strong dislocation of (in particular) the 350 m shoreline in upper Glen Roy is adjacent to the arcuate moraines at the western margin of the Turret fan, which have been interpreted as representing the maximum LLR glacial advance of the Gloy Glacier.

Hence the pattern of strongest dislocation of the Parallel Roads is consistently associated with inferred glacial limits, which suggests that changing ice and lake loads were responsible for the complex dislocation pattern.

It is also postulated that (i) the dislocation pattern detected in the surfaces of the Parallel Roads, along with (ii) the freshness of the surficial features associated with the landforms, and (iii) the association of landslips with the inferred retreat glacial limit for Alltnaray, are collectively best explained if the dislocation effects were imposed during the falling sequence of ice-dammed lakes. This fits the majority of the observations made from NEXTMap measurements with one exception: under this explanation, it is difficult to explain the scale of dislocation of the 350 m shoreline in upper Glen Roy, because by the time the 350 m lake had formed (at the maximum expanse of ice in Glen Roy), the ice in Turret had probably retreated into Glen Gloy. This element remains difficult to fit into the scenario just described.

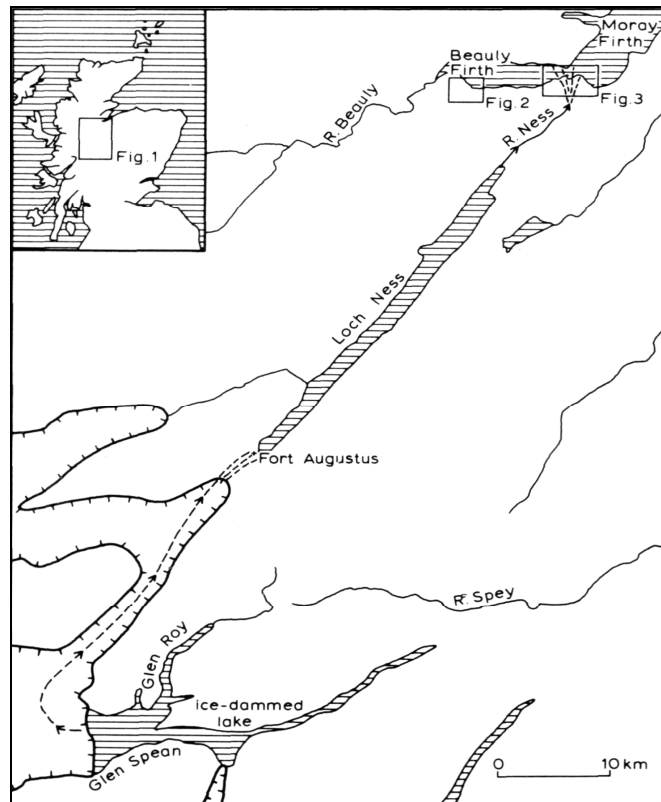
### **8.2.6 The locus and timing of major jökulhlaup events in the Roy-Gloy area**

Sissons (1979a) suggested that the final drainage of the 260 m Spean-Roy ice-dammed lake was conducted by a jökulhlaup event which lasted for a few days. Two years later (1981b), he further developed his jökulhlaup theory, by proposing that when the jökulhlaup took place, 5 km<sup>3</sup> of water escaped sub-glacially from the western Glen Spean valley, turned north-eastwards to flow along the Great Glen (Loch Lochy, Loch Oich and Loch Ness), depositing large gravel masses at Fort Augustus and Inverness, the latter covering at least 7 km<sup>2</sup> with a maximum recorded sediment thickness of 39 m (Figure 8.5). Following jökulhlaup drainage, lake water levels in Glen Spean dropped successively to 113 m, 99 m, 96.5 m, 90.5 m, 74.5 m and 71.5 m, always draining north-eastwards along the Great Glen, instead of south-westwards towards Loch Linnhe (Sissons 1979c; Figure 8.6).

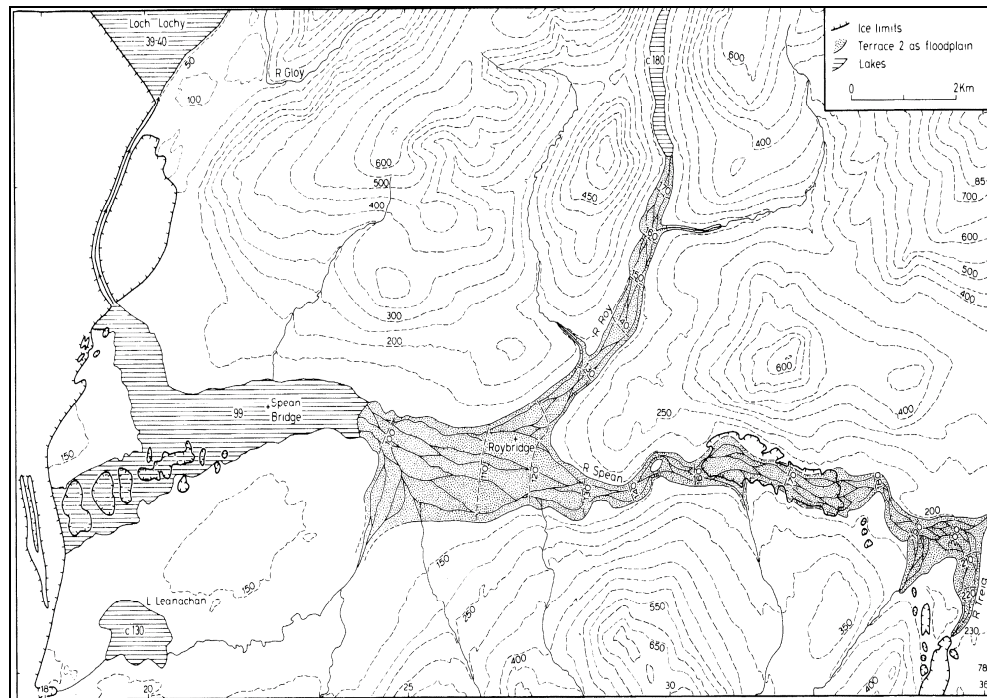


Russell *et al.*, (1998) examined new sedimentary evidence exposed in the Auchteraw terrace at Fort Augustus, linked by Sissons to the jökulhlaup event, and found the sedimentary deposits to be consistent with jökulhlaup deposition, showing a variety of lithofacies types that accorded with those of other studies of modern jökulhlaup deposits. Although that study supported the jökulhlaup mechanism that Sissons (1979a) proposed, it did not critically examine his model for its drainage routes.

The present author acknowledges that those very large gravel masses described from Fort Augustus and Inverness must have been deposited by a jökulhlaup flood that took place at a late stage during the Loch Lomond Stadial, but offers an alternative suggestion of the route that the drainage adopted. It is contended here that there is a higher probability that the major jökulhlaup event that led to the deposition of these fans originated from Glen Gloy, and not Glen Roy, for the following reasons:



**Figure 8.5 The Spean-Roy ice-dammed lake and proposed jökulhlaup route (arrows), with the locations of associated fan deposits at Fort Augustus and Inverness (Sissons 1981b).**



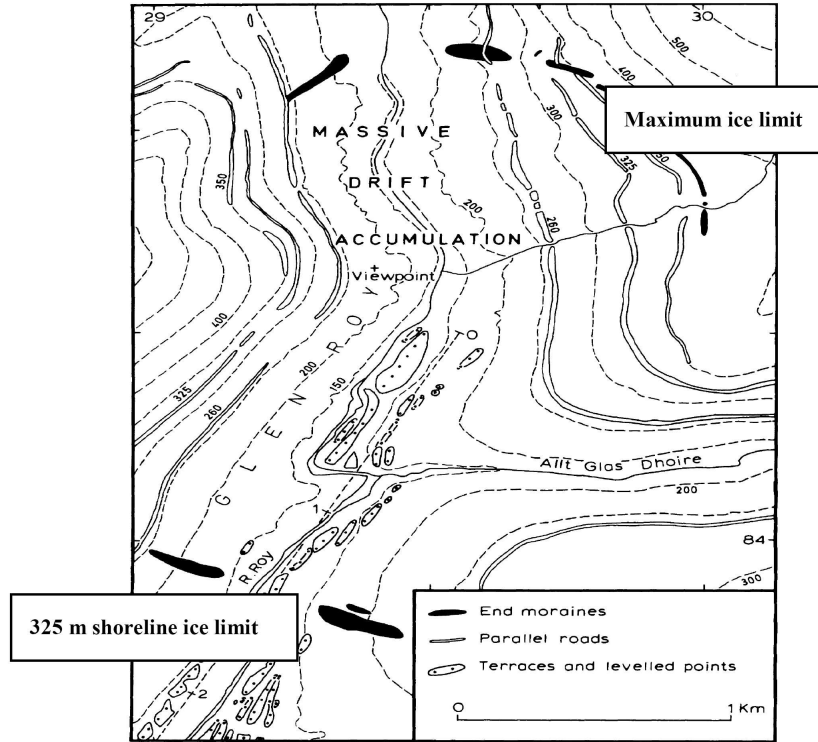
**Figure 8.6 Reconstructed lake water levels, glacier ice margin and associated fluvial terraces formed after jökulhlaup drainage according to Sissons (1979c).**

1. If the final drainage of the 260 m Spean-Roy ice-dammed lake was caused by a jökulhlaup that lasted several days, then it might be expected that the moraines and other mapped drift features below 260 m altitude in Glen Roy and Glen Spean would have suffered high velocity flood waters and been swept away or destroyed by them. Oddly, the massive drift of the LLR ice maximum limit in the vicinity of the Viewpoint and the cross-valley moraines associated with the 325 m lake further south (Figure 8.7A), as well as the various kettles, kames, kame- and river-terraces and cross-valley moraines that occupy much of Glen Spean (Figure 8.7 B, C and D), are all clearly well preserved.
2. Peacock and Cornish (1989) claimed that a small cross-valley moraine is preserved in Glen Gloy at about 2 km upstream of Glenfintaig Lodge, where the 355 m shoreline begins (p.14) (Figure 8.8, blue box b). They also pointed out mounds of till and gravel at Alltnaray, which they defined as the LLR ice limit in Glen Gloy (p.16) (Figure 8.8, blue box a). However these landforms are not

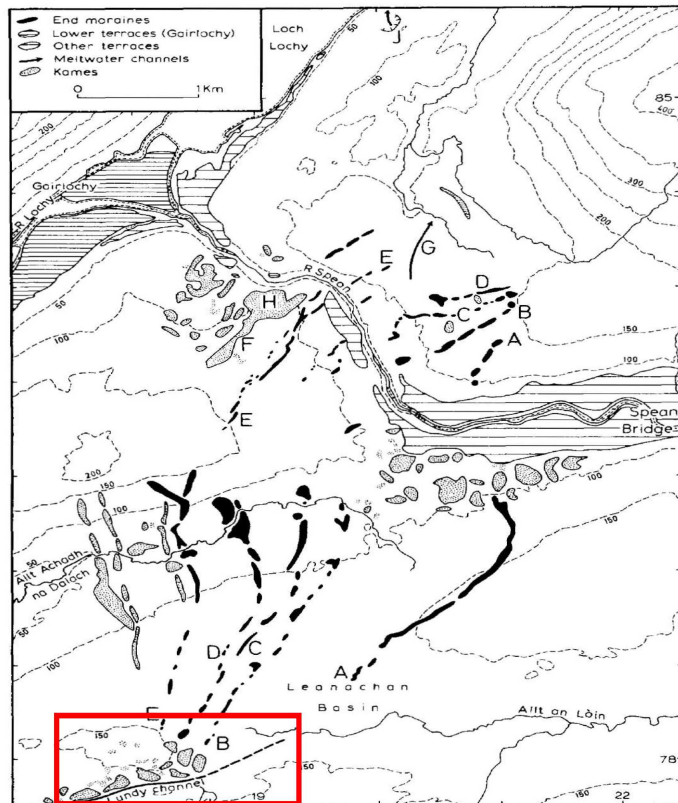
evident on NEXTMap DEM plots. What is very unusual is the insignificant size of the landforms in this vicinity compared with the scale and abundance of the moraine ridges in Roy (Figure 8.8, green box c) and Glen Turret/Coire Dubh. A reasonable inference, therefore, is that comparable landforms in Glen Gloy may have been swept away by large-scale lake drainage.

3. The present-day drainage route of the River Gloy runs SW initially, but then abruptly changes course to flow northwards around Glenfintaig Lodge to enter Loch Lochy. Yet the River Spean initially runs E-W but changes to a southwards course at Gairloch, to join the River Lochy and finally flow into Loch Linnhe (Figure 8.9). The difference in altitude between Loch Lochy (30 m OD) and Loch Linnhe (0 m OD) means that the floodwaters of a jökulhlaup event would have to have lifted up an ice mass and flow upstream to join Loch Lochy, if it originated in Glen Spean. Conversely, if the jökulhlaup event took place in Glen Gloy, the force of gravity would drive the floodwaters north-eastwards, into Loch Lochy and eventually along the Great Glen to the North Sea.

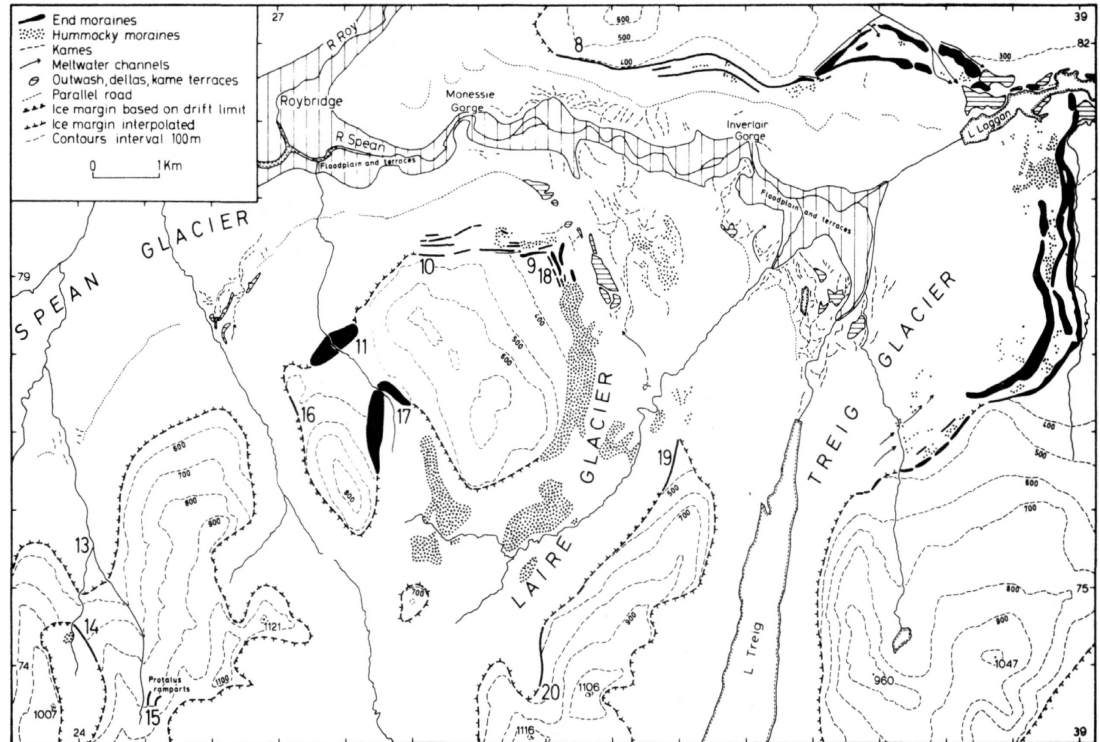
A.



B.



C.



D.

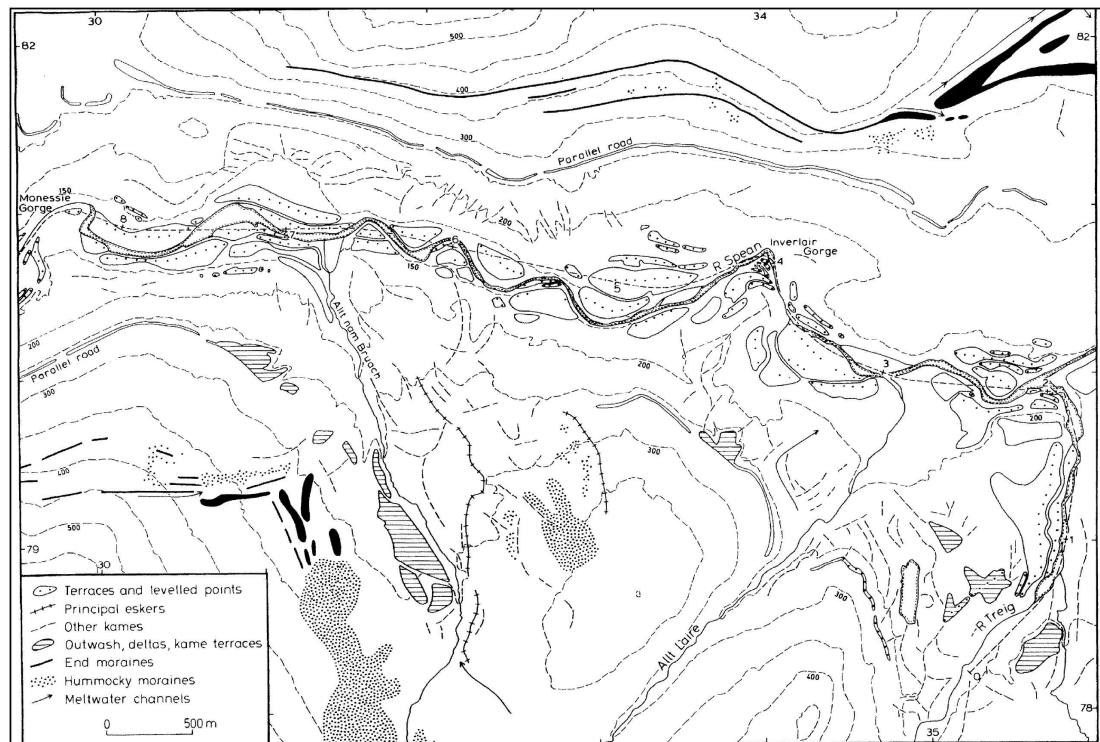


Figure 8.7 Landforms in the area around (A) the Glen Roy Viewpoint from Sissons, 1979c); (B) Spean Bridge and Gairloch (from Sissons, 1979a); (C) Loch Treig/Roybridge (from Sissons, 1979c; red box indicates position of Lundy Channell); (D) Triage valley and part of the Spean valley (from Sissons, 1979d).

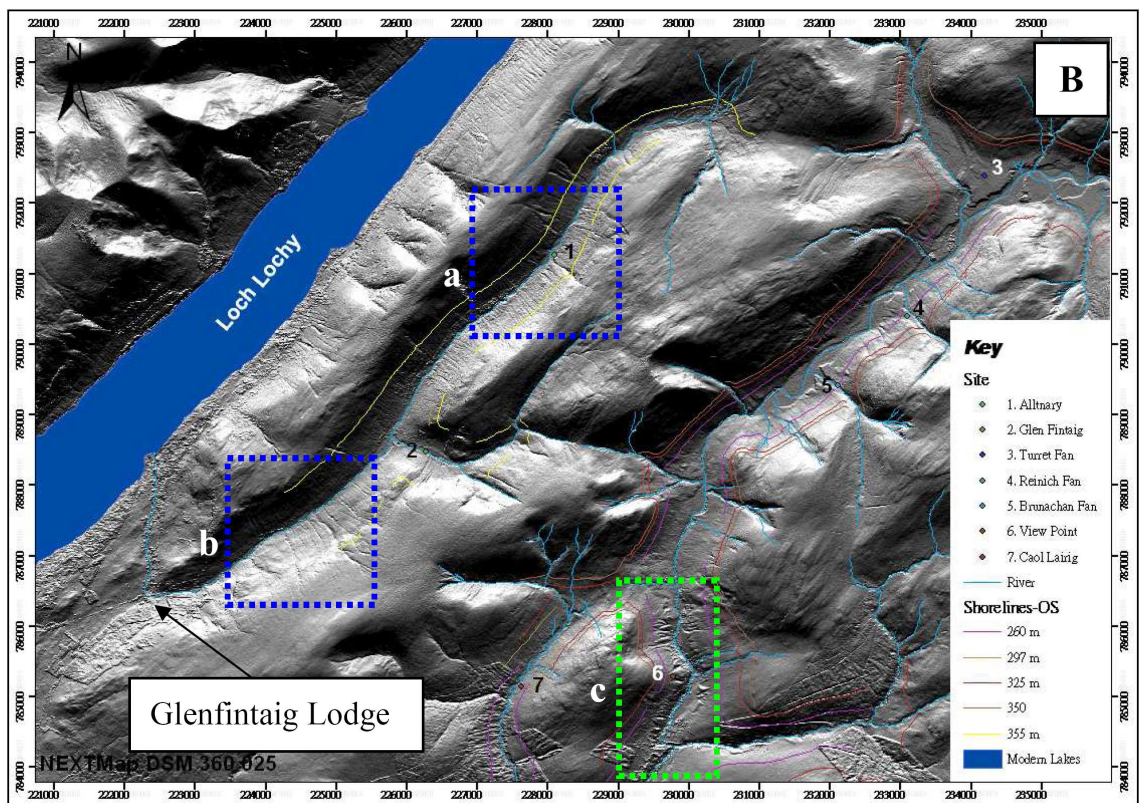
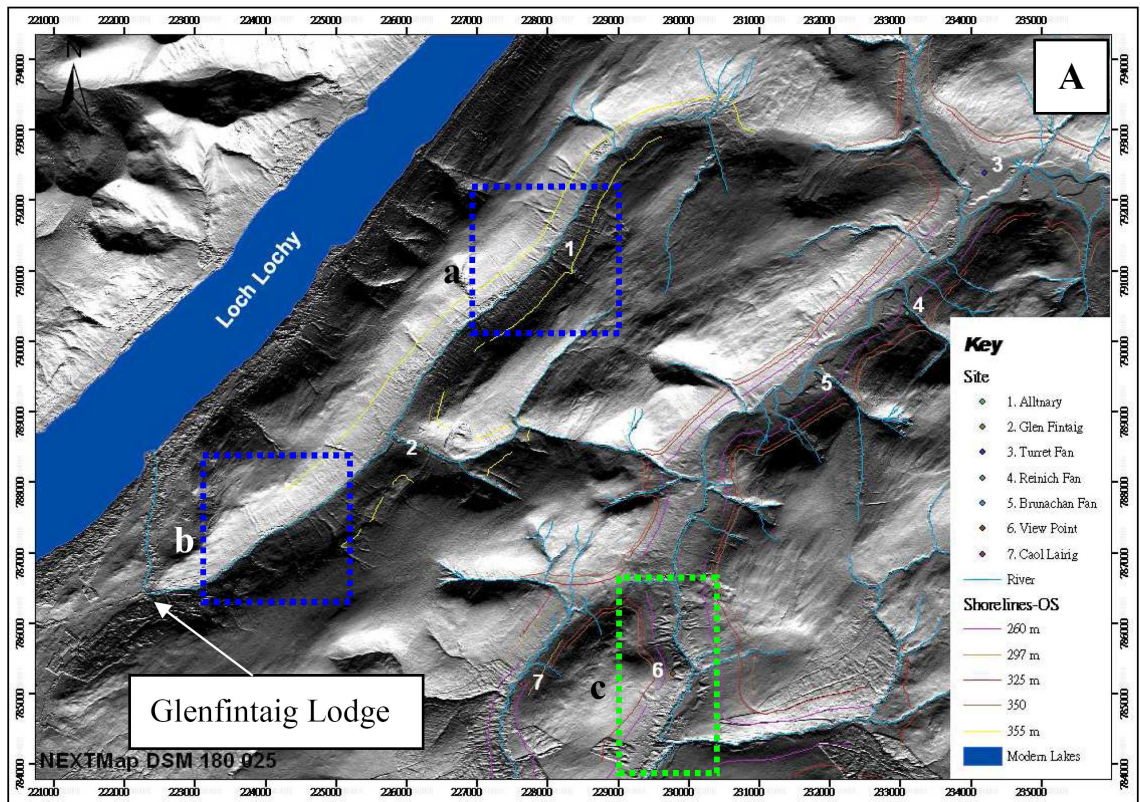
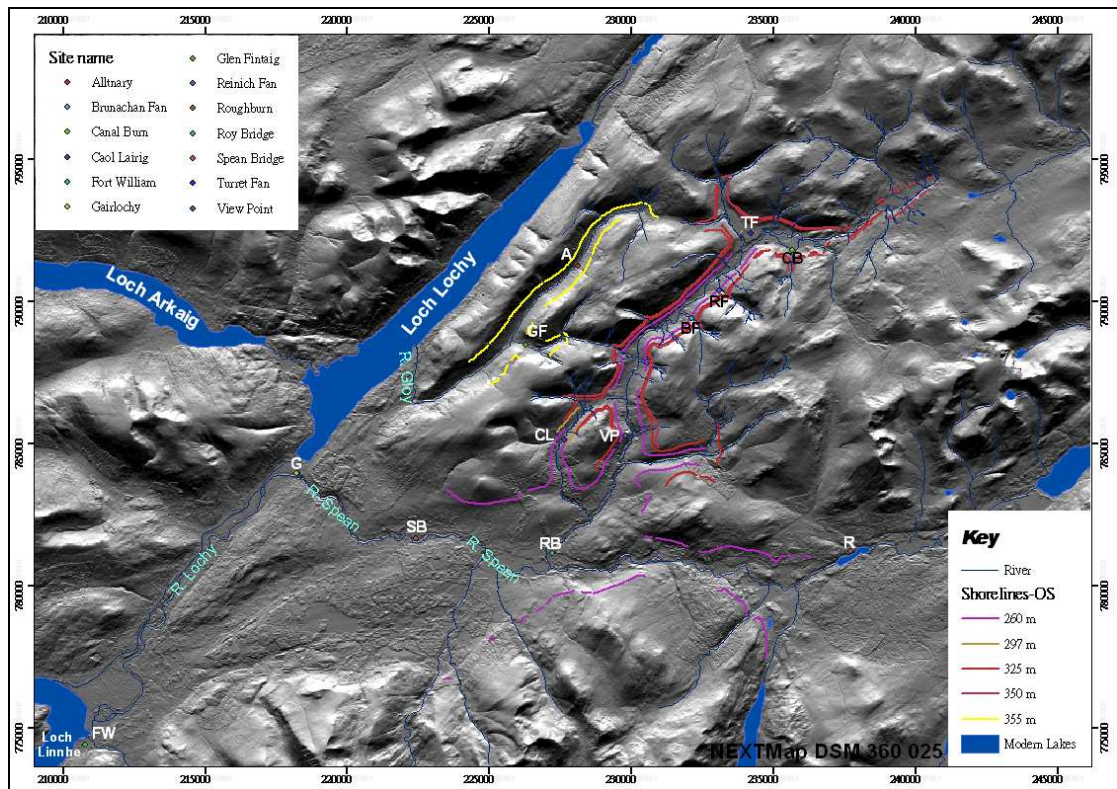


Figure 8.8 NEXMap DEM plot for the area around Glen Roy and Glen Gloy. A is illuminated from south, and B is illuminated from north. For comparisons of the detail in rectangular boxes a, b and c, see text.



**Figure 8.9** Modern catchment and topographic details in Glen Spean and Glen Gloy, on NEXTMap-derived DEM plot.

Sissons (1979a, 1979c and 1981b) did not provide much evidence to support his conclusion that the jökulhlaup deposits at Fort Augustus and Inverness originated from Glen Spean. He assumed a drainage route through the Lundy Channel near Creag Aoil, Spean Bridge (Figure 8.7 B, red box). Russell *et al.*, (2003) have investigated exposed sediment sequences on the northern flanks of the Lundy Channel, and have concluded that they reflect periodic jökulhlaup drainage from ice-dammed lakes with elevations between 260 m and 113 m, draining via the Lundy Channel. This implies that the final drainage of the 260 m lake waters may have flowed through the Lundy Channel to Loch Linnhe, rather than north to Fort Augustus and Inverness. The present author suggests the alternative Glen Gloy drainage model to be more likely, an explanation that deserves robust testing in future research.

### **8.3 The pattern and sequence of events in Glen Roy during the Loch Lomond Stadial**

Sissons (1978, 1979a 1981a and 1983) suggested that Loch Lomond Readvance glacier ice was generated in the mountains to the west of the Great Glen and advanced up Glen Gloy and Glen Spean, where it was joined by contemporaneous glaciers emerging from the Nevis mountain range. The resulting combined ice mass blocked the original river drainage flowing towards Loch Linnhe and caused the formation of the ice-dammed lakes. Continued advance of the ice led to rising lake levels controlled by four cols: the Patack/Mashie col at 260 m, the Roy/Laggan col at 325 m, the Roy/Spey col at 350 m and the Gloy/Turret col at 355 m, the corresponding heights of the principal lake shorelines preserved in the Roy and Gloy valleys (Figure 5.1 and 8.10). A further important col to note is that between Caol Lairig and Glen Roy at 297 m (Figure. 8.10), which temporarily controlled a lake at this level within Caol Lairig during the Loch Lomond Stadial. These cols controlled lake levels during both a rising sequence when the lower cols were successively blocked by ice, and a falling lake level sequence as the ice decayed. Other shorelines, noted in the literature and also observed by the author, occur at 334 m in Glen Roy, 295 m in Glen Gloy and 416 and 426 m in Glen Fintaig, which suggest additional short-lived lake levels. These are not considered in detail here because they are much less distinct and extensive than the better-known Parallel Roads, and also because the features controlling their overflow heights are uncertain.

While the cols that controlled the surface levels of the classic Parallel Roads are well established, less clear is the full picture of dynamic inter-linkage between the transient Loch Lomond Readvance ice margins and consequent adjustments in lake surface altitude. Taking all the evidence obtained from NEXTMap DEM data analysis and the arguments stemming from this evidence, discussed in chapters 6 and 7 and the earlier sections of this chapter, the author proposes a sequence of events during the Loch



Lomond Stadial for the Glen Roy area that in part confirms earlier interpretations, but with some important differences: the key stages are encapsulated in Figure 8.10 and reflect the evidence summarised in section 8.2. Ten key stages in ice margin position are indicated in Figure 8.10, covering the ice advance into the study area and a rising trend in lake levels (S1 in Glen Gloy and S2 to S6 in Glen Roy), followed by progressive ice decay and a falling trend in lake levels (S4, S5/6 and S10 in Glen Gloy; S7, S8, S9 and S11 in Glen Roy and Glen Spean). Key elements in this scheme are as follows.

### **Stage 1: LLR glacial ice maximum in Glen Gloy**

Glacier ice that advanced from west of the Great Glen during the LLR appears to have migrated up Glen Gloy, overflowed the 355 m Gloy-Roy col, and spread into Glen Turret, terminating at the Turret fan. At this time, the ice in lower Glen Spean may not have been sufficiently thick or competent to maintain a lake in upper Spean and Glen Roy at 260 m (see section 8.2).

### **Stage 2: Rising sequence of the 260 m lake in Glen Roy**

The ice became sufficiently thick in lower Glen Spean to create the 260 m lake, controlled by the 260 m Pattack-Mashie col, only after the Nevis ice joined the ice encroaching from west of the Great Glen. At this stage, the 260 m lake submerged much of Glen Spean and the Loch Laggan basin, the lower part of Coal Lairig and Glen Roy as far as its confluence with Glen Turret. The water of the 260 m lake probably came into contact with the margin of the glacier that had over-topped the Gloy-Turret col, causing it to recede (Figure 6.34).

### **Stage 3: Rising limb of the 297 m lake in Caol Lairig**

When the ice front advanced from the lower part of Glen Spean into the southern part of Glen Roy, it also invaded Caol Lairig. Further advance of the ice into both lower Glen

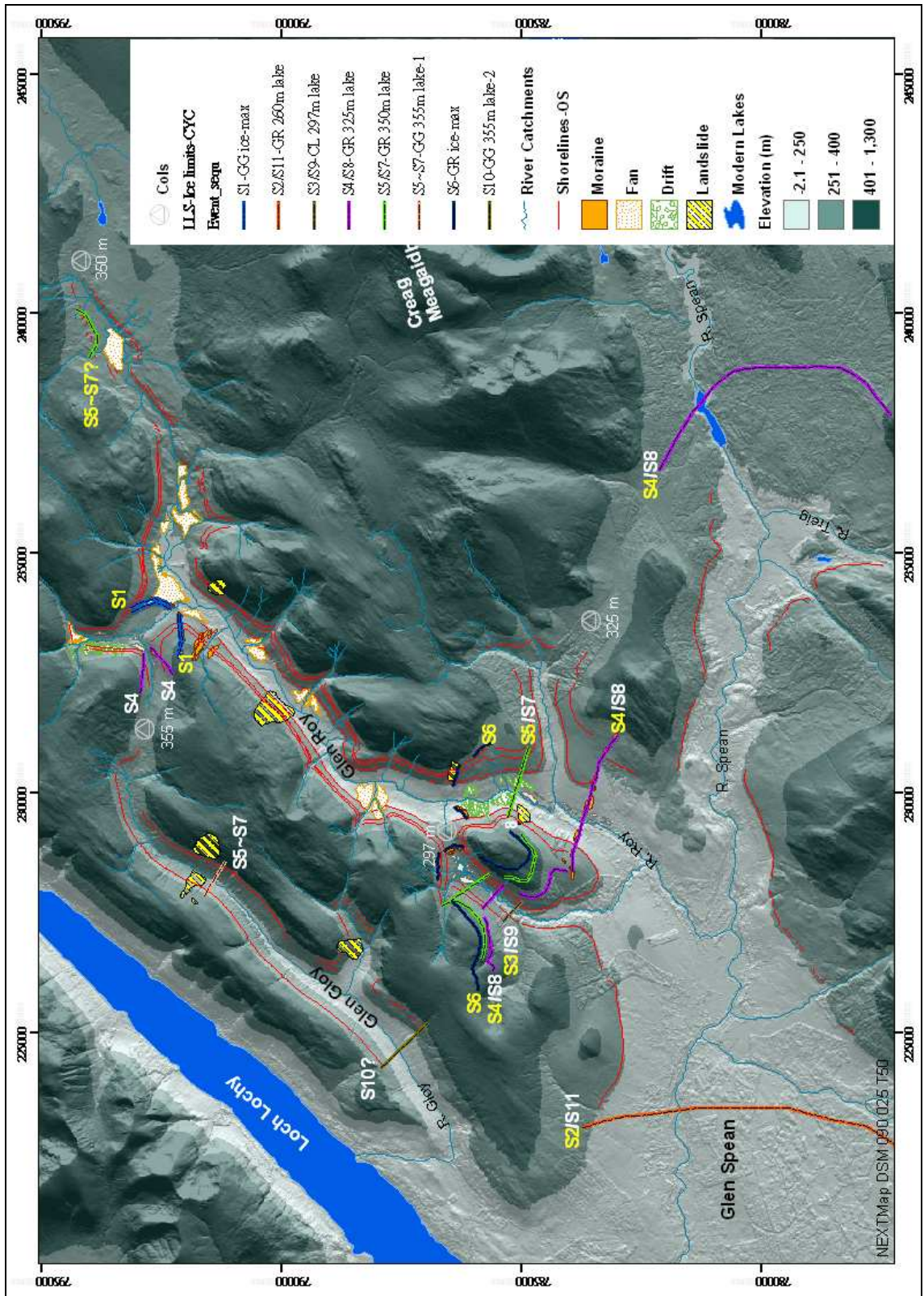


Figure 8.10 The sequence of ice advance and the rising lake sequence (labelled yellow) and of ice decay and the falling lake sequence (labelled white) in the Gloy-Roy-Spean area, according to the author's observations and interpretation.

Roy and Caol Lairig was sufficient to raise the level of the water in Caol Lairig above 260 m, after which its surface level became controlled by the next lowest overflow point – the 297 m col between Caol Lairig and Glen Roy (Figure 8.10).

#### **Stage 4: Rising stage of the 325 m lake**

The ice advanced further into the lower part of Glen Roy and the Coal Lairig valley, causing the lake water in Glen Roy to rise to 325 m, the height of the controlling col in Gleann Glas Doire (Figure 8.1). At this stage, water would have flowed from the Roy over the 297 m col into Caol Lairig, and over the Gleann Glas col into the 260 m lake in Loch Laggan, the height of which continued to be maintained by the Pattack-Mashie col (Figure 5.1). The ice margin of the Gloy Glacier at the Turret-Roy confluence was forced to retreat by the deeper waters of the 325 m lake, becoming stabilised at the mouth of the Allt a Chomlainn, where it formed an ice-contact delta (feature g, Figure 6.28; Figure 6.29), moraine (feature h, Figure 6.28; Figure 6.29A) and associated kame terrace (feature o, Figure 6.28; Figure 6.29A).

#### **Stage 5: Rising stage of the 350 m lake**

The ice in lower Glen Roy advanced further to block Gleann Glas Doire causing the lake level in upper Glen Roy to rise to the 350 m level in Caol Lairig, Glen Roy and Glen Turret. At this stage, the ice in Glen Spean reached its maximum position at Roughburn but the water surface level in the Loch Laggan basin remained at 260 m. The margin of the Gloy Glacier receded to a position near Alltnaray (Figure 5.5, H; S5-S7, Figure 8.10). There is independent evidence that suggests that glacier ice accumulated during the LLR on the Allt Dearg plateau, with a terminus close to Luib Chonnal (NN394937). The distribution of the 350 m shoreline in this vicinity suggests that the ice was at its margin at this stage, as the shoreline is absent from the ice-marginal landforms, but evident on adjacent slopes (Figure 7.17 and 7.18).

### **Stage 6: LLR ice maxima in Glen Roy, Caol Lairig and Allt Chonnal**

The ice reached its maximum position in Glen Roy at the Viewpoint and in Caol Lairig at the terminal moraine which lies close to the 297 m col (Figure 8.10). Stages 1 to 6 were termed the “rising sequence” by Palmer (2005), which was followed by what he termed the “falling sequence”, as the ice receded and the lake levels were progressively lowered. However, as discussed in section 8.2, the glaciers in Glen Roy, Glen Gloy and Caol Lairig did not act simultaneously, and the precise sequence of events is not always clear. As noted above, the Gloy Glacier started to retreat while the Roy Glacier was still advancing. Evidence is also presented in section 8.2 that indicates that the glacier in Caol Lairig receded more quickly than that which occupied lower Glen Roy.

### **Stage 7: Falling sequence: abandonment of the 350 m lake in Glen Roy and Caol Lairig**

At some point after the ice had reached its maximum position in Glen Roy, the ice would have started to retreat from its maximum position and when it had decayed sufficiently to enable water to flow over the col in Gleann Glas Dhoire, the lake level would have fallen to 325 m. Hence the Roy ice-front must have retreated from position S5/S7 to S4/S8 (Figure 8.10). It is not clear what was happening in Glen Gloy at this time, but the severe dislocation of the 350 m shoreline in Glen Roy close to landslip 3 (Figure 7.40) may have taken place soon after the shoreline was abandoned. This is inferred from the link previously made between landslips 5 and 6 in Glen Gloy and landslip 3 in Glen Roy. It is hypothesised that all three landslips, and the degree of dislocation of the 350 m shoreline in Glen Roy, were triggered by ice-front movements near Alltnaray. If correct, then the ice-front in Glen Gloy remained close to Alltnaray after the ice-front in Glen Roy had retreated sufficiently for the surface of the ice-dammed lake in Glen Roy to fall to 325 m. Furthermore, some ice retreat also

occurred in Caol Lairig, for the 325 m shoreline occupies parts of that valley that were previously occupied by ice during the maximum advance of the ice to the moraine at the col between Caol Lairig and Glen Roy.

#### **Stage 8: Formation of the 297 m lake in Caol Lairig during the falling sequence**

The ice margin in Caol Lairig continued to retreat but remained sufficiently thick to retain a lake in the upper part of the Caol Lairig valley after the Roy ice-dammed lake fell to 260 m. The 297 m shorelines in Caol Lairig are unique to that valley, its surface controlled by the lowest point on the col between Caol Lairig and Glen Roy. For the lake to exist therefore, water must have been able to flow over into Glen Roy, and that could only happen when the lake waters in Glen Roy were lower than those in Caol Lairig. Hence the 297 m lake during the falling sequence occurred after the lakes in Glen Roy had fallen from 325 to 260 m. The ice margin in Caol Lairig at this time is picked out by the southerly limits of the 297 m shoreline (line S3/S9, Figure 8.10).

#### **Stage 9: Abandonment of the 355 m lake in Glen Gloy**

There is no evidence for recessional ice-marginal positions in lower Glen Gloy, south-westwards of Alltnaray. A reasonable inference, therefore, is that the ice mass in lower Glen Spean and the Loch Lochy area remained thick enough to prevent drainage of the 355 m lake and the development of lower lake shorelines, and hence the ice margin appears to have been located somewhere between Alltnaray and the mouth of Glen Gloy (line S10, Figure 8.10) during the time of the falling lake sequence in Glen Roy (stages 7, 8, 10). It has been speculated that final drainage of the Gloy ice-dammed lake may have been by jökulhlaup (section 8.2.6); if this is correct, then ice in the lower part of Glen Spean and adjacent parts of the Great Glen must have retained sufficiently thick ice to prevent drainage towards the south-west, towards Loch Linnhe, which is the current natural drainage route. This would imply that as the ice dissipation in the region

gathered momentum, the ice front retreated from Glen Gloy faster than the ice-front in Glen Spean, which seems credible, since the ice tongue that penetrated Glen Gloy was much narrower and less massive than that in the Spean.

### **Stage 10: Final drainage of the 260 m lake in Glen Roy**

Sissons (1979c and 1981b) suggested that the final drainage of the ice-dammed lakes in the Roy-Spean catchment could be attributed to catastrophic floods or 'jökulhlaups' which were followed by several flood events of lower magnitude as the ice mass gradually shrank and the Spean-Roy lake system intermittently emptied(see above). Sissons (1979c) and Sissons and Cornish (1983) instrumentally measured the altitudes of the landforms of lower Glen Roy and the Glen Spean valley and found a series of terraces with surface altitudes at 113, 99, 96.5 and 90.5 m, which they concluded formed after catastrophic 'jökulhlaup' drainage, and during the time when the ice mass was gradually diminishing in size, with temporary halts in ice margin recession allowing the intermittent existence of lower ice-dammed lakes. A two km-long sector in Glen Spean, where kames and other dead-ice features abound, may mark the position of the ice margin at that time. A detailed analysis of these features and indeed this part of Glen Spean was not included in the present study; nevertheless, the evidence obtained from features in Glen Roy relating to the final drainage of the 260 m lake suggests a much gentler release of lake waters and therefore smaller-scale jökulhlaups from Glen Roy than envisaged by Sissons, as outlined in section 8.2.6.

A synopsis of the sequence of events summarised in the 10 stages outlined above is as follows:

1. Ice advances into lower Great Glen and northern flanks of Glen Nevis range, but develops quickest around the entrance to Glen Gloy.

2. The ice invades Glen Gloy, overtops the col into Glen Turret, and reaches the Turret Fan; the ice in Glen Spean at this stage is not sufficiently thick to prevent drainage towards Loch Linnhe, so that the Turret Fan forms subaerial deposits.
3. The ice advances into lower Glen Spean and becomes sufficiently thick to block drainage towards Loch Linnhe; at this point the 260 m ice-dammed lake is formed in Glen Roy, which affects the ice-front at the Turret Fan, causing a change to subaqueous deposition.
4. Further advance of the ice front into Glen Roy causes the lake level in Glen Roy to rise to 325 m; part of the Roy ice-front also invades Caol Lairig; the ice front at the Turret Fan is destabilised by the deeper lake waters, and recedes to the confluence between the Allt a Chomlainn and the Turret; ice has also been building up on the Carn Dearg plateau, with an ice-front tongue descending on to the floor of the upper Roy.
5. The ice reaches its maximum position in Glen Roy; the 350 m lake is formed in Glen Roy after the col in Gleann Glas Dhoire is blocked off by the advancing ice; a further increase in water depth causes the Gloy Glacier in Glen Turret to recede further and the ice front in Caol Lairig to start to recede; this rise in lake levels may also have destabilised the ice front at Allt Chonnal in the upper Roy, causing it to retreat.
6. Ice recession commences in Glen Roy and severe displacement of the 350 m lake shorelines takes place, accompanied by landslip activity; the ice-front in Glen Gloy is close to Alltnaray, where landslipping in Glen Gloy is concentrated.
7. The ice retreats further in Glen Roy, allowing the lake surface to fall to 325 m; the ice front in Caol Lairig recedes to enable the 325m lake to flood in; it is presumed that the 355 m lake still exists in Glen Gloy, and hence that the Gloy Glacier still blocks the valley.

8. Continued ice retreat in Glen Roy allows lake waters to escape through the col NE of Loch Laggan, and hence a fall in lake level to 260 m; the ice front in Caol Lairig is maintained at a sufficient thickness for the 297 m lake to develop within Caol Lairig.
9. The ice front in Glen Gloy recedes to a point where it fails to hold back the head of water in Glen Gloy, and one or more major jökulhlaups occur; in the author's opinion, this is the source of the flood waters that poured along the Great Glen towards Loch Ness.
10. The ice in Glen Spean recedes and or down-wastes sufficiently to enable drainage of meltwaters into Loch Linnhe, perhaps by jökulhlaup processes of diminishing magnitude.

#### **8.4 Key conclusions concerning the potential of NEXTMap DEM data**

The key conclusions to emerge from the experimental work undertaken in this PhD project, concerning the potential benefits of NEXTMap DEM data for geomorphological mapping, are as follows.

First, it has been shown that in broad terms, in both the Loch Lomond area (Chapter 4) and the Glen Roy area (Chapters 6 and 7), not only are surface forms of a range of glacial and associated landforms faithfully represented in NEXTMap, but they can be greatly enhanced by manipulation of light incidence, so that (a) features can be viewed under optimal light conditions and (b) some very subtle features in the landscape, that are not obvious in the field or are obscured by shadows on aerial photographs, become evident. This advantage of NEXTMap was applied systematically in the project to generate maps in which all features are represented under optimal light conditions. The results have provided a more complete picture on which to base



interpretations and inferences concerning the origins of, and relationships between, different suites of landforms. Some features that are either very small in scale (less than 1 or 2 metres in amplitude) or within the shadow of very steep hillsides are, however, difficult to resolve from the NEXTMap DEM plots, though this has been a problem encountered in less than 15% of the mapped areal cover reported here. Almost 100% non-obscured coverage with optimised light conditions can be achieved for areas of low relief that contain well formed glacial features, such as on the low ground to the south of Loch Lomond and in large parts of the Glen Roy area.

Second, NEXTMap appears to provide very precise representations of ground surface altitude variations, as shown by the experiments conducted on the Heathrow airport runways and the hydro-electric pipelines close to Fort William (Chapter 7). The ground surface appears to be reproducible to within an error of  $\pm 10$  cm for measurements obtained from flat, artificial surfaces (as for example the measurements made of the Heathrow runways), but for natural undulating terrain of the type encountered in the Glen Roy area, the errors are up to 0.5 m at maximum but more usually as low as 0.25 m. This conclusion is supported by the measurements made on terrace surfaces close to Loch Laggan, as well as on the adjacent lake surface (Figure 7.26 to 7.28), where the lake surface is represented as a straight horizontal line, while the terrace surface shows small variations considered to reflect natural ground undulations. The sub-horizontal form of the terrace is well represented, however, so that there is little doubt as to its terrace form. More difficulty was experienced with measurement of the ancient lake shorelines in Glen Roy, however, where several problems compound the application of NEXTMap measurements: these include variations caused by slope deposits slumping on to, and peat building on, the shoreline surfaces, gully erosion, and complex deformation of the surfaces as a result of glacial and lake loading/unloading. These difficulties make the measurement of the shoreline surfaces a trial using any approach,

including carefully controlled field measurements. Indeed, J.B. Sissons (pers. comm.) is of the opinion that precise measurement of these surfaces is unproductive, because of what he regards as overbearing problems of dislocation of their surfaces, an opinion the present author would not agree with, as developed next.

Third, and probably one of the greatest advantages of NEXTMap, is the potential it provides for making an enormous number of measurements of the ground surface in a relatively short time, in order to generate robust tests of particular geomorphological observations or proposals. This facility was applied in this thesis to make a comprehensive examination of the form of the surfaces of the Parallel Roads, and to test whether underlying along-shoreline gradients could be identified (i.e. the original, non-deformed trends), despite the highly distorted nature of their surfaces. Nearly 32,000 altitude measurements were made, the results presented in Chapter 7. This degree of analysis would take considerable effort and time if based on ground survey. The results suggest that, despite the perceived difficulties, some sustained trends can be discerned in the reconstructed along-shoreline gradients of all three Parallel Roads, and the fact that all three independently-measured surfaces show consistent gradient directions provides some confidence in the results. The inference is that the underlying along-shoreline gradients relate to large-scale regional isostatic tilting. In addition, however, the new data also show some local-scale off-sets to these trends, such as differences between the altitudes of the shorelines on the western side of middle Glen Roy compared with the eastern flank. The overall results for the form of the Parallel Roads presented in Chapter 7 have revealed a complex pattern of deformation that could only be discernible within such a comprehensive data-set.

It has also been shown, however (in section 7.11), that the direction and magnitude of maximum tilting of the shorelines are affected by the azimuth of the plane of projection

used. This is especially the case where the data used for trend surface analysis (TSA) are confined to within a single valley, and where the data are affected by major changes in the course of the valley and, correspondingly, in the alignment of the shoreline platforms. This has a number of implications for the application and interpretation of TSA procedures. It is argued in section 7.11 that a series of experiments should be run, to test the outcomes of systematic changes in axial projection, and by excluding data clearly affected by localised aberrant values. In other sections of Chapter 7, the data have also been analysed using other statistical measures, such as regression trends for individual sectors and mean and standard deviation values for individual 'stretches' of the shorelines. Due to limited time, the collective statistical data generated in this project has been under-utilised, and may hold important insights into the pattern of deformation of the shorelines. Systematic statistical tests of localised aberrant values and of the effects of changing axial projection direction are experiments planned by the author for the future. The important point to emphasise, however, is that NEXTMap DEM data enable these tests to be made more efficiently than by manual surveying methods, though the validity of the data that is generated needs to be tested still further.

Fourth, a facility that has been under-exploited in the present thesis because of constraints of time is the ability to represent (model) abstract elements, such as the former lake bodies at different stages in their development (Chapter 6). If time had permitted, this could have been exploited further, to reconstruct the former ice bodies, lakes, fans and local drainage features in order to illuminate their precise inter-relationships. The results might explain the origins of additional features in the landscape that escaped close examination in the present project.

All of the above approaches were adopted in the present study of the Glen Roy area to establish whether fresh light could be shone upon a number of disputed issues surrounding the age and sequential development of the famous Parallel Roads and associated glacial landforms. The key outcomes, summarised in section 8.3 above, broadly support the 'Sissons model' (Chapter 5) for the age of, and controls over, the form and distribution of the former ice-dammed lakes, but several new insights have also emerged, which have been outlined in earlier sections of this chapter. Most notable are (i) a possible resolution of the long-held dispute over the age and sedimentary context of the Turret Fan; (ii) a more complete picture of differences in timing of advance and retreat of the Loch Lomond glacier ice-fronts in the Gloy-Turret, Roy, Caol Lairig and Carn Dearg catchments; (iii) clarification of the mode of deformation and isostatically-controlled origins of the Parallel Roads; and (iv) a different origin for the jökulhlaup floods that drained into Loch Ness, which are thought to have been released from Glen Gloy, and not the Spean-Roy ice-dammed lakes.

Of course, these conclusions are difficult to confirm or reject using only geomorphological evidence, and need to be tested further by the application of independent stratigraphical and dating methods. In this regard, however, NEXTMap technology may also have a role to play, because the reconstructions of former glaciers and lakes during the Loch Lomond Readvance, summarised in this and earlier chapters of the thesis, have important physical implications. For example, it has been assumed that the effects of raising and lowering of lake levels would have had concomitant impacts on glacier margins, while the dislocation and deformation of the Parallel Roads have been attributed to differential loading and unloading caused by the expansion and reduction in the size of both local glaciers and ice-dammed lake bodies. These ideas might be testable by generating physical models of the spatial distribution of load, based on NEXTMap measurements of hypothesised glacier and lake volumes, and comparing

the results with the measured patterns of dislocation of the lake shorelines. The weight distribution of ice could be modelled using NEXTMap DEM data from the geomorphological evidence of terminal limits and lateral trimlines, while lake volumes and load impacts would be relatively easy to compute from the distribution of the lake shorelines. Future research should exploit this additional capability of NEXTMap technology, to test further the ideas presented in this PhD thesis.

## Bibliography

---

- Aarseth, I. and Fossen, H. (2004). A Holocene lacustrine rock platform around Storavatnet, Osterøy, western Norway. *The Holocene* **14**, 589-596.
- Agassiz, L. (1840). On glaciers, and the evidence of their having once existed in Scotland, Ireland and England. *Proceedings of the Geological Society of London* **3**, 327–332.
- Anderson, B. G., Mangerud, J., Sørensen, R., Reite, A., Sveian, H., Thoresen, M., and Bergstrom, B. (1995). Younger Dryas ice-marginal deposits in Norway. *Quaternary International* **28**, 147-169.
- Andrews, J.T. and Barnett, D.M. (1972). Analysis of strandline tilt directions in relation to ice centers and Postglacial crustal deformation, Laurentide Ice Sheet. *Geografiska Annaler. Series A, Physical Geography* **54**, 1-11.
- Aubrey, D. G., Emery, K. K., Uchupi, E. (1988). Changing coastal levels of South America and the Caribbean region from tide-gauge records. *Tectonophysics* **154**, 269-284.
- Ballantyne, C. K., and McCarroll, D. (1995). The vertical dimensions of Late Devensian glaciation on the mountains of Harris and southeast Lewis, Outer Hebrides, Scotland. *Journal of Quaternary Science* **10**, 211–223.
- Ballantyne, C. K., and Hallam, G. E. (2001). Maximum altitude of Late Devensian glaciation on South Uist, Outer Hebrides, Scotland. *Proceedings of the Geologists' Association* **112**, 155–167.
- Ballantyne, C. K., Schnabel, C., and Xu, S. (2009). Readvance of the last British–Irish Ice Sheet during Greenland Interstade 1 (GI-1): the Wester Ross Readvance, NW Scotland. *Quaternary Science Reviews* **28**, 783-789.
- Ballantyne, C. K., and Stone, J. (2012). Did large ice caps persist on low ground in north-west Scotland during the Lateglacial Interstade? *Journal of Quaternary Science* **27(3)**, 297-306.
- Balson, P. S., and Jeffrey, D. H. (1991). The glacial sequence of the southern North Sea. In “Glacial Deposits in Great Britain and Ireland” Ehlers, J., Gibbard, P. L., Rose, J. (Eds.), pp. 245–253. A. A. Balkema, Rotterdam.

Benn, D. I. (1997). Glacier fluctuations in western Scotland. *Quaternary International* **38-39**, 137-147.

Benn, D. I., and Evans, D. J. A. (1998). "Glaciers and Glaciation. " Edward Arnold, London.

Benn, D. I., and Ballantyne, C. K. (2005). Palaeoclimatic reconstruction from Loch Lomond Readvance glaciers in the West Drumochter Hills, Scotland. *Journal of Quaternary Science* **20**, 577-592.

Benn, D. I., and Evans, D. J. A. (2008). A Younger Dryas ice cap to the north of Glen Roy: a new perspective on the origin of the Turret Fan. *In* "The Quaternary of Glen Roy and vicinity: Field Guide." (A. P. Palmer, J. J. Lowe, and J. Rose, Eds.), pp. 158-161. Quaternary Research Association, London.

Benn, D. I., and Evans, D. J. A. (2010). "Glaciers and Glaciation. " (2<sup>nd</sup> edition). Hodder Education, London.

Björck, S. (1995). A review of the history of the Baltic Sea, 13.0-8.0 ka BP. *Quaternary International* **27**, 19-40.

Bondevik, S., and Mangerud, J. (2002). A calendar age estimate of a very late Younger Dryas ice sheet maximum in western Norway. *Quaternary Science Reviews* **21**, 1661-1676.

Boulton, G. S., Smith, G. D., Jones, A. S., and Newsome, J. (1985). Glacial geology and glaciology of the last mid-latitude ice sheets. *Journal of the Geological Society of London* **142**, 447-474.

Boulton, G. S., Peacock, J. D., and Sutherland, D. G. (1991). Quaternary. *In* "The Geology of Scotland (3rd edition)" (Craig, G. Y. Eds.), pp. 503-544. Geological Society of London, London.

Boulton, G., Hagdorn, M. (2006). Glaciology of the British Isles Ice Sheet during the last glacial cycle: form, flow, streams and lobes. *Quaternary Science Reviews* **25**, 3359-3390.

Bowen, D. Q. (1981). The South Wales End Moraine: fifty years after. *In* "The Quaternary in Britain" (Neale, J., Flenley, J. Eds.), pp. 60-67. Pergamon Press, Oxford.

Bowen, D. Q., Phillips, F. M., McCabe, A. M., Knutz, P. C., and Sykes, G. A. (2002). New data for the Last Glacial Maximum in Great Britain and Ireland. *Quaternary Science Reviews* **21**, 89–101.

Bradwell, T., Stoker, M. S., and Larter, R. (2007). Geomorphological signature and flow dynamics of The Minch palaeo-ice stream, NW Scotland. *Journal of Quaternary Science* **22**, 609–622.

Bradwell, T., Stoker, M., Krabbendam, M. (2008a). Megagrooves and streamlined bedrock in NW Scotland: The role of ice streams in landscape evolution. *Geomorphology* **97**, 135-156.

Bradwell, T., Fabel, D., Stoker, M., Mathers, H., McHargue, L., and Howe, J. (2008b). Ice caps existed throughout the Lateglacial Interstadial in northern Scotland. *Journal of Quaternary Science* **23**, 401-407.

Bradwell, T., Stoker, M. S., Golledge, N. R. et al. (12 authors). (2008c). The northern sector of the last British Ice Sheet: maximum extent and demise. *Earth-Science Reviews* **88**, 207-226.

BRITICE GIS-files, [http://www.shef.ac.uk/geography/staff/clark\\_chris/britice](http://www.shef.ac.uk/geography/staff/clark_chris/britice) (Accessed 11 August 2010).

Carr, S. J., Holmes, R., van der Meer, J. JM., and Rose, J. (2006). The Last Glacial Maximum in the North Sea Basin: micromorphological evidence of extensive glaciation. *Journal of Quaternary Science* **21**, 131-153.

Chen, C. Y., and Rose, J. (2008a). Assessment of remote sensed imagery on the analysis of landforms in Glen Roy. In "The Quaternary of Glen Roy and vicinity: Field Guide." (A. P. Palmer, J. J. Lowe, and J. Rose, Eds.), pp. 36-45. Quaternary Research Association, London.

Chen, C. Y., and Rose, J. (2008b). A DSM perspective on the geomorphology of the region around Glen Turret and the adjacent part of Glen Roy. In "The Quaternary of Glen Roy and vicinity: Field Guide." (A. P. Palmer, J. J. Lowe, and J. Rose, Eds.), pp. 150-157. Quaternary Research Association, London.

Chen, C. Y., and Rose, J. (2008c). A DSM perspective on the geomorphology of the region around Caol Lairig and the Viewpoint in the lower section of Glen Roy. In "The



Quaternary of Glen Roy and vicinity: Field Guide." (A. P. Palmer, J. J. Lowe, and J. Rose, Eds.), pp.166-173. Quaternary Research Association, London.

Chiverell, R. C., and Thomas, G. S. P. (2010). Extent and timing of the Last Glacial Maximum (LGM) in Britain and Ireland: a review. *Journal of Quaternary Science* **25**, 535-549.

Clark, C. D. (1997). Reconstructing the evolutionary dynamics of former ice sheets using multi-temporal evidence, remote sensing and GIS. *Quaternary Science Reviews* **16**, 1067-1092.

Clark, C. D., Evans, D.J.A., Khatwa, A., Bradwell, T., Jordan, C.J., Marsh, S. H., Mitchell, W. A., and Bateman, M. D. (2004). Map and GIS database of landforms and features related to the last British Ice Sheet. *Boreas* **33(4)**, 359-375.

Clark, C. D., Hughes, A. L. C., Greenwood, S. L., Spagnolo, M. and Ng, F.S.L. (2009) Size and shape characteristics of drumlins, derived from a large sample, and associated scaling laws. *Quaternary Science Reviews* **28**, 677–92.

Dackombe, R. V., and Thomas, G. S. P. (1991). Glacial deposits and Quaternary stratigraphy of the Isle of Man. In "Glacial Deposits in Great Britain and Ireland." (Ehlers, J., Gibbard, P. L., Rose, J., Eds.), pp. 333–344. Balkema, Rotterdam.

Darwin, C. (1839). Observations on the Parallel Roads of Glen Roy, and other parts of Lochaber in Scotland, with an attempt to prove that they are of marine origin. *Philosophical Transactions of the Royal Society* **129**, 39–81.

Dawson, A. G. (1989). Distribution and development of the Main Rock Platform, western Scotland: reply. *Scottish Journal of Geology* **25**, 233–238.

Dawson, A. G., Hampton, S., Fretwell, P, Harrison, S. and Greengrass, P. (2002). Defining the centre of glacio-isostatic uplift of the last Scottish ice-sheet: the Parallel Roads of Glen Roy, Scottish Highlands. *Journal of Quaternary Science* **17**, 527-533.

Denton, G. H., and Hughes, T. J. (1981). "The Last Great Ice Sheets" Wiley, New York.

Eaves, S. (2009). The Loch Lomond Readvance in the Creag Meagaidh area: glacier reconstruction and wider implications for the region around Glen Roy. Unpublished M.Sc. thesis. Royal Holloway, University of London.

Ehlers, J., and Gibbard, P. L. (2004). "Quaternary Glaciations – Extent and Chronology. Part I – Europe." Elsevier Press, Amsterdam, London.

Ehlers, J., Gibbard, P. L., and Hughes, P. D. (2011). "Quaternary Glaciations – Extent and Chronology: A Closer Look." Elsevier Press, Amsterdam, London.

Estes, J. E., Hajic, E. J., and Tinney, L. R. (1983). Fundamentals of image analysis: analysis of visible and thermal infrared data. *In* "Manual of Remote Sensing" (Colwell, R. N., Eds). American Society of Photogrammetry, Falls Church, Virginia.

Evans, D. J. A., Clark, C. D., and Mitchell, W. A. (2005). The last British Ice Sheet: a review of the evidence utilized in the compilation of the Glacial Map of Britain. *Earth-Science Reviews* **70**, 253-312.

Everest, J., Bradwell, T., and Golledge, N. (2005). Subglacial landforms of the Tweed palaeo-ice stream. *Scottish Geographical Magazine* **121**, 163-173.

Everest, J., Bradwell, T., Fogwell, C. J., and Kubik, P. W. (2006). Cosmogenic <sup>10</sup>Be age constraints for the Wester Ross Readvance Moraine: insights into British ice-sheet behaviour. *Geografiska Annaler: Series A, Physical Geography* **88**, 9-17.

Fabel, D., Small, D., Miguens-Rodriguez, M, and Freeman, S. P. H. T. (2010). Cosmogenic nuclide exposure ages from the 'Parallel Roads' of Glen Roy. *Journal of Quaternary Science* **25**, 597-603.

Fenton, C. H. (1991). "Neotectonics in NW Scotland: a Field Guide." University of Glasgow, Glasgow.

Fenton, C. H. and Ringrose P. S, (1992). Late Quaternary movement along the Kinloch Hourn fault, Inverness-shire, *In* " Neotectonics in Scotland: A Field Guide" (Fenton, C.H., Eds). pp. 54–60, University of Glasgow.

Firth, C. R., (1992). Loch Ness Shorelines: evidence for isostatic depression during the Loch Lomond (Younger Dryas) Stadial. *In* "Neotectonics in Scotland: A Field Guide" (Fenton, C. Eds.), pp. 72-75. University of Glasgow, Glasgow.

Firth, C. R., Smith D. E., and Cullingford R. A. (1993). Late Devensian and Holocene glacio-isostatic uplift patterns in Scotland. *In* "Neotectonics: Recent Advances" (Firth C. R. Eds.), pp. 1–14. Quaternary Proceedings 3.

Firth, C. R., and Stewart, I. S. (2000). Postglacial tectonics of the Scottish glacio-isostatic uplift centre. *Quaternary Science Reviews* **19**, 1469-1493.

Fjeldskaar, W. (1994). The amplitude and decay of the glacial forebulge in Fennoscandia. *Norsk Geologisk Tidsskrift* **74**, 2-8.

Fretwell, P. T., Peterson, I. R., and Smith, D. E. (2004). The use of Gaussian trend surfaces for modelling glacio-isostatic crustal rebound. *Scottish Journal of Geology* **40**, 175-179.

Fretwell, P. T., Smith, D. E. and Harrison, S. (2008). The Last Glacial Maximum British–Irish Ice Sheet: a reconstruction using digital terrain mapping. *Journal of Quaternary Science* **23(3)**, 241-248.

Gibbard, P. L., and Clark, C. D. (2011). Pleistocene glaciation limits in Great Britain. In "Quaternary Glaciations – Extent and Chronology: A Closer Look." (Ehlers, J. *et al.* Eds.), pp. 75-94. Elsevier Press, Amsterdam, London.

Golledge, N. R., and Hubbard, A. (2005). Evaluating Younger Dryas glacier reconstructions in part of the western Scottish Highlands: a combined empirical and theoretical approach. *Boreas* **34**, 274–286.

Golledge, N. R. (2006). The Loch Lomond Stadial glaciation south of Rannoch Moor: new evidence and palaeoglaciological insights. *Scottish Geographical Journal* **122**, 326–343

Golledge, N. R. (2007). An ice cap landsystem for palaeoglaciological reconstructions: characterizing the Younger Dryas in western Scotland. *Quaternary Science Reviews* **26**, 213–229.

Golledge, N. R., Hubbard, A., and Sugden, D. E. (2008). High-resolution numerical simulation of Younger Dryas glaciations in Scotland. *Quaternary Science Reviews* **27**, 888-904.

Golledge, N. R. (2010). Glaciation of Scotland during the Younger Dryas stadial: a review. *Journal of Quaternary Science* **25**, 550-566.

- Goodenough, K.M., Krabbendam, M., Bradwell, T., Finlayson, A., and Leslie, A.G. (2009). NEXTMap hill-shaded digital surface model of the Ullapool area, with inset showing the location within Scotland. *Scottish Journal of Geology* **45**, 99-105.
- Graham, D. F. and Grant, D. R. (1991). A test of airborne, side-looking synthetic aperture radar in central Newfoundland for geological reconnaissance. *Canadian Journal of Earth Sciences* **28**, 257-265.
- Graham, A. G. C., Lonergan, L., and Stoker, M. S. (2007). Evidence for Late Pleistocene ice stream activity in the Witch Ground Basin, central North Sea, from 3D seismic reflection data. *Quaternary Science Reviews* **26**, 627–643.
- Gray, J. M. (1974). The Main Rock Platform of the Firth of Lorn, western Scotland. *Transactions of the Institute of British Geographers* **61**, 81-99.
- Gray, J. M. (1978). Low-level shore platforms in the south-west Scottish Highlands: altitude, age and correlation. *Transactions of the Institute of British Geographers* **NS 3**, 151-164.
- Greenwood, S. L., Clark, C. D. and Hughes, A. L. C. (2007). Formalising an inversion methodology for reconstructing ice-sheet retreat patterns from meltwater channels: application to the British Ice Sheet. *Journal of Quaternary Science* **22**, 637-645.
- Hall, A. M. (1997). Quaternary stratigraphy: the terrestrial record. In "Reflections on the Ice Age in Scotland." (Gordon, J. E. Eds.), pp. 59–71. Scottish Natural Heritage.
- Heine, K., Reuther, A. U., Thieke, H. U., Schutz, R., Schlaak, N., and Kubik, P. (2009). Timing of Weichselian ice marginal positions in Brandenburg (northeastern Germany) using cosmogenic in situ <sup>10</sup>Be. *Zeitschrift für Geomorphologie N.F* **53**, 433-454.
- Hiemstra, J. F., Ecvans, D. J., Scourse, J. D., McCarroll, D., Furze, M. F. A., and Rhodes, E. (2006). New evidence for a grounded Irish Sea glaciation of the Isles of Scilly. *Quaternary Science Reviews* **25**, 299-309.
- Holmes, J., Lowe, J.J., Wolff, E., and Srokosz, M. (2011). Rapid climate change: lessons from the recent geological past. *Global and Planetary Change* **79**, 157-162.
- Houmark-Nielsen, M., (1989). The last interglacial- glacial cycle in Denmark. *Quaternary International* **3/4**, 31- 39.

Hubbard, A. (1999). High-resolution modeling of the advance of the Younger Dryas ice sheet and its climate in Scotland. *Quaternary Research* **52**, 27–43.

Huddart, D. (1991). The glacial history and glacial deposits of the North and West Cumbrian lowlands. In "Glacial Deposits in Great Britain and Ireland. Ehlers" (J., Gibbard, P.L., Rose, J. Eds.), pp. 151–167. Balkema, Rotterdam.

INTERMAP product handbook and quick start guide, version 3.3. (Accessed 25 November 2010) [www.centremapslive.co.uk/files/producthandbookver3\\_3.pdf](http://www.centremapslive.co.uk/files/producthandbookver3_3.pdf).

Jamieson, T. F. (1863). On the parallel roads of Glen Roy and their place in the history of the glacial period. *Geological Society of London Quarterly Journal* **19**, 235–239.

Jamieson, T. F. (1892). Supplementary remarks on Glen Roy. *Geological Society of London Quarterly Journal* **48**, 5–28.

Jarman, D. (2008). The Roy-Lochy rock slope failure cluster: implications for glacial breaching, ice movements, and Parallel Road dislocations. In "The Quaternary of Glen Roy and vicinity: Field Guide." (A. P. Palmer, J. J. Lowe, and J. Rose, Eds.), pp. 98-104. Quaternary Research Association, London.

Johnson, D. W. (1933). The correlation of ancient marine levels. *Comptes Rendus du Congrès International de Géographie Paris* **2**, 42-54.

Johnson-Ferguson, I., (2004). Glacial-lacustrine sediments and landforms in Glen Turret, western Scotland. Unpublished BSc dissertation, University of St Andrews.

Key, R. M., Clark, G. C., May, F., Phillips, E. R., Chacksfield, B. C. and Peacock J. D. (1997). "Geology of the Glen Roy District" Geological Memoir Sheet 63W. British Geological Survey. The Stationery Office, London.

Kleiber, H.-P., Knies, J., and Niessen, F. (2000). The Late Weichselian glaciation of the Franz Victoria Through, northern Barents Sea: ice sheet extent and timing. *Marine Geology* **168**, 25–44.

Lambeck, K. (1991). Glacial rebound and sea-level change in the British Isles. *Terra Nova* **3**, 379–389.

Lambeck, K. (1993a). Glacial rebound of the British Isles. I. Preliminary model results. *Geophysical Journal International* **115**, 941–959.

- Lambeck, K. (1993b). Glacial rebound of the British Isles. II. A high-resolution, high-precision model. *Geophysical Journal International* **115**, 960–990.
- Lambeck, K. (1995). Late Devensian and Holocene shorelines of the British Isles from models of glacio-isostatic rebound. *Journal of the Geological Society of London* **152**, 437–448.
- Lambeck, K., Smither, C., and Johnston, P. (1998). Sea-level change, glacial rebound and mantle viscosity for northern Europe. *Geophysical Journal International* **134**, 102–144.
- Landvik, J. Y., Bondevik, S., Elverhi, A., Fjeldskaar, W., Mangerud, J., Salvigsen, O., Siegert, M. J., Svendsen, J. I., and Vorren, T. O. (1998). The last glacial maximum of Svalbard and the Barents Sea Area: ice sheet extent and configuration. *Quaternary Science Reviews* **17**, 43–75.
- Lauder, T. D. (1823). On the parallel roads of Lochaber. *Transactions of the Royal Society of Edinburgh* **9**, 1-64
- Li, X., Baker, A. B. and Hutt, T. (2002). Accuracy of airborne IFSAR mapping. In "2002 FIG/ASPRS/ACSM Annual Conference" Society for Photogrammetry and Remote Sensing, American.
- Li, X., Tennant, J. K., and Lawrence, G. (2004). Three-dimensional mapping with airborne IFSAR based STAR technology – Intermap's experiences. In "Proceedings of XXth ISPRS Congress". Istanbul, Turkey.
- Lidmar-Bergström, K., Elvhage, C. and Ringberg, B. (1991). Landforms in Skane, south Sweden. *Geografiska Annaler* **73A**, 61-91.
- Lillesand, T. M., and Kiefer, R. W. (2004). "Remote Sensing and Image Interpretation" (5<sup>th</sup> edition). Wiley & Sons, New York.
- Lowe, J. J. and Walker, M. J. C. (1997). "Reconstructing Quaternary Environments" (2<sup>nd</sup> edition). Addison Wesley Longman Ltd.
- Lowe, J. J., Rasmussen, S. O., Björck, S., Hoek, W. Z., Steffensen, J. P., Walker, M. J. C., and Yu, Z., INTIMATE group. (2008a). Precise dating and correlation of events in

the North Atlantic region during the Last Termination: a revised protocol recommended by the INTIMATE group. *Quaternary Science Reviews* **27**, 6-17.

Lowe, J. J., Palmer, A. P. and MacLeod, A., (2008b). Setting the context. In "The Quaternary of Glen Roy and vicinity: Field Guide." (A. P. Palmer, J. J. Lowe, and J. Rose, Eds.), pp.8-35. Quaternary Research Association, London.

Lowe, J. J. and Cairns, P., (1991). New pollen-stratigraphic evidence for the deglaciation and lake drainage chronology of the Glen Roy-Glen Spean area, *Scottish Journal of Geology* **27**, 41 – 56.

Lowick, S. and Bailey, R. M., (2008). Application of luminescence methods to the dating of glacial sediments associated with the Parallel Roads of Glen Roy. In "The Quaternary of Glen Roy and vicinity: Field Guide." (A. P. Palmer, J. J. Lowe, and J. Rose, Eds.), pp.92-109. Quaternary Research Association, London.

Lubinski, D. J., Korsun, S., Polyak, L., Forman, S. L., Lehman, S. J., Herlihy, F. A., and Miller, G. H. (1996). The last deglaciation of the Franz Victoria Through, northern Barents Sea. *Boreas* **25**, 89–100.

Lundquist, J., and Wohlfarth, B. (2001). Timing and east–west correlation of south Swedish ice marginal lines during the Late Weichselian. *Quaternary Science Reviews* **20**, 1127-1148.

Lundqvist, J. (1986). Late Weichselian glaciation and deglaciation in Scandinavia. *Quaternary Science Reviews* **5**, 269–292.

MacLeod, A., Palmer, A., Lowe, J.J., Rose, J., Bryant, C., and Merritt, J. (2011). Timing of glacier response to Younger Dryas climatic cooling in Scotland. *Global and Planetary Change* **79** (3-4), 264-274.

Matthews, J. A., Dawson, A. G. and Shakesby, R. A. (1986). Lake shoreline development, frost weathering and rock platform erosion in an alpine periglacial environment, Jotunheimen, southern Norway. *Boreas* **15**, 33-50.

McCabe, M. (1987). Quaternary deposits and glacial stratigraphy in Ireland. *Quaternary Science Reviews* **6**, 259-299.

Mercer, B. (2001). Comparing LIDAR and IFSAR: what can you expect? In "Proceedings of Photogrammetric Week 2001", Stuttgart, Germany.

Miller, A. A. (1939). Attainable standards of accuracy in the determination of preglacial sea levels by physiographic methods. *Journal of Geomorphology* **2**, 95-115.

Milne, D. (1847). On polished and striated rocks, lately discovered on Arthur Seat, and other places near Edinburgh. *Edinburgh New Philosophical Journal* **42**, 154-72.

Nesje, A., and Sejrup, H.-P. (1988). Late Weichselian/Devensian ice sheets in the North Sea and adjacent land areas. *Boreas* **17**, 371-384.

O'Cofaigh, C., and Evans, D. J. A. (2007). Radiocarbon constraints on the age of the maximum advance of the British-Irish Ice sheet in the Celtic Sea. *Quaternary Science Reviews* **26**, 1197-1203.

Palmer, A. P. (2005). The micromorphological description, interpretation and palaeoenvironmental significance of lacustrine clastic laminated sediments. Unpublished PhD thesis, University of London.

Palmer, A. P. (2008a). Description of laminated sediments on the surface of the Glen Turret Fan (NN342 922). In "The Quaternary of Glen Roy and vicinity: Field Guide." (A. P. Palmer, J. J. Lowe, and J. Rose, Eds.), pp.127-133. Quaternary Research Association, London.

Palmer, A. P. (2008b). Developing a varve chronology for the Spean–Roy lakes: the Lochaber Master Varve Chronology (LMVC). In "The Quaternary of Glen Roy and vicinity: Field Guide." (A. P. Palmer, J. J. Lowe, and J. Rose, Eds.), pp.139-149. Quaternary Research Association, London.

Palmer, A. P., Rose, J., Lowe, J. J., and MacLeod, A. (2010). Annually-resolved dating of Younger Dryas glaciation and proglacial lake duration in Glen Roy and Glen Spean, Western Scottish Highlands. *Journal of Quaternary Science* **25** (4), 581–596.

Palmer, A. P., Rose, J., and Rasmussen, S. O. (2012). Evidence for phase-locked changes in climate between Scotland and Greenland during GS-1 (Younger Dryas) using micromorphology of glaciolacustrine varves from Glen Roy. *Quaternary Science Reviews* **36**, 114-123.

Peacock, J. D., (1986). Alluvial fans and an outwash fan in upper Glen Roy, Lochaber. *Scottish Journal of Geology* **22**, 347–366.



Peacock, J. D., and Cornish R. (1989). "Glen Roy Area: Field Guide." Quaternary Research Association, Cambridge.

Peacock, J. D., and May, F. (1993). Pre-Flandrian slope deformation in the Scottish Highlands: examples from Glen Roy and Glen Gloy. *Scottish Journal of Geology* **29**, 183-189.

Peltier, W. R., and Fairbanks, R. G. (2006). Global glacial ice volume and Last Glacial Maximum duration from an extended Barbados sea level record. *Quaternary Science Reviews* **25**, 3322-3337.

Pennant, T. (1771). "A Tour in Scotland 1769." John Monk, Chichester.

Phillips, W. M., Hall, A. M., Ballnatyne, C. K., Binnie, S., Kubik, P. W., and Freeman, S. (2008). Extent of the last ice sheet in northern Scotland tested with cosmogenic <sup>10</sup>Be exposure ages. *Journal of Quaternary Science* **23**, 101-108.

Polyak, L., Forman, S. L., Herlihy, F. A., Ivanov, G., and Krinitsky, P. (1997). Late Weichselian deglacial history of the Svyataya (Saint) Anna Through, northern Kara Sea, Arctic Russia. *Marine Geology* **143**, 169–188.

Prestwich, J. (1879). On the Origin of the Parallel Roads of Lochaber and Their Bearing on Other Phenomena of the Glacial Period. *Philosophical Transactions of the Royal Society of London* **170**, 663-726.

Punkari, M. (1982) Glacial geomorphology and dynamics in the eastern parts of the Baltic Shield interpreted using Landsat imagery. *Photogrammetric Journal of Finland* **9**, 77-93.

Rainio, H., Saarnisto, M., and Ekman, I. (1995). Younger Dryas end moraines in Finland and NW Russia. *Quaternary International* **28**, 179-192.

Rasmussen, S. O., Seierstad, I. K., Andersen, K. K., Bigler, M., Dahl-Jensen, D., and Johnsen, S. J. (2008). Synchronisation of the NGRIP, GRIP and GISP 2 ice cores across MIS2 and palaeoclimatic implications. *Quaternary Science Reviews* **27**, 18-28.

Ringrose, P. S. (1987). "Fault activity and palaeoseismicity during Quaternary time in Scotland." Unpublished PhD thesis, University of Strathclyde.

- Ringrose, P. S. (1989a). Palaeoseismic liquefaction event in late Quaternary lake sediments at Glen Roy, Scotland. *Terra Nova* **1**, 57–62.
- Ringrose, P. S. (1989b). Recent fault movement and paleoseismicity in western Scotland. *Tectonophysics* **163**, 305–314.
- Rinterknecht, V. R., Marks, L., Piotrowski, J. A., Raisbeck, G. M., Yiou, F., Brook, E. J., and Clark, P. U. (2005). Cosmogenic  $^{10}\text{Be}$  ages on the Pomeranian Moraine, Poland. *Boreas* **34**, 186–191.
- Rinterknecht, V. R., Clark, P. U., Raisbeck, G. M., Yiou, F., Bitinas, A., Brook, E. J., Marks, L., Zelcs, V., Lunkka, J-P., Pavlovskaya, I. E., Piotrowski, J. A., and Raukas, A. (2006). The last deglaciation of the southeastern sector of the Scandinavian Ice Sheet. *Science* **311**, 1449-1452.
- Rinterknecht, V. R., Pavlovskaya, I. E., and Clark, P. U. (2007). Timing of the last deglaciation in Belarus. *Boreas* **36**, 307-313.
- Rose, J., and Letzer, J. M. (1975). Drumlin measurements: a test of the reliability of data derived from 1:25,000 scale topographic maps. *Geological Magazine* **112**, 361-371.
- Rose, J. (1981). Field guide to the Quaternary geology of the southeastern part of the Loch Lomond basin. *Proceedings of the Geological Society of Glasgow* **123**, 12-28.
- Rose, J. (1985). The Dimlington Stadial/Dimlington Chronozone: a proposal for naming the main glacial episode of the Late Devensian in Britain. *Boreas* **14**, 225-230.
- Rose, J. (1987). Drumlins as part of a glacier bedform continuum. In "Drumlin Symposium" (Menzies, J., Rose, J. Eds.). Balkema, Rotterdam.
- Rose, J., Lowe, J. J., and Switsur, R. V. (1988). A radiocarbon date on plant detritus beneath till from the type area of the Loch Lomond Readvance, *Scottish Journal of Geology* **24**, 113-124.
- Rose, J. (1989). Stadial type sections in the British Quaternary. In "Quaternary Type Sections: Imagination or Reality." (Rose, J., and Schluchter, C. Eds.), pp. 45– 67. Balkema, Rotterdam.

Rose, J., and Lloyd-Davies, M. (2003). Croftamie: sediments and stratigraphy at the key section for the Loch Lomond Readvance. *In* "The Quaternary of the Western Highland Boundary." (D. J. A. Evans, Eds.), pp. 81-87. Quaternary Research Association, London.

Rose, J., and Smith, M. J. (2008). Glacial geomorphological maps of the Glasgow region, western central Scotland. *Journal of Maps* **v2008**, 399-416.

Röthlisberger, H. (1972). Water pressure in intra- and subglacial channels. *Journal of Glaciology* **11**, 177–203.

Rudwick, M. (2009). The Parallel Roads of Glen Roy: In the Footsteps of Charles Darwin - A Field Guide. History of Geology Group, Geological Society of London. [http://www.darwinproject.ac.uk/wp-content/uploads/2010/04/Rudwick\\_Glen-Roy-field-guide\\_DCP.pdf](http://www.darwinproject.ac.uk/wp-content/uploads/2010/04/Rudwick_Glen-Roy-field-guide_DCP.pdf) (Accessed 7 June 2010)

Russell, A. J. and Marren, P. M. (1998). A Younger Dryas (Loch Lomond Stadial) jökulhlaup deposit, Fort Augustus, Scotland. *Boreas* **27**, 231-242.

Schaetzl, R. J., Drzyzga, S. A., Weisenborn, B. N., Kincare, K. A., Lepczyk, X. C., Shein, K., Dowd, C. M., and Linker, J. (2002). Measurement, correlation, and mapping of glacial Lake Algonquin shorelines in northern Michigan. *Annals of the Association of American Geographers* **92** (3), 399-415.

Schreve R L. (1972). Movement of water in glaciers. *Journal of Glaciology* **11**, 205–214.

Scourse, J. D., and Furze, M. F. A. (2001). A critical review of the glaciomarine model for Irish Sea deglaciation: evidence from southern Britain, the Celtic shelf and adjacent continental slope. *Journal of Quaternary Science* **16** (5), 419–434.

Shackleton, N. J. (1987). Oxygen isotopes, ice volume and sea level. *Quaternary Science Reviews* **6**, 183-190.

Shennan, I., Lambeck, K., Horton, B. P., Innes, J. B., Lloyd, J. M., McArthur, J. J., Purcell, T., and Rutherford, M. M. (2000). Late Devensian and Holocene records of relative sea-level changes in northwest Scotland and their implications for glacio-hydro-isostatic modelling. *Quaternary Science Reviews* **19**, 1103-1136.

Shakesby, R. A. and Matthews, J. A. (1987). Frost weathering and rock platform erosion on periglacial lake shorelines: a test of a hypothesis. *Norsk geologisk Tidsskrift* **67**, 197-203.

Shennan, I., Peltier, W. R., Drummond, R., and Horton, B. P. (2002). Global to local scale parameters determining relative sea-level changes and the post-glacial isostatic adjustment of Great Britain. *Quaternary Science Reviews* **21**, 397–408.

Shin, R. A., and Barron, E. (1989). Climate sensitivity to continental ice sheet size and configuration. *Journal of Climate* **2**, 1517–1537.

Simpson, J. B. (1933). The Late-glacial readvance moraines of the Highland border west of the River Tay. *Transactions of the Royal Society of Edinburgh* **61**, 687-98.

Sissons, J. B. (1967). "The Evolution of Scotland's Scenery." Edinburgh, Oliver and Boyd.

Sissons, J. B. (1972). Dislocation and non-uniform uplift of raised shorelines in the western part of the Forth valley. *Transactions of the Institute of British Geographers* **55**, 145–159.

Sissons, J. B. (1974). A lateglacial ice cap in the central Grampians, Scotland. *Transactions of the Institute of British Geographers* **62**, 95-114.

Sissons, J. B. (1977). "The Parallel Roads of Glen Roy" Nature Conservancy Council, London.

Sissons, J.B. (1978). The parallel roads of Glen Roy and adjacent glens, Scotland. *Boreas* **7**, 229–244.

Sissons, J. B. (1979a). Catastrophic lake drainage in Glen Spean and the Great Glen, Scotland. *Journal of the Geological Society of London* **136**, 215–224.

Sissons, J. B. (1979b). The limit of the Loch Lomond Advance in Glen Roy and vicinity. *Scottish Journal of Geology* **15**, 31–42.

Sissons, J. B. (1979c). The later Lakes and associated fluvial terraces of Glen Roy, Glen Spean and vicinity. *Transactions of the Institute of British Geographers* **NS 4**, 12-29.

- Sissons, J. B. (1979d). Palaeoclimatic inferences from former glaciers in Scotland and the Lake District. *Nature* **278**, 518-21.
- Sissons, J. B. (1979e). The Loch Lomond Advance in the Cairngorm Mountains. *Scottish Geographical Magazine* **95**, 66-82.
- Sissons J. B. (1980a). Palaeoclimatic inferences from Loch Lomond Advance glaciers. In "Studies in the Lateglacial of North-west Europe", (Lowe J. J., Gray J. M., and Robinson J. E. Eds), pp. 31–44. Pergamon Press, Oxford.
- Sissons J. B. (1980b). The Loch Lomond Advance in the Lake District, northern England. Transactions of the Royal Society of Edinburgh. *Earth Sciences* **71**, 13–27.
- Sissons, J. B. (1981a). The last Scottish ice sheet: facts and speculative discussion. *Boreas* **10**, 1–17.
- Sissons, J. B. (1981b). Lateglacial marine erosion and a jökulhlaup deposit in the Beaully Firth. *Scottish Journal of Geology* **17**, 7–19.
- Sissons, J. B. (1982). A former ice-dammed lake and associated glacier limits in the Achnasheen area, central Ross-shire. *Transactions of the Institute of British Geographers* **NS 7**, 98-116.
- Sissons, J. B., and Cornish, R. (1982a). Rapid localised glacio-isostatic uplift at Glen Roy, Scotland. *Nature* **297**, 213–214.
- Sissons, J. B., and Cornish, R. (1982b). Differential glacio-isostatic uplift of crustal blocks at Glen Roy, Scotland. *Quaternary Research* **18**, 268–288.
- Sissons, J. B., and Cornish, R. (1983). Fluvial landforms associated with icedammed lake drainage in upper Glen Roy, Scotland. *Proceedings of the Geologists' Association* **94**, 45–52.
- Smith, D. E., Sissons, J. B., and Cullingford, R. A. (1969). Isobases for the Main Perth Raised Shoreline in south-east Scotland as determined by trend-surface analysis. *Transactions of the Institute of British Geographers* **46**, 45-52.
- Smith, D. E., Cullingford, R. A., and Firth, C. R. (2000). Patterns of isostatic land uplift during the Holocene: evidence from mainland Scotland. *Holocene* **10(4)**, 489–501.

Smith, D. E., Fretwell, P. T., Cullingford, R. A., and Firth, C. R. (2006). Towards improved empirical isobase models of Holocene land uplift for mainland Scotland, UK. *Philosophical Transactions of the Royal Society A* **364**, 949–972.

Smith, M. J. (2003). "Technical Developments for the Geomorphological Reconstruction of Palaeo Ice Sheets from Remotely Sensed Data" PhD Thesis, Sheffield University.

Smith, M. J., and Clark, C. D. (2005). Methods for the visualisation of digital elevation models for landform mapping. *Earth Surface Processes Landforms* **30(7)**, 885–900.

Smith, M. J., Rose, J., and Booth, S. (2006). Geomorphological mapping of glacial landforms from remotely sensed data: an evaluation of the principal data sources and an assessment of their quality. *Geomorphology* **76**, 148–165.

Smith, M. J. and Wise, S. M. (2007) Problems of bias in mapping linear landforms from satellite imagery. *Journal of Applied Earth Observation and Geoinformation* **9**, 65-78.

Stewart, I. S., Sauber, J., and Rose, J. (2000). Glacio-seismotectonics: ice sheets, crustal deformation and seismicity. *Quaternary Science Reviews* **19**, 1367–1389.

Stone, J. O., Ballantyne, C. K. (2006). Dimensions and deglacial chronology of the Outer Hebrides Ice Cap, northwest Scotland: implications of cosmic ray exposure dating. *Journal of Quaternary Science* **21**, 75–84.

Sutherland, D. G. (1984a). Modern glacier characteristics as a basis for inferring former climates with particular reference to the Loch Lomond Stadial. *Quaternary Science Reviews* **3**, 291–309.

Sutherland, D. G. (1984b). The Quaternary deposits and landforms of Scotland and the neighbouring shelves: a review. *Quaternary Science Reviews* **3**, 157–254.

Svendsen, J. I., Alexanderson, H., Astakhov, V. I., Demidov, I., Dowdeswell, J. A. et al. (30 authors) (2004). Late Quaternary ice sheet history of northern Eurasia. *Quaternary Science Reviews* **23**, 1229-1271.

Synge, F. M. (1977). Records of sea levels during the Late Devensian. *Philosophical Transactions of the Royal Society of London* **280**, 211–228.

Trenhaile, A. S. (2002). Rock coasts, with particular emphasis on shore platforms. *Geomorphology* **48**, 7-22.

Tye, G. (2007). "An investigation of the sediments in Caol Lairig valley, Scottish Highlands: implications for landscape evolution of the Glen Roy area during the Loch Lomond Stadial." Unpublished M.Sc. thesis, University of London.

Van Dam, T. M., Wahr, J., Chao, Y., Leuliette, E. (1997). Predictions of crustal deformation and of geoid and sea-level variability caused by oceanic and atmospheric loading. *Geophysical Journal International* **129**, 507-517.

Walcott, R. I. (1970). Isostatic response to loading of the crust in Canada. *Canadian Journal of Earth Sciences* **7**, 716-727.

## Appendix 1 Creating the rotating map

The rotating map in the present research is an animation based on the application of the Graphics Interchange Format techniques. The Graphics Interchange Format (refers as GIF in the following part) is a bitmap image format that was introduced by **CompuServe** (a Internet technique company) in 1987 to provide a colour image format for their file downloading areas, replacing their earlier run-length encoding (RLE) format, which was black and white only. Since it launched, it became very popular on the World Wide Web, because it used LZW data compression technique which was more efficient than the other formats such as PCX and MacPaint used in that time. It can save time in the downloading process and more importantly, it is widely supported for the World Wide Web environment.

The GIF was initially used for one static image until *Netscape* designed the Netscape Application Block in the 1990s which allow the static image to be transformed into an animation image. These application blocks were first applied to make animations in Netscape Navigator version 2.0, and then spread to other browsers. In general, the GIF file is suitable for sharp-edged line art (such as logos) with a limited number of colours. It can also be used to store low-colour sprite data for games or for small animations and low-resolution film clips. The reason I chose this technique in the present research is because it supports animations which can be used to simulate illumination changes and it is also easy to obtain in commercial or free image process software.

This technique was first applied by Smith (2003) to illustrate the illuminate azimuth bias effect in the Lough Gara, Ireland. In the present research, images generated with different illumination angles were organized in sequence and saved in a GIF formation to make it become an animation. The rotating map was then used as a mapped landform boundary testing platform to correct the landform boundary.

Detail procedures of making the rotating map are as follows:

The reason for using the rotating map is that the changes of illumination source on the DEM will affect the observer's visualization ability. No single hillshaded map can represent the whole features in one shot. Mapping result based on limited illumination source can not represent the true landform condition. Therefore, it is necessary to check the mapped landform boundary with image changing constantly in illumination source angle. In the present research, **Adobe ImageReady** was used to make a simple animation which can simulate the illumination source changing in sequence.



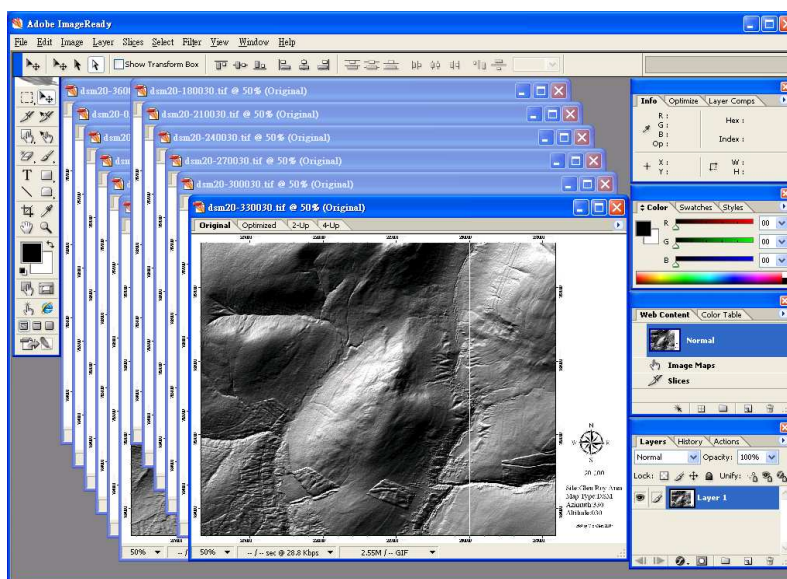
### Step 1: Generating hillshaded maps.

Hillshaded maps in the present research were generated using the **Spatial analyst** model in **Arc GIS**. The altitude and azimuth angle were parameters needed to be set up in this process. The rotating map is fixed in altitude angle and changes in azimuth angle in sequence. For low relief changing glacial landforms, such as drumlins, it is recommended to use a lower altitude angle (25° was used in the present research). However, this parameter is dependent on the mapping operator's eyesight; the best angle is the angle which allows the operator to visualize the majority of the mapping target. The azimuth angle was changed in 10° intervals in this research. Smaller azimuth angle intervals can be used but the size and complexity of the rotating map will also increase. Generated hillshaded maps were then put into a single folder for the next step.

### Step 2: Using Adobe ImageReady.

Start Adobe ImageReady by clicking your **Start** menu, then **Programs-> Adobe ImageReady CS2**

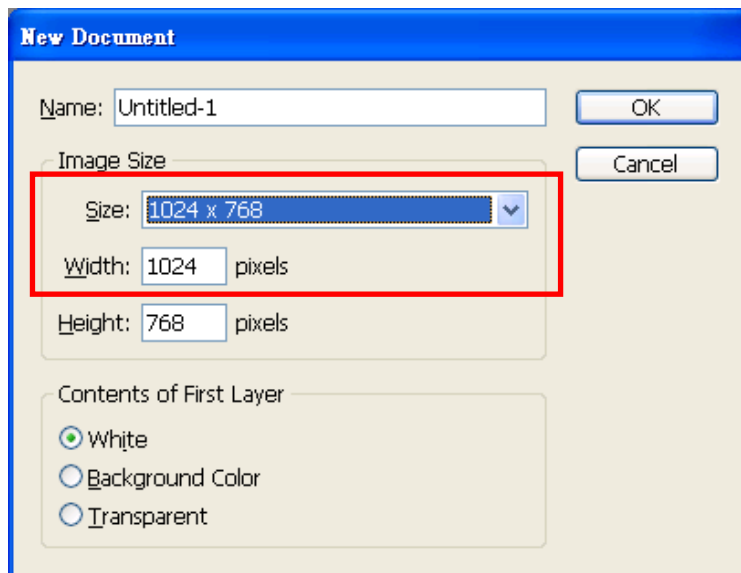
When the Adobe ImageReady dialog opens, clicking the **File->Open** from menu bar to open hillshaded maps generated in step 1.



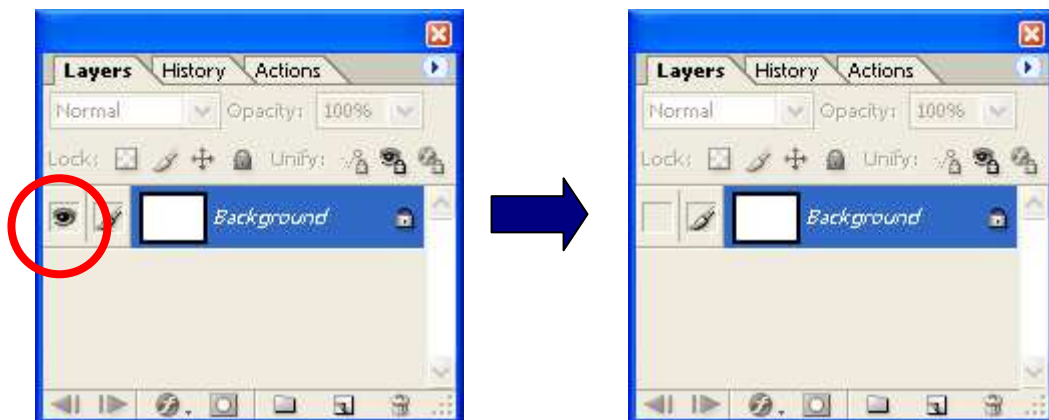
### Step 3: Create a new document.

- Click **File->New**, then the New Document dialog will appear as below.
- From **Size** dropdown arrow, select **1024 x 768** as your image size.
- Click **OK**.

This new document will be used as a base layer, all the hillshaded maps that opened in step 2 will be overlapping in this document.

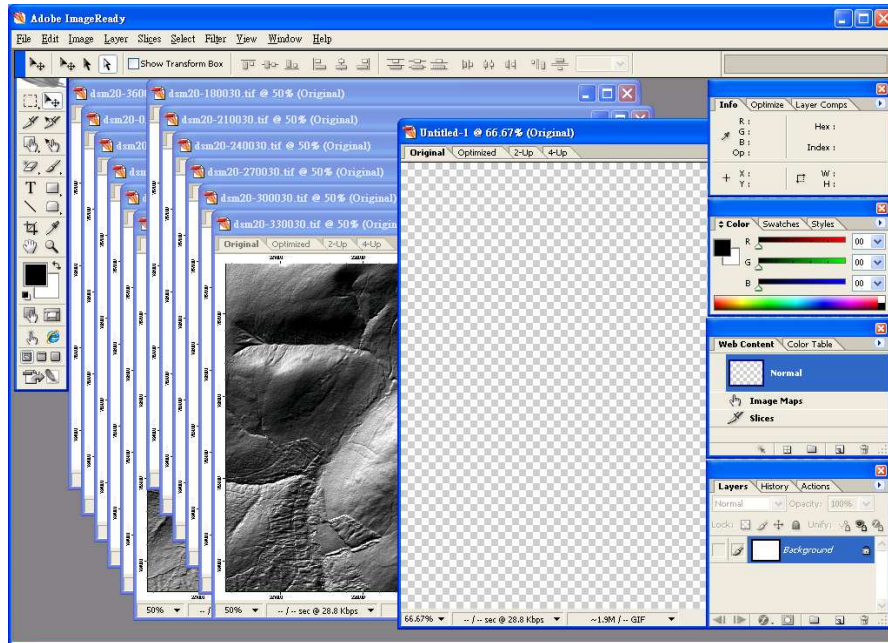


From the Layer dialog, on the right bottom of the Adobe ImageReady window, click the “eye” to make the base layer become invisible. This can help the operator adjust the map position in the overlapping process.



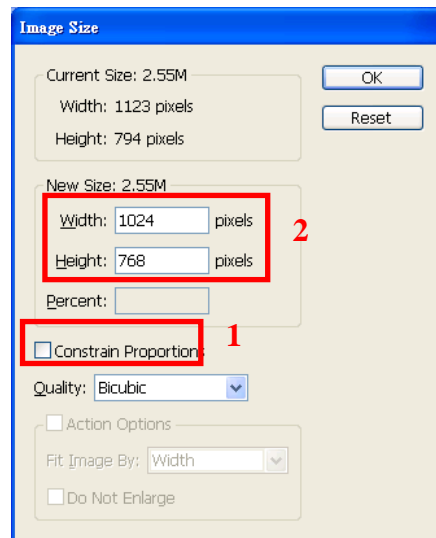
#### Step 4: Adjust each hillshaded map’s size.

- Click the hillshaded map to make it active(start from the smallest or largest azimuth angle and process in azimuth angle changing sequence)
- Open the Image Size edit dialog by clicking the **Image->Image Size**



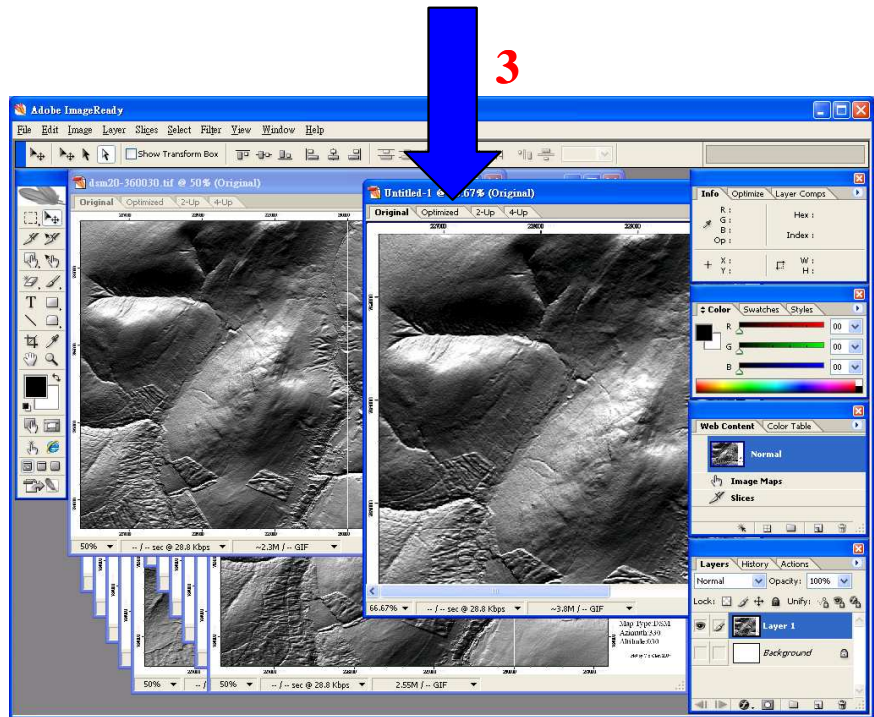
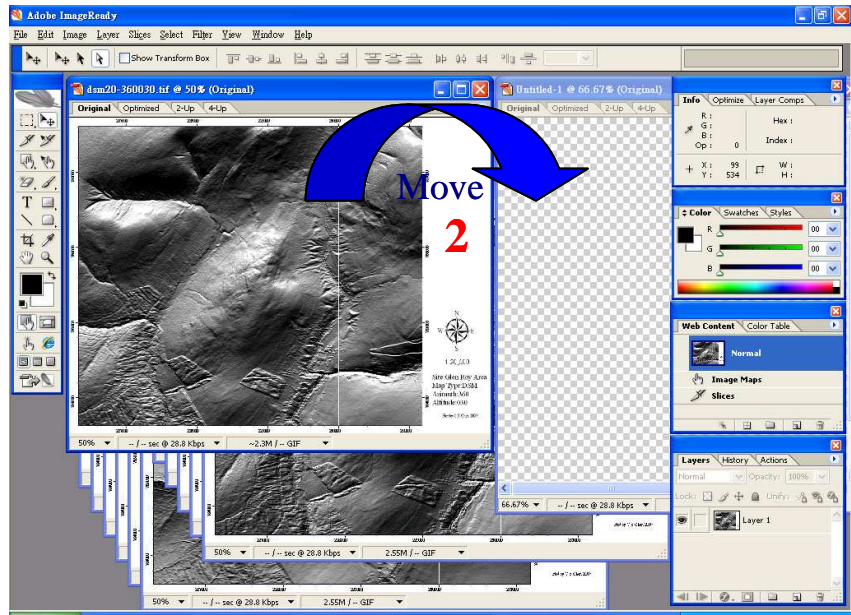
Setting the new size:

- Close the Constrain Proportions function.
- Width:1024 pixels, Height: 768 pixels.
- Click OK.

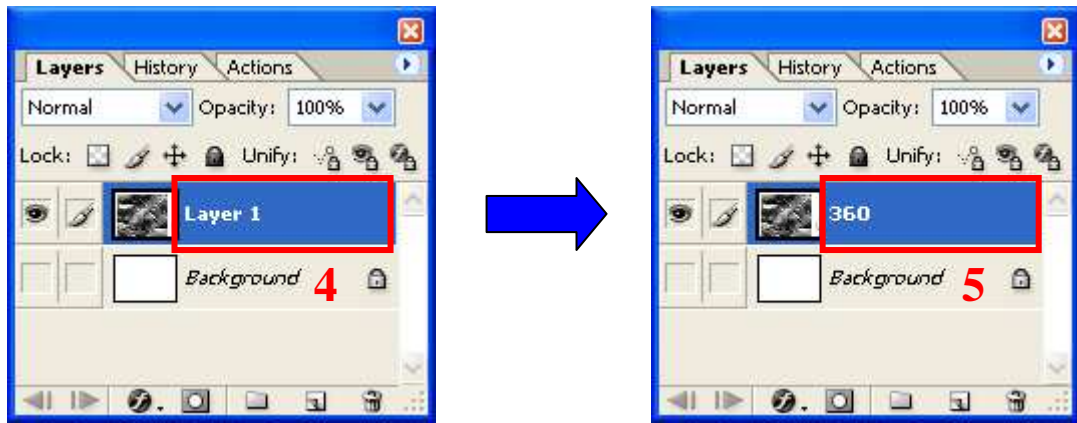


### Step 5: Overlapping images.

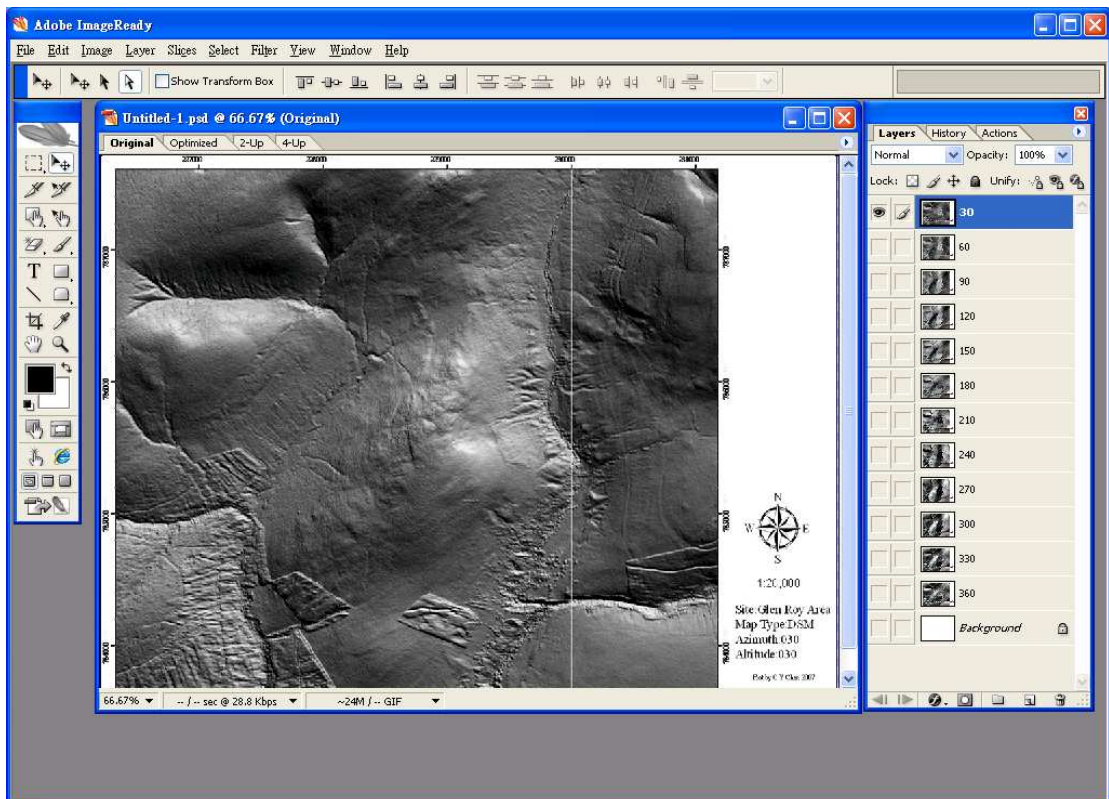
- Click the **Move Tool** button on the Tool palette.
- Move the mouse index on to the first hillshaded image, right click and hold on your mouse to move the hillshaded map on to the created new document.
- Adjust the map position in the new document.
- Close the edit image.



- Click the layer name in the Layer palette.
- Change the layer name from Layer1 to 360(It is recommend to use the illumination azimuth angle of this hillshaded map as the layer name).



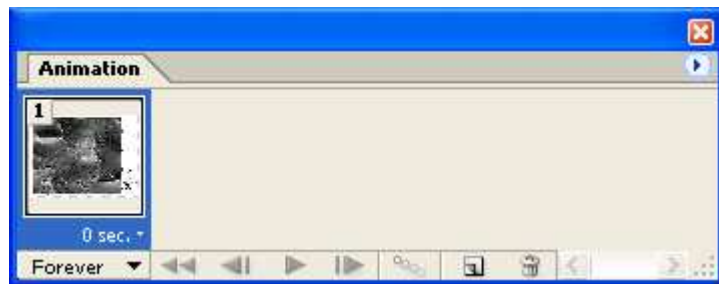
Repeat the same procedure until all hillshaded maps are well overlapped in the new document.



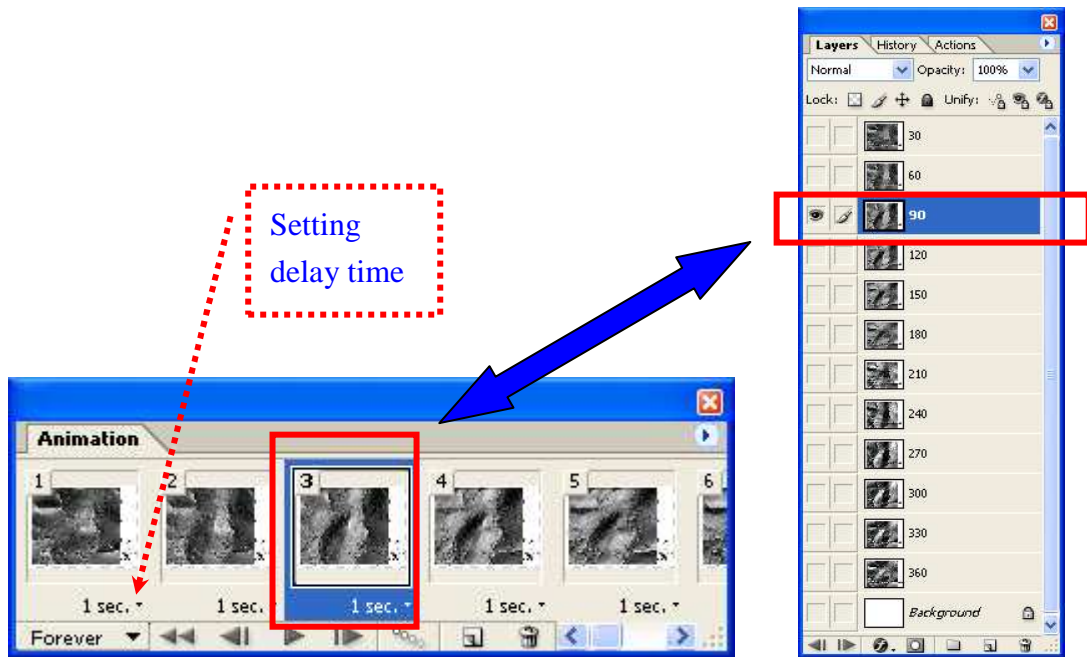
## Step 6: Creating an animation.

An animation is a sequence of images, or frames, that is displayed over time. Each frame varies slightly from the preceding frame, creating the illusion of movement when the frames are viewed in quick succession. In this step, the Animation palette and the Layers palette were used to create animation frames.

- From menu bar choose **Window-> Animation**, to turn on the animation pallet in the main workspace.
- Click the **Duplicates current frames** button and create **12** frames. (the number of frames depending on the number of hillshaded map used to make the animation; in this example azimuth angle interval is  $30^\circ$ )



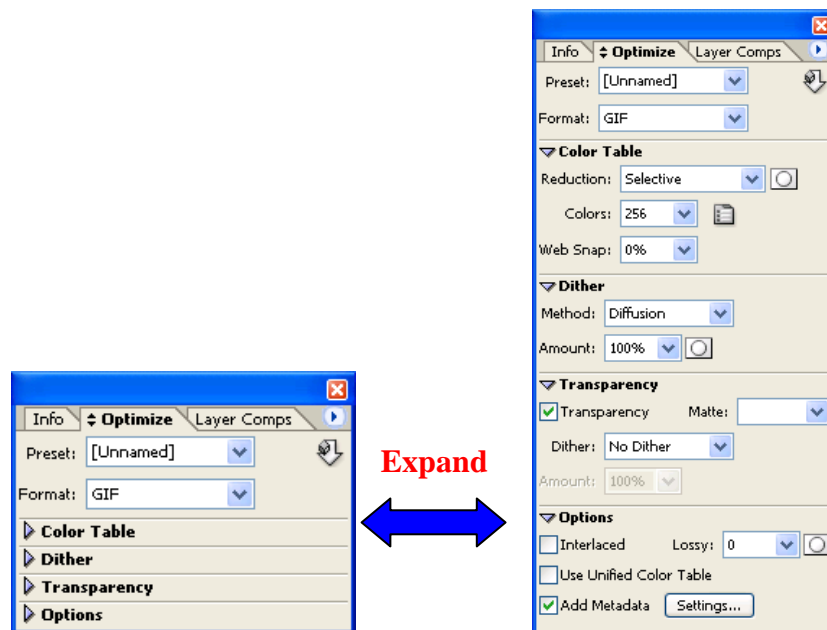
- Assign the delay time to each frame and specify looping so that the animation runs continuously. (For example, to represent the  $90^\circ$  azimuth hillshaded map on the third frame, we need to click the third frame in the Animation pallet to make it become active, then make sure that the  $90^\circ$  azimuth hillshaded map is the only one map opened in the Layer pallet).
- Delay time can be set by clicking the drop-down arrow on the bottom of each frame.



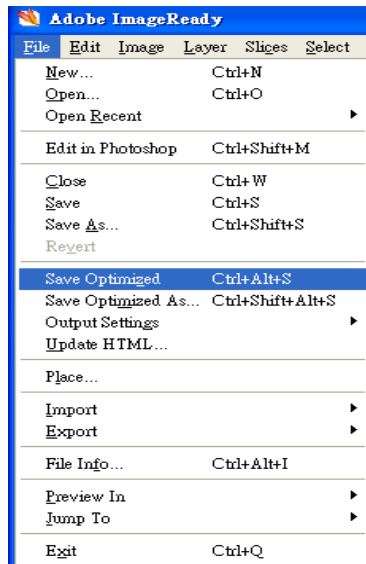
### Step 7: Output GIF file.

When we are satisfied with the animation we need to optimize the file before saving it.

- From the menu bar choose **Window-> Optimize**, to turn on the optimize pallet.
- Set the Format as **GIF**, Colour as **256**.



Choose **Save Optimized** from the main menu bar and save the finished animation as a GIF file.



The generated GIF file can be opened in image or picture viewer software such as the **Windows Picture and Fax Viewer** or **ACDSee**.

## **Appendix 2 Rotating maps (See CD):**

- 2.1 Drumlin mapping experiment
- 2.2 Kame and Kettle mapping experiment
- 2.3 Meltwater channel mapping experiment

## **Appendix 3 Shoreline surface analysis data (See CD):**

- 3.1 Analysis of shoeline width and slope
- 3.2 NEXTMap capability test 1 - Heathrow airport
- 3.3 NEXTMap capability test 2 - Loch Laggan
- 3.4 NEXTMap capability test 3 - Alcan Hydroelectrical pipes
- 3.5 Shoreline surface analysis-measure points
- 3.6 Shoreline surface trend analysis

## **Appendix 4 MSc students levelling of Parallel Road sections T and U., Glen Roy-Patrick Frings (See CD)**

## **Appendix 5 MSc students levelling of Parallel Road sections T and U., Glen Roy-Stephen Bate (See CD)**



**Appendix 6-Glen Roy - Shoreline surface gradient -260D\_325C\_350C  
(See CD)**

**Appendix 7- Glen Roy - Shoreline surface gradient -  
260-All\_325-All\_350-All (See CD)**

**Appendix 8 - Glen Roy - Overall landforms -NEXTMap (See CD)**

**Appendix 9 - Glen Roy - Overall landforms -OS map (See CD)**